frontiers | Research Topics

# Sex differences in immunometabolism, prophylaxis and therapy

**Edited by**
Suresh Mishra, Milica Vujičić and Ashley Fink

**Published in**
Frontiers in Immunology

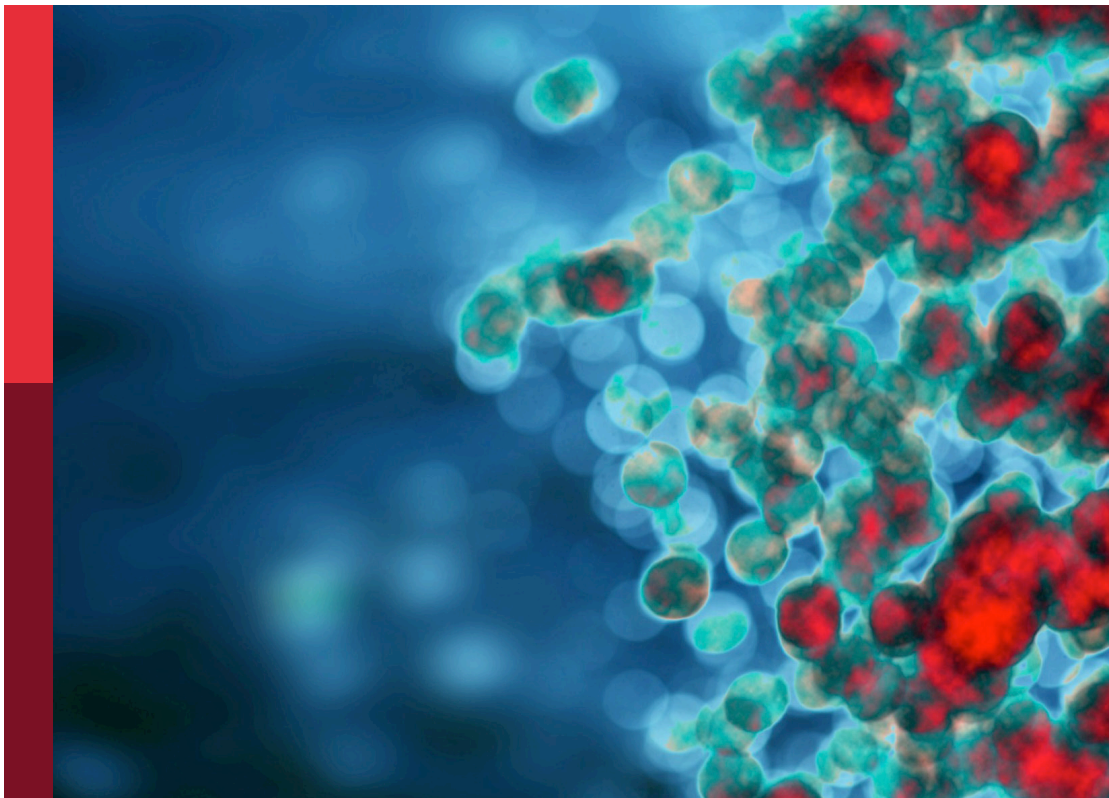

ISSN 1664-8714
ISBN 978-2-8325-3291-1
DOI 10.3389/978-2-8325-3291-1

## About Frontiers

Frontiers is more than just an open access publisher of scholarly articles: it is a pioneering approach to the world of academia, radically improving the way scholarly research is managed. The grand vision of Frontiers is a world where all people have an equal opportunity to seek, share and generate knowledge. Frontiers provides immediate and permanent online open access to all its publications, but this alone is not enough to realize our grand goals.

## Frontiers journal series

The Frontiers journal series is a multi-tier and interdisciplinary set of open-access, online journals, promising a paradigm shift from the current review, selection and dissemination processes in academic publishing. All Frontiers journals are driven by researchers for researchers; therefore, they constitute a service to the scholarly community. At the same time, the *Frontiers journal series* operates on a revolutionary invention, the tiered publishing system, initially addressing specific communities of scholars, and gradually climbing up to broader public understanding, thus serving the interests of the lay society, too.

## Dedication to quality

Each Frontiers article is a landmark of the highest quality, thanks to genuinely collaborative interactions between authors and review editors, who include some of the world's best academicians. Research must be certified by peers before entering a stream of knowledge that may eventually reach the public - and shape society; therefore, Frontiers only applies the most rigorous and unbiased reviews. Frontiers revolutionizes research publishing by freely delivering the most outstanding research, evaluated with no bias from both the academic and social point of view. By applying the most advanced information technologies, Frontiers is catapulting scholarly publishing into a new generation.

## What are Frontiers Research Topics?

Frontiers Research Topics are very popular trademarks of the *Frontiers journals series*: they are collections of at least ten articles, all centered on a particular subject. With their unique mix of varied contributions from Original Research to Review Articles, Frontiers Research Topics unify the most influential researchers, the latest key findings and historical advances in a hot research area.

Find out more on how to host your own Frontiers Research Topic or contribute to one as an author by contacting the Frontiers editorial office: frontiersin.org/about/contact

# Sex differences in immunometabolism, prophylaxis and therapy

**Topic editors**

Suresh Mishra — University of Manitoba, Canada

Milica Vujičić — University of Gothenburg, Sweden

Ashley Fink — College of Saint Benedict and Saint John's University, United States

**Citation**

Mishra, S., Vujičić, M., Fink, A., eds. (2023). *Sex differences in immunometabolism, prophylaxis and therapy*. Lausanne: Frontiers Media SA.

doi: 10.3389/978-2-8325-3291-1

# Table of contents

frontiers | Frontiers in Immunology

TYPE Editorial
PUBLISHED 07 August 2023
DOI 10.3389/fimmu.2023.1259382



OPEN ACCESS

EDITED AND REVIEWED BY
Josep Bassaganya-Riera,
Landos Biopharma, Inc., United States

*CORRESPONDENCE
Milica Vujičić
milica.vujicic@gu.se

RECEIVED 15 July 2023
ACCEPTED 21 July 2023
PUBLISHED 07 August 2023

CITATION
Fink A, Mishra S and Vujičić M (2023) Editorial: Sex differences in immunometabolism, prophylaxis and therapy.
*Front. Immunol.* 14:1259382.
doi: 10.3389/fimmu.2023.1259382



# Editorial: Sex differences in immunometabolism, prophylaxis and therapy

Ashley Fink[1], Suresh Mishra[2] and Milica Vujičić[3]*

[1]Department of Biology, College of Saint Benedict and Saint John's University, Collegeville, MN, United States, [2]Department of Internal Medicine, College of Medicine, Rady Faculty of Health Sciences, University of Manitoba, Winnipeg, MB, Canada, [3]Department of Physiology, Institute of Neuroscience and Physiology, The Sahlgrenska Academy at University of Gothenburg, Göteborg, Sweden

KEYWORDS

**sex difference, metabolism, immunity, therapy, immunometabolic dysregulation**

Editorial on the Research Topic
Sex differences in immunometabolism, prophylaxis and therapy

The immune system and metabolism are profoundly intertwined on a whole-body and cellular level, thus affecting homeostatic and pathological processes. Sex differences in immunometabolism have long been appreciated, yet not fully explored. The aim of this Research Topic was to reduce the knowledge gap in our understanding of sex differences in immunometabolism. Premenopausal females typically mount stronger innate and adaptive immune responses than males, which could lead to better protection against infections but also increase the risk for autoimmune disorders. As reviewed by Nytrova and Dolezal, sex bias in multiple sclerosis and neuromyelitis optica spectrum disorders affects the incidence, disease progression and risk of relapse. Biological sex also greatly affects whole-body metabolism. Premenopausal females expand subcutaneous fat whereas males, and females with polycystic ovary syndrome (PCOS), display visceral adiposity which is linked with a higher risk for metabolic disorders. Visceral adiposity is associated with chronic inflammation that attenuates immune responses to infection. It is therefore not surprising that sex differences in immunometabolism can shape responses to vaccines and therapeutic drugs. Several studies have reported that males have a higher risk for severe COVID-19 than females. As summarised in a review article by Rehman et al., this could be due to sex differences in estrogen receptor expression which can affect the HDL to LDL ratio, the nitric oxide synthesis, and others differently in males and females. Females with PCOS are also at higher risk for COVID-19 complications than non-PCOS females, further emphasising the intimate interactions between the immune system and metabolism on the outcome of infection. In a related study, Parker et al. found that induction of SARS-CoV2 antibody responses are more rapid in females. Earlier induction of an antibody response could confer faster clearance of the virus from the respiratory tract, thus explaining the sex-bias in disease severity. Sex-bias could also affect the treatment outcome. For instance, a study by Harnett et al. explored the impact of ES-62, a parasitic worm product, in a mouse model of obesity-accelerated aging. The authors found that ES-62 acts protectively in the male mice, but not in the female mice fed a high-fat diet. Specifically, ES-62 improved

aging-induced loss of bone structure. This was found to be primarily through the reduction of age-associated adipogenesis in bone marrow, thus increasing osteoblast differentiation. Furthermore, ES-62 increased the level of IL-10 producing regulatory B-cells in spleen and mesenteric lymph nodes of obese male, but not female mice. The study from Grabowski et al. brings important insight into sex-specific differences in behavioural and immunological responses to antibiotic and bacteriophage administration in mice. Of note, bacteriophage administration in tested concentrations seem to be safe for both male and female mice. Contrary to bacteriophages, Grabowski et al. showed that two common antibiotics- enrofloxacin and tetracycline, significantly impaired immune responses and central nervous system activity in female mice only. Since this effect was seen very early (two weeks of antibiotic administration), authors discuss the potential effect of early antibiotic exposure on metabolic disorders. The host microbiota and their metabolites act as signals regulating systemic and local immune responses. Meng et al. studied gonadal bacterial composition in swamp eels and found a significant difference between testes and ovaries. Even though major phyla were the same between sexes, their relative abundance showed difference with e.g., *Firmicutes* being more abundant in testes than ovaries. Authors further analysed function prediction of microbial genes expressed in testes and ovaries. Whereas metabolism of amino acids, vitamins and cofactors were significantly enriched in ovaries, testes microbiota genes were enriched for carbohydrate metabolism and immune system activation. It would be of value to translate these findings to the PCOS model. In a study by Balan et al., the authors tested the effect of pregnane neurosteroid interactions with toll like receptors. While neurosteroids are present in both males and females, they are specifically elevated during luteal phase of menstrual cycle and during pregnancy, possibly preventing overt immune system activation. Balan et al. reported that allopregnanolone inhibits TLR4 signalling in human marrow derived macrophages. However, allopregnanolone inhibited TLR7 specifically in female derived macrophages. Together, this highlights the importance of including both sexes in biological research of any kind to facilitate differential therapeutic options and treatment development more precisely. On the cellular level, immune cell phenotype is intimately connected with metabolic status. In states of high energy demand immune cells rely on glycolysis for producing ATP, while oxidative phosphorylation is the preferred energy source in resting and regulatory states. Along this line, Alharshawi et al. found that monocyte infiltration upon alcohol induced liver injury is dependent on interferon alpha receptor in females only. This study provides a cellular mechanism that could explain the sex disparity in alcohol induced liver injury that is more typical for women. On a similar note, Scott et al. explored the gain of function mutation in STAT1 by generating a mouse model carrying human STAT1 with the T385M mutation. Humans with the T385M mutation in STAT1 are more prone to autoimmunity, yet the mechanisms are not fully understood. Authors show that Stat1$^{t385m/+}$mice, in the absence of infection, display aberrant an adaptive immune response, with disrupted homeostasis and enhanced activation of T helper lymphocytes and atypical B cell activation, collectively leading to autoimmunity. Interestingly, these processes occurred earlier and were more robust in females. It would be interesting to assess cellular metabolism of such T helper and B lymphocytes, since it is known that STAT1, besides interferon signal transmission, regulates glycolysis, TCA cycle and oxidative phosphorylation. Crosstalk of interferon pathways and mitochondria is linked through mitochondrial NOD-like receptor X1 (NLRX1), as demonstrated in the study by Snäkä et al. Here the authors used the model of infection with parasitic worm *Leishmania guyanensis*, and showed that NLRX1 attenuated inflammation in females but not in males. Nlrx1-deficient macrophages from females were skewed towards a masculine phenotype with higher rates of glycolysis and OXPHOS, coupled with increased type I interferon production

In conclusion, we believe that this Research Topic expands our knowledge of sex-difference in immunometabolism. Understanding how biological sex can shape immune and metabolic responses will facilitate development of novel targets in immunometabolic disorders, targeted lifestyle interventions and modulations of existing therapies.

## Author contributions

AF: Writing – original draft, Writing – review & editing. SM: Writing – original draft, Writing – review & editing. MV: Writing – original draft, Writing – review & editing.

## Conflict of interest

The authors declare that the research was conducted in the absence of any commercial or financial relationships that could be construed as a potential conflict of interest.

## Publisher's note

frontiers in Immunology

ORIGINAL RESEARCH
published: 30 April 2021
doi: 10.3389/fimmu.2021.663548

# Alcohol Consumption Accumulation of Monocyte Derived Macrophages in Female Mice Liver Is Interferon Alpha Receptor Dependent

*Khaled Alharshawi*[†], *Holger Fey*[†], *Alyx Vogle*, *Tori Klenk*, *Miran Kim* and *Costica Aloman*[*]

*Division of Digestive Diseases and Nutrition, Section of Hepatology, Rush University, Chicago, IL, United States*

OPEN ACCESS

**Edited by:**
*Amiram Ariel,*
*University of Haifa, Israel*

**Reviewed by:**
*Reto Asmis,*
*Wake Forest School of Medicine, United States*
*Angela Amoruso,*
*Biolab S.r.l., Italy*

***Correspondence:**
*Costica Aloman*
*costica_aloman@rush.edu*

[†]*These authors have contributed equally to this work*

**Specialty section:**
*This article was submitted to Inflammation, a section of the journal Frontiers in Immunology*

**Received:** *03 February 2021*
**Accepted:** *20 April 2021*
**Published:** *30 April 2021*

**Citation:**
*Alharshawi K, Fey H, Vogle A, Klenk T, Kim M and Aloman C (2021) Alcohol Consumption Accumulation of Monocyte Derived Macrophages in Female Mice Liver Is Interferon Alpha Receptor Dependent. Front. Immunol. 12:663548. doi: 10.3389/fimmu.2021.663548*

Monocytes develop in the bone marrow from the hematopoietic stem cells and represent heterogeneous phagocyte cells in the circulation. In homeostatic and inflammatory conditions, after recruitment into tissues, monocytes differentiate into macrophages and dendritic cells. Alcohol use causes about 3.3 million worldwide deaths per year, which is about 5.9% of all deaths. In the United States and Europe, alcohol use disorders represent the fifth leading cause of death. Females are more susceptible to alcoholic liver injury in both humans and mice. Strikingly, we still do not know how much of this difference in tissue injury is due to the differential effect of alcohol and its toxic metabolites on a) parenchymal or resident cells and/or b) immune response to alcohol. Therefore, we used a model of chronic alcohol exposure in mice to investigate the dynamics of monocytes, an innate immune cell type showed to be critical in alcoholic liver injury, by using immunophenotypic characterization. Our data reveal a sex-dimorphism of alcohol response of hepatic monocytes in female mice that is interferon receptor alpha dependent. This dimorphism could shed light on potential cellular mechanism(s) to explain the susceptibility of females to alcoholic immunopathogenesis and suggests an additional targetable pathway for alcoholic liver injury in females.

**Keywords: monocytes, alcohol (EtOH), liver injury, mouse, female, male, Meadows-Cook model (MC)**

## INTRODUCTION

Monocytes originate in the bone marrow (BM) from the hematopoietic stem cells and represent a heterogeneous population of phagocytes in the circulation (1, 2). In homeostatic and inflammatory conditions, after recruitment into tissues, monocytes differentiate into macrophages and dendritic cells (DC) (1, 2). In both humans and mice, monocytes are classified into subsets based on differential expression of specific markers and function (3–5). In mice, monocytes are classified

based on the expression of lymphocyte antigen 6 complex, locus C1 (Ly-6C), C-C motif chemokine receptor 2 (CCR2), and C-X3-C motif chemokine receptor 1 (CX3CR1) (1, 2). Monocytes expressing high levels of Ly-6C and CCR2 (Ly-6C$^{hi}$CCR2$^{hi}$) and rapidly migrate to sites of inflammation to give rise to pro-inflammatory macrophages and DCs (1, 2, 4, 5). The locally patrolling monocytes (pro-repair) express high levels of CX3CR1 but low levels of both Ly-6C and CCR2 and described phenotypically as Ly-6C$^{lo}$CX3CR1$^{hi}$ (1, 2, 4, 5).

Alcohol use accounts for about 3.3 million worldwide deaths annually, which is about 5.9% of all deaths (6). In the United States and Europe, alcohol use disorders represent the fifth leading cause of death (6). Alcohol consumption induces damage to multiple organs, including the liver, brain, gut, pancreas, and lungs (7, 8). Alcohol use induces tissue injury by a complex interaction between toxic effects of alcohol metabolites, including acetaldehyde, reactive oxygen, and nitrogen species and the impact of alcohol on the immune system (8, 9). The primary metabolism of alcohol occurs in the liver; hence it suffers the most significant damage due to alcohol consumption (7, 8).

Evidence in the literature indicates that alcohol induces increased intestinal permeability that allows the intestinal bacterial production, i.e. endotoxins or lipopolysaccharide (LPS), to reach the portal circulation (10–12) and Kupffer cells (KC), tissue-resident macrophages in the liver. Portal and systemic bacterial products have a well validated critical role in alcoholic tissue injury by recruitment and activation of the immune cells, histologically documented by the accumulation of inflammatory cells (10, 11). Innate immune cells such as neutrophils and Ly-6C$^{hi}$ monocytes infiltrate liver tissues, are well defined participants in alcoholic tissue injury (6, 13, 14).

Mononuclear phagocytes, monocytes and macrophages, play a critical role in the pathogenesis of alcoholic liver disease (ALD) (15). KC represent the majority of liver macrophages in the steady-state (16). However, acute and chronic liver injury induces the recruitment of circulating monocytes into the liver, where they differentiate into macrophages and play a critical role in eliminating pathogens and induce tissue repair (16, 17).

The susceptibility of females to autoimmune diseases is well documented and was attributed at least partially to Interferon I signaling (18). Similarly, females are more susceptible to alcoholic liver injury in both humans and mice (19–21). Strikingly, we still do not know how much of this difference in susceptibility to alcohol tissue injury is due to the specific effect of alcohol and its toxic metabolites on a) parenchymal or resident hepatic cells and b) how much is due to sex specific immune response to alcohol (8, 9).

Therefore, we used a simple model of chronic alcohol exposure in mice to investigate the dynamics of monocytes, the most studied innate immune cell population, to alcohol exposure. Our data reveal a sex-dimorphism of alcohol response of hepatic monocyte-derived macrophages in female mice that is interferon receptor alpha dependent. This dimorphism sheds light on potential cellular mechanism(s) to explain the susceptibility of females to alcohol immunopathogenesis and suggest an additional targetable pathway for alcoholic liver injury in females.

**Abbreviations:** ALD, Alcoholic liver disease; BM, Bone marrow; CCR2, C-C motif chemokine receptor 2; cMoP, Common monocyte progenitor; CX3CR1, C-X3-C motif chemokine receptor 1; DC, Dendritic cells; EtOH, Alcohol (ethanol); GMP, Granulocyte-macrophage progenitor; HE, Hematoxylin and Eosin; IFN-I, Type 1 interferon; IFNR$^{KO}$, Interferon α/β receptor 1-knockout; KC, Kupffer cells; LD, Lieber DeCarli model; LPS, Lipopolysaccharide; Ly-6C, Lymphocyte antigen 6 complex, locus C1; MC, Meadows-Cook model; M-CSF, Monocyte/Macrophage colony-stimulating factor; MDM, Monocyte-derived macrophages; MDP, Macrophage-dendritic cell progenitor; TNFα, tumor necrosis factor alpha; WT, Wild type.

# MATERIALS AND METHODS

## Mice

Female and male Wild type (WT) C57BL/6 (stock # 000664) and Interferon α/β receptor 1-knockout (IFNR$^{KO}$) (stock # 32045-JAX) mice were purchased from Jackson Labs, Sacramento, CA. Six-week-old mice received ethanol (EtOH) (Pharmaco, Greenfield Global, Brookfield, CT) in water as per Meadows-Cook model (MC) and normal chow *ad libitum* for four weeks. EtOH concentration increased from 0% to 20% (v/v) gradually (5%, 10% and 15% for 4 days interval between each change then up to 20% in the 3$^{rd}$ week). Mice were placed on MC diet for 4 weeks. Liver and body weight were measured, and whole blood, BM, liver, spleen, and lungs were collected for analysis. All mice were kept in an infection-free environment, and only control mice had access to alcohol-free water. All experiments were approved by the Rush University Medical Center, Institutional Animal Care & Use Committee and performed following the guidelines of the National Institutes of Health.

## Leukocyte Isolation

Whole blood was obtained by cardiac puncture. After clot formation, samples were centrifuged and sera were obtained and used for analysis. Hepatic leukocyte isolation was performed as described previously (22) with minor modifications. Briefly, to eliminate circulating leukocytes in livers, each mouse was perfused with 10 mL of cold PBS (Fisher bioreagents, Pittsburgh, PA) *via* the portal vein. Lungs and livers were harvested and cut into small pieces (about 1 mm$^2$) on ice then pushed through a 70 μm filter (Biologix group limited, Shandong, China). After washing, pellets were resuspended in 8 ml of 40% Percoll (GE Healthcare, Waukesha, WI) and layered on top of 3 ml of 70% Percoll and centrifuged at 900 x g for 25 minutes at room temperature. Leukocytes were collected from the interface of 40% and 70% Percoll for counting and staining. Splenocytes were collected by mashing the spleen through a 70 μm filter. BM cells were flushed with 10 mL of cold PBS from the femur and tibia. Red cell lysis of spleen and BM cells were performed before counting and staining.

## Flow Cytometry

Samples were stained with fixable viability dye eFluor 506 eBioscience (Thermo Fisher Scientific, Waltham, MA) and fluorophore-conjugated antibodies against mouse CD16/32, CD45, CD45R/B220, CD3, CD19, NK1.1, Ly-6C, Ly-6G,

PDCA-1, MHC-II, CD11b, CD11c, CD103, CD115, CD117, CD127, CD135, F4/80, Gr-1, Ki-67, Sca-1, and TER-119 (**Supplementary Table 1**). Unless stated otherwise, all cell populations were gated as shown in **Supplementary Table 2**. Ki-67 relative mean fluorescent intensity (MFI) was calculated by dividing the MFI of each sample by the average MFI of the female control. Samples were acquired using an LSRFortessa flow cytometer (BD Bioscience, San Jose, CA). FlowJo software version 10.0.8r1 (FlowJo, LLC. Becton, Dickinson and Company, Franklin Lakes, NJ) was used for the analysis of the acquired flow cytometry data.

## ELISA

Blood was obtained by cardiac puncture at the time of euthanasia and centrifuged at 6,000 x g for 5 min for serum collection. Serum macrophage-colony stimulating factor (M-CSF) was measured by ELISA (MMC00, R&D systems, Minneapolis, MN). Serum alanine aminotransferase (ALT) and aspartate aminotransferase (AST) were measured using the ALT and AST Reagents (7526 and 7561, Pointe Scientific, Canton, MI). Serum LPS (endotoxins) was measured, according to manufacturer instruction, by PYROGENT-5000 Kinetic Turbidimetric LAL Assay (N383, Lonza, Morristown, NJ)

## Triglyceride Measurements

Hepatic triglycerides were measured using the triglyceride assay kit according to the protocol provided by the manufacturer (ab65336, Abcam, Cambridge, MA).

## Histology

### Hematoxylin and Eosin (HE) Staining

For assessment of steatosis by histological analysis, the liver tissue was fixed in 10% formalin for 24 h, paraffin-embedded, sectioned at 5 μm and stained with hematoxylin and eosin.

### Immunofluorescence

Cryo-sectioned 5 μm liver tissue slides were brought to room temperature and fixed with cold acetone for 8 min and then washed in PBS containing 0.05% Tween 20 (PBS-T). Nonspecific reactions were blocked with 5% normal goat serum (ab7481, Abcam, Cambridge, MA) and 5% TruStain fcX (BioLegend, San Diego, CA) in PBS-T for 1 h and then incubated with rabbit anti-mouse F4/80 (1:200, ab111101, Abcam) and rat anti-mouse Ly-6C (1:200, ab24973, Abcam) at 4°C overnight. After washing in PBS-T, the specimens were incubated with Alexa Fluor 488 goat anti-rat IgG (H+L) (1:400, #4416, Cell Signaling, Danvers, MA) and Alexa Fluor 555 goat anti-rabbit (1:400 #4413, Cell Signaling) for 1 hour at room temperature, washed again, treated with Vector TrueVIEW Autofluorescence Quenching Reagent and then counterstained with VECTASHIELD Mounting Medium with 4',6-diamino-2-phenylindole (DAPI) (both: Vector Labs, Burlingame, CA). The Zeiss Axio Observer Microscope (Carl Zeiss Micro Imaging, Inc., Thornwood, NY) equipped with the Zen pro 2.3 software was used to visualize the immunofluorescence staining for F4/80 and Ly-6C, and nuclear localization was provided by DAPI. The negative controls were obtained by incubating sections with non-specific rat IgG or rabbit IgG as described above.

## qRT-PCR

Total hepatic mRNA was isolated from flash frozen liver in liquid nitrogen. The University of Illinois at Chicago (UIC) Genomics Research Core processed the specimens for total mRNA extraction, cDNA synthesis. qRT-PCR for cytokines, chemokines, and adhesion molecules implicated in monocyte trafficking was done, using primers described in **Supplementary Table 3**, on the ViiA 7 Real-Time PCR System (Applied Biosystems, Foster City, CA). Fold change was calculated using the comparative Ct method. Housekeeping genes used are beta-Actin (*Actb*) and beta-2-microglobulin (*B2m*).

## Statistical Analysis

All figures generated and all statistical analyses were done using GraphPad Prism version 8.3.0 (GraphPad Software, Inc. San Diego, CA). Two way ANOVA with multiple comparisons is used to calculate the p-values. A p-value of $\leq 0.05$ was considered significant. The level of significance indicated by asterisks as follow: *p<0.05, **p<0.01, ***p<0.001, and ****p<0.0001. Unless stated otherwise, the data are presented as means ± standard error of the mean (SEM).

# RESULTS

## Consumption of Alcohol Resulted in an Increase in Recruited Monocytes/Macrophages in the Livers of Female Mice

To investigate the effect of alcohol consumption on monocytes homeostasis, female and male mice received alcohol in drinking water per Meadows-Cook (MC) model, a well-accepted mouse model of chronic alcohol consumption to characterize immunological effects of alcohol (23, 24). We chose MC, not Lieber DeCarli (LD), the most common mouse model of chronic alcoholic liver injury, because we are interested in studying the specific effect of alcohol on immune cells without the interference of the high fat and liquid diet used in LD model. Moreover, previous work published by our group demonstrated that LD model shared with alcohol exposure alone only a very restricted number of altered pathways (24).

Four weeks of alcohol consumption caused a significant reduction in the body weight, but not liver weight, of male mice; however, normalized liver/body weight ratio, surrogate for steatosis development, showed a significant increase only in female mice compared to controls (**Supplementary Figures 1A–C**). Despite no significant changes in liver triglycerides and liver enzymes, histological examination showed very mild small droplet steatosis in only alcohol-fed female mice compared to their controls (**Supplementary Figures 1D, E** and **Supplementary Figures 2A–C**). Serum levels of LPS in alcohol-fed female mice increased but did not reach statistical significance when compared with female control mice (**Supplementary Figure 2D**). Also, after alcohol consumption, the serum level of LPS in female mice is higher than in male mice but without statistical significance (**Supplementary Figure 2D**). Hepatic leukocytes did not increase in alcohol-fed mice in females and males (**Supplementary Figure 3**). Interestingly, female mice have more hepatic leukocytes than males in only alcohol-fed mice (**Supplementary Figure 3**).

The presence of small droplet discrete liver steatosis and increased liver/body weight ratio support early histological evidence of alcoholic liver injury in female mice, while the increase in number of hepatic leukocytes in alcohol-fed female mice compared to males may represent a potential modulator for susceptibility to alcoholic liver injury in females (19–21). We have shown that alcohol has a sex specific effect on innate immune cells after 3 months of alcohol exposure (25) so we wanted to further study innate immune cellular compartments affected during this earlier time points.

Hepatic leukocytes were isolated and stained for flow cytometry analysis and gated to identify hepatic monocytes, neutrophils, and DCs (**Supplementary Figure 4**). Females that consumed alcohol for four weeks showed a significantly greater increase in hepatic monocytes than controls and alcohol-fed male mice (**Figure 1A**). Since these hepatic monocytes were isolated from perfused livers we will refer to them from here on as monocyte derived macrophages (MDM). However, we observed no statistically significant change in hepatic neutrophils and DCs (**Supplementary Figure 5**) between alcohol-fed and control mice in both female and male groups at this early time point. These data demonstrated that one of the earliest immunological innate events induced by alcohol in mice is identified in the liver at the level of monocytes compartment and present only in females. This sex dependent immunological effect of alcohol on liver monocytes combined with the well-known dichotomy in susceptibility of alcoholic immune effects triggered us to explore the mechanism of alcohol exposure on hepatic monocytes.

## Hepatic MDM Increase in Female Mice Is Due to Increase of Both LY-6C$^{hi}$ and Ly-6C$^{lo}$ Subsets

Classically in mice, monocytes are divided into two primary subsets based on the phenotypic expression of Ly-6C, CCR2, and CX3CR1 (1, 2). Monocytes expressing high levels of Ly-6C and CCR2 (Ly-6C$^{hi}$CCR2$^{+}$) rapidly migrate to sites of inflammation to give rise to inflammatory macrophages and DCs and are known as "inflammatory monocytes" (1, 2). The locally patrolling monocytes express high levels of CX3CR1 but low levels of both Ly-6C and CCR2 and described phenotypically as Ly-6C$^{lo}$CX3CR1$^{+}$ (1, 2). Investigating the expression of Ly-6C on hepatic monocytes revealed a significant increase only in Ly-6C$^{hi}$ and Ly-6C$^{lo}$ MDMs in alcohol-fed female mice compared to controls (**Figures 1B, C**). Also, in alcohol consumed mice, females have more Ly-6C$^{hi}$ and Ly-6C$^{lo}$ MDMs than males (**Figures 1B, C**). Additionally, histological examination using immune-fluorescent microscopy showed a reduction in Ly-6C staining in the liver tissue from female mice consumed alcohol and controls compared to their male counterparts (**Figure 1D**). These data indicate that the hepatic MDMs increase is the result of the expansion of both Ly-6C$^{hi}$ and Ly-6C$^{lo}$ subset numbers.

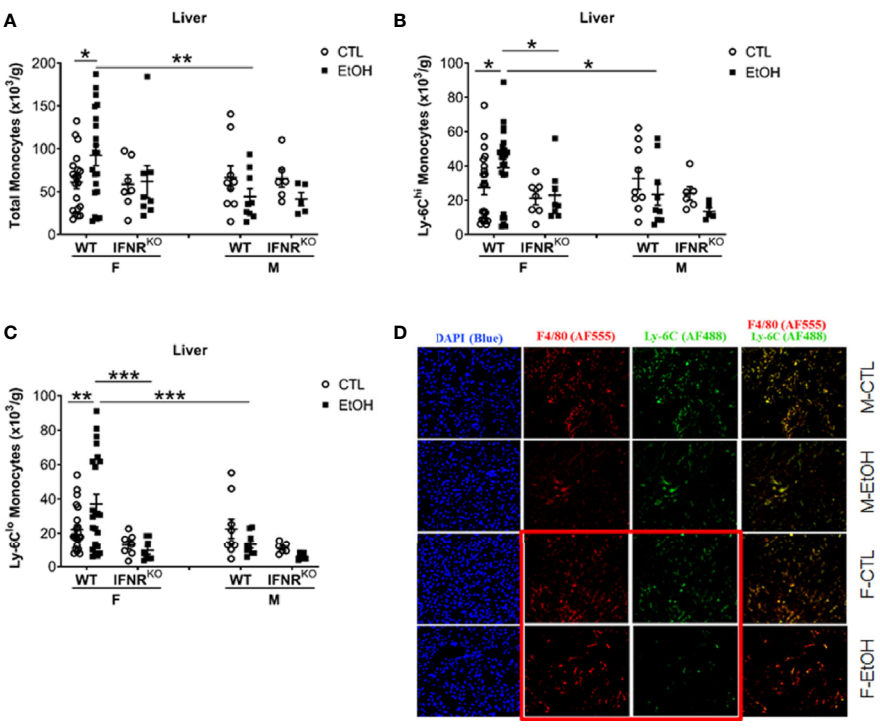


**FIGURE 1** | Alcohol induced increase in hepatic MDMs in female mice. Female (F) and male (M) From wild type (WT) and interferon α/β receptor 1-knockout (IFNR$^{KO}$) mice were provided a regular chow diet and ethanol in drinking water (EtOH) or ethanol-free water (CTL). After 4 weeks, mice were euthanized, and Liver harvested. **(A–C)** Hepatic leukocytes were stained and analyzed by flow cytometry. Dot graphs showing the numbers of total monocytes **(A)**, Ly-6C$^{hi}$ monocytes **(B)**, and Ly-6C$^{lo}$ monocytes **(C)** per gram of liver weight. Values are showing the mean ± SEM, *p<0.05, **p<0.01, ***p<0.001. n ≥ 5. **(D)** Images are showing liver tissue stained with fluorescent-labeled antibodies, anti-F4/80 (AF555/red), anti-Ly-6C (AF488/green), and DAPI (blue).

## Alcohol Consumption Induced a Reduction in the Serum Level of M-CSF but Did Not Alter the Numbers nor the Proliferation of BM Progenitors

Monocyte/Macrophage colony-stimulating factor (M-CSF), a growth factor shown to be essential for monocyte homeostasis and differentiation (2, 26). Mice deficient in CD115, the M-CSF receptor, have deficiencies in monocytes and macrophages (2, 26). Therefore, we tested the serum level of M-CSF. Alcohol consumption induced a reduction in the serum level of M-CSF only in female mice compared to controls (**Figure 2A**). Additionally, control female mice showed higher levels of serum M-CSF compared to their male counterparts (**Figure 2A**). Studying BM leukocytes did not show a significant increase in alcohol-fed mice compared to controls (**Supplementary Figure 6**). Interestingly, there was a significant decrease in BM leukocytes in females compared to males in control groups (**Supplementary Figure 6**). Considering the increase in hepatic leukocytes in females compared to males (**Supplementary Figure 3**), these data might indicate an organ-specific nature of the potential immune-cellular mechanism(s) that might explain the higher susceptibility of females to develop alcoholic tissue injury. We studied the classically identified BM progenitors gated as shown in **Supplementary Figures 7** and **8**. The data did not reveal a change in granulocyte-macrophage progenitor (GMP) (**Figure 2B**) and macrophage-dendritic cell progenitor (MDP) (**Figure 2C**) in alcohol-fed mice compared to controls. Investigating the expression of Ki-67, a cell proliferation marker (27), in GMP and MDP did not reveal significant changes after alcohol consumption (**Figures 2D, E**). These data suggest that the increase in monocytes found in female mice is not a result of alcohol interference in the development of BM classical progenitors.

## Alcohol Consumption in Female Mice Induced Increase in the Expression of Hepatic TNFα

We asked whether the increase in hepatic MDMs results in a change of hepatic cytokine expression and whether this reflects a change in the hepatic chemokines and adhesion molecules gradient implicated in the recruitment and migration of monocytes (28). The cytokine tumor necrosis factor alpha (TNFα) was upregulated in the livers of female mice fed alcohol compared to their control counterparts (**Figure 3A**). The expression of chemokines, chemokine receptors, and adhesion molecules tested did not reveal significant changes between alcohol-fed and control female mice (**Figures 3A–C**). The increase in TNFα data is consistent with overwhelming evidence in the literature about the implications of TNFα in alcohol-induced liver injury in both humans and mice and marks an early event in alcohol immunopathology (29–33).

## Alcohol Consumption Did Not Increase Hepatic MDMs in IFNR$^{KO}$ Mice as It Does in WT Mice

Our data did not reveal a disturbance in BM progenitors or recruitment and migration molecules that might explain the increase in MDMs we found in female mice that consumed alcohol. Published data showed regulation of emergent monocytopoiesis by type I interferon (IFN-I) signaling (34). Therefore, we used Interferon α/β receptor 1-deficient (IFNR$^{KO}$) mice to study the effect of alcohol on hepatic monocytes in the absence of IFN-I signaling. Interestingly, IFNR$^{KO}$ female mice consumed alcohol for four weeks failed to show an increase in their hepatic MDMs compared to control-fed mice, as did their WT counterparts (**Figures 1A–C**). In the livers of females, there are more Ly-6C$^{hi}$ and Ly-6C$^{lo}$ MDMs in WT compared to IFNR$^{KO}$, in alcohol-fed mice (**Figures 1B, C**). This data suggest a

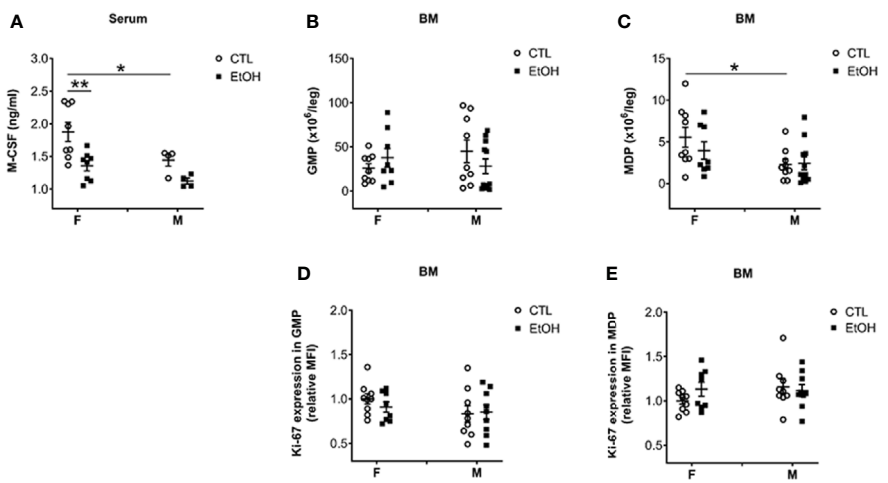


**FIGURE 2** | Alcohol consumption reduced M-CSF serum level in female mice but did not change the numbers nor the proliferation of classical BM progenitors. Female (F) and male (M) from wild type (WT) mice were provided a regular chow diet and ethanol in drinking water (EtOH) or ethanol-free water (CTL). After 4 weeks, mice were euthanized, and blood and BM collected. **(A)** Dot graphs showing the serum level of M-CSF. n ≥ 4. **(B–E)** BM cells counted then stained for flow cytometry analysis. BC) Dot graphs showing the numbers of GMP **(B)** and MDP **(C)** per leg. **(D, E)** Dot graphs showing Ki-67 expression (relative MFI) in GMP **(D)** and MDP **(E)**. n ≥ 8. Values are showing the mean ± SEM, *p<0.05, **p<0.01.

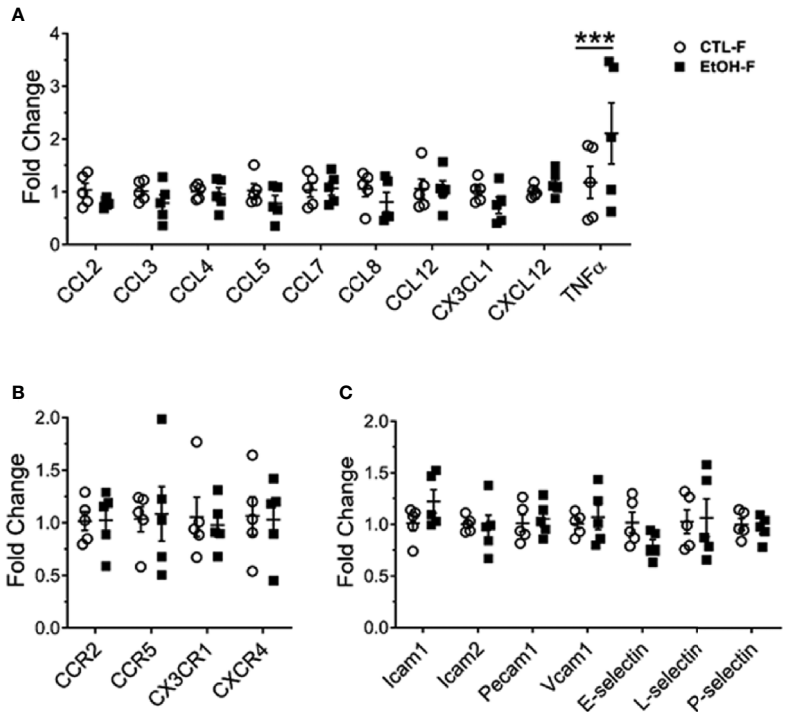


**FIGURE 3** | Increase in hepatic TNFα in alcohol-fed female mice. Female wild type mice were provided a regular chow diet and ethanol in drinking water (EtOH) or ethanol-free water (CTL). After 4 weeks, mice were euthanized, and liver harvested. Hepatic total mRNA extracted followed by qRT-PCR analysis of chemokines **(A)**, chemokine receptor **(B)**, and adhesion molecules **(C)** involved in monocyte recruitment. Dot graphs showing fold change in gene expression in alcohol-fed versus control mice calculated by comparative Ct method. n = 5. Values are showing the mean ± SEM ***p<0.001.

critical role for IFN-I signaling in the increase of MDMs induced by alcohol in female mice.

## IFNR$^{KO}$ Mice Have Fewer BM Monocyte Progenitors Than WT Mice

We further investigated the BM development of monocytes in both WT and IFNR$^{KO}$ mice. First, we investigated mature monocytes in the BM, and in both WT and IFNR$^{KO}$ mice, our data suggest no change in monocyte subsets between alcohol-fed mice and controls (**Figures 4A–C**). Comparing BM progenitors between alcohol-fed and control mice did not show significant changes in both WT and IFNR$^{KO}$ mice (**Figures 4D–F**). However, comparing the same progenitors between WT and IFNR$^{KO}$ mice revealed a significant reduction in MDP in IFNR$^{KO}$ female control mice (**Figure 4E**). In IFNR$^{KO}$, both control and alcohol-fed female mice, compared to WT, there is a reduction in common monocyte progenitors (cMoP), but it did not reach statistical significance (**Figure 4F**). These data further demonstrate a potential role of IFN-I signaling in the increase of Ly-6C$^{hi}$ and Ly-6C$^{lo}$ subsets in female mice early during alcohol consumption and preceding histological findings of alcoholic liver injury.

# DISCUSSION

Monocytes are innate immune cells recruited in sterile and pathogen induced inflamed tissues, critical in the clearance of pathogens and cellular debris as well as tissue return to steady-state condition (16). Multiple lines of evidence suggest the importance of monocytes in alcoholic tissue injury. Firstly, the elevation of neopterin and leukocyte-function-associated antigen 3, markers associated with monocyte activation, in patients with ALD (16, 35). Additionally, the expression of TNFα receptors and the spontaneous secretion of TNFα from circulating monocytes isolated from ALD patients and the association of high serum TNFα with poorer prognosis of acute alcoholic hepatitis patients all further suggests the critical role of monocytes in ALD (16). Furthermore, the migration of monocytes to the liver during inflammation and their conversion to a macrophage like phenotype, which play a critical role in eliminating pathogens and induce tissue repair (16, 17), indirectly further highlights the important role of monocytes in ALD.

In our experiments only very early and discrete signs of alcoholic liver injury are observed as increased small droplet steatosis without changes in liver triglycerides in alcohol-fed female mice after 4 weeks. This suggests rather early involvement of hepatocyte lipid transport and changes in non-triglyceride lipid fraction (sphingolipids, ceramides) by alcohol in female mice and less quantitative changes in triglycerides.

After alcohol consumption, female mice have higher leukocyte numbers compared with males and both, acute and chronic liver injuries, induce the recruitment of circulating monocytes into the liver (16). In our experiment, alcohol

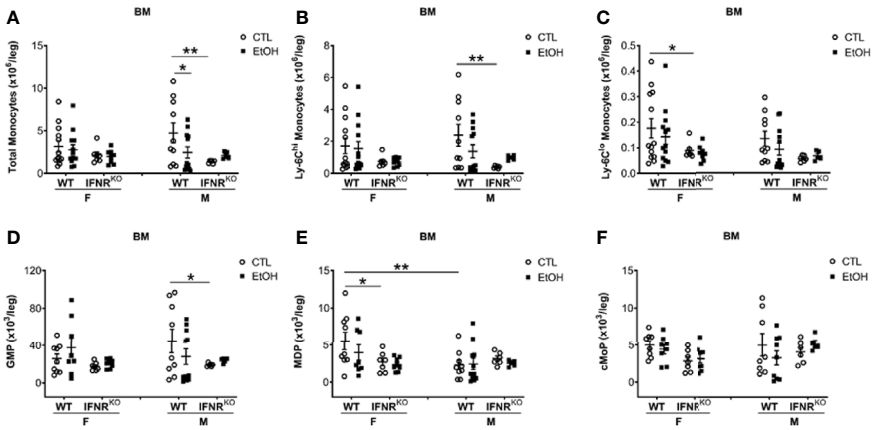


**FIGURE 4** | Reduction in MDP, a monocyte BM progenitor, in female IFNR$^{KO}$ mice. Female (F) and male (M) from wild type (WT) and interferon α/β receptor knockout (IFNR$^{KO}$) mice were provided a regular chow diet and ethanol in drinking water (EtOH) or ethanol-free water (CTL). After 4 weeks, mice were euthanized, and BM collected, cells counted, then stained for flow cytometry analysis. **(A–F)** Dot graphs showing the numbers per leg of total monocytes **(A)**, Ly-6C$^{hi}$ monocytes **(B)**, Ly-6C$^{lo}$ monocytes **(C)**, GMP **(D)**, MDP **(E)**, and cMoP **(F)**. n ≥ 5. Values showing the mean ± SEM, *p<0.05, **p<0.01.

exposure increased hepatic MDMs in female mice after only four weeks. No significant changes were found in other recruited examined phagocytes, DCs and neutrophils. Upon further investigation, the increase in hepatic MDMs in female mice after four weeks of alcohol consumption was due to a rise in both Ly-6C$^{hi}$ and Ly-6C$^{lo}$ subsets. The increase in hepatic MDM subsets is consistent with upregulation of TNFα mRNA as macrophages are known to produce it (16). It was reported that Ly-6C$^{hi}$ monocytes recruited following liver injury then undergo a phenotype switch to become Ly-6C$^{lo}$ monocytes within few days (5, 36, 37). Zigmond et al. showed in male mice, that liver injury induced by N-acetyl-p-aminophenol led to the recruitment of Ly-6C$^{hi}$ monocytes, which then differentiate into Ly-6C$^{lo}$ monocyte derived macrophages (36). Dal-Secco *et al.* showed that in sterile liver injury, Ly-6C$^{hi}$ (CCR2$^{hi}$ CX3CR1$^{lo}$) monocytes migrated to the injured area then transitioned to Ly-6C$^{lo}$ (CCR2$^{lo}$ CX3CR1$^{hi}$) monocytes (37). The data presented by both studies could support the concept that the increase in hepatic Ly-6C$^{hi}$ and Ly-6C$^{lo}$ in female mice after four weeks of alcohol consumption may be due to increased recruitment of Ly-6C$^{hi}$ then their conversion to Ly-6C$^{lo}$ MDMs. However, at this time, we cannot rule out the alternative hypothesis that the accumulation of hepatic Ly-6C$^{lo}$ MDMs may be, at least in part, due to increased hepatic recruitment or survival of Ly-6C$^{lo}$ MDMs.

To investigate the mechanism responsible for the early expansion of hepatic MDMs after alcohol exposure in female mice, we studied monocyte development. M-CSF is an important growth factor for the homeostasis and differentiation of monocytes (2, 26) and was found to be suppressed by alcohol. The reduction in the serum levels of M-CSF in alcohol-fed mice compared to controls in females is inconsistent with the reports on the non-alcoholic chronic liver disease where hepatic inflammation in female and male humans is associated with an increase in serum M-CSF (38, 39). However, our data is consistent with the observation that women have higher serum concentrations of M-CSF than men (40). The reduction of serum M-CSF in alcohol-fed female mice, suggests of a possible negative feedback effect on monocytopoiesis or direct alcohol effect on M-CSF sources. Studies on the effect of alcohol on M-CSF are scarce. Kottstorfer *et al.* found no significant correlation in humans between alcohol consumption and the expression of M-CSF (40). In spite of this suppressive effect of alcohol on circulating M-CSF levels, M-CSF levels in females are still significantly higher than males, which could potentially additionally explain the consistent increase in monocytes found in female mice after alcohol consumption. Analyzing classical BM progenitors such as GMP and MDP (2), we did not reveal significant changes in the bone marrow that could explain the increase in monocytes. Consistent with that, alcohol consumption for three months did not alter GMP progenitors in a Rhesus Monkey study (41).

Monocytes originate in the BM under the control of the growth factor M-CSF and circulate in the blood, and do not proliferate during steady state (26, 42). Monocyte development, monocytopoiesis, is regulated by the expression or suppression of transcription factors such as Transcription factor PU.1, Interferon regulatory factor-8, and Kruppel-like factor 4 (2). Induction of monocytopoiesis by IFN-I signaling during endotoxemia has been shown in the literature (34). Consistent with that, our data revealed the failure of IFNR$^{KO}$ mice exposed to alcohol to increase their hepatic Ly-6C$^{hi}$ and Ly-6C$^{lo}$ MDM subsets as did their WT counterparts. The data from the IFNR$^{KO}$ mice, compared to WT mice, also showed a reduction in mature Ly-6C$^{lo}$ monocytes in both liver and BM. In an acute model of sterile inflammation using a murine model of pristane-induced peritonitis the IFN-I signaling was responsible for monocyte recruitment and maturation during inflammation while mice deficient in TLR4, TNFα, IL-6, and IL1R failed to accumulate monocytes in the peritoneal cavity (43). This is consistent with our data that IFN-I signaling is critical for increasing hepatic MDMs upon alcohol consumption. However, in our case, the

increase was in both Ly-6C$^{hi}$ and Ly-6C$^{lo}$ subsets compared to the Ly-6C$^{hi}$ subset in the first phase of acute tissue injury model. In a second phase, the accumulation of Ly-6C$^{hi}$ monocytes was replaced by Ly-6C$^{lo}$ monocytes within 72 hours from the challenge, consistent with our finding (43).

MDP precursors and cMoP precursors in the BM are macrophage/monocyte progenitors (44). Studying MDP and cMoP progenitors in the BM of IFNR$^{KO}$ mice compared to WT revealed a reduction in MDP progenitors in female control mice, suggesting the importance of IFN-I signaling to maintain MDP progenitors at least during steady state. Lasseaux *et al.* reported a reduction in cMoP progenitors in mice 24 hours after intravenous injection with LPS, the sex of mice used in the experiments is not indicated (34), which is inconsistent with our data revealed no change in cMoP after alcohol consumption. This could be due to the fact that they used LPS compared to alcohol in our study. Interestingly, IFNR$^{KO}$ mice did not increase monocyte precursors after the LPS challenge, although the mice showed the reduction of cMoP progenitors (34), suggesting the IFN-I dependency of the monocytopoiesis during inflammation consistent with our data. It is important to state that more prolonged exposure to alcohol for 3 months in the same model in female mice expanded hepatic plasmacytoid DCs (25); whether that is an earlier event represented by bone marrow pDC expansion and paracrine source of IFNα for stimulation of monocytopoiesis by alcohol is under ongoing evaluation in our laboratory.

In summary, our data strongly suggest that alcohol exposure for four weeks in mice induces an increase of Ly-6C$^{hi}$ and Ly-6C$^{lo}$ MDMs in an IFN-I signaling-dependent manner only in female mice. Our data support the need for additional investigations of the cellular sources of IFNα and functional relevance of the hepatic MDM subsets expansion in female mice early upon alcohol exposure as a mechanism for increased susceptibility to alcoholic immunopathogenesis.

## DATA AVAILABILITY STATEMENT

The original contributions presented in the study are included in the article/**Supplementary Material**. Further inquiries can be directed to the corresponding author.

## ETHICS STATEMENT

The animal study was reviewed and approved by Rush University Medical Center, Institutional Animal Care & Use Committee.

## AUTHOR CONTRIBUTIONS

KA and HF conduct the experiments, analyzed the data, and wrote the manuscript. AV and TK conduct the experiments. MK conduct the experiment, analyzed the data, and reviewed the manuscript. CA obtained the funding, designed the project, analyzed the data, and edited and reviewed the manuscript. All authors contributed to the article and approved the submitted version.

## FUNDING

This work is supported by grant from the National Institutes of Health: AA024762 awarded CA.

## SUPPLEMENTARY MATERIAL

The Supplementary Material for this article can be found online at: https://www.frontiersin.org/articles/10.3389/fimmu.2021.663548/full#supplementary-material

## REFERENCES

1. Gao B, Ahmad MF, Nagy LE, Tsukamoto H. Inflammatory Pathways in Alcoholic Steatohepatitis. *J Hepatol* (2019) 70(2):249–59. doi: 10.1016/j.jhep.2018.10.023
2. Terry RL, Miller SD. Molecular Control of Monocyte Development. *Cell Immunol* (2014) 291(1-2):16–21. doi: 10.1016/j.cellimm.2014.02.008
3. Ziegler-Heitbrock L. The CD14+ CD16+ Blood Monocytes: Their Role in Infection and Inflammation. *J Leukoc Biol* (2007) 81(3):584–92. doi: 10.1189/jlb.0806510
4. Sunderkotter C, Nikolic T, Dillon MJ, Van Rooijen N, Stehling M, Drevets DA, et al. Subpopulations of Mouse Blood Monocytes Differ in Maturation Stage and Inflammatory Response. *J Immunol* (2004) 172(7):4410–7. doi: 10.4049/jimmunol.172.7.4410
5. Riva A, Mehta G. Regulation of Monocyte-Macrophage Responses in Cirrhosis-Role of Innate Immune Programming and Checkpoint Receptors. *Front Immunol* (2019) 10:167. doi: 10.3389/fimmu.2019.00167
6. Ohashi K, Pimienta M, Seki E. Alcoholic Liver Disease: A Current Molecular and Clinical Perspective. *Liver Res* (2018) 2(4):161–72. doi: 10.1016/j.livres.2018.11.002
7. Osna NA, Kharbanda KK. Multi-Organ Alcohol-Related Damage: Mechanisms and Treatment. *Biomolecules* (2016) 6(2):1–5. doi: 10.3390/biom6020020
8. Rusyn I, Bataller R. Alcohol and Toxicity. *J Hepatol* (2013) 59(2):387–8. doi: 10.1016/j.jhep.2013.01.035
9. Szabo G, Saha B. Alcohol's Effect on Host Defense. *Alcohol Res Curr Rev* (2015) 37(2):159–70.
10. Rao R. Endotoxemia and Gut Barrier Dysfunction in Alcoholic Liver Disease. *Hepatology* (2009) 50(2):638–44. doi: 10.1002/hep.23009
11. Rao RK, Seth A, Sheth P. Recent Advances in Alcoholic Liver Disease I. Role of Intestinal Permeability and Endotoxemia in Alcoholic Liver Disease. *Am J Physiol Gastrointestinal Liver Physiol* (2004) 286(6):G881–4. doi: 10.1152/ajpgi.00006.2004
12. Shukla PK, Meena AS, Manda B, Gomes-Solecki M, Dietrich P, Dragatsis I, et al. Lactobacillus Plantarum Prevents and Mitigates Alcohol-Induced Disruption of Colonic Epithelial Tight Junctions, Endotoxemia, and Liver Damage by an EGF Receptor-Dependent Mechanism. *FASEB J Off Publ Fed Am Soc Exp Biol* (2018) 32:fj201800351R. doi: 10.1096/fj.201800351R
13. Xu R, Huang H, Zhang Z, Wang FS. The Role of Neutrophils in the Development of Liver Diseases. *Cell Mol Immunol* (2014) 11(3):224–31. doi: 10.1038/cmi.2014.2
14. Osna NA, Donohue TM Jr., Kharbanda KK. Alcoholic Liver Disease: Pathogenesis and Current Management. *Alcohol Res Curr Rev* (2017) 38(2):147–61.
15. McClain CJ, Hill DB, Song Z, Deaciuc I, Barve S. Monocyte Activation in Alcoholic Liver Disease. *Alcohol* (2002) 27(1):53–61. doi: 10.1016/s0741-8329(02)00212-4

16. Ju C, Mandrekar P. Macrophages and Alcohol-Related Liver Inflammation. *Alcohol Res Curr Rev* (2015) 37(2):251–62.
17. Wang M, You Q, Lor K, Chen F, Gao B, Ju C. Chronic Alcohol Ingestion Modulates Hepatic Macrophage Populations and Functions in Mice. *J Leukoc Biol* (2014) 96(4):657–65. doi: 10.1189/jlb.6A0114-004RR
18. Klein SL, Flanagan KL. Sex Differences in Immune Responses. *Nat Rev Immunol* (2016) 16(10):626–38. doi: 10.1038/nri.2016.90
19. Wagnerberger S, Fiederlein L, Kanuri G, Stahl C, Millonig G, Mueller S, et al. Sex-Specific Differences in the Development of Acute Alcohol-Induced Liver Steatosis in Mice. *Alcohol Alcohol* (2013) 48(6):648–56. doi: 10.1093/alcalc/agt138
20. Fulham MA, Mandrekar P. Sexual Dimorphism in Alcohol Induced Adipose Inflammation Relates to Liver Injury. *PloS One* (2016) 11(10):e0164225. doi: 10.1371/journal.pone.0164225
21. Guy J, Peters MG. Liver Disease in Women: The Influence of Gender on Epidemiology, Natural History, and Patient Outcomes. *Gastroenterol Hepatol* (2013) 9(10):633–9.
22. Wintermeyer P, Cheng CW, Gehring S, Hoffman BL, Holub M, Brossay L, et al. Invariant Natural Killer T Cells Suppress the Neutrophil Inflammatory Response in a Mouse Model of Cholestatic Liver Damage. *Gastroenterology* (2009) 136(3):1048–59. doi: 10.1053/j.gastro.2008.10.027
23. Meyerholz DK, Edsen-Moore M, McGill J, Coleman RA, Cook RT, Legge KL. Chronic Alcohol Consumption Increases the Severity of Murine Influenza Virus Infections. *J Immunol* (2008) 181(1):641–8. doi: 10.4049/jimmunol.181.1.641
24. Vogle A, Qian T, Zhu S, Burnett E, Fey H, Zhu Z, et al. Restricted Immunological and Cellular Pathways are Shared by Murine Models of Chronic Alcohol Consumption. *Sci Rep* (2020) 10(1):2451. doi: 10.1038/s41598-020-59188-9
25. Alharshawi K, Fey H, Vogle A, Klenk T, Kim M, Aloman C. Sex Specific Effect of Alcohol on Hepatic Plasmacytoid Dendritic Cells. *Int Immunopharmacol* (2021) 90:107166. doi: 10.1016/j.intimp.2020.107166
26. Geissmann F, Manz MG, Jung S, Sieweke MH, Merad M, Ley K. Development of Monocytes, Macrophages, and Dendritic Cells. *Science* (2010) 327 (5966):656–61. doi: 10.1126/science.1178331
27. Sobecki M, Mrouj K, Camasses A, Parisis N, Nicolas E, Lleres D, et al. The Cell Proliferation Antigen Ki-67 Organises Heterochromatin. *eLife* (2016) 5: e13722. doi: 10.7554/eLife.13722
28. Shi C, Pamer EG. Monocyte Recruitment During Infection and Inflammation. *Nat Rev Immunol* (2011) 11(11):762–74. doi: 10.1038/nri3070
29. McClain CJ, Barve S, Barve S, Deaciuc I, Hill DB. Tumor Necrosis Factor and Alcoholic Liver Disease. *Alcohol Clin Exp Res* (1998) 22(5 Suppl):248S–52S. doi: 10.1097/00000374-199805001-00006
30. Kitazawa T, Nakatani Y, Fujimoto M, Tamura N, Uemura M, Fukui H. The Production of Tumor Necrosis Factor-Alpha by Macrophages in Rats With Acute Alcohol Loading. *Alcohol Clin Exp Res* (2003) 27(8 Suppl):72S–5S. doi: 10.1097/01.ALC.0000078611.55696.F0
31. Marcos M, Gomez-Munuera M, Pastor I, Gonzalez-Sarmiento R, Laso FJ. Tumor Necrosis Factor Polymorphisms and Alcoholic Liver Disease: A HuGE Review and Meta-Analysis. *Am J Epidemiol* (2009) 170(8):948–56. doi: 10.1093/aje/kwp236
32. Neuman MG, Maor Y, Nanau RM, Melzer E, Mell H, Opris M, et al. Alcoholic Liver Disease: Role of Cytokines. *Biomolecules* (2015) 5(3):2023–34. doi: 10.3390/biom5032023
33. Kawaratani H, Moriya K, Namisaki T, Uejima M, Kitade M, Takeda K, et al. Therapeutic Strategies for Alcoholic Liver Disease: Focusing on Inflammation and Fibrosis (Review). *Int J Mol Med* (2017) 40(2):263–70. doi: 10.3892/ijmm.2017.3015
34. Lasseaux C, Fourmaux MP, Chamaillard M, Poulin LF. Type I Interferons Drive Inflammasome-Independent Emergency Monocytopoiesis During Endotoxemia. *Sci Rep* (2017) 7(1):16935. doi: 10.1038/s41598-017-16869-2
35. Luna-Casado L, Diez-Ruiz A, Gutierrez-Gea F, Santos-Perez JL, Rico-Irles J, Wachter H, et al. Increased Peripheral Mononuclear Cells Expression of Adhesion Molecules in Alcoholic Cirrhosis: its Relation to Immune Activation. *J Hepatol* (1997) 27(3):477–83. doi: 10.1016/s0168-8278(97)80351-0
36. Zigmond E, Samia-Grinberg S, Pasmanik-Chor M, Brazowski E, Shibolet O, Halpern Z, et al. Infiltrating Monocyte-Derived Macrophages and Resident Kupffer Cells Display Different Ontogeny and Functions in Acute Liver Injury. *J Immunol* (2014) 193(1):344–53. doi: 10.4049/jimmunol.1400574
37. Dal-Secco D, Wang J, Zeng Z, Kolaczkowska E, Wong CH, Petri B, et al. A Dynamic Spectrum of Monocytes Arising From the in Situ Reprogramming of CCR2+ Monocytes At a Site of Sterile Injury. *J Exp Med* (2015) 212(4):447–56. doi: 10.1084/jem.20141539
38. Itoh Y, Okanoue T, Sakamoto S, Nishioji K, Kashima K. The Effects of Prednisolone and Interferons on Serum Macrophage Colony Stimulating Factor Concentrations in Chronic Hepatitis B. *J Hepatol* (1997) 26(2):244–52. doi: 10.1016/s0168-8278(97)80037-2
39. Itoh Y, Okanoue T, Ohnishi N, Nishioji K, Sakamoto S, Nagao Y, et al. Hepatic Damage Induced by Transcatheter Arterial Chemoembolization Elevates Serum Concentrations of Macrophage-Colony Stimulating Factor. *Liver* (1999) 19(2):97–103. doi: 10.1111/j.1478-3231.1999.tb00017.x
40. Kottstorfer J, Kaiser G, Thomas A, Gregori M, Kecht M, Domaszewski F, et al. The Influence of non-Osteogenic Factors on the Expression of M-CSF and VEGF During Fracture Healing. *Injury* (2013) 44(7):930–4. doi: 10.1016/j.injury.2013.02.028
41. Siggins RW, Molina P, Zhang P, Bagby GJ, Nelson S, Dufour J, et al. Dysregulation of Myelopoiesis by Chronic Alcohol Administration During Early SIV Infection of Rhesus Macaques. *Alcohol Clin Exp Res* (2014) 38 (7):1993–2000. doi: 10.1111/acer.12433
42. Auffray C, Sieweke MH, Geissmann F. Blood Monocytes: Development, Heterogeneity, and Relationship With Dendritic Cells. *Annu Rev Immunol* (2009) 27:669–92. doi: 10.1146/annurev.immunol.021908.132557
43. Lee PY, Li Y, Kumagai Y, Xu Y, Weinstein JS, Kellner ES, et al. Type I Interferon Modulates Monocyte Recruitment and Maturation in Chronic Inflammation. *Am J Pathol* (2009) 175(5):2023–33. doi: 10.2353/ajpath.2009.090328
44. Hettinger J, Richards DM, Hansson J, Barra MM, Joschko AC, Krijgsveld J, et al. Origin of Monocytes and Macrophages in a Committed Progenitor. *Nat Immunol* (2013) 14(8):821–30. doi: 10.1038/ni.2638

**Conflict of Interest:** The authors declare that the research was conducted in the absence of any commercial or financial relationships that could be construed as a potential conflict of interest.

frontiers in Immunology

REVIEW
published: 18 August 2021
doi: 10.3389/fimmu.2021.680845

# Immunity, Sex Hormones, and Environmental Factors as Determinants of COVID-19 Disparity in Women

*Suriya Rehman[1]*, Vijaya Ravinayagam[2], Insha Nahvi[3], Hanan Aldossary[1], Maha Al-Shammari[4], Mai Saad Al Amiri[5], Uday Kishore[6] and Ebtesam A. Al-Suhaimi[7]**

[1] Department of Epidemic Disease Research, Institute of Research and Medical Consultations (IRMC), Imam Abdulrahman Bin Faisal University, Dammam, Saudi Arabia, [2] Deanship of Scientific Research and Institute of Research and Medical Consultations (IRMC), Imam Abdulrahman Bin Faisal University, Dammam, Saudi Arabia, [3] Department of Basic Sciences, Preparatory Year Deanship, King Faisal University, Al Hofuf, Saudi Arabia, [4] Department of Public Health, Institute of Research and Medical Consultations (IRMC), Imam Abdulrahman Bin Faisal University, Dammam, Saudi Arabia, [5] Department of Obstetrics and Gynecology, Maternity and Children Hospital, Dammam, Saudi Arabia, [6] Biosciences, College of Health, Medicine and Life Sciences, Brunel University London, Uxbridge, United Kingdom, [7] Biology Department, College of Science and Institute of Research and Medical Consultations (IRMC), Imam Abdulrahman Bin Faisal University, Dammam, Saudi Arabia

OPEN ACCESS

**Edited by:**
Chaofeng Han,
Second Military Medical University, China

**Reviewed by:**
Leiliang Zhang,
Shandong First Medical University, China
Degang Yang,
Tongji University, China

***Correspondence:**
Suriya Rehman
surrehman@iau.edu.sa
Ebtesam A. Al-Suhaimi
ealsuhaimi@iau.edu.sa

**Specialty section:**
This article was submitted to Molecular Innate Immunity, a section of the journal Frontiers in Immunology

**Received:** 15 March 2021
**Accepted:** 29 July 2021
**Published:** 18 August 2021

**Citation:**
Rehman S, Ravinayagam V, Nahvi I, Aldossary H, Al-Shammari M, Amiri MSA, Kishore U and Al-Suhaimi EA (2021) Immunity, Sex Hormones, and Environmental Factors as Determinants of COVID-19 Disparity in Women. Front. Immunol. 12:680845. doi: 10.3389/fimmu.2021.680845

The current coronavirus disease 2019 (COVID-19), caused by severe acute respiratory syndrome virus 2 (SARS-CoV-2), has resulted in a major global pandemic, causing extreme morbidity and mortality. Few studies appear to suggest a significant impact of gender in morbidity and mortality, where men are reported at a higher risk than women. The infectivity, transmissibility, and varying degree of disease manifestation (mild, modest, and severe) in population studies reinforce the importance of a number of genetic and epigenetic factors, in the context of immune response and gender. The present review dwells on several contributing factors such as a stronger innate immune response, estrogen, angiotensin-converting enzyme 2 gene, and microbiota, which impart greater resistance to the SARS-CoV-2 infection and disease progression in women. In addition, the underlying importance of associated microbiota and certain environmental factors in gender-based disparity pertaining to the mortality and morbidity due to COVID-19 in women has also been addressed.

**Keywords: COVID-19, environment, estrogen, immunity, gender, hormones, microbiota**

## INTRODUCTION

The coronaviruses belong to the subfamily *Coronavirinae*, which cause respiratory and gastrointestinal infections (1). First discovered in 1960, the coronaviruses were ascribed to causing a mild respiratory symptom; these viruses include human CoV 229E (HCoV-229E) and HCoV-OC43 (2). The present coronavirus disease 2019 (COVID-19) pandemic by severe acute respiratory syndrome virus 2 (SARS-CoV-2) initially emerged from Wuhan Province, China at the seafood market (3). Various studies on the innate and adaptive immune responses to coronaviruses

have been carried out in recent years. The role of the immune responses is to initiate viral clearance, prevent viral replication, and help tissue repair. However, such immune responses play a crucial part in SARS-related pathogenicity. The SARS-CoV-2 is known to dysregulate cytokine-mediated inflammatory and immune responses (4). Innate immune humoral factors such as complement and coagulation-fibrinolysis systems, soluble proteins/naturally occurring antibodies, and cellular components (natural killer cells and other innate lymphocytes) seem to be fully engaged following viral infection. Dysregulation of these factors leads to viral replication in the lung airways and escalation of an adaptive immune response. Severity caused by SARS-CoV-2 infection thus may also be attributed to the degree of dysregulated immune and inflammatory response (5).

The virus has affected the global population; however, men seem to manifest more severe form of the disease than women, as per the onset of symptoms of the disease. The mortality in men is 2.4 times compared to women, although both gender have a similar susceptibility to transmission (6). One study that involved 425 COVID-19 patients reported 56% men (7), while another study reported 50.7% of 140 patients being men as infected individuals (8). Another study involving 1,019 COVID-19 patients revealed greater susceptibility of men compared to women to SARS-CoV-2, indicating that gender is as a risk factor for morbidity and mortality (6). One of the most noticeable differences is the mortality rates among men and women in the Western Europe, where 69% of men have died due to COVID-19. Even in the United States of America, a lesser percentage of women have died as compared to men (9). Similar patterns have been seen in China and other affected countries. According to one of the reports, the greatest sex disparity was seen in the death rate; it came to only 36.2% deaths in women as compared to men at the rate of 51.4%. Additionally, the analysis of COVID-19 cases documented in China showed a 2.8% case fatality in men as compared with a 1.7% rate in infected women (10) (**Figure 1**).

This is not the first time that coronaviruses have been found to affect women lesser than men. The epidemiological data from SARS-CoV (2003) and MERS-CoV (2012) epidemics also highlighted women at a lower risk of death from these deadly viruses (11). In Hong Kong, men were found to be affected more

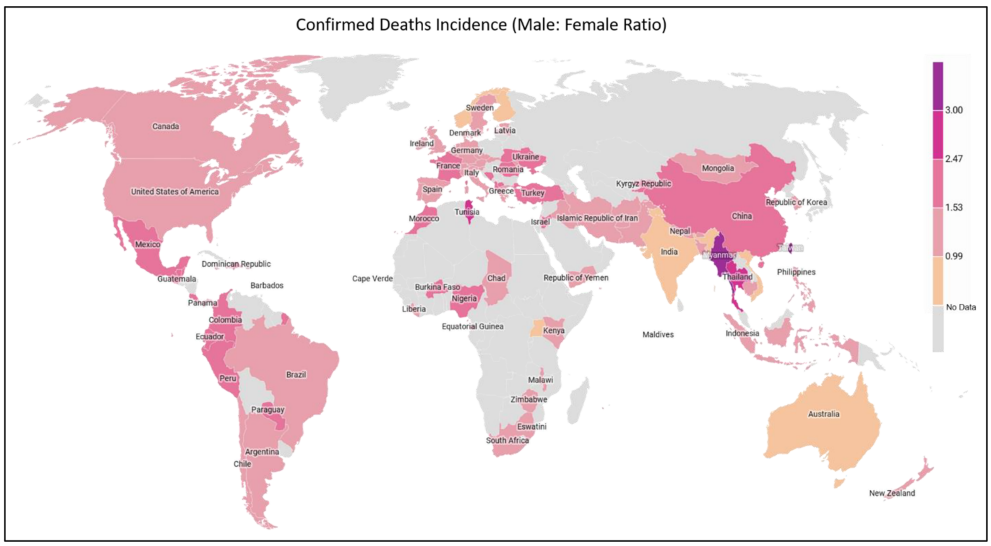


**Map key**

| | |
|---|---|
| Min Ratio | 0.54 (Vietnam) |
| Max Ratio | 6.73 (Saint Lucia) |
| Light Orange color | COVID 19 Deaths Ratio (Male: Female) < 1 |
| Dark Pink Color | COVID 19 Deaths Ratio (Male: Female) > 3 |
| No Data | No published confirmed COVID-19 deaths disaggregated according to sex |
| Period | The data collected from each official resource for each country, the starting period for each is different. However, this data is according to latest update on 2nd February 2021. |

Global Health 50/50. . https://globalhealth5050.org/covid19/sex-disaggregated-data-tracker/., n.d.)

**FIGURE 1** | Global map showing the confirmed COVID-19 death incidence (male and female ratio) in various countries.

severely than women by the SARS-CoV (12). Furthermore, men had a significantly higher fatality rate than women (21.9% *versus* 13.2%) (13). In 2012, when MERS-CoV hit Saudi Arabia, the disease occurrence among men (62%) was considerably higher than in women (38%) of the total confirmed infected cases (14). Thus, gender seems to play an important role in severity and fatality in SARS-related diseases.

## ESTROGEN ACTS AS AN IMMUNE-STIMULATING FACTOR

As men are worse affected by SARS-CoV-2, they require longer hospital stay and have a higher mortality rate when compared to women (15). The observed resistance to SARS-CoV-2 in women can be attributed to sex hormones, specifically estrogen, which is known to enhance the immune activity of both B as well as T-helper cells (16). Estrogen receptor alpha (ERα) is a steroid hormone receptor that controls physiological functions, including immunity. ERα has an effect on the subsets of T cells that includes Th1, Th2, Th17, and T regulatory cells, as well as follicular helper T (TFH) cells. It has been established that induced immunization by NP-conjugated ovalbumin produces specific antibodies that are elevated in CD4-ERα knock-out mice, under sufficient estrogen environment (17). Therefore, estrogen, the primary female sex hormone, stands out as a key biological factor making women's immune system more active against the virus (13).

There is a growing interest in studying the role of sex hormones in the tissue renin-angiotensin system (RAS). The expression of ACE2 (angiotensin-converting enzyme) in some organs, such as uterus, kidney, and heart, is regulated by 17β-estradiol. This occurs by increasing the locally existing ACE2 effect on the cardiac tissue and suppressing the RAS through catalytic cleavage of a particular residue of angiotensin II to increase the release of cardioprotective angiotensin 1–7 and upregulate anti-oxidative and anti-inflammatory effects (18) Estrogen level is inversely related with the regulation of cardiac troponin secreted during ischemic or anoxic condition, leading to irreversible injury to the cardiac cells (19). In few studies conducted on COVID-19 patients, it was seen that 51% patients died due to cardiac injury (20). The death rate in COVID-19 patients was 7.6% having normal cardiac troponin levels and without any cardiovascular disease. Mortality of 13.3% was seen in patients with underlying cardiovascular disease and normal cardiac troponin levels, 37.5% cardiovascular disease but elevated cardiac troponin levels, and 69.4% patients having both the conditions. A higher proportion of men (65.4%) had increased cardiac troponin as compared to women (42.2%) with COVID-19 (20).

The effect of estrogenic hormones could justify these observations, as this hormone has been reported to reduce low-density lipoprotein cholesterol and increase the high-density lipoprotein (21). 17β-estradiol, an estrogenic hormone, is also known to mediate the activation of early and late endothelial nitric oxide synthase *via* estrogen receptor interaction (22). Cardiomyocytes also carry the functional estrogen receptors that regulate the expression of nitric oxide synthase to prevent the cardiovascular system from damage by some factors such as suppression of the formation of thrombus, platelet stimulation, and adhesion of leukocyte-endothelial cell. It has been reported that male mice are more vulnerable to SARS-CoV compared to females. However, when the ovaries (an endocrine gland producing and releasing estrogen) from female mice were removed, their mortality from the SARS-CoV sharply increased (23).

COVID-19 affects men and women differently likely due to the difference in genetic nature and influence of sex hormones. COVID-19 enters the host body *via* the upper respiratory system, through contacting droplets. Estrogen has a beneficial impact on the entire respiratory tract system (16). Estrogen activates the response of mucosa of the nose by regulating turbinate hypertrophy and boosting secretion of nasal mucus containing anti-viral, antibacterial, and immune factors such as IgA, lysozyme, mucins, lactoferrin, electrolytes, and oligosaccharides, which are important for restricting upper airway infections (24). Besides, estrogen stimulates the synthesis of hyaluronic acid that preserves a suitable tropism of the cilia and the mucosal membrane (**Figure 2**). Additionally, estrogen stimulates the local nasal immune system that acts directly by stimulating phagocytic cells, antigen-presenting cells, and natural killer cells (25). Once stimulated, they can kill the virus protecting the body before its access to its target cells in the part of the respiratory system, thus reducing the pathological effect of the virus (26). In a study, it was indicated that G protein-coupled estrogen receptor (GPER) specifically supports the diminishing nasal symptoms, serum OVA-specific IgE, and Th2 cell immune response, but boosts the Treg immune response in mice (27). In addition to its indigenous impact in the nasal cavity, estrogen provides the required level of hyaluronic acid secretion needed for the mouth's hydration by promoting the function of the lower respiratory system as it acts directly on the bronchial epithelial membrane to secrete more mucus. At this stage, the effective role of estrogen is promoted by the progesterone (PG) physiological function as it upregulates amphiregulin (epidermal growth factor) to maintain the histological integrity of the lung tissue if the viral infection occurs. PG also improves the onset of the symptoms of respiratory disease, when given to women at menopause phase (28). Estradiol (E2) and PG support a reduced case of a naive immune-inflammatory reaction, *via* increasing the immune tolerance and synthesis of immunoglobulins. It has been reported that the combination of E2 and PG could enhance the anti-viral immunity, but downplay cytokine storms in COVID-19 (29).

E2 has been found to have a protective activity against the disease severity, as revealed by higher levels of cytokines such as IL-6 and IL-8 in severe cases. E2 corresponded to COVID-19 severity, because of the regulation of such cytokines associated with inflammation (30). Also, regulatory proteins (Cardiac troponin T and troponin I) play a key role in calcium regulation (7).

Estrogen has anti-inflammatory and anti-oxidative actions on the effectors of the renin-angiotensin system-like pro-oxidative

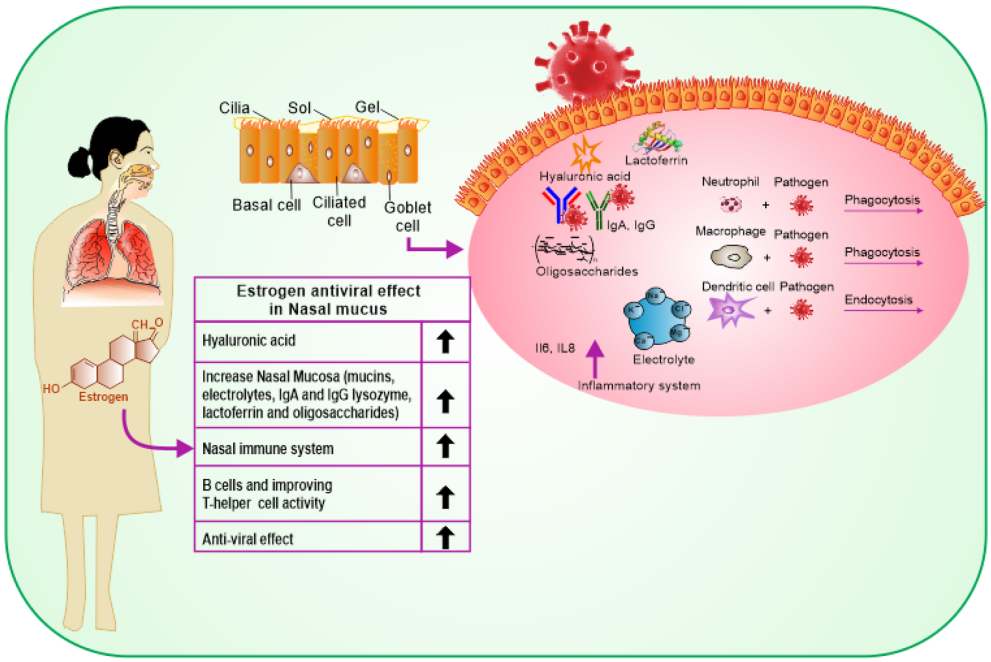


**FIGURE 2** | Schematic representation showing the protective effects of estrogen on the upper and lower respiratory tract cells and its benefits on the immune response.

LOX-1 and pro-inflammatory ICAM-1. Estrogen alters the homeostasis of the local RAS and offers protection in the atrial myocardium (31). Moreover, other studies have indicated the anti-viral activity of two selective estrogen receptor modulators against viral infection like Ebola. Primary differentiated human nasal epithelial cell cultures obtained from healthy men and women demonstrated the action of estrogenic receptors on the human cellular response to influenza A virus (IAV) infections. Nasal epithelial cells are the primary cell type infected with IAV, and these cultures allowed to investigate IAV infection and pathogenesis based on the sex and hormonal milieu of the donor cultures (32).

Menopause is an individual risk factor for COVID-19 as it causes a sudden reduction in estrogen levels which could minimize the risk difference between men and women, although the case studies have revealed that the gender disparity still exists in elderly people. In postmenopausal women, the ovaries produce estrone, the inactive form of estrogen, in high quantities. Additionally, estrogen is no longer the only endocrine factor in the postmenopausal stage. A number of extragonadal tissues such as adipose tissue, bone chondrocytes and osteoblasts, aortic and endothelium, vascular smooth muscle cells, skin, skeletal muscle, and several brain regions produce estrogen, to act locally as a paracrine and intracrine factor (33). Therefore, circulating estrogen levels explain its effect in menopausal women because estrogen escapes from local metabolism and gets into the main circulation (33, 34). It is still unclear if the estrogen circulation and expression in the local tissue play a part in the reduced COVID-19 mortality in menopausal women compared to age-matched men (35). Therefore, the role of estrogen is fascinating.

## DIFFERENCE IN INNATE AND ADAPTIVE IMMUNITY

Women show reduced susceptibility to viral infections due to their varying nature of innate immunity, hormones, and other factors associated with sex chromosomes. Sex-related hormones regulate the range of the immune responses distinctively in men and women (36). The estrogen and ER-α influence the activation and proliferation of T-lymphocytes and initiate elevation of IFN-γ level in Th1 lymphocytes. A gradual IFN reciprocation by mismatched dsRNA or exogenous IFN-α treatment has been found to inhibit SARS-CoV multiplication in the lungs of mice (37). Studies have reported that IFN-β and IFN-γ can significantly suppress the replication of SARS-CoV, and a symbiotic anti-SARS-CoV action was attained with the synthesis of the IFN-β and IFN-γ (38). As discussed earlier, treatment with estrogen suppresses the inflammatory response and reduces SARS-CoV load that leads to an increased survival in mice (23). Contrary to estrogen, testosterone have a general inhibitory action on the immune response, specifically to viral antigens (39). In a study, murine macrophage treatment with testosterone suppressed the nitrate oxidase synthetase (40).

Studies have shown suppressive effects of testosterone on the activation of dendritic cells, antigen presentation to T-lymphocytes, and initiation of immune response (41). Th1 cells

have a crucial part to play in protection against viral infections by secreting IFN-γ (42). Androgens can influence the thymocyte response by suppressing the Th1 proliferation and reducing IFN-γ synthesis (43–45).

Among women, in order to reduce the duplication of X-linked genes, the second X chromosome is silenced *via* X chromosome inactivation (XCI), although many genes escape this inactivation. A location on Xp22.2, which is for the ACE2 gene, also bypasses X-inactivation, resulting in the phenotypic differences between the genders. The other XCI escaping regions are IRAK1 (Interleukin-1 receptor-associated kinase 1) and IKKγ (inhibitor of nuclear factor Kappa-B kinase subunit gamma) that might influence the immune response against the COVID-19 infection in women. Numerous genes are involved with the X chromosome. Mutations occurring in a single gene may lead to two different alleles with a distinct mechanism of response, suggesting that women could not only escape the outcome of deterrent mutations but also help to fight against infectious challenges such as SARS-CoV-2. Additionally, estrogen and estrogen receptor signaling confer an important potency to innate as well as adaptive immunity and the process of tissue repair during and after the viral infection (7, 36, 39) (**Figure 3**).

In SARS-CoV-2 infected women, T cells, especially $CD8^+$ T cells, were found much more activated. When their clinical trajectory was analyzed, it was revealed that elevated cytokine levels in women patients were related to the worsening condition

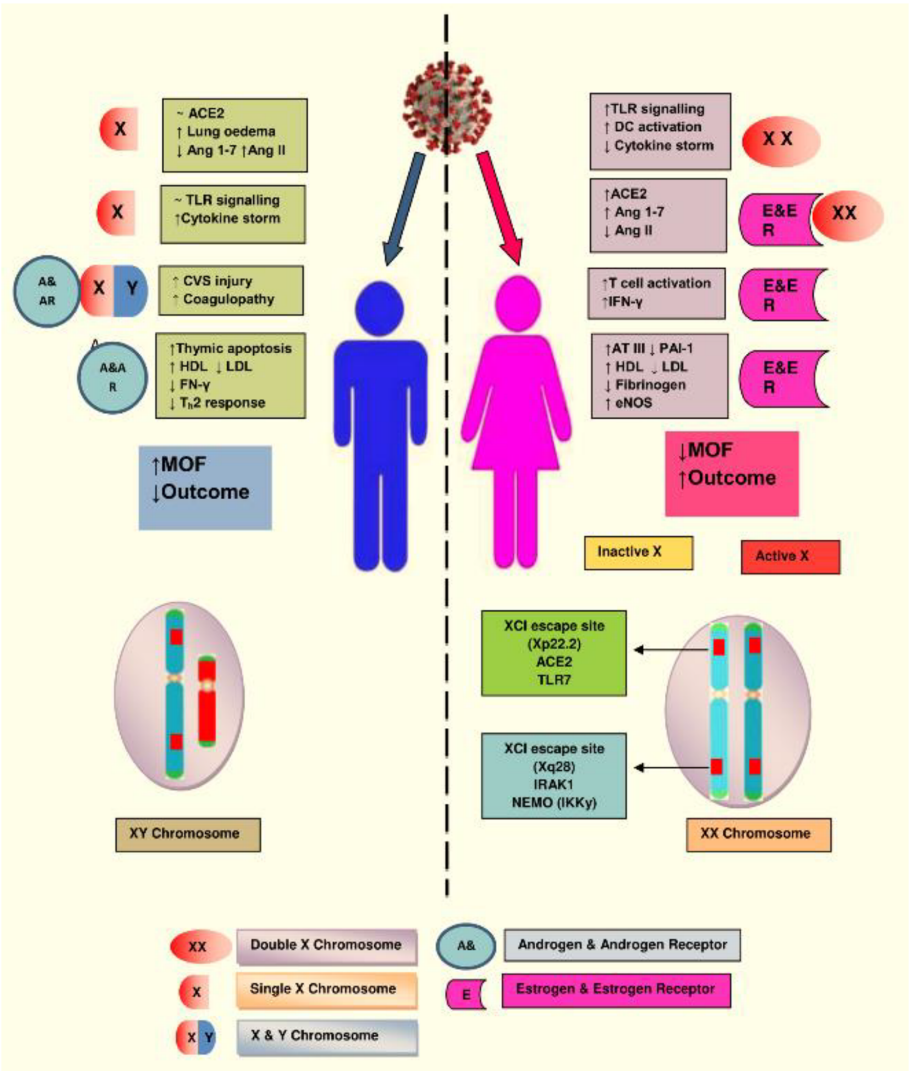


**FIGURE 3** | The X chromosome in females has various genes associated with immunity. Natural mutation in one copy of X gene may lead to two different alleles with distinct regulatory mechanism, which protect the women from implications of deleterious mutations and confers advantage in facing novel immunogens, like SARS-CoV-2. Illustration presents the genes encoded on the X-chromosome involved in the increased immune response in females during COVID-19. (Abbreviations used: TLR7, Toll-like receptor 7; DC, dendritic cell; CVS, cardiovascular system; IFN-γ, interferon gamma; LDL, low-density lipoprotein; HDL, high-density lipoprotein; ATIII, antithrombin III; IRAK1, Interleukin-1 receptor-associated kinase 1; MOF, multiorgan failure).

of COVID-19 disease (36). Most COVID-19 affected patients have higher plasma levels of pro-inflammatory cytokines/chemokines (IL-6, IL-2, IL-8, IL-7, CCL2, CCL3, and TNF) (3). This may lead to tissue damage and subsequent organ failure. Elevated levels of plasma cytokines are correlated with a decrease in lymphocytes which leads to the progression of COVID-19 disease. Dysfunction of T cells with age is also associated with worse COVID-19 disease outcomes (46). However, even though elderly women develop a strong T-cell immune response, majority develop anti-Spike IgG at the initial stage of infection that helps in suppressing proinflammatory cytokines, and hence, worsening of disease does not occur (47).

It is equally pertinent to mention that women are at no lesser risk of getting infected with coronavirus, especially during pregnancy, as women fall at higher risk of severe illness from other respiratory infections. COVID-19 infection in pregnant women did not differ much from non-pregnant women (48). Reports have suggested that pregnancy and childbirth do not seem to contribute to an increased risk of contracting SARS-CoV-2 infection; it also does not increase the severity of the clinical course of COVID-19, compared to non-pregnant women of the same age (49–51).

COVID-19 infection during pregnancy may have more unfavorable results in comparison with the non-pregnant group (52). Additionally, COVID-19 and pregnancy increase the chance of internal clotting that increases the risk of thrombosis (53). During the period of pregnancy, a large variety of immune cells, mostly natural killer (NK) cells, macrophages, and regulatory T cells (Treg), are activated. The accumulation of macrophages and NK cells takes place around trophoblastic cells during the first trimester of pregnancy protecting miscarriage of the allogeneic fetus (19). Hence, the maternal immune system shields fetus from the damage by environmental insults. Likewise, the fetus also modifies the maternal immune system. During pregnancy, PG has immunomodulatory effects that influence the Th1 response. In pregnancy, an enhancement in anti-inflammatory factors like interleukin-1 receptor antagonist (IL-RA) and TNF-α receptor (TNF-R) is recorded; conversely, a decrease in IL-1β and TNF-α is found (20).

Variations in the estrogen and PG levels during pregnancy may cause respiratory, cardiovascular, reversible degeneration in the thymus, with a reduction in $CD4^+$ and $CD8^+$ T cells that may lead to more susceptibility of women to SARS-CoV-2 infection. The PG on nasal mucosa acts as a facilitator in the attachment of the virus and prevents its elimination. Additionally, an increase in oxygen consumption due to vascular congestion and reduction in the capacity of the lung may increase the risk for severity of COVID-19 in pregnant women (54). Another risk factor is the higher ACE2 expression during pregnancy, and hence increased risk of complications from COVID-19 infection (55). An increase in ACE2 receptors in the kidneys during pregnancy may contribute to effective regulation of blood pressure, although it can favor the attachment and facilitate the virus entry into the host cells (54).

Androgens might lead to severe COVID-19 disease among men through raising neutrophil count and increasing the production of cytokines (IL-1β, IL-10, IL-2), altering TGF-β production by immune cells, and decreasing the antibody production (47). This event is crucial as the patients with severe COVID-19 exhibit cytokine storm syndrome due to neutrophils. One of the androgen pathways in COVID-19 infection is the transmembrane protease, serine 2 (TMPRSS2) gene that is expressed mainly in the adult prostate (56), and in metastatic prostate cancers; it is also found in tissues like lung, kidney, pancreas, colon, small intestine, and liver (56). The TMPRSS2 gene is transcribed and regulated by the androgen receptor, and the main target of TMPRSS2 expression in COVID-19 is the lungs, kidneys, and liver (57). In one retrospective study, increased levels of testosterone in most women (60%) having COVID-19 disease were recorded; a positive correlation between the levels of testosterone and pro-inflammatory cytokines among women with COVID-19 was also noted (58).

In view of a higher mortality in men from COVID-19 compared to women, it has recently been pointed out that testosterone may affect disease severity. This notion is supported by the evidence that the primer protease for SARS-CoV-2 spike protein, TIMPRSS2, as well as the virus entry receptor, ACE2, are upregulated by testosterone (59). Although debated, androgen-deprivation therapy in prostate cancer patients infected with SARS-CoV-2 has been suggested (60). However, hypogonadism can also be a risk factor for severe COVID-19 (61). It is worth noting that women suffering from polycystic ovarian syndrome (PCOS), which is characterised by heightened androgen levels (hyperandrogenism), have been found to be at a significantly higher risk of COVID-19 compared to non-PCOS women (62, 63).

## ROLE OF ANGIOTENSIN-CONVERTING ENZYME 2 (ACE2)

The ACE2 gene that is found on the X chromosome (location: Xp22.2; nucleotides 15 494 402–15 602 148, GRCh38.hg38 version) has been reported to work differently in men and women (64). ACE2 carries out its important functions by dissociating angiotensin I into angiotensin II. Angiotensin II, being a small peptide, is of huge importance in the case of vasoconstriction and sodium balance. ACE2 breaks angiotensin I and II into dissociated peptides that possibly lead to vasodilatation and, hence, countering angiotensin II (65, 66). The entry route for SARS-CoV-2 is *via* ACE2, similar to the SARS-CoV virus, bearing a spike protein that binds with ACE2 to invade the cells (20, 46, 67). The location of the ACE2 gene on Xp22.2 is a site of genes that escapes XCI, leading to phenotypic dissimilarities between genders (68, 69). SARS-CoV-2 possesses 16 residues of receptor binding motif (RBM), and binds to 16 of the 20 ACE2 residues present in men. In women, the same RBM of SARS-CoV-2 may be detected by ACE2 on any of the two X chromosomes. The possibility becomes less for the similar residue sequences of ACE2 present on the second chromosome to bind efficiently to the RBM of SARS-CoV-2, leading to the

breakdown of Ang II to form Ang 1–7 by unbound ACE2, and therefore might reduce the chance of respiratory edema during SARS-CoV-2 infection. Men, with only one X chromosome, are deficient in the alternative mechanisms that could impart cellular protection during COVID-19 infection (70, 71).

Several significant divergences in the prevalence of ACE2 variants have been reported among diverse races and ethnicity. Recently, a single-cell RNA sequencing (RNA-seq) study reported that Asian men could express tissue ACE2 at a higher level (72). During a study on the northeastern Chinese Han population, the serum ACE2 activity was found to have a negative correlation with body mass index, pulse pressure, and estrogen levels among hypertensive women (6). Such studies indicate a protective mechanism of circulating ACE2 and the participation of estrogens in the expression and upregulation of ACE2 activity levels (73).

ACE2 is present in epithelial cells of the lung, intestine, blood vessels, and kidney (74). The angiotensin system plays a vital role in cardiovascular homeostasis, acute inflammation, and autoimmune disorders (75). The presence of high ACE2 receptors may lead to a higher risk of contracting SARS-CoV2. It has been reported that men have elevated levels of circulating ACE2 than women, and also in patients having diabetes and cardiovascular ailments (76). People with cardiovascular failure have the plasma ACE2 elevated in men compared to women, which correlates with increased SARS-CoV infection (65, 77). Among the hypertensive women, blood pressure and body mass index inversely correspond to ACE2, whereas there is a direct correlation of blood sugar and estrogen levels to ACE2 level (65, 78). As mentioned above, estrogen also downregulates the renin-angiotensin system components acting as an anti-inflammatory and anti-oxidative agent (67, 78). Significant functional regulation of ACE2 by estrogen may explain the gender differences in COVID-19 associated morbidity and mortality (79).

## Microbiota

Development of a pronounced innate and adaptive immune response is greatly influenced by the composition of the human gut microbiota. The human gut possesses a diverse and complex microbial consortium that reciprocates by establishing the persistent host immune homeostasis (80–82). The human gut harbors complex communities of microorganisms that includes holobiont (composite organism) and hologenome (collective genome of all bionts) (83). This complex composition offers a crucial genomic and metabolic capability that has an important impact on the initiation, development, and action of the host immune system, thereby protecting against infections and safeguarding the ecosystem of gut flora (84). The homeostatic cascades existing between the immune system and gut microbiota of the host play a crucial role in modulating the activation of host cells and tissues involved in response to infectious agents (85). The interaction of virus and microbiota has been studied in several viral infections. For example, surfactin, a molecule on a *Bacillus subtilis* surface, is known to disintegrate many viruses including influenza A (85). Thus, the gut microbiota is likely to influence COVID-19 pathogenicity, and conversely, SARS-CoV-2 may influence the gut microbiota leading to dysbiosis and other unpleasant consequences (86). Therefore, the alteration of the composition of existing microbiota and health conditions during SARS-CoV-2 infection is likely to have a major role in establishing the susceptibility and resilience of an individual to COVID-19. However, most of the COVID-19 severe symptoms and fatalities occur in individuals having some risk factors such as aging, preexisting comorbidities, and, to some extent, gender, which are indirectly characterized by disrupted microbiome status (87).

Like gastrointestinal system, the respiratory microbiome constitutes the community of differentiated bacterial phyla like *Bacteroidetes*, *Firmicutes*, and *Proteobacteria* and has a protective role in the host immunity (44, 88) (**Figure 4A**). Han et al. showed that the COVID-19 infection can alter the lung microbiome (89). A severe dysbiosis was found among COVID-19 patients, with a higher prevalence of pathogenic microbes such as *Klebsiella oxytoca*, *Faecalibacterium prausnitzii*, *Lactic Acid Bacteria*, and *Tobacco mosaic virus* (TMV) (**Figure 4B**). The serious inflammatory environment in the lungs correlated with *Rothia mucilaginosa*, TMV level, and SARS-CoV-2, suggesting a key role of respiratory microbiota in COVID-19 disease. Other studies also reported fecal microbial changes in 15 subjects infected with COVID-19 that correlated with high severity and abundance of *Coprobacillus*, *Clostridium ramosum*, and *Clostridium hathewayi*, and reduced levels of *Faecalibacterium prausnitzii* and *Alistipes onderdonkii* (90, 91) (**Figures 4A, B**).

The microbiota existing outside of the reproductive tract is significantly mediated by the sex steroid hormones. Many studies conducted on mice, fish, and humans have analyzed the sex difference in gut microbiota. This subject of whether the sex difference in gut microbiome in humans has any involvement in the disparity of viral infection is an interesting area to study (92). In a study, gender differences correlated with the overall composition of gut microbiota. The gut microbiome in women was found to have a lower occurrence of *Bacteroidetes* compared to men (93). An animal study evaluated gender-specific variations in the composition of gut microbiota (94, 95). The systemic estrogen levels may be influenced by dietary fiber, which is the main energy source of gut microbial fermentation and, hence, formulates the gut microbiota (94, 96).

# ENVIRONMENTAL MEDIATORS

In addition to biological differences accounting for a significant gender disparity of COVID-19, the influence of environmental factors could also play a part (97).

## Lifestyle

Lifestyle choices among the genders possibly makes a huge difference. Historically, it has been noticed that men are more habitual of smoking than women. Smokers tend to have weakened lungs leading to chronic lung and heart diseases that could be the worst outcome, if infected with COVID-19 (97–100). In China, the smoking prevalence in men is 57.6% which is nearly 10 times more than the women with 6.7% (101).

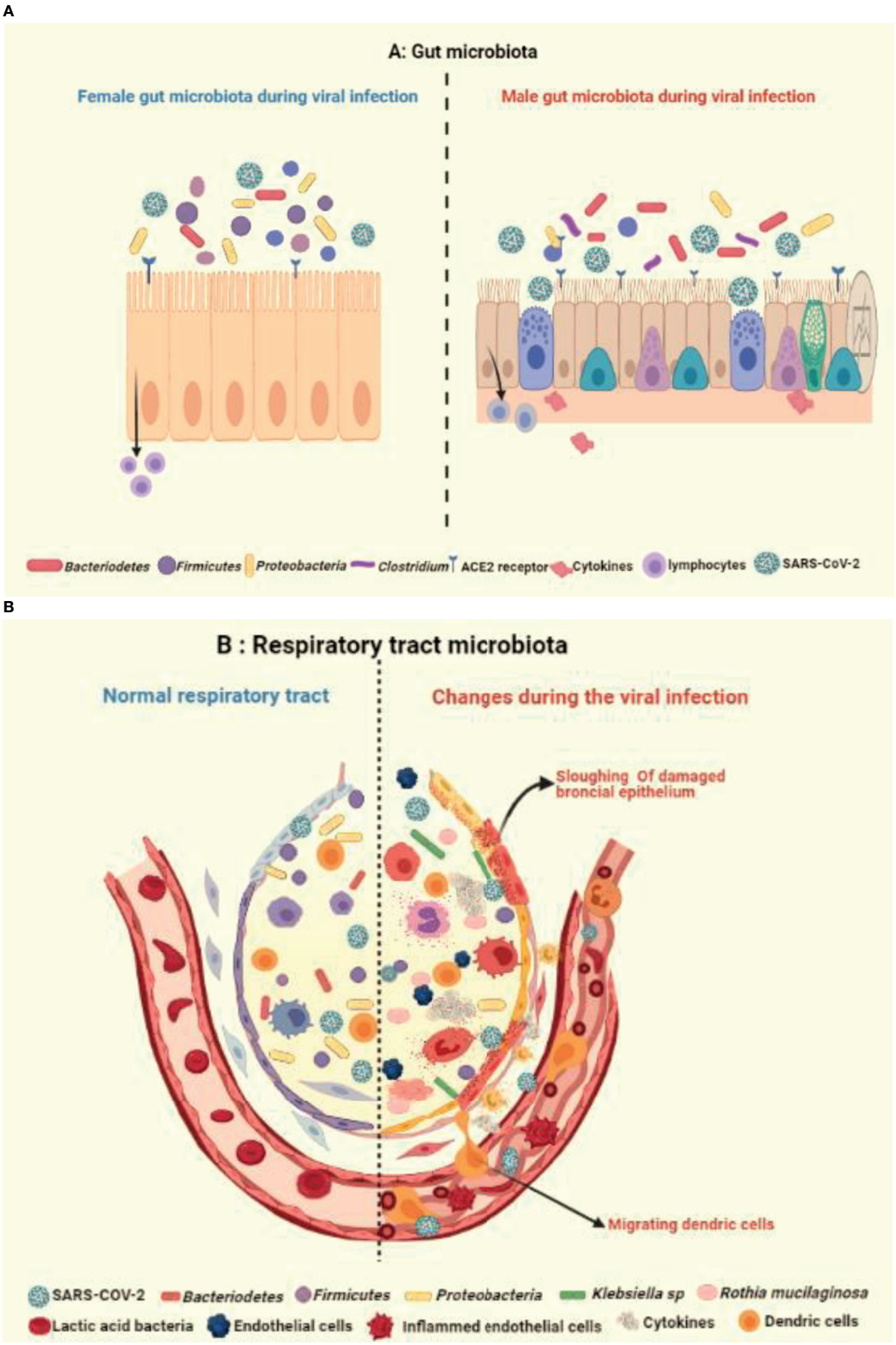


**FIGURE 4** | Illustration showing the impact of healthy and unhealthy microbiota on respiratory tract infection. The complex relationship *via* gut-lung axis might be crucial in determining the vulnerability of respiratory tract to COVID-19, as an outcome of potential variation and crosstalk between **(A)** healthy gut microbiota with occurrence of fewer *Bacteriodetes* and **(B)** respiratory microbiota with prevalence of more *Klebsiella* and *Ruthia sps* in virus infected alveolus.

The lower airways of smokers have shown a higher expression of ACE2, suggesting a higher risk for COVID-19 (102, 103). Such findings are an indication of one of the factors behind the increased mortality in men with COVID-19 which needs further validation.

### Exercise

The decreased incidence rate of COVID-19 symptoms in women can be also related to the physical activity engaging from moderate-to-vigorous one. Women are considered to be physically more active when compared with men who prefer prolonged and intensive exercises (1, 104). Prolonged and vigorous exercise may lead to immunosuppression; on the contrary, mild and moderate exercise enhances immune response and significantly minimizes the risk and severity of respiratory viral infection. This is supported by a number of studies that explain a moderate level of exercise lowers inflammation and boosts the immune function. Regular mild physical activity influences the level of hormones related to stress, which downregulates intense inflammation of the respiratory tract and helps in activating the anti-viral innate immunity polarising the immune function towards a Th2 profile, extensive research is needed to study cellular and molecular cascades through which exercise regulates immune response (104–106).

### Nutrition

A study shows nutritional environment during the post and prenatal period is associated with a reduced mortality rate among females in case of HIV, for example, high-fat diet and the micronutrients like Vitamin B, C, and E supplements have a reduction of 32% (107). Another study suggests the benefits of supplementary maternal micronutrients in women compared to men (108, 109).

## CONCLUSIONS AND PERSPECTIVE

Immunity, X-chromosome associated genes, and sex hormones are the main distinguishing factors that are likely to offer greater resistance against SARS-CoV-2 in women. The evidence suggesting important decisive factors of gender-related disparity in immunity may impact on the onset of COVID-19 and vaccination outcomes.

## AUTHOR CONTRIBUTIONS

SR: conceptualized, drafted, figures, and revised. VN contributed to figure, environmental factors, and reference formatting. IN: contributed to epidemiology part. HA: contributed to environmental part. MS: contributed to mortality and map part. MA contributed to severity and manifestation part. UK: reviewed, edited, and revised the manuscript. EAl-S: conceptualized, drafted, revised, and edited. All authors read the article and approved the submitted version.

## FUNDING

Institute for Research and Medical Consultation (IRMC) is highly acknowledged for the research facilities.

## ACKNOWLEDGMENTS

The figures have been created using Biorender software.

## REFERENCES

1. Khan S, Tombuloglu H, Hassanein SE, Rehman S, Bozkurt A, Cevik E, et al. Coronavirus Diseases 2019: Current Biological Situation and Potential Therapeutic Perspective. *Eur J Pharmacol* (2020) 886:173447. doi: 10.1016/j.ejphar.2020.173447
2. Cleri DJ, Ricketti AJ, Vernaleo JR. Severe Acute Respiratory Syndrome (SARS). *Infect Dis Clin North Am* (2010) 24:175–202. doi: 10.1016/j.idc.2009.10.005
3. Huang C, Wang Y, Li X, Ren L, Zhao J, Hu Y, et al. Clinical Features of Patients Infected With 2019 Novel Coronavirus in Wuhan, China. *Lancet* (2020) 395:497–506. doi: 10.1016/S0140-6736(20)30183-5
4. Hosseini A, Hashemi V, Shomali N, Asghari F, Gharibi T, Akbari M, et al. Innate and Adaptive Immune Responses Against Coronavirus. *BioMed Pharmacother* (2020) 132:110859. doi: 10.1016/j.biopha.2020.110859
5. Boechat JL, Chora I, Morais A, Delgado L. The Immune Response to SARS-CoV-2 and COVID-19 Immunopathology – Current Perspectives. *Pulmonology* (2021) 9:S2531–0437(21)00084-2. doi: 10.1016/j.pulmoe.2021.03.008
6. Jin JM, Bai P, He W, Wu F, Liu XF, Yang JK. Gender Differences in Patients With COVID-19: Focus on Severity and Mortality. *Front Public Health* (2020) 8:152. doi: 10.3389/fpubh.2020.00152
7. Li Q, Guan X, Wu P, Wang X, Zhou L, Tong Y, et al. Early Transmission Dynamics in Wuhan, China, of Novel Coronavirus-Infected Pneumonia. *N Engl J Med* (2020) 382:1199–207. doi: 10.1056/NEJMOa2001316
8. Zhang J, Xiang D, Cao YY, Yuan YD, Yang YB, Yan YQ, et al. Clinical Characteristics of 140 Patients Infected With SARS-CoV-2 in Wuhan, China. *Allergy* (2020) 75(7):1730–41. doi: 10.1111/all.14238
9. Rabin RC. In N.Y.C., the Coronavirus Is Killing Men at Twice the Rate of Women. *N Y Time* (2020).
10. The Novel Coronavirus Pneumonia Emergency Response Epidemiology Team. The Epidemiological Characteristics of an Outbreak of 2019 Novel Coronavirus Diseases (COVID-19) in China. *Zhonghua Liu Xing Bing Xue Za Zhi* (2020) 41(2):145. doi: 10.46234/ccdcw2020.032
11. Aleanizy FS, Mohmed N, Alqahtani FY, El Hadi Mohamed RA. Outbreak of Middle East Respiratory Syndrome Coronavirus in Saudi Arabia: A Retrospective Study. *BMC Infect Dis* (2017) 17(1):23. doi: 10.1186/s12879-016-2137-3
12. Peiris JSM, Lai ST, Poon LLM, Guan Y, Yam LYC, Lim W, et al. Coronavirus as a Possible Cause of Severe Acute Respiratory Syndrome. *Lancet* (2003) 361(9366):1319–25. doi: 10.1016/S0140-6736(03)13077-2
13. Karlberg J, Chong DSY, Lai WYY. Do Men Have a Higher Case Fatality Rate of Severe Acute Respiratory Syndrome Than Women Do? *Am J Epidemiol* (2004) 159(3):229–31. doi: 10.1093/aje/kwh056
14. Alghamdi IG, Hussain II, Almalki SS, Alghamdi MS, Alghamdi MM, El-Sheemy MA. The Pattern of Middle East Respiratory Syndrome Coronavirus in Saudi Arabia: A Descriptive Epidemiological Analysis of Data From the Saudi Ministry of Health. *Int J Gen Med* (2014) 7:417. doi: 10.2147/IJGM.S67061
15. Graziano O, Rezza G, Brusaferro S. Case-Fatality Rate and Characteristics of Patients Dying in Relation to COVID-19 in Italy. *JAMA* (2020) 323 (18):1775–6. doi: 10.1001/jama.2020.4683
16. Taneja V. Sex Hormones Determine Immune Response. *Front Immunol* (2018) 9:1931. doi: 10.3389/fimmu.2018.01931
17. Kim DH, Park HJ, Park HS, Jae UL, Che MK, Myung CG, et al. Estrogen Receptor α in T Cells Suppresses Follicular Helper T Cell Responses and

Prevents Autoimmunity. *Exp Mol Med* (2019) 51(4):1–9. doi: 10.1038/s12276-019-0237-z

18. Joyner J, Neves LAA, Granger JP, Alexander BT, Merrill DC, Chappell MC, et al. Temporal-Spatial Expression of ANG-(1-7) and Angiotensin-Converting Enzyme 2 in the Kidney of Normal and Hypertensive Pregnant Rats. *Am J Physiol Regul Integr Comp Physiol* (2007) 293(1): R169–77. doi: 10.1152/ajpregu.00387.2006
19. Mingels AMA, Kimenai DM. Sex-Related Aspects of Biomarkers in Cardiac Disease. *Adv Exp Med Biol* (2018) 1065:545–64. doi: 10.1007/978-3-319-77932-4_33
20. Guo T, Fan Y, Chen M, Wu X, Zhang L, He T, et al. Cardiovascular Implications of Fatal Outcomes of Patients With Coronavirus Disease 2019 (COVID-19). *JAMA Cardiol* (2020) 5:811–8. doi: 10.1001/jamacardio.2020.1017
21. Mebane S, Irma L. Effects of Estrogen or Estrogen/Progestin Regimens on Heart Disease Risk Factors in Postmenopausal Women: The Postmenopausal Estrogen/Progestin Interventions (PEPI) Trial. *JAMA* (1995) 273(3):199–208. doi: 10.1001/jama.273.3.199
22. Fontaine C, Morfoisse F, Tatin F, Zamora A, Zahreddine R, Henrion D, et al. The Impact of Estrogen Receptor in Arterial and Lymphatic Vascular Diseases. *Int J Mol Sci* (2020) 21(9):3244. doi: 10.3390/ijms21093244
23. Channappanavar R, Fett C, Mack M, Ten Eyck PP, Meyerholz DK, Perlman S. Sex-Based Differences in Susceptibility to Severe Acute Respiratory Syndrome Coronavirus Infection. *J Immunol* (2017) 198(10):4046–53. doi: 10.4049/jimmunol.1601896
24. Paulsson B, Gredmark T, Burian P, Bende M. Nasal Mucosal Congestion During the Menstrual Cycle. *J Laryngol Otol* (1997) 111(4):337–9. doi: 10.1017/s0022215100137259
25. Costa HO, de Castro Neto NP, Rossi LM, Millas I, Coelho F, da Silva L. Influence of Estradiol Administration on Estrogen Receptors of Nasal Mucosa: An Experimental Study on Guinea Pigs. *Braz J Otorhinolaryngol* (2014) 80(1):18–23. doi: 10.5935/1808-8694.20140006
26. Kozlowski PA, Williams SB, Lynch RM, Flanigan TP, Patterson RR, Cu-Uvin S, et al. Differential Induction of Mucosal and Systemic Antibody Responses in Women After Nasal, Rectal, or Vaginal Immunization: Influence of the Menstrual Cycle. *J Immunol* (2002) 169(1):566–74. doi: 10.4049/jimmunol.169.1.566
27. Wang YX, Gu ZW, Hao LY. The Environmental Hormone Nonylphenol Interferes With the Therapeutic Effects of G Protein-Coupled Estrogen Receptor Specific Agonist G-1 on Murine Allergic Rhinitis. *Int Immunopharmacol* (2020) 78:106058. doi: 10.1016/j.intimp.2019.106058
28. Tam A, Wadsworth S, Dorscheid D, Man SF, Sin DD. Estradiol Increases Mucus Synthesis in Bronchial Epithelial Cells. *PloS One* (2014) 9(6):e100633. doi: 10.1371/journal.pone.0100633
29. Mauvais-Jarvis F, Klein SL, Levin ER. Estradiol, Progesterone, Immunomodulation, and COVID-19 Outcomes. *Endocrinology* (2020) 161(9):bqaa127. doi: 10.1210/endocr/bqaa127
30. Ting D, Zhang J, Wang T, Cui P, Chen Z, Jiang J, et al. A Multi-Hospital Study in Wuhan, China: Protective Effects of Non-Menopause and Female Hormones on SARS-CoV-2 Infection. *medRxiv* (2020), 20043943. doi: 10.1101/2020.03.26.20043943
31. Bukowska A, Spiller L, Wolke C, Lendeckel U, Weinert S, Hoffmann J, et al. Protective Regulation of the ACE2/ACE Gene Expression by Estrogen in Human Atrial Tissue From Elderly Men. *Exp Biol Med* (2017) 242(14):14. doi: 10.1177/1535370217718808
32. Peretz J, Pekosz A, Lane AP, Klein SL. Estrogenic Compounds Reduce Influenza A Virus Replication in Primary Human Nasal Epithelial Cells Derived From Female, But Not Male, Donors. *Am J Physiol Lung Cell Mol Physiol* (2016) 310:415–25. doi: 10.1152/ajplung.00398.2015.-Influenza
33. Simpson ER. Sources of Estrogen and Their Importance. *J Steroid Biochem Mol Biol* (2003) 86:225–30. doi: 10.1016/S0960-0760(03)00360-1
34. Murata Y, Robertson KM, Jones MEE, Simpson ER. Effect of Estrogen Deficiency in the Male: The ArKO Mouse Model. *Mol Cell Endocrinol* (2002) 193:7–12. doi: 10.1016/s0303-7207(02)00090-4
35. Di Stadio A, Della Volpe A, Ralli AM, Ricci G. Gender Differences in COVID-19 Infection. The Estrogen Effect on Upper and Lower Airways. Can It Help to Figure Out a Treatment? *Eur Rev Med Pharmacol Sci* (2020) 24:5195–6. doi: 10.26355/eurrev_202005_21298
36. Takahashi T, Ellingson MK, Wong P, Israelow B, Lucas C, Klein J, et al. Sex Differences in Immune Responses to SARS-CoV-2 That Underlie Disease Outcomes. *Nature* (2020) 588:315–20. doi: 10.1038/s41586-020-2700-3
37. Barnard DL, Craig WD, Bailey K, Heiner M, Montgomery R, Lauridsen L, et al. Evaluation of Immunomodulators, Interferons and Known *In Vitro* SARS-CoV Inhibitors for Inhibition of SARS-CoV Replication in BALB/c Mice. *Antivir Chem Chemother* (2006) 17:275–84. doi: 10.1177/095632020601700505
38. Sainz BJr., Mossel EC, Peters CJ, Garry RF. Interferon-Beta and Interferon-Gamma Synergistically Inhibit the Replication of Severe Acute Respiratory Syndrome-Associated Coronavirus (SARS-CoV). *Virology* (2004) 329 (1):11–7. doi: 10.1016/j.virol.2004.08.011
39. Torcia MG, Nencioni L, Clemente AM, Civitelli L, Celestino I, Limongi D, et al. Sex Differences in the Response to Viral Infections: TLR8 and TLR9 Ligand Stimulation Induce Higher IL10 Production in Males. *PloS One* (2012) 7(6):e39853. doi: 10.1371/journal.pone.0039853
40. Friedl R, Brunner M, Moeslinger T, Spieckermann PG. Testosterone Inhibits Expression of Inducible Nitric Oxide Synthase in Murine Macrophages. *Life Sci* (2000) 68(4):417–29. doi: 10.1016/S0024-3205(00)00953-X
41. Trigunaite A, Dimo J, Jørgensen TN. Suppressive Effects of Androgens on the Immune System. *Cell Immunol* (2015) 294(2):87–94. doi: 10.1016/j.cellimm.2015.02.004
42. Micallef MJ, Ohtsuki T, Kohno K, Tanabe F, Ushio S, Namba M, et al. Interferon-γ-Inducing Factor Enhances T Helper 1 Cytokine Production by Stimulated Human T Cells: Synergism With Interleukin-12 for Interferon-γ Production. *Eur J Immunol* (1996) 26(7):1647–51. doi: 10.1002/eji.1830260736
43. Kissick HT, Sanda MG, Dunn LK, Pellegrini KL, On ST, Noel JK, et al. Androgens Alter T-Cell Immunity by Inhibiting T-Helper 1 Differentiation". *Proc Natl Acad Sci USA* (2014) 111(27):9887–92. doi: 10.1073/pnas.1402468111
44. Giamarellos-Bourboulis EJ, Netea MG, Rovina N, Akinosoglou K, Antoniadou A, Antonakos N, et al. Complex Immune Dysregulation in COVID-19 Patients With Severe Respiratory Failure. *Cell Host Microbe* (2020) 27(6):992–1000.e3. doi: 10.1016/j.chom.2020.04.009
45. Grasselli G, Zangrillo A, Zanella A, Antonelli M, Cabrini L, Castelli A, et al. Baseline Characteristics and Outcomes of 1591 Patients Infected With SARS-CoV-2 Admitted to ICUs of the Lombardy Region, Italy. *JAMA* (2020) 323(16):1574–81. doi: 10.1001/jama.2020.5394
46. Zhang X, Yun T, Yun L, Gang L, Feng L, Zhigang Y, et al. Viral and Host Factors Related to the Clinical Outcome of COVID-19. *Nature* (2020) 323 (16):1574–81. doi: 10.1038/s41586-020-2355-0
47. Klein SL, Flanagan KL. Sex Differences in Immune Responses. *Nat Rev Immunol* (2016) 16:626–38. doi: 10.1038/nri.2016.90
48. Harman S. Ebola, Gender and Conspicuously Invisible Women in Global Health Governance. *Third World Q* (2016) 16(10):626–38. doi: 10.1080/01436597.2015.1108827
49. Breslin N, Baptiste C, Gyamfi-Bannerman C, Miller R, Martinez R, Bernstein K, et al. Coronavirus Disease 2019 Infection Among Asymptomatic and Symptomatic Pregnant Women: Two Weeks of Confirmed Presentations to an Affiliated Pair of New York City Hospitals. *Am J Obstet Gynecol MFM* (2020) 37(3):100118. doi: 10.1016/j.ajogmf.2020.100118
50. Garg S, Kim L, Whitaker M, O'Halloran A, Cummings C, Holstein R, et al. Hospitalization Rates and Characteristics of Patients Hospitalized With Laboratory-Confirmed Coronavirus Disease 2019 - Covid-Net, 14 States, March 1–30, 2020. *Morbid Mortal Wkly Rep* (2020) 2(2):100118. doi: 10.15585/MMWR.MM6915E3
51. Sutton D, Fuchs K, D'Alton M, Goffman D. Universal Screening for SARS-CoV-2 in Women Admitted for Delivery. *N Engl J Med* (2020) 382 (22):2163–4. doi: 10.1056/NEJMc2009316
52. Kotlar B, Gerson E, Petrillo S, Langer A, Tiemeier H. The Impact of the COVID-19 Pandemic on Maternal and Perinatal Health: A Scoping Review. *Reprod Health* (2021) 1(18):1–39. doi: 10.1186/s12978-021-01070-6
53. Guasch E, Brogly N, Gilsanz F. COVID in Obstetrics: Labor Analgesia and Cesarean Section. *Curr Opin Anaesthesiol* (2021) 34(1):62–8. doi: 10.1097/ACO.0000000000000949
54. Spiezia L, Boscolo A, Poletto F, Cerruti L, Tiberio I, Campello E, et al. COVID-19-Related Severe Hypercoagulability in Patients Admitted to

Intensive Care Unit for Acute Respiratory Failure. *Thromb Haemost* (2020) 120(6):998–1000. doi: 10.1055/s-0040-1710018
55. Nabulsi AA, Folsom AR, White A, Patsch W, Heiss G, Wu KK, et al. Association of Hormone-Replacement Therapy With Various Cardiovascular Risk Factors in Postmenopausal Women. The Atherosclerosis Risk in Communities Study Investigators. *N Engl J Med* (1993) 328(15):1069–75. doi: 10.1056/NEJM199304153281501
56. Wambier CG, Goren A, Vaño-Galván S, Ramos PM, Ossimetha A, Nau G, et al. Androgen Sensitivity Gateway to COVID-19 Disease Severity. *Drug Dev Res* (2020) 81(7):771–6. doi: 10.1002/ddr.21688
57. Moradi F, Behnaz E, Ghadiri-Anari A. The Role of Androgens in COVIcD-19. *Diabetes Metab Syndr* (2020) 14(6):2003–6. doi: 10.1016/j.dsx.2020.10.014
58. Schroeder M, Tuku B, Jarczak D, Nierhaus A, Bai T, Jacobsen H, et al. The Majority of Male Patients With COVID-19 Present Low Testosterone Levels on Admission to Intensive Care in Hamburg, Germany: A Retrospective Cohort Study. *medRxiv* (2020) 14(6):20073817. doi: 10.1101/2020.05.07.20073817
59. Mohamed MS, Moulin TC, Schiöth HB. Sex Differences in COVID-19: The Role of Androgens in Disease Severity and Progression. *Endocrine* (2020) 71(1):3–8. doi: 10.1007/s12020-020-02536-6
60. Salciccia S, Del Giudice F, Eisenberg ML, Mastroianni CM, De Berardinis E, Ricciuti GP, et al. Androgen-Deprivation Therapy and SARS-Cov-2 Infection: The Potential Double-Face Role of Testosterone. *Ther Adv Endocrinol Metab* (2020) 11:2042018820969019. doi: 10.1177/204201882096901
61. Rastrelli G, Di Stasi V, Inglese F, Beccaria M, Garuti M, Di Costanzo D, et al. Low Testosterone Levels Predict Clinical Adverse Outcomes in SARS-CoV-2 Pneumonia Patients. *Andrology* (2020) 9(1):88–98. doi: 10.1111/andr.12821
62. Subramanian A, Anand A, Adderley NJ, Okoth K, Toulis KA, Gokhale K, et al. Increased COVID-19 Infections in Women With Polycystic Ovary Syndrome: A Population-Based Study. *Eur J Endocrinol* (2021) 184(5):637–45. doi: 10.1530/EJE-20
63. Kyrou I, Karteris E, Robbins T, Chatha K, Drenos F, Randeva HS. Polycystic Ovary Syndrome (PCOS) and COVID-19: An Overlooked Female Patient Population at Potentially Higher Risk During the COVID-19 Pandemic. *BMC Med* (2020) 18(1):220. doi: 10.1186/s12916-020-01697-5
64. Culebras E, Hernández F. ACE2 Is on the X Chromosome: Could This Explain COVID-19 Gender Differences? *Eur Heart J* (2020) 41(32):3095. doi: 10.1093/eurheartj/ehaa521
65. Purdie A, Hawkes S, Buse K, Onarheim K, Aftab W, Low N, et al. Sex, Gender and Covid-19: Disaggregated Data and Health Disparities. *BMJ Glob Health Blogs* (2020) 41(32):3095.
66. Sama IE, Ravera A, Santema BT, van Goor H, Ter Maaten JM, Cleland JGF, et al. Circulating Plasma Concentrations of Angiotensin-Converting Enzyme 2 Inmen and Women With Heart Failure and Effects of Renin-Angiotensin-Aldosterone Inhibitors. *Eur Heart J* (2020) 41(19):1810–7. doi: 10.1093/eurheartj/ehaa373
67. Majdic G. Could Sex/Gender Differences in ACE2 Expression in the Lungs Contribute to the Large Gender Disparity in the Morbidity and Mortality of Patients Infected With the SARS-CoV-2 Virus? *Front Cell Infect Microbiol* (2020) 10:327. doi: 10.3389/fcimb.2020.00327
68. Carrel L, Willard HF. X-Inactivation Profile Reveals Extensive Variability in X-Linked Gene Expression in Females. *Nature* (2005) 434(7031):400–4. doi: 10.1038/nature03479
69. Talebizadeh Z, Simon SD, Butler MG. X Chromosome Gene Expression in Human Tissues: Male and Female Comparisons. *Genomics* (2006) 88(6):675–81. doi: 10.1016/j.ygeno.2006.07.016
70. Lan J, Ge J, Yu J, Shan S, Zhou H, Fan S, et al. Structure of the SARS-CoV-2 Spike Receptor-Binding Domain Bound to the ACE2 Receptor. *Nature* (2020) 581(7807):215–20. doi: 10.1038/s41586-020-2180-5
71. Kuba K, Imai Y, Rao S, Gao H, Guo F, Guan B, et al. A Crucial Role of Angiotensin Converting Enzyme 2 (ACE2) in SARS Coronavirus-Induced Lung Injury. *Nat Med* (2005) 11(8):875–9. doi: 10.1038/nm1267
72. Zhao Y, Zhao Z, Wang Y, Zhou Y, Ma Y, Zuo W. Single-Cell RNA Expression Profiling of ACE2, the Putative Receptor of Wuhan 2019-NCov. *bioRxiv* (2020) 11(8):919985. doi: 10.1101/2020.01.26.919985
73. da Silva JS, Gabriel-Costa D, Wang H, Ahmad S, Xuming S, Jasmina V, et al. Blunting of Cardioprotective Actions of Estrogen in Female Rodent Heart Linked to Altered Expression of Cardiac Tissue Chymase and ACE2. *J Renin Angiotensin Aldosterone Syst* (2017) 18(3):1470320317722270. doi: 10.1177/1470320317722270
74. Rehman S, Majeed T, Azam Ansari M, Ali U, Sabit H, Al-Suhaimi EA. Current Scenario of COVID-19 in Pediatric Age Group and Physiology of Immune and Thymus Response. *Saudi J Biol Sci* (2020) 27(10):2567–73. doi: 10.1016/j.sjbs.2020.05.024
75. Aztatzi-Aguilar OG, Uribe-Ramírez M, Montaño JA, Barbier O, De Vizcaya-Ruiz A. Acute and Subchronic Exposure to Air Particulate Matter Induces Expression of Angiotensin and Bradykinin-Related Genes in the Lungs and Heart: Angiotensin-II Type-I Receptor as a Molecular Target of Particulate Matter Exposure. *Part Fibre Toxicol* (2015) 12:17. doi: 10.1186/s12989-015-0094-4
76. Patel SK, Velkoska K, Burrell LM. Emerging Markers in Cardiovascular Disease: Where Does Angiotensin-Converting Enzyme 2 Fit in? *Clin Exp Pharmacol Physiol* (2013) 40(8):551–9. doi: 10.1111/1440-1681.12069
77. Leong HN, Earnest A, Lim HH, Chin CF, Tan C, Puhaindran ME, et al. SARS in Singapore - Predictors of Disease Severity. *Ann Acad Med Singap* (2006) 35(5):326–31. doi: 10.1111/1440-1681.12069
78. Gagliardi MC, Tieri P, Ortona E, Ruggieri A. ACE2 Expression and Sex Disparity in COVID-19. *Cell Death Discov* (2020) 6:37. doi: 10.1038/s41420-020-0276-1
79. Groban L, Wang H, Sun X, Ahmad S, Ferrario CM. Is Sex a Determinant of COVID-19 Infection? Truth or Myth? *Curr Hypertens Rep* (2020) 22(9):62. doi: 10.1007/s11906-020-01073-x
80. Raoult D, Hsueh PR, Stefani S, Rolain JM. COVID-19 Therapeutic and Prevention. *Int J Antimicrob Agents* (2020) 55(4):105937. doi: 10.1016/j.ijantimicag.2020.105937
81. Maslowski KM, Charles RM. Diet, Gut Microbiota and Immune Responses. *Nat Immunol* (2011) 12(1):5–9. doi: 10.1038/ni0111-5
82. Thaiss CA, Zmora N, Levy M, Elinav E. The Microbiome and Innate Immunity. *Nature* (2016) 535(7610):65–74. doi: 10.1038/nature18847
83. Postler TS, Ghosh S. Understanding the Holobiont: How Microbial Metabolites Affect Human Health and Shape the Immune System. *Cell Metab* (2017) 26(1):110–30. doi: 10.1016/j.cmet.2017.05.008
84. Blander JM, Longman RS, Iliev ID, Sonnenberg GF, Artis D. Regulation of Inflammation by Microbiota Interactions With the Host. *Nat Immunol* (2017) 18:851–60. doi: 10.1038/ni.3780
85. Johnson BA, Hage A, Kalveram B, Mears M, Plante JA, Rodriguez SE, et al. Peptidoglycan-Associated Cyclic Lipopeptide Disrupts Viral Infectivity. *J Virol* (2019) 93(22):e01282. doi: 10.1128/JVI.01282-19
86. Donati Zeppa S, Agostini D, Piccoli G, Stocchi V, Sestili P. Gut Microbiota Status in COVID-19: An Unrecognized Player? *Front Cell Infect Microbiol* (2020) 10:576551. doi: 10.3389/fcimb.2020.576551
87. Belkaid Y, Harrison OJ. Homeostatic Immunity and the Microbiota. *Immunity* (2017) 18(46):562–76. doi: 10.1016/j.immuni.2017.04.008
88. Zhang D, Li S, Wang N, Tan HY, Zhang Z, Feng Y. The Cross-Talk Between Gut Microbiota and Lungs in Common Lung Diseases. *Front Microbiol* (2020) 11:301. doi: 10.3389/fmicb.2020.00301
89. Han Y, Jia Z, Shi J, Wang W, He K. The Active Lung Microbiota Landscape of COVID-19 Patients. *medRxiv* (2020) 11:20144014. doi: 10.1101/2020.08.20.20144014
90. Zhou F, Yu T, Du R, Fan G, Liu Y, Liu Z, et al. Clinical Course and Risk Factors for Mortality of Adult Inpatients With COVID-19 in Wuhan, China: A Retrospective Cohort Study. *Lancet* (2020) 395(10229):1054–62. doi: 10.1016/S0140-6736(20)30566-3
91. Zuo T, Zhang F, Lui GCY, Yeoh YK, Li AYL, Zhan H, et al. Alterations in Gut Microbiota of Patients With COVID-19 During Time of Hospitalization. *Gastroenterology* (2020) 159(3):944–55. doi: 10.1053/j.gastro.2020.05.048
92. Yurkovetskiy L, Burrows M, Khan AA, Graham L, Volchkov P, Becker B, et al. Gender Bias in Autoimmunity Is Influenced by Microbiota. *Immunity* (2013) 39:400–12. doi: 10.1016/j.immuni.2013.08.013
93. Dominianni C, Sinha R, Goedert JJ, Pei Z, Yang L, Hayes RB, et al. Sex, Body Mass Index, and Dietary Fiber Intake Influence the Human Gut Microbiome. *PloS One* (2015) 10:e0124599. doi: 10.1371/journal.pone.0124599
94. Org E, Mehrabian M, Parks BW, Shipkova P, Liu X, Drake TK, et al. Sex Differences and Hormonal Effects on Gut Microbiota Composition in Mice. *Gut Microbes* (2016) 7(4):313–22. doi: 10.1080/19490976.2016.1203502

95. Kim YS, Unno T, Kim BY, Park MS. Sex Differences in Gut Microbiota. *World J Mens Health* (2020) 38:48–60. doi: 10.5534/wjmh.190009
96. Santos-Marcos JA, Haro C, Vega-Rojas A, Alcala-Diaz JF, Molina-Abril H, Leon-Acuña A, et al. Sex Differences in the Gut Microbiota as Potential Determinants of Gender Predisposition to Disease. *Mol Nutr Food Res* (2019) 63(7):e1800870. doi: 10.1002/mnfr.201800870
97. Oakes JM, Fuchs RM, Gardner JD, Lazartigues E, Yue X. Nicotine and the Renin-Angiotensin System. *Am J Physiol Regul Integr Comp Physiol* (2018) 315:R895–906. doi: 10.1152/ajpregu.00099.2018
98. Yue X, Basting TM, Flanagan TW, Xu J, Lobell TD, Gilpin NW, et al. Nicotine Downregulates the Compensatory Angiotensin-Converting Enzyme 2/ Angiotensin Type 2 Receptor of the Renin-Angiotensin System. *Ann Am Thorac Soc* (2018) 15:S126–7. doi: 10.1513/AnnalsATS.201706-464MG
99. World Health Organization (WHO) and Global Adult Tobacco Survey (GATS). *Fact Sheet China 2018*. Annals of the American Thoracic Society (2018).
100. Klein SL. The Effects of Hormones on Sex Differences in Infection: From Genes to Behavior. *Neurosci Biobehav Rev* (2000) 24:627–38. doi: 10.1016/ S0149-7634(00)00027-0
101. Yang T, Barnett R, Jiang S, Yu L, Xian H, Ying J, et al. Gender Balance and Its Impact on Male and Female Smoking Rates in Chinese Cities. *Soc Sci Med* (2016) 154:9–17. doi: 10.1016/j.socscimed.2016.02.035
102. Leung JM, Yang CX, Tam A, Shaipanich T, Hackett TL, Singhera GK, et al. ACE-2 Expression in the Small Airway Epithelia of Smokers and COPD Patients: Implications for COVID-19. *Eur Respir J* (2020) 55:2000688. doi: 10.1183/13993003.00688-2020
103. Nasiri MJ, Haddadi S, Tahvildari A, Farsi Y, Arbabi M, Hasanzadeh S, et al. COVID-19 Clinical Characteristics, and Sex-Specific Risk of Mortality: Systematic Review and Meta-Analysis. *Front Med* (2020) 7:459. doi: 10.3389/fmed.2020.00459
104. Martin SA, Pence BD, Woods JA. Exercise and Respiratory Tract Viral Infections. *Exerc Sport Sci Rev* (2009) 37:157–64. doi: 10.1097/ JES.0b013e3181b7b57b
105. Brown AS, Davis JM, Murphy EA, Carmichael MD, Carson JA, Ghaffar A, et al. Gender Differences in Macrophage Antiviral Function Following Exercise Stress. *Med Sci Sports Exerc* (2006) 38:859–63. doi: 10.1249/ 01.mss.0000218125.21509.cc
106. Brown AS, . Davis MM, Murphy EA, Carmichael MD, Ghaffar A, Mayer EP. Gender Differences in Viral Infection After Repeated Exercise Stress. *Med Sci Sports Exerc* (2004) 36:1290–5. doi: 10.1249/01.MSS.0000135798.72735.B3
107. Kawai K, Msamanga G, Manji K, Villamor E, Bosch RJ, Hertzmark E, et al. Sex Differences in the Effects of Maternal Vitamin Supplements on Mortality and Morbidity Among Children Born to HIV-Infected Women in Tanzania. *Br J Nutr* (2010) 103:1784–91. doi: 10.1017/S0007114509993862
108. Prentice S. They Are What You Eat: Can Nutritional Factors During Gestation and Early Infancy Modulate the Neonatal Immune Response? *Front Immunol* (2017) 8:1641. doi: 10.3389/fimmu.2017.01641
109. Maggini S, Pierre A, Calder PC. Immune Function and Micronutrient Requirements Change Over the Life Course. *Nutrients* (2018) 10(10):1531. doi: 10.3390/nu10101531


**Conflict of Interest:** The authors declare that the research was conducted in the absence of any commercial or financial relationships that could be construed as a potential conflict of interest.

**Publisher's Note:** All claims expressed in this article are solely those of the authors and do not necessarily represent those of their affiliated organizations, or those of the publisher, the editors and the reviewers. Any product that may be evaluated in this article, or claim that may be made by its manufacturer, is not guaranteed or endorsed by the publisher.

frontiers | Frontiers in Immunology

ORIGINAL RESEARCH
published: 16 May 2022
doi: 10.3389/fimmu.2022.882867

# Sex-Biased Control of Inflammation and Metabolism by a Mitochondrial Nod-Like Receptor

*Tiia Snäkä[1], Amel Bekkar[1], Chantal Desponds[1], Florence Prével[1], Stéphanie Claudinot[1], Nathalie Isorce[1], Filipa Teixeira[1], Coline Grasset[1], Ioannis Xenarios[2,3], Isabel C. Lopez-Mejia[3], Lluis Fajas[3] and Nicolas Fasel[1]**

[1] Department of Biochemistry, University of Lausanne, Epalinges, Switzerland, [2] Agora Center, Center Hospitalier Universitaire (CHUV), Lausanne, Switzerland, [3] Center for Integrative Genomics, University of Lausanne, Lausanne, Switzerland

Mitochondria regulate steroid hormone synthesis, and in turn sex hormones regulate mitochondrial function for maintaining cellular homeostasis and controlling inflammation. This crosstalk can explain sex differences observed in several pathologies such as in metabolic or inflammatory disorders. Nod-like receptor X1 (NLRX1) is a mitochondria-associated innate receptor that could modulate metabolic functions and attenuates inflammatory responses. Here, we showed that in an infectious model with the human protozoan parasite, *Leishmania guyanensis*, NLRX1 attenuated inflammation in females but not in male mice. Analysis of infected female and male bone marrow derived macrophages showed both sex- and genotype-specific differences in both inflammatory and metabolic profiles with increased type I interferon production, mitochondrial respiration, and glycolytic rate in *Nlrx1*-deficient female BMDMs in comparison to wild-type cells, while no differences were observed between males. Transcriptomics of female and male BMDMs revealed an altered steroid hormone signaling in *Nlrx1*-deficient cells, and a "masculinization" of *Nlrx1*-deficient female BMDMs. Thus, our findings suggest that NLRX1 prevents uncontrolled inflammation and metabolism in females and therefore may contribute to the sex differences observed in infectious and inflammatory diseases.

**Keywords: inflammation, innate immunity, metabolism, sex, nod-like receptor X1**

OPEN ACCESS

***Edited by:***
*Thomas A. Kufer, University of Hohenheim, Germany*

***Reviewed by:***
*Damien Arnoult, INSERM U1197 Unité Mixte de Recherche Interactions Cellules Souches-Niches, France*
*Willie Brickey, University of North Carolina at Chapel Hill, United States*

***Correspondence:**
*Nicolas Fasel*
*Nicolas.Fasel@unil.ch*

***Specialty section:***
*This article was submitted to Molecular Innate Immunity, a section of the journal Frontiers in Immunology*

***Received:*** *24 February 2022*
***Accepted:*** *05 April 2022*
***Published:*** *16 May 2022*

***Citation:***
*Snäkä T, Bekkar A, Desponds C, Prével F, Claudinot S, Isorce N, Teixeira F, Grasset C, Xenarios I, Lopez-Mejia IC, Fajas L and Fasel N (2022) Sex-Biased Control of Inflammation and Metabolism by a Mitochondrial Nod-Like Receptor. Front. Immunol. 13:882867. doi: 10.3389/fimmu.2022.882867*

## INTRODUCTION

Different factors including XY-encoded genes and sex hormones contribute to sex-dependent variations in the incidence of different infectious and inflammatory diseases (1). Transcriptional analysis of unstimulated female and male immune cells has revealed sex-specific gene expression patterns, with differences mainly in type I interferon (IFN)-response genes that were enriched in females (2–4). In addition, immune cells express receptors for sex hormones: estrogens (17-β-estradiol), androgens (testosterone) and progesterone. These hormones are modulators of immune cells and contribute to differences in cell activation and functionality (5–7). Binding of estrogens to their nuclear receptors, estrogen receptor alpha and beta (ERα and ERβ, respectively) promotes or

dampens immune signaling in innate immune cells in a dose-dependent manner. While physiological levels of estrogens tend to promote type I IFN responses, higher doses are immunosuppressive (1, 5, 8). Moreover, estrogens play a key role in the resolution of inflammation and cutaneous repair by promoting anti-inflammatory macrophage activation (9–11).

To respond to infection and cellular damage, immune cells are able to adapt their functional profiles not only by activation of different transcriptional profiles but also by engaging specific metabolic pathways. Indeed, the regulation of energy metabolism is crucial for innate immune cell function and for example plays a major role in macrophage activation and polarization to either pro-inflammatory M1 or anti-inflammatory M2 macrophage subtypes allowing adaptation to different environments. While M1 macrophages are characterized by a high glycolytic rate and play a role in pathogen clearance, M2 macrophages rely on mitochondrial oxidative phosphorylation (OXPHOS) and promote tissue repair (12–14). Mitochondria are key organelles in energy metabolism and sex- and tissue-specific differences in mitochondrial function and morphology have been reported (15–17). Mitochondrial enzymes play a key role in sex hormone biosynthesis, and in turn sex hormones, mainly estrogens, regulate mitochondrial function and morphology *via* nuclear or mitochondrial ERs to promote mitochondrial metabolism (18, 19).

Nod-like receptor X1 (NLRX1) is a unique mitochondrial NOD-like receptor (NLR) implicated in the control of inflammation and metabolism in both infectious and inflammatory diseases. It was first described as a traditional RNA-binding pathogen recognition receptor (PRR) involved in mitochondrial antiviral immunity mainly by attenuating type I IFN or nuclear factor-κB (NF-κB) signaling (20–23). However, recent studies have shown that NLRX1 plays an important role in the control of inflammation in several models of cancer and tissue injury, independently of its role in pathogen recognition (24–27). In addition, due to its localization at the mitochondria, the central hub of metabolism and immunity, several studies suggest a role for NLRX1 in the maintenance of mitochondrial physiology, function, and reactive oxygen species (mtROS) production following infection or injury (28–31). Interestingly, sex differences in all these aspects have been described, however, no studies have reported a potential link to an NLR.

To investigate the role of NLRX1, we used an experimental murine model based on a protozoan parasite, *Leishmania guyanensis* (*Lgy*), inducing cutaneous lesions at the site of the infection. This causative agent of human cutaneous leishmaniasis can induce a more exacerbated hyperinflammatory form of the disease when carrying in its cytoplasm an endosymbiont virus, *Leishmania* RNA Virus 1 (LRV1) with a double-stranded viral RNA as genome (32–35). Upon phagocytosis of the parasite into macrophages, the viral double stranded RNA (dsRNA) is recognized by the macrophage endosomal Toll-like receptor 3 (TLR3) and induces a strong type I IFN mediated antiviral response and NF-κB mediated pro-inflammatory cytokines such as interleukin 6 (IL-6) and as tumor-necrosis factor α (TNFα) leading to an exacerbated disease outcome (36, 37). This experimental model allowed us to investigate not only the inflammatory response in *in vitro* infected macrophages but also the *in vivo* development of exacerbated lesions in mice. Here, we showed that NLRX1 controlled viral mediated inflammation and metabolism in a sex-dependent manner.

# MATERIALS AND METHODS

## Ethics Statement

All animal experimentation protocols described in this study were approved by the Swiss Federal Veterinary Office (SFVO), under authorization numbers VD2113.2 and VD3551. Animal handling and experimental procedures were undertaken with strict adherence to the ethical guidelines given by the SFVO and under inspection by the Department of Security and Environment of the State of Vaud, Switzerland.

## Mice

Wild-type (WT) (C57BL/6JOlaHsd) mice were purchased from Envigo (Netherlands) and *Nlrx1*-deficient mice (*Nlrx1*$^{-/-}$) (B6.129-Nlrx1tm1 Tsc) were generated previously by replacing the first four coding exons with a neomycin cassette, that was later removed (38). The mice were previously backcrossed onto the C57BL/6JOlaHsd background for at least 5 generations. Mice were genotyped by PCR using tissue-isolated genomic DNA using the KAPA Mouse Genotyping Kit (KAPA Biosystems). Mice were maintained at the animal facility of the Center for Immunity and Immunology Lausanne (CIIL) (Switzerland) in a pathogen-free environment. Males and females (6-9 weeks old) were used for experiments. *In vivo* experiments were performed at a biosafety level 2 (BSL-2) animal facility at the CIIL. Cages were enriched with one igloo, two carboard tubes, one wood stick, and tissues. Experiments were performed after one week of acclimation in the BSL-2 animal facility. Food (SAFE or KLIBA NAGAF) and water were provided ad libitum. Light cycle was maintained at 13 hours light and 11 hours darkness, temperature was set at 21°C ± 2 and humidity was kept at 55% ± 10. The oligonucleotides used for genotyping of *Nlrx1*-deficient mice were:

*Nlrx1* "WT For": 5'-TTA GAC TGG TGT TAC GGG AGA CTG-3'

*Nlrx1* "Common Rev": 5'-CCC AGG CAC TGT TGT CCT ACA-3'

*Nlrx1* "KO For": 5'-TAA GGG TTC GCG TAC GGT G-3'

## Strains

Two isogenic clones of *Leishmania guyanensis* (*Lgy*) were used. A LRV1-bearing (LRV1$^{+}$ *Lgy*M4147/SSU : IR2SAT-LUC(b)c3) and LRV1-cured (LRV1$^{-}$ *Lgy*M4147/SSU : IR2SAT-LUC(b)c3) *Lgy* (named *Lgy*LRV1+ and *Lgy*LRV1-, respectively) were obtained by drug treatment of LRV1+ strain of *Lgy* M4147 (MHOM/BR/75/M4147) containing a firefly luciferase (ffLUC) gene as described previously (39). *Lgy* parasites were cultured at 26°C in Schneider's Drosophila medium (Gibco) supplemented with 20% of Fetal Bovine Serum (FBS, Gibco), 1% penicillin/

streptomycin (BioConcept), 2% HEPES buffer (BioConcept) and 0.6 µg/ml 6-Biopterin (Sigma-Aldrich) and 0.2% Hemin folate (Sigma-Aldrich, Fluka). For infection, parasites were cultured for 6 days to obtain stationary phase infectious metacyclic promastigotes.

## Bone Marrow Derived Macrophage (BMDM) Culture, Infection and Stimulation

BMDMs were isolated from tibias and femurs of non-infected female and male WT and *Nlrx1*$^{-/-}$ mice. Macrophages were cultured at 37°C and 5% $CO_2$ in complete Dulbecco's modified Eagle Medium (DMEM) supplemented with 10% FBS, 1% penicillin/streptomycin, 1% HEPES buffer and 50 ng/ml of murine recombinant mouse macrophage colony stimulating factor (rmM-CSF, Immunotools) for 6 days. At day 3, fresh complete DMEM supplemented with rm-MCSF was added. At day 6, adherent BMDMs were isolated and plated at a concentration of 1.25 x $10^6$ cells/ml one day prior of infection. BMDMs were infected at 35°C and 5% $CO_2$ with stationary phase parasites with a multiplicity of infection (MOI) of 5 parasites per macrophage or stimulated with 2 µg/ml of polyinosinic-polycytidylic acid (poly I:C) (Immunotools).

## Mice Infection and Quantification of Inflammation and Parasite Burden by Bioluminescence

Age-matched (6-9 weeks old) female or male mice were injected in the hind footpads with 3 x $10^6$ stationary phase *Lgy* promastigotes in 50 µl of Dulbecco's Phosphate-Buffered Saline (dPBS, Gibco). To follow disease progression, footpad swelling was measured weekly using a Vernier caliper. When required, to quantify inflammation and parasite burden, mice were injected intraperitoneally (i.p.) with 200 mg/kg of Luminol sodium salt (Carbosynth) or 150 mg/kg of VivoGlo Luciferin (Promega) diluted in dPBS, respectively. Bioluminescence from mouse footpads was measured by *In-vivo* Xtreme II (BRUKER) and quantified using Molecular Imaging (MI) software (BRUKER) as described previously (40).

## Histology and Immunohistochemistry (IHC)

Footpads were collected and fixed overnight at 4°C with 4% paraformaldehyde (PFA, Fluka). Following fixation, tissue samples were dehydrated and included in paraffin. 3.5 µm paraffin sections were generated using a Microm HM355 microtome (Thermo Scientific) and stained with hematoxylin (J.T Baker) and eosin (Merck) stain. Sections were visualized using a NanoZoomer S60 (Hamamatsu Photonics K.K.) scanner with Nikon Plan Apochromat 40x objective using brightfield contrast and analyzed using NPD.scan3.3 (Hamamatsu Photonics K.K.). Representative images of the sections are shown.

## RNA Extraction From Footpads and qRT-PCR

Footpads from infected WT or *Nlrx1*$^{-/-}$ mice were collected and snap-frozen in liquid nitrogen and kept at -80°C for storage. For RNA extraction, tissues were lysed in TRI Reagent (Molecular Research Center, inc) using a TissueLyser system (Qiagen). RNA was isolated by chloroform/isopropanol/ethanol phase separation protocol as described previously (41). RNA was quantified using NanoDrop 2000 (ThermoFisher Scientific) and 2000 ng/µl of RNA was used for cDNA synthesis. Alternatively, BMDMs were lysed with PRImeZOL Reagent (Canvax) and RNA was isolated using Direct-zol-96 RNA (Zymo Research) according to the manufacturer's instructions. cDNA was synthesized using SuperScript II Reverse Transcriptase (Invitrogen). Real-time quantitative PCR (qRT-PCR) was performed using the LightCycler 480 (Roche). The results were analyzed using the threshold cycle ($C_T$) method ($2^{-\Delta\Delta Ct}$) for relative quantification of gene expression and normalized to *L32* housekeeping gene encoding for 60S ribosomal protein. The oligonucleotides used were:

*L32:* 5′-AAG CGA AAC TGG CGG AAA C-3' and 5′-TAA CCG ATG TTG GGC ATC AG-3'

*Il6*: 5'-TCC AGT TGC CTT CTT GGG AC-3' and 5'-GTC TAA TTA AGC CTC CGA CT-3'

*Tnfa:* 5'-CAT CTT CTC AAA ATT CGA GTG ACA A-3' and 5'- TGG GAG TAG ACA AGG TAC AAC CC-3'

*Ifnb:* 5'-AAC CTC ACC TAC AGG GC-3' and 5′-CAT TCT GGA GCA TCT CTT GG-3'

*Nlrx1:* 5'-CAT GGA AAC TCG GCA GAC AG-3' and 5'-GGC TAA ACC ACT CGG TGA GG-3'

## Western Blot Analysis

BMDMs were lysed with 1.5x Laemmli's Sample Buffer in $H_2O$ and incubated at 95°C for 3 min. Cell lysates were size-fractioned by 8% SDS-PAGE and wet-transferred to a nitrocellulose membrane. Membranes were blocked with 5% non-fat dry milk in Tris buffered saline with 0.1% Tween-20 (TBST) at room temperature. Western blotting was performed using the following antibodies: anti-NLRX1 (1/1000, Proteintech, 17215-1-AP), anti-y-TUBULIN (1/10 000, Sigma-Aldrich, T5326), goat anti-rabbit IgG (H+L) HRP (1/2500, Promega, W4011) and goat anti-mouse IgG (H+L) HRP (1/2500, Promega, W4021). ECL Western Blotting detection reagent (GE Healthcare Life Sciences) was used for revelation.

## Enzyme-Linked Immuno-Sorbent Assay (ELISA)

The concentrations of IFNβ (Thermo Fisher, 424001), IL-6 (Invitrogen, 88-7064-88) and TNF-α (Invitrogen, 88-7324-88) in collected cell-free supernatants at 24 hours from infected or stimulated BMDMs were determined by ELISA following the manufacturer's instructions. Optical density was read on a Synergy HT Multi-Mode Plate Reader (BioTek Instruments) at 450/570 nm.

## High Throughput Microscopy

BMDMs were seeded in µ-Plate 96 Well Black (Ibidi) at a concentration of 1.25 x $10^6$ cells/ml. Cells were infected or stimulated for 8 and 24 hours and fixed with 4% PFA (Fluka). Cells were subsequently stained with 4′,6-diamidino-2-

phenylindole (DAPI) (Molecular Probes) and Alexa Fluor 488 phalloidin (Molecular probes) to stain the nuclei and cytoplasm, respectively. Images were acquired using ImageXpress Micro Confocal (Molecular Devices) with a 40x objective. Parasite and cell number per well were quantified using MetaExpress custom Module Editor (Molecular Devices) as described previously (42).

## RNA Sequencing of BMDMs and Bioinformatics Analysis

BMDMs from age-matched WT and *Nlrx1*$^{-/-}$ mice were infected with *Lgy* parasites or stimulated with poly I:C for 8 and 24 hours. RNA was extracted using a RNeasy Kit (Qiagen) following manufacturer's instructions. RNA quality and concentrations were determined by Fragment Analyzer and Ribogreen QubIT quantification, respectively, and libraries for sequencing were then prepared at the Lausanne Genomic Technologies Facility (GTF). Statistical analysis was performed for genes independently in R (R version 4.0.3). Genes with low counts were filtered out according to the rule of 1 count(s) per million (cpm) in at least 1 sample. Differential expression was computed with limma by fitting data to a linear model (43). Weighted gene co-expression network analysis (WGCNA) was performed on normalized data in R (package WGCNA 1.69). Modules were identified by dynamic tree cut with a minimum module size=20. Module eigengenes (MEs) that are the first principal component of the module were calculated and relationship of module eigengenes with infection status was assessed with a regression analysis. Module eigengenes average predictions were plotted as a heatmap. Gene Ontology (GO) enrichment analysis was performed for gene co-expression modules against GO categories using the topGO R package (topGO 2.26.0) and gene ontology database (07.2019). Only biological processes (BP) were considered for the analysis. For all modules, genes were ranked according to their connectivity within a single module as measured by the kwithin-index.

## Metabolism Assessment by Seahorse Analyzer

Metabolism measurement was performed with a Seahorse XFe96 Extracellular Flux Analyzer (Agilent). BMDMs were plated in a Seahorse XF96 cell culture microplate (Agilent) overnight. Cells were then infected with *Lgy* parasites for 8 hours and then pre-incubated in assay medium (Seahorse XF DMEM pH 7.4, Agilent) supplemented with 2 mM L-glutamine (Gibco), 1 mM pyruvate (Gibco) and 25 mM glucose (Gibco) for 1h at 37°C without $CO_2$. To measure mitochondrial metabolism and glycolysis, a Mito Stress Test and a Glycolytic Rate Assay were performed, respectively, according to manufacturer's instructions. Cells were treated with 1 µM Oligomycin (Sigma), 2 µM FCCP (Sigma), 0.5 µM/0.5 µM Rotenone/Antimycin A (Sigma) and 50 mM 2-deoxy-D-glucose (Sigma). Results were analyzed using Wave Desktop software (Agilent) and data was normalized to total protein concentration per well. Briefly, post-assay, cells were lysed with a mixture of RIPA Buffer IV (Biotech) and a complete protease inhibitor cocktail tablet (Roche) in $H_2O$. Protein concentration was quantified using Pierce BCA Protein Assay Kit (Thermo Fisher Scientific) following manufacturer's instructions. To assess the effect of estradiol, cells were pre-treated with 200 pg/ml of 17-β estradiol (Sigma) for 2 hours and estradiol was kept in the assay medium for the duration of the assay.

## Measurement of ROS Production

Intracellular and mitochondrial ROS production were measured by the superoxide indicator dihydroethidium (DHE) (Thermo Fisher Scientific) and the mitochondrial superoxide indicator MitoSOX Red (Thermo Fisher Scientific). Briefly, cells were infected with *Lgy* parasites or treated with poly I:C for 8 hours, after which cells were labelled with 5µM DHE or 5 µM MitoSOX Red in PBS with 5 mM glucose (Gibco) for 20 min at 37°C. After incubation, cells were washed, and fluorescence was measured at 518/606 nm (MitoSOX Red) and 510/590 nm (DHE) using the Spectramax i3 plate reader (Molecular Devices). Measures were normalized to total protein concentration per well using Pierce BCA Protein Assay Kit (Thermo Fisher Scientific) following manufacturer's instructions.

## Electron Microscopy Analysis of Mitochondria

After 8 hours of infection, cells were fixed in 2.5% glutaraldehyde solution (Fluka) in PBS for 1 hour at room temperature (RT), then postfixed with a mixture of 1% osmium tetroxide (EMS) and 1.5% of potassium ferrocyanide (Sigma) in PBS for 1 hour at RT. Samples were washed in distilled water, spin down in low melting 2% agarose (Sigma) in $H_2O$ (Sigma), let to solidify on ice, cut in 1 $mm^3$ cube and dehydrated in acetone solution (Sigma) at graded concentrations (30%, 40 min; 50%, 40 min; 70%, 40 min; 100%, 2x1 hour). This was followed by infiltration in Epon (Sigma) at graded concentrations (Epon 1/3 acetone, 2 hours; Epon 3/1 acetone, 2 hours; Epon 1/1, 4 hours; Epon 1/1, 12 hours) and finally polymerized for 48 hours at 60°C. Ultrathin sections of 50 nm were cut on a Leica Ultracut (Leica Mikrosysteme GmbH) and picked up on a copper slot grid 2x1 mm (EMS) coated with a polystyrene film (Sigma). Sections were poststained with 2% uranyl acetate (Sigma) in $H_2O$ for 10 minutes, rinsed several times with $H_2O$ followed by Reynold's lead citrate in $H_2O$ (Sigma) for 10 minutes and rinsed several times with $H_2O$. Singles micrographs were taken with a transmission electron microscope Philips CM100 (Thermo Fisher Scientific) at an acceleration voltage of 80kV with a TVIPS TemCam-F416 digital camera (TVIPS GmbH). To determine the percentage of mitochondria volume per cell volume, a grid (500 nm spacing) was applied on each micrograph and each intersection was defined as being part of the mitochondria, nucleus, or cytoplasm. The stereology analysis was performed using 3dmod and its stereology plugin (44).

## Statistical Analysis

All graphs and statistical tests were generated in GraphPad Prism [version 9.3.1 (350)]. Either unpaired Student's t-test or two-way ANOVA with multiple comparisons was used for bar graphs,

while repeated-measure two-way ANOVA with Bonferroni's post-test correction was used for x/y curves. Significance was reached with p values ≤ 0.05. p values are shown as * for $p < 0.05$, ** for $p < 0.01$, *** for $p < 0.001$ and **** for $p < 0.0001$.

# RESULTS

## Loss of NLRX1 Exacerbated Inflammation and Tissue Damage Following *Lgy*LRV1+ Infection of Female Mice

To investigate whether NLRX1 modulated the pathogenicity of *Lgy* and affected disease progression, we first infected female C57BL/6 wild-type (WT) or NLRX1-deficient (*Nlrx1*$^{-/-}$) mice with *Lgy* parasites containing the dsRNA LRV1 virus (*Lgy*LRV1 +) and monitored lesion development weekly. In comparison to WT female mice, *Nlrx1*$^{-/-}$ infected female mice showed significantly increased footpad swelling (**Figure 1A**) and signs of inflammation as measured by *in vivo* bioluminescence imaging following luminol injection (**Figure 1B**). However, no significant differences were observed in parasite load as measured by bioluminescence of luciferase expressing parasites (**Figure 1C**). Thus, in female mice, NLRX1 seemed to attenuate LRV1 mediated inflammation independently of the parasite load.

To further confirm the role of NLRX1 in regulation of inflammation, we collected non-infected and infected footpads at the peak of infection. We did not observe any differences or abnormalities in skin structure of non-infected *Nlrx1*-deficient mice compared to WT (**Figure 1D**, upper panel). However, correlating to the lesion severity, we observed an important increase in thickness and in immune cell infiltration in the dermis ("D") of *Lgy*LRV1+ infected *Nlrx1*$^{-/-}$ mice (**Figure 1D**, bottom panel) compared to WT mice. In addition, we observed that at the peak of infection pro-inflammatory markers *Ifnb* and

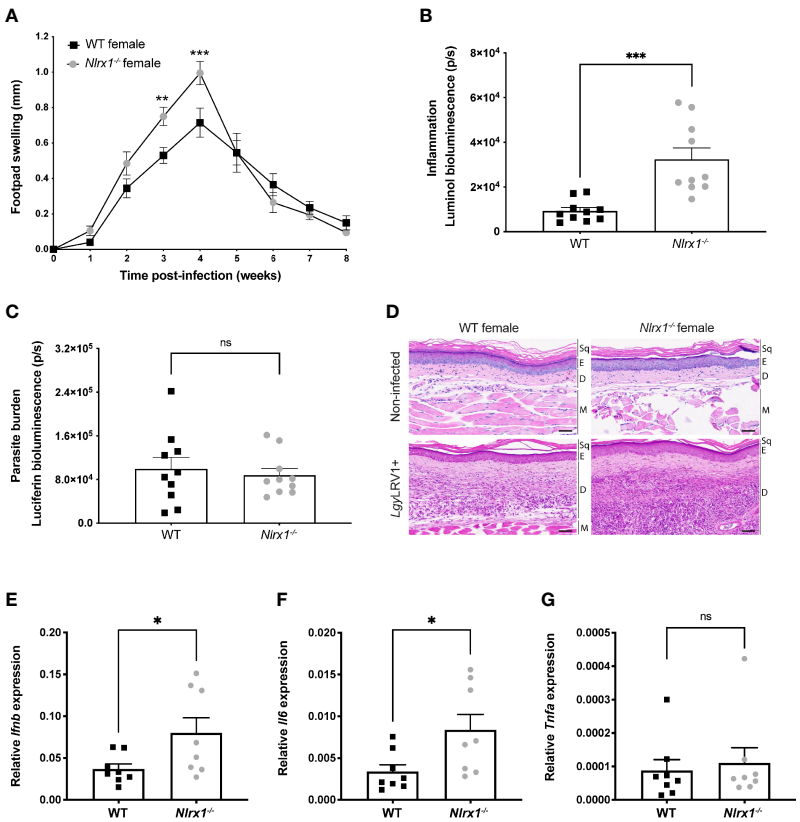


**FIGURE 1** | NLRX1 attenuated inflammation and tissue damage in infected female mice. Wild-type (WT) and *Nlrx1*-deficient (*Nlrx1*$^{-/-}$) C57BL/6 female mice (n=5 mice per group) were infected in both hind footpads with $3x10^6$ stationary phase *Lgy*LRV1+ parasites containing a luciferase gene. **(A)** Footpad swelling was measured weekly as a proxy of disease progression. At the peak of infection [4 weeks post-infection (p.i.)] **(B)** *in vivo* inflammation and **(C)** parasite burden was visualized and quantified by bioluminescence imaging after luminol and luciferin injection, respectively. Graphs are presented as mean +- SEM and are representative of three independent experiments. **(D)** Representative images of hematoxylin and eosin (H&E) staining of footpad sections. Upper panel show normal histological appearance of the epidermis and dermis of female WT and *Nlrx1*$^{-/-}$ mouse footpads. Bottom panel: lesions from hind footpads of *Lgy*LRV1+ infected female mice were dissected at 4 weeks p.i. and cell recruitment to lesion site was visualized. Magnification: 40x, scale bar: 50 µm. Sq, squames. E, epidermis. D, dermis. M, muscle. (n=5 mice per group). Relative mRNA levels of pro-inflammatory genes **(E)** *Ifnb*, **(F)** *Il6* and **(G)** *Tnfa* were quantified in the lesions of infected WT and *Nlrx1*$^{-/-}$ female mice at 4 weeks p.i. using RT-qPCR. Graphs are presented as mean +- SEM (n=8 mice per group). Statistical significance was assessed by two-way ANOVA with multiple comparisons **(A)** or unpaired, parametric t-test (B-C, E-G). ns = non-significant, *p ≤ 0.05 **p ≤ 0.01, ***p ≤ 0.001.

*Il6* (**Figures 1E, F**) were significantly upregulated in lesions of *Nlrx1*$^{-/-}$ mice infected with *Lgy*LRV1+ parasites, while no differences were observed in *Tnfa* expression as measured by qRT-PCR (**Figure 1G**). Thus, taken together these results supported a role for NLRX1 in controlling inflammation by limiting immune cell infiltration and tissue damage as well as type I IFN and IL-6 expression in lesions of female mice, while not affecting TNFα expression known to be responsible for parasite killing (36).

## *In Vitro* Analysis of Female BMDMs Suggested a Role for NLRX1 in the Regulation of Inflammation, Infection, Metabolism, and Sex Hormone Signaling

Several studies have reported a downregulation of NLRX1 in different experimental models such as viral and bacterial infections and brain injury (27, 45, 46). Therefore, we investigated whether infection with *Lgy* regulated *Nlrx1* expression. Thus, we infected bone marrow derived macrophages (BMDMs) isolated from WT female mice with *Lgy*LRV1+ parasites or stimulated them with polyinosinic-polycytidylic acid (poly I:C), a known synthetic dsRNA agonist of TLR3. We observed a downregulation of *Nlrx1* mRNA in both infected and poly I:C treated BMDMs at 8 hours post-infection (p.i.) when infection is established, however with a fold-change inferior to 2 (**Figure 2A**). This downregulation was no longer observed at 24 hours p.i. (**Supplementary Figure S1A**). Similarly, we did not observe any significant changes in NLRX1 protein levels at 8 or 24 hours p.i. (**Supplementary Figure S1B**), suggesting a transcriptional regulation of NLRX1 only in the early phase of infection with *Lgy*LRV1+ parasites or after poly I:C treatment.

To further characterize the increased tissue damage and inflammation observed in *Nlrx1*$^{-/-}$ female mice, we next sought to determine any possible effect of NLRX1-deficiency on inflammation and *Lgy* infection in *in vitro* infected BMDMs. Thus, we infected WT and *Nlrx1*$^{-/-}$ female BMDMs with *Lgy*LRV1+ or stimulated them with poly I:C and measured pro-inflammatory cytokines in the cell-free supernatant at 24 hours post-infection. As expected, no cytokines were detected in non-infected cells. In contrast, NLRX1-deficiency resulted in a significantly increased production of IFNβ in *Lgy*LRV1+ infected or poly I:C treated cells (**Figure 2B**). We did not observe any differences in IL-6 or TNFα production (**Figures 2C, D**) suggesting that IFNβ was produced by infected macrophages whereas, upon tissue damage, *Il6* up-regulation measured in lesions was likely produced by other sources such as keratinocytes, dendritic cells and fibroblasts (47).

In infectious models, loss of NLRX1 has been reported to promote either pathogen survival or clearance depending on the model (46, 48–52). To investigate whether NLRX1 affected the number of parasites per BMDM, we infected WT and *Nlrx1*-/- female BMDMs with *Lgy*LRV1+ parasites for 8 and 24 hours. We did not observe differences in parasite burden in the establishment of infection (8 hours p.i.) (**Supplementary Figure S1C**) suggesting that NLRX1 did not affect the phagocytic capacity of BMDMs. In contrast, at 24 hours post infection, the absence of NLRX1 resulted in a decreased number of parasites per cell (**Figure 2E**). This decrease was associated to an increased macrophage survival in absence of NLRX1 that was observed only at 24 hours p.i. (**Supplementary Figures S1D, E**) (27, 53). However, as shown in **Figures 1A, C**, despite an increased macrophage survival with a lower number of parasites per cell *in vitro, in vivo Nlrx1*-deficient female mice developed larger lesions independently of the parasite load.

To better define the role of this mitochondrial sensor in macrophages isolated from female mice, we performed a transcriptomics analysis of WT and *Nlrx1*$^{-/-}$ female BMDMs infected with *Lgy*LRV1+ parasites or stimulated with poly I:C for 8 or 24 hours. We then performed a global weighted correlation network analysis (WGCNA) to group genes with similar expression patterns into modules. WGCNA has been used previously to identify key biological processes and gene modules associated with the studied disease (54–57). The underlying hypothesis is that genes involved in the same function or pathway or that are co-regulated are expected to be in the same module named by a color. Genes that do not group to any module form the "grey" module and are discarded from the analysis. The association of the WGCNA modules with the different conditions is represented as heatmaps at 8 and 24 hours (**Figure 2F**, **Supplementary Figure S1F**). The genes in each module are listed in **Supplementary Tables 1, 2**. We performed a gene ontology (GO) enrichment analysis for each module to identify the biological processes associated to each module. For each module GO terms are listed in **Supplementary Tables 3 and 4**. Based on the GO analysis, we could group most of the modules into 2 main categories of GO terms (1): inflammation and infection and (2) mitochondria and metabolism (**Supplementary Figure S1G**). These categories were based on a selection of several keywords such as "interleukin" or "biosynthesis", respectively. Identification of such biological processes was not surprising because of the choice of an infectious model and a knock-out gene for a mitochondrial receptor described to play a role in both categories. In contrast, both at 8 and 24 hours p.i., more than a third of the modules (34.8% and 45.5%, respectively) were enriched in GO terms associated to sex hormone signaling (**Figure 2F**, **Supplementary Figures S1F, G**) such as "regulation of androgen receptor signaling pathway" (GO:0060765) or "cellular response to estrogen stimulus" (GO:0071391). These GO terms were rather unexpected and suggested a potential sex-bias in the NLRX1 phenotype.

## In Male Mice Loss of NLRX1 Did Not Affect Lesion Severity

Although no association between NLRX1 and sex hormone signaling has been described to our knowledge, many studies have shown that sex hormones may play a role in the regulation of innate immune cell activation, inflammation, and mitochondrial function (1, 58). Based on the transcriptomics analysis of female BMDMs, we decided to investigate whether the *Nlrx1*$^{-/-}$ phenotype was dependent on sex. Thus, we infected male

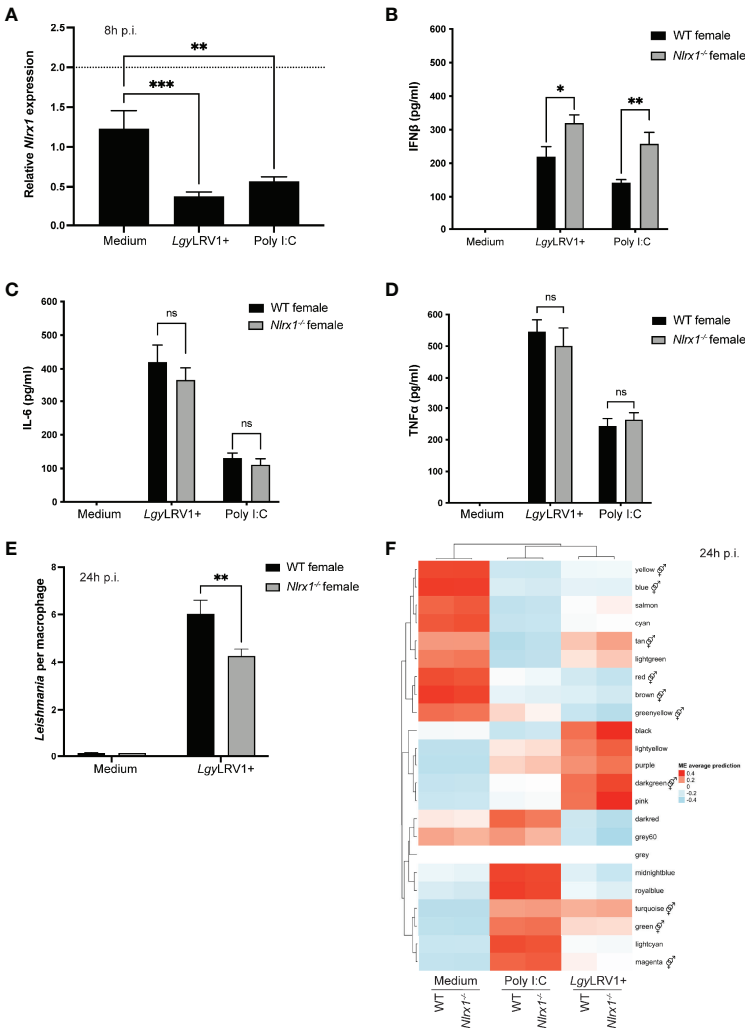


**FIGURE 2** | Inflammatory profile and transcriptomics analysis of female BMDMs. Bone marrow derived macrophages (BMDMs) from WT and *Nlrx1*$^{-/-}$ female mice were isolated and infected with stationary phase *Lgy*LRV1+ parasites or stimulated with the TLR3 agonist poly I:C (2 µg/ml). *Nlrx1* mRNA levels were quantified by qRT-PCR **(A)** at 8 hours p.i. (n=3 independent experiments). **(B–D)** After 24 hours, supernatants were collected and IFNβ, IL-6 and TNFα secretion was quantified by ELISA in *Lgy*LRV1+ or poly I:C stimulated BMDMs. (n=3 independent experiments). **(E)** At 24 hours p.i., BMDMs were fixed with 4% PFA and stained with DAPI and phalloidin. Cells were visualized with a high content microscope (40x) and intracellular parasite load was quantified using a MetaXpress software (n=2 independent experiments). **(F)** Transcriptomics analysis of WT and *Nlrx1*$^{-/-}$ female BMDMs (n=3 mice per group) infected with *Lgy*LRV1+ parasites or stimulated with poly I:C (2 µg/ml) for 24 hours. The heatmap represents the global weighted correlation network analysis (WGCNA) and module names are represented by a color. A gene ontology (GO) enrichment analysis for each module was performed to identify the biological processes associated to each module. ♂ represents modules enriched in GO terms associated with sex hormone signaling. Graphs are presented as mean +- SEM and significance was tested by two-way ANOVA with multiple comparisons (A-F). ns = non-significant, *p ≤ 0.05, **p ≤ 0.01, ***p ≤ 0.001.

C57BL/6 WT or *Nlrx1*$^{-/-}$ mice with *Lgy*LRV1+ parasites. In contrast to female mice, we found no significant differences in the development of lesions (**Figure 3A**). Moreover, at the peak of infection, male mice did not display any differences in inflammation as measured by *in vivo* bioluminescence imaging (**Figure 3B**). However, we observed a reduced parasite burden in *Nlrx1*$^{-/-}$- mice in comparison to WT (**Figure 3C**) that we did not observe in female mice (**Figure 1C**). Consistent with the absence of difference in inflammation and contrary to female mice, we observed no significant differences in skin structure, dermal thickness or immune cell infiltration between non-infected (**Figure 3D**, upper panel) or *Lgy*LRV1+ infected male mice (**Figure 3D**, bottom panel). Finally, we observed a significant reduction in *Ifnb* mRNA levels in the lesions of *Nlrx1*$^{-/-}$ male mice infected with *Lgy*LRV1+ (**Figure 3E**) in comparison to WT, but no differences in *Il6* or *Tnfa* mRNA levels as measured by qRT-PCR (**Figures 3F, G**). Taken together, NLRX1 did not modulate lesion development or inflammation in male mice contrarily to results obtained with female mice suggesting a strong sex bias in the function of NLRX1.

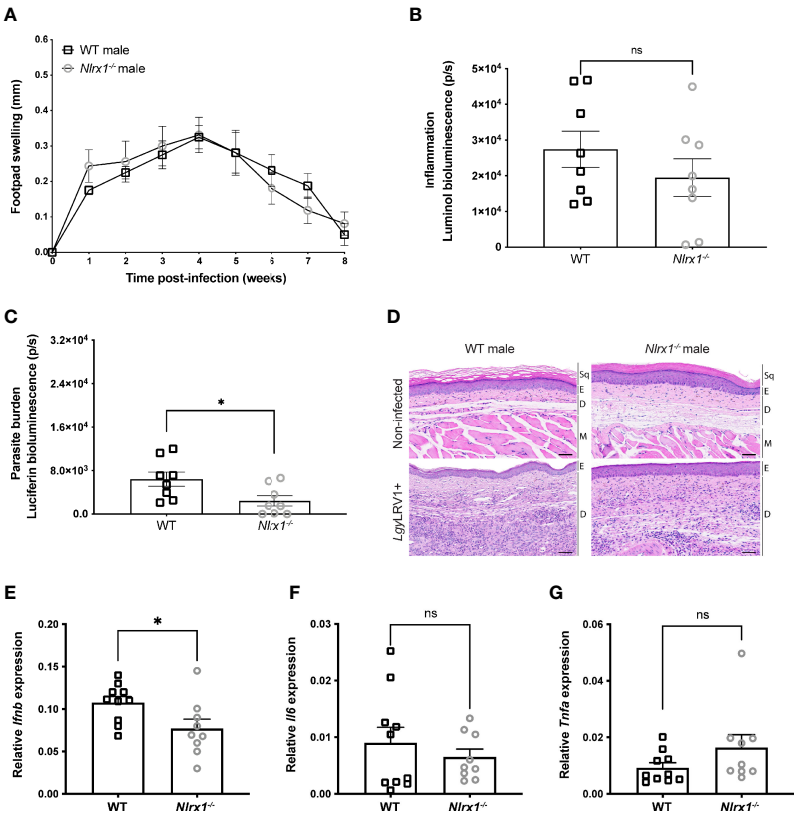


**FIGURE 3** | In male mice NLRX1 did not regulate inflammation or tissue damage. Wild-type (WT) and *Nlrx1*-deficient (*Nlrx1*$^{-/-}$) C57BL/6 male mice (n=4 mice per group) were infected in both hind footpads with 3x10$^6$ stationary phase *Lgy*LRV1+ parasites **(A)** Footpad swelling was measured weekly as a proxy of disease progression. At the peak of infection (4 weeks p.i.), **(B)** *in vivo* inflammation and **(C)** parasite burden was visualized and quantified by bioluminescence imaging after luminol and luciferin injection, respectively. Graphs are presented as mean +- SEM and are representative of three independent experiments. **(D)** Representative images of hematoxylin and eosin (H&E) staining of footpad sections. Upper panel show normal histological appearance of the epidermis and dermis of male mouse footpads. Bottom panel: lesions from hind footpads of *Lgy*LRV1+ infected male mice were dissected at 4 weeks p.i. and cell recruitment to lesion site was visualized. Magnification: 40x, scale bar: 50 µm. Sq, squames. E, epidermis. D, dermis. M, muscle. (n=5 mice per group). Relative mRNA levels of pro-inflammatory genes **(E)** *Ifnb*, **(F)** *Il6* and **(G)** *Tnfa* were quantified in the lesions of infected WT and *Nlrx1*$^{-/-}$ male mice at 4 weeks p.i. using RT-qPCR. Graphs are presented as mean +- SEM. (n=9-10 mice per group). Statistical significance was assessed by two-way ANOVA with multiple comparisons **(A)** or unpaired, parametric t-test **(B, C, E–G)**. ns = non-significant, *p ≤ 0.05.

## Female and Male BMDMs Showed Differences in Inflammation and Infectivity in Absence of NLRX1

To better understand the sex-bias in NLRX1 function, we decided to investigate whether isolated macrophages also displayed a sex-dependent phenotype. First, we infected both female and male WT BMDMs with *Lgy* parasites or stimulated them with poly I:C for 8 and 24 hours to analyze whether NLRX1 expression was affected by sex. At 8 or 24 hours p.i., we did not observe any significant differences in *Nlrx1* mRNA (**Figures 4A, B**) and protein levels (**Supplementary Figure S2A**) between females and males, suggesting that biological sex did not directly affect NLRX1 expression in BMDMs. Based on the *in vivo* data, the role of NLRX1 in the regulation of inflammation and infection was highly dependent on sex. Thus, we measured IFNβ, IL-6 and TNFα cytokine production at 24 hours post-infection in both female and male WT and *Nlrx1*$^{-/-}$ BMDMs infected with *Lgy*LRV1+ parasites or stimulated with poly I:C. No cytokines were detected in non-infected cells. Consistent with the lesions, increased IFNβ production (**Figure 4C**; **Supplementary Figure S3A**) was specific to female *Nlrx1*$^{-/-}$ BMDMs infected with *Lgy*LRV1+ or treated with poly I:C, whereas we did not observe any differences between male BMDMs. Interestingly, the Nlrx1$^{-/-}$ female BMDMs showed a similar IFNβ production compared to males. Surprisingly and in contrast to the lesions, NLRX1-deficiency resulted in a significantly increased production of both IL-6 and TNFα levels (**Figures 4D, E**; **Supplementary Figures S2B, S3B, C**) in *Nlrx1*$^{-/-}$ male BMDMs in comparison to WT male BMDMs.

Since we observed differences in cytokine profiles of female and male BMDMs, we investigated whether also parasite burden in BMDMs was affected by sex. As previously, we infected WT and *Nlrx1*$^{-/-}$ female and male BMDMs with *Lgy*LRV1+ parasites for 8 and 24 hours. At 8 hours p.i. female and male BMDMs showed similar parasite burdens independently of the genotype

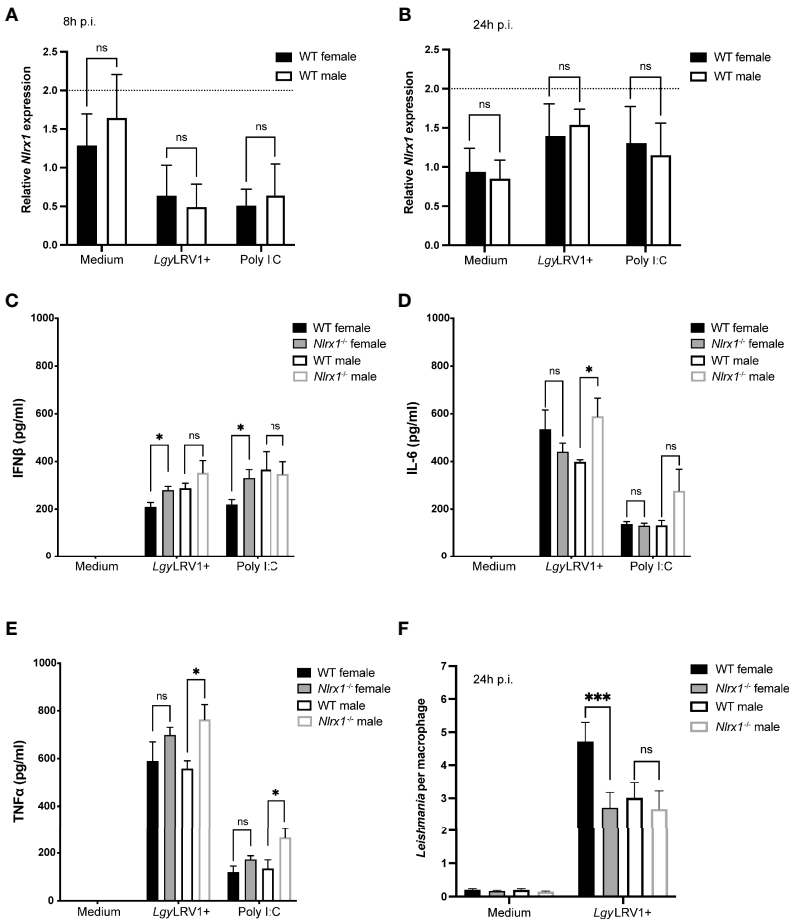


**FIGURE 4** | Sex bias in inflammation and infection in absence of NLRX1. BMDMs from female and male WT and *Nlrx1*$^{-/-}$ mice were isolated simultaneously and infected with *Lgy*LRV1+ parasites or stimulated with TLR3 agonist poly I:C (2 μg/ml). After 8 hours **(A)** and 24 hours p.i. **(B)**, *Nlrx1* mRNA levels were quantified by qRT-PCR (n=3 independent experiments). **(C–E)** After 24 hours, proinflammatory cytokines IFNβ, IL-6 and TNFα were quantified in cell-free supernatants by ELISA in *Lgy*LRV1+ infected or poly I:C stimulated BMDMs. (n=3-4 independent experiments). **(F)** At 24 hours p.i., BMDMs were fixed with 4% PFA and stained with DAPI and phalloidin. Cells were visualized with a high content microscope (40x) and intracellular parasite load was quantified using a MetaXpress software. (n=3 independent experiments). Graphs are presented as mean +- SEM and significance was tested by two-way ANOVA with multiple comparisons **(A–F)**. ns = non-significant, *p ≤ 0.05, ***p ≤ 0.001.

(**Supplementary Figure S2C**). However, at 24 hours p.i. WT female BMDMs maintained a higher parasite burden, whereas female *Nlrx1*$^{-/-}$ BMDMs and both male BMDMs showed a significantly reduced and similar parasite burden (**Figure 4F**; **Supplementary Figure S3D**). Although we did not observe statistically significant differences in macrophage survival, at 24 hours but not at 8 hours p.i., both male BMDMs and *Nlrx1*-deficient female BMDMs seemed to survive better in comparison to WT female cells correlating to the lower parasite burden observed in these cells (**Figure S2D, E**). Taken together, these results supported a strong association between sex and NLRX1 function.

## Both Sex and Genotype Affected Metabolic Profiles and Mitochondria of BMDMs

NLRX1 was shown to play a role in the regulation of both OXPHOS and glycolysis, the two major metabolic pathways for energy production (31, 59). In addition, based on the transcriptomics analysis of female BMDMs, NLRX1 seemed to have a strong effect on cellular metabolism and mitochondrial function. Thus, we sought to investigate whether the loss of NLRX1 resulted in a change in OXPHOS or glycolysis, the two major energetic pathways of the cell. To examine if NLRX1 affected OXPHOS, we determined the oxygen consumption rate (OCR) in both female and male WT and *Nlrx1*$^{-/-}$ BMDMs infected with *Lgy*LRV1+ parasites for 8 hours. In non-infected BMDMs, we observed very low OCR levels and no differences between groups, suggesting a low metabolic activity in unstimulated cells after 8 hours (**Figure 5A**). Moreover, NLRX1-deficient female BMDMs infected with *Lgy*LRV1+ showed a significantly increased basal mitochondrial respiration compared to WT female, but that was comparable to basal respiration of male BMDMs. In contrast we did not observe differences in basal respiration between WT and *Nlrx1*-

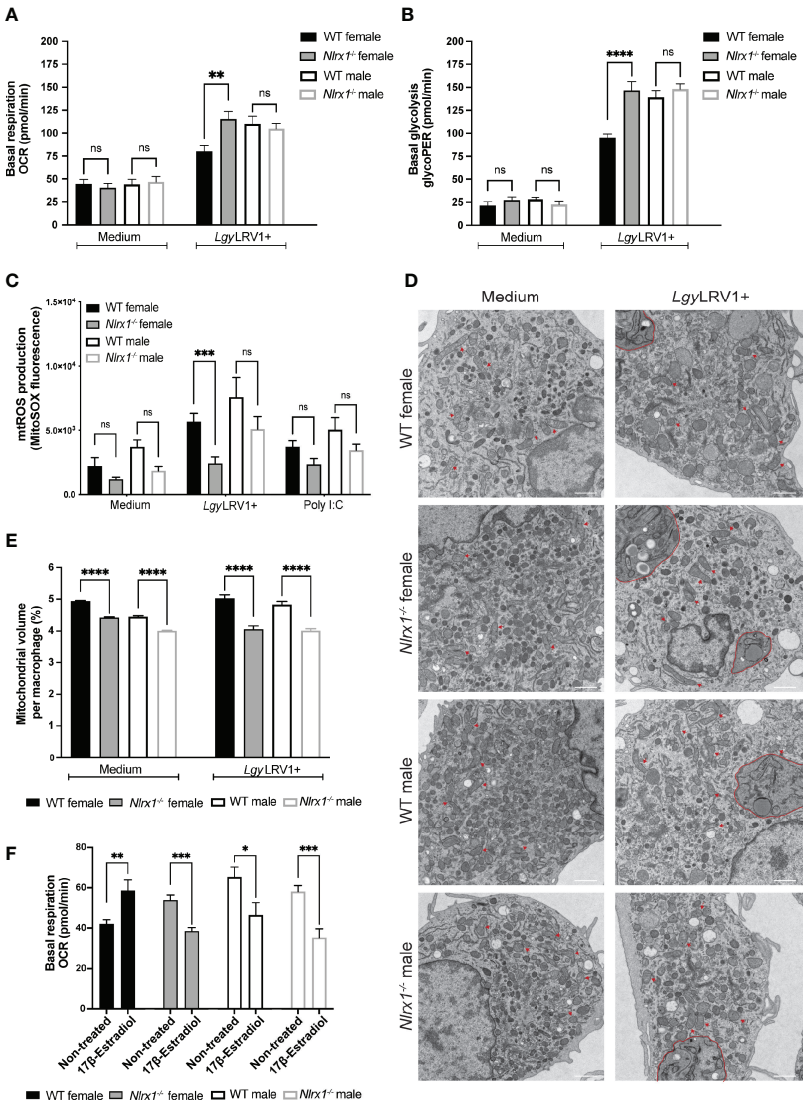


**FIGURE 5** | In absence of NLRX1 female BMDMs had a male-like metabolic response. BMDMs from female and male WT and *Nlrx1*$^{-/-}$ mice were isolated simultaneously and infected with *Lgy*LRV1+ parasites for 8 hours. After 8 hours, **(A)** basal mitochondrial respiration and **(B)** basal glycolytic rate were assessed by Seahorse XFe96 analyzer and adjusted to protein concentration per well (n=3-4 independent experiments). **(C)** Mitochondrial ROS (mtROS) production was quantified in female and male BMDMs infected with *Lgy*LRV1+ parasites or treated with poly I:C (2 μg/ml) for 8 hours. Cells were stained with MitoSOX Red (5 μM) for 20 min at 37°C. Fluorescence was measured using a Spectramax i3 plate reader and adjusted to protein concentration per well. (n=3 independent experiments). **(D)** Mitochondria structure and **(E)** the percentage of mitochondria volume per cell of female and male BMDMs infected with *Lgy*LRV1+ parasites for 8 hours were analyzed by transmission electron microscopy. Representative images are shown. Red arrows show examples of normal mitochondrial structure. *Lgy*LRV1+ parasites are contoured in red (n=2 independent experiments, total of minimum 60 cells analyzed per group). Magnification: 4800x. Scale bar: 1 μm. **(F)** BMDMs from female and male WT and *Nlrx1*$^{-/-}$ mice were pre-treated with 17β-estradiol (200 pg/ml) for 2 hours and estradiol was kept in the assay medium for the duration of the assay. Basal mitochondrial respiration was assessed by Seahorse XFe96 analyzer and adjusted to protein concentration per well (n=4 independent experiments). Graphs are presented as mean +- SEM and significance was assessed by two-way ANOVA with multiple comparisons **(A–C)** or unpaired, parametric t-test **(E, F)**. ns = non-significant, *p ≤ 0.05, **p ≤ 0.01, ***p ≤ 0.001, ****p ≤ 0.0001.

deficient male BMDMs infected with *Lgy*LRV1+ (**Figure 5A**; **Supplementary Figures S4A**, **S5A**). To investigate whether NLRX1 also affected glycolysis in BMDMs, we measured the basal glycolytic rate in the same conditions. In non-infected cells, we observed a very low glycolytic rate, and no differences between groups (**Figure 5B**). Similarly to the pattern observed for mitochondrial respiration, female *Nlrx1*$^{-/-}$ BMDMs infected with LgyLRV1+ showed a significantly increased glycolytic rate compared to WT female, but that was similar to the glycolytic rate of male BMDMs. As before for mitochondrial respiration, we did not observe differences in glycolytic rate between WT and *Nlrx1*-deficient male BMDMs (**Figure 5B**;

**Supplementary Figure S5B**). Taken together, these results suggested a global effect of NLRX1 on female, but not on male macrophage metabolism.

NLRX1 is localized at the mitochondria, and its function in the control of inflammation has been linked to mitochondria and in the modulation of mtROS production (21, 23, 24, 50, 60, 61). This modulation occurs potentially through the interaction with Ubiquinol-Cytochrome C Reductase Core Protein 2 (UQCRC2), a subunit of the complex III of the respiratory chain (38, 62). We measured mtROS and cellular ROS accumulation, by MitoSOX Red and DHE respectively, in female and male BMDMs infected with *Lgy*LRV1+ parasites or treated with poly I:C for 8 hours. Globally mtROS was reduced in *Nlrx1*$^{-/-}$ BMDMs independently of sex, whereas no differences were observed in cellular ROS (**Figure 5C**; **Supplementary Figure S4B, S5C**). To verify whether mitochondrial morphology was affected by NLRX1-defiency, we performed transmission electron microscopy (TEM) on non-infected and *Lgy*LRV1+ infected female and male BMDMs. We did not observe any differences in mitochondrial morphology between WT and *Nlrx1*$^{-/-}$ BMDMs and no mitochondrial defects were observed (**Figure 5D**). On the other hand, quantification of TEM images revealed a reduced mitochondrial density and number in both female and male *Nlrx1*$^{-/-}$ BMDMs compared to WT (**Figure 5E ; Supplementary Figure S4C, S5D**) potentially explaining the reduced mtROS production observed in these cells.

Since neither mtROS production nor mitochondrial structure could explain differences observed in metabolism, we examined whether sex differences in cellular bioenergetics could be modified by the female hormone 17-β estradiol. Similarly to the study done by Gupta et al. (2020) (3), estradiol treatment of male BMDMs significantly reduced mitochondrial respiration (**Figure 5F**). Surprisingly, estradiol treatment increased basal respiration of WT female BMDMs but reduced basal respiration of *Nlrx1*-deficient female BMDMs similarly to males (**Figure 5F**). This male-like pattern of *Nlrx1*-deficient female cells after estradiol treatment was specific to mitochondrial respiration since estradiol increased the glycolytic rate only in females but not in male BMDMs (**Supplementary Figure S4D**). Taken together, these results suggested that macrophage metabolism can be modulated by the female sex hormone and differences in estradiol response might contribute to the sex bias observed in the bioenergetics between WT and *Nlrx1*-deficient BMDMs.

## In Female Mice NLRX1 Deficiency Resulted in a "Masculinization" of the BMDM Transcriptomic Profile

To better understand the complex interplay between NLRX1 genotype and sex, we decided to perform a second RNA sequencing and WGCNA analysis including both female and male BMDMs. To further confirm the role of NLRX1 in the control of TLR3- and type I IFN-mediated inflammation, we added a non-inflammatory strain of *Lgy* that does not carry the LRV1 virus (*Lgy*LRV1-) to the analysis. Infection with *Lgy*LRV1- strain does not induce NF-κB mediated pro-inflammatory cytokines nor a potent type I IFN response thus leading to a less severe form of the disease (37, 63). We infected BMDMs with both *Lgy* parasites or stimulated them with poly I:C for 8 or 24 hours. The relationship between the different modules and the experimental conditions was assessed with a regression analysis and module eigengenes average predictions are shown as heatmaps at 24 and 8 hours (**Figure 6A**; **Supplementary Figure S6A**, respectively). The genes in each module are listed in **Supplementary Tables 5, 6**. In each condition, the heatmap clusters the groups according to their similarity. Supporting the male-like behavior of *Nlrx1*-deficient female cells, we could observe that at 24 hours post-infection, in all condition except with poly I:C treatment, the *Nlrx1*$^{-/-}$ female BMDMs clustered more closely to the WT and *Nlrx1*-deficient male BMDMs than to the WT female (**Figure 6A**). At 8 hours p.i., this clusterization pattern was only observed with infection with *Lgy*LRV1+ (**Supplementary Figure S6A**). As previously, we performed a gene ontology (GO) enrichment analysis for each module to identify the biological processes associated to each module. For each module GO terms are listed in **Supplementary Tables 7, 8**. As expected, GO enrichment analysis of the different modules revealed that most modules were enriched in GO terms associated to (1) Inflammation and infectivity and (2) Mitochondria and metabolism. In addition, at 8 hours p.i. more than half of the modules (60%) were enriched in GO terms associated to (3) sex hormone signaling, while at 24 hours p.i. we observed this enrichment in all modules, except the *green* module (**Figure 6A**; **Supplementary Figure S6A, S6B**).

We next performed pairwise comparisons between the different groups and plotted the number of significantly differentially expressed genes both at 8 and 24 hours using a cut-off of fold-change [-2:2] and an adjusted p-value < 0.05 (**Figure 6B–D**; **Supplementary Figures S6C–G**). We identified only a few sex- or genotype-specific genes except in non-infected BMDMs in which at 8 hours p.i. we identified a significant number of genotype-specific genes (**Supplementary Figure S6C**). In the last two comparisons, we compared opposite genotypes with opposite sex. Interestingly, we observed a common pattern that when we compared *Nlrx1*$^{-/-}$ female BMDMs to a WT male, independently of the condition or time-point, we observed less differences than when *Nlrx1*$^{-/-}$ male BMDMs were compared to a WT female, suggesting that the transcriptomic profile of female *Nlrx1*$^{-/-}$ cells was closer to a male, as suggested by the WGCNA analysis.

To investigate whether we would be able to explain why *Nlrx1*$^{-/-}$ female BMDMs had a male-like transcriptomics profile, we wanted to identify genes that in *Nlrx1*$^{-/-}$ female BMDMs were expressed at a similar level than in male BMDMs. To do so, we looked for genes that were differentially expressed only in the WT female BMDMs, but not between the three other groups, *Nlrx1*$^{-/-}$ female, *Nlrx1*$^{-/-}$ male and WT male BMDMs. We used a threshold of adjusted p-value inferior to 0.1. The analysis identified only 3 genes in non-infected BMDMs at 8 hours timepoint (**Figure 6E**): the lysophosphatidic acid receptor 1 (*Lpar1*), the vascular endothelial growth receptor factor 2 (*Kdr*) and the cyclic AMP-responsive element-binding protein 3-like protein 2 (*Creb3l2*). These genes play a role in

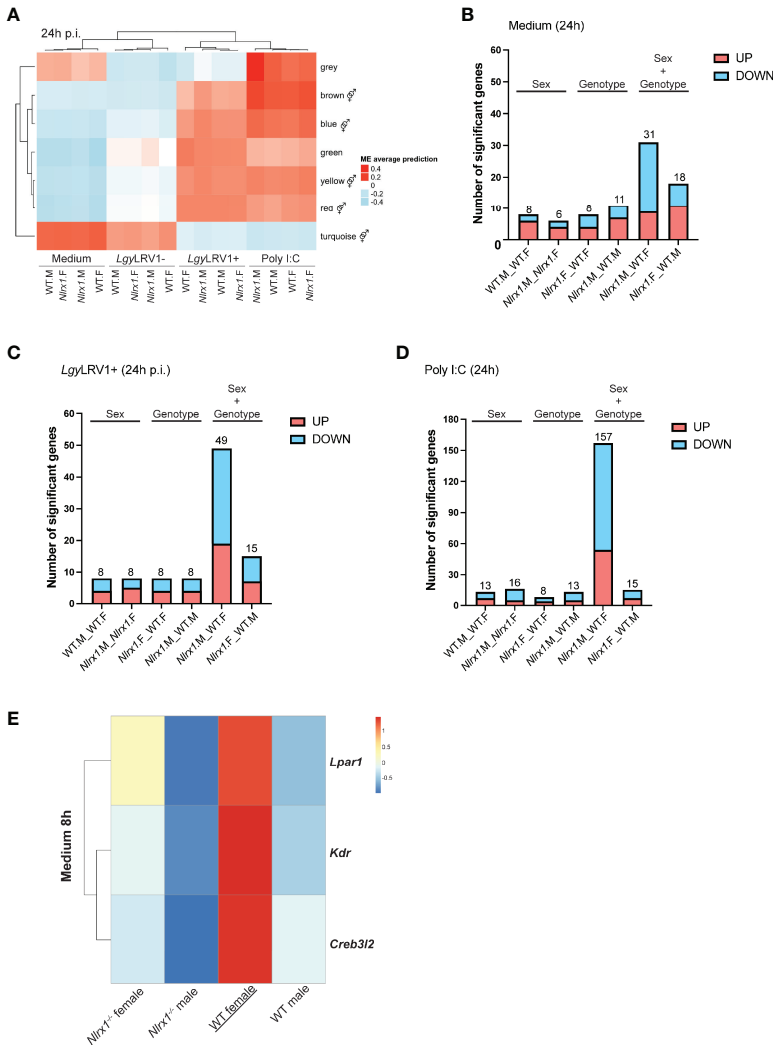


**FIGURE 6** | Transcriptomics analysis of female and male BMDMs revealed a male-like phenotype of *Nlrx1*$^{-/-}$ female BMDMs. **(A)** Transcriptomics analysis of both female and male WT and *Nlrx1*$^{-/-}$ BMDMs (n=3 mice per group) infected with *Lgy*LRV1+ and *Lgy*LRV1- parasites or stimulated with poly I:C (2 µg/ml) for 24 hours. The heatmap represents the global weighted correlation network analysis (WGCNA) and module names are represented by a color. A gene ontology (GO) enrichment analysis for each module was performed to identify the biological processes associated to each module. represents modules enriched in GO terms associated with sex hormone signaling. At 24 hours, the number of differentially expressed genes between groups in **(B)** non-infected, **(C)** *Lgy*LRV1+ infected and **(D)** poly I:C treated conditions is plotted. On each barplot the number represents the total number of differentially upregulated (in red) and downregulated (in blue) genes. Pairwise comparisons are done by "sex" (same genotype, different sex, "WT.F._WT.M" and "*Nlrx1*.F_*Nlrx1.M*"), by "genotype" (same sex, different genotype ("*Nlrx1*.F_WT.F" and "*Nlrx1*.M_WT.M"), or by combining both "sex and genotype" ("*Nlrx1*.M_WT.F" and "*Nlrx1*.F_WT.M"). See **Supplementary Tables 9–11** for the list of significantly differentially expressed genes. **(E)** Identification of WT female specific genes. Genes that were differentially expressed in only in WT female BMDMs but not between the other three groups (*Nlrx1-/-* female, *Nlrx1-/-* male and WT male BMDMs) were identified in non-infected samples at 8 hours.

inflammation (64–66), angiogenesis (67) and collagen synthesis (68, 69), respectively, aspects that are hallmarks of *Leishmania* infection (70, 71) and where in other experimental models sex differences have been described (72–74).

## DISCUSSION

It is well established that females and males differ in their clinical manifestations of both infectious and inflammatory diseases due to differences in the development and strength of the immune response (75, 76). In this study, we provided evidence that NLRX1 limited inflammation and tissue damage in female mice infected with the human protozoan parasite *Lgy* carrying an endosymbiotic dsRNA virus, LRV1, activating TLR3. We showed that in presence of this TLR3 agonist, *Nlrx1*-deficient female mice developed a more severe pathology with increased inflammation and immune cell recruitment to the site of infection compared to WT mice independently of the parasite burden measured in the lesions, suggesting a role in the control

of inflammation. Here, inflammation in the lesion was mediated by an increased expression of the pro-inflammatory *Il6* and *Ifnb*, but not *Tnfa*. Surprisingly, we did not observe any difference in IL-6 production between *in vitro* female WT and *Nlrx1*-deficient macrophages infected with *Lgy*LRV1+, but only an increased production of IFNβ. Thus, our results suggested that infected macrophages contributed to increased IFNβ, but other cell types in the skin lesion also contributed to increased IL-6 production and to the *in vivo* exacerbated phenotype observed in *Nlrx1*-deficient female mice.

In *Lgy*LRV1+ infection, the exact mechanism of type I IFN regulation by NLRX1 is yet to be further elucidated. Different mechanisms of anti-viral regulation by NLRX1 have been proposed, including inhibition of retinoic acid-inducible gene (RIG)-I-like receptor-mitochondrial antiviral-signaling (RIG-I-MAVS) protein interaction (20, 22), sequestration of the DNA sensor stimulator of interferon genes (STING) (77, 78), competition with the dsRNA activated protein kinase (PKR) (79), or binding to the autophagy complex formed of mitochondrial Tu translation elongation factor and autophagy related proteins 5 and 12 (TUFM/ATG5/ATG12) (52, 80). Several studies support that NLRX1 is located at the mitochondrial matrix rather than at the mitochondrial outer membrane (MOM) as suggested by the first study by Moore *et al.* (20, 62). Therefore, it raises the question how interaction with proteins located on the MOM or in the cytoplasm, such as MAVS or STING, respectively, would occur within the mitochondrial matrix unless disruption of the mitochondria occurs in the experimental model in question. Although we did not observe any mitochondrial structural damage *in vitro* in BMDMs, we cannot exclude that the hypoxic conditions in the lesions in *Lgy* infection would lead to a mitochondrial functional decline as it is often described in injury and ischemia (81–83). However, in a previous study, we have shown that LRV1 does not activate the cytoplasmic RNA sensors such as RIG-I-MAVS signaling and viral RNA recognition occurs only *via* the TLR3 pathway (37, 63, 84). Thus, in our study NLRX1 controlled IFNβ production downstream of TLR3.

To better understand the role of NLRX1 in our model system of infection, we first performed a transcriptomics analysis of infected female BMDMs. Bioinformatic analysis revealed a significant number of modules enriched in GO terms associated to sex hormone signaling. Even if still quite controversial, sex differences in clinical outcome to viral infections have been reported and differences in susceptibility may be attributed to both sex hormones and sex chromosome encoded genes. Although previous reports have not described a link between sex and NLRX1, oppositely to females, infection of *Nlrx1*-deficient male mice did not result in an exacerbated disease outcome. Indeed, male mice did not exhibit any significant differences in lesion size or cell recruitment. Conversely to *in vivo* where *Nlrx1*-deficient male mice showed a slight reduction in *Ifnb* and *Il6* expression, *in vitro Lgy*LRV1+ infected male BMDMs produced higher levels of IL-6 and TNFα, but not IFNβ, in comparison to females, suggesting a role for other inflammatory cells or mediators *in vivo*.

Several PRRs, including TLRs and NLRs, are able to activate multiple metabolic pathways that lead to a metabolic switch from OXPHOS to glycolytic ATP production which is often critical for innate immune cell activation (85, 86). Given its mitochondrial localization, NLRX1 has been suggested to play a role in the maintenance of mitochondrial function and metabolism (31, 81). However, its impact on cellular metabolism seem to depend on the cell type and to our knowledge no studies have investigated the role of NLRX1 on macrophage colony stimulating factor (M-CSF) primed BMDM metabolism (87). *Leishmania* and other intracellular pathogens are known to manipulate host metabolism and *Leishmania* infection seems to favor a switch to aerobic glycolysis (88, 89). Here we showed that infection with *Lgy* parasites induced glycolysis in infected BMDMs while maintaining a high OXPHOS activity. Interestingly, WT male BMDMs showed a higher metabolic activity in comparison to WT females. This is in line with a previous study showing that neutrophils, another innate immune cell type, isolated from males had a higher mitochondrial respiration in comparison to females (3). However, no sex differences in metabolism were observed between female and male *Nlrx1*-deficient BMDMs. Interestingly, the OXPHOS and glycolytic activity of the BMDMs, the parasite burden, the *in vitro* IFNβ production and response to 17β-estradiol all showed a similar pattern: female *Nlrx1*-deficient cells had a profile similar to male cells. Differences in metabolic rates were not linked to mitochondrial numbers or to impairment of mitochondrial structure since *Nlrx1*-deficient cells had less mitochondria and produced less mtROS than WT cells independently of sex and no structural defects were observed upon *Lgy*LRV1+ infection.

Since BMDMs were able to respond to 17β-estradiol, the differences in bioenergetic profiles of male and female BMDMs may be potentially driven by sex hormones. In neutrophils, a higher OXPHOS profile observed in males has been linked to immature state neutrophils (3). How these differences in metabolic profiles impact the macrophage function, should however be further studied. Estrogens have been shown to impact macrophage metabolism directly. Erα-mediated signaling in macrophages have been shown to promote anti-inflammatory M2-polarization and promote wound healing and cutaneous repair by enhancing angiogenesis and collagen synthesis (9, 10, 90–92). Estrogens not only play a role in mitochondrial biogenesis and in the regulation of mitochondrial function, but several studies have shown that estrogens may also play a role in glucose metabolism and may also stimulate glycolysis (93, 94). Reports are still conflicting on the role of NLRX1 on cell metabolism. Therefore, the effect of sex hormones on BMDMs metabolism and on NLRX1 would be of great interest for future studies.

Trying to provide novel insight on the sex-related differences observed in *Nlrx1*-deficient cells, we performed a second transcriptomic analysis of both female and male BMDMs. Interestingly, at 8 hours post-infection, *Nlrx1*-deficient cells clustered together with males with *Lgy*LRV1+ infection, while at 24 hours this clustering occurred in all conditions except treatment with poly I:C. Similarly, pairwise comparisons of

significantly differentially expressed genes between groups confirmed a male-like transcriptomic profile of *Nlrx1*-/- female cells. Our analysis identified three WT female signature genes in non-infected BMDMs at 8 hours timepoint: *Lpar1*, *Kdr* and *Creb3l2*. The role and contribution of *Lpar1* to the observed sex differences may be of great interest for future studies. The synthesis of its ligand, lysophosphatidic acid (LPA), was shown to be type I IFN dependent in an autocrine and paracrine manner in response to TLR3 signaling (95). Differential levels of secreted LPA may contribute to differences in inflammation and pathology observed *in vivo* and *in vitro*, since LPA is produced by several cell types. Of note, sex differences in response to LPA have been described in a model of osteoarthritis (96).

NLRX1 is a unique mitochondria-associated innate immune receptor of the NLR family, and its role extends from the traditional pathogen recognition to the regulation of different cellular functions to control inflammation. However, as highlighted by the diverse effects of NLRX1 that have been described, the mechanism through which NLRX1 influences inflammation, the immune response or the metabolism is still under debate. One might speculate that some of the discrepancies observed in the function of NLRX1 may be attributed to the sex of the animal model used in their research. Interestingly, it was shown that the C-terminal leucine-rich repeat domain (LRR) of NLRX1 could bind several polyunsaturated lipids that mediated the anti-inflammatory effects of NLRX1 (31, 97). In serum LPA is most often found in its unsaturated forms and polyunsaturated forms of LPA are synthetized for example in mouse models of allergic airway inflammation (98, 99). Screening of compounds also predicted that other lipids including sterol lipids could modulate NLRX1 activity (97). All sex steroid hormones are derived from cholesterol, the main sterol synthetized in animal cells, and although *Nlrx1* expression did not differ between males and females, it remains to be determined whether sex hormones could bind and modulate NLRX1 function and its downstream signaling.

In addition to cellular and lipid metabolism, infection with *Leishmania* may lead to modifications of the extracellular matrix (ECM) and collagen composition of the dermis at the site of infection (70, 100). In addition, cutaneous leishmaniasis is also characterized by vascular remodeling and lymphangiogenesis mediated by the vascular endothelial growth factor A (VEGF-A)/VEGF receptor 2 (VEGFR-2) signaling pathway that is essential for lesion resolution (71, 101, 102). Interestingly, in addition the *Lpar1*, two other gene candidates were identified in our transcriptomic analysis to be upregulated only in WT females, *Creb3l2* and *Kdr* that play a role in collagen synthesis (68) and angiogenesis (67), respectively. NLRX1 has been shown to affect both. Overexpression of NLRX1 human nucleus pulposus cells in the intervertebral disc resulted in increased collagen synthesis and decreased ECM decomposing enzymes (103). On the other hand, *Nlrx1*-deficiency led to increased expression of wound healing factors epidermal growth factor (EGF) and TGFβ in epithelial cells in a mouse model of DSS-induced colitis (104). Thus, both angiogenesis and collagen composition could be further investigated in infected footpad sections of both female and male wild-type and *Nlrx1*-deficient mice.

Taken together, our study provides novel insight on the relevance of the first mitochondrial NLR and its connection to the control of inflammation specifically in females. There is accumulating evidence that in human diseases innate immune response, inflammation, and energy metabolism are regulated in a sex-dependent manner (105, 106). Increasing number of studies have shown altered expression of NLRX1 in human patients. For example, high NLRX1 expression positively correlated with HIV-1 viremia in patients (107), or conversely low expression was associated to low prognosis of hepatocellular carcinoma (108) and gastric cancer (109). Similarly, expression of NLRX1 was reduced in aneurysm-induced brain injury (27) and in chronic obstructive pulmonary disease (COPD) (110). Interestingly, in COPD, disease prevalence does not seem to differ between men and women, however the clinical presentation is different and more severe in women (111). Whether NLRX1 contributes to sex differences observed in these pathologies remains to be determined. Taken together, NLRX1 represents a promising therapeutic target as a regulator of inflammation as already shown in several mice models (112–114). However, only the research approaches that consider both sexes will provide a complete understanding of the regulation of inflammation and metabolism and provide new insights for sex-specific drug development.

## DATA AVAILABILITY STATEMENT

The data presented in this study are deposited in NCBI's Gene Expression Omnibus (GEO) repository and are accessible through GEO Series accession numbers GSE201120 and GSE201066.

## ETHICS STATEMENT

The animal study was reviewed and approved by Swiss Federal Veterinary Office (SFVO).

## AUTHOR CONTRIBUTIONS

TS and NF designed the study. TS performed experiments, analyzed the data, and wrote the first draft of the manuscript. SC, CD, FP, NI, and FT performed experiments. AB, IX, NI, FT, and CG analyzed data. IL, LF, AB, IX, SC, and NF interpreted and discussed the data. NF reviewed and edited the manuscript. All authors contributed to the article and approved the submitted version.

## FUNDING

This work was funded by the grants from the Swiss National fund for research to NF (Grant No. 310030_173180, and

IZRJZ3_164176/1) and by Fondation Pierre Mercier pour la science.

## ACKNOWLEDGMENTS

We thank the veterinary and animal facility staff at Center for Immunity and Infection (CIIL) for ensuring the highest possible animal welfare and ethical standards for animal experimentation. We thank the ACCESS Geneva high throughput screening facility and Dr. Dimitri Moreau for his assistance with the experiments and data analysis. We thank the electron microscopy facility of Lausanne, Dr. Christel Genoud and Jean Daraspe for their assistance in sample preparation and image analysis. We thank Jean-Christophe Stehle and Janine Horlbeck from the Mouse pathology facility (UNIL) for the preparation of histology sections. Finally, we thank the Lausanne Genomic Technologies Facility and Leonore Wigger for RNAseq data analysis.

## SUPPLEMENTARY MATERIAL

The Supplementary Material for this article can be found online at: https://www.frontiersin.org/articles/10.3389/fimmu.2022.882867/full#supplementary-material

## REFERENCES

1. Klein SL, Flanagan KL. Sex Differences in Immune Responses. *Nat Rev Immunol* (2016) 16(10):626–38. doi: 10.1038/nri.2016.90
2. Gal-Oz ST, Maier B, Yoshida H, Seddu K, Elbaz N, Czysz C, et al. Immgen Report: Sexual Dimorphism in the Immune System Transcriptome. *Nat Commun* (2019) 10(1):4295. doi: 10.1038/s41467-019-12348-6
3. Gupta S, Nakabo S, Blanco LP, O'Neil LJ, Wigerblad G, Goel RR, et al. Sex Differences in Neutrophil Biology Modulate Response to Type I Interferons and Immunometabolism. *Proc Natl Acad Sci USA* (2020) 117(28):16481–91. doi: 10.1073/pnas.2003603117
4. So J, Tai AK, Lichtenstein AH, Wu D, Lamon-Fava S. Sexual Dimorphism of Monocyte Transcriptome in Individuals With Chronic Low-Grade Inflammation. *Biol Sex Differ* (2021) 12(1):43. doi: 10.1186/s13293-021-00387-y
5. Kovats S. Estrogen Receptors Regulate Innate Immune Cells and Signaling Pathways. *Cell Immunol* (2015) 294(2):63–9. doi: 10.1016/j.cellimm.2015.01.018
6. Moulton VR. Sex Hormones in Acquired Immunity and Autoimmune Disease. *Front Immunol* (2018) 9:2279. doi: 10.3389/fimmu.2018.02279
7. Kadel S, Kovats S. Sex Hormones Regulate Innate Immune Cells and Promote Sex Differences in Respiratory Virus Infection. *Front Immunol* (2018) 9:1653. doi: 10.3389/fimmu.2018.01653
8. Ruggieri A, Anticoli S, D'Ambrosio A, Giordani L, Viora M. The Influence of Sex and Gender on Immunity, Infection and Vaccination. *Ann Ist Super Sanita* (2016) 52(2):198–204. doi: 10.4415/ANN_16_02_11
9. Villa A, Rizzi N, Vegeto E, Ciana P, Maggi A. Estrogen Accelerates the Resolution of Inflammation in Macrophagic Cells. *Sci Rep* (2015) 5:15224. doi: 10.1038/srep15224
10. Campbell L, Emmerson E, Williams H, Saville CR, Krust A, Chambon P, et al. Estrogen Receptor-Alpha Promotes Alternative Macrophage Activation During Cutaneous Repair. *J Invest Dermatol* (2014) 134 (9):2447–57. doi: 10.1038/jid.2014.175
11. Routley CE, Ashcroft GS. Effect of Estrogen and Progesterone on Macrophage Activation During Wound Healing. *Wound Repair Regener* (2009) 17(1):42–50. doi: 10.1111/j.1524-475X.2008.00440.x
12. Di Conza G, Ho PC. Metabolic Adaptation of Macrophages in Chronic Diseases. *Cancer Lett* (2018) 414:250–6. doi: 10.1016/j.canlet.2017.11.023
13. Galvan-Pena S, O'Neill LA. Metabolic Reprograming in Macrophage Polarization. *Front Immunol* (2014) 5:420. doi: 10.3389/fimmu.2014.00420
14. Viola A, Munari F, Sanchez-Rodriguez R, Scolaro T, Castegna A. The Metabolic Signature of Macrophage Responses. *Front Immunol* (2019) 10:1462. doi: 10.3389/fimmu.2019.01462
15. Gaignard P, Frechou M, Liere P, Therond P, Schumacher M, Slama A, et al. Sex Differences in Brain Mitochondrial Metabolism: Influence of Endogenous Steroids and Stroke. *J Neuroendocrinol* (2018) 30(2):e12497. doi: 10.1111/jne.12497
16. Khalifa AR, Abdel-Rahman EA, Mahmoud AM, Ali MH, Noureldin M, Saber SH, et al. Sex-Specific Differences in Mitochondria Biogenesis, Morphology, Respiratory Function, and Ros Homeostasis in Young Mouse Heart and Brain. *Physiol Rep* (2017) 5(6):e13125. doi: 10.14814/phy2.13125
17. Ventura-Clapier R, Moulin M, Piquereau J, Lemaire C, Mericskay M, Veksler V, et al. Mitochondria: A Central Target for Sex Differences in Pathologies. *Clin Sci (Lond)* (2017) 131(9):803–22. doi: 10.1042/CS20160485
18. Klinge CM. Estrogenic Control of Mitochondrial Function and Biogenesis. *J Cell Biochem* (2008) 105(6):1342–51. doi: 10.1002/jcb.21936
19. Klinge CM. Estrogenic Control of Mitochondrial Function. *Redox Biol* (2020) 31:101435. doi: 10.1016/j.redox.2020.101435
20. Moore CB, Bergstralh DT, Duncan JA, Lei Y, Morrison TE, Zimmermann AG, et al. Nlrx1 Is a Regulator of Mitochondrial Antiviral Immunity. *Nature* (2008) 451(7178):573–7. doi: 10.1038/nature06501
21. Tattoli I, Carneiro LA, Jehanno M, Magalhaes JG, Shu Y, Philpott DJ, et al. Nlrx1 Is a Mitochondrial Nod-Like Receptor That Amplifies Nf-Kappab and Jnk Pathways by Inducing Reactive Oxygen Species Production. *EMBO Rep* (2008) 9(3):293–300. doi: 10.1038/sj.embor.7401161
22. Allen IC, Moore CB, Schneider M, Lei Y, Davis BK, Scull MA, et al. Nlrx1 Protein Attenuates Inflammatory Responses to Infection by Interfering With the Rig-I-Mavs and Traf6-Nf-Kappab Signaling Pathways. *Immunity* (2011) 34(6):854–65. doi: 10.1016/j.immuni.2011.03.026
23. Hong M, Yoon SI, Wilson IA. Structure and Functional Characterization of the Rna-Binding Element of the Nlrx1 Innate Immune Modulator. *Immunity* (2012) 36(3):337–47. doi: 10.1016/j.immuni.2011.12.018
24. Singh K, Poteryakhina A, Zheltukhin A, Bhatelia K, Prajapati P, Sripada L, et al. Nlrx1 Acts as Tumor Suppressor by Regulating Tnf-Alpha Induced Apoptosis and Metabolism in Cancer Cells. *Biochim Biophys Acta* (2015) 1853(5):1073–86. doi: 10.1016/j.bbamcr.2015.01.016
25. Soares F, Tattoli I, Rahman MA, Robertson SJ, Belcheva A, Liu D, et al. The Mitochondrial Protein Nlrx1 Controls the Balance Between Extrinsic and Intrinsic Apoptosis. *J Biol Chem* (2014) 289(28):19317–30. doi: 10.1074/jbc.M114.550111
26. Eitas TK, Chou WC, Wen H, Gris D, Robbins GR, Brickey J, et al. The Nucleotide-Binding Leucine-Rich Repeat (Nlr) Family Member Nlrx1 Mediates Protection Against Experimental Autoimmune Encephalomyelitis and Represses Macrophage/Microglia-Induced Inflammation. *J Biol Chem* (2014) 289(7):4173–9. doi: 10.1074/jbc.M113.533034
27. Theus MH, Brickler T, Meza AL, Coutermarsh-Ott S, Hazy A, Gris D, et al. Loss of Nlrx1 Exacerbates Neural Tissue Damage and Nf-Kappab Signaling Following Brain Injury. *J Immunol* (2017) 199(10):3547–58. doi: 10.4049/jimmunol.1700251
28. Imbeault E, Mahvelati TM, Braun R, Gris P, Gris D. Nlrx1 Regulates Neuronal Cell Death. *Mol Brain* (2014) 7:90. doi: 10.1186/s13041-014-0090-x
29. Jaworska J, Coulombe F, Downey J, Tzelepis F, Shalaby K, Tattoli I, et al. Nlrx1 Prevents Mitochondrial Induced Apoptosis and Enhances Macrophage Antiviral Immunity by Interacting With Influenza Virus Pb1-F2 Protein. *Proc Natl Acad Sci USA* (2014) 111(20):E2110-9. doi: 10.1073/pnas.1322118111
30. Singh K, Sripada L, Lipatova A, Roy M, Prajapati P, Gohel D, et al. Nlrx1 Resides in Mitochondrial Rna Granules and Regulates Mitochondrial Rna Processing and Bioenergetic Adaptation. *Biochim Biophys Acta Mol Cell Res* (2018) 1865(9):1260–76. doi: 10.1016/j.bbamcr.2018.06.008

31. Stokman G, Kors L, Bakker PJ, Rampanelli E, Claessen N, Teske GJD, et al. Nlrx1 Dampens Oxidative Stress and Apoptosis in Tissue Injury *Via* Control of Mitochondrial Activity. *J Exp Med* (2017) 214(8):2405–20. doi: 10.1084/jem.20161031
32. Ives A, Masina S, Castiglioni P, Prevel F, Revaz-Breton M, Hartley MA, et al. Myd88 and Tlr9 Dependent Immune Responses Mediate Resistance to Leishmania Guyanensis Infections, Irrespective of Leishmania Rna Virus Burden. *PloS One* (2014) 9(5):e96766. doi: 10.1371/journal.pone.0096766
33. Brettmann EA, Shaik JS, Zangger H, Lye LF, Kuhlmann FM, Akopyants NS, et al. Tilting the Balance Between Rna Interference and Replication Eradicates Leishmania Rna Virus 1 and Mitigates the Inflammatory Response. *Proc Natl Acad Sci USA* (2016) 113(43):11998–2005. doi: 10.1073/pnas.1615085113
34. Cantanhede LM, da Silva Junior CF, Ito MM, Felipin KP, Nicolete R, Salcedo JM, et al. Further Evidence of an Association Between the Presence of Leishmania Rna Virus 1 and the Mucosal Manifestations in Tegumentary Leishmaniasis Patients. *PloS Negl Trop Dis* (2015) 9(9):e0004079. doi: 10.1371/journal.pntd.0004079
35. Ito MM, Catanhede LM, Katsuragawa TH, Silva Junior CF, Camargo LM, Mattos Rde G, et al. Correlation Between Presence of Leishmania Rna Virus 1 and Clinical Characteristics of Nasal Mucosal Leishmaniosis. *Braz J Otorhinolaryngol* (2015) 81(5):533–40. doi: 10.1016/j.bjorl.2015.07.014
36. Reverte M, Eren RO, Jha B, Desponds C, Snaka T, Prevel F, et al. The Antioxidant Response Favors Leishmania Parasites Survival, Limits Inflammation and Reprograms the Host Cell Metabolism. *PloS Pathog* (2021) 17(3):e1009422. doi: 10.1371/journal.ppat.1009422
37. Rossi M, Castiglioni P, Hartley MA, Eren RO, Prevel F, Desponds C, et al. Type I Interferons Induced by Endogenous or Exogenous Viral Infections Promote Metastasis and Relapse of Leishmaniasis. *Proc Natl Acad Sci USA* (2017) 114(19):4987–92. doi: 10.1073/pnas.1621447114
38. Rebsamen M, Vazquez J, Tardivel A, Guarda G, Curran J, Tschopp J. Nlrx1/Nod5 Deficiency Does Not Affect Mavs Signalling. *Cell Death Differ* (2011) 18(8):1387. doi: 10.1038/cdd.2011.64
39. Kuhlmann FM, Robinson JI, Bluemling GR, Ronet C, Fasel N, Beverley SM. Antiviral Screening Identifies Adenosine Analogs Targeting the Endogenous Dsrna Leishmania Rna Virus 1 (Lrv1) Pathogenicity Factor. *Proc Natl Acad Sci USA* (2017) 114(5):E811–E9. doi: 10.1073/pnas.1619114114
40. Reverte M, Fasel N. Leishmania Parasite Quantification by Bioluminescence in Murine Models. *Bio Protoc* (2019) 9(22):e3431. doi: 10.21769/BioProtoc.3431
41. Rio DC, Ares MJr., Hannon GJ, Nilsen TW. Purification of Rna Using Trizol (Tri Reagent). *Cold Spring Harb Protoc* (2010) 2010(6):pdb prot5439. doi: 10.1101/pdb.prot5439
42. Eren RO, Fasel N. Macrophage Survival Assay Using High Content Microscopy. *Bio Protoc* (2017) 7(16):e2509. doi: 10.21769/BioProtoc.2509
43. Ritchie ME, Phipson B, Wu D, Hu Y, Law CW, Shi W, et al. Limma Powers Differential Expression Analyses for Rna-Sequencing and Microarray Studies. *Nucleic Acids Res* (2015) 43(7):e47. doi: 10.1093/nar/gkv007
44. Kremer JR, Mastronarde DN, McIntosh JR. Computer Visualization of Three-Dimensional Image Data Using Imod. *J Struct Biol* (1996) 116 (1):71–6. doi: 10.1006/jsbi.1996.0013
45. Nasi M, De Biasi S, Bianchini E, Digaetano M, Pinti M, Gibellini L, et al. Analysis of Inflammasomes and Antiviral Sensing Components Reveals Decreased Expression of Nlrx1 in Hiv-Positive Patients Assuming Efficient Antiretroviral Therapy. *AIDS* (2015) 29(15):1937–41. doi: 10.1097/QAD.0000000000000830
46. Philipson CW, Bassaganya-Riera J, Viladomiu M, Kronsteiner B, Abedi V, Hoops S, et al. Modeling the Regulatory Mechanisms by Which Nlrx1 Modulates Innate Immune Responses to Helicobacter Pylori Infection. *PloS One* (2015) 10(9):e0137839. doi: 10.1371/journal.pone.0137839
47. Velazquez-Salinas L, Verdugo-Rodriguez A, Rodriguez LL, Borca MV. The Role of Interleukin 6 During Viral Infections. *Front Microbiol* (2019) 10:1057. doi: 10.3389/fmicb.2019.01057
48. Allen I, Simmons A, Capria V, LeRoith T, Robbins G, Heid B, et al. Nlrx1 Attenuates Tumorigenesis Through the Negative Regulation of Akt and Nf-Kappa B Signaling. *J Immunol* (2014) 192(1 supplement):203–6.
49. Huang JH, Liu CY, Wu SY, Chen WY, Chang TH, Kan HW, et al. Nlrx1 Facilitates Histoplasma Capsulatum-Induced Lc3-Associated Phagocytosis for Cytokine Production in Macrophages. *Front Immunol* (2018) 9:2761. doi: 10.3389/fimmu.2018.02761
50. Hung SC, Huang PR, Almeida-da-Silva CLC, Atanasova KR, Yilmaz O, Ojcius DM. Nlrx1 Modulates Differentially Nlrp3 Inflammasome Activation and Nf-Kappab Signaling During Fusobacterium Nucleatum Infection. *Microbes Infect* (2017) 20(9–10):615–25. doi: 10.1016/j.micinf.2017.09.014
51. Kastelberg B, Tubau-Juni N, Ayubi T, Leung A, Leber A, Hontecillas R, et al. Nlrx1 Is a Key Regulator of Immune Signaling During Invasive Pulmonary Aspergillosis. *PloS Pathog* (2020) 16(9):e1008854. doi: 10.1371/journal.ppat.1008854
52. Lei Y, Wen H, Yu Y, Taxman DJ, Zhang L, Widman DG, et al. The Mitochondrial Proteins Nlrx1 and Tufm Form a Complex That Regulates Type I Interferon and Autophagy. *Immunity* (2012) 36(6):933–46. doi: 10.1016/j.immuni.2012.03.025
53. Coutermarsh-Ott S, Simmons A, Capria V, LeRoith T, Wilson JE, Heid B, et al. Nlrx1 Suppresses Tumorigenesis and Attenuates Histiocytic Sarcoma Through the Negative Regulation of Nf-Kappab Signaling. *Oncotarget* (2016) 7(22):33096–110. doi: 10.18632/oncotarget.8861
54. Pan J, Weng Z, Xue C, Lin B, Lin M. The Bioinformatics-Based Analysis Identifies 7 Immune-Related Genes as Prognostic Biomarkers for Colon Cancer. *Front Oncol* (2021) 11:726701. doi: 10.3389/fonc.2021.726701
55. Maertens A, Tran V, Kleensang A, Hartung T. Weighted Gene Correlation Network Analysis (Wgcna) Reveals Novel Transcription Factors Associated With Bisphenol a Dose-Response. *Front Genet* (2018) 9:508. doi: 10.3389/fgene.2018.00508
56. Langfelder P, Horvath S. Wgcna: An R Package for Weighted Correlation Network Analysis. *BMC Bioinf* (2008) 9:559. doi: 10.1186/1471-2105-9-559
57. Gardinassi LG, Garcia GR, Costa CH, Costa Silva V, de Miranda Santos IK. Blood Transcriptional Profiling Reveals Immunological Signatures of Distinct States of Infection of Humans With Leishmania Infantum. *PloS Negl Trop Dis* (2016) 10(11):e0005123. doi: 10.1371/journal.pntd.0005123
58. Di Florio DN, Sin J, Coronado MJ, Atwal PS, Fairweather D. Sex Differences in Inflammation, Redox Biology, Mitochondria and Autoimmunity. *Redox Biol* (2020) 31:101482. doi: 10.1016/j.redox.2020.101482
59. Leber A, Hontecillas R, Tubau-Juni N, Zoccoli-Rodriguez V, Hulver M, McMillan R, et al. Nlrx1 Regulates Effector and Metabolic Functions of Cd4+ T Cells. *J Immunol* (2017) 198(6):2260–8. doi: 10.4049/jimmunol.1601547
60. Unger BL, Ganesan S, Comstock AT, Faris AN, Hershenson MB, Sajjan US. Nod-Like Receptor X-1 Is Required for Rhinovirus-Induced Barrier Dysfunction in Airway Epithelial Cells. *J Virol* (2014) 88(7):3705–18. doi: 10.1128/JVI.03039-13
61. Yin H, Sun G, Yang Q, Chen C, Qi Q, Wang H, et al. Nlrx1 Accelerates Cisplatin-Induced Ototoxity in Hei-Oc1 Cells *Via* Promoting Generation of Ros and Activation of Jnk Signaling Pathway. *Sci Rep* (2017) 7:44311. doi: 10.1038/srep44311
62. Arnoult D, Soares F, Tattoli I, Castanier C, Philpott DJ, Girardin SE. An N-Terminal Addressing Sequence Targets Nlrx1 to the Mitochondrial Matrix. *J Cell Sci* (2009) 122(Pt 17):3161–8. doi: 10.1242/jcs.051193
63. Ives A, Ronet C, Prevel F, Ruzzante G, Fuertes-Marraco S, Schutz F, et al. Leishmania Rna Virus Controls the Severity of Mucocutaneous Leishmaniasis. *Science* (2011) 331(6018):775–8. doi: 10.1126/science.1199326
64. Fransson J, Gomez-Conde AI, Romero-Imbroda J, Fernandez O, Leyva L, de Fonseca FR, et al. Activation of Macrophages by Lysophosphatidic Acid Through the Lysophosphatidic Acid Receptor 1 as a Novel Mechanism in Multiple Sclerosis Pathogenesis. *Mol Neurobiol* (2021) 58(2):470–82. doi: 10.1007/s12035-020-02130-x
65. Lin CI, Chen CN, Lin PW, Chang KJ, Hsieh FJ, Lee H. Lysophosphatidic Acid Regulates Inflammation-Related Genes in Human Endothelial Cells Through Lpa1 and Lpa3. *Biochem Biophys Res Commun* (2007) 363 (4):1001–8. doi: 10.1016/j.bbrc.2007.09.081
66. Zhao J, He D, Su Y, Berdyshev E, Chun J, Natarajan V, et al. Lysophosphatidic Acid Receptor 1 Modulates Lipopolysaccharide-Induced Inflammation in Alveolar Epithelial Cells and Murine Lungs. *Am J Physiol Lung Cell Mol Physiol* (2011) 301(4):L547–56. doi: 10.1152/ajplung.00058.2011
67. Paradowska-Gorycka A, Stypinska B, Pawlik A, Malinowski D, Romanowska-Prochnicka K, Manczak M, et al. Kdr (Vegfr2) Genetic Variants and Serum Levels in Patients With Rheumatoid Arthritis. *Biomolecules* (2019) 9(8):355. doi: 10.3390/biom9080355

68. Khan HA, Margulies CE. The Role of Mammalian Creb3-Like Transcription Factors in Response to Nutrients. *Front Genet* (2019) 10:591. doi: 10.3389/fgene.2019.00591
69. Li YH, Tardif G, Hum D, Kapoor M, Fahmi H, Pelletier JP, et al. The Unfolded Protein Response Genes in Human Osteoarthritic Chondrocytes: Perk Emerges as a Potential Therapeutic Target. *Arthritis Res Ther* (2016) 18:172. doi: 10.1186/s13075-016-1070-6
70. de Menezes JP, Saraiva EM, da Rocha-Azevedo B. The Site of the Bite: Leishmania Interaction With Macrophages, Neutrophils and the Extracellular Matrix in the Dermis. *Parasites Vectors* (2016) 9(1):264. doi: 10.1186/s13071-016-1540-3
71. Weinkopff T, Konradt C, Christian DA, Discher DE, Hunter CA, Scott P. Leishmania Major Infection-Induced Vegf-A/Vegfr-2 Signaling Promotes Lymphangiogenesis That Controls Disease. *J Immunol* (2016) 197(5):1823–31. doi: 10.4049/jimmunol.1600717
72. Barcena ML, Niehues MH, Christiansen C, Estepa M, Haritonow N, Sadighi AH, et al. Male Macrophages and Fibroblasts From C57/Bl6j Mice Are More Susceptible to Inflammatory Stimuli. *Front Immunol* (2021) 12:758767 (4714). doi: 10.3389/fimmu.2021.758767
73. Dworatzek E, Mahmoodzadeh S, Schriever C, Kusumoto K, Kramer L, Santos G, et al. Sex-Specific Regulation of Collagen I and Iii Expression by 17beta-Estradiol in Cardiac Fibroblasts: Role of Estrogen Receptors. *Cardiovasc Res* (2019) 115(2):315–27. doi: 10.1093/cvr/cvy185
74. Sieveking DP, Lim P, Chow RW, Dunn LL, Bao S, McGrath KC, et al. A Sex-Specific Role for Androgens in Angiogenesis. *J Exp Med* (2010) 207(2):345–52. doi: 10.1084/jem.20091924
75. Jaillon S, Berthenet K, Garlanda C. Sexual Dimorphism in Innate Immunity. *Clin Rev Allergy Immunol* (2019) 56(3):308–21. doi: 10.1007/s12016-017-8648-x
76. Lotter H, Altfeld M. Sex Differences in Immunity. *Semin Immunopathol* (2019) 41(2):133–5. doi: 10.1007/s00281-018-00728-x
77. Guo H, Konig R, Deng M, Riess M, Mo J, Zhang L, et al. Nlrx1 Sequesters Sting to Negatively Regulate the Interferon Response, Thereby Facilitating the Replication of Hiv-1 and DNA Viruses. *Cell Host Microbe* (2016) 19 (4):515–28. doi: 10.1016/j.chom.2016.03.001
78. Luo X, Donnelly CR, Gong W, Heath BR, Hao Y, Donnelly LA, et al. Hpv16 Drives Cancer Immune Escape *Via* Nlrx1-Mediated Degradation of Sting. *J Clin Invest* (2020) 130(4):1635–52. doi: 10.1172/JCI129497
79. Feng H, Lenarcic EM, Yamane D, Wauthier E, Mo J, Guo H, et al. Nlrx1 Promotes Immediate Irf1-Directed Antiviral Responses by Limiting Dsrna-Activated Translational Inhibition Mediated by Pkr. *Nat Immunol* (2017) 18 (12):1299–309. doi: 10.1038/ni.3853
80. Lei Y, Wen H, Ting JP. The Nlr Protein, Nlrx1, and Its Partner, Tufm, Reduce Type I Interferon, and Enhance Autophagy. *Autophagy* (2013) 9 (3):432–3. doi: 10.4161/auto.23026
81. Chu X, Wu S, Raju R. Nlrx1 Regulation Following Acute Mitochondrial Injury. *Front Immunol* (2019) 10:2431. doi: 10.3389/fimmu.2019.02431
82. Zhou H, Zhu P, Wang J, Zhu H, Ren J, Chen Y. Pathogenesis of Cardiac Ischemia Reperfusion Injury Is Associated With Ck2alpha-Disturbed Mitochondrial Homeostasis *Via* Suppression of Fundc1-Related Mitophagy. *Cell Death Differ* (2018) 25(6):1080–93. doi: 10.1038/s41418-018-0086-7
83. Schatz V, Neubert P, Rieger F, Jantsch J. Hypoxia, Hypoxia-Inducible Factor-1alpha, and Innate Antileishmanial Immune Responses. *Front Immunol* (2018) 9:216. doi: 10.3389/fimmu.2018.00216
84. Hartley MA, Eren RO, Rossi M, Prevel F, Castiglioni P, Isorce N, et al. Leishmania Guyanensis Parasites Block the Activation of the Inflammasome by Inhibiting Maturation of Il-1beta. *Microb Cell* (2018) 5(3):137–49. doi: 10.15698/mic2018.03.619
85. Arnoult D, Soares F, Tattoli I, Girardin SE. Mitochondria in Innate Immunity. *EMBO Rep* (2011) 12(9):901–10. doi: 10.1038/embor.2011.157
86. Chou WC, Rampanelli E, Li X, Ting JP. Impact of Intracellular Innate Immune Receptors on Immunometabolism. *Cell Mol Immunol* (2021) 19 (3):337–51. doi: 10.1038/s41423-021-00780-y
87. Fekete T, Bencze D, Biro E, Benko S, Pazmandi K. Focusing on the Cell Type Specific Regulatory Actions of Nlrx1. *Int J Mol Sci* (2021) 22(3):1316. doi: 10.3390/ijms22031316
88. Bichiou H, Bouabid C, Rabhi I, Guizani-Tabbane L. Transcription Factors Interplay Orchestrates the Immune-Metabolic Response of Leishmania Infected Macrophages. *Front Cell Infect Microbiol* (2021) 11:660415. doi: 10.3389/fcimb.2021.660415
89. Moreira D, Rodrigues V, Abengozar M, Rivas L, Rial E, Laforge M, et al. Leishmania Infantum Modulates Host Macrophage Mitochondrial Metabolism by Hijacking the Sirt1-Ampk Axis. *PloS Pathog* (2015) 11(3): e1004684. doi: 10.1371/journal.ppat.1004684
90. Souza C, Barbosa CD, Coelho H, Santos Junior MN, Barbosa EN, Queiroz EC, et al. Effects of 17beta-Estradiol on Monocyte/Macrophage Response to Staphylococcus Aureus: An *in Vitro* Study. *Front Cell Infect Microbiol* (2021) 11:701391. doi: 10.3389/fcimb.2021.701391
91. Trenti A, Tedesco S, Boscaro C, Trevisi L, Bolego C, Cignarella A. Estrogen, Angiogenesis, Immunity and Cell Metabolism: Solving the Puzzle. *Int J Mol Sci* (2018) 19(3):859. doi: 10.3390/ijms19030859
92. Rzepecki AK, Murase JE, Juran R, Fabi SG, McLellan BN. Estrogen-Deficient Skin: The Role of Topical Therapy. *Int J Womens Dermatol* (2019) 5(2):85–90. doi: 10.1016/j.ijwd.2019.01.001
93. Brinton RD. Estrogen Regulation of Glucose Metabolism and Mitochondrial Function: Therapeutic Implications for Prevention of Alzheimer's Disease. *Adv Drug Delivery Rev* (2008) 60(13-14):1504–11. doi: 10.1016/j.addr.2008.06.003
94. Cai Q, Lin T, Kamarajugadda S, Lu J. Regulation of Glycolysis and the Warburg Effect by Estrogen-Related Receptors. *Oncogene* (2013) 32 (16):2079–86. doi: 10.1038/onc.2012.221
95. Song J, Guan M, Zhao Z, Zhang J. Type I Interferons Function as Autocrine and Paracrine Factors to Induce Autotaxin in Response to Tlr Activation. *PloS One* (2015) 10(8):e0136629. doi: 10.1371/journal.pone.0136629
96. O'Brien MS, Philpott HTA, McDougall JJ. Targeting the Nav1.8 Ion Channel Engenders Sex-Specific Responses in Lysophosphatidic Acid-Induced Joint Neuropathy. *Pain* (2019) 160(1):269–78. doi: 10.1097/j.pain.0000000000001399
97. Lu P, Hontecillas R, Abedi V, Kale S, Leber A, Heltzel C, et al. Modeling-Enabled Characterization of Novel Nlrx1 Ligands. *PloS One* (2015) 10(12): e0145420. doi: 10.1371/journal.pone.0145420
98. Ackerman SJ, Park GY, Christman JW, Nyenhuis S, Berdyshev E, Natarajan V. Polyunsaturated Lysophosphatidic Acid as a Potential Asthma Biomarker. *biomark Med* (2016) 10(2):123–35. doi: 10.2217/bmm.15.93
99. Knowlden S, Georas SN. The Autotaxin-Lpa Axis Emerges as a Novel Regulator of Lymphocyte Homing and Inflammation. *J Immunol* (2014) 192 (3):851–7. doi: 10.4049/jimmunol.1302831
100. Cardoso FO, Zaverucha-do-Valle T, Almeida-Souza F, Abreu-Silva AL, Calabrese KDS. Modulation of Cytokines and Extracellular Matrix Proteins Expression by Leishmania Amazonensis in Susceptible and Resistant Mice. *Front Microbiol* (2020) 11:1986. doi: 10.3389/fmicb.2020.01986
101. Bowlin A, Roys H, Wanjala H, Bettadapura M, Venugopal G, Surma J, et al. Hypoxia-Inducible Factor Signaling in Macrophages Promotes Lymphangiogenesis in Leishmania Major Infection. *Infect Immun* (2021) 89(8):e0012421. doi: 10.1128/IAI.00124-21
102. Weinkopff T, Roys H, Bowlin A, Scott P. Leishmania Infection Induces Macrophage Vascular Endothelial Growth Factor a Production in an Arnt/Hif-Dependent Manner. *Infect Immun* (2019) 87(11):e00088–19. doi: 10.1128/IAI.00088-19
103. Xu H, Ji L, Yu C, Chen Q, Ge Q, Lu Y. Mir-423-5p Regulates Cells Apoptosis and Extracellular Matrix Degradation *Via* Nucleotide-Binding, Leucine-Rich Repeat Containing X1 (Nlrx1) in Interleukin 1 Beta (Il-1beta)-Induced Human Nucleus Pulposus Cells. *Med Sci Monit* (2020) 26:e922497. doi: 10.12659/MSM.922497
104. Tattoli I, Killackey SA, Foerster EG, Molinaro R, Maisonneuve C, Rahman MA, et al. Nlrx1 Acts as an Epithelial-Intrinsic Tumor Suppressor Through the Modulation of Tnf-Mediated Proliferation. *Cell Rep* (2016) 14(11):2576–86. doi: 10.1016/j.celrep.2016.02.065
105. Arnold AP. Promoting the Understanding of Sex Differences to Enhance Equity and Excellence in Biomedical Science. *Biol Sex Differ* (2010) 1(1):1. doi: 10.1186/2042-6410-1-1
106. Morrow EH. The Evolution of Sex Differences in Disease. *Biol Sex Differ* (2015) 6:5. doi: 10.1186/s13293-015-0023-0
107. Guo H, Wang Q, Ghneim K, Wang L, Rampanelli E, Holley-Guthrie E, et al. Multi-Omics Analyses Reveal That Hiv-1 Alters Cd4(+) T Cell Immunometabolism to Fuel Virus Replication. *Nat Immunol* (2021) 22 (4):423–33. doi: 10.1038/s41590-021-00898-1

108. Hu B, Ding GY, Fu PY, Zhu XD, Ji Y, Shi GM, et al. Nod-Like Receptor X1 Functions as a Tumor Suppressor by Inhibiting Epithelial-Mesenchymal Transition and Inducing Aging in Hepatocellular Carcinoma Cells. *J Hematol Oncol* (2018) 11(1):28. doi: 10.1186/s13045-018-0573-9
109. Fan Z, Pan J, Wang H, Zhang Y. Nod-Like Receptor X1, Tumor Necrosis Factor Receptor-Associated Factor 6 and Nf-Kappab Are Associated With Clinicopathological Characteristics in Gastric Cancer. *Exp Ther Med* (2021) 21(3):208. doi: 10.3892/etm.2021.9640
110. Kang MJ, Yoon CM, Kim BH, Lee CM, Zhou Y, Sauler M, et al. Suppression of Nlrx1 in Chronic Obstructive Pulmonary Disease. *J Clin Invest* (2015) 125 (6):2458–62. doi: 10.1172/JCI71747
111. Zysman M, Raherison-Semjen C. Women's Copd. *Front Med (Lausanne)* (2021) 8:600107. doi: 10.3389/fmed.2021.600107
112. Koo JH, Kim DH, Cha D, Kang MJ, Choi JM. Lrr Domain of Nlrx1 Protein Delivery by Dnp2 Inhibits T Cell Functions and Alleviates Autoimmune Encephalomyelitis. *Theranostics* (2020) 10(7):3138–50. doi: 10.7150/thno.43441
113. Koo JH, Kim SH, Jeon SH, Kang MJ, Choi JM. Macrophage-Preferable Delivery of the Leucine-Rich Repeat Domain of Nlrx1 Ameliorates Lethal Sepsis by Regulating Nf-Kappab and Inflammasome Signaling Activation. *Biomaterials* (2021) 274:120845. doi: 10.1016/j.biomaterials.2021.120845
114. Leber A, Hontecillas R, Zoccoli-Rodriguez V, Bienert C, Chauhan J, Bassaganya-Riera J. Activation of Nlrx1 by Nx-13 Alleviates Inflammatory Bowel Disease Through Immunometabolic Mechanisms in Cd4(+) T Cells. *J Immunol* (2019) 203(12):3407–15. doi: 10.4049/jimmunol.1900364

**Conflict of Interest:** The authors declare that the research was conducted in the absence of any commercial or financial relationships that could be construed as a potential conflict of interest.

frontiers | Frontiers in Immunology

TYPE Original Research
PUBLISHED 29 July 2022
DOI 10.3389/fimmu.2022.940095



OPEN ACCESS

EDITED BY
Michael V. Volin,
Midwestern University, United States

REVIEWED BY
Sadiq Umar,
University of Illinois at Chicago, United States
Suprabhat Mukherjee,
Kazi Nazrul University, India

*CORRESPONDENCE
A. Leslie Morrow
morrow@med.unc.edu

†Present Address:
Kimberly S. Williams,
Environmental and Health Sciences Program, Spelman College, Atlanta, GA, United States

SPECIALTY SECTION
This article was submitted to Inflammation, a section of the journal Frontiers in Immunology

RECEIVED 09 May 2022
ACCEPTED 07 July 2022
PUBLISHED 29 July 2022

CITATION
Balan I, Aurelian L, Williams KS, Campbell B, Meeker RB and Morrow AL (2022) Inhibition of human macrophage activation *via* pregnane neurosteroid interactions with toll-like receptors: Sex differences and structural requirements. *Front. Immunol.* 13:940095. doi: 10.3389/fimmu.2022.940095



# Inhibition of human macrophage activation *via* pregnane neurosteroid interactions with toll-like receptors: Sex differences and structural requirements

Irina Balan[1], Laure Aurelian[2], Kimberly S. Williams[3†], Brian Campbell[4], Rick B. Meeker[3] and A. Leslie Morrow[1*]

[1]Department of Psychiatry, Department of Pharmacology, Bowles Center for Alcohol Studies, University of North Carolina at Chapel Hill, School of Medicine, Chapel Hill, NC, United States, [2]Stanford University School of Medicine, Stanford, CA, United States, [3]Department of Neurology, University of North Carolina at Chapel Hill, School of Medicine, Chapel Hill, NC, United States, [4]Translational Sciences, Sage Therapeutics Inc., Cambridge, MA, United States

We recently discovered that (3α,5α)3-hydroxypregnan-20-one (allopregnanolone) inhibits pro-inflammatory toll-like receptor (TLR) activation and cytokine/chemokine production in mouse macrophage RAW264.7 cells. The present studies evaluate neurosteroid actions upon TLR activation in human macrophages from male and female healthy donors. Buffy coat leukocytes were obtained from donors at the New York Blood Center (http://nybloodcenter.org/), and peripheral blood mononuclear cells were isolated and cultured to achieve macrophage differentiation. TLR4 and TLR7 were activated by lipopolysaccharide (LPS) or imiquimod in the presence/absence of allopregnanolone or related neurosteroids and pro-inflammatory markers were detected by ELISA or western blotting. Cultured human monocyte-derived-macrophages exhibited typical morphology, a mixed immune profile of both inflammatory and anti-inflammatory markers, with no sex difference at baseline. Allopregnanolone inhibited TLR4 activation in male and female donors, preventing LPS-induced elevations of TNF-α, MCP-1, pCREB and pSTAT1. In contrast, 3α,5α-THDOC and SGE-516 inhibited the TLR4 pathway activation in female, but not male donors. Allopregnanolone completely inhibited TLR7 activation by imiquimod, blocking IL-1-β, IL-6, pSTAT1 and pIRF7 elevations in females only. 3α,5α-THDOC and SGE-516 partially inhibited TLR7 activation, only in female donors. The results indicate that allopregnanolone inhibits TLR4 and TLR7 activation in cultured human macrophages resulting in diminished cytokine/chemokine production. Allopregnanolone inhibition of TLR4 activation was found in males and females, but inhibition of TLR7 signals exhibited specificity for female donors. 3α,5α-THDOC and SGE-516 inhibited TLR4 and TLR7 pathways only in females. These studies demonstrate anti-inflammatory effects of allopregnanolone in

human macrophages for the first time and suggest that inhibition of pro-inflammatory cytokines/chemokines may contribute to its therapeutic actions.

KEYWORDS

allopregnanolone (3α, 5α-THP), SGE-516, cytokines, chemokine, neurosteroid (3α, 5α)-3 21-dihydroxypregnan-20-one (3α, 5α-THDOC)

# 1 Introduction

Inflammation is associated with the pathogenesis of numerous systemic, neurodegenerative and psychiatric diseases (1–3). Furthermore, inflammation may arise from bacterial and fungal infections (4–7), leading to long-lasting complications of infectious disease, such as long COVID-19 or sepsis (8, 9). The contribution of mononuclear phagocytes (macrophages/microglia) to inflammatory and neuroinflammatory diseases is well documented (10–13), but so too are many pro-survival and repair actions that favor survival and recovery. While strong immune suppressants have been available for decades (14), progress in the development of agents that provide control of specific macrophage functions (specifically inflammation) have lagged behind. The ability to regulate macrophage functions with greater precision is necessary to facilitate efforts to suppress deleterious inflammation while retaining supportive functions.

Toll-like receptors (TLRs) play an important role in various activities of macrophages (15). TLRs belong to a family of pattern recognition receptors that can recognize and respond to molecular signatures referred to as pathogen-associated molecular patterns (PAMPs) and danger-associated molecular patterns (DAMPs) (16). At least 10 human TLRs have been identified (17). TLRs share common structural domains, which define their ability to recruit the adaptor proteins that regulate signaling. Recognition of PAMPs and DAMPs by TLRs initiate signaling pathways that involve phosphorylation (activation) of transcription factors, their translocation to the nucleus and culminate in the production of inflammatory cytokines such as tumor necrosis factor alpha (TNF-α), interleukins 1 and 6 (IL-1; IL-6) and chemokines such as monocyte chemoattractant protein-1 (MCP-1) (5, 15, 18–21). Excessive TLR activation contributes to the development of many inflammatory and neuroinflammatory diseases, such as systemic lupus erythematosus, infection-associated sepsis, atherosclerosis, asthma (22), ischemia (23), depression (24, 25), alcohol use disorders (26, 27), traumatic brain injury (28), neurodegeneration (29, 30), and epilepsy (31, 32).

There is a growing appreciation for potential interactions between systemic immune activation and brain TLRs that facilitate detrimental inflammatory activity. Thus, blocking TLR signals may be useful to regulate overactive systemic and CNS responses (22). We recently discovered that endogenous neurosteroid (3α,5α)3-hydroxypregnan-20-one (allopregnanolone, 3α,5α-THP) inhibits myeloid differentiation primary response 88 (MyD88)-dependent TLR2, TLR4, and TLR7 (but not TIR-domain-containing adapter-inducing interferon-β dependent TLR3) pro-inflammatory signal activation and the production of cytokines/chemokines through its ability to block TLR-MyD88 binding in the mouse macrophage RAW264.7 cell line and the alcohol-preferring (P) rat brain (33, 34). Since inflammatory conditions are ubiquitous hallmarks of human disease (vide infra), it is essential to establish the validity of this work in human macrophages and to examine sex as a biological variable in the studies. Here, we examine the effect of allopregnanolone as well as the endogenous neurosteroid (3α,5α)-3,21-dihydroxypregnan-20-one (3α,5α-THDOC) and a synthetic analog of allopregnanolone, SGE-516, on cultured human monocyte-derived macrophages (hMDM), obtained from both male and female healthy donors.

Allopregnanolone and 3α,5α-THDOC display minimal activity at nuclear genomic receptors (35), but are potent positive modulators of γ-aminobutyric acid type A ($GABA_A$) receptors (36–38). They have anesthetic, anticonvulsant, sedative, and anxiolytic effects (39), and modulate the hypothalamic pituitary adrenal axis to reduce stress activation (40). Significantly, allopregnanolone and/or its precursors progesterone and pregnenolone, were shown to be effective in clinical studies of schizophrenia (41) and cocaine craving (42). A proprietary formulation of allopregnanolone, Brexanolone i.v., is a fast-and long-acting antidepressant and the only FDA specifically approved treatment for post-partum depression (43–45). Further, allopregnanolone has putative therapeutic activity in animal models of alcoholism (46–48), traumatic brain injury (49, 50), multiple sclerosis (51, 52), and Alzheimer's disease (53). The synthetic compound SGE-516, a 1,2,5-triazole analog of allopregnanolone, was reported to display better aqueous solubility while maintaining efficacy as an allosteric modulator at $GABA_A$ receptors (54). SGE-516 has been reported to exhibit anticonvulsant activity as demonstrated in experimental seizure and epilepsy animal models (55–57). In addition, SGE-516 has recently been shown to protect mice from chronic stress-induced behavioral deficits including restoration

of theta power ratios indicative of normalized network activity in brain (58).

Many effects of neurosteroids have been attributed to actions at $GABA_A$ receptors. Here, however, we demonstrate unique inhibitory effects of allopregnanolone on the modulation of pro-inflammatory MyD88-dependent TLR4 and TLR7 signaling pathways in hMDMs resulting in diminished cytokine production. Inhibition of TLR4 pathways was observed in males and females, however inhibition of TLR7 pathways was only observed in hMDM from female subjects. We further observed the structural specificity of allopregnanolone in the inhibition of these signals, suggesting that D ring modifications may be detrimental to the anti-inflammatory efficacy of this class of compounds in both males and females.

# 2 Materials and methods

## 2.1 Culture of hMDMs

Human buffy coat leukocytes were obtained from healthy donors at the New York Blood Center (http://nybloodcenter.org/), a non-profit organization for the collection and distribution of blood for clinical and research purposes. No personal identifiers were sent with the shipment. The NY Blood Center maintains IRB approval for their blood collection procedures and UNC School of Medicine issued an IRB waiver for this work since no personal identifiers were made available to investigators.

Culture of hMDM was as previously described (59–61) with minor modifications. Blood was diluted 2:1 with phosphate buffered saline (PBS), layered on top of Ficoll-Paque (GE Healthcare 17-1440-03), and centrifuged at 500 X g for 20 min. The peripheral blood mononuclear cells (PBMCs) were collected from the PBS/Ficoll-Paque interface and transferred to a tube containing PBS to a total volume of 40 ml. The resulting PBMCs were incubated in red blood cell lysis buffer (Sigma R7757, CSH protocols) to remove any red blood cell contamination. PBS was added to a volume of 40 ml, the PBMCs were re-suspended and centrifuged at 150 X g for 20 min. The wash step was repeated once and the final pellet was re-suspended in Dulbecco's modified Eagle medium (DMEM) with high glucose, 10% fetal bovine serum (FBS, Gibco 160000-044) and 20 µg/ml gentamicin (Gibco 15750-60). Cells were counted and aliquoted into low adhesion 6 well plates (Corning 3471) at a density of approximately $10^6$ cells/$cm^2$. Media was changed 2-3 times weekly to maintain optimal cell heath. Cells were cultured for 5-7 days to allow monocyte attachment, then remaining white blood cells were then washed from the plate, yielding a pure macrophage culture. To minimize any differentiation bias, the adherent cells were grown in complete DMEM without colony stimulating factor (CSF) supplements for one to two weeks to achieve 70-80% coverage of the plate, indicative of macrophage differentiation. Previous studies indicated that the macrophages can secrete significant amounts of both M-CSF and/or GM-CSF to support their own growth (59) although basal GM-CSF is typically very low.

## 2.2 Immune protein profile of macrophage conditioned medium

Basal characteristics of hMDM cultured under the above conditions were determined in the initial establishment of the culture protocol. Medium was collected and centrifuged at 1000 X g for 5 min to remove any floating cells or debris in the medium. The cell free medium was added to a RayBiotech human antibody array L-507 (RayBiotech Life, Inc., Peachtree, GA) and processed according to the human antibody array protocol. Slide arrays were scanned using an Agilent technologies DNA microarray scanner and the analysis was carried out using MetaMorph® software. A representative example of results from the analysis of the hMDM secretome on the RayBiotech L-507 cytokine array is shown in the Supplementary Material (Figure S1). Internal negative controls were used to establish basal fluorescence and variation across the array. The minimum threshold for a positive fluorescence signal was set at 2.57 standard deviation units above the average background to give a probability of 0.005 that a protein signal would be identified as positive by chance. The linearity of signal detection was verified from internal positive standards. Since signal intensity varied between different arrays, protein expression was normalized to the total fluorescent signal for all proteins on the array. A relative fluorescence value increase of 6500 represented the $p<0.005$ cutoff compared to negative controls, providing a moderately stringent index for proteins to be considered as actively secreted.

## 2.3 Flow cytometry

Flow cytometry of hMDM at baseline was performed as previously described (60, 61). The hMDM were removed from low adhesion wells in ice cold, calcium-free HBSS and centrifuged for 5 min at 450 x g. Cellular pellets were re-suspended and fixed in a Fluorfix solution (Biolegend 420801) for 20 min at room temperature. Fixed cells were then treated with permeabilization buffer (EBioscience 020-8333-56) and centrifuged for 5 min at 450 x g at 4° C. The wash step was repeated followed by re-suspension in 100 µl of permeabilization buffer plus 5 µl antibody (CD 206 Biolegend 321114; 5 µl CD16 Biolegend 302008 and 5 µl CD163 Biolegend 333607, CD14, Biolegend 301817; CD80, Biolegend 305207; CD86 Biolegend 305420; CD192 Biolegend 335303; CD197 Biolegend 353203, 353205) at room temperature for 20 min. The stained cells were washed three times in cell staining buffer (Biolegend 420201). Flow cytometry was performed on a FACS Calibur (Becton

Dickinson, San Jose, CA) using direct immunofluorescence with at least 10,000 events. All cells were gated to remove debris. Three color staining analysis was utilized. Cells were analyzed according to side scatter and receptor bound fluorescence, and data was collected with logarithmic amplifiers. Fluorescence spillover compensation was estimated using single-stained and unstained samples with the Cell Quest software (BD). After collection, data was further analyzed with FlowJo software (TreeStar Inc., Ashland, OR).

## 2.4 Cell treatment

The selective agonists for TLR4 [lipopolysaccharide (LPS); 1 μg/ml] (Cat. #L9641, Lot # 071M4120V, Sigma-Aldrich, Saint Louis, MO, USA), and TLR7 [imiquimod (IMQ); 30 μg/ml] (Cat. #tlrl-imqs, *In vivo*Gen, San Diego, CA, USA) were added to the cultures alone, or together with allopregnanolone (1.0 μM) or 3α,5α-THDOC (1.0 μM) or SGE-516 (1.0 μM) in DMEM (without FBS and antibiotics) 24 h before cell collection. Synthetized allopregnanolone and 3α,5α-THDOC were gifts from Dr. Purdy (62, 63) and SGE-516 was a gift from Sage Therapeutics (54). The ligand and neurosteroid concentrations were selected based on previous findings of maximal effects (33, 34). The effects of the neurosteroids on cells that were not treated with the TLR agonists were studied in parallel.

## 2.5 Protein extraction for immunoblotting and ELISA

Protein extraction and assay were as previously described (33, 34, 64, 65). Cells were lysed with radioimmunoprecipitation (RIPA) buffer (Sigma, Cat. # R0278) supplemented with protease and phosphatase inhibitor cocktails (Sigma, Cat. # P8340 and P0044, respectively). The lysates were sonicated twice for 30 seconds at 25% output power with a Sonicator ultrasonic processor (Misonix, Inc., Farmingdale, NY) and centrifuged (14,000 g; 4°C) for 30 min. Total protein levels were determined by the bicinchoninic acid assay (BCA, Thermo Fisher Scientific, Waltham, MA, USA, Cat.# 23228 and Cat.# 1859078).

## 2.6 Immunoblotting

The proteins (50 μg/lane) were denatured at 95°C (5 min) in 4x Laemmli denaturing buffer (Bio-Rad, Cat. # 1610747) with 10% β-mercaptoethanol and resolved by SDS-polyacrylamide gel (SDS-PAGE) electrophoresis as previously described (33, 34). Briefly, the 10% separation gels (16x18cm) and 3% stacking gels were freshly prepared from acrylamide/bisacrylamide (ratio 29:1) stock solution (Bio-Rad, Cat. # 161-0156) and were polymerized by the addition of 0.025% tetramethylethylenediamine (TEMED; BioRad, Cat. # 1610800EDU) and ammonium persulphate (Bio-Rad, Cat. # 7727540). Electrophoresis was carried out with a current of 25 mA per gel for 4-5 hours. Electrophoretically separated samples were transferred to a polyvinylidene difluoride membrane (PVDF; Bio-Rad Cat. #1620177). Blots were blocked for 2 hrs at room temperature (RT) with 5% blotting-grade blocker (Bio-Rad, Cat. # 1706404) or 5% bovine serum albumin (for phosphorylated primary antibodies) and exposed to primary antibodies overnight (4°C), followed by horseradish peroxidase-labeled secondary antibodies (1 hr, RT). Primary and secondary antibodies were diluted with 5% blotting-grade blocker buffer or 5% BSA (for phosphorylated primary antibodies). Tris-buffered saline with 0.05% Tween-20 (TNT) was used to wash the blots 3 times (10 min each) after incubation with primary and secondary antibodies. Immunoreactive bands were visualized with the PlusECL kit reagents (Perkin Elmer, Waltham, MA, USA, Cat.# NEL105001EA) followed by detection with enhanced chemiluminescence (ImageQuant LAS4000, GE Healthcare, Amersham, UK). Densitometric analysis was conducted using ImageQuant TL v8.1.0.0. Each densitometric measurement was divided by the corresponding β-actin densitometric measurement and the results are expressed as the mean β-actin adjusted densitometric units ± SEM. The primary antibodies, their clonality, host species, dilution and supplier are listed in SM (Table S1). All antibodies were validated by the supplier and by us, as previously described (33, 34, 64, 65). Specific protein detection used full length gels (33, 34, 64, 65). Horseradish peroxidase-labeled secondary antibodies were anti-rabbit (Cat. # 7074, RRID: AB_2099233, Cell Signaling Technology), anti-mouse (Cat# 7076, RRID: AB_330924, Cell Signaling Technology) and anti-goat IgG (Cat# A24452, RRID: AB_2535921, Thermo Fisher Scientific, Waltham, MA, USA).

## 2.7 ELISA

Protein extracts were assayed with ELISA kits (Raybiotech, Norcross, GA, USA) for MCP-1 (Cat. # ELH-MCP1-1), TNF-α (Cat. # ELH-TNFa-CL-1), IL-6 (Cat. # ELH-IL6-CL-1), IL-1β (Cat. # ELH-IL1b-1), IFN-γ (Cat. # ELH-IFNg-CL-1), IL-1ra (Cat. # ELH-IL1ra-CL-1), IL-13 (Cat. # ELH-IL13-1), and TGF-β1 (Cat. # ELH-TGFb1-1) as per the manufacturer's instructions. Results are expressed as picograms/milligram total protein (pg/mg).

## 2.8 Statistics

Two-way analysis of variance (ANOVA) followed by Tukey's *post-hoc* test (GraphPad Prism 8.3.1.) was used for the statistical analysis of hMDM cells treated with TLR agonists with/without the neurosteroids. hMDM cultures (n ≥ 12/group)

were obtained from 3-5 donors per group. Results are from a total of 27 donors, 11 females and 16 males. P<0.05 was considered statistically significant.

# 3 Results

## 3.1 Characteristics of hMDM

The hMDM represent a typical macrophage morphology (Figure 1A) as previously described (66). Based on specific expression of cellular surface markers and the secretion of certain cytokines, macrophages can be classified into classically activated, pro-inflammatory macrophages (67–69), and alternatively activated, anti-inflammatory macrophages (68–70). Surface expression of CD14 and CD16 are used to distinguish classical, intermediate, and nonclassical macrophage subsets (71, 72). The basal hMDM secretome was assessed by RayBiotech human antibody array L-507 (Figure 1B) and illustrates a mixed profile of the pro-inflammatory (TNF-α, IL-6, IFN-γ), and anti-inflammatory (IL-13, TGF-β1, IL-1ra) mediators (13, 68, 69), in the baseline state. To determine potential sex differences at baseline, hMDM cell lysates obtained from female and male donors were analyzed by ELISA for both pro-inflammatory (TNF-α, IL-6, IL-1β, MCP-1, IFN-γ) and anti-inflammatory (IL-13, TGF-β1, IL-1ra) mediators, with no evidence of sex differences (Figure 1C). Surface markers determined by flow cytometry (Figure 1D) revealed basal expression of CD14 as well as a mix of markers sensitive to both M1 (CD80, CD86, CD68, CD197) or M2 (CD16, CD163, CD206) polarization and CCL2/MCP-1 chemotaxis (CD192/CCR2). Because previous studies indicate that rodent macrophages and human peripheral blood mononuclear cells express RNAs of some $GABA_A$ receptor subunits (73, 74) we examined $GABA_A$ receptor subunit α1, α2, α4, and δ protein expression at baseline or after treatments with lipopolysaccharide (LPS) and/or allopregnanolone in hMDM. $GABA_A$ receptor subunits investigated were undetectable at baseline or following treatment with LPS and/or allopregnanolone indicating that responses observed in the current studies were not related to GABAergic pharmacology (Figure 1E). Positive controls for $GABA_A$ receptor subunit expression are shown from the amygdala of male and female P rats intraperitoneally injected with vehicle (45% w/v 2-hydroxypropyl-β-cyclodextrin; 30 min) or allopregnanolone (15 mg/kg; 30 min) (33, 34).

The endogenous neurosteroids allopregnanolone and 3α,5α-THDOC are positive allosteric modulators of the $GABA_A$ receptors (36–38, 54) and have similar chemical structures at A, B, and C rings. 3α,5α-THDOC differs from the allopregnanolone by a C-21-hydroxyl group at the D-ring. SGE-516 is a synthetic neuroactive steroid that differs from the allopregnanolone by a C-3 cis-methyl and cis-hydrogens at C-5 and C-19 in the A-ring, and a C-21-1,2,5-triazole group at the D-ring (Figure 1F).

## 3.2 Inhibitory effects of allopregnanolone on the TLR4 signaling pathway in male and female hMDM

We have previously shown that allopregnanolone inhibits the activated TLR4 signaling pathway in the mouse macrophage RAW264.7 cell line and the P rat brain (33, 34). Pathway inhibition included blocking of the phosphorylation (activation) of canonical signaling members including cAMP-response element binding protein (CREB), nuclear factor kappa B (NF-kB) p65 and the resulting expression of inflammatory MCP-1, high mobility group box 1 (HMGB1) and TNF-α (33). hMDM were treated with LPS (1 μg/ml; 24h) in the absence or presence of allopregnanolone (1.0 μM), 3α,5α-THDOC (1.0 μM) or SGE-516 (1.0 μM). Cell lysates were assayed for established members of the activated TLR4 pathway, including activated (phosphorylated) pCREB, signal transducer and activator of transcription 1 (pSTAT1), the cytokine TNF-α, and chemokine MCP-1 (21, 33, 75, 76). The ligand and neurosteroid concentrations were selected based on previous findings of maximal effects (33, 34). The effects of allopregnanolone, 3α,5α-THDOC, and SGE-516 on cells that were not treated with the TLR4 agonist LPS were analogously studied.

LPS caused a significant increase in the levels of TNF-α [~70% in hMDM from both female ($F(1,51)=71.40$, $p<0.0001$) and male ($F(1,57)=102.5$, $p<0.0001$) donors] and MCP-1 [~65% in hMDM from both female donors ($F(1,75)=21.17$, $p<0.0001$) and male donors ($F(1,78)=154.8$, $p<0.0001$)], relative to vehicle control (Figures 2A, B). The increases of TNF-α were partially inhibited by allopregnanolone [~55% and ~35% inhibition in hMDM from female donors ($F(1,51)=9.064$, $p=0.0040$) (Figure 2A) and male donors ($F(1, 57)=8.004$, $p=0.0064$) (Figure 2B), respectively]. The LPS-induced elevation of TNF-α and the inhibitory effect of allopregnanolone on TNF-α were similar in hMDM derived from both male donors and female donors (Figure S2A). The increases of MCP-1 were completely inhibited by allopregnanolone in hMDM from female donors ($F(1,75)=5.039$, $p=0.0277$) (Figure 2A) and by ~40% in hMDM from male donors ($F(1,78)=5.094$, $p=0.0268$) (Figure 2B). The LPS-induced elevation of MCP-1 is higher and the inhibitory effect of 3α,5α-THP on MCP-1 is lesser in hMDM from male donors than female donors (Figure S2B). LPS and/or allopregnanolone did not affect TLR4 expression in hMDM from both male and female donors and there are no sex differences in the expression of TLR4 at baseline, after LPS and/or allopregnanolone treatments (Figure S3).

LPS activated the TLR4 pathways through increases in pCREB [~40% and ~60% in hMDM from female ($F(1,48)=20.77$, $p<0.0001$)

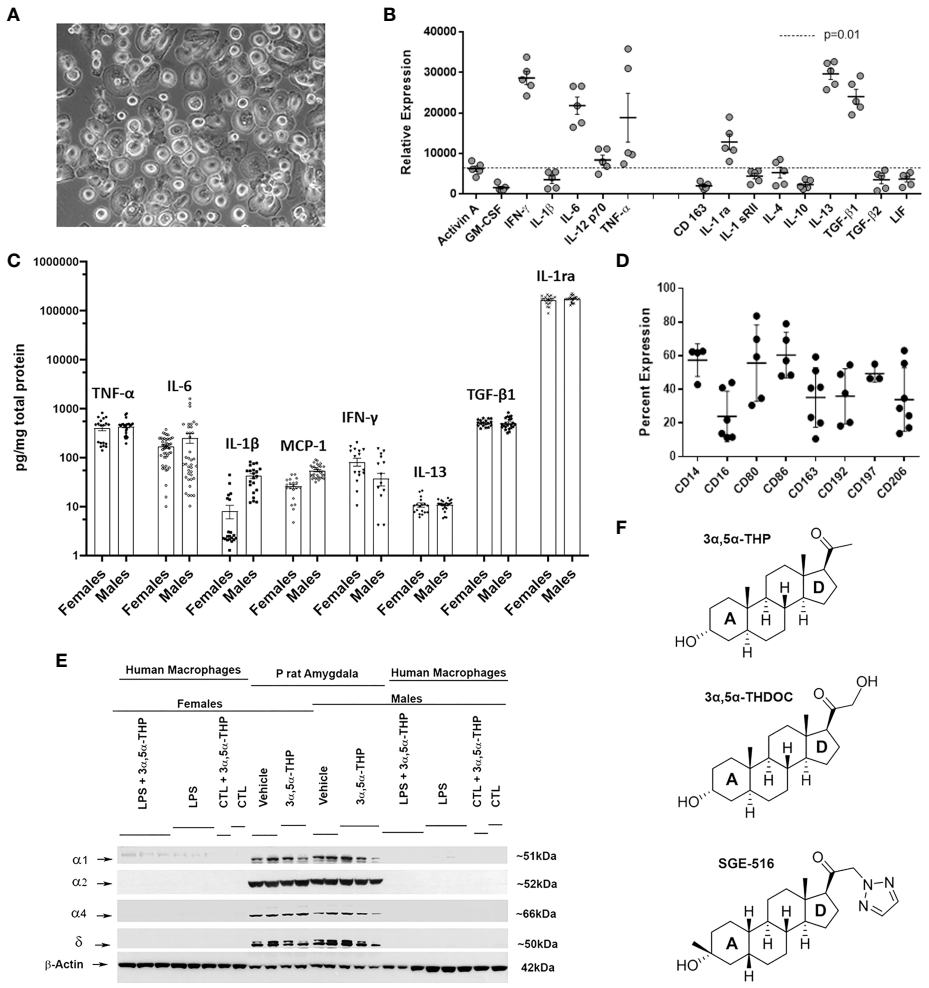


FIGURE 1
Characteristics of cultured human monocyte-derived macrophages. **(A)** Example of a monolayer of human monocyte-derived macrophages (hMDM) grown on ultralow adhesion plastic. **(B)** Basal hMDM secretome from 5 independent mixed sex cultures detected by RayBiotech human antibody array L-507 illustrating a mixed inflammatory and anti-inflammatory cytokine profile. **(C)** hMDM cell lysates analyzed by ELISA express both inflammatory (TNF-α, IL-6, IL-1β, MCP-1, IFN-γ) and anti-inflammatory (IL-13, TGF-β1, IL-1ra) mediators with no evidence of sex differences at baseline. Each hMDM culture is shown as a single symbol (n ≥ 18), obtained from at least 3 male or 3 female donors. **(D)** hMDM surface markers determined by flow cytometry using direct immunofluorescence in 4-7 independent mixed sex cultures. **(E)** Western blot image shows that hMDM from both male and female donors (n=9 cultures from 3 donors/sex) lack γ-aminobutyric acid type A ($GABA_A$) receptor subunits α1, α2, α4, and δ at baseline (CTL) or after treatments with lipopolysaccharide (LPS) and/or allopregnanolone (3α,5α-THP). As a positive control, the amygdala from male and female alcohol preferring P rats intraperitoneally injected with vehicle (45% w/v 2-hydroxypropyl-β-cyclodextrin; 30 min) or allopregnanolone (15 mg/kg; 30 min) was used. **(F)** Chemical structures of endogenous neurosteroids allopregnanolone and 3α,5α-THDOC (tetrahydrodeoxycorticosterone) and the synthetic 1,2,5-triazole analog of the allopregnanolone, SGE-516. 3α,5α-THDOC differs from the allopregnanolone by a C-21-hydroxyl group at the D-ring. SGE-516 differs from the allopregnanolone by a C-3 cis-methyl and cis-hydrogens at C-5 and C-19, and a C-21-1,2,5-triazole group at the D-ring.

and male (F(1,48)=10.62, p=0.0021) donors, respectively] and pSTAT1 [~60% in hMDM from both female (F(1,51)=81.58, p<0.0001) and male (F(1,49)=48.79, p<0.0001) donors] (Figure 3). No effects of LPS (p>0.05) on NF-kB p50 or NF-kB p65 were detected (Figure S4). The increases in pCREB were completely inhibited by allopregnanolone in hMDM from both female (F(1,48) =4.428, p=0.0406) (Figure 3A) and male (F(1,48)=4.665, p=0.0358) (Figure 3B) donors. The increases of pSTAT1 were partially inhibited by allopregnanolone [~35% and ~45% inhibition in hMDM from female (F(1,51)=4.193, p=0.0458) (Figure 3A) and male (F(1,49)=4.530, p=0.0384) (Figure 3B) donors, respectively]. Consistent with our previous studies (33), allopregnanolone did not change the levels of pCREB, pSTAT1, TNF-α or MCP-1 in hMDM that were not treated with the TLR4 agonist LPS, indicating that allopregnanolone specifically targets the activated TLR4 signal (Figures 2, 3).

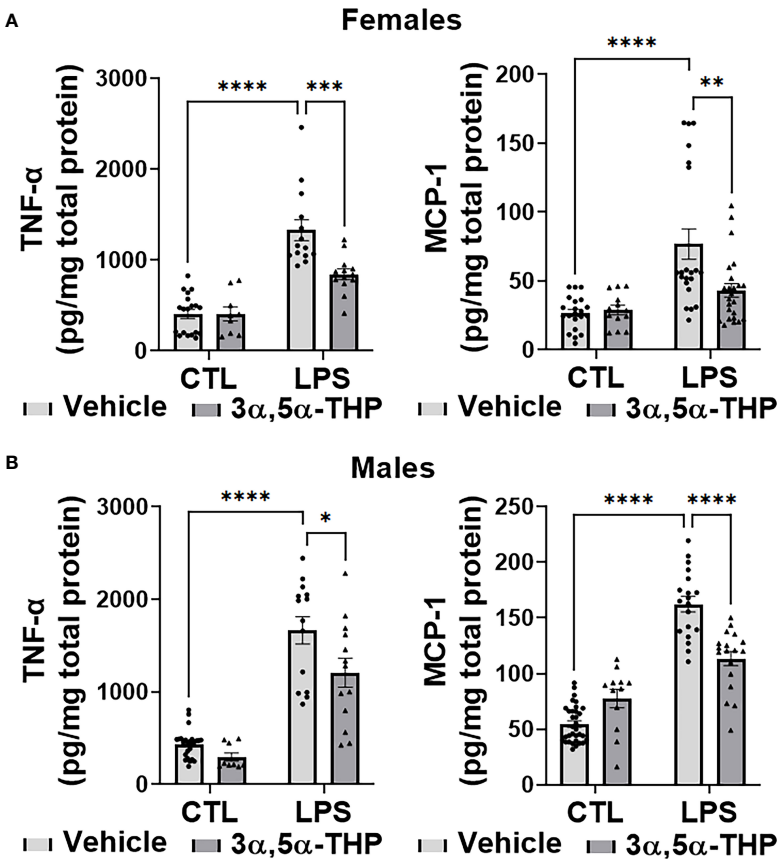


FIGURE 2
Allopregnanolone (3α,5α-THP) inhibits LPS-induced increases of inflammatory cytokine TNF-α and chemokine MCP-1 in human monocyte-derived macrophages (hMDM) from both female and male donors. Each hMDM culture (n ≥12 cultures from 3-5 female **(A)** or 3-5 male **(B)** donors/grp) is shown as a single symbol. Cells were treated with the TLR4 agonist lipopolysaccharide (LPS) (1 μg/ml; 24h) with or without allopregnanolone (1 μM; 24h). LPS caused a significant increase in the levels of TNF-α (~70% in hMDM from both female and male donors) and MCP-1 (~65% in hMDM from both female and male donors) relative to vehicle control (CTL). The increases of TNF-α were partially inhibited by allopregnanolone (~55% and ~35% inhibition in hMDM from female **(A)** and male **(B)** donors, respectively) (Two-way ANOVA, Tukey's *post hoc* test: *$p < 0.05$, ***$p < 0.001$, ****$p < 0.0001$). The increases of MCP-1 were completely inhibited by allopregnanolone in hMDM from female **(A)** and by ~40% in hMDM from male **(B)** donors (Two-way ANOVA, Tukey's *post hoc* test: **$p < 0.01$, ****$p < 0.0001$). Allopregnanolone did not change the levels of TNF-α and MCP-1 in hMDM that were not treated with the TLR4 agonist LPS ($p>0.05$).

## 3.3 3α,5α-THDOC and SGE-516 inhibition of TLR4 pathways in hMDM of female, but not male donors

LPS caused a significant increase in the levels of TNF-α [~80% in hMDM from both female ($F(1,63)=88.35$, $p<0.0001$ and $F(1,47)=132.7$, $p<0.0001$ for experiments with 3α,5α-THDOC and SGE-516, respectively) and male ($F(1,60)=131.3$, $p<0.0001$ and $F(1,40)=25.84$, $p<0.0001$ for experiments with 3α,5α-THDOC and SGE-516, respectively) donors] and MCP-1 [~65% in hMDM from both female ($F(1,86)=5.067$, $p=0.0269$ and $F(1,42)=13.20$, $p=0.0008$ for experiments with 3α,5α-THDOC and SGE-516, respectively) and male ($F(1,56)=6.714$, $p=0.0122$ and $F(1,55)=48.02$, $p<0.0001$ for experiments with 3α,5α-THDOC and SGE-516, respectively) donors] relative to vehicle control (Figures 4A, B). The increases of TNF-α were partially inhibited by 3α,5α-THDOC and SGE-516 [~30% and ~35% inhibition, respectively] in hMDM derived from female donors ($F(1,63)=7.132$, $p=0.0096$ and $F(1,47)=10.12$, $p=0.0026$ for experiments with 3α,5α-THDOC and SGE-516, respectively) (Figure 4A), but not male donors ($F(1,60)=0.6948$, $p=0.4078$ and $F(1,40)=0.09574$; $p=0.7586$ for experiments with 3α,5α-THDOC and SGE-516, respectively) (Figure 4B). The increases of MCP-1 were completely inhibited by 3α,5α-THDOC or SGE-516 in hMDM from female donors ($F(1,86)=3.981$, $p=0.0492$ and $F(1,42)=15.88$, $p=0.0003$ for experiments with 3α,5α-THDOC and SGE-516, respectively) (Figure 4A), but not male donors ($F(1,56)=0.9187$, $p=0.3419$ and $F(1,55)=0.02609$, $p=0.8723$ for experiments with 3α,5α-THDOC and SGE-516, respectively) (Figure 4B).

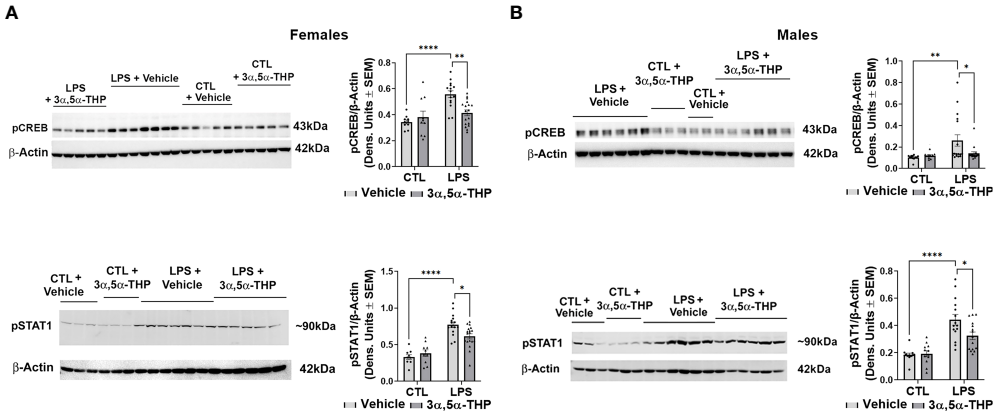


FIGURE 3
Allopregnanolone (3α,5α-THP) inhibits LPS-induced activation of MyD88-dependent TLR4 pro-inflammatory signal and does not target non-activated TLR4 signal in human monocyte-derived macrophages (hMDM) from both female and male donors. hMDM cultures were treated with LPS (1 μg/ml; 24 h) with or without allopregnanolone (1 μM; 24 h). Representative western blot images and summary data of densitometric scatter dot plots show the levels of pCREB and pSTAT1 in females **(A)** and males **(B)**. Each data point represents an individual hMDM culture (n≥12 cultures from 3 female **(A)** or 3 male **(B)** donors/grp). β-Actin was used as protein loading control. LPS caused a significant increase in the levels of pCREB (~40% and ~60% in MDM from female **(A)** and male **(B)** donors, respectively) and pSTAT1 (~60% in hMDM from both female **(A)** and male **(B)** donors) relative to vehicle control (CTL). The increases of pCREB were completely inhibited by allopregnanolone in hMDM from both female **(A)** and male **(B)** donors. The increases of pSTAT1 were partially inhibited by allopregnanolone (~35% and ~45% inhibition in hMDM from female **(A)** and male **(B)** donors, respectively). Allopregnanolone did not change the levels of pCREB and pSTAT1 in hMDM that were not treated with the TLR4 agonist LPS (A, B), indicating that allopregnanolone specifically targets the activated TLR4 signal. Two-way ANOVA, Tukey's *post hoc* test: *p < 0.05, **p < 0.01, ****p < 0.0001.

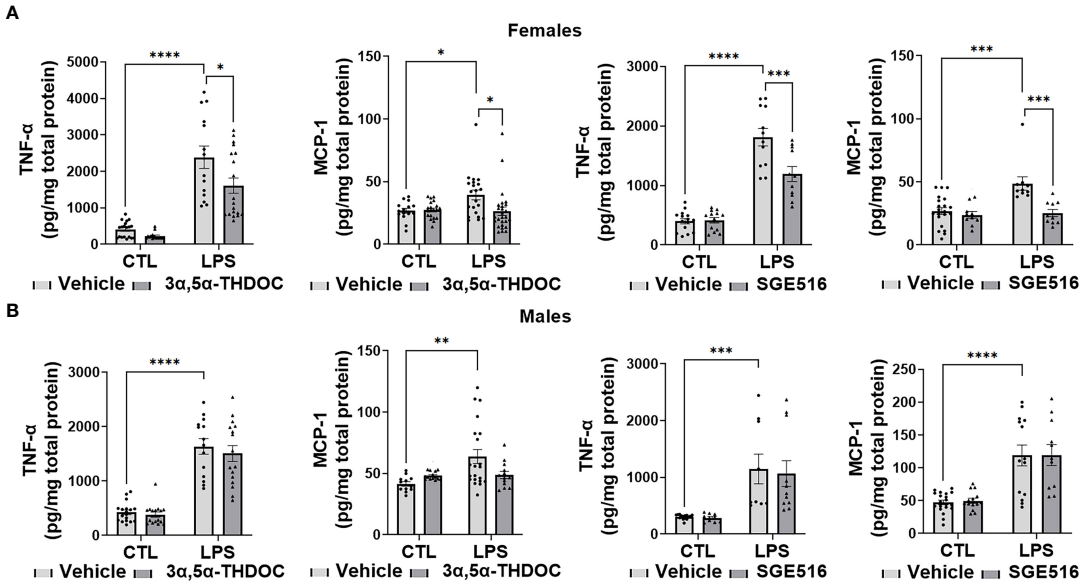


FIGURE 4
3α,5α-THDOC and SGE-516 inhibit LPS-induced increases of TNF-α and MCP-1 in human monocyte-derived macrophages (hMDM) from female, but not male donors. Each hMDM culture (n≥12 from 3 female **(A)** or 3 male **(B)** donors/grp) is shown as a single symbol. Cells were treated with LPS (1 μg/ml; 24h) with or without 3α,5α-THDOC (1 μM; 24h) or SGE-516 (1 μM; 24h). LPS caused a significant increase in the levels of TNF-α (~80% in hMDM from both female **(A)** and male **(B)** donors) and MCP-1 (~65% in hMDM from both female **(A)** and male **(B)** donors) relative to vehicle control (CTL). The increases of TNF-α were partially inhibited by 3α,5α-THDOC and SGE-516 (~30% and ~35% inhibition, respectively) in hMDM derived from female **(A)** but not male **(B)** donors. The increases of MCP-1 were completely inhibited by 3α,5α-THDOC or SGE-516 in hMDM from female **(A)** but not male **(B)** donors. Two-way ANOVA, Tukey's *post hoc* test: *p < 0.05, **p < 0.01, ***p < 0.001, ****p < 0.0001.

Since both 3α,5α-THDOC and SGE-516 inhibited LPS-induced increases of TNF-α and MCP-1 in hMDM from female donors, we examined their effects on LPS activation of the TLR4 pathway transcription factors. The levels of pCREB [~35%; F(1,20)=17.13, p=0.0005 and F(1,27)=7.040, p=0.0132 for experiments with 3α,5α-THDOC and SGE-516, respectively] and pSTAT1 [~60%; F(1,30)=28.87, p<0.0001 and F(1,28)=23.92, p<0.0001 for experiments with 3α,5α-THDOC and SGE-516, respectively] were also significantly increased in LPS-treated hMDM from female donors (Figure 5). The increases of pCREB were completely inhibited by 3α,5α-THDOC (F(1,20)=4.354, p=0.0499) and SGE-516 (F(1,27) =5.991, p=0.0212). The increases of pSTAT1 were completely inhibited by 3α,5α-THDOC (F(1,30)=7.172, p=0.0119) and partially inhibited by SGE-516 [~30%; F(1,28)=4.732, p=0.0382] (Figure 5). Consistent with the allopregnanolone effect, neither 3α,5α-THDOC nor SGE-516 changed the levels of pCREB, pSTAT1, as well as TNF-α or MCP-1 (p>0.05) in hMDM that were not treated with the TLR4 agonist LPS, indicating that both 3α,5α-THDOC and SGE-516 specifically target the activated TLR4 signal (Figures 4, 5).

Collectively, and consistent with our previous studies (33, 34), the data indicate that allopregnanolone inhibits activation of the TLR4 signal and cytokine/chemokine increases in hMDM from both female and male donors. In contrast, 3α,5α-THDOC and SGE-516 inhibit the TLR4 signaling pathway in hMDM from female, but not male donors, indicating a distinct structural requirement for neurosteroids in the inhibition of TLR4 pathways in male macrophages that was not observed in female macrophages.

## 3.4 Inhibitory effects of neurosteroids on the TLR7 signaling pathway are dependent upon sex in hMDM

We have previously shown that allopregnanolone inhibits the activated TLR7 signaling pathway in the mouse macrophage RAW264.7 cell line and the brain of female P rats (34). To examine whether allopregnanolone as well as 3α,5α-THDOC and SGE-516 also inhibit activation of TLR7 signal and pathway members in hMDM, cells were treated with the TLR7 agonist imiquimod (IMQ) (30 μg/ml; 24 hrs) in the absence or presence of allopregnanolone (1.0 μM), 3α,5α-THDOC (1.0 μM) or SGE-516 (1.0 μM). Cell lysates were assayed for established members of the activated TLR7 pathway, including the TLR7-associated activated (phosphorylated) transcription factor interferon regulatory factor 7 (pIRF7), pSTAT1, as well as cytokines IL-6 and IL-1β (19, 34, 77–79). The effect of allopregnanolone, 3α,5α-THDOC or SGE-516 on cells that were not treated with the TLR7 agonist IMQ was analogously studied.

### 3.4.1 Allopregnanolone, 3α,5α-THDOC and SGE-516 inhibition of TLR7 pathways in hMDM of female, but not male donors

IMQ caused a significant increase in the levels of IL-6 [~45-90% and 60-80% in hMDM from female donors (F(1,82)=4.648, p=0.0340; F(1,42)=49.41, p<0.0001 and F(1,38)=56.34, p<0.0001 for experiments with allopregnanolone, 3α,5α-THDOC and SGE-516, respectively) (Figures 6A, 8A) and male donors (F (1,88)=15.55, p=0.0002; F(1,32)=21.25, p<0.0001 and F(1,22) =33.00, p<0.0001 for experiments with allopregnanolone,

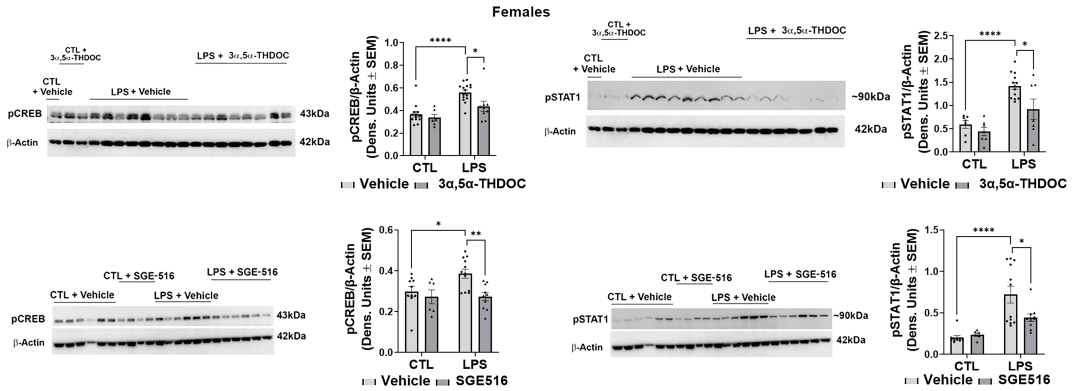


FIGURE 5
3α,5α-THDOC and SGE-516 inhibit LPS-induced activation of MyD88-dependent TLR4 pro-inflammatory signal in human monocyte-derived macrophages (hMDM) from female donors. hMDM cultures were treated with LPS (1 μg/ml; 24 h) with or without 3α,5α-THDOC (1 μM; 24 h) or SGE-516 (1 μM; 24 h). Representative western blot images and summary data of densitometric scatter dot plots show the levels of pCREB and pSTAT1 in females. Each data point represents an individual hMDM culture (n≥9 from 3 female donors/grp). β-Actin was used as protein loading control. LPS caused a significant increase in the levels of pCREB (~35%) and pSTAT1 (~60%) in hMDM from female donors relative to vehicle control (CTL). The increases of pCREB were completely inhibited by 3α,5α-THDOC and SGE-516. The increases of pSTAT1 were completely inhibited by 3α,5α-THDOC and partially inhibited by SGE-516 (~30%). Two-way ANOVA, Tukey's *post hoc* test: *p < 0.05, **p < 0.01, ****p < 0.0001.

3α,5α-THDOC and SGE-516, respectively)] (Figures 6B, 8B). Likewise, IMQ caused a significant increase in the levels of IL-1β [~95% in hMDM from both female donors ($F(1,44)=8.416$, $p=0.0058$; $F(1,58)=127.0$, $p<0.0001$ and $F(1,51)=47.46$, $p<0.0001$ for experiments with allopregnanolone, 3α,5α-THDOC and SGE-516, respectively) (Figures 6A, 8A) and male donors ($F(1,63)=73.33$, $p<0.0001$; $F(1,59)=40.79$, $p<0.0001$ and $F(1,43)=553.6$, $p<0.0001$ for experiments with allopregnanolone, 3α,5α-THDOC and SGE-516, respectively)] (Figures 6B, 8B). IMQ activated the TLR7 pathways through increases in pIRF7 [~35% and ~25% in hMDM from female donors ($F(1,52)=18.15$, $p<0.0001$) (Figure 7A) and male donors ($F(1,24)=18.45$, $p=0.0002$)] (Figure 7B) and pSTAT1 [~35% and ~40% in hMDM from female donors ($F(1,42)=13.64$, $p=0.0006$) (Figure 7A) and male donors ($F(1,45)=15.61$, $p=0.0003$)] (Figure 7B).

The increases of IL-6 were completely inhibited by allopregnanolone in hMDM from female donors ($F(1,82)=12.45$, $p=0.0007$) (Figure 6A), but not male donors ($F(1,88)=0.5031$, $p=0.4800$) (Figure 6B). The increases of IL-1β were completely inhibited by allopregnanolone in hMDM from female donors ($F(1,44)=4.148$, $p=0.0477$) (Figure 6A), but not male donors ($F(1,63)=0.6435$, $p=0.4254$) (Figure 6B). The increases of pIRF7 were completely inhibited by allopregnanolone in hMDM from female donors ($F(1,52)=6.619$, $p=0.0130$) (Figure 7A), but not male donors ($F(1,24)=0.1615$, $p=0.6913$) (Figure 7B). The increases of pSTAT1 were completely inhibited by allopregnanolone in hMDM from

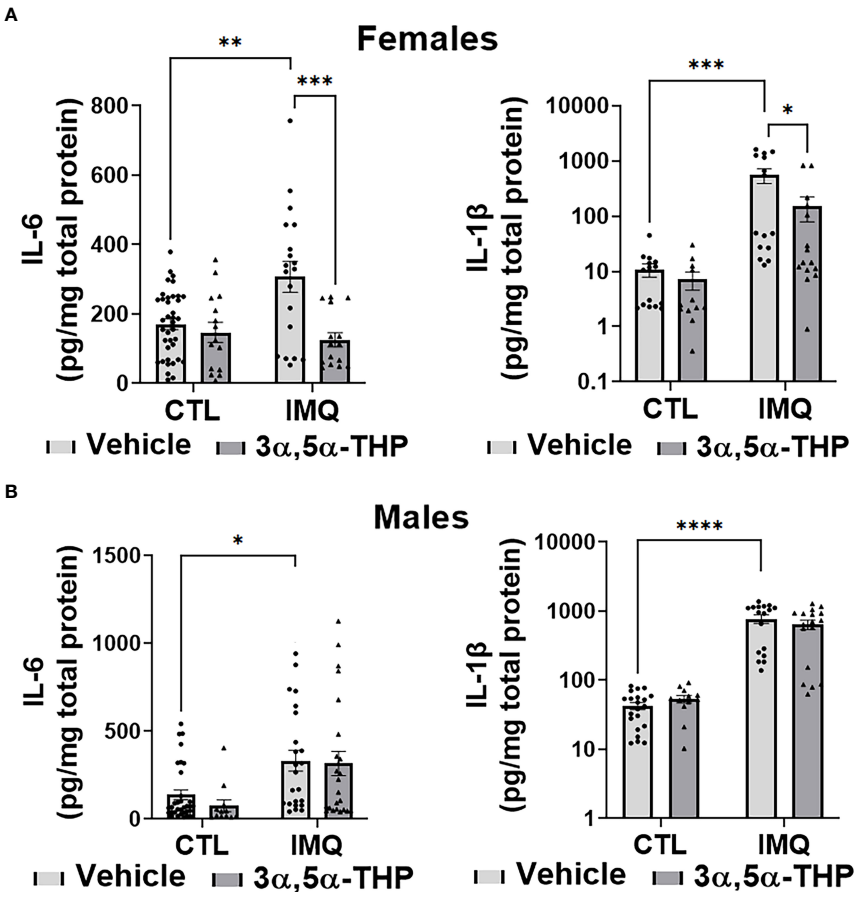


FIGURE 6
Allopregnanolone (3α,5α-THP) inhibits imiquimod-induced increases of inflammatory cytokines IL-6 and IL-1β in human monocyte-derived macrophages (hMDM) from female but not male donors. Each hMDM culture (n≥12 cultures from 3-5 female **(A)** or 3-5 male **(B)** donors/grp) is shown as a single symbol. Cells were treated with TLR7 agonist imiquimod (IMQ; 30 μg/ml) with or without allopregnanolone (1 μM). Cells were harvested at 24 h after treatment initiation and examined for the expression of inflammatory cytokines IL-6 and IL-1β. IMQ caused a significant increase in the levels of IL-6 (~45% and ~60% in hMDM from female **(A)** and male **(B)** donors, respectively) and IL-1β (~95% in hMDM from both female **(A)** and male **(B)** donors), relative to vehicle control (CTL) (Two-way ANOVA, Tukey's *post hoc* test: *$p < 0.05$, **$p < 0.01$, ***$p < 0.001$, ****$p < 0.0001$). The increases of IL-6 and IL-1β, were completely inhibited by allopregnanolone in hMDM from female donors (Two-way ANOVA, Tukey's *post hoc* test: *$p < 0.05$, ***$p < 0.001$) but not male donors ($p > 0.05$). Allopregnanolone did not change the levels of IL-6 and IL-1β ($p>0.05$) in hMDM that were not treated with the TLR7 agonist IMQ.

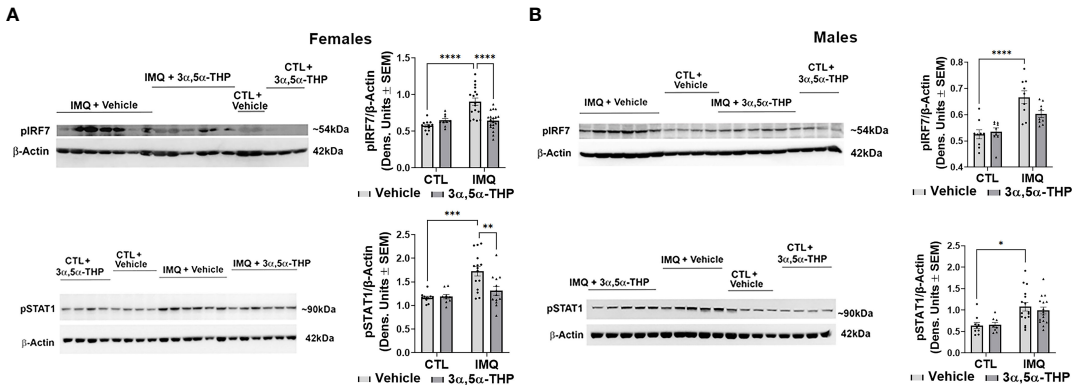


FIGURE 7
Allopregnanolone (3α,5α-THP) inhibits imiquimod-induced activation of MyD88-dependent TLR7 pro-inflammatory signal in human monocyte-derived macrophages (hMDM) from female but not male donors. hMDM were treated with TLR7 agonist imiquimod (IMQ; 30 μg/ml) with or without allopregnanolone (1 μM). Cells were harvested at 24 h after treatment initiation and examined for the expression of MyD88-dependent activated (phosphorylated) interferon regulatory factor 7 (pIRF7) and transcription factor pSTAT1. Representative western blot images and summary data of densitometric scatter dot plots show the levels of pIRF7 and pSTAT1 in females **(A)** and males **(B)**. Each data point represents an individual hMDM culture (n≥12 cultures from 3 female **(A)** or 3 male **(B)** donors/grp). β-Actin was used as protein loading control. IMQ caused a significant increase in the levels of pIRF7 (~35% and ~25% in hMDM from female **(A)** and male **(B)** donors, respectively) and pSTAT1 (~35% and ~40% in hMDM from female **(A)** and male **(B)** donors, respectively) relative to vehicle control (CTL) (Two-way ANOVA, Tukey's *post hoc* test: *p < 0.05, ***p < 0.001, ****p < 0.0001). The increases of pIRF7 and pSTAT1 were completely inhibited by allopregnanolone in hMDM from female donors (Two-way ANOVA, Tukey's *post hoc* test: **p < 0.01, ****p < 0.0001) but not male donors (Two-way ANOVA, Tukey's *post hoc* test, p>0.05). Allopregnanolone did not change the levels of pIRF7 and pSTAT1 (p>0.05) in hMDM that were not treated with the TLR7 agonist IMQ indicating that allopregnanolone specifically targets the activated TLR7 signal.

female donors (F(1,42)=4.489, p=0.0401) (Figure 7A), but not male donors (F(1,45)=0.2987, p=0.5874) (Figure 7B). IMQ and/or allopregnanolone did not affect TLR7 expression in hMDM from both male and female donors and there are no sex differences in the expression of TLR7 at baseline, after IMQ and/or allopregnanolone treatments (Figure S5).

Consistent with the inhibitory effect of allopregnanolone, 3α,5α-THDOC and SGE-516, albeit to a lesser extent, also inhibited IMQ-induced cytokine increases in hMDM derived from female donors, but not male donors (Figures 8A, B). The increases of IL-1β were partially inhibited by 3α,5α-THDOC and SGE-516 [~30% and ~35% inhibition, respectively] in hMDM derived from female donors (F(1,58)=4.702, p=0.0343 and F(1,51)=4.744, p=0.0340, for experiments with 3α,5α-THDOC and SGE-516, respectively) (Figure 8A), but not male donors (F(1,59)=0.04079, p=0.8406 and F(1,43)=1.924, p=0.1725 for experiments with 3α,5α-THDOC and SGE-516, respectively) (Figure 8B). The increases of IL-6 were partially inhibited by 3α,5α-THDOC [~30% inhibition] in hMDM derived from female donors (F(1,42)=4.202, p=0.0467) (Figure 8A), but not male donors (F(1,32)=0.006, p=0.9396) (Figure 8B), but were not inhibited by SGE-516 in hMDM from either female donors (F(1,38)=1.094, p=0.3022) (Figure 8A) or male donors (F(1,22)=0.011, p=0.9174) (Figure 8B).

Consistent with our previous studies (34), in the absence of the TLR7 agonist IMQ, allopregnanolone did not change the levels of pIRF7, pSTAT1, IL-6 or IL-1β and 3α,5α-THDOC and SGE-516 did not change the levels of IL-6 or IL-1β in hMDM, indicating that the neurosteroids specifically target the activated TLR7 signal (Figures 6–8).

Collectively, these results extend our previous studies in the mouse RAW264.7 macrophage cell line (34) to primary human macrophages, indicating that allopregnanolone inhibits activation of the TLR7 signal and cytokine increases. However, we show here that its effects are selective for hMDM from female donors. Correspondingly, although with lesser efficacy, 3α,5α-THDOC and SGE-516 also inhibit the TLR7 signaling pathway in hMDM from female, but not male donors, indicating sex specificity favoring females in the inhibition of TLR7 pathways by all the neurosteroids tested.

## 4 Discussion

The current findings indicate that allopregnanolone inhibits activation of the TLR4 and TLR7 signals and cytokine/chemokine increases in hMDM. However, we show here that its effects in hMDM are distinct from RAW264.7 cells (29), as the inhibition of TLR7 pathways are selective for female donors. We further observe that two steroids with C-21 structural modifications, 3α,5α-THDOC and SGE-516 inhibit the TLR4 pathway in hMDM from female, but not male donors, indicating different structural specificity for neurosteroid inhibition of TLR4 pathways in male vs. female donors. We also

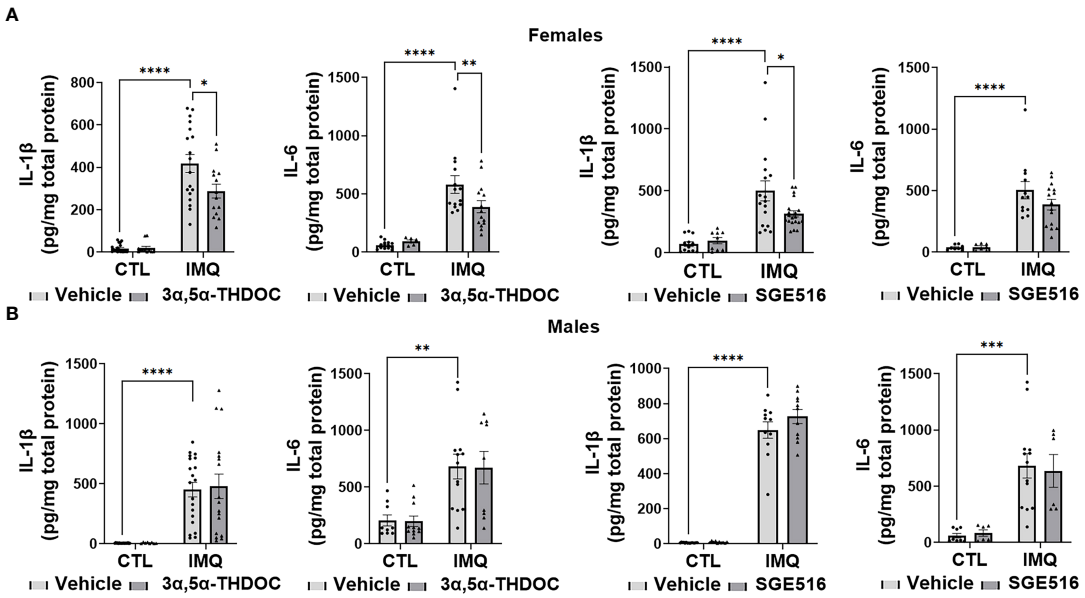


FIGURE 8
3α,5α-THDOC partially inhibits imiquimod-induced increases of IL-1β and IL-6 and SGE-516 partially inhibits IL-1β in human monocyte-derived macrophages (hMDM) from female but not male donors. Each hMDM culture (n≥12 from 3 female **(A)** or 3 male **(B)** donors/grp) is shown as a single symbol. Cells were treated with imiquimod (IMQ) (30 μg/ml; 24h) with or without 3α,5α-THDOC (1 μM; 24h) or SGE-516 (1 μM; 24h). IMQ caused a significant increase in the levels of IL-1β (~95% in hMDM from both female **(A)** and male **(B)** donors) and IL-6 (~90% and ~80% in MDM from female **(A)** and male **(B)** donors, respectively) relative to vehicle control (CTL). The increases of IL-1β were partially inhibited by 3α,5α-THDOC and SGE-516 (~30% and ~35% inhibition, respectively) in hMDM derived from female **(A)** but not male **(B)** donors. The increases of IL-6 were partially inhibited by 3α,5α-THDOC in hMDM from female (~30% inhibition) **(A)** but not male **(B)** (p>0.05) donors and were not inhibited by SGE-516 in hMDM from both female **(A)** and male **(B)** donors (p>0.05). Two-way ANOVA, Tukey's *post hoc* test: *p < 0.05, **p < 0.01, ***p < 0.001, ****p < 0.0001.

demonstrate that allopregnanolone, 3α,5α-THDOC and SGE-516 inhibit the activated TLR signaling pathways in hMDM, but they have no effect on the unstimulated pathways.

The TLR4 agonist LPS increased multiple markers of TLR4 activation, including the phosphorylated (activated) transcription factors CREB, STAT1, as well as TNF-α and MCP-1, in hMDM. All these effects were inhibited by allopregnanolone in hMDM from both male and female donors. In contrast 3α,5α-THDOC and SGE-516 inhibit these TLR4 pathway members in hMDM from female, but not male donors, indicating different structural requirements of neurosteroids for inhibiting TLR4 signaling between sexes. We previously demonstrated that allopregnanolone inhibits TLR4 binding to both MyD88 and MD2 to prevent TLR4 pathway activation and the production of MCP-1, HMGB1 and TNF-α in RAW264.7 cells (33). The present results suggest that TLR4 pathway activation mechanisms may differ in female vs. male hMDM, such that 3α,5α-THDOC and SGE-516 are unable to block their activation in males. This might involve sex differences in TLR4 adaptor protein expression that alter the structural requirements for inhibition of pathway activation. Further studies are needed to elucidate the mechanism of this sex difference.

The TLR7 agonist IMQ increased markers of TLR7 activation, phosphorylated (activated) transcription factors STAT1 and IRF7, as well as IL-6 and IL-1β, in hMDM. All these effects were inhibited by allopregnanolone in hMDM from female, but not male donors. Correspondingly, 3α,5α-THDOC inhibits IL-6 and IL-1β and SGE-516 inhibits IL-1β in hMDM from female, but not male donors. The mechanism of the sex specificity in TLR7 signal inhibition by neurosteroids in hMDM is unknown and additional studies will be required for elucidation. Since allopregnanolone inhibits the TLR7 interaction with MyD88 (34), it is likely that other TLR7 adaptor proteins as well as sex hormone receptors, chaperons, or proteins that enhance or suppress TLR7 signals may be involved.

Even though the endogenous neurosteroids allopregnanolone and 3α,5α-THDOC, and synthetic compound SGE-516 are all allosteric modulators of $GABA_A$ receptors (36–38, 54), the present data suggests that GABAergic activity may not be necessary or sufficient for TLR4 inhibition in hMDM, similar to our previous report in RAW264.7 cells (33). We previously found that allopregnanolone and pregnenolone (which lacks GABAergic actions) both completely inhibit TLR4 pathway activation and the production of MCP-1, HMGB1 and

TNF-α in RAW264.7 cells (33). These two steroids have distinct A ring properties, with identical D ring structure, suggesting structural specificity at ring D for inhibition of TLR4 signaling in RAW264.7 cells (33). Since the structures of both 3α,5α-THDOC and SGE-516 differ from the allopregnanolone by additional C-21-hydroxyl and C-21-1,2,5-triazole groups, respectively (54, 62, 80), modifications such as these at the D-ring could be detrimental for neurosteroid inhibition of TLR activation in hMDM from male donors as well as RAW264.7 cells. Further additional studies with a greater number of structural modifications are needed to adequately assess the structural requirements for TLR inhibition. Moreover, the effects of these structural modifications on neurosteroid inhibition of TLRs in the brain also remain unstudied.

Even though these data indicate that there are no sex differences in the expression of both TLR4 and TLR7 at baseline, or pathway activation by agonists, we observed differential inhibitory effects of neurosteroids in female vs. male macrophages. Numerous sex differences in innate and adaptive immunity have been identified in various studies (81–85). Sex differences in immune function can be attributed in many cases to regulatory effects of gonadal hormones *in vivo* (86). Other sex differences include reduced sensitivity to the effects of LPS, greater phagocytic activity, production of more anti-inflammatory prostanoids, and more efficient antigen presentation in female macrophages (86, 87). The present data indicate that female macrophages had reduced sensitivity to LPS, as defined by the level of MCP-1, compared to male macrophages (Figure S1). This factor may explain the greater inhibition of LPS-induced elevation of MCP-1 by allopregnanolone in female macrophages when compared with male macrophages. Thus, neurosteroid regulation may represent an additional mechanism for sex dependent immune regulation.

We previously showed that allopregnanolone inhibits TLR4 binding to MD-2 and MyD88, and TLR7 binding to MyD88 in RAW264.7 cells (33, 34). However, the exact mechanism of allopregnanolone inhibition remains unclear. Allopregnanolone and pregnenolone have also been shown to enhance the degradation of bound adaptor proteins, which promote ubiquitination and degradation of the toll/interleukin-1 receptor domain-containing adapter protein and TLR2 in HEK293T cells (88). Further studies are needed to identify the protein-protein interactions that are inhibited by neurosteroids and enable kinetic analysis.

Pro-inflammatory signaling through TLRs plays a major role in the detrimental activities of macrophages (15). The TLR4-specific ligand LPS, causes receptor oligomerization with multiple adaptor proteins at the cell membrane, inducing a cascade of protein-protein interactions that produce proinflammatory cytokines and chemokines (16, 19, 75, 89–91). TLR7 is located on the endosome and recognizes single-stranded RNA molecules (ssRNAs) (92, 93) and imidazoquinoline derivatives such as IMQ, which directly bind TLR7, induce its dimer formation, MyD88 binding and subsequent production of proinflammatory cytokines (16, 94, 95). The ability of allopregnanolone to simultaneously inhibit both TLR4 and TLR7 pathway activation could offer much needed control of inflammatory signaling and may offer a unique approach to the treatment of inflammatory conditions. Thus, the demonstration of TLR4 and TLR7 inhibition by various neurosteroids in hMDM has clear therapeutic relevance.

Macrophages promote neuroinflammation following traumatic brain injury (96), in multiple sclerosis (97, 98), ischemic stroke and intracerebral hemorrhage (98), and contribute to systemic inflammation in many other disease states (10). In addition, systemic inflammation is thought to contribute to the development and progression of neurodegenerative diseases (99). Moreover, various proinflammatory cytokines and chemokines derived from TLR4 and TLR7 activation are now recognized as potential markers of psychiatric conditions, including depression (24, 25), postpartum depression (100, 101), post-traumatic stress disorders (102–104) and alcohol use disorders (26, 27, 105). Thus, it seems plausible that the ability of allopregnanolone to inhibit both TLR4 and TLR7 interactions with MyD88 and their pathways contribute to its therapeutic actions in the treatment of post-partum depression (43) and post-traumatic stress disorders (106) and may have beneficial actions in other inflammatory conditions.

In conclusion, the present results show that endogenous neuroactive steroids regulate both TLR4 and TLR7 activation in cultured human macrophages, but with specificity for female donors. Because these steroids are present in circulation of both males and females, but are elevated during the luteal phase of the menstrual cycle as well as during pregnancy in women (39), they may play an integral role in the modulation of pro-inflammatory signaling across the lifespan and contribute to protection from both systemic and neuroinflammatory disease. Further work is needed to establish the contribution of their anti-inflammatory effects in the treatment of post-partum depression as well as other inflammatory conditions.

## Data availability statement

The original contributions presented in the study are included in the article/Supplementary Material. Further inquiries can be directed to the corresponding author.

## Ethics statement

The studies involving human participants were reviewed and approved by Human buffy coat leukocytes were obtained from healthy donors at the New York Blood Center (http://nybloodcenter.org/), a non-profit organization for the

collection and distribution of blood for clinical and research purposes. No personal identifiers were sent with the shipment. The patients/participants provided their written informed consent to participate in this study.

## Author contributions

IB, LA and ALM conceived project; IB, KW and RBM conducted experiments and analyzed data, ALM, RBM and BC provided funding, IB, RBM and ALM drafted manuscript, all authors contributed to the experimental design and editing of manuscript.

## Funding

This work was supported by NIH grant R01-AA024095, Sage Therapeutics Inc., and the Bowles Center for Alcohol Studies at UNC School of Medicine to ALM and R01-NS108808 to RBM.

## Acknowledgements

We would like to thank Ashley Suchy for her work in support of these studies. We dedicate this work to Dr. Laure Aurelian who passed away in May 2021 in the middle of these studies. Her knowledge, inspiration and insight were instrumental in this work and in our efforts.

## Conflict of interest

ALM, LA and IB hold a provisional patent on the anti-inflammatory actions of allopregnanolone and related steroids on Toll-like receptor pathways in the immune system and brain. BC was employed by Sage Therapeutics and the study received partial funding from Sage Therapeutics. Sage Therapeutics contributed the compound SGE-516 for these studies, but had no other involvement in the study.

The remaining authors declare that the research was conducted in the absence of any commercial or financial relationships that could be construed as a potential conflict of interest.

## Publisher's note



## Supplementary material

The Supplementary Material for this article can be found online at: https://www.frontiersin.org/articles/10.3389/fimmu.2022.940095/full#supplementary-material

## References

1. Chen L, Deng H, Cui H, Fang J, Zuo Z, Deng J, et al. Inflammatory responses and inflammation-associated diseases in organs. *Oncotarget* (2018) 9(6):7204–18. doi: 10.18632/oncotarget.23208

2. Chitnis T, Weiner HL. CNS inflammation and neurodegeneration. *J Clin Invest* (2017) 127(10):3577–87. doi: 10.1172/JCI90609

3. Yuan N, Chen Y, Xia Y, Dai J, Liu C. Inflammation-related biomarkers in major psychiatric disorders: a cross-disorder assessment of reproducibility and specificity in 43 meta-analyses. *Trans Psychiatry* (2019) 9(1):233. doi: 10.1038/s41398-019-0570-y

4. Mukherjee S, Mukherjee S, Maiti TK, Bhattacharya S, Sinha Babu SP. A novel ligand of toll-like receptor 4 from the sheath of wuchereria bancrofti microfilaria induces proinflammatory response in macrophages. *J Infect Dis* (2017) 215(6):954–65. doi: 10.1093/infdis/jix067

5. Vijay K. Toll-like receptors in immunity and inflammatory diseases: Past, present, and future. *Int Immunopharmacol* (2018) 59:391–412. doi: 10.1016/j.intimp.2018.03.002

6. Takeuchi O, Akira S. Pattern recognition receptors and inflammation. *Cell* (2010) 140(6):805–20. doi: 10.1016/j.cell.2010.01.022

7. Bourgeois C, Kuchler K. Fungal pathogens–a sweet and sour treat for toll-like receptors. *Front Cell Infect Microbiol* (2012) 2. doi: 10.3389/fcimb.2012.00142

8. Del Valle DM, Kim-Schulze S, Huang HH, Beckmann ND, Nirenberg S, Wang B, et al. An inflammatory cytokine signature predicts COVID-19 severity and survival. *Nat Med* (2020) 26(10):1636–43. doi: 10.1038/s41591-020-1051-9

9. Wittebole X, Castanares-Zapatero D, Laterre PF. Toll-like receptor 4 modulation as a strategy to treat sepsis. *Mediators Inflamm* (2010) 2010:568396. doi: 10.1155/2010/568396

10. Murray PJ, Wynn TA. Protective and pathogenic functions of macrophage subsets. *Nat Rev Immunol* (2011) 11(11):723–37. doi: 10.1038/nri3073

11. Raggi F, Pelassa S, Pierobon D, Penco F, Gattorno M, Novelli F, et al. Regulation of human macrophage M1–M2 polarization balance by hypoxia and the triggering receptor expressed on myeloid cells-1. *Front Immunol* (2017) 8. doi: 10.3389/fimmu.2017.01097

12. Oishi Y, Manabe I. Macrophages in inflammation, repair and regeneration. *Int Immunol* (2018) 30(11):511–28. doi: 10.1093/intimm/dxy054

13. Atri C, Guerfali FZ, Laouini D. Role of human macrophage polarization in inflammation during infectious diseases. *Int J Mol Sci* (2018) 19(6):1801. doi: 10.3390/ijms19061801

14. Rathee P, Chaudhary H, Rathee S, Rathee D, Kumar V. Immunosuppressants: A review. *Pharma Innovation* (2013) 1(12, Part A):90–101.

15. McCoy CE, O'Neill LA. The role of toll-like receptors in macrophages. *Front Biosci* (2008) 13:62–70. doi: 10.2741/2660

16. Takeda K, Kaisho T, Akira S. Toll-like receptors. *Annu Rev Immunol* (2003) 21:335–76. doi: 10.1146/annurev.immunol.21.120601.141126

17. Zarember KA, Godowski PJ. Tissue expression of human toll-like receptors and differential regulation of toll-like receptor mRNAs in leukocytes in response to microbes, their products, and cytokines. *J Immunol* (2002) 168(2):554–61. doi: 10.4049/jimmunol.168.2.554

18. Pandey S, Agrawal DK. Immunobiology of toll-like receptors: emerging trends. *Immunol Cell Biol* (2006) 84(4):333–41. doi: 10.1111/j.1440-1711.2006.01444.x

19. Kawasaki T, Kawai T. Toll-like receptor signaling pathways. *Front Immunol* (2014) 5:461. doi: 10.3389/fimmu.2014.00461

20. Akhter N, Madhoun A, Arefanian H, Wilson A, Kochumon S, Thomas R, et al. Oxidative stress induces expression of the toll-like receptors (TLRs) 2 and 4 in the human peripheral blood mononuclear cells: Implications for metabolic inflammation. *Cell Physiol Biochem* (2019) 53(1):1–18. doi: 10.33594/000000117

21. Grassin-Delyle S, Abrial C, Salvator H, Brollo M, Naline E, Devillier P. The role of toll-like receptors in the production of cytokines by human lung macrophages. *J Innate Immun* (2020) 12(1):63–73. doi: 10.1159/000494463

22. Gao W, Xiong Y, Li Q, Yang H. Inhibition of toll-like receptor signaling as a promising therapy for inflammatory diseases: A journey from molecular to nano therapeutics. *Front Physiol* (2017) 8:508. doi: 10.3389/fphys.2017.00508

23. Gesuete R, Kohama SG, Stenzel-Poore MP. Toll-like receptors and ischemic brain injury. *J Neuropathol Exp Neurol* (2014) 73(5):378–86. doi: 10.1097/NEN.0000000000000068

24. Bullmore E. The art of medicine: Inflamed depression. *Lancet* (2018) 392 (10154):1189–90. doi: 10.1016/S0140-6736(18)32356-0

25. Liu J, Buisman-Pijlman F, Hutchinson MR. Toll-like receptor 4: innate immune regulator of neuroimmune and neuroendocrine interactions in stress and major depressive disorder. *Front Neurosci* (2014) 8. doi: 10.3389/fnins.2014.00309

26. Crews FT, Lawrimore CJ, Walter TJ, Coleman LG Jr. The role of neuroimmune signaling in alcoholism. *Neuropharmacology* (2017) 122:56–73. doi: 10.1016/j.neuropharm.2017.01.031

27. Vetreno RP, Qin L, Coleman LGJr., Crews FT. Increased toll-like receptor-MyD88-NFkappaB-Proinflammatory neuroimmune signaling in the orbitofrontal cortex of humans with alcohol use disorder. *Alcohol Clin Exp Res* (2021) 45 (9):1747–61. doi: 10.1111/acer.14669

28. Shi K, Zhang J, Dong JF, Shi FD. Dissemination of brain inflammation in traumatic brain injury. *Cell Mol Immunol* (2019) 16(6):523–30. doi: 10.1038/s41423-019-0213-5

29. Okun E, Griffioen KJ, Lathia JD, Tang SC, Mattson MP, Arumugam TV. Toll-like receptors in neurodegeneration. *Brain Res Rev* (2009) 59(2):278–92. doi: 10.1016/j.brainresrev.2008.09.001

30. Lehnardt S, Massillon L, Follett P, Jensen FE, Ratan R, Rosenberg PA, et al. Activation of innate immunity in the CNS triggers neurodegeneration through a toll-like receptor 4-dependent pathway. *Proc Natl Acad Sci* (2003) 100(14):8514–9. doi: 10.1073/pnas.1432609100

31. Vezzani A, Ruegg S. The pivotal role of immunity and inflammatory processes in epilepsy is increasingly recognized: introduction. *Epilepsia* (2011) 52 Suppl 3:1–4. doi: 10.1111/j.1528-1167.2011.03028.x

32. Maroso M, Balosso S, Ravizza T, Liu J, Bianchi ME, Vezzani A. Interleukin-1 type 1 receptor/Toll-like receptor signalling in epilepsy: the importance of IL-1beta and high-mobility group box 1. *J Internal Med* (2011) 270(4):319–26. doi: 10.1111/j.1365-2796.2011.02431.x

33. Balan I, Beattie MC, O'Buckley TK, Aurelian L, Morrow AL. Endogenous neurosteroid (3α,5α)3-Hydroxypregnan-20-one inhibits toll-like-4 receptor activation and pro-inflammatory signaling in macrophages and brain. *Sci Rep* (2019) 9(1):1220. doi: 10.1038/s41598-018-37409-6

34. Balan I, Aurelian L, Schleicher R, Boero G, O'Buckley T, Morrow AL. Neurosteroid allopregnanolone (3alpha,5alpha-THP) inhibits inflammatory signals induced by activated MyD88-dependent toll-like receptors. *Transl Psychiatry* (2021) 11(1):145. doi: 10.1038/s41398-021-01266-1

35. McEwen BS. Non-genomic and genomic effects of steroids on neural activity. *Trends Pharmacol Sci* (1991) 12(4):141–7. doi: 10.1016/0165-6147(91)90531-V

36. Majewska MD, Harrison NL, Schwartz RD, Barker JL, Paul SM. Steroid hormone metabolites are barbiturate-like modulators of the GABA receptor. *Science* (1986) 232:1004–7. doi: 10.1126/science.2422758

37. Morrow AL, Suzdak PD, Paul SM. Steroid hormone metabolites potentiate GABA receptor-mediated chloride ion flux with nanomolar potency. *Eur J Pharmacol* (1987) 142:483–5. doi: 10.1016/0014-2999(87)90094-X

38. Stell BM, Brickley SG, Tang CY, Farrant M, Mody I. Neuroactive steroids reduce neuronal excitability by selectively enhancing tonic inhibition mediated by delta subunit-containing GABAA receptors. *Proc Natl Acad Sci U S A* (2003) 100 (24):14439–44. doi: 10.1073/pnas.2435457100

39. Paul SM, Purdy RH. Neuroactive steroids. *FASEB J* (1992) 6:2311–22. doi: 10.1096/fasebj.6.6.1347506

40. Boero G, Porcu P, Morrow AL. Pleiotropic actions of allopregnanolone underlie therapeutic benefits in stress-related disease. *Neurobiol Stress* (2020) 12:100203. doi: 10.1016/j.ynstr.2019.100203

41. Marx CE, Lee J, Subramaniam M, Rapisarda A, Bautista DC, Chan E, et al. Proof-of-concept randomized controlled trial of pregnenolone in schizophrenia. *Psychopharmacol (Berl)* (2014) 231(17):3647–62. doi: 10.1007/s00213-014-3673-4

42. Milivojevic V, Fox HC, Sofuoglu M, Covault J, Sinha R. Effects of progesterone stimulated allopregnanolone on craving and stress response in cocaine dependent men and women. *Psychoneuroendocrinology* (2016) 65:44–53. doi: 10.1016/j.psyneuen.2015.12.008

43. Meltzer-Brody S, Colquhoun H, Riesenberg R, Epperson CN, Deligiannidis KM, Rubinow DR, et al. Brexanolone injection in post-partum depression: two multicentre, double-blind, randomised, placebo-controlled, phase 3 trials. *Lancet* (2018) 392(10152):1058–70. doi: 10.1016/S0140-6736(18)31551-4

44. Pinna G. Allopregnanolone, the neuromodulator turned therapeutic agent: Thank you, next? *Front Endocrinol (Lausanne)* (2020) 11:236. doi: 10.3389/fendo.2020.00236

45. Morrow AL, Balan I, Boero G. Mechanisms underlying recovery from postpartum depression following brexanolone therapy. *Biol Psychiatry* (2022) 91 (3):252–3. doi: 10.1016/j.biopsych.2021.11.006

46. Morrow AL. Recent developments in the significance and therapeutic relevance of neuroactive steroids - introduction to the special issue. *Pharmacol Ther* (2007) 116(1):1–6. doi: 10.1016/j.pharmthera.2007.04.003

47. Morrow AL, Porcu P. Neuroactive steroid biomarkers of alcohol sensitivity and alcoholism risk. In: M Ritsner, editor. *Neuropsychiatric biomarkers, endophenotypes, and genes*. Dordrecht: Springer Science + Business Media B.V (2009). p. 47–57.

48. Morrow AL, Boero G, Porcu P. A rationale for allopregnanolone treatment of alcohol use disorders: Basic and clinical studies. *Alcohol Clin Exp Res* (2020) 44 (2):320–39. doi: 10.1111/acer.14253

49. He J, Evans CO, Hoffman SW, Oyesiku NM, Stein DG. Progesterone and allopregnanolone reduce inflammatory cytokines after traumatic brain injury. *Exp Neurol* (2004) 189(2):404–12. doi: 10.1016/j.expneurol.2004.06.008

50. He J, Hoffman SW, Stein DG. Allopregnanolone, a progesterone metabolite, enhances behavioral recovery and decreases neuronal loss after traumatic brain injury. *Restorative Neurol Neurosci* (2004) 22(1):19–31.

51. Noorbakhsh F, Baker GB, Power C. Allopregnanolone and neuroinflammation: a focus on multiple sclerosis. *Front Cell Neurosci* (2014) 8:134. doi: 10.3389/fncel.2014.00134

52. Schumacher M, Guennoun R, Stein DG, De Nicola AF. Progesterone: therapeutic opportunities for neuroprotection and myelin repair. *Pharmacol Ther* (2007) 116(1):77–106. doi: 10.1016/j.pharmthera.2007.06.001

53. Brinton RD. Neurosteroids as regenerative agents in the brain: therapeutic implications. *Nat Rev Endocrinol* (2013) 9(4):241–50. doi: 10.1038/nrendo.2013.31

54. Martinez Botella G, Salituro FG, Harrison BL, Beresis RT, Bai Z, Shen K, et al. Neuroactive steroids. 1. positive allosteric modulators of the (γ-aminobutyric Acid)A receptor: Structure–activity relationships of heterocyclic substitution at c-21. *J Med Chem* (2015) 58(8):3500–11. doi: 10.1021/acs.jmedchem.5b00032

55. Hammond RS, Althaus AL, Ackley MA, Maciag C, Martinez Botella G, Salituro FG, et al. Anticonvulsant profile of the neuroactive steroid, SGE-516, in animal models. *Epilepsy Res* (2017) 134:16–25. doi: 10.1016/j.eplepsyres.2017.05.001

56. Hawkins NA, Lewis M, Hammond RS, Doherty JJ, Kearney JA. The synthetic neuroactive steroid SGE-516 reduces seizure burden and improves survival in a dravet syndrome mouse model. *Sci Rep* (2017) 7(1):15327. doi: 10.1038/s41598-017-15609-w

57. Althaus AL, McCarren HS, Alqazzaz A, Jackson C, McDonough JH, Smith CD, et al. The synthetic neuroactive steroid SGE-516 reduces status epilepticus and neuronal cell death in a rat model of soman intoxication. *Epilepsy Behav* (2017) 68:22–30. doi: 10.1016/j.yebeh.2016.12.024

58. Antonoudiou P, Colmers PLW, Walton NL, Weiss GL, Smith AC, Nguyen DP, et al. Allopregnanolone mediates affective switching through modulation of oscillatory states in the basolateral amygdala. *Biol Psychiatry* (2022) 91(3):283–93. doi: 10.1016/j.biopsych.2021.07.017

59. Killebrew DA, Williams KS, Xie Y, Longo F, Meeker RB. Suppression of HIV-associated macrophage activation by a p75 neurotrophin receptor ligand. *J Neuroimmune Pharmacol* (2021). doi: 10.1007/s11481-021-10002-x

60. Williams KS, Killebrew DA, Clary GP, Meeker RB. Opposing effects of NGF and proNGF on HIV induced macrophage activation. *J Neuroimmune Pharmacol* (2016) 11(1):98–120. doi: 10.1007/s11481-015-9631-z

61. Williams KS, Killebrew DA, Clary GP, Seawell JA, Meeker RB. Differential regulation of macrophage phenotype by mature and pro-nerve growth factor. *J Neuroimmunol* (2015) 285:76–93. doi: 10.1016/j.jneuroim.2015.05.016

62. Purdy RH, Morrow AL, Blinn JR, Paul SM. Synthesis, metabolism, and pharmacological activity of 3 alpha-hydroxy steroids which potentiate GABA-receptor-mediated chloride ion uptake in rat cerebral cortical synaptoneurosomes. *J Med Chem* (1990) 33:1572–81. doi: 10.1021/jm00168a008

63. Purdy RH, Moore PH, Morrow AL, Paul SM. The 3a-hydroxy ring-a-reduced metabolites of progesterone and deoxycorticosterone: Natural ligands of central GABAA receptors. In: E Costa, SM Paul, editors. *Neurosteroids and brain function*. New York: Raven Press (1991). p. 95–102.

64. Balan I, Warnock KT, Puche A, Gondre-Lewis MC, Aurelian L. Innately activated TLR4 signal in the nucleus accumbens is sustained by CRF amplification loop and regulates impulsivity. *Brain Behavior Immun* (2018) 69:139–53. doi: 10.1016/j.bbi.2017.11.008

65. Balan I, Warnock KT, Puche A, Gondre-Lewis MC, June H, Aurelian L. The GABAA receptor α2 subunit activates a neuronal TLR4 signal in the ventral tegmental area that regulates alcohol and nicotine abuse. *Brain Sci* (2018) 8(4). doi: 10.3390/brainsci8040072

66. Rostam HM, Reynolds PM, Alexander MR, Gadegaard N, Ghaemmaghami AM. Image based machine learning for identification of macrophage subsets. *Sci Rep* (2017) 7(1):3521. doi: 10.1038/s41598-017-03780-z

67. Pace JL, Russell SW, Schreiber RD, Altman A, Katz DH. Macrophage activation: priming activity from a T-cell hybridoma is attributable to interferon-gamma. *Proc Natl Acad Sci* (1983) 80(12):3782–6. doi: 10.1073/pnas.80.12.3782

68. Viola A, Munari F, Sánchez-Rodríguez R, Scolaro T, Castegna A. The metabolic signature of macrophage responses. *Front Immunol* (2019) 10. doi: 10.3389/fimmu.2019.01462

69. Tarique AA, Logan J, Thomas E, Holt PG, Sly PD, Fantino E. Phenotypic, functional, and plasticity features of classical and alternatively activated human macrophages. *Am J Respir Cell Mol Biol* (2015) 53(5):676–88. doi: 10.1165/rcmb.2015-0012OC

70. Stein M, Keshav S, Harris N, Gordon S. Interleukin 4 potently enhances murine macrophage mannose receptor activity: a marker of alternative immunologic macrophage activation. *J Exp Med* (1992) 176(1):287–92. doi: 10.1084/jem.176.1.287

71. Ziegler-Heitbrock L. Blood monocytes and their subsets: Established features and open questions. *Front Immunol* (2015) 6. doi: 10.3389/fimmu.2015.00423

72. Thomas GD, Hamers AAJ, Nakao C, Marcovecchio P, Taylor AM, McSkimming C, et al. Human blood monocyte subsets: A new gating strategy defined using cell surface markers identified by mass cytometry. *Arterioscler Thromb Vasc Biol* (2017) 37(8):1548–58. doi: 10.1161/ATVBAHA.117.309145

73. Reyes-García MG, Hernández-Hernández F, Hernández-Téllez B, García-Tamayo F. GABA (A) receptor subunits RNA expression in mice peritoneal macrophages modulate their IL-6/IL-12 production. *J Neuroimmunol* (2007) 188 (1-2):64–8. doi: 10.1016/j.jneuroim.2007.05.013

74. Alam S, Laughton DL, Walding A, Wolstenholme AJ. Human peripheral blood mononuclear cells express GABAA receptor subunits. *Mol Immunol* (2006) 43(9):1432–42. doi: 10.1016/j.molimm.2005.07.025

75. Luu K, Greenhill CJ, Majoros A, Decker T, Jenkins BJ, Mansell A. STAT1 plays a role in TLR signal transduction and inflammatory responses. *Immunol Cell Biol* (2014) 92(9):761–9. doi: 10.1038/icb.2014.51

76. Toshchakov V, Jones BW, Perera PY, Thomas K, Cody MJ, Zhang S, et al. TLR4, but not TLR2, mediates IFN-beta-induced STAT1alpha/beta-dependent gene expression in macrophages. *Nat Immunol* (2002) 3(4):392–8. doi: 10.1038/ni774

77. Moynagh PN. TLR signalling and activation of IRFs: revisiting old friends from the NF-kappaB pathway. *Trends Immunol* (2005) 26(9):469–76. doi: 10.1016/j.it.2005.06.009

78. Wong CK, Cheung PF, Ip WK, Lam CW. Intracellular signaling mechanisms regulating toll-like receptor-mediated activation of eosinophils. *Am J Respir Cell Mol Biol* (2007) 37(1):85–96. doi: 10.1165/rcmb.2006-0457OC

79. Vogelsang P, Karlsen M, Brun JG, Jonsson R, Appel S. Altered phenotype and Stat1 expression in toll-like receptor 7/8 stimulated monocyte-derived dendritic cells from patients with primary sjögren's syndrome. *Arthritis Res Ther* (2014) 16(4):R166. doi: 10.1186/ar4682

80. Reddy DS. Role of anticonvulsant and antiepileptogenic neurosteroids in the pathophysiology and treatment of epilepsy. *Front Endocrinol (Lausanne)* (2011) 2. doi: 10.3389/fendo.2011.00038

81. Cunningham MA, Naga OS, Eudaly JG, Scott JL, Gilkeson GS. Estrogen receptor alpha modulates toll-like receptor signaling in murine lupus. *Clin Immunol* (2012) 144(1):1–12. doi: 10.1016/j.clim.2012.04.001

82. Seillet C, Laffont S, Trémollières F, Rouquié N, Ribot C, Arnal J-F, et al. The TLR-mediated response of plasmacytoid dendritic cells is positively regulated by estradiol *in vivo* through cell-intrinsic estrogen receptor α signaling. *Blood* (2012) 119(2):454–64. doi: 10.1182/blood-2011-08-371831

83. Calippe B, Douin-Echinard V, Delpy L, Laffargue M, Lélu K, Krust A, et al. 17Beta-estradiol promotes TLR4-triggered proinflammatory mediator production through direct estrogen receptor alpha signaling in macrophages *in vivo*. *J Immunol* (2010) 185(2):1169–76. doi: 10.4049/jimmunol.0902383

84. Kovats S. Estrogen receptors regulate innate immune cells and signaling pathways. *Cell Immunol* (2015) 294(2):63–9. doi: 10.1016/j.cellimm.2015.01.018

85. Seillet C, Rouquié N, Foulon E, Douin-Echinard V, Krust A, Chambon P, et al. Estradiol promotes functional responses in inflammatory and steady-state dendritic cells through differential requirement for activation function-1 of estrogen receptor α. *J Immunol* (2013) 190(11):5459–70. doi: 10.4049/jimmunol.1203312

86. Klein SL, Flanagan KL. Sex differences in immune responses. *Nat Rev Immunol* (2016) 16(10):626–38. doi: 10.1038/nri.2016.90

87. Marriott I, Bost KL, Huet-Hudson YM. Sexual dimorphism in expression of receptors for bacterial lipopolysaccharides in murine macrophages: a possible mechanism for gender-based differences in endotoxic shock susceptibility. *J Reprod Immunol* (2006) 71(1):12–27. doi: 10.1016/j.jri.2006.01.004

88. Murugan S, Jakka P, Namani S, Mujumdar V, Radhakrishnan G. The neurosteroid pregnenolone promotes degradation of key proteins in the innate immune signaling to suppress inflammation. *J Biol Chem* (2019) 294(12):4596–607. doi: 10.1074/jbc.RA118.005543

89. Gay NJ, Symmons MF, Gangloff M, Bryant CE. Assembly and localization of toll-like receptor signalling complexes. *Nat Rev Immunol* (2014) 14(8):546–58. doi: 10.1038/nri3713

90. Lu Y-C, Yeh W-C, Ohashi PS. LPS/TLR4 signal transduction pathway. *Cytokine* (2008) 42(2):145–51. doi: 10.1016/j.cyto.2008.01.006

91. Guha M, Mackman N. LPS induction of gene expression in human monocytes. *Cell Signal* (2001) 13(2):85–94. doi: 10.1016/S0898-6568(00)00149-2

92. Diebold SS, Kaisho T, Hemmi H, Akira S, Reis e Sousa C. Innate antiviral responses by means of TLR7-mediated recognition of single-stranded RNA. *Science* (2004) 303(5663):1529–31. doi: 10.1126/science.1093616

93. Heil F, Hemmi H, Hochrein H, Ampenberger F, Kirschning C, Akira S, et al. Species-specific recognition of single-stranded RNA *via* toll-like receptor 7 and 8. *Science* (2004) 303(5663):1526–9. doi: 10.1126/science.1093620

94. Tanji H, Ohto U, Shibata T, Miyake K, Shimizu T. Structural reorganization of the toll-like receptor 8 dimer induced by agonistic ligands. *Science* (2013) 339 (6126):1426–9. doi: 10.1126/science.1229159

95. Zhang Z, Ohto U, Shibata T, Krayukhina E, Taoka M, Yamauchi Y, et al. Structural analysis reveals that toll-like receptor 7 is a dual receptor for guanosine and single-stranded RNA. *Immunity* (2016) 45(4):737–48. doi: 10.1016/j.immuni.2016.09.011

96. Morganti JM, Jopson TD, Liu S, Riparip LK, Guandique CK, Gupta N, et al. CCR2 antagonism alters brain macrophage polarization and ameliorates cognitive dysfunction induced by traumatic brain injury. *J Neurosci* (2015) 35(2):748–60. doi: 10.1523/JNEUROSCI.2405-14.2015

97. Rawji KS, Yong VW. The benefits and detriments of Macrophages/Microglia in models of multiple sclerosis. *Clin Dev Immunol* (2013) 2013:948976. doi: 10.1155/2013/948976

98. Zhao M, Tuo H, Wang S, Zhao L. The roles of monocyte and monocyte-derived macrophages in common brain disorders. *BioMed Res Int* (2020) 2020:9396021. doi: 10.1155/2020/9396021

99. Xie J, Van Hoecke L, Vandenbroucke RE. The impact of systemic inflammation on alzheimer's disease pathology. *Front Immunol* (2022) 12:796867. doi: 10.3389/fimmu.2021.796867

100. Achtyes E, Keaton SA, Smart L, Burmeister AR, Heilman PL, Krzyzanowski S, et al. Inflammation and kynurenine pathway dysregulation in post-partum women with severe and suicidal depression. *Brain Behavior Immun* (2020) 83:239–47. doi: 10.1016/j.bbi.2019.10.017

101. Sha Q, Madaj Z, Keaton S, Escobar Galvis ML, Smart L, Krzyzanowski S, et al. Cytokines and tryptophan metabolites can predict depressive symptoms in pregnancy. *Transl Psychiatry* (2022) 12(1):35. doi: 10.1038/s41398-022-01801-8

102. Kim TD, Lee S, Yoon S. Inflammation in post-traumatic stress disorder (PTSD): A review of potential correlates of PTSD with a neurological perspective. *Antioxid (Basel)* (2020) 9(2):107. doi: 10.3390/antiox9020107

103. Miller MW, Lin AP, Wolf EJ, Miller DR. Oxidative stress, inflammation, and neuroprogression in chronic PTSD. *Harv Rev Psychiatry* (2018) 26(2):57–69. doi: 10.1097/HRP.0000000000000167

104. Michopoulos V, Powers A, Gillespie CF, Ressler KJ, Jovanovic T. Inflammation in fear- and anxiety-based disorders: PTSD, GAD, and beyond. *Neuropsychopharmacology* (2017) 42(1):254–70. doi: 10.1038/npp.2016.146

105. Crews FT, Walter TJ, Coleman LGJr., Vetreno RP. Toll-like receptor signaling and stages of addiction. *Psychopharmacol (Berl)* (2017) 234(9-10):1483–98. doi: 10.1007/s00213-017-4560-6

106. Rasmusson AM, Marx CE, Pineles SL, Locci A, Scioli-Salter ER, Nillni YI, et al. Neuroactive steroids and PTSD treatment. *Neurosci Lett* (2017) 649:156–63. doi: 10.1016/j.neulet.2017.01.054

frontiers | Frontiers in Immunology

TYPE Mini Review
PUBLISHED 09 August 2022
DOI 10.3389/fimmu.2022.933415



OPEN ACCESS

EDITED BY
Jacqueline Palace,
Oxford University Hospitals NHS Trust,
United Kingdom

REVIEWED BY
Eoin Flanagan,
Mayo Clinic, United States
Sasitorn Siritho,
Bumrungrad International Hospital,
Thailand

*CORRESPONDENCE
Petra Nytrova
Petra.Nytrova@lf1.cuni.cz

SPECIALTY SECTION
This article was submitted to
Multiple Sclerosis
and Neuroimmunology,
a section of the journal
Frontiers in Immunology

RECEIVED 03 May 2022
ACCEPTED 19 July 2022
PUBLISHED 09 August 2022

CITATION
Nytrova P and Dolezal O (2022) Sex bias in multiple sclerosis and neuromyelitis optica spectrum disorders: How it influences clinical course, MRI parameters and prognosis. *Front. Immunol.* 13:933415. doi: 10.3389/fimmu.2022.933415



# Sex bias in multiple sclerosis and neuromyelitis optica spectrum disorders: How it influences clinical course, MRI parameters and prognosis

Petra Nytrova[1]* and Ondrej Dolezal[2]

[1]Department of Neurology and Centre of Clinical Neuroscience, First Faculty of Medicine, Charles University in Prague and General University Hospital, Prague, Czechia, [2]Department of Neurology, Dumfries and Galloway Royal Infirmary, NHS Scotland, Dumfries, United Kingdom

This review is a condensed summary of representative articles addressing the sex/gender bias in multiple sclerosis (MS) and neuromyelitis optica spectrum disorders (NMOSD). The strong effects of sex on the incidence and possibly also the activity and progression of these disorders should be implemented in the evaluation of any phase of clinical research and also in treatment choice consideration in clinical practice and evaluation of MRI parameters. Some relationships between clinical variables and gender still remain elusive but with further understanding of sex/gender-related differences, we should be able to provide appropriate patient-centered care and research.

KEYWORDS

**multiple sclerosis, neuromyelitis optica spectrum disorders, sex bias, pregnancy, magnetic resonance imaging, brain atrophy, disease progression**

## Introduction

The predominance of females among patients with autoimmune central nervous system disorders such as multiple sclerosis (MS) and neuromyelitis optica spectrum disorders (NMOSD) is well recognized. Several sex-specific factors, including sex hormones themselves and genetics - the presence of two X chromosomes versus one X and one Y chromosome, and environmental and societal factors including dietetic habits might play an important role in susceptibility and manifestation of autoimmune disorders (1–3). Furthermore, these factors can influence each other in the interconnected functional network. In this review, we discuss current views on sex bias in MS and NMOSD and their impact on disease course, prognosis, and MRI findings.

Previous research naturally focused on the influence of sex hormones, but it seems that hormonal variances between sexes explain clinical differences only to some extent as

female sex bias is frequently observed even in autoimmune diseases with onset in childhood when estrogen levels do not differ between sexes, or in postmenopausal women (4). A possible explanation for these differences could be hidden in sex chromosomes, which were studied on animal models of different autoimmune disorders (5, 6). Several X chromosome genes are known to be involved in immune responses (7), one of which is Forkhead box p3 (Foxp3) (5). This gene is important for the development and function of CD4+CD25hi T regulatory cells (Treg) (8, 9), which might contribute to the relative resistance to experimental autoimmune encephalomyelitis in males (10). Foxp3 expression during the induction of Treg function is controlled by epigenetic mechanisms at the transcriptional level that involve Foxp3 DNA methylation (11, 12). Furthermore, there are not only X-linked genes that could influence the sex bias but also X-linked control mechanisms like non-coding microRNA (miRNA), which is involved in the regulation of gene expression by suppressing mRNA translation or triggering mRNA degradation (13–15). The upregulation of X-linked miR-18 during relapse in patients with MS was described (16). The reason for the absence of miRNA in the Y chromosome is unknown (14).

## Sex bias in epidemiology and pathophysiology of MS and NMOSD

MS is an acquired inflammatory demyelinating disorder predominantly affecting young females in 2-3:1 female to male (F:M) ratio for relapsing MS in developed countries (17–19). Furthermore, several studies have shown that multiple sclerosis F:M ratio of cases increases over time when serial cross-sectional comparisons were made (17). In contrast, primary progressive MS affects men and women equally (20, 21). Previously, the cellular immunology of relapsing multiple sclerosis was considered to be principally T-cell driven. However, recent research revealed that autoimmune pathological processes in MS are more complex and involve multiple cell types and their functionally distinct subsets. Particularly in relapsing multiple sclerosis pathological mechanisms involve imbalanced interactions between T cells, myeloid cells, B cells, and their effector and regulatory subpopulations (22). There is likely no qualitative difference in the pathology between relapsing and progressive MS and to some extent including primary progressive MS. However, the contribution of the pathological processes and alterations differs quantitatively. Focal new and active white matter lesions (representing inflammation) are most numerous in early (acute and relapsing) MS and lesional volume changes are of less dominance when patients enter the progressive stage (23). Diffuse changes in the normal-appearing white matter are sparse in early MS but very pronounced in patients with progressive MS (24). These changes eventually lead to localized (e.g. cortical) and global brain atrophy which can be seen on brain MRI. Therefore, the most commonly used MRI marker for monitoring inflammatory activity is the number or volume of MRI hyperintense lesions (on T2 weighted or FLAIR images). Modern techniques can successfully detect cortical lesions as well (25). Neuromyelitis optica spectrum disorders are rare inflammatory disorders of the central nervous system, manifesting clinically as optic neuritis, myelitis, and certain brain and brainstem syndromes (26). NMOSD may include aquaporin 4 (AQP4)-antibody seropositive autoimmune astrocytopathic disease and AQP4-antibody seronegative patients as well (27). A part of those seronegative patients with clinical NMO phenotype have antibodies to myelin oligodendrocyte glycoprotein (MOG) (28, 29) and represents a relatively new disease entity called myelin oligodendrocyte glycoprotein-antibody associated disease (MOGAD) (30, 31). AQP4-antibody seropositive NMOSD has a high female to male ratio (up to 9:1) with later onset (at the average age above 40) compared to multiple sclerosis (32, 33).

## The effect of sex on the age of clinical onset and diseases course in MS and NMOSD

The relationship between age of onset and sex ratio in different life periods can help to explain the role of sex hormones in MS and NMOSD disease pathogenesis. Sex hormones can affect the function of the immune cells directly *via* binding to the steroid receptors and have various effects on cells of both the adaptive and innate immune systems (3, 34–37). Relapsing MS and NMOSD can sometimes manifest in children and adolescents as well, although rarely. It can be difficult to differentiate MS from other inflammatory demyelinating diseases at an early age. Multiple sclerosis presents with its typical female predominance from puberty onwards, corresponding with reproductive maturing, whilst males seem to be over-represented at very young ages (38). It seems that within the relapsing MS group there are sex differences in relapse characteristics and in the extent of recovery where males show more incomplete recovery from a relapse and more persistent disability (traditionally represented by the Expanded Disability Status Scale, EDSS) (39–41). These sex differences in disability were not observed in late-onset MS or in primary progressive form (41, 42). Kalincik et al. showed that women tend to present with visual and sensory relapses more frequently than men, who are relatively more likely to present with pyramidal (motor), brainstem, and cerebellar relapses (43). Although several studies have evaluated the effect of menopause on MS disease course, including relapse rates, disability progression, and patient-reported outcomes. Data are inconclusive so far but might indicate some increase in disability when comparing before

and after menopause stages (44–46). A systemic hormone treatment used in postmenopausal MS patients was associated with the better physical quality of life in postmenopausal women (47). The effect of hormone therapy (estriol or estroprogestins) combined with glatiramer acetate or interferon beta was also analysed in clinical trials in women with relapsing MS (48–50).

Relatively little is also known about transgender (TGD) issues in patients with multiple sclerosis, who face substantial challenges stemming from chronic illness in combination with psychosocial and other health factors related to transgender issues (51). Gender-affirming exogenous hormone use must be considered because it can influence the risk of MS. The main pattern of treatment for TGD female to male (TrM) is lifelong testosterone (52) and for TGD male to female (TrW), oral or transdermal estrogens, progesterone, and an antiandrogen (cyproterone acetate) are used (53). Pakpoor et al. provided some evidence supporting a potential role for low testosterone and/or feminising hormones on MS risk in TGD males to females (54).

The female predominance in NMOSD occurring in children and adolescents is seen at the ratio of 1.5:1 and 3.25:1 respectively (55). The other study has shown a 5:1 F:M ratio of AQP4-antibody seropositive patients younger than 12 years (56). This being said, elderly individuals are also at risk of developing NMOSD. The proportion of AQP4-antibody seropositive individuals (detection rate), defined by a decade of age, increased exponentially in women after the age of 50. This was not observed in men of the same age (57). How menopause may affect the age of manifestation of NMOSD and the role of sex hormones has not been studied in detail. Increasing age was associated with a decreased risk of relapse in AQP4-antibody seropositive patients (58). Some patients with typical clinical manifestations for neuromyelitis optica are consistently seronegative for AQP4-IgG. The French and German studies and Mayo group reported almost equal or slightly increased F:M ratio (1.2:1; 1.9:1; respectively 1:1) in these cohorts when Wingerchuk criteria for NMO from 2006 were applied (59–61). The proportion of seropositive MOG-IgG patients with NMO phenotype varies between different studies based on applied diagnostic criteria and sensitivity of the cell-based assay used for the antibody assessment. MOG-antibody seropositive patients can account for about 40% of AQP4-antibody seropositive patients who were diagnosed according to the 2015 International panel on NMOSD diagnosis when the highly sensitive live cell-based assay was used (62). The clinical manifestation of MOGAD differs between age groups. The most common presentation in children is acute disseminated encephalomyelitis (ADEM) compared to adults, who typically suffer from optic neuritis at the onset. In the youngest cohort (age <10 years) of MOGAD, we cannot see much difference between males and females but there is a slight female predominance in adolescents and adults (63). Kim et al. have shown an impact of sex on disease onset age and site of relapse when AQP4-antibody seropositive male NMOSD patients had a higher age at onset than women and were less likely to develop optic neuritis as the initial symptom (64). Kitley et al. described a UK-Japanese cohort of patients with disease onset < 30 years of age in which 61% of patients first presented with optic neuritis compared with only 18% presenting with longitudinally extensive transverse myelitis (LETM). In older groups (50 years of age) we see almost the opposite picture as 66% presented with LETM compared with 28% presenting with optic neuritis (65). Whether sex hormones might influence (directly or indirectly) a development or severity of optic neuritis and protect the spinal cord remains unanswered. On the other hand, the protective effects of sex hormones on remyelination after optic neuritis were studied in several works (66–68).

## Radiological aspects of sex difference in MS and NMOSD

Brain atrophy, including grey matter and white matter atrophy measurement, is recently becoming a routine marker to monitor the disease in clinical studies and clinical practice. Over the last 20 years, different studies reported significant differences between sexes in variable measures. Generally, it seems that males are showing more, traditionally associated with degenerative processes, grey matter pathology, and atrophy (69). It seems that grey matter atrophy is affecting not only cortical regions but also deep grey matter represented by the reduction of neuronal mass in basal ganglia (putamen) and thalamus resulting in impairment of cognitive functions (70). Therefore, you can find a very different extent of atrophy in male and female patients with almost identical clinical histories. The brain atrophy dominant in males has been reported in groups of different ethnic origins (71). These sex-specific differences in atrophy measures are seemingly not as prominent early in the disease (72), but changes in those variables, however discreet, are likely pre-dating changes in the clinical picture (73). More questionable results were obtained while studying lesion volume/lesion load in MS patients (74, 75). This would not be surprising as lesion load varies significantly between individuals irrespective of gender. See schematic diagram (Figure 1) summarizing theoretical differences of sex bias in lesion volume, EDSS (clinical scale), and brain atrophy.

Lesions, predominantly present in white matter, would have an impact on white matter (WM) volume too. This obvious relationship between white matter lesions and white matter volume would explain why studies looking at white matter atrophy are showing more contradictory findings. In some studies, it seems that males show more prominent white matter changes associated with axonal loss than females (76). In other work, WM atrophy was even more prominent in females (69). Atrophy of all compartments is seen even in the

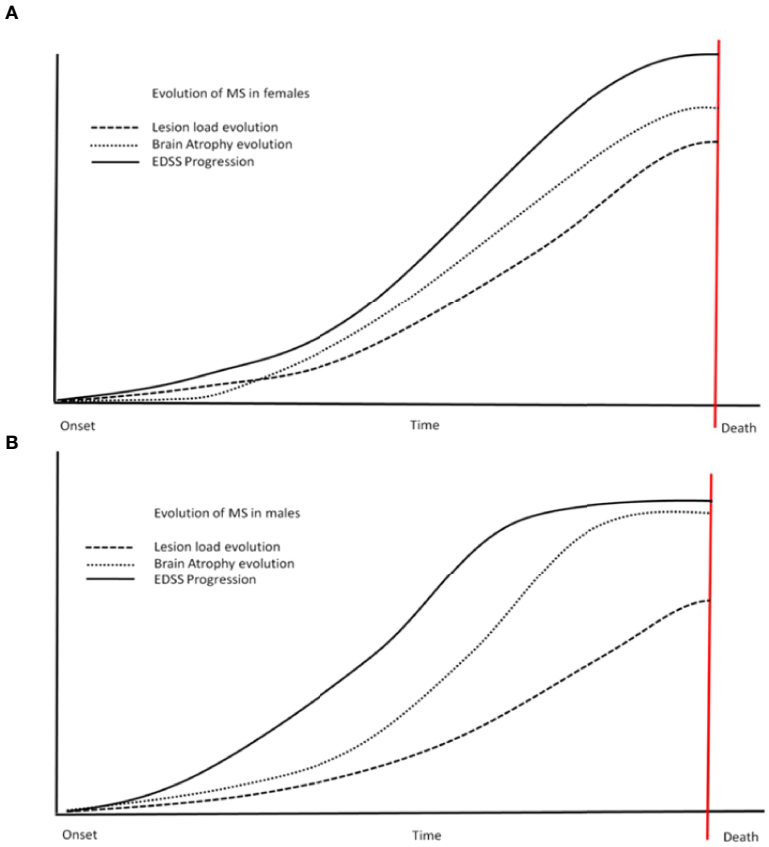


FIGURE 1
Steeper progress for males? This schematic diagram shows the differences in different variables between the sexes (females - **A**, males - **B**). Steeper changes are more obvious in males **(B)** - including atrophy and EDSS. Males also reach a plateau of variables sooner than females (the scheme is not to scale regarding time and values, reflecting trends only). EDSS, expanded disability status scale.

early stages of PPMS (77). Artificial intelligence approaches have been recently tried to evaluate future risks, estimate disability progression, and most importantly monitor response to medication (atrophy-led v. lesion-led estimation) (78).

Unfortunately, no representative studies are focusing on MRI differences between sexes in NMOSD nor the impact of pregnancy on MRI parameters. In recent decades research paid attention to the role of iron and its metabolism in MS and NMOSD. Brain iron homeostasis is known to be disturbed in multiple sclerosis (79–81). The progression of disability in MS seems to inversely correlate with iron concentration, especially in a deep grey matter on MRI imaging (quantitative susceptibility mapping), which could have prognostic and diagnostic value (e.g., helping to differentiate between relapsing or primary progressive MS and in AQP4-antibody seropositive NMOSD) (82–84). The relationship between the clinical stage of MS, disease progression, and amount of iron differs between brain structures examined (putamen, caudate, inflammatory lesions, thalamus, normal-appearing white matter, etc.) (82–86). A correlation was found between the disability (EDSS) and magnetic susceptibility in the putamen in remitting MS (84). However, it is unclear if iron concentration changes are instead related to atrophy and loss of structure with lower concentrations of iron (e.g. myelin and calcium-rich structures) (85). Dedicated research looking at iron levels and sex differences is still to be done as many conducted studies did not analyse that relationship.

## Disease severity during pregnancy and the postpartum period in MS and NMOSD

The influence of sex hormones on autoimmune diseases including the changes in disease severity and activity during or

after pregnancy has been reported in many autoimmune disorders such as systemic lupus erythematosus, myasthenia gravis, etc. (87, 88). Since high levels of hormones during pregnancy enhance Th2 response, this may suppress MS which is driven by Th1 response (89). Pregnancy is not associated with an increased risk of a flare of disease activity in MS. On the contrary, during the post-partum period lesion volume and inflammatory activity can increase T1 lesion volume "black holes" as well as T2 lesion volume in MS. It is usually followed by the clinical activity of the disease (90). While short-term consequences of pregnancy in MS are deemed proven it remains contentious what impact this has on brain atrophy and disability progression in the long term (91–93). Assisted reproductive techniques using gonadotropin-releasing hormone analogues (GnRH; either agonists or antagonists) might be associated with clinical (increased annualized relapse rate during the 3 months following *in vitro* fertilisation) and MRI visible inflammatory activity in MS (94–96). The administration of GnRH antagonist over agonist mainly in females <40 years of age is preferred (97, 98).

Less known is about NMO and pregnancy. NMOSD is mediated mostly by Th2 lymphocytes therefore a higher risk of relapse can be expected. Women with NMO also have an elevated rate of pregnancy complications including preeclampsia, which are associated with increased Th17 cells and reduction of T-regulatory cells (99). These in turn can enhance inflammation in NMOSD and be associated with increased relapse rates and disability in patients with NMOSD during pregnancy, and especially in the early postpartum period (100–102). Increased risk of relapse in those periods in NMOSD patients is also associated with discontinued or insufficient immunosuppressive treatment (101). Pregnancy complications in AQP4-autoantibody seropositive patients might be also related to other autoimmune comorbidity or the presence of autoantibodies such as antiphospholipid antibodies, which have been described in combination (or in absence) of SLE in NMOSD patients (103–106). Aquaporin-4 is expressed by the human placenta (107) and it has been demonstrated that AQP4-IgG could be a causative agent in increased miscarriages in females with AQP4-antibody seropositive NMOSD (105, 108, 109).

Although pregnancy in MS patients is not associated with increased disease activity as mentioned above, it is necessary to consider the disease activity before pregnancy, especially the type of therapy. One of the aspects that must be considered during the reproductive age of MS patients is the teratogenicity of the disease-modifying therapies. Teriflunomide is classified as a teratogen of category X (for both females and males), therefore expected benefits from this treatment do not outweigh drug-associated risks, and its use in pregnant women is contraindicated (110). There was so far no evidence of increased rates of spontaneous abortion, decreased birth weight or congenital malformation in human trials or retrospective pharmacovigilance observation (111, 112). Teriflunomide plasma levels of less than 0.02 mg/L are expected to have no teratogenic impact (112), therefore the rapid elimination procedure of teriflunomide in case of pregnancy is recommended. Another important aspect of

TABLE 1 Summary of sex bias in relapsing multiple sclerosis (MS) and AQP4-antibody seropositive neuromyelitis optica spectrum disorders (NMOSD).

| | Relapsing MS | AQP4-IgG$^{pos}$NMOSD | Possible explanation/association |
|---|---|---|---|
| Epidemiology (female to male ratio) | 2-3:1 in adults (17–19)<br>women show earlier onset (117) | up to 9:1 in adults (32, 33)<br>up to 5:1 in children younger < 12 years (56) | sex hormones affect directly or indirectly function of immune cells ; X dosage compensation and escape from X-inactivation; imprinting of X chromosome genes; epigenetics; X-linked non-coding microRNA (1–16); |
| Clinical features | visual and sensory relapses more frequent in women;<br>motor, brainstem, and cerebellar relapses more frequent in men (43) | male patients have higher age at onset and are more likely to develop myelitis as a first symptom (64) | unknown |
| Imaging | GM and central atrophy are more advanced in male patients, whereas lesion load or gadolinium enhancing lesions are more advanced in female patients (69, 70, 118) | unknown | men develop a lower number of inflammatory lesions in the CNS, but a higher number of degenerative lesions with extensive axonal loss; males have a higher incidence of cortical GM lesions compared to females (120) |
| Disability progression | males show more incomplete recovery from a relapse and more persistent disability (119) | probably not related to sex; influenced by age of disease onset and by delay in diagnosis/treatment (64) | absence of protective effects of females hormones; Y gene presence or absence;differences in parental X imprinting of X chromosome genes (1–7) – f.e. a different expression of TLR7 by cortical neurons in males (121) is also considered in MS |
| Risk of relapse | higher in women (119) | not studied but the risk of relapse is more likely to be associated with younger age (64) | effects of females hormones on the immune system and other sex-related factors that can play role in higher susceptibility for MS in women (1–5) |

GM, grey matter; WM, white matter; TLR7, toll-like receptor 7.

pregnancy planning in MS patients is to consider discontinuation of highly effective therapies such as fingolimod or natalizumab. It has been reported that stopping fingolimod and natalizumab may be a cause of worsening neurological status (113). Disease reactivation following fingolimod cessation is more common in younger patients, those with greater disease activity before cessation, and those who switch to a low-efficacy therapy (114). Fingolimod discontinuation could be a cause of life-threatening relapse, although this is a rare situation (115). Saying all this we have to bear in mind that fingolimod is teratogenic in animals, therefore, would not be a suitable treatment in pregnancy contrary to natalizumab which can be used until the 34th week of gestation in the case of patients with high disease activity (116). Neurologists and obstetricians must be aware of the potential complications of a pregnancy in a woman who has MS but specifically NMOSD.

## Summary

As seen above, sex bias is an extremely important factor (summarized in Table 1). In many cases it defines the prognosis and fate of individual patients. Current up-to-date research is helping us to understand the relationships between the pathophysiology of MS and NMOSD and gender stands in three main areas: clinical (experience of treating clinicians); immuno-chemical (basic and applied research); and radiographic (MRI studies, volumetry, etc.). The key to understanding is a multidisciplinary approach covering all these areas. Sex/gender effect on the incidence, activity, and progression of these disorders should be implemented in the evaluation of any phase of clinical research and treatment choice consideration in clinical practice and evaluation of MRI parameters. Some relationships between clinical variables and sexes remain elusive but with further understanding of sex/gender related differences, we should be able to provide appropriate patient-centered care and research.

## Author contributions

PN has been involved in source collection and wrote the clinical and immunology section of the article. OD was involved in source collection and wrote the radiology section. Both authors participated equally in the graphic and clinical sections. All authors read and approved the final manuscript.

## Funding

The work was supported by the Czech Ministry of Education – project Cooperatio LF1, research area Neuroscience, by Czech Ministry of Health – project NU22-04-00193, and the project of National Institute for Neurological Research (Programme EXCELES, ID project No LX22NPO5107- funded by the European Union-Next Generation EU.

## Conflict of interest

PN has received speaker honoraria and consultant fees from Biogen, Novartis, Merck, Roche, and financial support for research activities from Roche and Merck. OD has received in the past funding for research, speaking honoraria, advisory boards, travel or educational support from Bristol-Myers Squibb, Sanofi Genzyme, Novartis, Biogen and Merck Serono pharmaceuticals.

## Publisher's note



## References

1. Klein SL, Flanagan KL. Sex differences in immune responses. *Nat Rev Immunol* (2016) 16(10):626–38. doi: 10.1038/nri.2016.90

2. Jacobson DL, Gange SJ, Rose NR, Graham NM. Epidemiology and estimated population burden of selected autoimmune diseases in the United States. *Clin Immunol Immunopathol* (1997) 84(3):223–43. doi: 10.1006/clin.1997.4412

3. Rubtsova K, Marrack P, Rubtsov AV. Sexual dimorphism in autoimmunity. *J Clin Invest* (2015) 125(6):2187–93. doi: 10.1172/JCI78082

4. Billi AC, Kahlenberg JM, Gudjonsson JE. Sex bias in autoimmunity. *Curr Opin Rheumatol* (2019) 31(1):53–61. doi: 10.1097/BOR.0000000000000564

5. Voskuhl RR, Sawalha AH, Itoh Y. Sex chromosome contributions to sex differences in multiple sclerosis susceptibility and progression. *Mult Scler* (2018) 24 (1):22–31. doi: 10.1177/1352458517737394

6. Smith-Bouvier DL, Divekar AA, Sasidhar M, Du S, Tiwari-Woodruff SK, King JK, et al. A role for sex chromosome complement in the female bias in autoimmune disease. *J Exp Med* (2008) 205(5):1099–108. doi: 10.1084/jem.20070850

7. Brooks WH. X Chromosome inactivation and autoimmunity. *Clin Rev Allergy Immunol* (2010) 39(1):20–9. doi: 10.1007/s12016-009-8167-5

8. Fontenot JD, Gavin MA, Rudensky AY. Foxp3 programs the development and function of CD4+CD25+ regulatory T cells. *Nat Immunol* (2003) 4(4):330–6. doi: 10.1038/ni904

9. Hori S, Nomura T, Sakaguchi S. Control of regulatory T cell development by the transcription factor Foxp3. *Science* (2003) 299(5609):1057–61. doi: 10.1126/science.1079490

10. Reddy J, Waldner H, Zhang X, Illes Z, Wucherpfennig KW, Sobel RA, et al. Cutting edge: CD4+CD25+ regulatory T cells contribute to gender differences in susceptibility to experimental autoimmune encephalomyelitis. *J Immunol* (2005) 175(9):5591–5. doi: 10.4049/jimmunol.175.9.5591

11. Polansky JK, Kretschmer K, Freyer J, Floess S, Garbe A, Baron U, et al. DNA Methylation controls Foxp3 gene expression. *Eur J Immunol* (2008) 38(6):1654–63. doi: 10.1002/eji.200838105

12. Floess S, Freyer J, Siewert C, Baron U, Olek S, Polansky J, et al. Epigenetic control of the foxp3 locus in regulatory T cells. *PloS Biol* (2007) 5(2):e38. doi: 10.1371/journal.pbio.0050038

13. Schurz H, Salie M, Tromp G, Hoal EG, Kinnear CJ, Moller M. The X chromosome and sex-specific effects in infectious disease susceptibility. *Hum Genomics* (2019) 13(1):2. doi: 10.1186/s40246-018-0185-z

14. Bianchi I, Lleo A, Gershwin ME, Invernizzi P. The X chromosome and immune associated genes. *J Autoimmun* (2012) 38(2-3):J187–92. doi: 10.1016/j.jaut.2011.11.012

15. Carissimi C, Fulci V, Macino G. MicroRNAs: Novel regulators of immunity. *Autoimmun Rev* (2009) 8(6):520–4. doi: 10.1016/j.autrev.2009.01.008

16. Mohamed MS, Nahrery E, Shalaby N, Hussein M, Aal RAE, Mohamed MM. Micro-RNA 18b and interleukin 17A profiles in relapsing remitting multiple sclerosis. *Mult Scler Relat Disord* (2019) 28:226–9. doi: 10.1016/j.msard.2018.12.013

17. Orton SM, Herrera BM, Yee IM, Valdar W, Ramagopalan SV, Sadovnick AD, et al. Sex ratio of multiple sclerosis in Canada: A longitudinal study. *Lancet Neurol* (2006) 5(11):932–6. doi: 10.1016/S1474-4422(06)70581-6

18. Dobson R, Giovannoni G. Multiple sclerosis - A review. *Eur J Neurol* (2019) 26(1):27–40. doi: 10.1111/ene.13819

19. Izquierdo G, Venegas A, Sanabria C, Navarro G. Long-term epidemiology of multiple sclerosis in the northern Seville district. *Acta Neurol Scand* (2015) 132 (2):111–7. doi: 10.1111/ane.12363

20. Miller DH, Leary SM. Primary-progressive multiple sclerosis. *Lancet Neurol* (2007) 6(10):903–12. doi: 10.1016/S1474-4422(07)70243-0

21. Tremlett H, Zhao Y, Devonshire V, Neurologists UBC. Natural history comparisons of primary and secondary progressive multiple sclerosis reveals differences and similarities. *J Neurol* (2009) 256(3):374–81. doi: 10.1007/s00415-009-0039-7

22. Bar-Or A, Li R. Cellular immunology of relapsing multiple sclerosis: interactions, checks, and balances. *Lancet Neurol* (2021) 20(6):470–83. doi: 10.1016/S1474-4422(21)00063-6

23. Lassmann H. Multiple sclerosis pathology. *Cold Spring Harb Perspect Med* (2018) 8(3):a028936. doi: 10.1101/cshperspect.a028936

24. Kutzelnigg A, Lucchinetti CF, Stadelmann C, Bruck W, Rauschka H, Bergmann M, et al. Cortical demyelination and diffuse white matter injury in multiple sclerosis. *Brain* (2005) 128(Pt 11):2705–12. doi: 10.1093/brain/awh641

25. Bouman PM, Strijbis VI, Jonkman LE, Hulst HE, Geurts JJ, Steenwijk MD. Artificial double inversion recovery images for (juxta)cortical lesion visualization in multiple sclerosis. *Mult Scler* (2022) 28(4):541–9. doi: 10.1177/13524585211029860

26. Wingerchuk DM, Banwell B, Bennett JL, Cabre P, Carroll W, Chitnis T, et al. International consensus diagnostic criteria for neuromyelitis optica spectrum disorders. *Neurology* (2015) 85(2):177–89. doi: 10.1212/WNL.0000000000001729

27. Fujihara K. Neuromyelitis optica spectrum disorders: still evolving and broadening. *Curr Opin Neurol* (2019) 32(3):385–94. doi: 10.1097/WCO.0000000000000694

28. Kitley J, Waters P, Woodhall M, Leite MI, Murchison A, George J, et al. Neuromyelitis optica spectrum disorders with aquaporin-4 and myelin-oligodendrocyte glycoprotein antibodies: A comparative study. *JAMA Neurol* (2014) 71(3):276–83. doi: 10.1001/jamaneurol.2013.5857

29. Papp V, Langkilde AR, Blinkenberg M, Schreiber K, Jensen PEH, Sellebjerg F. Clinical utility of anti-MOG antibody testing in a Danish cohort. *Mult Scler Relat Disord* (2018) 26:61–7. doi: 10.1016/j.msard.2018.09.010

30. Fujihara K. MOG-antibody-associated disease is different from MS and NMOSD and should be classified as a distinct disease entity - commentary. *Mult Scler* (2020) 26(3):276–8. doi: 10.1177/1352458519895236

31. Hegen H, Reindl M. Recent developments in MOG-IgG associated neurological disorders. *Ther Adv Neurol Disord* (2020) 13:1756286420945135. doi: 10.1177/1756286420945135

32. Papp V, Illes Z, Magyari M, Koch-Henriksen N, Kant M, Pfleger CC, et al. Nationwide prevalence and incidence study of neuromyelitis optica spectrum disorder in Denmark. *Neurology* (2018) 91(24):e2265–e75. doi: 10.1212/WNL.0000000000006645

33. Flanagan EP, Cabre P, Weinshenker BG, Sauver JS, Jacobson DJ, Majed M, et al. Epidemiology of aquaporin-4 autoimmunity and neuromyelitis optica spectrum. *Ann Neurol* (2016) 79(5):775–83. doi: 10.1002/ana.24617

34. Greene GL, Sobel NB, King WJ, Jensen EV. Immunochemical studies of estrogen receptors. *J Steroid Biochem* (1984) 20(1):51–6. doi: 10.1016/0022-4731(84)90188-2

35. Banchereau J, Briere F, Caux C, Davoust J, Lebecque S, Liu YJ, et al. Immunobiology of dendritic cells. *Annu Rev Immunol* (2000) 18:767–811. doi: 10.1146/annurev.immunol.18.1.767

36. Mor G, Sapi E, Abrahams VM, Rutherford T, Song J, Hao XY, et al. Interaction of the estrogen receptors with the fas ligand promoter in human monocytes. *J Immunol* (2003) 170(1):114–22. doi: 10.4049/jimmunol.170.1.114

37. Bhatia A, Sekhon HK, Kaur G. Sex hormones and immune dimorphism. *Sci World J* (2014) 2014:159150. doi: 10.1155/2014/159150

38. Tintore M, Arrambide G. Early onset multiple sclerosis: The role of gender. *J Neurol Sci* (2009) 286(1-2):31–4. doi: 10.1016/j.jns.2009.07.016

39. Debouverie M, Pittion-Vouyovitch S, Louis S, Guillemin F, Group L. Natural history of multiple sclerosis in a population-based cohort. *Eur J Neurol* (2008) 15(9):916–21. doi: 10.1111/j.1468-1331.2008.02241.x

40. Kalincik T. Multiple sclerosis relapses: Epidemiology, outcomes and management. A systematic review. *Neuroepidemiology* (2015) 44(4):199–214. doi: 10.1159/000382130

41. Ribbons KA, McElduff P, Boz C, Trojano M, Izquierdo G, Duquette P, et al. Male Sex is independently associated with faster disability accumulation in relapse-onset MS but not in primary progressive MS. *PloS One* (2015) 10(6):e0122686. doi: 10.1371/journal.pone.0122686

42. Bove RM, Healy B, Augustine A, Musallam A, Gholipour T, Chitnis T. Effect of gender on late-onset multiple sclerosis. *Mult Scler* (2012) 18(10):1472–9. doi: 10.1177/1352458512438236

43. Kalincik T, Buzzard K, Jokubaitis V, Trojano M, Duquette P, Izquierdo G, et al. Risk of relapse phenotype recurrence in multiple sclerosis. *Mult Scler* (2014) 20(11):1511–22. doi: 10.1177/1352458514528762

44. Bove R, Okai A, Houtchens M, Elias-Hamp B, Lugaresi A, Hellwig K, et al. Effects of menopause in women with multiple sclerosis: An evidence-based review. *Front Neurol* (2021) 12:554375. doi: 10.3389/fneur.2021.554375

45. Bove R, Healy BC, Musallam A, Glanz BI, De Jager PL, Chitnis T. Exploration of changes in disability after menopause in a longitudinal multiple sclerosis cohort. *Mult Scler* (2016) 22(7):935–43. doi: 10.1177/1352458515606211

46. Baroncini D, Annovazzi PO, De Rossi N, Mallucci G, Torri Clerici V, Tonietti S, et al. Impact of natural menopause on multiple sclerosis: a multicentre study. *J Neurol Neurosurg Psychiatry* (2019) 90(11):1201–6. doi: 10.1136/jnnp-2019-320587

47. Bove R, White CC, Fitzgerald KC, Chitnis T, Chibnik L, Ascherio A, et al. Hormone therapy use and physical quality of life in postmenopausal women with multiple sclerosis. *Neurology* (2016) 87(14):1457–63. doi: 10.1212/WNL.0000000000003176

48. De Giglio L, Marinelli F, Barletta VT, Pagano VA, De Angelis F, Fanelli F, et al. Effect on cognition of estroprogestins combined with interferon beta in multiple sclerosis: Analysis of secondary outcomes from a randomised controlled trial. *CNS Drugs* (2017) 31(2):161–8. doi: 10.1007/s40263-016-0401-0

49. Voskuhl RR, Wang H, Wu TC, Sicotte NL, Nakamura K, Kurth F, et al. Estriol combined with glatiramer acetate for women with relapsing-remitting multiple sclerosis: A randomised, placebo-controlled, phase 2 trial. *Lancet Neurol* (2016) 15(1):35–46. doi: 10.1016/S1474-4422(15)00322-1

50. Pozzilli C, De Giglio L, Barletta VT, Marinelli F, Angelis FD, Gallo V, et al. Oral contraceptives combined with interferon beta in multiple sclerosis. *Neurol Neuroimmunol Neuroinflamm* (2015) 2(4):e120. doi: 10.1212/NXI.0000000000000120

51. Sullivan A, Kane A, Valentic G, Rensel M. Recommendations to address the unique clinical and psychological needs of transgender persons living with multiple sclerosis. *Int J MS Care* (2022) 24(1):35–40. doi: 10.7224/1537-2073.2021-066

52. Irwig MS. Testosterone therapy for transgender men. *Lancet Diabetes Endocrinol* (2017) 5(4):301–11. doi: 10.1016/S2213-8587(16)00036-X

53. Tangpricha V, den Heijer M. Oestrogen and anti-androgen therapy for transgender women. *Lancet Diabetes Endocrinol* (2017) 5(4):291–300. doi: 10.1016/S2213-8587(16)30319-9

54. Pakpoor J, Wotton CJ, Schmierer K, Giovannoni G, Goldacre MJ. Gender identity disorders and multiple sclerosis risk: A national record-linkage study. *Mult Scler* (2016) 22(13):1759–62. doi: 10.1177/1352458515627205

55. Chitnis T, Ness J, Krupp L, Waubant E, Hunt T, Olsen CS, et al. Clinical features of neuromyelitis optica in children: US network of pediatric MS centers report. *Neurology* (2016) 86(3):245–52. doi: 10.1212/WNL.0000000000002283

56. Camera V, Messina S, Elhadd KT, Sanpera-Iglesias J, Mariano R, Hacohen Y, et al. Early predictors of disability of paediatric-onset AQP4-IgG-seropositive neuromyelitis optica spectrum disorders. *J Neurol Neurosurg Psychiatry* (2022) 93 (1):101–11. doi: 10.1136/jnnp-2021-327206

57. Quek AM, McKeon A, Lennon VA, Mandrekar JN, Iorio R, Jiao Y, et al. Effects of age and sex on aquaporin-4 autoimmunity. *Arch Neurol* (2012) 69 (8):1039–43. doi: 10.1001/archneurol.2012.249

58. Kunchok A, Malpas C, Nytrova P, Havrdova EK, Alroughani R, Terzi M, et al. Clinical and therapeutic predictors of disease outcomes in AQP4-IgG+ neuromyelitis optica spectrum disorder. *Mult Scler Relat Disord* (2020) 38:101868. doi: 10.1016/j.msard.2019.101868

59. Marignier R, Bernard-Valnet R, Giraudon P, Collongues N, Papeix C, Zephir H, et al. Aquaporin-4 antibody-negative neuromyelitis optica: distinct assay sensitivity-dependent entity. *Neurology* (2013) 80(24):2194–200. doi: 10.1212/WNL.0b013e318296e917

60. Jiao Y, Fryer JP, Lennon VA, Jenkins SM, Quek AM, Smith CY, et al. Updated estimate of AQP4-IgG serostatus and disability outcome in neuromyelitis optica. *Neurology* (2013) 81(14):1197–204. doi: 10.1212/WNL.0b013e3182a6cb5c

61. Jarius S, Ruprecht K, Wildemann B, Kuempfel T, Ringelstein M, Geis C, et al. Contrasting disease patterns in seropositive and seronegative neuromyelitis optica: A multicentre study of 175 patients. *J Neuroinflammation* (2012) 9:14. doi: 10.1186/1742-2094-9-14

62. Hamid SHM, Whittam D, Mutch K, Linaker S, Solomon T, Das K, et al. What proportion of AQP4-IgG-negative NMO spectrum disorder patients are MOG-IgG positive? A cross sectional study of 132 patients. *J Neurol* (2017) 264 (10):2088–94. doi: 10.1007/s00415-017-8596-7

63. Marignier R, Hacohen Y, Cobo-Calvo A, Probstel AK, Aktas O, Alexopoulos H, et al. Myelin-oligodendrocyte glycoprotein antibody-associated disease. *Lancet Neurol* (2021) 20(9):762–72. doi: 10.1016/S1474-4422(21)00218-0

64. Kim SM, Waters P, Woodhall M, Kim YJ, Kim JA, Cheon SY, et al. Gender effect on neuromyelitis optica spectrum disorder with aquaporin4-immunoglobulin G. *Mult Scler* (2017) 23(8):1104–11. doi: 10.1177/1352458516674366

65. Kitley J, Leite MI, Nakashima I, Waters P, McNeillis B, Brown R, et al. Prognostic factors and disease course in aquaporin-4 antibody-positive patients with neuromyelitis optica spectrum disorder from the United Kingdom and Japan. *Brain* (2012) 135(Pt 6):1834–49. doi: 10.1093/brain/aws109

66. Kim RY, Mangu D, Hoffman AS, Kavosh R, Jung E, Itoh N, et al. Oestrogen receptor β ligand acts on CD11c+ cells to mediate protection in experimental autoimmune encephalomyelitis. *Brain* (2018) 141(1):132–47. doi: 10.1093/brain/awx315

67. Nuzzi R, Scalabrin S, Becco A, Panzica G. Sex hormones and optic nerve disorders: A review. *Front Neurosci* (2019) 13:57. doi: 10.3389/fnins.2019.00057

68. Hussain R, Ghoumari AM, Bielecki B, Steibel J, Boehm N, Liere P, et al. The neural androgen receptor: A therapeutic target for myelin repair in chronic demyelination. *Brain* (2013) 136(Pt 1):132–46. doi: 10.1093/brain/aws284

69. Antulov R, Weinstock-Guttman B, Cox JL, Hussein S, Durfee J, Caiola C, et al. Gender-related differences in MS: A study of conventional and nonconventional MRI measures. *Mult Scler* (2009) 15(3):345–54. doi: 10.1177/1352458508099479

70. Voskuhl RR, Patel K, Paul F, Gold SM, Scheel M, Kuchling J, et al. Sex differences in brain atrophy in multiple sclerosis. *Biol Sex Differ* (2020) 11(1):49. doi: 10.1186/s13293-020-00326-3

71. Rojas JI, Patrucco L, Besada C, Funes J, Cristiano E. [Sex-related differences in atrophy and lesion load in multiple sclerosis patients]. *Neurologia* (2013) 28 (7):389–93. doi: 10.1016/j.nrl.2012.10.008

72. Dolezal O, Gabelic T, Horakova D, Bergsland N, Dwyer MG, Seidl Z, et al. Development of gray matter atrophy in relapsing-remitting multiple sclerosis is not gender dependent: results of a 5-year follow-up study. *Clin Neurol Neurosurg* (2013) 115 Suppl 1:S42–8. doi: 10.1016/j.clineuro.2013.09.020

73. Hanninen K, Viitala M, Paavilainen T, Karhu JO, Rinne J, Koikkalainen J, et al. Thalamic atrophy without whole brain atrophy is associated with absence of 2-year NEDA in multiple sclerosis. *Front Neurol* (2019) 10:459. doi: 10.3389/fneur.2019.00459

74. Ng Kee Kwong KC, Mollison D, Meijboom R, York EN, Kampaite A, Thrippleton MJ, et al. The prevalence of paramagnetic rim lesions in multiple sclerosis: A systematic review and meta-analysis. *PloS One* (2021) 16(9):e0256845. doi: 10.1371/journal.pone.0256845

75. Marschallinger R, Muhlau M, Pongratz V, Kirschke JS, Marschallinger S, Schmidt P, et al. Geostatistical analysis of white matter lesions in multiple sclerosis identifies gender differences in lesion evolution. *Front Mol Neurosci* (2018) 11:460. doi: 10.3389/fnmol.2018.00460

76. Klistorner A, Wang C, Yiannikas C, Graham SL, Parratt J, Barnett MH. Progressive injury in chronic multiple sclerosis lesions is gender-specific: A DTI study. *PloS One* (2016) 11(2):e0149245. doi: 10.1371/journal.pone.0149245

77. Sastre-Garriga J, Ingle GT, Chard DT, Ramio-Torrenta L, Miller DH, Thompson AJ. Grey and white matter atrophy in early clinical stages of primary progressive multiple sclerosis. *Neuroimage* (2004) 22(1):353–9. doi: 10.1016/j.neuroimage.2004.02.008

78. Eshaghi A, Young AL, Wijeratne PA, Prados F, Arnold DL, Narayanan S, et al. Identifying multiple sclerosis subtypes using unsupervised machine learning and MRI data. *Nat Commun* (2021) 12(1):2078. doi: 10.1038/s41467-021-22265-2

79. Stankiewicz JM, Neema M, Ceccarelli A. Iron and multiple sclerosis. *Neurobiol Aging* (2014) 35 Suppl 2:S51–8. doi: 10.1016/j.neurobiolaging.2014.03.039

80. Craelius W, Migdal MW, Luessenhop CP, Sugar A, Mihalakis I. Iron deposits surrounding multiple sclerosis plaques. *Arch Pathol Lab Med* (1982) 106(8):397–9.

81. Paling D, Tozer D, Wheeler-Kingshott C, Kapoor R, Miller DH, Golay X. Reduced R2' in multiple sclerosis normal appearing white matter and lesions may reflect decreased myelin and iron content. *J Neurol Neurosurg Psychiatry* (2012) 83 (8):785–92. doi: 10.1136/jnnp-2012-302541

82. Schweser F, Hagemeier J, Dwyer MG, Bergsland N, Hametner S, Weinstock-Guttman B, et al. Decreasing brain iron in multiple sclerosis: The difference between concentration and content in iron MRI. *Hum Brain Mapp* (2021) 42 (5):1463–74. doi: 10.1002/hbm.25306

83. Burgetova A, Dusek P, Vaneckova M, Horakova D, Langkammer C, Krasensky J, et al. Thalamic iron differentiates primary-progressive and relapsing-remitting multiple sclerosis. *AJNR Am J Neuroradiol* (2017) 38 (6):1079–86. doi: 10.3174/ajnr.A5166

84. Pudlac A, Burgetova A, Dusek P, Nytrova P, Vaneckova M, Horakova D, et al. Deep Gray matter iron content in neuromyelitis optica and multiple sclerosis. *BioMed Res Int* (2020) 2020:6492786. doi: 10.1155/2020/6492786

85. Hagemeier J, Zivadinov R, Dwyer MG, Polak P, Bergsland N, Weinstock-Guttman B, et al. Changes of deep gray matter magnetic susceptibility over 2 years in multiple sclerosis and healthy control brain. *NeuroImage Clin* (2018) 18:1007–16. doi: 10.1016/j.nicl.2017.04.008

86. Haider L, Simeonidou C, Steinberger G, Hametner S, Grigoriadis N, Deretzi G, et al. Multiple sclerosis deep grey matter: the relation between demyelination, neurodegeneration, inflammation and iron. *J Neurol Neurosurg Psychiatry* (2014) 85(12):1386–95. doi: 10.1136/jnnp-2014-307712

87. Doria A, Iaccarino L, Sarzi-Puttini P, Ghirardello A, Zampieri S, Arienti S, et al. Estrogens in pregnancy and systemic lupus erythematosus. *Ann N Y Acad Sci* (2006) 1069:247–56. doi: 10.1196/annals.1351.022

88. Varner M. Myasthenia gravis and pregnancy. *Clin Obstet Gynecol* (2013) 56 (2):372–81. doi: 10.1097/GRF.0b013e31828e92c0

89. Saito S, Nakashima A, Shima T, Ito M. Th1/Th2/Th17 and regulatory T-cell paradigm in pregnancy. *Am J Reprod Immunol* (2010) 63(6):601–10. doi: 10.1111/j.1600-0897.2010.00852.x

90. Anderson A, Krysko KM, Rutatangwa A, Krishnakumar T, Chen C, Rowles W, et al. Clinical and radiologic disease activity in pregnancy and postpartum in MS. *Neurol Neuroimmunol Neuroinflamm* (2021) 8(2). doi: 10.1212/NXI.0000000000000959

91. Khalid F, Healy BC, Dupuy SL, Chu R, Chitnis T, Bakshi R, et al. Quantitative MRI analysis of cerebral lesions and atrophy in post-partum patients with multiple sclerosis. *J Neurol Sci* (2018) 392:94–9. doi: 10.1016/j.jns.2018.06.025

92. Uher T, Kubala Havrdova E, Vodehnalova K, Krasensky J, Capek V, Vaneckova M, et al. Pregnancy-induced brain magnetic resonance imaging changes in women with multiple sclerosis. *Eur J Neurol* (2022) 29(5):1446–56. doi: 10.1111/ene.15245

93. Portaccio E, Ghezzi A, Hakiki B, Sturchio A, Martinelli V, Moiola L, et al. Postpartum relapses increase the risk of disability progression in multiple sclerosis: The role of disease modifying drugs. *J Neurol Neurosurg Psychiatry* (2014) 85 (8):845–50. doi: 10.1136/jnnp-2013-306054

94. Michel L, Foucher Y, Vukusic S, Confavreux C, de Seze J, Brassat D, et al. Increased risk of multiple sclerosis relapse after *in vitro* fertilisation. *J Neurol Neurosurg Psychiatry* (2012) 83(8):796–802. doi: 10.1136/jnnp-2012-302235

95. Hellwig K, Schimrigk S, Beste C, Muller T, Gold R. Increase in relapse rate during assisted reproduction technique in patients with multiple sclerosis. *Eur Neurol* (2009) 61(2):65–8. doi: 10.1159/000177937

96. Correale J, Farez MF, Ysrraelit MC. Increase in multiple sclerosis activity after assisted reproduction technology. *Ann Neurol* (2012) 72(5):682–94. doi: 10.1002/ana.23745

97. Kaisey M, Sicotte N, Giesser B. Multiple sclerosis management and reproductive changes: A guide for general neurologists. *Neurol Clin Pract* (2018) 8(2):142–7. doi: 10.1212/CPJ.0000000000000436

98. Toftager M, Bogstad J, Bryndorf T, Lossl K, Roskaer J, Holland T, et al. Risk of severe ovarian hyperstimulation syndrome in GnRH antagonist versus GnRH agonist protocol: RCT including 1050 first IVF/ICSI cycles. *Hum Reprod* (2016) 31 (6):1253–64. doi: 10.1093/humrep/dew051

99. Davoudi V, Keyhanian K, Bove RM, Chitnis T. Immunology of neuromyelitis optica during pregnancy. *Neurol Neuroimmunol Neuroinflamm* (2016) 3(6):e288. doi: 10.1212/NXI.0000000000000288

100. Kim W, Kim SH, Nakashima I, Takai Y, Fujihara K, Leite MI, et al. Influence of pregnancy on neuromyelitis optica spectrum disorder. *Neurology* (2012) 78(16):1264–7. doi: 10.1212/WNL.0b013e318250d812

101. Shimizu Y, Fujihara K, Ohashi T, Nakashima I, Yokoyama K, Ikeguch R, et al. Pregnancy-related relapse risk factors in women with anti-AQP4 antibody positivity and neuromyelitis optica spectrum disorder. *Mult Scler* (2016) 22 (11):1413–20. doi: 10.1177/1352458515583376

102. Fragoso YD, Adoni T, Bichuetti DB, Brooks JB, Ferreira ML, Oliveira EM, et al. Neuromyelitis optica and pregnancy. *J Neurol* (2013) 260(10):2614–9. doi: 10.1007/s00415-013-7031-y

103. Mehta LR, Samuelsson MK, Kleiner AK, Goodman AD, Anolik JH, Looney RJ, et al. Neuromyelitis optica spectrum disorder in a patient with systemic lupus erythematosus and anti-phospholipid antibody syndrome. *Mult Scler* (2008) 14 (3):425–7. doi: 10.1177/1352458507084107

104. Iyer A, Elsone L, Appleton R, Jacob A. A review of the current literature and a guide to the early diagnosis of autoimmune disorders associated with neuromyelitis optica. *Autoimmunity* (2014) 47(3):154–61. doi: 10.3109/08916934.2014.883501

105. Squatrito D, Colagrande S, Emmi L. Devic's syndrome and primary APS: a new immunological overlap. *Lupus* (2010) 19(11):1337–9. doi: 10.1177/0961203310368968

106. Komolafe MA, Komolafe EO, Sunmonu TA, Olateju SO, Asaleye CM, Adesina OA, et al. New onset neuromyelitis optica in a young Nigerian woman with possible antiphospholipid syndrome: A case report. *J Med Case Rep* (2008) 2:348. doi: 10.1186/1752-1947-2-348

107. Escobar J, Gormaz M, Arduini A, Gosens K, Martinez A, Perales A, et al. Expression of aquaporins early in human pregnancy. *Early Hum Dev* (2012) 88 (8):589–94. doi: 10.1016/j.earlhumdev.2012.01.009

108. Nour MM, Nakashima I, Coutinho E, Woodhall M, Sousa F, Revis J, et al. Pregnancy outcomes in aquaporin-4-positive neuromyelitis optica spectrum disorder. *Neurology* (2016) 86(1):79–87. doi: 10.1212/WNL.0000000000002208

109. Reuss R, Rommer PS, Bruck W, Paul F, Bolz M, Jarius S, et al. A woman with acute myelopathy in pregnancy: Case outcome. *BMJ* (2009) 339:b4026. doi: 10.1136/bmj.b4026

110. Lu E, Wang BW, Guimond C, Synnes A, Sadovnick AD, Dahlgren L, et al. Safety of disease-modifying drugs for multiple sclerosis in pregnancy: Current challenges and future considerations for effective pharmacovigilance. *Expert Rev Neurother* (2013) 13(3):251–60. doi: 10.1586/ern.13.12

111. Kieseier BC, Benamor M. Pregnancy outcomes following maternal and paternal exposure to teriflunomide during treatment for relapsing-remitting multiple sclerosis. *Neurol Ther* (2014) 3(2):133–8. doi: 10.1007/s40120-014-0020-y

112. Aly L, Hemmer B, Korn T. From leflunomide to teriflunomide: Drug development and immunosuppressive oral drugs in the treatment of multiple sclerosis. *Curr Neuropharmacol* (2017) 15(6):874–91. doi: 10.2174/1570159X14666161208151525

113. Papeix C, Vukusic S, Casey R, Debard N, Stankoff B, Mrejen S, et al. Risk of relapse after natalizumab withdrawal: Results from the French TYSEDMUS cohort. *Neurol Neuroimmunol Neuroinflamm* (2016) 3(6):e297. doi: 10.1212/NXI.0000000000000297

114. Malpas CB, Roos I, Sharmin S, Buzzard K, Skibina O, Butzkueven H, et al. Multiple sclerosis relapses following cessation of fingolimod. *Clin Drug Investig* (2022) 42(4):355–64. doi: 10.1007/s40261-022-01129-7

115. Lapucci C, Baroncini D, Cellerino M, Boffa G, Callegari I, Pardini M, et al. Different MRI patterns in MS worsening after stopping fingolimod. *Neurol Neuroimmunol Neuroinflamm* (2019) 6(4):e566. doi: 10.1212/NXI.0000000000000566

116. Varyte G, Arlauskiene A, Ramasauskaite D. Pregnancy and multiple sclerosis: an update. *Curr Opin Obstet Gynecol* (2021) 33(5):378–83. doi: 10.1097/GCO.0000000000000731

117. Miclea A, Salmen A, Zoehner G, Diem L, Kamm CP, Chaloulos-Iakovidis P, et al. Age-dependent variation of female preponderance across different phenotypes of multiple sclerosis: A retrospective cross-sectional study. *CNS Neurosci Ther* (2019) 25(4):527–31. doi: 10.1111/cns.13083

118. Weatherby SJ, Mann CL, Davies MB, Fryer AA, Haq N, Strange RC, et al. A pilot study of the relationship between gadolinium-enhancing lesions, gender effect and polymorphisms of antioxidant enzymes in multiple sclerosis. *J Neurol* (2000) 247(6):467–70. doi: 10.1007/s004150070179

119. Kalincik T, Vivek V, Jokubaitis V, Lechner-Scott J, Trojano M, Izquierdo G, et al. Sex as a determinant of relapse incidence and progressive course of multiple sclerosis. *Brain* (2013) 136(Pt 12):3609–17. doi: 10.1093/brain/awt281

120. Gilli F, DiSano KD, Pachner AR. SeXX matters in multiple sclerosis. *Front Neurol* (2020) 11:616. doi: 10.3389/fneur.2020.00616

121. Du S, Itoh N, Askarinam S, Hill H, Arnold AP, Voskuhl RR. XY sex chromosome complement, compared with XX, in the CNS confers greater neurodegeneration during experimental autoimmune encephalomyelitis. *Proc Natl Acad Sci U S A* (2014) 111(7):2806–11. doi: 10.1073/pnas.1307091111

frontiers | Frontiers in Immunology

TYPE Original Research
PUBLISHED 24 August 2022
DOI 10.3389/fimmu.2022.938326



OPEN ACCESS

EDITED BY
Jiong Chen,
Ningbo University, China

REVIEWED BY
Xuemei Li,
Chinese Academy of Fishery Sciences (CAFS), China
Haipeng Guo,
Ningbo University, China

*CORRESPONDENCE
Daji Luo
luodaji@ihb.ac.cn

SPECIALTY SECTION
This article was submitted to Comparative Immunology, a section of the journal Frontiers in Immunology

RECEIVED 07 May 2022
ACCEPTED 08 August 2022
PUBLISHED 24 August 2022

CITATION
Meng K, Lin X, Liu H, Chen H, Liu F, Xu Z, Sun Y and Luo D (2022) Gonadal bacterial community composition is associated with sex-specific differences in swamp eels *Monopterus albus*. *Front. Immunol.* 13:938326. doi: 10.3389/fimmu.2022.938326



# Gonadal bacterial community composition is associated with sex-specific differences in swamp eels *(Monopterus albus)*

Kaifeng Meng[1,2], Xing Lin[1,3], Hairong Liu[1], Huijie Chen[1,2], Fei Liu[1,3], Zhen Xu[1,3], Yonghua Sun[1,3] and Daji Luo[1,2,3]*

[1]State Key Laboratory of Freshwater Ecology and Biotechnology, Institute of Hydrobiology, The Innovative Academy of Seed Design, Hubei Hongshan Laboratory, Chinese Academy of Sciences, Wuhan, China, [2]College of Fisheries, Huazhong Agricultural University, Wuhan, China, [3]College of Advanced Agricultural Sciences, University of Chinese Academy of Sciences, Beijing, China

Organisms are colonized by microorganism communities and play a pivotal role in host function by influencing physiology and development. In mammals, bacterial community may alter gonadal maturation and drive sex-specific differences in gene expression and metabolism. However, bacterial microbiota diversity in the gonads of early vertebrates has not been fully elucidated. Here, we focused on the swamp eel (*Monopterus albus*), which naturally undergoes sex reversal, and systematically analyzed the bacterial microbiota profiles between females and males using 16S rRNA gene sequences. Specifically, the microbial abundance and community diversity of gonads in males were higher than in females. Although Proteobacteria, Firmicutes, Bacteroidetes, and Actinobacteria were characterized as the dominating phyla in ovary and testis, the relative abundance of Firmicutes was significantly higher in males than females. Detailed analysis of the microbial community revealed that *Bacilli* were the dominant bacteria in ovaries and *Clostridium* in testes of *M. albus*. More importantly, we proposed that differences in the microbial composition and distribution between ovaries and testes may be linked to functional categories in *M. albus*, especially metabolism. These findings represent a unique resource of bacterial community in gonads to facilitate future research about the mechanism of how microbiota influence sex-specific differences and sex reversal in vertebrates.

KEYWORDS

**bacterial community, sex-specific differences, gonads, swamp eel (*monopterus albus*), 16S rRNA gene sequences**

## Highlights

1. Microbial abundance and community diversity of gonads in *M. albus* are present at higher levels in males than females;
2. *Bacilli* may be the dominant bacteria in ovaries and *Clostridium* in testes of *M. albus*;
3. Bacterial community may be linked to gonadal development and function in *M. albus*.

## Introduction

Vertebrate surfaces are inhabited by dense and complex microbial populations characterized by remarkable dynamism and exceptional stability (1, 2). Shaped by millennia of evolution, beneficial and balanced relationships have developed between hosts and microbes, where microbes play essential roles in many biological functions, including development, nutrition, and immune responses (3–5). Thus, a balanced microbiome helps maintain normal host physiology, and imbalances may be linked to physiological disorders (6). Evidence is accumulating about the microbiome's roles in various sexual dimorphisms and sex-specific rhythms in mammals (7). The commensal microbial community alters testosterone, a gonadal steroid related to the gonadal transition in species that undergo sex reversal (8, 9). Besides that, it is bacterial microbiota (*Lactobacillus* and *Clostridia*) that is responsible for semen quality and fertility status in mammals (10, 11). Changes in the abundance of multiple bacteria from the Bacteroidetes and Firmicutes phyla are associated with polycystic ovary syndrome (PCOS) (12). However, how sex-specific differences influence bacterial microbiota diversity in early vertebrates has not been fully elucidated.

Water is a microbial-rich environment that promotes bacterial growth compare to air. In other words, the vertebrate transition from water to land likely affected the relationships between hosts and their microbial community (13). Thus, studies on bacterial microbiome of fish may provide a broader understanding of vertebrate microbiomes due to the complexity and diversity of the microbes in fish habitats. At present, most studies have focused on the compositions of bacterial communities on teleost mucosal surfaces and found that different tissues are inhabited by unique microbial communities and proportions of specific bacteria (13, 14). In addition, it was illustrated that gender was one of the factors influencing the intestinal microbial composition in *D. rerio*, *M. albus*, *B. pectinirostris* and *C. guichenoti* (15–18). A recent study identified that the cloaca of Atlantic salmon (*Salmon salar*) was an additional teleost mucosa-associated lymphoid tissue (MALT), and we hypothesized that gonads connecting the cloaca also harbor abundant microbial communities as a matter of course (19, 20). Although preliminary descriptions of testicular microbiota compositions in zebrafish have shown that *Pseudomonas*, *Lactobacillus*, and *Bifidobacterium* are the main genera (21), the gonadal microorganisms driven by sex differences remain to be elucidated in most teleost species.

The swamp eel (*Monopterus albus*) is a typical protogynous hermaphrodite fish that undergoes sexual reversal from female to male during its lifecycle (22). The sex reversal process involves coordinated transformations across multiple factors, including primordial germ cells and neuroendocrine and molecular axes (23–27). Several studies have reported that the bacterial community is critical to sex-specific differences in gene expression and metabolism in mammals (7). These findings suggest a new mechanism that the bacterial community might affect host sexual maturation (28). Sexual fate can no longer be considered an irreversible deterministic process in many fish. Exploring whether the bacterial community is required for the underlying biological processes of sex is a worthy scientific endeavor. In brief, comparing the microbial differences in *M. albus* from the perspective of the essential tissues, gonads, will increase our understanding of sex-specific differences.

In the present study, *M. albus* of the same age were chosen as our experimental animal and kept under identical conditions (e.g., environment, diet). Sex identification showed that male individuals appeared in the population of *M. albus* through artificial propagation. Moreover, dramatic differences of the bacterial composition and distribution between testis and ovary in *M. albus*, suggesting that gonadal microbiota may be sex-specific differences. In addition, key bacterial community in ovary and testis were screened, providing favorable practical significance for the production of *M. albus*.

## Materials and methods

### Fish maintenance

The *M. albus* was originally purchased from Baishazhou Agricultural Market, Wuhan, China (22). After domestication under laboratory conditions, healthy and mature *M. albus* were selected as parents to generate the F1 sibling generation offspring using artificial insemination (Figure 1A). After artificial insemination, embryos were incubated in the incubator of cell culture room until the mouth-opening stage of larval *M. albus*. Hatching occurred 7 dpf (days post fertilization) at 27 ± 1°C. After the juveniles could eat the bloodworms, they were randomly divided into 3 groups (Dup1, Dup2 and Dup3 as parallel experiments) and transferred to the indoor circulating system involving appropriate temperature (25-28°C), pH value (7.2-8.0), and dissolved oxygen over 14 months (Figure 1B).

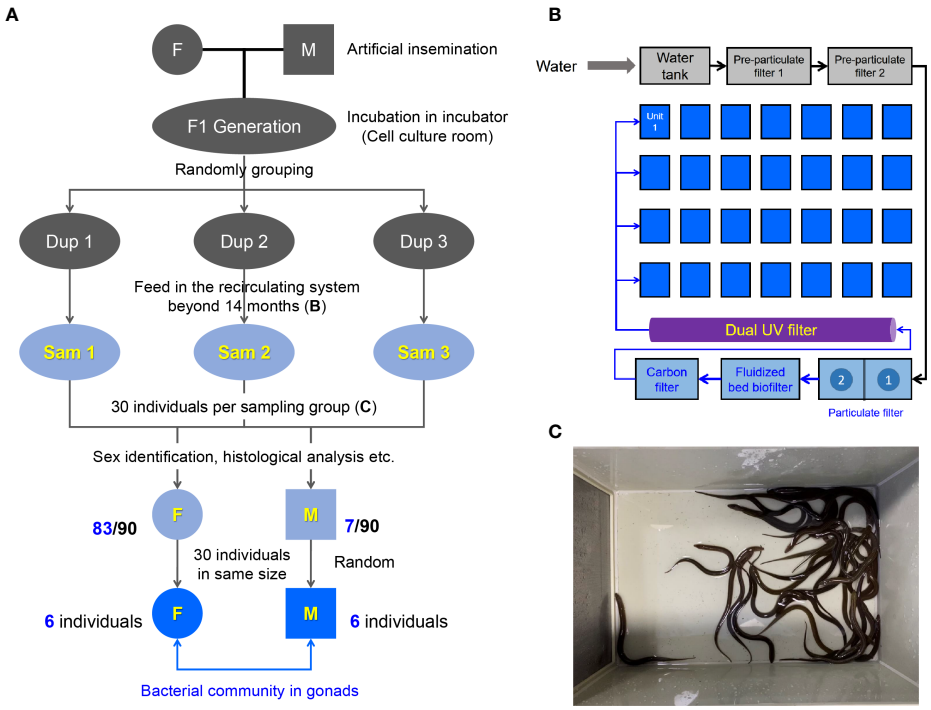


FIGURE 1
Design and sampling of this study. **(A)** Generation of sibling population in *M. albus* and experimental sampling design. **(B)** Schematic diagram of the recirculating system. **(C)** 30 individuals were randomly selected as the sampling group from the unit of the recirculating system.

Frozen bloodworm at a rate of 0.5%-1% body weight was fed twice a day (9:00 a.m. and 4:00 p.m.) during the whole feeding process in the indoor recirculating system. Experimental fish (30 individuals per group) were randomly selected from each Dup group and transferred to plastic boxes one week prior to sampling (Sam1, Sam2 and Sam3 group as experimental duplication) (Figure 1C). During this period, fish were terminated from feeding and half of the culture water was replaced with ultrapure water every three days. After sex identification, 30 individuals of similar size including females and males were screened according to the size of fish for the subsequent study. All animal procedures were carried out in accordance with the Guiding Principles for the Care and Use of Laboratory Animals and approved by the Institute of Hydrobiology, Chinese Academy of Sciences.

## Sample collection

Before sampling, the water of fish living (3 replicate water samples) was firstly collected for 16S rRNA gene sequencing to obtain the background composition of bacterial community in water environment (Supplementary Figure 1). Subsequently, the *M. albus* were anesthetized with MS-222 and the length and weight were measured. After the fish body surface was swabbed with 75% ethanol, the blood then was collected and immediately transferred to a 2 ml sterile blood collection vessel and centrifuged at 3000 rpm for 30 min to obtain serum. After sterile dissection, the gonads were collected, weighed, and divided into three parts. One of them was fixed immediately at 4% (v/v) neutral buffer paraformaldehyde for sex identification. The other part was collected in sterile micro-centrifuge tubes with 1 ml TRIZol for RNA extraction and quantitative real-time PCR (qRT-PCR). The last part was stored in sterile freezing tubes for bacteria 16S rRNA gene sequencing. The weight relationship between gonads and body was represented by GSI (Wgonad/Wbody×100%). All of these tissues collected for RNA or DNA analyses were immediately frozen with liquid nitrogen and stored at -80°C for further study.

## Measurement and analysis of sex hormones

The serum samples were thawed on ice, and separated into two centrifuge tubes. One of the duplicate samples was used for estradiol analysis and the other for testosterone. The concentrations of estradiol and testosterone in serum were determined by using fish-specific enzyme-linked immunosorbent assay (ELISA) kits (MEIMIAN, China)

according to the manufacturer's instructions. Briefly, the serum was incubated in microelisa stripplate at 37°C for 30 min. After washing five times with wash solution, 50 µl HRP-Conjunction reagent was added and incubated at 37°C for 30 min. The 50 µl chromogen solution was added for 10 min followed by 50 µl stop solution. The OD values of each well were detected at 450 nm absorbance (MD SpectraMax M5 Microplate Reader, USA) after adding the stop solution.

## Histology and light microscopy studies

After fixed in 4% neutral formalin buffer more than 24 hours, the gonads were dehydrated through a series of ethanol gradient, washed with xylene, embedded in paraffin, and then sectioned into 4 µm pieces. The paraffin pieces were stained with classic hematoxylin and eosin (H&E) as follows: dewaxed in xylene, rehydrated through a graded ethanol series, stained the nucleus with hematoxylin solution and cytoplasm with eosin solution, finally sealed by resin. Subsequently, images were acquired in a microscope (Nikon, Japan) using the CaseViewer software.

## Micro-CT scanning

To distinguish the anatomical relationships between the gonads and the gut in *M. albus*, we performed the CT investigations. Specifically, *M. albus* was fixed in 4% neutral formalin buffer more than 24 hours, then dehydrated through a series of ethanol gradient for 4 days. After gradient dehydration, *M. albus* was immersed in phosphotungstic acid (6 mg/ml) diluted with ethanol at 37°C for 10 days. Subsequently, *M. albus* was subjected to fixed bed and scanned with Skyscan High Resolution Micro-CT Imaging System (Bruker, Belgium). The Data Viewer software and CTvox software was used for post-processing and capture of pictures (Supplementary Figure 2).

## RNA extraction and quantitative real-time PCR analysis

Total RNA was extracted from gonads which were homogenized in 1 mL TRIZol (Invitrogen, USA) by shaking (60 HZ for 1 min) with 3 mm beads following the manufacturer's instructions. To normalize gene expression levels for each sample, equivalent amounts of the total RNA (1000 ng) were used for cDNA synthesis with the SuperScript first-strand synthesis system for qRT-PCR (Monad, China) in a 20 µl reaction volume. The synthesized cDNA was diluted 5 times and then was used as a template for qRT-PCR analysis. The qRT-PCR was performed in a Bio-Rad CFX96 Touch Detection System (BioRad, USA) by using the 2× SYBR qPCR Master mix (Monad, China) as the following conditions: 95°C for 5 min, followed by 40 cycles at 95°C for 10 s and at 58°C for 30 s. Relative fold changes of genes were calculated by the methods of -ΔΔCt and the housekeeping gene elongation factor (EF-1α) was used as control gene for normalization of expression. Primers used for qRT-PCR are listed in Supplementary Table S1.

## DNA extraction and PCR amplification

Following the manufacturer's instructions, the total genomic DNA from twelve gonads (six testis and six ovaries) was extracted using MagPure Stool DNA KF kit B (Magen, China). Then the quantity and quality of extracted DNA were measured with a Qubit Fluorometer by using the Qubit dsDNA BR Assay kit (Invitrogen, USA) and checked by running aliquot on 1% agarose gel, respectively.

Variable regions V3–V4 of bacterial 16S rRNA gene was amplified with universal PCR primers, 338F (5'-ACTCCTACGGGAGGCAGCAG-3') and 806R (5'-GGACTACHVGGGTWTCTAAT-3'). Both forward and reverse primers were tagged with Illumina adapter, pad, and linker sequences. PCR enrichment was performed in a 50 µl reaction containing 30ng template, fusion PCR primer, and PCR master mix as following conditions: 94°C for 3 min, followed by 30 cycles of 94°C for 30 s, 50°C for 45 s, 72°C for 45 s and final extension for 10 min at 72°C. The PCR products were purified with AmpureXP beads and eluted in Elution buffer. Libraries were qualified by the Agilent 2100 bioanalyzer (Agilent, USA). The validated libraries were used for sequencing on the Illumina HiSeq 2500 platform (BGI, China) following the standard pipelines of Illumina, and generating 2 × 300 bp pairedend reads.

## Illumina MiSeq sequencing and bioinformatics analysis

Raw reads were filtered to remove adaptors and low-quality and ambiguous bases, and then paired-end reads were added to tags by the Fast Length Adjustment of Short reads program (FLASH) to get the tags. The tags were clustered into OTUs with a cutoff value of 97% using UPARSE software and chimera sequences were compared with the Gold database using UCHIME to detect. Then, OTU representative sequences were taxonomically classified using Ribosomal Database Project (RDP) Classifier with a minimum confidence threshold of 0.6, and trained on the RDP Release16 database by QIIME (29). The USEARCH global was used to compare all tags back to OTU to get the OTU abundance statistics table of each sample. Alpha and beta diversity were estimated by MOTHUR and QIIME at the OTU level, respectively. Principal component analysis (PCA) in OTUs was plotted with R package "ade4". Principal

Coordinate Analysis (PCoA) was performed by QIIME (v1.8.0). Nonmetric multidimensional scaling ordination (NMDS) was performed by R package. UPGMA cluster was performed by phytools and R package version 3.5.1. Wilcox Test results of species difference were performed by R/Bioconductor package DESeq. Significant differences were considered between the two groups when p-vaule and FDR values were less than 0.05. LEfSe cluster or LDA analysis was conducted by LEfSe. KEGG functions were predicted using the PICRUSt software (30). Barplot and heatmap of different classification levels were plotted with R package v3.4.1 and R package "gplots", respectively. The sequence information for this study has been uploaded to NCBI with the accession number PRJNA832434.

## Identification and analysis of gonadal bacteria

To verify the key bacteria in the gonadal tissue, we sampled the gonadal tissue of *M. albus* under the same background. After homogenization by bead beating for 2 min at 60 Hz, 100 µl homogenate was absorbed onto the plate preparation of Brain Heart Infusion Agar. Subsequently, single colonies were selected to culture for further enrichment post nearly 12 hours. Bacterial universal primers were used for further amplification in a 50 µl reaction including 25 µl 2× PCR master mix, 2 µl bacteria template, and 2 µl primers as following conditions: 94°C for 10 min, followed by 35 cycles of 94°C for 30 s, 58°C for 30 s, 72°C for 1 min and final extension for 10 min at 72°C. After being analyzed by agarose gel electrophoresis and photographed, PCR products were purified and sequenced.

## Statistical analysis

An unpaired Student's *t*-test (Prism version 8.0; GraphPad) was used for analysis of differences between groups. *P* values of 0.05 or less were considered statistically significant.

# Results

## Sex identification of *M. albus*

Genetic background, nutrition, and environment may affect the microbial community (3). To explore the difference of gonadal bacterial community between female and male in *M. albus*, the sibling F1 generation was generated for eliminating the interference of genetic background (Figure 1A). Embryos and larval *M. albus* were incubated in the incubator of cell culture room (Figure 1A), then, the juveniles were feed in the indoor circulating system over fourteen months (Figure 1B). The influence of nutrition and living environment on individual microbial community is minimized between female and male *M. albus*. To further exclude differences due to individual size, after sex identification, 30 individuals of similar size including females and males were selected for the subsequent study (Figures 1C, 2A).

As a natural female-to-male sex reversal freshwater economic fish, the sex of *M. albus* individuals were truly identified. Unexpectedly, the majority of *M. ablus* had female oocytes, but seven individuals had male characteristics, such as the appearance of genital folds and spermatogenic cells (Figures 1A, 2A). Given the morphological differences between gonads, we statistically analyzed the growth parameters of the identified *M. albus*. Although no significant differences were observed in body length or weight, a remarkable difference in GSI was detected between female groups and male *M. albus* (Figure 2B). Changes in gonadal steroid concentrations typically accompany gonadal transition in species that undergo sex reversal. In the present study, serum estradiol was approximately 2-fold higher in females (85.74 ± 24.30 ng/µL) than in males (45.50 ± 7.59 ng/µL). However, serum testosterone in males reached 19.58 ± 3.05 nmol/L, which was significantly higher than measured in females (14.59 ± 2.88 nmol/L) (Figure 2C).

Several genes were then quantified in testis and ovary samples *via* RT-qPCR, including sexual-related genes (cyp19a1a, foxl-2, sox-9, and dmrt-1), physical barrier-related genes (occludin, claudin-12, and claudin-15), and immune-related genes (polymeric immunoglobulin receptor (pIgR), toll-like receptor (TLR-3, TLR-7 and TLR-8), lysozyme and hepcidin) (Figure 2D). As expected, the female-related gene foxl-2 was highly expressed in ovaries, whereas the expression levels of male-related genes sox-9 and dmrt-1 are significantly higher in testes than in ovaries. Tight junctions are vital to the structure of the blood-testicular barrier. We found mRNA level of occludin was significantly downregulated whereas claudin-12 and claudin-15 were upregulated in testes, suggesting that structural integrity differed between testis and ovary. Similarly, higher expression levels of TLR-7, TLR-8, and pIgR transcripts were observed in testis than in ovary. Importantly, lysozyme, an antimicrobial peptide, has higher expression in the testes than in ovaries, hinting that the microbial environment may be unique between testes and ovaries.

## 16S rDNA gene sequencing and diversity analysis in *M. albus*

To distinguish the anatomical relationships between the gonads and the gut in *M. albus*, Micro-CT investigations was performed and presented the gonad abutted the gut and sequentially terminated in the cloaca, respectively (Supplementary Figure 2). Subsequently, testes and ovaries of *M. albus* were collected for 16S rRNA sequencing to verify

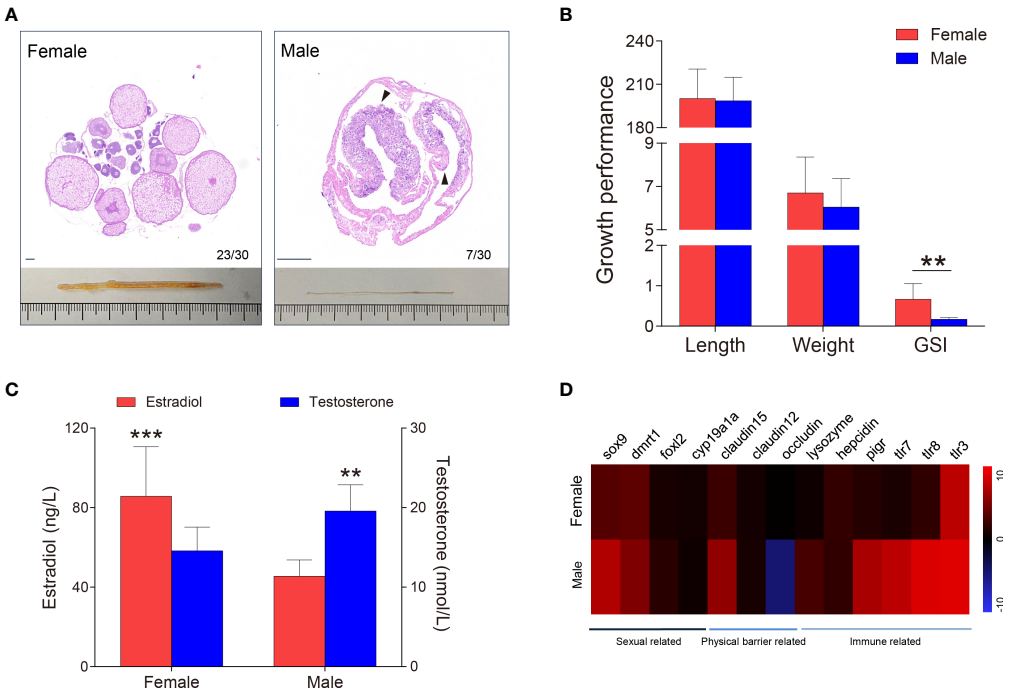


FIGURE 2
Sex identification of *M. albus*. **(A)** Representative histology graphs (upper) and morphology (lower) from ovary and testis of *M. albus* under the same background. Black triangles indicate genital folds. Scale bar, 100 μm. **(B)** Relationships among body length (mm), weight (g), and GSI (%) of *M. albus*. **(C)** Serum concentrations of estradiol (left) and testosterone (right) in female and male *M. albus*. **(D)** Heat map depicting the relative expression levels of genes in ovary (n=22) and testis (n=5) tissues. $^{**}P < 0.01$, $^{***}P < 0.001$, unpaired Student's *t*-test. The data are expressed as the mean values ± standard deviation (SD).

whether gonadal microorganisms are related to sex. After quality filtering and normalization to remove adaptors and low-quality or ambiguous bases, a total of 672,573 high-quality sequences were obtained, equivalent to an average of 56,047 reads per sample. Valid sequences were then clustered, resulting in 619 OTUs with a cutoff value of 97% identity. Sequences were classified taxonomically for downstream analysis. Males and females shared 150 OTUs; males had 240 unique OTUs, and females had 229 (Figure 3A). A rarefaction curve and coverage indices were applied to evaluate the depth of sequencing and species richness. Our result revealed that most of the OTUs were detected in all samples, and all samples reached saturation (Figure 3B). Meanwhile, coverage indices among all samples were as high as 99%, indicating that the sequencing depth was sufficient (Table 1). OTUs were then used to analyze differences in the gonadal microbial abundance, and community diversity was compared between female and male fish. Chaos and Sob indices were substantially higher in testis than in ovary samples. Although the difference did not reach significance, the Shannon index was higher in testis than in ovary samples (Figure 3C, Table 1). These results suggest that sex influences the microbial richness and diversity of gonadal flora in the *M. albus*.

Based on the OTU abundance of each sample, non-metric multidimensional scaling analysis ordination was performed to define the relationship between the female and male groups. We found testis samples were similar to each other and could be distinguished from ovary samples, indicating that significant differences in community structure exist between male and female *M. albus* (Figure 3D). Hierarchical clustering trees and heat map analysis revealed that samples were clustered into two distinct groups depending on sex (Figures 3E, F). In addition, PCA and PCoA yielded similar results, suggesting that differences between samples were primarily due to sex (Supplementary Figure 3).

## Composition of gonadal microflora in female and male *M. albus*

To further analyze the microbial composition differences between the female and male *M. albus*, microbial sequences from testis and ovary tissues were classified by phylum, class, order, family, and genus. The results showed that eleven phyla were predominantly observed in ovary and testis samples, with

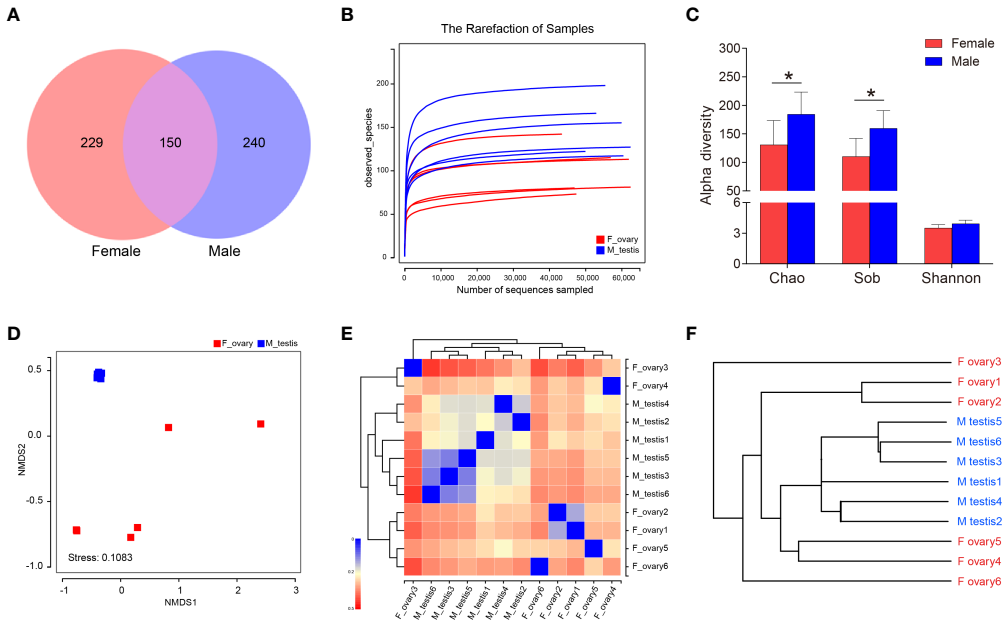


FIGURE 3
Diversity analysis in *M. albus*. **(A)** Venn diagram displays the number of shared and unique OTUs in the gonads of female and male *M. albus*. **(B)** Rarefaction analysis of female and male gonads. **(C)** Histograms represent alpha diversity analyses in the gonads of male and female gonads M. albus, including Chao, Sob, and Shannon indices. **(D)** NMDS shows the relationship between females and males. **(E)** heat map analysis shows the relationship among female and male samples. **(F)** Hierarchical cluster analysis of weighted-unifrac distances generated from ovary and testis was constructed by UPGMA. *$P < 0.05$, unpaired Student's *t*-test. The data are expressed as the mean values ± standard deviation (SD).

Firmicutes, Proteobacteria, Bacteriodetes, and Actinobacteria being the most dominant phyla among females and males. Notably, Proteobacteria, Actinobacteria, and Cyanobacteria were more abundant in the ovarian bacterial community (35.3%, 6.4%, and 5.8%, respectively) compared with the bacterial community in testis (24.5%, 3.2%, and 2.4%, respectively) (Figures 4A, B). In turn, a more abundant number of Firmicutes were more abundant in testis (51.0%) than in ovary samples (32.4%). Although the differences between groups did not reach significance, Bacteroidetes was predominant and accounted for 12.0% of the diversity in the ovarian bacterial community and 15.3% in the testis. It is worth noting that Fusobacteria was detected only in female individuals, although its abundance was low (2.8%) (Figures 4A, C).

At the order level, potentially pathogenic bacteria were detected in ovary and testis samples, including members of the orders Burkholderiales (11.4% in ovary versus 8.2% in testis) and Pseudomonadales (9.3% in ovary versus 7.9% in testis). In contrast, the orders Erysipelotrichales and Enterobacteriales were significantly enriched in the testis (6.5% and 4.2%, respectively) compared to the ovary (1.3% and 3.1%, respectively) (Figures 4D-F and Supplementary Figure 4). The testis microbial community was also enriched in potentially beneficial taxa known to produce short-chain fatty acids (SCFAs), including Clostridiales (39.3% in testis versus 23.0% in ovary), Bacteroidales (15.1% in testis versus 9.7% in ovary), and Lactobacillales (2.1% in testis versus 1.5% in ovary). Other SCFA-producing bacteria were enriched in ovaries, such as

TABLE 1 Alpha diversity of the gonad microbial community in *M. albus*.

| | F_ovary | M_testis | *P*-vaule |
|---|---|---|---|
| sobs | 110.33 ± 28.88 | 159.67 ± 28.45 | 0.0215* |
| chao | 130.89 ± 38.80 | 184.33 ± 35.54 | 0.0465* |
| ace | 134.02 ± 29.43 | 178.72 ± 25.84 | 0.0288* |
| shannon | 3.51 ± 0.30 | 3.93 ± 0.33 | 0.0600 |
| simpson | 0.06 ± 0.03 | 0.04 ± 0.02 | 0.2631 |
| coverage | 0.999 ± 0.0001 | 0.999 ± 0.00001 | 0.0663 |

The data are expressed as the mean values ± standard deviation (SD). P-values were determined using Student's t-test (*P < 0.05).

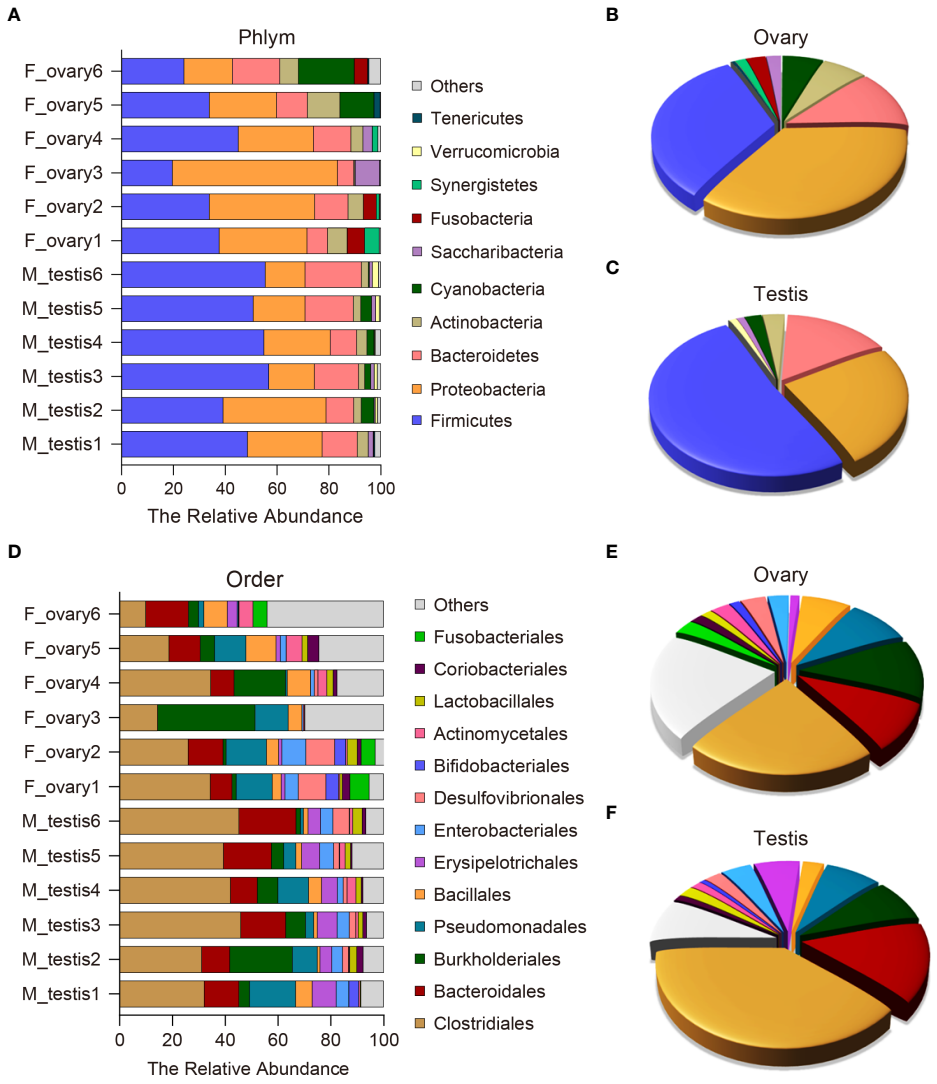


FIGURE 4
Composition and distribution of bacterial microbiomes in *M. albus* gonads. **(A)** Comparison of the composition and relative abundance of dominant bacterial taxa between ovary and testis at the phylum level. **(B, C)** Pie graphs represent the average relative abundance of each phylum in ovarian **(B)** or testicle **(C)** bacterial community. **(D)** Comparison of the composition and relative abundance of dominant bacterial taxa between ovary and testis at the order level. **(E, F)** Pie graphs represent the average relative abundance of each order in ovarian **(E)** or testicle **(F)** bacterial community.

Bacillales (2.9% in testis versus 7.1% in ovary) (Figures 4D-F and Supplementary Figure 4). These results indicate that broad, well-defined ranges of bacteria with beneficial and pathogenic characteristics exist in M. albus gonads, and notable differences are related to sex.

## Dominant bacterial community analysis between testis and ovary of *M. albus*

Differences in the microbial communities at the class and genus level were displayed with histograms for the top 10 abundant OTUs from female and male *M. albus*. The relative abundances of *Clostridia* and *Erysipelotrichia* are significantly higher in males than females ($P < 0.01$) at the class level (Figure 5A and Supplementary Figure 5A). Interestingly, not only are *Clostridium XIVa* and *Bacteroides* significantly different (confirming former studies), but *Escherichia*, a more potentially pathogenic bacterial genus, was identified in testis tissue. Moreover, the beneficial taxa *Romboutsia* were detected significantly in males (Supplementary Figure 5B).

Dominant microbiomes that contribute to bacteria differences were also investigated by linear discriminant analysis of effect size (LEfSe). In contrast to male *M. albus*, we

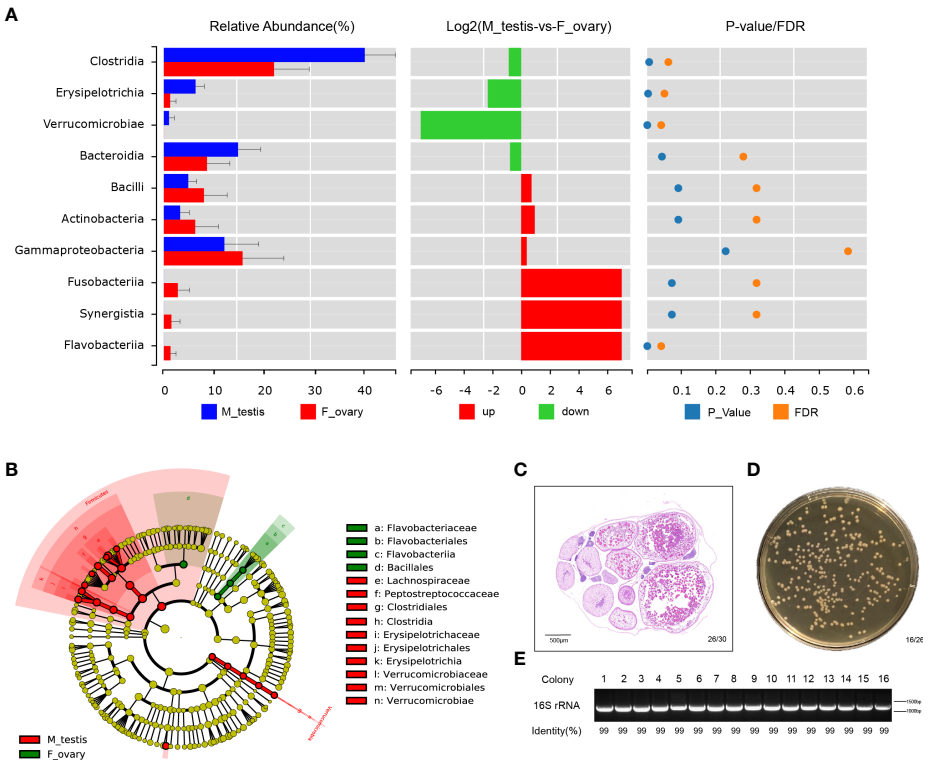


FIGURE 5
Bacterial community are significantly different between ovary and testis in *M. albus*. **(A)** Differences in microbial communities at the class level. **(B)** Cladogram representation of LEfSe analysis shows that bacterial taxa are significantly associated with the ovary (green) or testis (red). **(C)** Representative graphs of ovary histology in *M. albus*. **(D)** Culture plates from gonads of *M. albus*. Black triangles indicate single colonies of *Bacillus*. **(E)** Agarose gel electrophoresis of colony PCR samples. PCR products were verified by agarose gel electrophoresis and sequencing.

observed that the genus *Flavobacteriaceae*, the order *Flavobacteriales*, and the class *Flavobacteriia* were predominant in the female *M. albus*. Meanwhile, the order *Bacillales* (a member of the Firmicutes phylum) was also enriched in the ovary (Figure 5B). However, three other members of Firmicutes (*Clostridiales* and *Erysipelotrichales*) were more prevalent in the testis. *Verrucomicrobiales* was other orders that are more predominant in *M. albus* testis (Figure 5B). Gonads of *M. albus* propagated under identical conditions were randomly selected for bacterial identification on coating plates to verify the dominant gonadal bacteria. Sex identification revealed ovarian characteristics in almost all gonads, so the tissue homogenates of ovaries were cultured on Brain Heart Infusion Agar, and bacterial colonies with the characteristic white, large and flat morphology were detected on most plates (Figures 5C, D). Subsequently, single colonies were isolated and sequenced using 16S rRNA universal primers. The results revealed that the similarity with *Bacillus* was over 99%, which provided additional support that *Bacillus* may be the dominant bacteria in *M. albus* ovaries (Figure 5E). These findings indicate that sex exerts profound and complex effects on the microbial community composition and affects dominant bacteria in gonads of *M. albus*.

## Functional prediction of microbial communities in *M. albus*

PICRUSt was carried out to predict the functions of genes expressed in the microbial communities in *M. albus* gonads. Using level 1 KEGG ortholog function predictions, three functional categories were significantly different ($P < 0.05$) between females and males: metabolism, cellular processes, and organismal systems (Figure 6A and Supplementary Figure 6). Concretely, metabolism was more abundant in females, whereas categories involved in cellular processes and organismal systems were more abundant in males. Additional differences between males and females were identified when metabolic pathways were characterized at level 2 KEGG. The functional categories enriched in female bacterial microbiota included the metabolic pathways of xenobiotics biodegradation and metabolism, amino acid metabolism, and metabolism of

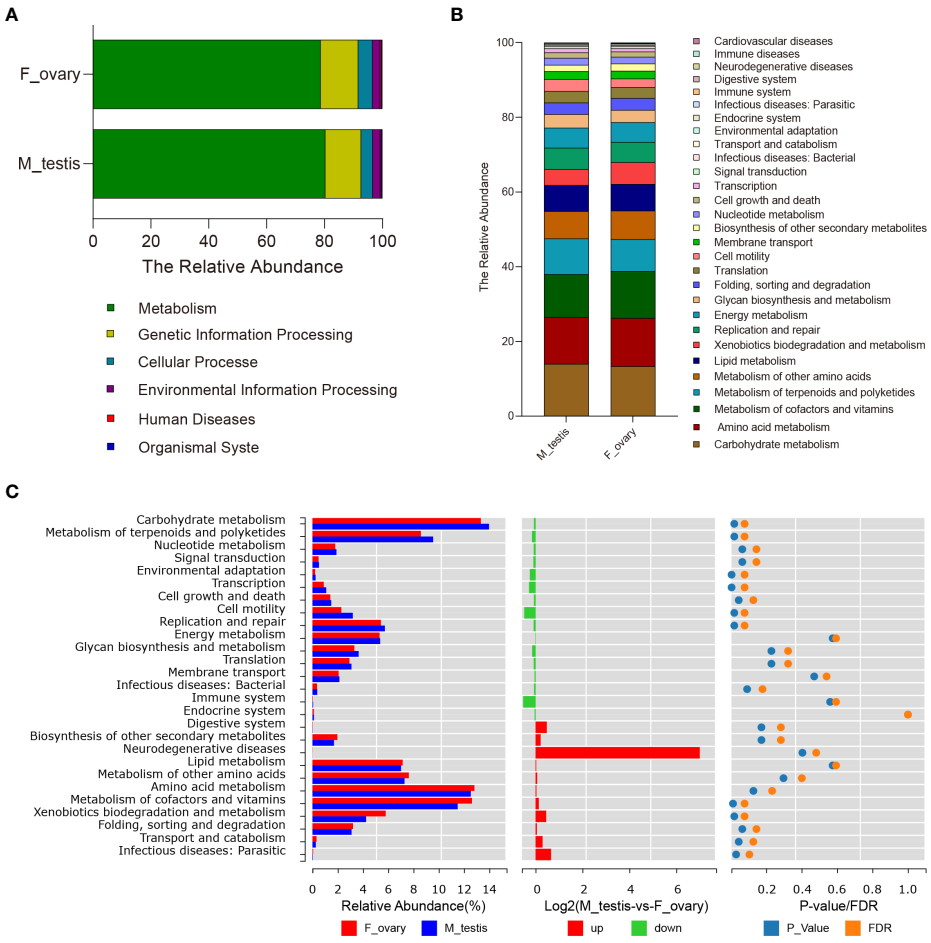


FIGURE 6
Predictive analysis of microbiota function in gonads of the *M. albus*. **(A)** Average relative abundances in predicted functional genes of gonadal bacterial community at KEGG level 1. **(B)** Average relative abundances in predicted functional genes of gonadal bacterial community at KEGG level 2. **(C)** Average relative abundances and differences in predicted functional genes of gonadal bacterial community at KEGG level 2.

cofactors and vitamins, whereas the functional categories enriched in males were carbohydrate metabolism and metabolism of terpenoids and polyketides. Interestingly, in males, functional genes in enzyme families, transcription, and cell motility categories were more concentrated. Although the difference between males and females did not reach statistical significance, genes associated with bacterial community involved in immune system function were substantially higher in males, whereas genes involved in immune diseases were enriched in females (Figures 6B, C).

## Discussion

Microbiomes in vertebrates vary in a tissue-specific manner and play vital roles in many biological functions, including growth enhancement, nutrition, development, metabolism, and immune responses (31, 32). In mammals, bacterial microbiota could alter gonadal maturation and drive sex-specific differences in gene expression and metabolism (7, 10–12). Although teleost bacterial microbiomes have been extensively studied (5, 20), the diversity present in gonads for most teleost species remains unexplored. In this study, we compared the microbial community compositions of female and male *M. albus*, a teleost that undergoes sex reversal naturally, and predicted the corresponding functional differences.

Environmental and host genetic factors shape individual variations in host-associated microbiota community structures (33). In this study, *M. albus* with identical genetic backgrounds were hatched from embryos and kept under identical conditions (e.g., environment, diet), to minimize any effects caused by environment and heredity. It is generally believed that it takes more than two years for *M. albus* to undergo sex reversal in natural environments (22). Unexpectedly, seven individuals with

male characteristics (e.g., genital folds and spermatogenic cells) emerged approximately one-year post-hatching. Previous studies found that temperature affects sex differentiation in various teleost species, so one reason for the early reversal in *M. albus* might be the suitable indoor temperature (34, 35). In our study, significantly higher serum testosterone in males than females provided additional support to the facticity that males had emerged. However, lower average concentrations of estradiol and testosterone were detected in our study, a finding that is at odds with the content of sex hormones reported in a previous study. On the one hand, the environment may be associated with the synthesis, secretion, or transport of hormones (36). On the other hand, differences in the weight and shape of *M. albus* individuals can cause differences in serum hormones according to previous study (37). As assessed in several species, a shared characteristic among fish species in which temperature can alter sex ratios is that exposure to heat during early development upregulates the expression of genes related to testis differentiation with a concomitant down-regulation of genes related to ovarian differentiation (38, 39). We also observed substantially elevated expression of sox-9 and dmrt-1 genes in male testis, further suggesting temperature may have an effect on sexual reversal. Meanwhile, consistent with the previous studies on sex regulated genes, a lower expression of sox-9 and dmrt-1 were also detected in the ovary, which may be caused by the same genome shared between female and male individuals (40, 41). The claudin family of membrane proteins play vital roles in tight junctions structure, an intercellular junction critical for building the epithelial barrier and maintaining epithelial polarity (42). Previous studies in fish have found that upregulation of occludin mRNA levels stabilizes intercellular structural integrity, whereas upregulation of claudin mRNA levels disrupts the structural integrity of cells (43). In this study, we observed that claudin-15 mRNA levels were significantly upregulated and occludin mRNA levels were downregulated in *M. albus* testes, implying that the physical barrier integrity in testis was less than that in ovaries. In vertebrates, TLRs can distinguish among classes of pathogens and serve an important role in orchestrating the appropriate adaptive immune responses. It has been illustrated that TLR3, TLR7, and TLR8 are primarily located in the endoplasmic reticulum and in lysosomal-like vesicles and are thought to have a vital role in anti-viral immunity (44). In the present study, higher expression levels of these TLRs in testis suggest the microbial immune environment may be different between testes and ovaries. Interestingly, pIgR, a gene involved in teleost mucosal defense, exhibited significantly higher expression in testis than in ovary, providing additional support that genes associated with immune responses differ between the sexes, similar to mammals, and these differences likely contribute to sex-specific vaccine outcomes (45). Whether there is a relationship between physical barrier integrity and immune environments, and the specific mechanism needs additional research and development. Lysozyme is an antimicrobial peptide that is widely distributed in teleost and contributes greatly to antibacterial defense due to its ability to cleave the glycosidic bond between N-acetylmuramic acid and N-acetylglucosamine residues in bacterial cell wall peptidoglycans (5, 46). Our data showed that the lysozyme expression increased significantly in testis, indicating that more potential bacterial microorganisms inhabited in testis.

To further investigate the precise differences of gonadal microorganisms, the testis and ovaries of *M. albus* were collected for 16S rRNA sequencing and analyzed, respectively. In contrast to results reported for *M. albus* intestinal flora, this study found that gonadal tissues exhibited higher Alpha diversity in males than females (16). It supported that different tissues are inhabited by uniquely different microbial communities and proportions of specific bacteria (13, 14). Therefore, it was the body site that led to the difference of diversity and richness to a large extent, and it does not rule out that group differences contribute a small amount to the observed diversity. Meanwhile, Beta diversity analysis where the male sample was clustered while the female sample was scattered indicates that the gonadal flora of *M. albus* changes at different developmental stages. The more obvious differences between male and female *M. albus* were reflected in the composition of gonadal microflora (Figure 4). Gonad tissues from humans are characterized by Proteobacteria, Firmicutes, Bacteroidetes, and Actinobacteria as the dominating phyla, similar to the microbial compositions observed in this study on *M. albus* (11, 47). However, there are significant differences in the proportion of these microorganisms between testis and ovary. In our study, Firmicutes was the most prominent bacterial community in testis, whereas the relative abundance of Bacteroidetes had no significant difference between the two groups. Although the concept that an increment in the relative abundance of Firmicutes and Bacteroidetes may be associated with obesity has been consistently supported by numerous studies, a recent meta-analysis concluded that there were no statistically significant differences in the Firmicutes/Bacteroidetes ratio between obese and normal-weight adults (48, 49). Combined with our previous results on weight and the recently published meta-analysis, it may further strengthen the deduction that the Firmicutes/Bacteroidetes ratio may not be a robust marker for obesity (50). However, an increased prevalence of the bacterial phylum Proteobacteria is a sensitive marker for an unstable microbial community (dysbiosis) and a potential diagnostic criterion for disease (51). Whether females may suffer from more diseases than males deserves additional study to understand due to the higher proportion of Proteobacteria in females than males observed in the present study. In addition to Proteobacteria, Cyanobacteria also produce a wide variety of potentially toxic secondary metabolites and various other cyanobacterial bioactive compounds that could affect fish

health. Previous studies have shown that Cyanobacteria may be related to the effect of environmental stress on metabolic divergences in fish (52). The design of this study eliminated environmental differences; therefore, the relative abundance of Cyanobacteria in ovary relative to testis indicates that there may be intrinsic metabolic differences between *M. albus* males and females.

SCFA synthesized from carbohydrates and indigestible oligosaccharides are rich energy sources for the host metabolism. Intestinal members of the orders *Clostridiales, Bacteroidales*, and *Lactobacillales* are correlated with the biosynthesis and absorption of SCFA by enzymes such as glycosyl transferases, glycoside hydrolases, and polysaccharide lyases (53). Moreover, a compensatory relationship between testicular and intestinal microbiota has been reported (21); therefore, we speculate that gonadal bacterial microbiota are also involved in host metabolism and homeostasis maintenance. Significant differences in the metabolism between the ovary and testis are suggested by the overrepresentation or underrepresentation of the predicted KEGG pathways associated with different metabolic processes and biosynthesis in the ovary and testis. For example, higher levels of microbial functional genes associated with the metabolism of cofactors and vitamins were detected in ovaries, whereas the level of carbohydrate, terpenoids and polyketides metabolism was significantly elevated in testis. Because activated T cells mediate metabolic reprogramming, promote the production of glycolytic flux and lactate, and elevate the production of lipids, proteins, nucleic acids, and other carbohydrates (i.e., induction of biomass), we surmise that these metabolic differences between male and female *M. albus* may be related to their correlative immune function (54). Evidence is accumulating to support specific roles for bacterial community in the development and function of T cells and T regulatory (Treg) cells (53, 55). In the case of distinct *Clostridia* clusters, it could be either independent of pattern recognition receptors (PRRs) or dependent on My-D88 dependent mechanisms (56). In the case of *Bacillus*, induction of Treg cells appears to be mediated by polysaccharide A-induced TLR2 signaling (57). The higher relative abundance of these immune-related bacteria in testis may indicate that males have a more active immune response. Moreover, microbial cell wall peptidoglycans were reported to maintain tight junctions by TLR2-mediated signaling, suggesting that *Bacillus* may be responsible for the integrity of ovary (58). More importantly, certain SCFAs (e.g., butyrate) have been implicated in the development and function of Tregs. Whether there is a certain relationship among microbiota, metabolism, and immunity in male and female *M. albus* needs to be further explored. In addition to *Bacillus*, *Lactobacillus* has also been reported as an aquaculture probiotic, and this study found it to be more abundant in *M. albus* testes. Previous studies have reported that *Lactobacillus* and *Clostridia* are associated with semen quality and fertility status (10, 11). In view of the special characteristic of sexual reversal in *M. albus*, additional studies should focus on the relationship between probiotics and sperm quality in *M. albus*.

This study is the first comprehensive characterization of the microbial communities in *M. albus* gonads to our knowledge. To summarize, this study found significant differences in the microbial composition and distribution of *M. albus* between testis and ovary, which may be relevant to the difference in the metabolism, immune modulation, and host-microbe interactions between female and male groups. These findings provided unique resources for further explore how gonadal bacterial community influences sex-specific differences. Meanwhile, it also provides theoretical support for the improvement of polycystic ovary syndrome.

## Data availability statement

The datasets presented in this study can be found in online repositories. The names of the repository/repositories and accession number(s) can be found in NCBI with the accession number PRJNA832434.

## Ethics statement

The animal study was reviewed and approved by Institute of Hydrobiology, Chinese Academy of Sciences.

## Author contributions

DL conceived the project. DL and KM designed the study. KM performed most of experiment and analyses. XL helped in breeding and sampling. HL and FL helped in analyzed the image data. HC, ZX and YS helped in data analyses. KM and DL prepared the draft and final version of the manuscript. All authors read and approved the final manuscript.

## Acknowledgments

We would like to thank Yuanli Zhao, Rui Li and Meidi Hu for their help in experimental process; Xin Wang, Yuan Xiao and Yan Wang (The Analysis and Testing Center of Institute of Hydrobiology, Chinese Academy of Sciences) for their support of instrument platform and technical. This work was supported by grants from the National Natural Science Foundation of China (Grant No.31922085 to DL), and Natural Science Foundation of Hubei Province (Grant No. 2020CFA056 to DL).

## Conflict of interest

The authors declare that the research was conducted in the absence of any commercial or financial relationships that could be construed as a potential conflict of interest.

## Publisher's note

All claims expressed in this article are solely those of the authors and do not necessarily represent those of their affiliated organizations, or those of the publisher, the editors and the reviewers. Any product that may be evaluated in this article, or claim that may be made by its manufacturer, is not guaranteed or endorsed by the publisher.

## Supplementary material

The Supplementary Material for this article can be found online at: https://www.frontiersin.org/articles/10.3389/fimmu.2022.938326/full#supplementary-material

## References

1. Coyte KZ, Rakoff-Nahoum S. Understanding competition and cooperation within the mammalian gut microbiome. *Curr Biol* (2019) 29(11):R538–R44. doi: 10.1016/j.cub.2019.04.017

2. Yassour M, Vatanen T, Siljander H, Hamalainen AM, Harkonen T, Ryhanen SJ, et al. Natural history of the infant gut microbiome and impact of antibiotic treatment on bacterial strain diversity and stability. *Sci Transl Med* (2016) 8 (343):343ra81. doi: 10.1126/scitranslmed.aad0917

3. Round JL, Mazmanian SK. The gut microbiota shapes intestinal immune responses during health and disease. *Nat Rev Immunol* (2009) 9(5):313–23. doi: 10.1038/nri2515

4. Ley RE, Peterson DA, Gordon JI. Ecological and evolutionary forces shaping microbial diversity in the human intestine. *Cell* (2006) 124(4):837–48. doi: 10.1016/j.cell.2006.02.017

5. Yu YY, Ding LG, Huang ZY, Xu HY, Xu Z. Commensal bacteria-immunity crosstalk shapes mucosal homeostasis in teleost fish. *Rev Aquacult* (2021) 13 (4):2322–43. doi: 10.1111/raq.12570

6. Biragyn A, Ferrucci L. Gut dysbiosis: A potential link between increased cancer risk in ageing and inflammaging. *Lancet Oncol* (2018) 19(6):e295–304. doi: 10.1016/s1470-2045(18)30095-0

7. Weger BD, Gobet C, Yeung J, Martin E, Jimenez S, Betrisey B, et al. The mouse microbiome is required for sex-specific diurnal rhythms of gene expression and metabolism. *Cell Metab* (2019) 29(2):362–82.e8. doi: 10.1016/j.cmet.2018.09.023

8. Markle JGM, Frank DN, Mortin-Toth S, Robertson CE, Feazel LM, Rolle-Kampczyk U, et al. Sex differences in the gut microbiome drive hormone-dependent regulation of autoimmunity. *Science* (2013) 339(6123):1084–8. doi: 10.1126/science.1233521

9. Yurkovetskiy L, Burrows M, Khan AA, Graham L, Volchkov P, Becker L, et al. Gender bias in autoimmunity is influenced by microbiota. *Immunity* (2013) 39(2):400–12. doi: 10.1016/j.immuni.2013.08.013

10. Lundy SD, Vij SC, Rezk AH, Cohen JA, Bajic P, Ramasamy R. The microbiome of the infertile Male. *Curr Opin Urol* (2020) 30(3):355–62. doi: 10.1097/MOU.0000000000000742

11. Alfano M, Ferrarese R, Locatelli I, Ventimiglia E, Ippolito S, Gallina P, et al. Testicular microbiome in azoospermic men-first evidence of the impact of an altered microenvironment. *Hum Reprod* (2018) 33(7):1212–7. doi: 10.1093/humrep/dey116

12. Thackray VG. Sex, microbes, and polycystic ovary syndrome. *Trends Endocrinol Metab* (2019) 30(1):54–65. doi: 10.1016/j.tem.2018.11.001

13. Lowrey L, Woodhams DC, Tacchi L, Salinas I. Topographical mapping of the rainbow trout (*Oncorhynchus mykiss*) microbiome reveals a diverse bacterial community with antifungal properties in the skin. *Appl Environ Microbiol* (2015) 81(19):6915–25. doi: 10.1128/AEM.01826-15

14. Meng KF, Ding LG, Wu S, Wu ZB, Cheng GF, Zhai X, et al. Interactions between commensal microbiota and mucosal immunity in teleost fish during viral infection with svcv. *Front Immunol* (2021) 12:654758. doi: 10.3389/fimmu.2021.654758

15. Liu Y, Yao Y, Li H, Qiao F, Wu J, Du ZY, et al. Influence of endogenous and exogenous estrogenic endocrine on intestinal microbiota in zebrafish. *PLoS One* (2016) 11(10):e0163895. doi: 10.1371/journal.pone.0163895

16. Wang Y, Zhang J, Zhou Q, Wang Z, Gao M, Yang X, et al. Analysis of the intestinal flora in Male versus female swamp eels (*Monopterus albus*). *Front Microbiol* (2020) 11:699. doi: 10.3389/fmicb.2020.00699

17. Ma R, Wang S, Zhao F, Xu C, Ji Y, Song C, et al. Comparative study on intestinal bacterial communities of *Boleophthalmus pectinirostris* and *Periophthalmus magnuspinnatus* with different sexes and feeding strategies. *Ann Microbiol* (2018) 68(3):123–33. doi: 10.1007/s13213-018-1324-4

18. Li X, Yan Q, Ringo E, Wu X, He Y, Yang D. The influence of weight and gender on intestinal bacterial community of wild largemouth bronze gudgeon (*Coreius guichenoti*, 1874). *BMC Microbiol* (2016) 16(1):191. doi: 10.1186/s12866-016-0809-1

19. Loken OM, Bjorgen H, Hordvik I, Koppang EO. A teleost structural analogue to the avian bursa of fabricius. *J Anat* (2020) 236(5):798–808. doi: 10.1111/joa.13147

20. Salinas I, Fernandez-Montero A, Ding Y, Sunyer JO. Mucosal immunoglobulins of teleost fish: A decade of advances. *Dev Comp Immunol* (2021) 121:104079. doi: 10.1016/j.dci.2021.104079

21. Su Y, He L, Hu Z, Li Y, Zhang Y, Fan Z, et al. Obesity causes abrupt changes in the testicular microbiota and sperm motility of zebrafish. *Front Immunol* (2021) 12:639239. doi: 10.3389/fimmu.2021.639239

22. Chen H, Liu H, Li R, Lin X, Luo H, Ji S, et al. Blood cell identification and hematological analysis during natural sex reversal in rice field eel (*Monopterus albus*). *Aquaculture* (2021) 538:736543. doi: 10.1016/j.aquaculture.2021.736543

23. Zhang Y, Zhang S, Liu Z, Zhang L, Zhang W. Epigenetic modifications during sex change repress gonadotropin stimulation of Cyp19a1a in a teleost ricefield eel (*Monopterus albus*). *Endocrinology* (2013) 154(8):2881–90. doi: 10.1210/en.2012-2220

24. Gao Y, Jia D, Hu Q, Li D. Foxl3, a target of mir-9, stimulates spermatogenesis in spermatogonia during natural sex change in *Monopterus albus*. *Endocrinology* (2016) 157(11):4388–99. doi: 10.1210/en.2016-1256

25. Feng K, Luo H, Hou M, Li Y, Chen J, Zhu Z, et al. Alternative splicing of Gnrh2 and Gnrh2-associated peptide plays roles in gonadal differentiation of the rice field eel. *Monopterus Albus Gen Comp Endocrinol* (2018) 267:9–17. doi: 10.1016/j.ygcen.2018.05.021

26. Wang X, Lai F, Shang D, Cheng Y, Lan T, Cheng H, et al. Cellular fate of intersex differentiation. *Cell Death Dis* (2021) 12(4):388. doi: 10.1038/s41419-021-03676-x

27. Hou M, Feng K, Luo H, Jiang Y, Xu W, Li Y, et al. Complete depletion of primordial germ cells results in masculinization of *Monopterus albus*, a protogynous hermaphroditic fish. *Mar Biotechnol (NY)* (2022) 24(2):320–34. doi: 10.1007/s10126-022-10106-2

28. Morris A. Microbiota drives sex-specific differences. *Nat Rev Endocrinol* (2018) 15(1):4. doi: 10.1038/s41574-018-0127-9

29. Caporaso JG, Kuczynski J, Stombaugh J, Bittinger K, Bushman FD, Costello EK, et al. Qiime allows analysis of high-throughput community sequencing data. *Nat Methods* (2010) 7(5):335–6. doi: 10.1038/nmeth.f.303

30. Wilkinson TJ, Huws SA, Edwards JE, Kingston-Smith AH, Siu-Ting K, Hughes M, et al. Cowpi: A rumen microbiome focussed version of the picrust functional inference software. *Front Microbiol* (2018) 9:1095. doi: 10.3389/fmicb.2018.01095

31. Mendes R, Garbeva P, Raaijmakers JM. The rhizosphere microbiome: Significance of plant beneficial, plant pathogenic, and human pathogenic microorganisms. *FEMS Microbiol Rev* (2013) 37(5):634–63. doi: 10.1111/1574-6976.12028

32. Rao C, Coyte KZ, Bainter W, Geha RS, Martin CR, Rakoff-Nahoum S. Multi-kingdom ecological drivers of microbiota assembly in preterm infants. *Nature* (2021) 591(7851):633–8. doi: 10.1038/s41586-021-03241-8

33. Org E, Mehrabian M, Parks BW, Shipkova P, Liu X, Drake TA, et al. Sex differences and hormonal effects on gut microbiota composition in mice. *Gut Microbes* (2016) 7(4):313–22. doi: 10.1080/19490976.2016.1203502

34. Yamaguchi T, Yamaguchi S, Hirai T, Kitano T. Follicle-stimulating hormone signaling and Foxl2 are involved in transcriptional regulation of aromatase gene during gonadal sex differentiation in Japanese flounder, *Paralichthys olivaceus*. *Biochem Biophys Res Commun* (2007) 359(4):935–40. doi: 10.1016/j.bbrc.2007.05.208

35. Poonlaphdecha S, Pepey E, Canonne M, de Verdal H, Baroiller JF, D'Cotta H. Temperature induced-masculinisation in the Nile tilapia causes rapid up-regulation of both Dmrt1 and amh expressions. *Gen Comp Endocrinol* (2013) 193:234–42. doi: 10.1016/j.ygcen.2013.06.007

36. Song Y, Li R. Effects of environment and lifestyle factors on anovulatory disorder. *Adv Exp Med Biol* (2021) 1300:113–36. doi: 10.1007/978-981-33-4187-6_5

37. Jerez S, Rodriguez C, Cejas JR, Bolanos A, Lorenzo A. Lipid dynamics and plasma level changes of 17beta-estradiol and testosterone during the spawning season of gilthead seabream (*Sparus aurata*) females of different ages. *Comp Biochem Physiol B Biochem Mol Biol* (2006) 143(2):180–9. doi: 10.1016/j.cbpb.2005.11.002

38. Ribas L, Liew WC, Diaz N, Sreenivasan R, Orban L, Piferrer F. Heat-induced masculinization in domesticated zebrafish is family-specific and yields a set of different gonadal transcriptomes. *Proc Natl Acad Sci U.S.A.* (2017) 114(6):E941–E50. doi: 10.1073/pnas.1609411114

39. Diaz N, Piferrer F. Lasting effects of early exposure to temperature on the gonadal transcriptome at the time of sex differentiation in the European Sea bass, a fish with mixed genetic and environmental sex determination. *BMC Genomics* (2015) 16:679. doi: 10.1186/s12864-015-1862-0

40. Zhou R, Liu L, Guo Y, Yu H, Cheng H, Huang X, et al. Similar gene structure of two Sox9a genes and their expression patterns during gonadal differentiation in a teleost fish, rice field eel (*Monopterus albus*). *Mol Reprod Dev* (2003) 66(3):211–7. doi: 10.1002/mrd.10271

41. Sheng Y, Chen B, Zhang L, Luo M, Cheng H, Zhou R. Identification of dmrt genes and their up-regulation during gonad transformation in the swamp eel (*Monopterus albus*). *Mol Biol Rep* (2014) 41(3):1237–45. doi: 10.1007/s11033-013-2968-6

42. Otani T, Furuse M. Tight junction structure and function revisited. *Trends Cell Biol* (2020) 30(10):805–17. doi: 10.1016/j.tcb.2020.08.004

43. Shi Y, Zhong L, Liu Y, Zhang J, Lv Z, Li Y, et al. Effects of dietary andrographolide levels on growth performance, antioxidant capacity, intestinal immune function and microbioma of rice field eel (*Monopterus albus*). *Anim (Basel)* (2020) 10(10):1744. doi: 10.3390/ani10101744

44. Palti Y. Toll-like receptors in bony fish: From genomics to function. *Dev Comp Immunol* (2011) 35(12):1263–72. doi: 10.1016/j.dci.2011.03.006

45. Klein SL, Flanagan KL. Sex differences in immune responses. *Nat Rev Immunol* (2016) 16(10):626–38. doi: 10.1038/nri.2016.90

46. Kumaresan V, Bhatt P, Ganesh MR, Harikrishnan R, Arasu M, Al-Dhabi NA, et al. A novel antimicrobial peptide derived from fish goose type lysozyme disrupts the membrane of salmonella enterica. *Mol Immunol* (2015) 68(2 Pt B):421–33. doi: 10.1016/j.molimm.2015.10.001

47. Miles SM, Hardy BL, Merrell DS. Investigation of the microbiota of the reproductive tract in women undergoing a total hysterectomy and bilateral salpingo-oopherectomy. *Fertil Steril* (2017) 107(3):813–20.e1. doi: 10.1016/j.fertnstert.2016.11.028

48. Ley RE, Turnbaugh PJ, Klein S, Gordon JI. Microbial ecology - human gut microbes associated with obesity. *Nature* (2006) 444(7122):1022–3. doi: 10.1038/4441022a

49. Walters WA, Xu Z, Knight R. Meta-analyses of human gut microbes associated with obesity and ibd. *FEBS Lett* (2014) 588(22):4223–33. doi: 10.1016/j.febslet.2014.09.039

50. Riva A, Borgo F, Lassandro C, Verduci E, Morace G, Borghi E, et al. Pediatric obesity is associated with an altered gut microbiota and discordant shifts in firmicutes populations. *Environ Microbiol* (2017) 19(1):95–105. doi: 10.1111/1462-2920.13463

51. Shin NR, Whon TW, Bae JW. Proteobacteria: Microbial signature of dysbiosis in gut microbiota. *Trends Biotechnol* (2015) 33(9):496–503. doi: 10.1016/j.tibtech.2015.06.011

52. Sotton B, Paris A, Le Manach S, Blond A, Duval C, Qiao Q, et al. Specificity of the metabolic signatures of fish from cyanobacteria rich lakes. *Chemosphere* (2019) 226:183–91. doi: 10.1016/j.chemosphere.2019.03.115

53. Koh A, De Vadder F, Kovatcheva-Datchary P, Backhed F. From dietary fiber to host physiology: Short-chain fatty acids as key bacterial metabolites. *Cell* (2016) 165(6):1332–45. doi: 10.1016/j.cell.2016.05.041

54. Maciolek JA, Pasternak JA, Wilson HL. Metabolism of activated T lymphocytes. *Curr Opin Immunol* (2014) 27:60–74. doi: 10.1016/j.coi.2014.01.006

55. Park J, Kim M, Kang SG, Jannasch AH, Cooper B, Patterson J, et al. Short-chain fatty acids induce both effector and regulatory T cells by suppression of histone deacetylases and regulation of the mtor-S6k pathway. *Mucosal Immunol* (2015) 8(1):80–93. doi: 10.1038/mi.2014.44

56. Geuking MB, Cahenzli J, Lawson MA, Ng DC, Slack E, Hapfelmeier S, et al. Intestinal bacterial colonization induces mutualistic regulatory T cell responses. *Immunity* (2011) 34(5):794–806. doi: 10.1016/j.immuni.2011.03.021

57. Round JL, Lee SM, Li J, Tran G, Jabri B, Chatila TA, et al. The toll-like receptor 2 pathway establishes colonization by a commensal of the human microbiota. *Science* (2011) 332(6032):974–7. doi: 10.1126/science.1206095

58. Jandhyala SM, Talukdar R, Subramanyam C, Vuyyuru H, Sasikala M, Nageshwar Reddy D. Role of the normal gut microbiota. *World J Gastroenterol* (2015) 21(29):8787–803. doi: 10.3748/wjg.v21.i29.8787

frontiers | Frontiers in Immunology

TYPE Original Research
PUBLISHED 29 August 2022
DOI 10.3389/fimmu.2022.953053



OPEN ACCESS

EDITED BY
Giamila Fantuzzi,
University of Illinois at Chicago,
United States

REVIEWED BY
Joseph Anthony Lorenzo,
UCONN Health, United States
Maria Pini,
Alira Health, United States

*CORRESPONDENCE
Margaret M. Harnett
Margaret.Harnett@glasgow.ac.uk
William Harnett
W.Harnett@strath.ac.uk

SPECIALTY SECTION
This article was submitted to Inflammation, a section of the journal Frontiers in Immunology

RECEIVED 25 May 2022
ACCEPTED 11 August 2022
PUBLISHED 29 August 2022

CITATION
Harnett MM, Doonan J, Lumb FE, Crowe J, Damink RO, Buitrago G, Duncombe-Moore J, Wilkinson DI, Suckling CJ, Selman C and Harnett W (2022) The parasitic worm product ES-62 protects the osteoimmunology axis in a mouse model of obesity-accelerated ageing.
*Front. Immunol.* 13:953053.
doi: 10.3389/fimmu.2022.953053



# The parasitic worm product ES-62 protects the osteoimmunology axis in a mouse model of obesity-accelerated ageing

Margaret M. Harnett[1]*, James Doonan[2], Felicity E. Lumb[2], Jenny Crowe[1], Roel Olde Damink[2], Geraldine Buitrago[2], Josephine Duncombe-Moore[1], Debbie I. Wilkinson[3], Colin J. Suckling[4], Colin Selman[5] and William Harnett[2]*

[1]Institute of Infection, Immunity and Inflammation, University of Glasgow, Glasgow, United Kingdom, [2]Strathclyde Institute of Pharmacy and Biomedical Sciences, University of Strathclyde, Glasgow, United Kingdom, [3]Institute of Medical Sciences, University of Aberdeen, Aberdeen, United Kingdom, [4]Department of Pure and Applied Chemistry, University of Strathclyde, Glasgow, United Kingdom, [5]Glasgow Ageing Research Network (GARNER), Institute of Biodiversity, Animal Health and Comparative Medicine, University of Glasgow, Glasgow, United Kingdom

Despite significant increases in human lifespan over the last century, adoption of high calorie diets (HCD) has driven global increases in type-2 diabetes, obesity and cardiovascular disease, disorders precluding corresponding improvements in healthspan. Reflecting that such conditions are associated with chronic systemic inflammation, evidence is emerging that infection with parasitic helminths might protect against obesity-accelerated ageing, by virtue of their evolution of survival-promoting anti-inflammatory molecules. Indeed, ES-62, an anti-inflammatory secreted product of the filarial nematode *Acanthocheilonema viteae*, improves the healthspan of both male and female C57BL/6J mice undergoing obesity-accelerated ageing and also extends median lifespan in male animals, by positively impacting on inflammatory, adipose metabolic and gut microbiome parameters of ageing. We therefore explored whether ES-62 affects the osteoimmunology axis that integrates environmental signals, such as diet and the gut microbiome to homeostatically regulate haematopoiesis and training of immune responses, which become dysregulated during (obesity-accelerated) ageing. Of note, we find sexual dimorphisms in the decline in bone health, and associated dysregulation of haematopoiesis and consequent peripheral immune responses, during obesity-accelerated ageing, highlighting the importance of developing sex-specific anti-ageing strategies. Related to this, ES-62 protects trabecular bone structure, maintaining bone marrow (BM) niches that counter the ageing-associated decline in haematopoietic stem cell (HSC) functionality highlighted by a bias towards myeloid lineages, in male but not female, HCD-fed mice. This is evidenced by the ability of ES-62 to suppress the adipocyte and megakaryocyte bias and correspondingly promote increases in B lymphocytes in the BM. Furthermore, the consequent prevention of ageing-associated myeloid/

lymphoid skewing is associated with reduced accumulation of inflammatory $CD11c^+$ macrophages and IL-1β in adipose tissue, disrupting the perpetuation of inflammation-driven dysregulation of haematopoiesis during obesity-accelerated ageing in male HCD-fed mice. Finally, we report the ability of small drug-like molecule analogues of ES-62 to mimic some of its key actions, particularly in strongly protecting trabecular bone structure, highlighting the translational potential of these studies.

KEYWORDS

ageing, B lymphocyte, ES-62, inflammation, obesity, osteoimmunology

## Introduction

The dramatic increase in lifespan, resulting from advances in medicine, better nutrition and improved sanitation over the last century, has not been mirrored by a similar increase in late-life health and well-being (healthspan). This disconnect reflects that the ageing process appears to have been accelerated by adoption of the Western life-style, incorporating a high calorie diet (HCD) and sedentary behaviours, resulting in dysfunction of immunometabolic networks and promotion of age-associated co-morbidities such as type 2 diabetes (T2D), stroke, cardiovascular disease, and cancers (1). Moreover, there is increasing evidence that HCD-induced obesity (2) acts as a reciprocal risk factor with autoimmune conditions in promoting dysbiosis of the microbiome and disruption of gut barrier integrity, with the resulting inflammation inducing dysregulation of the key cellular sensor that integrates metabolism and inflammation, mTOR (3, 4). This triggers canonical biological ageing processes (1, 5, 6), including the premature ageing of haematopoietic stem cells (HSC) and consequent immune system dysfunction (5, 6). Indeed, we have recently shown that the extended health- and life-span exhibited by mTOR mutant (S6Kinase1-null) mice is associated with preservation of HSC function during ageing (7).

The pivotal role of chronic low-grade inflammation in driving age-associated co-morbidities and (accelerating) ageing *per se* also resonates with the Hygiene Hypothesis in which the evolutionary-rapid eradication of pathogens, including helminths, has left us with unbalanced hyperactive immune systems that may have contributed to the recent alarming increase in prevalence of allergic and autoimmune disorders (8, 9). Consistent with this, evidence from both epidemiological studies and animal models of inflammatory disease suggests that parasitic helminth infection might protect humans from developing chronic inflammatory conditions and indeed, live helminths have undergone trials as therapeutics in a range of immune-mediated diseases (8, 9). Certainly, we have shown that ES-62, a phosphorylcholine (PC)-containing immunomodulator secreted by the filarial nematode, *Acanthocheilonema viteae*, protects against allergic and autoimmune pathology in various mouse models by subverting TLR4-signalling to downregulate aberrant MyD88 responses and restore the regulatory:effector immune system balance, thereby allowing it to homeostatically resolve aberrant inflammation irrespective of its phenotype [reviewed in reference (10)]. Collectively such findings led us to hypothesise that ES-62 might increase health- and lifespan by targeting inflamm-ageing.

We therefore embarked on an age- and sex-matched longitudinal survival study, combined with evaluation of parallel interventional cross-sectional cohorts at various time-points across the life-course that allowed us to analyse effects of ES-62 (when administered at 1 μg/week) on >120 inflammatory and metabolic parameters in C57BL/6J mice fed a HCD diet (11). Male and female mice were found to exhibit distinct pathological responses in this model of obesity-accelerated ageing, with female mice typically showing more exaggerated inflammatory responses whilst the male animals exhibited more pronounced metabolic defects including visceral adipocyte hypertrophy, insulin resistance and loss of pancreatic β-cell function (11). This sexual dimorphism extended to ES-62-responsiveness, with sex-specific improvements in healthspan apparent and strikingly, increasing median lifespan recorded in male, but not female, HCD-fed mice (11). Mathematical modelling identified (as expected) that anti-inflammatory activities were amongst the signatures most predictive of ES-62 action (11). However, this analysis also highlighted the importance of additional protective effects targeting intestinal integrity in male HCD-cohorts. These actions reflected normalisation of the gut microbiome (11) with, in particular, profound depletion of proteobacteria species previously associated with promoting ageing (12, 13). Of note, we have also shown the protection against joint inflammation and bone damage afforded by ES-62, in the collagen-induced arthritis (CIA) mouse model of rheumatoid arthritis, to be associated

with its normalisation of the gut microbiome and intestinal barrier integrity (14).

Collectively, these findings may be pertinent to the ability of ES-62 to promote healthspan as gut health impacts not only on the "training" of immune responses and skeletal health (osteoimmunology) (15–17), but also on inflamm-ageing, age-associated comorbidities, frailty and the ageing process *per se* (18–20). This reflects that the combination of cumulative exposure to pathogens and Western-style diets causes changes in the gut microbiota during obesity and ageing that drives the dysregulation of haematopoiesis. Such dysregulation is typically characterised by an increase in HSC numbers but a decline in HSC functionality (HSC exhaustion/senescence) and a bias towards myeloid lineages (21–23). Generation of the resultant inflammatory network termed the senescence-associated secretory phenotype (SASP) impacts on long-term HSC functionality, perpetuating dysregulation of haematopoiesis (24, 25). The SASP is thus manifested by anaemia, immunosenescence and thrombocytosis, as well as elevated systemic levels of cytokines and chemokines (e.g., IL-1α and β, IL-6 and TNFα; CXCL1 and CXCL2) (22, 24). The impact of such decline in HSC functionality is underlined by the evidence that BM Transfer (BMT) from young to old mice can extend lifespan (26, 27), as well as protect against obesity and age-associated comorbidities like cardiovascular and neurodegenerative disease (28, 29). SASP arises due to HSCs responding both directly to microbiota-derived molecules and indirectly, *via* the impairment of the haematopoiesis-supporting BM microenvironment resulting from the impact of inflammation and metabolic stress on mesenchymal lineages (22, 23, 25). As TLR/MyD88 signalling, which is a key target of ES-62, plays an important role in these events, we therefore investigated whether, by modulating bone structure and the BM microenvironment, ES-62 acted to reduce dysregulation of haematopoiesis to suppress inflamm-ageing and promote healthspan during HCD-accelerated ageing of male and female mice.

# Methods

## Ethics statement

All procedures were performed in accordance with UK Home Office Project Licences (60/4504 and PDBDC/7568), following the "principles of laboratory animal care" (NIH Publication No. 86-23, revised 1985) and approval by the University of Glasgow Animal Welfare and Ethical Review Board.

## The obesity-accelerated mouse model

Male and female C57BL/6J mice (Envigo, UK) were housed (in same sex groups of 2 to 4, randomly allocated on arrival at 4 weeks of age) in the Central Research Facility (University of Glasgow, UK) and maintained, under specific pathogen-free conditions, at 22°C under a 12-h light/dark cycle with *ad libitum* access to water and Chow (CRM-P) and High Calorie (Western Diet RD) diets from Special Diet Services, UK as described previously (11, 30). Briefly, from 4 weeks of age, all mice were fed normal Chow CRM-P diet (comprising Oil, 3.36%; Protein 18.35%; Fibre, 4.23%: Sugar 3.9%; Atwater fuel energy from Oil, 9.08%; Protein, 22.03%: Carbohydrate, 68.9%) plus 150 ppm Fenbendazole. Mice were administered PBS, purified endotoxin-free ES-62 (1 μg (31);) or a combination of SMAs 11a plus 12b (both 1 μg (32)) weekly *via* the subcutaneous route from 9 weeks of age (30, 31). At 10 weeks of age, the HCD cohorts received Western Diet RD (Fat, 21.4%; Protein, 17.5%; Fibre, 3.5%; Sucrose 33%; Atwater fuel energy from Fat, 42%; Protein, 15%: Carbohydrate, 43%) plus 150 ppm Fenbendazole.

For the ES-62 time-course study, male and female cohorts of mice were culled at the following ages (days; (d)), d56 (8 weeks); d160 (22-23 weeks); d340 (48-49 weeks) and d500 (71-72 weeks). The group sizes were: d56 (Chow + PBS, n=6), d160 (HCD + PBS/ES-62, n=10/group; Chow + PBS, n=6), d340 (HCD + PBS/ES-62, n=12/group; Chow + PBS, n=6) and d500 (HCD + PBS/ES-62, n=6/group; Chow + PBS, n=5). For analysis of the effect of ES-62 on ageing Chow-fed mice, additional male and female cohorts of mice were culled at 340 days (48-49 weeks) of age (Chow + PBS/ES-62, n=8; HCD + PBS, n=8) and, in the SMA study, male and female cohorts of mice were culled at 160 days (22-23 weeks) of age (Chow + PBS, n=4; HCD + PBS/ES-62, n=6).

Following fasting overnight (~16 h), blood was collected between 8-10 am from mice after cervical dislocation and rapid decapitation of the animals from the severed carotid artery. Blood was either immediately aliquoted into FACS buffer (PBS containing 2.5% BSA and 0.5 mM EDTA) and kept on ice for processing for flow cytometric analysis or following clotting at room temperature, centrifuged and the isolated serum stored at-20°C in endotoxin-free Eppendorf tubes for analysis of IL-1β and TNF-α by ELISA (BD Biosciences, Oxford UK).

## Bone histology and micro computed tomography (μCT)

Paws and femurs were fixed in 4% paraformaldehyde prior to decalcification and paraffin wax embedding for H&E staining (7 μm sections) of joints as described previously (14, 33). Joint histopathology was determined by semi-quantitative scoring of cell infiltration/pannus formation, cartilage and bone erosion, each scored on a 0-3 severity scale (34) and then averaged, with the mean values representing the histopathology scores for individual mice. In bone sections, adipocytes were identified visually in the BM by their spherical, amorphous and white appearance. BM adipocytes were enumerated in 3 images from each mouse and the numbers of adipocytes normalised to the area of the BM, calculated using ImageJ software (pixel to

10.3389/fimmu.2022.953053

micron conversion) for each field of view, with the mean values calculated as the data point for each individual animal.

Femurs were subjected to μCT analysis at the Microscopy and Histology Core Facility at the Institute of Medical Sciences, University of Aberdeen (https://www.abdn.ac.uk/ims/facilities/ microscopy-histology/services-and-equipment-1872.php#panel1876), using a Skyscan1072 x-ray Microtomograph (Skyscan, Aartselaar, Belgium) and NRecon version 1.4.4. (3D images) and CTan version 1.0.7.2 Skyscan software using protocols described previously (35–37).

## Flow cytometry

Flow cytometric analysis was performed as described previously (11, 14, 30, 33). Briefly, following red cell-lysis (with 0.8% $NH_4Cl$ buffer), BM, blood, spleen, MLN and adipose tissue cells were suspended in FACS buffer (PBS containing 2.5% BSA and 0.5 mM EDTA) and phenotyped using the following antibodies:

| Tissue | Specificity | Conjugate | Clone | Supplier | Catalogue # |
|---|---|---|---|---|---|
| BM | CD3 | PE | 17A2 | BioLegend | #100205 |
| | B220 | PE | RA36B2 | BioLegend | #103207 |
| | Ter119 | PE | TER-119 | BioLegend | #116207 |
| | CD11b | FITC | M1/70 | BioLegend | #101206 |
| | Sca-1 | FITC | D7 | BioLegend | #108116 |
| | Ly6C | PerCP-Cy5.5 | HK1.4 | BioLegend | #128011 |
| | Ly6G | APC | 1A8 | BioLegend | #127613 |
| | CD11b | APC | M1/70 | BioLegend | #101212 |
| | CD45 | APC | 30-F11 | BioLegend | #103112 |
| | RANKL | Biotin | IK22/5 | BioLegend | #510003 |
| | CD117 | Biotin | 2B6 | BioLegend | #105803 |
| | Streptavidin | APC-Cy7 | | BioLegend | #405208 |
| | CD115 | Biotin | AFS98 | eBioscience | #13-1152-82 |
| | CD117 | APC | 2B8 | eBioscience | #17-1171-82 |
| Other tissues | CD3 | FITC | 146-2C11 | BioLegend | #100305/6 |
| | CD3 | FITC | 17A2 | BioLegend | #100203 |
| | CD3 | PE | 17A2 | ImmunoTools | #22150034 |
| | CD4 | PE | GK1.5 | BioLegend | #100407 |
| | CD4 | APC-ef780 | RM4-5 | eBioscience | #47-0042-82 |
| | CD8 | PE-Cy7 | 53-6.7 | eBioscience | #25-0081-82 |
| | CD44 | PerCP | IM7 | BioLegend | #103036 |
| | CD45RB | FITC | C363-16A | BioLegend | #103305 |
| | CD45RB | APC-ef780 | 30-F11 | Invitrogen | #47-0451-82 |
| | CD19 | AF700 | 6D5 | BioLegend | #115527/8 |
| | CD11c | FITC | N418 | BioLegend | #117305 |
| | CD11c | PE-Cy7 | N418 | BioLegend | #117318 |

HSC analysis involved use of a dump channel (PE-conjugated lineage cocktail) in combination with FITC anti-Sca-1 and APC or biotin anti-CD117 antibodies. For surface marker staining, antibodies were used at 0.2 μg/$10^6$ cells (1/100 dilution) except for anti-CD45 (1/200 dilution). Streptavidin was used at 1/500 dilution. Cell death was assessed by fixed viability stain (APC-ef780) or 7AAD (BD Bioscience, UK) staining. Data were acquired using FACS Canto or BD LSRII flow cytometers and analysed using FlowJo Software (Tree Star In, OR USA, version 8.8.7) and populations were gated using isotype and fluorescence minus one (FMO) controls (11, 14, 30, 33). Exemplar gating strategies are shown in Supplementary Figure 1.

## Osteoclast (OC) differentiation *in vitro*

OC differentiation was determined as we described previously (14, 33). Briefly, BM was flushed from the tibias and femurs using a sterile 23-gauge needle and syringe and aspirated to create a single cell suspension in PBS which, following filtering through a 20 μm cell strainer, was centrifuged (400 x g), washed in PBS and resuspended ($10^6$/ml) in "complete" αMEM medium (containing 50 U/ml penicillin, 50 μg/ml streptomycin and 10% FCS). Cells were incubated overnight with M-CSF (30 ng/ml; Peprotech, London, UK) at 37°C in 5% $CO_2$ and then following removal of non-adherent cells, re-suspended in fresh complete αMEM medium supplemented with 30 ng/ml M-CSF and 50 ng/ml RANKL and OC differentiation initiated by seeding cells ($10^5$) in 96-well tissue-culture plates, with the medium refreshed on day 4. Functional maturation was assessed by TRAP staining (Leukocyte Acid Phosphatase Kit, Sigma, UK) on day 5, with $TRAP^+$ cells containing ≥ 3 nuclei counted as OCs. The size of individual OCs per field of view (FOV) was calculated from images (x4 magnification; scale bars 1000 μm) generated by an EVOS FL Auto Cell Imaging System using Image J software.

## qRT-PCR

As described previously (14, 33), BM cells ($10^6$) were lysed in RNeasy Lysis Buffer prior to mRNA extraction using RNeasy Plus Mini kit (Qiagen, Germany) and cDNA generated using the High Capacity cDNA Reverse Transcriptase kit (Applied Biosystems, Life Technology) and amplified using the StepOne Plus™ real-time PCR system (Applied Biosystems). KiCqStart® qPCR Ready Mix (Sigma-Aldrich) was used in conjunction with the following primer pairs:

10.3389/fimmu.2022.953053

| Gene | Forward Primer | Reverse Primer |
|---|---|---|
| RANK, *tnfrsf11a* | GAAATAAGGAGTCCTCAGGG | TAGAATCTCTGACTTCTGCC |
| RANKL, *tnfsf11* | TCTGTTCCTGTACTTTCGAG | TTCATGGAGTCTCAGGATTC |
| OPG, *tnfrsf11b* | GAAGATCATCCAAGACATTGAC | TCCTCCATAAACTGAGTAGC |
| IL-1β *il1b* | GTGATATTCTCCATGAGCTTTG | TCTTCTTTGGGTATTGCTTG |
| β-actin, *actb* | GATGTATG AAGGCTTTGGTC | TGTGCACTTTTATTGGTCTC |

Data were normalised to the reference gene β-actin to obtain the ΔCT values and expressed as Rq (2^-ΔCt).

## Statistical analysis

All data were analysed by GraphPad Prism 9 software using unpaired student T-tests, one or two-way ANOVA with Fishers LSD post-test for parametric data or Kruskal-Wallis test for non-parametric/ordinal data. The data presented in scatter plots are the mean values (of triplicate images/assays) or, for flow cytometric analysis, the % live cells or Mean Fluorescence Intensity (MFI) values of the individual mice in the group (bar is the mean value for the group) and analysed by one-way ANOVA. For time-courses, the data are presented as the mean ± SEM values for the group (n values presented in legends) derived from the mean values for the individual mice and analysed by two-way ANOVA. Significant differences between the cohorts are shown on the figures, where significance is denoted by $^{*}p < 0.05$, $^{**}p < 0.01$, $^{***}p < 0.001$ and $^{****}p<0.0001$ or $^{\#}p < 0.05$, $^{\#\#}p < 0.01$, $^{\#\#\#}p < 0.001$ and $^{\#\#\#\#}p<0.0001$.

# Results

We hypothesised that ES-62 acts to normalise the osteoimmunology axis in its suppression of inflamm-ageing and promotion of healthspan during obesity-accelerated ageing. Thus, we analysed the impact of HCD-feeding on ~70 parameters of osteoimmunology - ranging through bone structure and pathology to BM cellularity, differentiation, lineage skewing and consequent peripheral immune responses – across the lifecourse in male and female C57BL/6J mice and determined whether ES-62 could modulate any altered responses back towards those exhibited by Chow-fed controls. The data obtained exhibited, sex-, diet- and age-associated signatures that displayed sexual dimorphism with respect to ES-62 responsiveness (summarised in Figure 1). The key findings are detailed below (Figures 2–8), with the remainder of the data provided in the Supplementary Information (Supplementary Figures 2-13).

## ES-62 protects against ageing-induced loss of bone structure in male HCD-fed mice

Bone remodelling, balancing the actions of osteoclasts (OCs) and osteoblasts (OBs) in controlling bone resorption and synthesis respectively, is a normal and necessary physiological process during adulthood, but one which becomes dysregulated during obesity and ageing, resulting in loss of bone mass and development of osteolytic diseases such as arthritis and osteoporosis (38–40). In our study, histological analysis of paw synovial joints indicated a trend for limited damage to develop between d160 and d340, but there were no statistically significant differences amongst any of the groups in either sex over this time period (Figures 2A, B).

Obesity and ageing have also been reported to impact on trabecular bone architecture with consequent perturbation of the bone marrow niche supporting stem cell function (25), resulting in the skewing of immune responses and development of inflamm-ageing/SASP, with in turn, the further fostering of osteolytic disease and frailty (38–40). Imaging by micro-computed tomography (μCT) revealed clear ageing-associated loss of trabecular bone structure (as indicated by transverse 2D and deconvolved 3D images), in the femurs of Chow-fed male and particularly female mice (Figures 2C, D respectively). This process was substantially accelerated by HCD-feeding in male mice whereas the female mice showed profound changes by d160 even when fed a normal Chow diet, confirming the early onset and profound deterioration in trabecular architecture previously reported for this sex of C57BL/6 mouse (41). By contrast, and perhaps consistent with the marginal articular pathology observed (Figures 2A, B), changes in cortical (as evidenced by cross-sectional 2D images) bone were much less pronounced, with no dramatic effects observed amongst the groups in either sex at least over the 500 days monitored (Figures 2C, D). Quantitative μCT analysis of key parameters of bone health (Supplementary Figures 2A-O; Table 1) showed that those associated with bone integrity, mechanical function and strength, such as high bone/tissue volume ratios (%BV/TV), bone density (BS/TV), trabecular number (Tb.N), bone intersection surface (contact with trabecular nodes) and fractal dimension, declined during (obesity-accelerated) ageing of the mice. By contrast, the scores for parameters positively associated with osteopenia and osteoporosis (42–44) such as Degrees of Anistropy, Structural Model Index (SMI; plate to rod transition) and trabecular thickness (Tb.Th), separation (Tb.Spn) and pattern (Tb.PF; disconnected trabecular lattice) increased. Noteworthy, loss of bone structure was evident in both sexes of Chow- and HCD-fed ageing mice: however, female mice exhibited a significantly more profound decline than their male

10.3389/fimmu.2022.953053

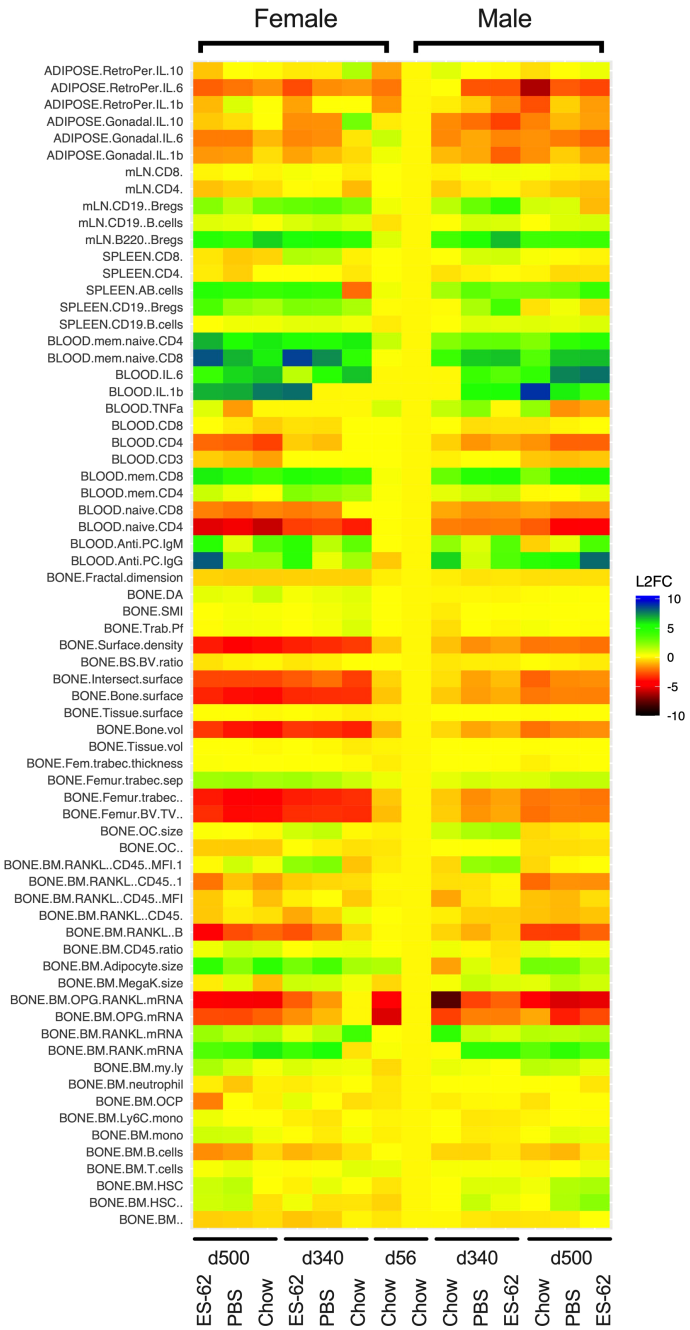


FIGURE 1
Heatmap analysis of the effects of HCD-feeding and exposure to ES-62 on parameters associated with the osteoimmunology axis. Characterisation of the indicated features of bone structure, bone marrow cellularity, differentiation and myeloid/adipocyte skewing and consequent systemic and peripheral inflammatory responses was carried out on tissues derived from individual young (d56) and ageing (d340 and d500) male and female mice fed normal Chow or a HCD (from d70) diet, the HCD groups being administered (s/c) PBS or ES-62 (1 µg) weekly from d63. The mean responses of the groups were determined and normalised to those of the male d56 group and the data presented in heatmap form in terms of the log2 fold response for each parameter.

10.3389/fimmu.2022.953053

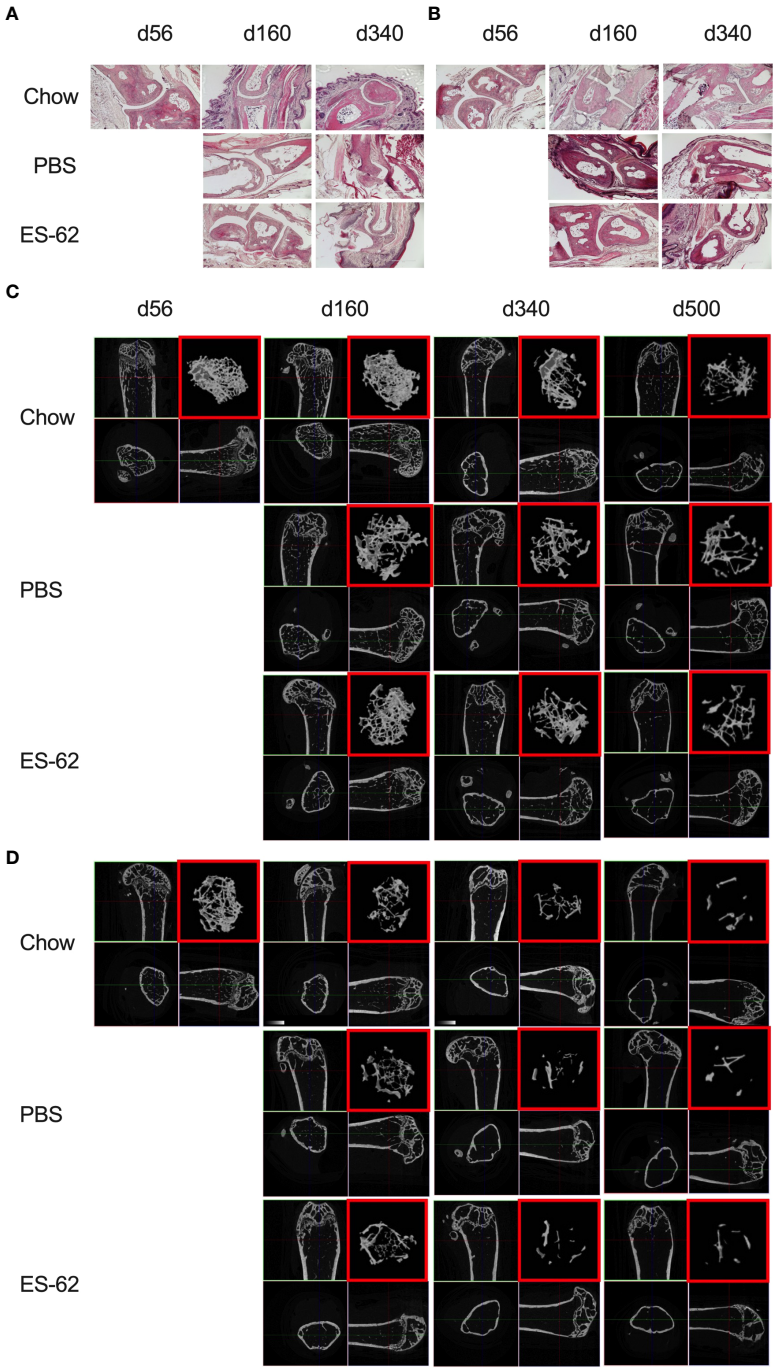


FIGURE 2
Impact of HCD-feeding and exposure to ES-62 on trabecular bone structure. Representative sections of H & E staining of paw joint sections (scale bar 400 µm) are shown for the indicated groups of male **(A)** and female **(B)** mice and where tissue damage was not significantly different across the groups. Scores: for male mice, d56: 0, n=3, Chow: 0.48 ± 0.09, n=11; PBS-HCD: 0.58 ± 0.08, n=4; ES-62: 0.25 ± 0.08, n=4; for female mice, d56: 0.11 ± 0.11, n=3; Chow: 0.50 ± 0.14, n=10; PBS-HCD: 0.66 ± 0.24, n=4; ES-62: 0.44 ± 0.22, n=3. MicroCT analysis of femurs from the indicated groups of male **(C)** and female **(D)** mice was performed and representative 2D images of transverse sections through femurs illustrating the reference growth plate and the downstream area (~200 slices of pixel size 5 µm) of analysis of trabecular parameters (upper left and lower right boxes) are shown. Reconstruction of the image stack provided 3D images of the trabecular structure (red box) whilst cross-sectional analysis provides a 2D image of the cortical bone (lower left box).

10.3389/fimmu.2022.953053

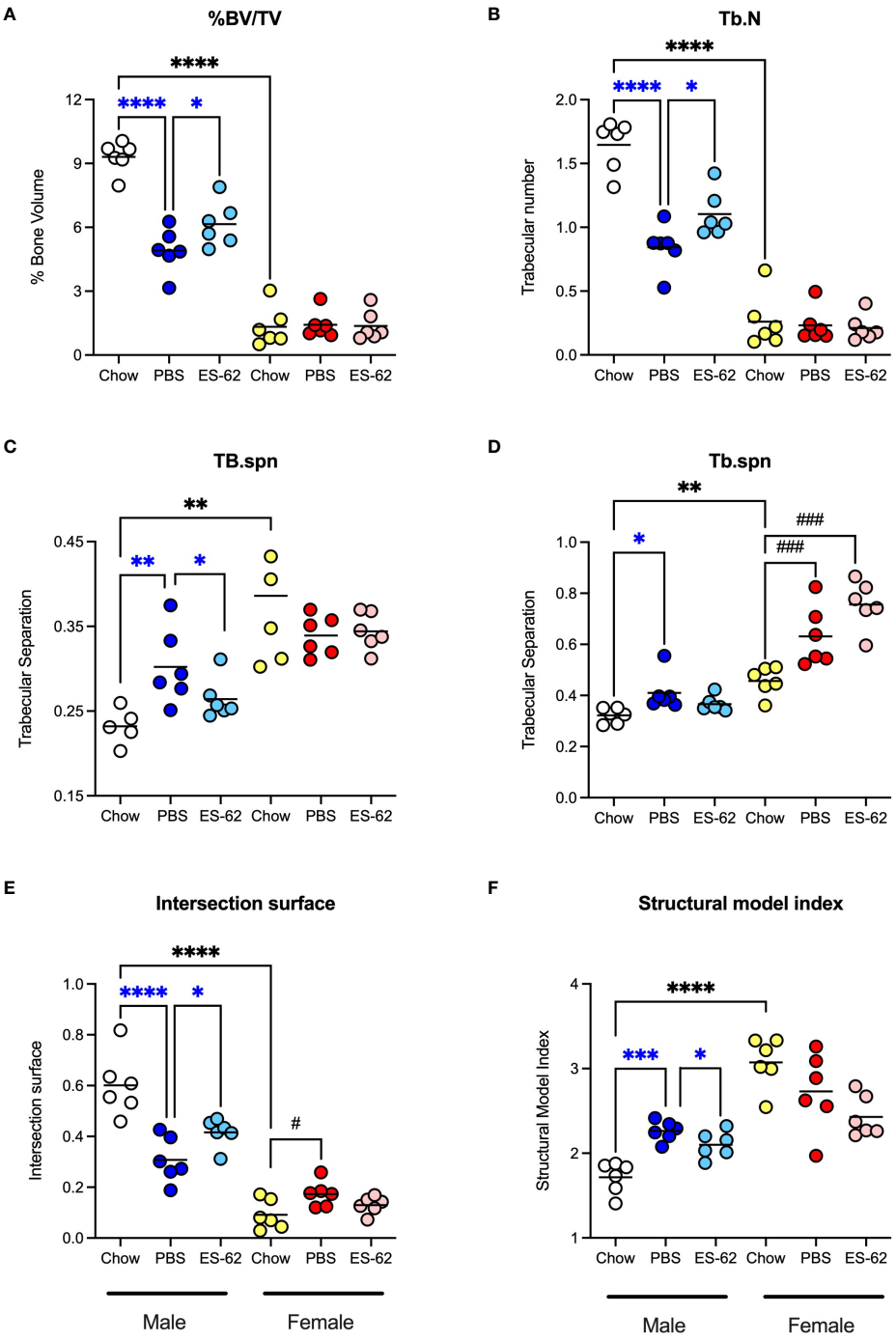


FIGURE 3
ES-62 protects against the HCD-accelerated changes in parameters of trabecular bone architecture in male mice. The effects of ES-62 on HCD (PBS)- and ageing-induced decline in bone structure homeostasis as evidenced by changes in **(A)** % Bone Volume/Tissue Volume (BV/TV) at d340; **(B)** Trabecular Number (Tb.N) at d340; **(C)** Trabecular Separation (Tb.spn) at d160; **(D)** Trabecular Separation (Tb.spn) at d340; **(E)** Intersection Surface at d340 and **(F)** Structure Model Index (SMI) at d340. The data shown are the values of femurs from individual mice (symbols) with the mean value for the group represented by the bar and significant differences indicated by blue****=p<0.0001 for male PBS v male Chow, blue***= p<0.001 for male PBS v male Chow, blue**=p<0.01 for PBS v male Chow, blue*=p<0.05 for male PBS v male Chow and blue*= p<0.05 for male PBS v male ES-62 **(A–F)**, black****= p<0.0001 for male Chow v female Chow and black**=p<0.01 for male Chow v female Chow **(A–F)**, black$^{\#\#\#}$ = p<0.001 for female Chow v female PBS or female ES-62 **(D)** and black$^{\#}$ = p<0.05 for female Chow v female PBS **(E)** groups.

counterparts such that their loss of bone structure was not accelerated by HCD administration (Supplementary Figures 2A-O). ES-62 was able to significantly reduce a number of the obesity-accelerated changes in trabecular architecture (Figures 2C, D; Figures 3A–F; Table 1) in the male HCD-fed mice, delaying the decline in %BV/TV, Tb.N and intersection surface (Figures 3A, B, E) and the increase in trabecular separation and SMI values (Figures 3C, D, F).

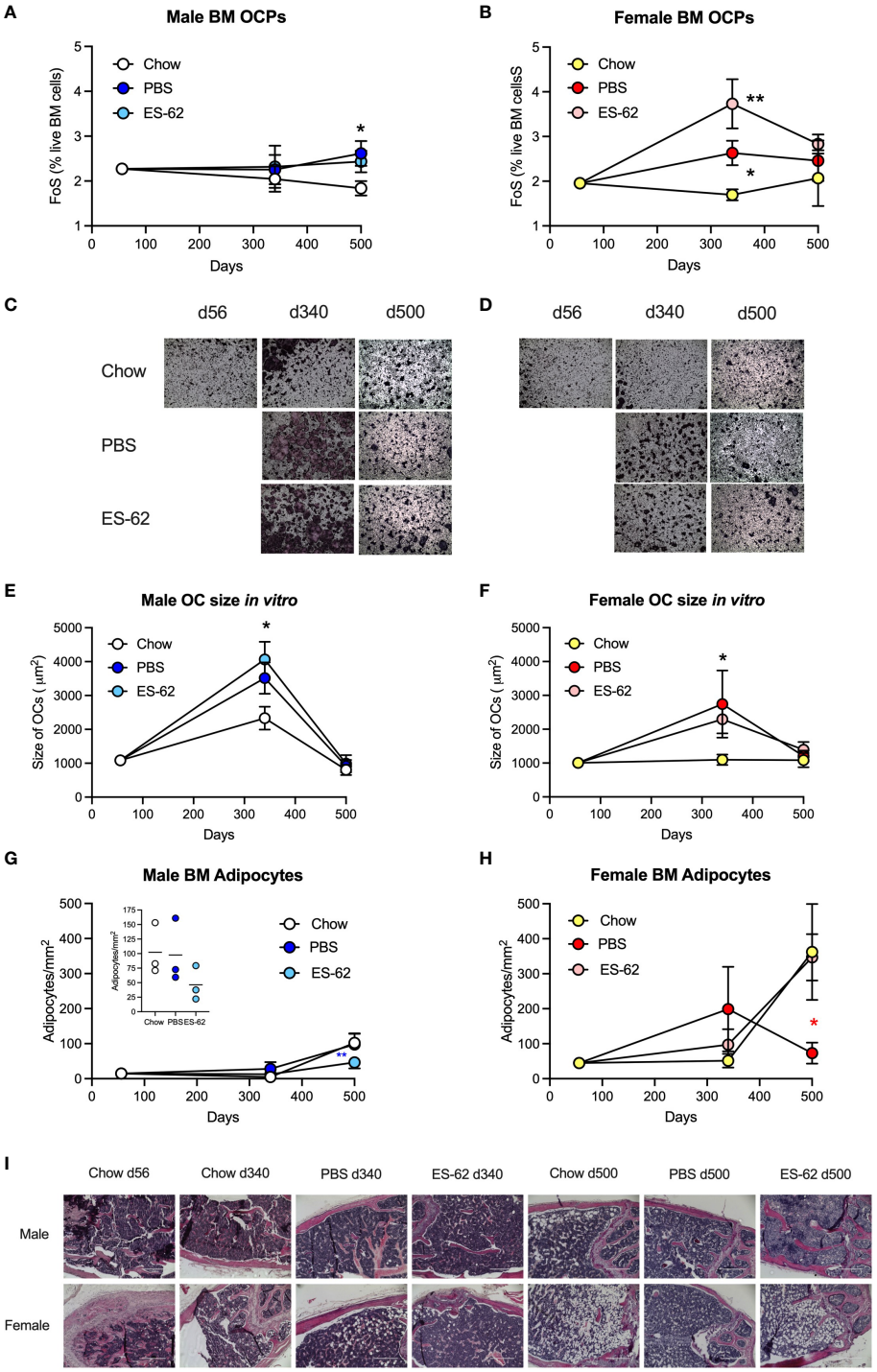


FIGURE 4 (Continued)

FIGURE 4 (Continued)
Obesity-accelerated ageing is associated with enhanced osteoclastogenic potential and BM adipocyte accumulation. The levels of BM $CD3^-B220^-Ter119^-Ly6G^-Ly6C^{high}$ $CD11b^{low}$ OCPs were determined as the frequency of single cells (FoS) expressed as % live BM cells at the indicated timepoints in **(A)** male and **(B)** female mice fed Chow or HCD, the latter cohort treated with either PBS or ES-62. The data are presented as the mean ± SEM values for the indicated group, where for male mice, at d56: n=6; d340: Chow, n=6; PBS, n=7; ES-62, n=8; d500, Chow, n=5; PBS, n=5; ES-62, n=5 individual mice and for female mice, at d56: n=6; d340: Chow, n=6; PBS, n=8; ES-62, n=8; d500, Chow, n= 3; PBS, n=5; ES-62, n=6 individual mice. Significant differences are indicated by *=p<0.05, male Chow v male PBS or ES-62 **(A)** and female Chow v female PBS **(B)** and **=p<0.01, female Chow v female ES-62 **(B)** groups. **(C–F)** OC differentiation at day 5 was assessed by TRAP staining and the size of multinucleated OCs (>3 nuclei) determined by Image J analysis. Representative images (x4 magnification) of OCs of the indicated groups of male **(C)** and female **(D)** mice are shown and the mean group OC size ± SEM determined from the mean values of triplicate cultures of individual male mice at each time point where for male mice **(E)**, at d56: n=6; d340: Chow, n=6; PBS, n=3; ES-62, n=4; d500, Chow, n=5; PBS, n=5; ES-62, n=5 individual mice and for female mice **(F)**, at d56: n=6; d340: Chow, n=6; PBS, n=3; ES-62, n=4; d500, Chow, n=4, PBS, n=5; ES-62, n=5 individual mice. Significant differences are indicated by *=p<0.05, Chow v PBS or ES-62 for male **(E)** and female **(F)** mice. **(G–I)** BM adipocytes were visualised (x10 magnification, scale bars 400 μm) and quantitated by Image J analysis where the mean group number/$mm^2$ ± SEM is determined from the mean values of triplicate fields of view (FoV) of the individual mice at each time point. For male mice **(G)**, d500 data scale expanded in insert), d56: n=6; d340: Chow, n=6; PBS, n=6; ES-62, n=6; d500, Chow, n=3; PBS, n=3; ES-62, n=3 individual mice and for female mice **(H)**, d56: n=6; d340: Chow, n=5, PBS, n=5; ES-62, n=6; d500, Chow, n=3; PBS, n=3; ES-62, n=3 individual mice. Significant differences are indicated by blue**=p<0.01 for male PBS v male ES-62 **(G)** and red*=p<0.05, female PBS v female ES-62 **(H)** groups. Representative images are shown for each group **(I)**.

However, perhaps reflecting the deterioration associated with these parameters noted even in the Chow-fed female group, there was no evidence that ES-62 exerted such protective actions in HCD-fed mice of this sex (Figures 3A–F; Table 1).

To determine whether the observed bone damaging changes were associated with dysregulation of bone remodelling towards osteoclastogenesis, we first examined the levels of BM osteoclast progenitors (OCPs; $CD3^-B220^-Ter119^-Ly6G^-Ly6C^{high}$ $CD11b^{low}$ BM cells (14, 33). This revealed that although OCP levels remained relatively constant in Chow-fed mice of both sexes up to 500 days of age, they were significantly increased in female, and to a lesser extent in male, HCD-fed mice. However, this HCD-induced increase was not significantly reduced by exposure to ES-62 in either case (Figures 4A, B). Rather, we observed a stronger upregulation of OCP levels driven by ES-62 in the BM of HCD-fed female mice (Figures 4A, B). Whilst the HCD-induced increase in OCP levels was confirmed in additional cohorts of female mice (Supplementary Figure 3A, B), the ES-62 effect was not recapitulated in the "normal" Chow-fed (cES-62) ageing context (Supplementary Figure 3A, B). Next, analysis of *in vitro* differentiation of BM OCPs to large, active multinucleated OCs (14, 33), showed that OCPs from both sexes of HCD-fed mice exhibited a greater increase in osteoclastogenic potential at d340 than their Chow-fed counterparts. Again, these HCD-induced changes in OCP functionality were not modulated by *in vivo* exposure to ES-62, but in all groups, declined towards or below the levels exhibited by young mice at d500 (Figures 4C–F; Supplementary Figure 3C, D). Further evidence that the parasitic worm product was not modulating osteoclastogenesis was provided by the findings that whilst the expression of the OC-promoting factor RANKL (cell surface intensity; MFI) and its receptor, RANK (mRNA) were similarly increased at d340 in BM cells from both sexes of HCD-fed mice, relative to their Chow-fed controls, again, these responses were generally not modulated by ES-62 (Supplementary Figure 3E-J).

Collectively these data suggested that the ES-62-mediated protection against the accelerated decline in bone health observed in male HCD-fed mice did not reflect modulation of OCP levels or osteoclastogenesis. Interestingly therefore, and presumably reflecting the mesenchymal stem cell (MSC) impairment that results in an ageing-associated BM adipocyte bias (at the expense of osteoblasts) (45), adipocyte numbers increased in both male and particularly, female mice as they aged (Figures 4G–I). Exposure to ES-62 reduced adipocyte numbers in male HCD-fed mice (Figures 4G, I), suggesting it may support the osteoblastic niche in mediating its protective effects. Rather surprisingly however, whilst BM adipocyte numbers peaked at d340 in the female HCD-fed mice, the highest numbers of BM adipocytes were found in Chow- and ES-62-HCD-fed female mice at d500 (Figures 4H, I). Clearly therefore, sexual dimorphism exists in ageing-associated adipogenesis in the BM.

## ES-62 normalises the ageing-associated myeloid/lymphoid bias of male HCD-fed mice

As the bone stromal microenvironment impacts on HSC functionality, we next investigated how HCD-feeding and exposure to ES-62 impacted on haematopoiesis and subsequent immune responses. Whilst it has been widely reported that the levels of $Lin^-Sca\text{-}1^+c\text{-}Kit^+$ (LSK) HSCs are dramatically increased in "old" C57BL/6 mice (6-17x fold for mice at >730, relative to 60-90, days old), due to exhaustion/senescence (21, 25, 46, 47), their levels were not elevated in the BM of Chow-fed mice of either sex by day 500 in our study (Figures 5A, B). However, and consistent with the ability of obesity to accelerate ageing, the levels of LSK-HSCs observed in the BM from ageing male and female HCD-fed mice were significantly higher than those of their Chow-fed counterparts

by this time point (Figures 5A, B; males, ~2.5x fold; females, ~3x fold). Exposure to ES-62 did not significantly modify these elevated levels of HSCs in either male or female HCD-fed mice (Figures 5A, B).

Although the d500 Chow-fed mice did not exhibit elevated levels of LSK-HSCs, BM from the Chow-fed animals showed an increased myeloid/lymphoid cell ratio that was evident by d340 in both male and female chow-fed mice (Figures 5C, D), findings indicative of the well-established ageing-associated myeloid skewing. This myeloid bias was not modulated by HCD in either male or female animals but interestingly, showed sexual dimorphism in terms of the impact of exposure to ES-62 (Figures 5C, D). Thus, whilst ES-62 acted to suppress the myeloid bias in ageing male mice, it perhaps surprisingly strongly promoted it in female HCD-fed animals at d500 (Figures 5C, D). The protective effect of ES-62 against this myeloid bias in male mice reflected both a limiting of the HCD-induced decline in B cells (Figure 5E) and associated increases of various myeloid lineages (Figures 6A, E, H). By contrast, and perhaps consistent with the adipocyte skewing away from the B cell-promoting osteoblastic (or their mesenchymal progenitors) niche (48–50) observed in female mice (Figures 4H, I), exposure to ES-62 did not impact on the profound HCD-accelerated decline in B cells (Figure 5F) and resulted in enhanced levels of certain myeloid cells in the BM of d500 HCD-fed female animals (Figures 6B, F). These differential effects of ES-62 on the ageing-associated myeloid bias in male and female HCD-fed mice were broadly corroborated in terms of absolute numbers of the relevant cell populations (Supplementary Figure 4).

Although ES-62-treated HCD-fed mice also exhibited less myeloid/lymphoid skewing than their Chow-fed counterparts, these effects of ES-62 appear generally to be restricted to the accelerated inflammation-induced pathology associated with HCD-feeding. Thus, in separate cohorts of Chow-, HCD- and ES-62-Chow (cES-62)-fed mice (PBS treated, HCD-fed mice were also included as obesity-accelerated ageing controls), we found that treatment with the helminth product had no effect on the BM levels of LSK-HSCs or any myeloid/lymphoid bias pertaining at the d340 time point in the male Chow-fed animals (Supplementary Figures 5A-D). By contrast, the d340 female HCD-fed mice exhibited reduced levels of B and T cells, providing corroboration of the sexual dimorphisms in haematopoiesis we have identified during ageing of HCD-fed mice (Supplementary Figures 5E-L).

## ES-62 and lymphoid cells

Whilst male Chow- and HCD-fed mice showed a comparable substantial age-associated decline in BM B cells that was significantly mitigated in the ES-62-treated HCD cohort, the reduction observed in female Chow-fed mice was profoundly accelerated in both the PBS- and ES-62-treated HCD cohorts (Figures 5E, F). By contrast, levels of BM T cells were relatively stable in all cohorts, although treatment with ES-62 tended to enhance their levels, relative to those exhibited by their PBS-HCD- and Chow-fed male, but not female, counterparts, at d500 (Figures 5G, H). Perhaps, given the evidence that RANKL may provide a crucial autocrine factor for B cell development (39), the inverse effects of ES-62 on the proportions of B cells expressing RANKL (Figures 5I, J) provide a potential mechanism contributing to its prevention of this myeloid bias in male, but not female HCD-fed mice.

Despite the observed age-associated decline in BM B cells in Chow and HCD-fed male and female mice (Figures 5E, F), we found the total levels of splenic and MLN $CD19^+$ B cells to increase with age, and this was accelerated and exacerbated by HCD-feeding in male animals, but not modulated by ES-62 in either sex (Supplementary Figures 6A-D). Rather, ES-62 increased the levels of "regulatory" IL-10 producing B cells (Bregs) in the spleens (Supplementary Figure 6E) and MLNs (11) of HCD-fed male, but not female mice. These "regulatory" actions of ES-62 were again restricted to the HCD-fed animals as its administration to Chow-fed animals was not associated with any significant change in the levels of MLN or splenic Bregs or the levels of $CD19^+CD21^-CD23^-CD11c^+$ ageing-associated B cells (ABCs) in the spleens of such animals (Supplementary Figures 6F-H). Likewise, ES-62 had little or no effect on naïve and memory $CD4^+$ and $CD8^+$ T cell populations in the blood, spleen or MLNs of Chow- or HCD-fed mice of either sex (Supplementary Figures 7-9).

## ES-62 and myeloid lineages

Neutrophils constitute a major myeloid population in the BM and it has been proposed that the hyperglycemia and hyperlipidemia resulting from HCD/obesity induce enhanced BM production of (primed) neutrophils that contribute to adipose tissue inflammation and development of diabetes and cardiovascular conditions (51). Consistent with previous findings that neutrophil levels are broadly similar in the BM of young and old healthy mice (52), we found that BM neutrophil levels in male Chow-fed mice rise only marginally with age. Whilst this was also true of PBS-HCD-fed male animals, this ageing effect was somewhat countered in the ES-62-treated HCD cohort at d500 (Figure 6A). Moreover, in female mice there was no overall change in the levels of neutrophils in Chow- and ES-62-HCD-fed animals over the time course of the experiment, although a significant decrease in their levels was observed in the BM of PBS-HCD-fed female mice at d500 (Figure 6B). Likewise, the levels of BM monocytes showed only limited changes during ageing of male and female mice, with HCD-feeding both reducing (d340) and enhancing (d500, albeit not significantly in the case of the female animals)

the levels of these cells, regardless of exposure to ES-62 (Figures 6C, D). Deeper analysis revealed that the classical, inflammatory Ly6C$^{hi}$ sub-population of monocytes did not exhibit the d500 increase in any of the cohorts of HCD-fed mice (Figures 6E, F), perhaps suggesting the HCD-induced decrease (in both total and Ly6C$^{hi}$ monocytes) at d340 reflected the mobilisation of these monocytes associated with obesity-programming of peripheral inflammation.

ES-62 also impacted on the megakaryocyte component of the ageing-associated skewing towards the myeloid lineages that is promoted by the obesity-driven BM adipocyte bias and contributes to the production of platelets with increased inflammatory and thrombotic activity recently implicated in the development of cardiovascular comorbidities (53). Histological analysis revealed increased numbers of megakaryocytes evident even in the bones of ageing Chow-fed mice. Whilst male mice fed a HCD diet displayed significantly more of these cells at d340 and d500, these were reduced by exposure to ES-62 towards the levels seen in Chow-fed animals and a similar modulatory pattern was observed in female mice, particularly at d500 (Figures 6G–I). Megakaryocytes have also recently been implicated in promoting HSC quiescence during ageing (49, 50) and thus, together with its enhancement of B and T lymphocytes and decrease in neutrophils, the ES-62-mediated suppression of the rise in megakaryocytes likely contributes to its ability to block the myeloid/lymphoid bias exhibited in the BM of ageing male HCD-fed mice (Figure 5C).

Although the ageing myeloid bias is associated with chronic low-grade inflammation in terms of systemic IL-1β and TNFα levels (22), there was no clear pattern regarding effect of sex, HCD or ES-62 on the serum levels of these cytokines across our mouse cohorts. Perhaps of more relevance in the context of obesity, however, increased levels of inflammatory CD11c$^{+}$ macrophages were evident at d340 in the gonadal fat of male PBS-HCD, but not ES-62-HCD-, fed male mice (Figure 6J), with the protective effect of ES-62 correlating with a reduction in the mRNA levels of IL-1β and TNFα (Figures 6K, L) in this tissue. Experiments involving additional d340 cohorts of PBS-Chow-, ES-62-Chow- and, as an obesity-accelerated ageing control, PBS-HCD-fed mice, showed that treatment with ES-62 had no effect on the levels of these adipose CD11c$^{+}$ macrophages or Bregs in either male Chow-fed mice (Figures 6M, N). However, they corroborated the finding that enhanced levels of CD11c$^{+}$ macrophages are found in the gonadal fat pads of male, but not female, HCD-fed mice relative to their Chow-fed counterparts (Figure 6M) and in addition, identified HCD-induced depletion of Bregs from this adipose tissue in female, but not male, mice at d340 (Figure 6N).

## Small molecule analogues (SMAs) of ES-62 target trabecular bone and the BM niche

Although the findings reported above have potential translational impact, ES-62 itself is not suitable for drug development as it is a large, "foreign" and hence immunogenic glycoprotein. Rather, we have addressed translational potential by designing a library of SMAs of which at least two (11a, 12b) mimic ES-62's primary mechanism of action in downregulating MyD88 and also recapitulate many of its protective effects in mouse models of chronic inflammatory disease including asthma, arthritis and SLE (10, 32, 54). Crucially, treating mice with 11a plus 12b (combined due to subtle but complementary differences in their immunomodulatory actions), also promotes their healthspan by improving gut and metabolic homeostasis in the HCD model of obesity-accelerated ageing (30). We therefore investigated whether such treatment could recapitulate the impact of ES-62 on the bone microenvironment, focusing on the d160 time-point when much of the (obesity-accelerated) loss of trabecular bone structure was already apparent (Figures 2, 3; Supplementary Figure 2). Again, although no significant differences in articular joint pathology (Figure 7A) were determined, the profound loss of trabecular bone architecture in all cohorts of female mice and the HCD-acceleration of such pathology in male mice (Figures 2, 3; Table 1; Supplementary Figure 2) was confirmed. μCT analysis of these d160 cohorts indicated that treatment with the SMA combination clearly mimicked the actions of ES-62 in protecting against trabecular bone loss (Figures 7B, 8), again by preventing the decline in % BV/TV, Tb.N and intersection surface (Figures 8A, B, J) and the increase in T.PF and SMI in male, but not female, HCD-fed mice (Figures 8L, O).

Such trabecular bone loss and/or its protection by exposure to the SMAs, was again not associated with any substantial effects on the levels of OCPs or their osteoclastic potential (Supplementary Figures 10A-G) and consistent with this, there were no significant differences amongst the cohorts in their BM expression of RANK, RANKL or OPG. However, the elevated levels in BM adipocytes generally observed in female, relative to male, mice at d340 and d500 (Figures 4G–I) were also evident at the d160 timepoint, although these were not further increased by HCD-feeding (Figures 7C–E). Moreover, whilst HCD-feeding increased the levels of BM adipocytes in male mice at this timepoint, this enhancement was countered by their exposure to the SMAs (Figures 7C, D). Collectively, these data suggest that trabecular bone loss at this stage may also predominantly reflect dysregulation of BM adipocyte homeostasis and that this regulatory checkpoint exhibits sexual dimorphism in its ES-62/SMAs responsiveness.

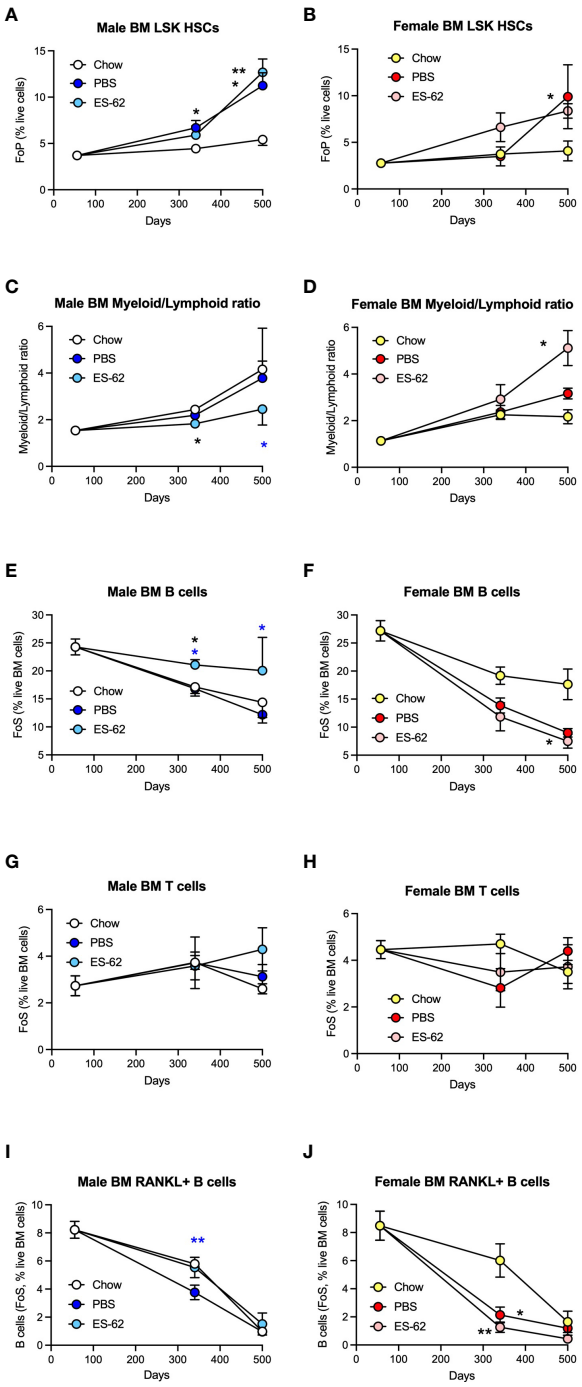


FIGURE 5
ES-62 protects against myeloid/lymphoid skewing and maintains B cell levels in the BM of male HCD-fed mice. The levels of $Lin^{-}Sca\text{-}1^{+}c\text{-}kit^{+}$ (LSK) HSC (**A**, male; **B**, female; as % $Lin^{-}$ cells [frequency of precursor (FoP)]) and the ratios of Myeloid/Lymphoid lineages (**C**, male; **D**, female) are shown. The levels of $CD19^{+}$ B cells **(E, F)**, $CD3^{+}$ T cells **(G, H)** and $RANKL^{+}$ B cells **(I, J)** were determined as the frequency of single cells (FoS) expressed as % live BM cells at the indicated timepoints in male **(E, G, I)** and female **(F, H, J)** mice fed Chow or HCD, the latter cohort treated with either PBS or ES-62. The data are presented as the mean ± SEM values for individual mice in each group, where for male mice, at d56: n=6; d340: Chow, n=6; PBS, n=7; ES-62, n=8; and at d500, Chow, n=5; PBS, n=5; ES-62, n=5 and for female mice, at d56: n=6; d340: Chow, n=6; PBS, n=8; ES-62, n=8; and at d500, Chow, n= 3; PBS, n=5; ES-62, n=6. Significant differences are indicated by black*=p<0.05 for Chow v PBS or ES-62 in male **(A, C, E)** or female **(B, D, F, J)** mice; black**=p<0.01 for Chow v PBS or ES-62 in male **(A)** and female **(J)** mice; blue*=p<0.05 for male PBS v male ES-62 **(C, E)** and blue **=p<0.01 for male PBS v male ES-62 **(I)** groups.

10.3389/fimmu.2022.953053

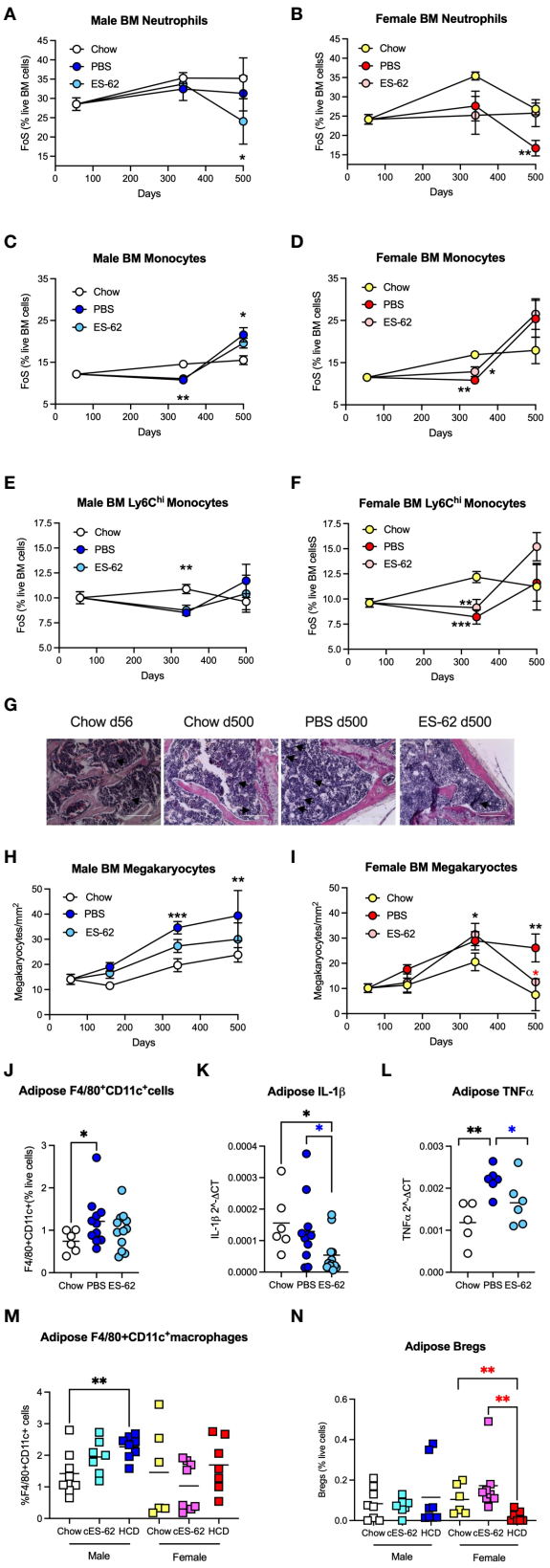


FIGURE 6 (Continued)

FIGURE 6 (Continued)
ES-62 modulates levels of BM myeloid lineages in male HCD-fed mice. The levels of $Ly6C^+Ly6G^+$ neutrophils **(A, B)**, $Ly6C^+Ly6G^-$ monocytes **(C, D)** and $Ly6C^{high}$ monocytes **(E, F)** were determined as the frequency of single cells (FoS) expressed as % live BM cells at the indicated timepoints in male **(A, C, E)** and female **(B, D, F)** mice fed Chow or HCD, the latter cohort treated with either PBS or ES-62. The data are presented as the mean ± SEM values for individual mice in each group, where for male mice, at d56: n=6; d340: Chow, n=6; PBS, n=7; ES-62, n=8 and at d500, Chow, n=5; PBS, n=5; ES-62, n=5 and for female mice, at d56: n=6; d340: Chow, n=6; PBS, n=8; ES-62, n=8 and at d500, Chow, n= 3, PBS, n=5; ES-62, n=6. Significant differences are indicated by black*=p<0.05 for Chow v PBS or ES-62 in male **(A, C)** or female **(D)** mice; black**=p<0.01 for Chow v PBS or ES-62 in male **(C, E)** and female **(B, D, F)** mice and black***=p<0.001 for Chow v PBS in female mice **(F)** groups. **(G–I)** BM megakaryocytes were visualised (x20 magnification, scale bars 200 µm), with representative images shown for the indicated groups of male mice **(G)**. Quantitation was by Image J analysis where the mean group number/$mm^2$ ± SEM is determined from the mean values of triplicate field of view (FoV) of individual male **(H)** and female **(I)** mice at each time point. For male mice, at d56: n=6; d340: Chow, n=6; PBS, n=6; ES-62, n=6; and at d500, Chow, n=3; PBS, n=3; ES-62, n=3 and for female mice, at d56: n=6; d340: Chow, n=5; PBS, n=5; ES-62, n=6 and at d500, Chow, n=3; PBS, n=3; ES-62, n=3. Significant differences are indicated by black**=p<0.01 and black***=p<0.001 for male Chow v male PBS but not male ES-62 **(H)** and black*=p<0.05 for female Chow v female PBS or female ES-62; black**=p<0.01 for female Chow v female PBS and red*=p<0.05 for female PBS v female ES-62 **(I)** groups. Levels of $F4/80^+CD11c^+$ macrophages **(J, M)**, IL-1β **(K)** and TNFα **(L)** mRNA and $IL\text{-}10^+CD19^+$ Bregs **(N)** were determined in gonadal adipose tissue of each of Chow-, HCD-PBS and HCD-ES-62 male mice **(J–L)** and in separate d340 studies investigating the effect of ES-62 in a non-obese setting involving Chow-, Chow-ES-62 (cES-62) and, as a confirmatory obesity-accelerated ageing control, HCD-PBS male and female mice cohorts **(M, N).** The data shown are mean values for individual mice (symbols) and the group means are indicated by the bars. Significant differences are indicated by black*=p < 0.05 for male Chow v male PBS **(J)** or ES-62 **(K)**; black**=p<0.01 for male Chow v PBS **(L)**; blue*=p<0.05 for male PBS v male ES-62 **(K, L)**; black**=p<0.01 for male Chow v HCD **(M)** and red**=p<0.01 for female HCD v female Chow and female cES-62 **(N)** groups.

Although there were no significant differences between the groups in terms of LSK-HSCs, myeloid/lymphoid skewing or various myeloid lineages in either sex at d160 (Supplementary Figures 11A, B, E-H), the HCD-induced decrease in B and T cells in the BM of female mice (Supplementary Figures 11C, D) likely reflects adipocyte disruption of the osteoblastic/CXCL12 abundant reticular (CAR) niches that support lymphoid lineages. However, the levels of B and T cells in the blood, spleen or MLNs were not modulated by SMA treatment in either sex (Supplementary Figure 12; Supplementary Figures 13A-F). Interestingly, given the inflammatory ($CD11c^+$ macrophages and IL-1β) nature of adipose tissue in male HCD-fed mice that we identified at d160 (11) and d340 (Figures 6J–L), we have also found significant rises in TNFα (at the mRNA level) in the gonadal fat pads of male but not female HCD-mice, which were not reduced by exposure to either ES-62 or SMAs at d160 (Supplementary Figures 13G, H). However, whilst the mRNA levels of IL-1β likewise appear to be elevated in these fat pads of male HCD-fed mice at this time point, in this case, ES-62 appears to be able to reduce production of this cytokine in this adipose tissue. A similar pattern tended to be observed in the female animals, although this did not reach statistical significance (Supplementary Figure 13I). Nevertheless, collectively these data indicate that the SMAs mimic ES-62's ability to retrain the BM microenvironment and that their anti-inflammatory actions are associated with their capacity to promote healthspan during obesity-accelerated ageing (11, 30).

## Discussion

Collectively, our analyses of the impact of HCD-feeding on the BM microenvironment and consequent skewing of immune responses across the life-course in male and female C57BL/6J mice underlines the central role that dysregulation of the osteoimmunology axis plays in driving inflamm-ageing and associated metabolic comorbidities, loss of skeletal health, frailty and (obesity-induced acceleration of) the ageing process *per se* (15–20). Moreover, they have highlighted pronounced sexual dimorphisms in these processes with female mice exhibiting more dramatic dysfunction in each of loss of skeletal health, disruption of the BM niche and consequent haematopoiesis towards a more pro-inflammatory phenotype, factors likely contributing to the observed sex differences in the immune system with ageing, particularly with respect to development of autoimmunity and in addition, efficacy of vaccination and cancer immunotherapy (55). Further to this sexual dimorphism, exposure to ES-62 predominately ameliorates such dysregulation in male HCD-fed mice, a differential effect perhaps contributing to our observation that whilst it can promote healthspan in both sexes of obese mice, it is only able to extend the median lifespan of male HCD-fed mice (11).

Such protection in male HCD-fed mice appears to reflect that ES-62 harnesses its immunomodulatory properties to counteract the aberrant training of BM progenitors triggered by the chronic low-grade inflammation associated with obesity, rather than acting on the ageing processes within these cells, *per se*, as it had little effect on the, albeit more limited, dysregulation of haematopoiesis evidenced by Chow-fed mice at 340 days of age. Nevertheless, in reducing the myeloid/adipocyte skewing and loss of BM B cells associated with both "normal" and obesity-accelerated ageing (17, 21–25) in male mice, ES-62 acts to maintain a BM phenotype more consistent with that of young mice. Thus, as it is increasingly evident that all ageing characteristics do not (i) occur synchronously, or indeed linearly, (ii) exhibit sexual dimorphism and (iii) are impacted by acute and chronic exposure to environmental factors such as diet and smoking (56–60), any clear protective effects of ES-62 against dysregulation of the osteoimmunology axis in Chow-fed

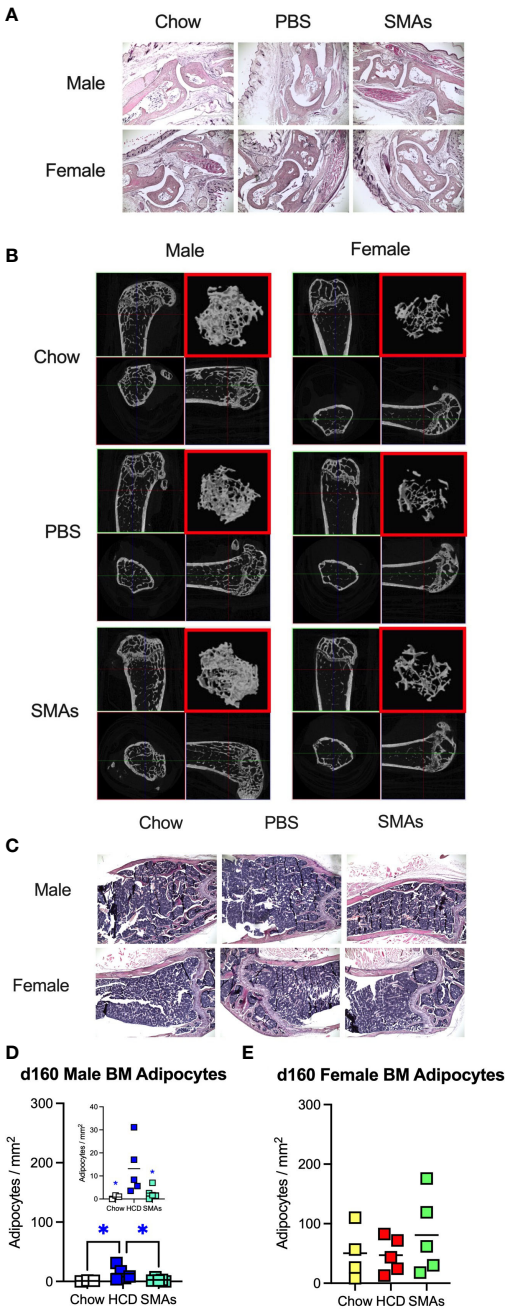


FIGURE 7
ES-62-based SMAs protect against disruption of the BM niche in male HCD-fed mice at d160, a time-point when substantial (obesity-accelerated) loss of trabecular bone structure is established. **(A)** Representative sections of H & E staining of paw joint sections (scale bar 1000 µm) are shown for the indicated groups of d160 male and female mice and where tissue damage was not significantly different across the groups. Scores: for male mice, Chow: 0.66 ± 0.19, n=4; PBS-HCD: 0.38 ± 0.10, n=6; SMAs-HCD: 0.50 ± 0.17, n=6; for female mice, Chow: 0.58 ± 0.16, n=4; PBS-HCD: 0.53 ± 0.17, n=5; SMAs-HCD: 0.33 ± 0.15, n=5. **(B)** MicroCT analysis of femurs from the indicated groups of d160 male and female mice was performed and representative 2D images of transverse sections through femurs illustrating the reference growth plate and the downstream area (~200 slices of pixel size 5 µm) of analysis of trabecular parameters (upper left and lower right boxes) are shown. Reconstruction of the image stack provided 3D images of the trabecular structure (red box) whilst cross-sectional analysis provides a 2D image of the cortical bone (lower left box). **(C)** Representative images of BM adipocytes (x10 magnification, scale bars 400 µm) in male and female Chow-, HCD-PBS- and HCD-SMAs-fed mice at d160 are shown. **(D, E)** Quantitation is by Image J analysis where the mean group number/mm$^2$ ± SEM is determined from the mean values (of triplicate FoV values) of the individual mice (symbols) and the group means are indicated by the bars for male (D; insert shows expanded scale) and female **(E)** mice. Significant differences are indicated by blue*=p < 0.05 for male HCD-PBS v male Chow or male HCD-SMAs mice **(D)**.

male mice might not be apparent until a much later age. ES-62 might therefore exhibit protection in much older Chow-fed mice when the "biological" (rather than chronological) ages of key functional responses of such animals correspond to those of younger HCD-fed mice and/or the eventual chronic inflammation resulting from gut dysbiosis and loss of barrier integrity in Chow-fed animals impacts on the ageing process (11–13). Hence, whilst our data indicate a dramatic increase in

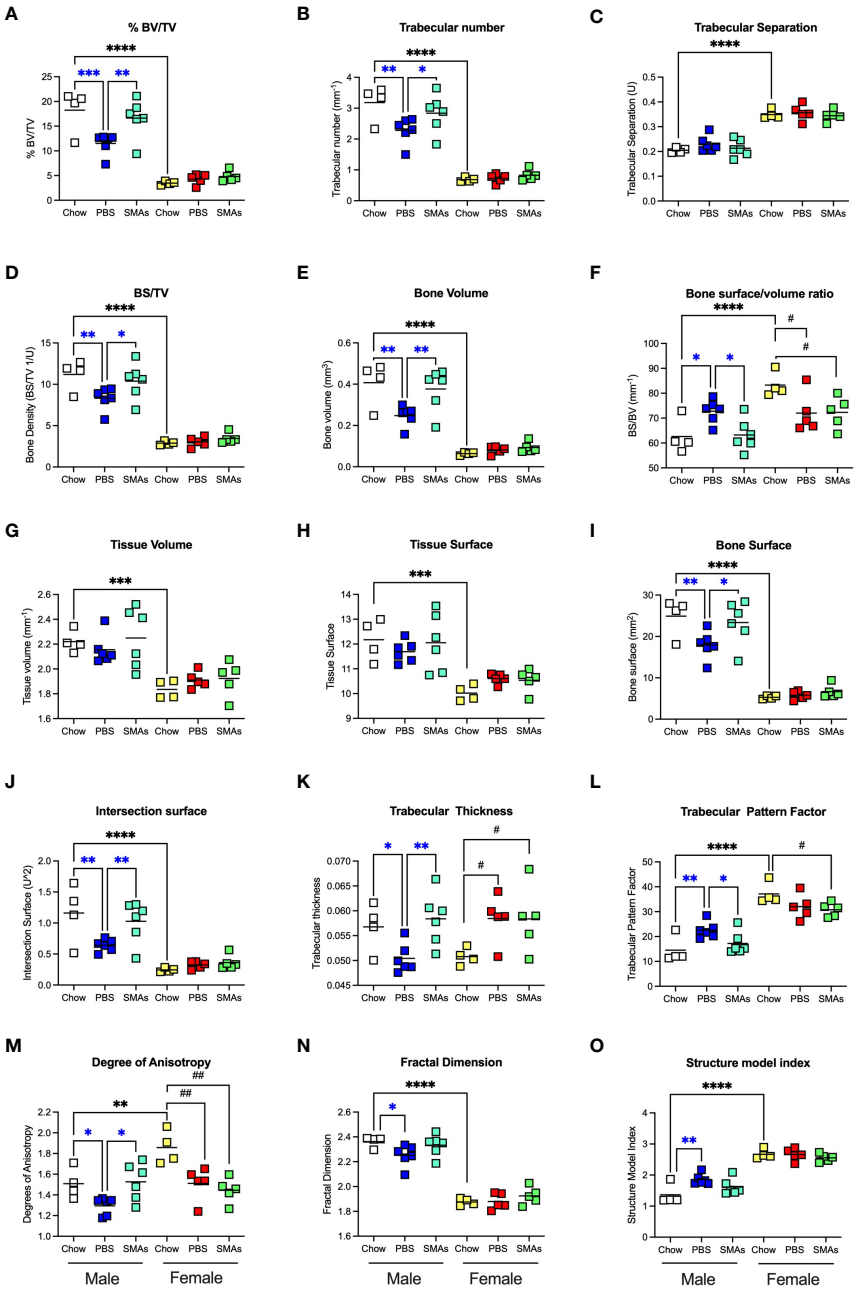


FIGURE 8
ES-62-based SMAs protect against the HCD-accelerated decline in trabecular bone structure in male HCD-fed mice. The effects of ES-62-based SMAs on the HCD (PBS)- accelerated decline in bone structure homeostasis, as evidenced by changes in the indicated parameters of trabecular architecture in femurs from Chow-, HCD-PBS (PBS)- and HCD-SMAs (SMAs) groups of male and female mice **(A–O)** at d160. The data shown are the values of femurs from individual mice (symbols) with the mean value for the group represented by the bar. Significant differences are indicated by blue***=p<0.001 for male PBS v male Chow, blue**=p<0.01 for male PBS v male Chow or male SMAs, and blue*=p<0.05 for male PBS v male Chow or male SMAs **(A, B, D–F, I–O)**; black****=p<0.0001, black***=p<0.001 and black**=p<0.01 for male Chow v female Chow **(A–J, L–O)** and black$^{\#\#}$=p<0.01 and black$^{\#}$=p<0.05 for female Chow v female PBS or female SMAs **(F, K–M)** groups.

TABLE 1 µct analysis of femur bone structure during HCD accelerated in ageing male and female C57BL/6J mice.

| | Male | | | | | | | | | Female | | | | | | | | | Male v Female Chow | | Male Chow v HCD | Female Chow v HCD | Male v Female HCD |
|---|---|---|---|---|---|---|---|---|---|---|---|---|---|---|---|---|---|---|---|---|---|---|---|
| | Chow Mean±SEM | | | HCD Mean ±SEM | | | HCD-ES-62 Mean±SEM | | | Chow Mean ±SEM | | | HCD Mean ±SEM | | | HCD-ES-62 Mean±SEM | | | d56 | | Age-related change (d56-500) | | |
| | d56 | d340 | % d56* | d340 | % d56* | % d340† | d340 | % d56* | % d340† | d56 | d340 | % d56* | d340 | % d56* | % d340† | d340 | % d56* | % d340† | p‡ | p§ | p§ | p§ | p§ |
| BV/TV (%) | 14.48 ± 0.99 | 9.30 ± 0.30 | 64 | 4.91 ± 0.43 | 34 | 53 | 6.15 ± 0.43 | 42 | 66 | 7.72 ± 0.65 | 1.33 ± 0.38 | 17 | 1.42 ± 0.26 | 18 | 107 | 1.37 ± 0.70 | 18 | 103 | <0.0001 | <0.0001 | 0.0004 | ns | <0.0001 |
| Tb.N ($mm^{-1}$) | 2.74 ± 0.13 | 1.64 ± 0.08 | 60 | 0.84 ± 0.07 | 31 | 51 | 1.10 ± 0.07 | 40 | 67 | 1.63 ± 0.14 | 0.26 ± 0.09 | 16 | 0.23 ± 0.05 | 14 | 89 | 0.21 ± 0.04 | 13 | 81 | <0.0001 | <0.0001 | <0.0001 | ns | <0.0001 |
| Tb.spn (µm) | 202 ± 0.34 | 322 ± 1.21 | 159 | 410 ± 2.94 | 203 | 128 | 366 ± 2.99 | 181 | 114 | 307 ± 2.42 | 457 ± 2.28 | 149 | 632 ± 4.79 | 206 | 138 | 756 ± 3.80 | 246 | 166 | 0.0008 | <0.0001 | 0.0004 | 0.0066 | <0.0001 |
| IS | 0.77 ± 0.04 | 0.60 ± 0.05 | 78 | 0.31 ± 0.04 | 40 | 52 | 0.42 ± 0.02 | 54 | 69 | 0.54 ± 0.03 | 0.09 ± 0.02 | 17 | 0.17 ± 0.02 | 32 | 189 | 0.13 ± 0.01 | 24 | 142 | 0.0008 | <0.0001 | 0.0001 | ns | <0.0001 |
| SMI | 1.92 ± 0.06 | 1.72 ± 0.08 | 90 | 2.26 ± 0.05 | 118 | 132 | 2.10 ± 0.06 | 110 | 122 | 2.14 ± 0.5 | 3.07 ± 0.12 | 144 | 2.73 ± 0.19 | 128 | 88 | 2.43 0.10 | 113 | 79 | 0.0057 | <0.0001 | 0.0081 | ns | <0.0001 |

*Treatment value at d340 as % of day d56 value, calculated by regression of mean values.
†Treatment value at d340 as % of d340 Chow control.
‡p value as assessed by Sudent's t-test.
§p value of sex-by age interaction across time course (d56-500) as determined by 2-way ANOVA.
BV/TV, bone volume/tissue volume; Tb. N, trabecular number; Tb.spn, trabecular bone separation; IS, intersection surface; SMI, structural model index.



10.3389/fimmu.2022.953053

the levels of HSCs between d340 and d500 in HCD-fed animals, previous studies on C57BL/6 mice showed that Chow-fed mice typically exhibited elevated levels of HSCs displaying loss of functionality between 18-24 months (d547-730), at which point such dysregulation was not further enhanced in mice experiencing a lifelong HCD (61, 62). Interestingly, whilst calorie restriction reduced these elevated HSC levels, it had no effect on their functionality in these old mice (61–63). By contrast, reduced myeloid/lymphoid skewing, improved HSC quiescence and repopulating capacity (partially reversed by insulin-like growth factor-1) has been reported in calorie-restricted "middle age" (9 months old) mice (64). However, perhaps surprisingly therefore, these "middle-aged" calorie-restricted mice also demonstrated suppressed lymphoid differentiation (rescued by provision of IL-6/IL-7), resulting specifically in decreased B cell immunity (64). Collectively, these studies emphasise the lack of correlation/synchronicity amongst various ageing parameters and the disconnect between biological and chronological age (56–60). It is also worth noting, given the profound sexual dimorphisms we have uncovered in the osteoimmunology axis, that these previous studies were either performed on undefined (61, 64) or mixed male and female (63) cohorts, potentially confounding the interpretation of at least some of these functional responses.

Alternatively, and consistent with our wealth of data suggesting that ES-62 acts to resolve chronic inflammation rather than suppressing steady-state or "emergency" responses, it is possible that ES-62 only targets "hyper-responsive" cells, the cross-talk between signals generated by ES-62 and the pathogenic microenvironment generating a unique, modulated phenotype. Supporting this idea, whilst ES-62 similarly has little or no effect on the functionality of fibroblasts in the synovial joints of healthy mice, it induces a stable epigenetically rewired, inflammation-resolving/tissue repair phenotype of synovial fibroblast in mice undergoing collagen-induced arthritis (CIA; a model of rheumatoid arthritis), that is distinct from that found in naïve animals (65). Interestingly, IL-1β signalling, a key factor in driving the pathogenic transformation of synovial fibroblasts in CIA and rheumatoid arthritis that is targeted by ES-62 (65), is crucial to the pro-inflammatory training of both BM and migratory "surveillance" haemopoietic stem and progenitor cells (HSCPs) and their resultant accumulation and differentiation into adipose tissue-resident myeloid cells that perpetuates the inflammatory osteoimmunology cycle in obesity (24, 66–68). Pertinent to this, we have now shown the levels of IL-1β, TNFα and $CD11c^+$ inflammatory macrophages to be reduced in the gonadal adipose tissue of male, but not female, HCD-mice by ES-62 at d340. Associated with this, we have previously reported that the helminth product reduces the levels of pro-inflammatory $CD11c^+$ macrophages whilst increasing those of anti-inflammatory $CD11c^-CD301^+$ macrophages found in these fat depots at d160 and in addition, counteracts the elevated levels of IL-1β in the liver in male, but not female HCD-fed animals at d500 (11).

ES-62's key actions in combating dysregulation of the osteoimmunology axis in male HCD-fed mice focus on slowing the ageing-related myeloid/lymphoid bias and associated loss of B lineage cells, as well as protecting the BM niche by suppressing the mesenchymal skewing towards adipocyte accumulation. These actions are likely interconnected as adipocyte skewing results in the depletion of the osteoblasts (or progenitors) proposed to be important, *via* their generation of IL-7 and CXCL12 (SDF-1), for B cell differentiation (39), as well as disrupting the BM niche and inducing pathogenic bone remodelling (25, 69–71). Given the increasing evidence that LPS-stimulated TLR4/MyD88 signalling is critical in driving both emergency pro-inflammatory myelopoiesis to fight infection and the myeloid/lymphoid skewing associated with (obesity-accelerated) ageing (66), our working model is that ES-62 harnesses its ability to subvert TLR4 signalling and downregulate MyD88 in order to counteract such dysregulation of HSCs, both in the BM and the periphery. Moreover, the central role of sensing of LPS (66), elevated in serum as a consequence of microbiota dysbiosis and loss of gut barrier integrity in each of infection and obesity, conditions associated with chronic inflammation and ageing *per se*, underlines the key contributions of the TLR4/MyD88 signalling cassette and the gut-osteoimmunology axis in the (dys)regulation of health and well-being over the life-course (11–14, 17–19, 25, 69–71).

Strikingly, impairment of HSC function has now been reported to occur prior to the onset of obesity-induced accumulation of adipose tissue $CD11c^+$ macrophages and the inflammation associated with the IL-1β- and TNFα-driven myeloid/lymphoid skewing of BM progenitors (24). This led to the discovery that LPS impacts directly on the functionality of (TLR4 expressing) BM HSCs (66), with deeper analysis revealing MyD88 signalling to be responsible for expansion of granulocyte/macrophage precursors and contributing to the accumulation of adipose tissue macrophages (72). LPS-TLR4/MyD88 signalling likewise similarly impacts on (migratory) Haematopoietic Stem and Progenitor Cells (HSPCs) (67), mobilised to the periphery in response to obesity where they also differentiate and accumulate as adipose tissue macrophages (68) to perpetuate inflammation and, *via* IL-1β release, further biasing of differentiation of BM cells (24, 66). HCD-depletion of the Common Lymphoid Progenitor (CLP) and B cell-differentiation-promoting CXCL12 abundant reticular (CAR) cells in the BM (25) additionally reinforces the myeloid/lymphoid bias (66) as does the HCD enhancement of $Nestin^+$ MSCs, which drive the adipocyte bias of the BM niche in obesity (25). Further to the osteoimmunology axis-targeting actions of ES-62 in the BM, MSCs also express TLRs and whilst LPS promotes differentiation of the proinflammatory (IL-6/IL-8-producing) MSC1 subset, by contrast TLR3 signalling promotes

differentiation of an immunosuppressive MSC2 subset (73, 74). Intriguingly therefore, as ES-62 can desensitize TLR4/MyD88 but not TLR3 signalling (10), by shifting the TLR4/TLR3 and hence MSC1/MSC2 functional balance it could effectively reset homeostasis of the osteoimmunology axis to promote healthspan. Certainly, TLR3 agonists are being explored for their potential to repair the BM niche and direct MSC2 to repair cardiac damage and cardiovascular disease in obesity (75–77).

Interestingly, MyD88 has also proven important in the regulation of functional responses of B cells in the periphery as, whilst MyD88-deficient B cells were impaired in upregulation of CD86 and proliferation, they exhibited increased synthesis of DNP-specific IgG1 antibodies (78), an isotype consistent with the modified (regulatory) TH2 immune response to ES-62 (79). Likewise, B cell depletion of MyD88 results in abrogation of pathogenic autoantibody responses (80–82) and is associated with the ES-62-induction of Bregs in mouse models of systemic lupus erythematosus, asthma and RA (14, 83, 84). Notably, treatment of HCD-fed male mice with ES-62 results in increased levels of splenic Bregs, reflecting our previous report of a similar induction of Bregs in the MLNs of these animals (11). Interestingly therefore, adoptive transfer of a splenic $CD9^+$ Breg population derived from mice infected with the parasitic trematode *Schistosoma japonicum* has recently been shown to promote metabolic health and suppress inflammation in young female C57BL/6 mice acutely fed (from 4 weeks of age) a high fat diet for up to 9 weeks (85). Moreover, whilst ES-62 also results in the upregulation of ABCs (high PC-reactivity) and anti-PC antibodies, this is likely to be beneficial in countering the declining immunity to (PC-containing) pneumococcal infection in ageing (HCD-fed) males (11, 86). Such natural antibodies have also been implicated in the induction of Bregs (87, 88), which by interacting with (dietary, endogeneous and microbiota-derived) lipid-sensing NKT cells, potentially provide an additional mechanism to counter the chronic pathogenic inflammation occurring in autoimmunity (89, 90) and obesity-accelerated ageing (11).

Nevertheless, despite even our young (d56) female Chow-fed mice exhibiting profoundly disrupted trabecular bone structure that presumably predisposes them to potentially irreversible dysregulation of the BM niche and consequent immune responses, our TLR4/MyD88-targeting mechanistic model leaves the key question, of why the osteoimmunology axis of female HCD-fed mice is relatively unresponsive to ES-62, unanswered. Indeed, given that our original hypothesis was that ES-62 would combat the chronic inflammation that causes retraining of BM progenitors, it might have been predicted that it would be more effective in female mice as they typically make stronger inflammatory responses than male animals (55). However, we found some surprising data with, for example, female HCD-fed mice exhibiting the lowest levels of neutrophils in the BM at d500: whilst this may simply reflect their mobilisation to the periphery under the conditions of chronic inflammation associated with obesity (91), it is also possible that these reduced levels could be due to the loss of $CD62L^{lo}CD11b^{hi}$ neutrophils that are a subpopulation of myeloid suppressor cells that normally home to the BM (92). Likewise, the highest numbers of adipocytes accumulated in the BM were observed in Chow- and ES-62-HCD-fed female mice at d500. However, increasing evidence that BM adipose tissue (MAT) functions as an endocrine organ (and hence may be differentially responsive to sex hormones) that can promote metabolic adaptation and bone homeostasis, whilst generally exerting detrimental effects on haematopoiesis and osteogenesis (93, 94), makes these findings more complicated to interpret without deeper characterisation of their functional phenotype. For example, BM accumulation of adipocytes can be a stress response acting to protect cells from lipotoxicity and providing a mobilisable reservoir during energy deficit (95), with brown MAT driving the energy balance, adaptive thermogenesis and releasing IGF-1 and leptin, factors that promote osteogenesis and bone mass (95). By contrast, sensing of obesity-induced oxidative stress could disrupt the brown/white MAT balance, leading to further release of cytokines and free fatty acids perpetuating inflammation (95–97). Intriguingly therefore, a novel bone-specific, ageing-associated adipogenesis pathway has recently been identified that, under conditions of metabolic stress, results in the accumulation of lipid-storing adipocytes within the haematopoietic niche, particularly in female mice (98).

Turning once again to osteogenesis, in terms of the proposed roles of leptin and adiponectin in promoting this [by increasing osteoblastic and suppressing osteoclastic activities (99–101)] and modulating haematopoiesis and inflammatory responses in mouse models, we had previously measured the effects of exposure to ES-62 on serum levels of these adipokines in our cohorts of ageing male and female mice (11). As obesity induces bone loss, it was not surprising that we found HCD-feeding to suppress serum adiponectin levels in both sexes. However, and perhaps rather unexpectedly from an osteogenic viewpoint, obesity was found to be associated with enhanced leptin levels. Nevertheless, this may simply reflect that chronic exposure to HCD induced a state of leptin resistance in these animals (11). Moreover, whilst ES-62 did not significantly reduce the HCD-induced gain in body mass and had no effect on HCD-associated adiponectin levels, it suppressed serum leptin levels in both sexes of HCD-fed mice at d500 (11). These data perhaps suggest that rather than targeting adipokine levels to promote osteogenesis, ES-62 might be acting to counter the inflammatory metabolic actions of leptin at this time point. Alternatively, as leptin can act directly on MSCs to promote BM adipogenesis (102), the reduction of serum leptin by ES-62 could contribute to the significant reduction of adipocyte skewing and disruption of the

bone marrow osteoblastic niche observed in male HCD-fed mice at d500. However, once again, sexual dimorphism is evident, as this adipocyte reduction is not found in female animals.

Thus, to further dissect the mechanisms underpinning the sexual dimorphism in ES-62 -protection of bone health and the haematopoiesis-supporting BM niche, we suggest that extensive bone histomorphometry (103) and measurement of more definitive serum biomarkers (104) of bone resorption (e.g., CTX-1) and formation (e.g., P1NP) could be employed. These techniques could help determine how the structural changes in the bones of our ageing mouse cohorts determined by μCT relate to dysregulation of the OC/OB balance controlling bone resorption and formation. Complementing these approaches, we aim to gain a fuller understanding of the divergent functional rewiring of BM populations underlying the sexual dimorphisms in dysregulation of haematopoiesis induced by HCD-accelerated ageing and their differential ES-62 responsiveness. To achieve this, we are currently embarked on a program of RNAseq (single cell and bulk) and adoptive transfer/reconstitution *in vivo* studies which, in concert with bioinformatic analyses, aims to identify the key functional and cellular BM phenotypes involved. Certainly, knowledge of these ageing BM phenotypes is imperative for exploiting the potential for ES-62 (and other interventions) to differentially target inflammatory and stromal cells (and progenitors) in the BM and periphery, to tailor inflammatory responses appropriate to the sexual dimorphisms evolved by the immune system to promote the health and lifespan of male and female individuals.

Finally, in terms of translating these actions of ES-62 to the clinic, we are encouraged by the ability of the SMAs to mimic not only its key gut and metabolic effects (30) but also certain of its impacts on the osteoimmunology axis, most notably in strong protection of the trabecular bone structure and BM niche. Such protection augurs well for their potential as starting points in the identification of novel ES-62-based anti-ageing interventions, particularly those targeting osteolytic diseases and chronic inflammatory disorders and comorbidities. Moreover, these studies once again underline the importance of targeted drug development in terms of addressing the sexual dimorphisms associated with ageing and inflammation-based comorbidities.

## Data availability statement

The original contributions presented in the study are included in the article/Supplementary Material. Further inquiries can be directed to the corresponding authors.

## Ethics statement

The animal study was reviewed and approved by University of Glasgow Animal Welfare and Ethical Review Board.

## Author contributions

JD, FL, JC, ROD, GB, JD-M, and DW performed the experiments and/or contributed to the analysis of the data for the study that MH, WH, and CS conceived. JD and FL prepared ES-62 and CJS produced the ES-62-based SMAs. MH, WH, and CS supervised the study and experimental design and contributed to data analysis. MH and WH prepared the manuscript and all authors were involved in its review and revision and have approved the final version.

## Funding

This work was funded by awards to MH, WH and CS from the BBSRC (BB/M029662/1, BB/M029727/1, BB/V001027/1 and BB/V000993/1).

## Acknowledgments

The authors would like to thank Kevin Mackenzie at the Microscopy and Histology Core Facility at the Institute of Medical Sciences, University of Aberdeen for his help in the processing and analysis of the femur microCT samples.

## Conflict of interest

The authors declare that the research was conducted in the absence of any commercial or financial relationships that could be construed as a potential conflict of interest

## Publisher's note



## Supplementary material

The Supplementary Material for this article can be found online at: https://www.frontiersin.org/articles/10.3389/fimmu.2022.953053/full#supplementary-material

# References


1. Jin C, Flavell RA. Innate sensors of pathogen and stress: linking inflammation to obesity. *J Allergy Clin Immunol* (2013) 132(2):287–94. doi: 10.1016/j.jaci.2013.06.022

2. Versini M, Aljadeff G, Jeandel PY, Shoenfeld Y. Obesity: an additional piece in the mosaic of autoimmunity. *Isr Med Assoc J* (2014) 16(10):619–21.

3. Cheng SC, Quintin J, Cramer RA, Shepardson KM, Saeed S, Kumar V, et al. mTOR- and HIF-1alpha-mediated aerobic glycolysis as metabolic basis for trained immunity. *Science* (2014) 345(6204):1250684. doi: 10.1126/science.1250684

4. O'Neill LA, Hardie DG. Metabolism of inflammation limited by AMPK and pseudo-starvation. *Nature* (2013) 493(7432):346–55. doi: 10.1038/nature11862

5. Laplante M, Sabatini DM. mTOR signaling in growth control and disease. *Cell* (2012) 149(2):274–93. doi: 10.1016/j.cell.2012.03.017

6. Cornu M, Albert V, Hall MN. mTOR in aging, metabolism, and cancer. *Curr Opin Genet Dev* (2013) 23(1):53–62. doi: 10.1016/j.gde.2012.12.005

7. Selman C, Sinclair A, Pedroni SM, Irvine EE, Michie AM, Withers DJ. Evidence that hematopoietic stem cell function is preserved during aging in long-lived S6K1 mutant mice. *Oncotarget* (2016) 7(21):29937–43. doi: 10.18632/oncotarget.8729

8. Elliott DE, Weinstock JV. Nematodes and human therapeutic trials for inflammatory disease. *Parasite Immunol* (2017) 39(5):10.1111/pim.12407. doi: 10.1111/pim.12407

9. Douglas B, Oyesola O, Cooper MM, Posey A, Tait Wojno E, Giacomin PR, et al. Immune system investigation using parasitic helminths. *Annu Rev Immunol* (2021) 39:639–65. doi: 10.1146/annurev-immunol-093019-122827

10. Harnett MM, Harnett W. Can parasitic worms cure the modern world's ills? *Trends Parasitol* (2017) 33(9):694–705. doi: 10.1016/j.pt.2017.05.007

11. Crowe J, Lumb FE, Doonan J, Broussard M, Tarafdar A, Pineda MA, et al. The parasitic worm product ES-62 promotes health- and life-span in a high calorie diet-accelerated mouse model of ageing. *PloS Pathog* (2020) 16(3):e1008391. doi: 10.1371/journal.ppat.1008391

12. Zhang C, Li S, Yang L, Huang P, Li W, Wang S, et al. Structural modulation of gut microbiota in life-long calorie-restricted mice. *Nat Commun* (2013) 4:2163. doi: 10.1038/ncomms3163

13. Clark RI, Salazar A, Yamada R, Fitz-Gibbon S, Morselli M, Alcaraz J, et al. Distinct shifts in microbiota composition during drosophila aging impair intestinal function and drive mortality. *Cell Rep* (2015) 12(10):1656–67. doi: 10.1016/j.celrep.2015.08.004

14. Doonan J, Tarafdar A, Pineda MA, Lumb FE, Crowe J, Khan AM, et al. The parasitic worm product ES-62 normalises the gut microbiota bone marrow axis in inflammatory arthritis. *Nat Commun* (2019) 10(1):1554. doi: 10.1038/s41467-019-09361-0

15. Dar HY, Azam Z, Anupam R, Mondal RK, Srivastava RK. Osteoimmunology: The nexus between bone and immune system. *Front Biosci (Landmark Ed)* (2018) 23:464–92. doi: 10.2741/4600

16. Hsu E, Pacifici R. From osteoimmunology to osteomicrobiology: How the microbiota and the immune system regulate bone. *Calcif Tissue Int* (2018) 102 (5):512–21. doi: 10.1007/s00223-017-0321-0

17. Tu Y, Yang R, Xu X, Zhou X. The microbiota-gut-bone axis and bone health. *J Leukoc Biol* (2021) 110(3):525–37. doi: 10.1002/JLB.3MR0321-755R

18. Guedj A, Volman Y, Geiger-Maor A, Bolik J, Schumacher N, Kunzel S, et al. Gut microbiota shape 'inflamm-ageing' cytokines and account for age-dependent decline in DNA damage repair. *Gut* (2020) 69(6):1064–75. doi: 10.1136/gutjnl-2019-318491

19. Bischoff SC. Microbiota and aging. *Curr Opin Clin Nutr Metab Care* (2016) 19(1):26–30. doi: 10.1097/MCO.0000000000000242

20. Soysal P, Arik F, Smith L, Jackson SE, Isik AT. Inflammation, frailty and cardiovascular disease. *Adv Exp Med Biol* (2020) 1216:55–64. doi: 10.1007/978-3-030-33330-0_7

21. Rundberg Nilsson A, Soneji S, Adolfsson S, Bryder D, Pronk CJ. Human and murine hematopoietic stem cell aging is associated with functional impairments and intrinsic Megakaryocytic/Erythroid bias. *PloS One* (2016) 11(7):e0158369. doi: 10.1016/j.exphem.2016.06.205

22. Caiado F, Pietras EM, Manz MG. Inflammation as a regulator of hematopoietic stem cell function in disease, aging, and clonal selection. *J Exp Med* (2021) 218(7):e20201541. doi: 10.1084/jem.20201541

23. Dorshkind K, Hofer T, Montecino-Rodriguez E, Pioli PD, Rodewald HR. Do haematopoietic stem cells age? *Nat Rev Immunol* (2020) 20(3):196–202. doi: 10.1038/s41577-019-0236-2

24. Pietras EM. Inflammation: a key regulator of hematopoietic stem cell fate in health and disease. *Blood* (2017) 130(15):1693–8. doi: 10.1182/blood-2017-06-780882

25. Luo Y, Chen GL, Hannemann N, Ipseiz N, Kronke G, Bauerle T, et al. Microbiota from obese mice regulate hematopoietic stem cell differentiation by altering the bone niche. *Cell Metab* (2015) 22(5):886–94. doi: 10.1016/j.cmet.2015.08.020

26. Shen J, Tsai YT, Dimarco NM, Long MA, Sun X, Tang L. Transplantation of mesenchymal stem cells from young donors delays aging in mice. *Sci Rep* (2011) 1:67. doi: 10.1038/srep00067

27. Kovina MV, Zuev VA, Kagarlitskiy GO, Khodarovich YM. Effect on lifespan of high yield non-myeloablating transplantation of bone marrow from young to old mice. *Front Genet* (2013) 4:144. doi: 10.3389/fgene.2013.00144

28. Ikehara S, Li M. Stem cell transplantation improves aging-related diseases. *Front Cell Dev Biol* (2014) 2:16. doi: 10.3389/fcell.2014.00016

29. Das MM, Godoy M, Chen S, Moser VA, Avalos P, Roxas KM, et al. Young bone marrow transplantation preserves learning and memory in old mice. *Commun Biol* (2019) 2:73. doi: 10.1038/s42003-019-0298-5

30. Lumb FE, Crowe J, Doonan J, Suckling CJ, Selman C, Harnett MM, et al. Synthetic small molecule analogues of the immunomodulatory acanthocheilonema viteae product ES-62 promote metabolic homeostasis during obesity in a mouse model. *Mol Biochem Parasitol* (2019) 234:111232. doi: 10.1016/j.molbiopara.2019.111232

31. McInnes IB, Leung BP, Harnett M, Gracie JA, Liew FY, Harnett W. A novel therapeutic approach targeting articular inflammation using the filarial nematode-derived phosphorylcholine-containing glycoprotein ES-62. *J Immunol* (2003) 171 (4):2127–33. doi: 10.4049/jimmunol.171.4.2127

32. Al-Riyami L, Pineda MA, Rzepecka J, Huggan JK, Khalaf AI, Suckling CJ, et al. Designing anti-inflammatory drugs from parasitic worms: a synthetic small molecule analogue of the acanthocheilonema viteae product ES-62 prevents development of collagen-induced arthritis. *J Med Chem* (2013) 56(24):9982–10002. doi: 10.1021/jm401251p

33. Doonan J, Lumb D, Pineda MA, Tarafdar A, Crow J, Khan AM, et al. Protection against arthritis by the parasitic worm project ES-62, and its drug-like small molecule analogues, is associated with inhibition of osteoclastogenesis. *Front Immunol* (2018) 9:1016. doi: 10.3389/fimmu.2018.01016

34. Hayer S, Vervoordeldonk MJ, Denis MC, Armaka M, Hoffmann M, Backlund J, et al. 'SMASH' recommendations for standardised microscopic arthritis scoring of histological sections from inflammatory arthritis animal models. *Ann Rheum Dis* (2021) 80(6):714–26. doi: 10.1136/annrheumdis-2020-219247

35. Khalid AB, Goodyear SR, Ross RA, Aspden RM. Mechanical and material properties of cortical and trabecular bone from cannabinoid receptor-1-null (Cnr1 (-/-)) mice. *Med Eng Phys* (2016) 38(10):1044–54. doi: 10.1016/j.medengphy.2016.06.024

36. Selman C, Lingard S, Choudhury AI, Batterham RL, Claret M, Clements M, et al. Evidence for lifespan extension and delayed age-related biomarkers in insulin receptor substrate 1 null mice. *FASEB J* (2008) 22(3):807–18. doi: 10.1096/fj.07-9261com

37. Selman C, Tullet JM, Wieser D, Irvine E, Lingard SJ, Choudhury AI, et al. Ribosomal protein S6 kinase 1 signaling regulates mammalian life span. *Science* (2009) 326(5949):140–4. doi: 10.1126/science.1177221

38. Guder C, Gravius S, Burger C, Wirtz DC, Schildberg FA. Osteoimmunology: A current update of the interplay between bone and the immune system. *Front Immunol* (2020) 11:58. doi: 10.3389/fimmu.2020.00058

39. Ponzetti M, Rucci N. Updates on osteoimmunology: What's new on the cross-talk between bone and immune system. *Front Endocrinol (Lausanne)* (2019) 10:236. doi: 10.3389/fendo.2019.00236

40. Faienza MF, D'Amato G, Chiarito M, Colaianni G, Colucci S, Grano M, et al. Mechanisms involved in childhood obesity-related bone fragility. *Front Endocrinol (Lausanne)* (2019) 10:269. doi: 10.3389/fendo.2019.00269

41. Glatt V, Canalis E, Stadmeyer L, Bouxsein ML. Age-related changes in trabecular architecture differ in female and male C57BL/6J mice. *J Bone Miner Res* (2007) 22(8):1197–207. doi: 10.1359/jbmr.070507

42. Farkasdi S, Pammer D, Racz R, Hriczo-Koperdak G, Szabo BT, Dobo-Nagy C, et al. Development of a quantitative preclinical screening model for implant osseointegration in rat tail vertebra. *Clin Oral Investig* (2019) 23(7):2959–73. doi: 10.1007/s00784-018-2661-1

43. Brunet-Imbault B, Lemineur G, Chappard C, Harba R, Benhamou CL. A new anisotropy index on trabecular bone radiographic images using the fast Fourier transform. *BMC Med Imaging* (2005) 5:4. doi: 10.1186/1471-2342-5-4

44. Cesar R, Boffa RS, Fachine LT, Leivas TP, Silva AMH, Pereira CAM, et al. Evaluation of trabecular microarchitecture of normal osteoporotic and osteopenic human vertebrae. *Proc Eng* (2013) 59:6–15. doi: 10.1016/j.proeng.2013.05.087

45. Benova A, Tencerova M. Obesity-induced changes in bone marrow homeostasis. *Front Endocrinol (Lausanne)* (2020) 11:294. doi: 10.3389/fendo.2020.00294

46. Li X, Zeng X, Xu Y, Wang B, Zhao Y, Lai X, et al. Mechanisms and rejuvenation strategies for aged hematopoietic stem cells. *J Hematol Oncol* (2020) 13(1):31. doi: 10.1186/s13045-020-00864-8

47. Dykstra B, de Haan G. Hematopoietic stem cell aging and self-renewal. *Cell Tissue Res* (2008) 331(1):91–101. doi: 10.1007/s00441-007-0529-9

48. Zehentmeier S, Pereira JP. Cell circuits and niches controlling b cell development. *Immunol Rev* (2019) 289(1):142–57. doi: 10.1111/imr.12749

49. Ho YH, Mendez-Ferrer S. Microenvironmental contributions to hematopoietic stem cell aging. *Haematologica* (2020) 105(1):38–46. doi: 10.3324/haematol.2018.211334

50. Yang D, de Haan G. Inflammation and aging of hematopoietic stem cells in their niche. *Cells* (2021) 10(8):1849. doi: 10.3390/cells10081849

51. Rosales C. Neutrophil: A cell with many roles in inflammation or several cell types? *Front Physiol* (2018) 9:113. doi: 10.3389/fphys.2018.00113

52. Ortmann W, Kolaczkowska E. Age is the work of art? impact of neutrophil and organism age on neutrophil extracellular trap formation. *Cell Tissue Res* (2018) 371(3):473–88. doi: 10.1007/s00441-017-2751-4

53. Valet C, Batut A, Vauclard A, Dortignac A, Bellio M, Payrastre B, et al. Adipocyte fatty acid transfer supports megakaryocyte maturation. *Cell Rep* (2020) 32(1):107875. doi: 10.1016/j.celrep.2020.107875

54. Suckling CJ, Alam S, Olson MA, Saikh KU, Harnett MM, Harnett W. Small molecule analogues of the parasitic worm product ES-62 interact with the TIR domain of MyD88 to inhibit pro-inflammatory signalling. *Sci Rep* (2018) 8(1):2123. doi: 10.1038/s41598-018-20388-z

55. Gubbels Bupp MR, Potluri T, Fink AL, Klein SL. The confluence of sex hormones and aging on immunity. *Front Immunol* (2018) 9:1269. doi: 10.3389/fimmu.2018.01269

56. Fischer KE, Hoffman JM, Sloane LB, Gelfond JA, Soto VY, Richardson AG, et al. A cross-sectional study of male and female C57BL/6Nia mice suggests lifespan and healthspan are not necessarily correlated. *Aging (Albany NY)* (2016) 8 (10):2370–91. doi: 10.18632/aging.101059

57. Yanai S, Endo S. Functional aging in Male C57BL/6J mice across the life-span: A systematic behavioral analysis of motor, emotional, and memory function to define an aging phenotype. *Front Aging Neurosci* (2021) 13:697621. doi: 10.3389/fnagi.2021.697621

58. Fahlstrom A, Zeberg H, Ulfhake B. Changes in behaviors of male C57BL/6J mice across adult life span and effects of dietary restriction. *Age (Dordr)* (2012) 34 (6):1435–52. doi: 10.1007/s11357-011-9320-7

59. Tavoian D, Lozier NR, de Lacalle S. Age of peak performance differs by functional task in mice tracked over 2 years. *J Gerontol A Biol Sci Med Sci* (2021) 76 (7):1179–83. doi: 10.1093/gerona/glab048

60. Schultz MB, Kane AE, Mitchell SJ, MacArthur MR, Warner E, Vogel DS, et al. Age and life expectancy clocks based on machine learning analysis of mouse frailty. *Nat Commun* (2020) 11(1):4618. doi: 10.1038/s41467-020-18446-0

61. Lazare S, Ausema A, Reijne AC, van Dijk G, van Os R, de Haan G. Lifelong dietary intervention does not affect hematopoietic stem cell function. *Exp Hematol* (2017) 53:26–30. doi: 10.1016/j.exphem.2017.06.002

62. Dykstra B, Olthof S, Schreuder J, Ritsema M, de Haan G. Clonal analysis reveals multiple functional defects of aged murine hematopoietic stem cells. *J Exp Med* (2011) 208(13):2691–703. doi: 10.1084/jem.20111490

63. Ho TT, Dellorusso PV, Verovskaya EV, Bakker ST, Flach J, Smith LK, et al. Aged hematopoietic stem cells are refractory to bloodborne systemic rejuvenation interventions. *J Exp Med* (2021) 218(7):e20210223. doi: 10.1084/jem.20210223

64. Tang D, Tao S, Chen Z, Koliesnik IO, Calmes PG, Hoerr V, et al. Dietary restriction improves repopulation but impairs lymphoid differentiation capacity of hematopoietic stem cells in early aging. *J Exp Med* (2016) 213(4):535–53. doi: 10.1084/jem.20151100

65. Corbet M, Pineda MA, Yang K, Tarafdar A, McGrath S, Nakagawa R, et al. Suppression of inflammatory arthritis by the parasitic worm product ES-62 is associated with epigenetic changes in synovial fibroblasts. *PloS Pathog* (2021) 17 (11):e1010069. doi: 10.1371/journal.ppat.1010069

66. Liu A, Chen M, Kumar R, Stefanovic-Racic M, O'Doherty RM, Ding Y, et al. Bone marrow lympho-myeloid malfunction in obesity requires precursor cell-autonomous TLR4. *Nat Commun* (2018) 9(1):708. doi: 10.1038/s41467-018-03145-8

67. Massberg S, Schaerli P, Knezevic-Maramica I, Kollnberger M, Tubo N, Moseman EA, et al. Immunosurveillance by hematopoietic progenitor cells trafficking through blood, lymph, and peripheral tissues. *Cell* (2007) 131(5):994–1008. doi: 10.1016/j.cell.2007.09.047

68. Luche E, Robert V, Cuminetti V, Pomie C, Sastourne-Arrey Q, Waget A, et al. Corrupted adipose tissue endogenous myelopoiesis initiates diet-induced metabolic disease. *Elife* (2017) 6:e23194. doi: 10.7554/eLife.23194

69. Li Q, Wu Y, Kang N. Marrow adipose tissue: Its origin, function, and regulation in bone remodeling and regeneration. *Stem Cells Int* (2018) 2018:7098456. doi: 10.1155/2018/7098456

70. Li Z, Hardij J, Bagchi DP, Scheller EL, MacDougald OA. Development, regulation, metabolism and function of bone marrow adipose tissues. *Bone* (2018) 110:134–40. doi: 10.1016/j.bone.2018.01.008

71. Lu L, Tang M, Li J, Xie Y, Li Y, Xie J, et al. Gut microbiota and serum metabolic signatures of high-Fat-Induced bone loss in mice. *Front Cell Infect Microbiol* (2021) 11:788576. doi: 10.3389/fcimb.2021.788576

72. Griffin C, Eter L, Lanzetta N, Abrishami S, Varghese M, McKernan K, et al. TLR4, TRIF, and MyD88 are essential for myelopoiesis and CD11c(+) adipose tissue macrophage production in obese mice. *J Biol Chem* (2018) 293(23):8775–86. doi: 10.1074/jbc.RA117.001526

73. Waterman RS, Tomchuck SL, Henkle SL, Betancourt AM. A new mesenchymal stem cell (MSC) paradigm: polarization into a pro-inflammatory MSC1 or an immunosuppressive MSC2 phenotype. *PloS One* (2010) 5(4):e10088. doi: 10.1371/journal.pone.0010088

74. Kota DJ, DiCarlo B, Hetz RA, Smith P, Cox CSJr., Olson SD. Differential MSC activation leads to distinct mononuclear leukocyte binding mechanisms. *Sci Rep* (2014) 4:4565. doi: 10.1038/srep04565

75. Mastri M, Shah Z, McLaughlin T, Greene CJ, Baum L, Suzuki G, et al. Activation of toll-like receptor 3 amplifies mesenchymal stem cell trophic factors and enhances therapeutic potency. *Am J Physiol Cell Physiol* (2012) 303(10): C1021–33. doi: 10.1152/ajpcell.00191.2012

76. Ankrum JA, Ong JF, Karp JM. Mesenchymal stem cells: immune evasive, not immune privileged. *Nat Biotechnol* (2014) 32(3):252–60. doi: 10.1038/nbt.2816

77. Ndumele CE, Matsushita K, Lazo M, Bello N, Blumenthal RS, Gerstenblith G, et al. Obesity and subtypes of incident cardiovascular disease. *J Am Heart Assoc* (2016) 5(8):e003921. doi: 10.1161/JAHA.116.003921

78. Yanagibashi T, Nagai Y, Watanabe Y, Ikutani M, Hirai Y, Takatsu K. Differential requirements of MyD88 and TRIF pathways in TLR4-mediated immune responses in murine b cells. *Immunol Lett* (2015) 163(1):22–31. doi: 10.1016/j.imlet.2014.11.012

79. Houston KM, Wilson EH, Eyres L, Brombacher F, Harnett MM, Alexander J, et al. Presence of phosphorylcholine on a filarial nematode protein influences immunoglobulin G subclass response to the molecule by an interleukin-10-dependent mechanism. *Infect Immun* (2000) 68(9):5466–8. doi: 10.1128/IAI.68.9.5466-5468.2000

80. Teichmann LL, Schenten D, Medzhitov R, Kashgarian M, Shlomchik MJ. Signals *via* the adaptor MyD88 in b cells and DCs make distinct and synergistic contributions to immune activation and tissue damage in lupus. *Immunity* (2013) 38(3):528–40. doi: 10.1016/j.immuni.2012.11.017

81. Lamagna C, Hu Y, DeFranco AL, Lowell CA. B cell-specific loss of Lyn kinase leads to autoimmunity. *J Immunol* (2014) 192(3):919–28. doi: 10.4049/jimmunol.1301979

82. Hua Z, Gross AJ, Lamagna C, Ramos-Hernandez N, Scapini P, Ji M, et al. Requirement for MyD88 signaling in b cells and dendritic cells for germinal center anti-nuclear antibody production in Lyn-deficient mice. *J Immunol* (2014) 192 (3):875–85. doi: 10.4049/jimmunol.1300683

83. Rodgers DT, McGrath MA, Pineda MA, Al-Riyami L, Rzepecka J, Lumb F, et al. The parasitic worm product ES-62 targets myeloid differentiation factor 88-dependent effector mechanisms to suppress antinuclear antibody production and proteinuria in MRL/lpr mice. *Arthritis Rheumatol* (2015) 67(4):1023–35. doi: 10.1002/art.39004

84. Coltherd JC, Rodgers DT, Lawrie RE, Al-Riyami L, Suckling CJ, Harnett W, et al. The parasitic worm-derived immunomodulator, ES-62 and its drug-like small molecule analogues exhibit therapeutic potential in a model of chronic asthma. *Sci Rep* (2016) 6:19224. doi: 10.1038/srep19224

85. Li M, Wang H, Ni Y, Li C, Xu X, Chang H, et al. Helminth-induced CD9(+) b-cell subset alleviates obesity-associated inflammation *via* IL-10 production. *Int J Parasitol* (2022) 52(2-3):111–23. doi: 10.1016/j.ijpara.2021.08.009

86. Webster SE, Ryali B, Clemente MJ, LT N, Holodick NE. Sex influences age-related changes in natural antibodies and CD5(+) b-1 cells. *J Immunol* (2022) 208 (7):1755–71. doi: 10.4049/jimmunol.2101150

87. Lobo PI, Schlegel KH, Bajwa A, Huang L, Okusa MD. Natural IgM and TLR agonists switch murine splenic pan-b to "Regulatory" cells that suppress ischemia-induced innate inflammation *via* regulating NKT-1 cells. *Front Immunol* (2017) 8:974. doi: 10.3389/fimmu.2017.00974

88. Slobodkin MR, Elazar Z. The Atg8 family: multifunctional ubiquitin-like key regulators of autophagy. *Essays Biochem* (2013) 55:51–64. doi: 10.1042/bse0550051

89. Oleinika K, Rosser EC, Matei DE, Nistala K, Bosma A, Drozdov I, et al. CD1d-dependent immune suppression mediated by regulatory b cells through modulations of iNKT cells. *Nat Commun* (2018) 9(1):684. doi: 10.1038/s41467-018-02911-y

90. Oleinika K, Mauri C, Salama AD. Effector and regulatory b cells in immune-mediated kidney disease. *Nat Rev Nephrol* (2019) 15(1):11–26. doi: 10.1038/s41581-018-0074-7

91. Furze RC, Rankin SM. Neutrophil mobilization and clearance in the bone marrow. *Immunology* (2008) 125(3):281–8. doi: 10.1111/j.1365-2567.2008.02950.x

92. Nauseef WM, Borregaard N. Neutrophils at work. *Nat Immunol* (2014) 15 (7):602–11. doi: 10.1038/ni.2921

93. Ambrosi TH, Schulz TJ. The emerging role of bone marrow adipose tissue in bone health and dysfunction. *J Mol Med (Berl)* (2017) 95(12):1291–301. doi: 10.1007/s00109-017-1604-7

94. Ambrosi TH, Scialdone A, Graja A, Gohlke S, Jank AM, Bocian C, et al. Adipocyte accumulation in the bone marrow during obesity and aging impairs stem cell-based hematopoietic and bone regeneration. *Cell Stem Cell* (2017) 20 (6):771–84.e6. doi: 10.1016/j.stem.2017.02.009

95. Muruganandan S, Govindarajan R, Sinal CJ. Bone marrow adipose tissue and skeletal health. *Curr Osteoporos Rep* (2018) 16(4):434–42. doi: 10.1007/s11914-018-0451-y

96. Suchacki KJ, Tavares AAS, Mattiucci D, Scheller EL, Papanastasiou G, Gray C, et al. Bone marrow adipose tissue is a unique adipose subtype with distinct roles in glucose homeostasis. *Nat Commun* (2020) 11(1):3097. doi: 10.1038/s41467-020-16878-2

97. Turner RT, Martin SA, Iwaniec UT. Metabolic coupling between bone marrow adipose tissue and hematopoiesis. *Curr Osteoporos Rep* (2018) 16(2):95–104. doi: 10.1007/s11914-018-0422-3

98. Zhang X, Robles H, Magee KL, Lorenz MR, Wang Z, Harris CA, et al. A bone-specific adipogenesis pathway in fat-free mice defines key origins and adaptations of bone marrow adipocytes with age and disease. *Elife* (2021) 10: e66275. doi: 10.7554/elife66275

99. Turner RT, Kalra SP, Wong CP, Philbrick KA, Lindenmaier LB, Boghossian S, et al. Peripheral leptin regulates bone formation. *J Bone Miner Res* (2013) 28 (1):22–34. doi: 10.1002/jbmr.1734

100. Karsenty G, Khosla S. The crosstalk between bone remodeling and energy metabolism: A translational perspective. *Cell Metab* (2022) 34(6):805–17. doi: 10.1016/j.cmet.2022.04.010

101. Lewis JW, Edwards JR, Naylor AJ, McGettrick HM. Adiponectin signalling in bone homeostasis, with age and in disease. *Bone Res* (2021) 9(1):1. doi: 10.1038/s41413-020-00122-0

102. Yue R, Zhou BO, Shimada IS, Zhao Z, Morrison SJ. Leptin receptor promotes adipogenesis and reduces osteogenesis by regulating mesenchymal stromal cells in adult bone marrow. *Cell Stem Cell* (2016) 18(6):782–96. doi: 10.1016/j.stem.2016.02.015

103. Malhan D, Muelke M, Rosch S, Schaefer AB, Merboth F, Weisweiler D, et al. An optimized approach to perform bone histomorphometry. *Front Endocrinol (Lausanne)* (2018) 9:666. doi: 10.3389/fendo.2018.00666

104. Mentzel J, Kynast T, Kohlmann J, Kirsten H, Bluher M, Simon JC, et al. Reduced serum levels of bone formation marker P1NP in psoriasis. *Front Med (Lausanne)* (2021) 8:730164. doi: 10.3389/fmed.2021.730164

frontiers | Frontiers in Immunology

TYPE Original Research
PUBLISHED 15 March 2023
DOI 10.3389/fimmu.2023.1146702



OPEN ACCESS

EDITED BY
Ann Chahroudi,
Emory University, United States

REVIEWED BY
Stephen Crooke,
Centers for Disease Control and Prevention (CDC), United States
Rebecca M. Lynch,
George Washington University, United States
Anne Piantadosi,
Emory University, United States

*CORRESPONDENCE
Georgios Pollakis
pollakis@liverpool.ac.uk

†These authors have contributed equally to this work

SPECIALTY SECTION
This article was submitted to Viral Immunology, a section of the journal Frontiers in Immunology

RECEIVED 17 January 2023
ACCEPTED 27 February 2023
PUBLISHED 15 March 2023

CITATION
Parker E, Thomas J, Roper KJ, Ijaz S, Edwards T, Marchesin F, Katsanovskaja K, Lett L, Jones C, Hardwick HE, Davis C, Vink E, McDonald SE, Moore SC, Dicks S, Jegatheesan K, Cook NJ, Hope J, Cherepanov P, McClure MO, Baillie JK, Openshaw PJM, Turtle L, Ho A, Semple MG, Paxton WA, Tedder RS, Pollakis G and ISARIC4C Investigators (2023) SARS-CoV-2 antibody responses associate with sex, age and disease severity in previously uninfected people admitted to hospital with COVID-19: An ISARIC4C prospective study.
*Front. Immunol.* 14:1146702.
doi: 10.3389/fimmu.2023.1146702

# SARS-CoV-2 antibody responses associate with sex, age and disease severity in previously uninfected people admitted to hospital with COVID-19: An ISARIC4C prospective study

Eleanor Parker[1†], Jordan Thomas[2†], Kelly J. Roper[2†], Samreen Ijaz[3†], Tansy Edwards[4†], Federica Marchesin[1], Ksenia Katsanovskaja[1], Lauren Lett[2], Christopher Jones[2], Hayley E. Hardwick[2], Chris Davis[5], Elen Vink[5], Sarah E. McDonald[5], Shona C. Moore[2], Steve Dicks[3,6], Keerthana Jegatheesan[3,6], Nicola J. Cook[7], Joshua Hope[7], Peter Cherepanov[7], Myra O. McClure[1], J. Kenneth Baillie[8], Peter J. M. Openshaw[9], Lance Turtle[2], Antonia Ho[5], Malcolm G. Semple[2†], William A. Paxton[2†], Richard S. Tedder[1†], Georgios Pollakis[2*†] and ISARIC4C Investigators

[1]Department of Infectious Disease, Imperial College London, London, United Kingdom, [2]National Institute of Health and Care Research (NIHR) Health Protection Research Unit in Emerging and Zoonotic Infections, Department of Clinical Infection, Microbiology and Immunology, Institute of Infection, Veterinary and Ecological Sciences, University of Liverpool, Liverpool, United Kingdom, [3]Blood Borne Virus Unit, Reference Department, UK Health Security Agency, London, United Kingdom, [4]Medical Research Council (MRC) International Statistics and Epidemiology Group, London School of Hygiene and Tropical Medicine, London, United Kingdom, [5]Medical Research Council, University of Glasgow Centre for Virus Research, Glasgow, United Kingdom, [6]National Health Service (NHS) Blood and Transplant, London, United Kingdom, [7]Chromatin Structure and Mobile DNA Laboratory, The Francis Crick Institute, London, United Kingdom, [8]Roslin Institute, University of Edinburgh, Edinburgh, United Kingdom, [9]National Heart & Lung Institute, Imperial College, London, United Kingdom

The SARS-CoV-2 pandemic enables the analysis of immune responses induced against a novel coronavirus infecting immunologically naïve individuals. This provides an opportunity for analysis of immune responses and associations with age, sex and disease severity. Here we measured an array of solid-phase binding antibody and viral neutralising Ab (nAb) responses in participants (n=337) of the ISARIC4C cohort and characterised their correlation with peak disease severity during acute infection and early convalescence. Overall, the responses in a Double Antigen Binding Assay (DABA) for antibody to the receptor binding domain (anti-RBD) correlated well with IgM as well as IgG responses against viral spike, S1 and nucleocapsid protein (NP) antigens. DABA reactivity also correlated with nAb. As we and others reported previously, there is greater risk of severe disease and death in older men, whilst the sex ratio was found to be equal within each severity grouping in younger people. In older males with

severe disease (mean age 68 years), peak antibody levels were found to be delayed by one to two weeks compared with women, and nAb responses were delayed further. Additionally, we demonstrated that solid-phase binding antibody responses reached higher levels in males as measured *via* DABA and IgM binding against Spike, NP and S1 antigens. In contrast, this was not observed for nAb responses. When measuring SARS-CoV-2 RNA transcripts (as a surrogate for viral shedding) in nasal swabs at recruitment, we saw no significant differences by sex or disease severity status. However, we have shown higher antibody levels associated with low nasal viral RNA indicating a role of antibody responses in controlling viral replication and shedding in the upper airway. In this study, we have shown discernible differences in the humoral immune responses between males and females and these differences associate with age as well as with resultant disease severity.

KEYWORDS

SARS-CoV-2, immunology, COVID-19, virus, disease, serology, neutralisation

# 1 Introduction

Individual risk of COVID-19 severity is heterogenous and determined by several factors including the host's clinical characteristics and genetics (1–4). The most important predictors of severe disease are advanced age and male sex followed by the presence of co-morbidities including cardiac disease, metabolic disorders such as obesity and diabetes, hypertension and respiratory diseases (2, 5–11). Further, recent studies have identified several genetic correlates of disease severity (4, 12–14).

Disease outcome may also be determined by the timing and magnitude of humoral immune responses (15–19). Generally, antibody responses to acute infection in SARS-CoV-2-naïve individuals are rapid; the majority of patients seroconvert for virus-specific IgM and then IgG between 10-19 days post-symptom onset (20–22). The primary viral targets of humoral responses to SARS-CoV-2 are the Spike (S) glycoprotein (including the RBD domain) and the nucleocapsid (N) protein (23). The majority of virus neutralisation activity is provided by antibodies directed against the receptor binding domain (RBD) of the spike protein S1 sub-unit, which blocks the interaction between S and ACE2 (24–27). Mild cases of COVID-19 have previously been associated with higher ratios of antibodies directed against RBD as opposed to N, as well as rapid reduction of respiratory tract viral RNA concomitant with rises in anti-RBD IgG (16, 24). Faster production of both total and RBD-specific IgG has been observed in female patients (28, 29), and early upregulation of specific IgM responses (24, 30) and neutralising RBD specific responses (31) have been associated with improved disease outcome. In response to vaccination, elderly patients generate weaker humoral responses, characterised by slower induction of antibody production, lower magnitude Ab titres at peak and quicker Ab decline, when compared to younger adults (32–35). Whilst several reports have shown that elderly patients are able to generate robust and neutralising antibody responses during acute infection (7, 36, 37), there is less evidence of early antibody kinetics impacting on disease outcome in elderly patients.

Using serum samples from patients hospitalised during the first wave of the COVID-19 pandemic in the United Kingdom (UK), we have performed an extensive analysis of the serological responses generated to SARS-CoV-2 in an immune-naïve population. Anti-RBD reactivity, neutralising function and class specific antibodies to S and N proteins were measured using a hybrid double antigen binding assay (DABA) (38), a pseudo-virus particle (PVP) neutralisation assay and Ig capture assays respectively. This portfolio of assay formats was used previously in the characterisation of the antibody response kinetics in Ebola virus survivors following the Sierra Leone outbreak of 2014-2016 (38, 39). By comparing serological responses in hospitalised patients of different age groups and sexes in the context of the early UK outbreak when the virus population was relatively homogenous, we have been able to identify host characteristics that contribute to the risk of severe disease. Additionally, repeat sampling starting from early in hospital admission through to convalescence has provided greater insights into the influence of sex and age on early antibody kinetics, and their association with outcome.

# 2 Materials and methods

## 2.1 Study cohort patients and samples

This analysis included sera from 337 patients admitted to UK hospitals with COVID-19 between February and June 2020 before vaccines were made available and therefore describing a new infection in a naïve human population. The patients were enrolled in the International Severe Acute Respiratory and emerging Infections Consortium (ISARIC) World Health

Organization (WHO) Clinical Characterisation Protocol UK (CCP-UK) study. Study participants were confirmed SARS-CoV-2 positive by reverse transcription polymerase chain (PCR) reaction or were highly suspected cases based on clinical presentation and providing a serological response in one or more of the described assays being recorded. Acute infection samples were collected within 21 days of the onset of symptoms and convalescent samples were collected when SARS-CoV-2 PCR showed undetectable viral burden. A number of patients underwent serial sampling (2/n=129, 3/n=91, 4/n=12, 5/n=1), with not all follow up specimens tested in every assay implemented. Samples with repeated measures were included in a mixed effect regression model to analyse the antibody responses over time (section 3.5).

Patients were stratified into five categories of peak illness severity based on the World Health Organization (WHO) COVID-19 ordinal scale (40): 1) no oxygen requirement (WHO score 3); 2) patient requiring oxygen by face mask or nasal prongs (WHO score 4); 3) patient requiring high-flow nasal oxygen (HFNO) or non-invasive ventilation (NIV) (WHO score 5); 4) patients requiring mechanical ventilation (WHO score 6/7) and 5) patients who died within 28 days. (WHO score 8).

## 2.2 Anti-SARS-CoV-2 S1, spike and NP IgM and IgG capture ELISAs

Three viral antigens all based on the hCoV-19/Australia/VIC01/202 (Accession MT007544) lineage were tested. The SARS-CoV-2 full length spike glycoprotein (Spike/amino acids 1–1211; His-tag) and the nucleoprotein (NP) conjugated to Horseradish peroxidase (HRP) were purchased from The Native Antigen Company (Kidlington, Oxford, UK). The SARS-CoV-2 S1 antigen (spanning Wuhan-Hu-1 SARS-CoV-2 Spike residues 1–530, C-terminal twin Strep tag) (41, 42) was produced and gifted by The Francis Crick Institute and conjugated to HRP using the Bio-Rad LYNX HRP conjugation kit, in accordance with the manufacturer's instructions. Recombinant NP antigens from seasonal coronavirus NL63, OC43, HKU1 and 229E were used to block non-specific NP responses as previously described (43). These proteins were produced in *Escherichia coli* with N-terminal hexahistidine-SUMO and C-terminal Twin Strep tags and purified by tandem immobilised metal and StrepTactin® affinity chromatography. The IgM and IgG capture ELISAs for the detection of antibody to S1, Spike and NP were undertaken as described previously (43).

## 2.3 SARS-CoV-2 RNA quantitative reverse transcriptase polymerase chain reaction

SARS-CoV-2 RNA was quantified using a NEB Luna Universal Probe One-Step RT-qPCR Kit (New England Biolabs, E3006) and 2019-nCoV CDC N1 primers and probes (IDT, 10006713)). Genome copy numbers were quantified using a standard curve generated from serial dilutions of a plasmid containing the target N protein gene fragment. The standard was quantified and quality controlled using QX600 droplet digital PCR system (Bio-rad, UK).

## 2.4 Anti-RBD hybrid DABA immunoassay

Antibodies targeting SARS-CoV-2 were measured using a hybrid double antigen bridging assay (DABA) that was previously developed to detect Ebola virus (EBOV) glycoprotein targeting antibodies (38) and recently adapted and validated to detect SARS-CoV-2 directed antibodies, using the same methodology for performance and analysis as described previously (44). Briefly, an S1 antigen coated onto a solid phase was used to bind all reactive immunoglobulins present in a sample, after a which an HRP conjugated RBD antigen was added to detect antibody binding which was expressed as arbitrary units (AU)/ml (44). Owing to the use of an antigen as the detector, the DABA detects all classes of antibody that target a specific antigen, unlike methods which discriminate between IgM or IgG.

## 2.5 Generation of SARS-CoV-2 pseudovirus particle, infectivity and neutralisation assay

### 2.5.1 Cell culture

HEK293T (ATCC® CRL-3216™) cells were cultivated in Dulbecco's modified eagle medium (Invitrogen) and supplemented with 10% heat-treated FCS (Sigma), 2mM/ml L-glutamine (Invitrogen), 100 U/ml penicillin (Invitrogen) and 100 mg/ml streptomycin (Invitrogen), termed complete DMEM (Thermofisher). HEK293T/ACE-2 cells were used to monitor PVP infectivity and in performing serum neutralisation assays. All cells were cultured at 37°C and at 5% $CO_2$.

### 2.5.2 SARS-CoV-2 PVP production and infection

The ancestral SARS-CoV-2 S glycoprotein (Accession MN908947) was cloned into the pCDNA3.1 expression plasmid (produced by GeneArt Gene Synthesis) and was used in generating PVP stocks *via* a lentiviral system to generate single-cycle infectious viral particles as previously described (45, 46). HEK293T cells ($5.0x10^5$ in each well of a 6-well tissue culture flask) (Corning) were grown in 2.0 ml of complete DMEM overnight. Cells were transfected with 750 ng of the lentiviral luciferase reporter construct, pCSFLW, along with 450 ng of the SARS-CoV-2 S expression plasmid and 500 ng of the lentiviral backbone, p8.91, using cationic polymer transfection reagent (Polyethylenimine) (Polysciences) and in the presence of OptiMEM (Invitrogen). OptiMEM/plasmid mix was removed 16 h post transfection and 2.0 ml complete DMEM added with the single-cycle infectious SARS-CoV-2 stock harvested 48 h later, passed through a 0.45μM filter, aliquoted and stored at −80°C. PVP infection was monitored on HEK293T/ACE-2 cells through measuring luciferase activity (expressed from the HIV-1 LTR promoter) under control of Tat expression from the HIV-1 backbone. 100 μl of virus stock was used to infect $1.5x10^4$ cells/well for 6 h in a white 96 well plate (Corning). Following infection 100 μl DMEM complete medium was added to each well. 48 h post infection, media was discarded from the wells and the cells washed with PBS (Thermofisher), lysed with 30 μl cell lysis buffer (Promega) and luciferase activity determined utilising

the commercially available luciferase assay (Promega) and measured using a BMGLabtech FluoroStar Omega luminometer.

### 2.5.3 SARS-CoV-2 S PVP neutralisation assay

SARS-CoV-2 enveloped PVP was thawed and pooled and subsequently diluted 1/20 in complete DMEM. Serum samples from SARS-CoV-2 individuals were serially diluted 2-fold with complete DMEM; 28 µl serum dilution was incubated with 420 µl diluted SARS-CoV-2 PVP for 30 min at RT. 200 µl of virus/serum dilution mix was used to infect HEK293T/ACE-2 cells. Luciferase activity readings of neutralised virus were analysed i) by considering 0% inhibition as the infection values of the virus in the absence of convalescent plasma included in each experiment, ii) by considering 0% inhibition as the infection values of two consecutive high dilutions not inhibiting virus entry. The neutralisation activity defined as the serum dilution that reduced viral infectivity by 50%, 70% or 90% ($IC_{50}$, $IC_{70}$ or $IC_{90}$, respectively).

## 2.6 Statistical analyses

Statistical analyses were performed using GraphPad Prism 6.0 software. Unpaired sample comparisons were conducted for all data; however, individual figures state the corresponding statistical test performed. These include parametric and non-parametric t-tests (student t-test and Mann-Whitney U test) and non-parametric ANOVA (Kruskal-Wallis test). Significant P values < 0.05 were depicted by * or a horizontal line above the groups compared. Repeated measures linear regression was used to model antibody levels over time, including a random intercept term to account for within-individual correlation, age and a time-sex interaction to predict trajectories for males and females separately, adjusted for age.

# 3 Results

## 3.1 Patient demographics

We analysed the patient demograhics of individuals within our cohort, specifically age and sex, to determine the risk of severe disease across these groups. A higher proportion of the 337 study participants were male (63.0%, n=210). Median age was 57 years (range: 15–94) with no age difference observed between sexes (male median age = 57.3 years/range: 19–90 and female median age = 57.7 years/range: 15–94). As this was a hospital study, no asymptomatic individuals were enrolled. Participants were grouped into categories S1-S5 according to disease severity (Supplementary Figure 1) (40). The ratio of males to females increased within the higher disease severity groupings, from 47% of participants in S1, to 66% of participants in S4, and with only three females (8.1%) in S5 (individuals that died within 28 days of disease onset) (Figure 1A). There were no age differences between sexes within severity groupings, and the age range narrowed as disease severity increased (Figure 1A). The average participant age across severity groups was similar with S5 being an exception, where participants tended to be older.

We next anlysed the time between the onset of symptoms and hospital presentation to compare the rate of deteriation across different patient groupings. No difference was found between males and females in the time between symptom onset and hospital presentation (Figure 1B). When the cohort was stratified by 10 yearly age categories, participants between 50 and 70 years old were recruited later than participants <50 years or >70 years (Figure 1C), reflecting a delay from disease onset to when participants presented at the hospital. In this cohort we found that overall, males developed more severe disease than females (Figure 1D), which was shown in all age categories above 50 years (Figure 1E).

## 3.2 Antibody responses by gender and age

When measuring anti-RBD using the hybrid DABA (an antibody class neutral assay) high antibody levels were measured within one week following onset of symptoms and were maintained at high levels for 3 to 4 weeks (Figure 2A). Anti-RBD titres reached a peak around day 21 following symptom onset for both males and females, and peak antibody levels were higher in males. Neutralising antibodies (nAb) ($IC_{50}$, $IC_{70}$ or $IC_{90}$), measured using the PVP neutralisation assay, revealed a similar serological profile to anti-RBD with a sharp initial increase reaching the peak at around day 26 post symptom onset (Figure 2B). When comparing anti-RBD with nAb responses ($IC_{70}$) a correlation was observed during the first 21-day period ($P<0.0001$, $r_p=0.6476$). This correlation remained but was lower in magnitude after 21 days following disease onset ($P<0.0001$, $r_p=0.3666$) (Figure 2C).

At recruitment to the study, corresponding to the time that a participant was hospitalized, no significant differences were identified between males and females in anti-RBD (DABA) or nAb responses (Supplementary Figures 2A, B). However, when divided into age groups, significant differences were observed in the antibody responses between age groupings for both males and females (Supplementary Figures 2C, D). Specifically, individuals between 51-70 years of age demonstrated higher anti-RBD levels and nAb responses ($IC_{70}$) than those aged 20-49 or those >70 years old. (Supplementary Figures 2C, D).

We further studied responses against the two main immunogenic viral proteins, the spike and the non-envelope nucleoprotein (NP). The S1 region of spike that includes the RBD was was also studied individually considering it is the primary target of nuetralising antibodies. In samples taken at recruitment, which represents a range of days between patients since the onset of symptoms and hospital presentation, IgM and IgG antibody binding responses to spike, S1 and NP were not significantly different between males and females for most age groupings, except for the IgM responses to S1, which were higher in men aged 60-70 (Supplementary Figures 3A-F). The IgM responses to the S1, Spike, and NP proteins all demonstrated higher levels in individuals aged between 41-60 in comparison to the <40 or >70 age groupings (Supplementary Figures 3A-C, respectively), with a

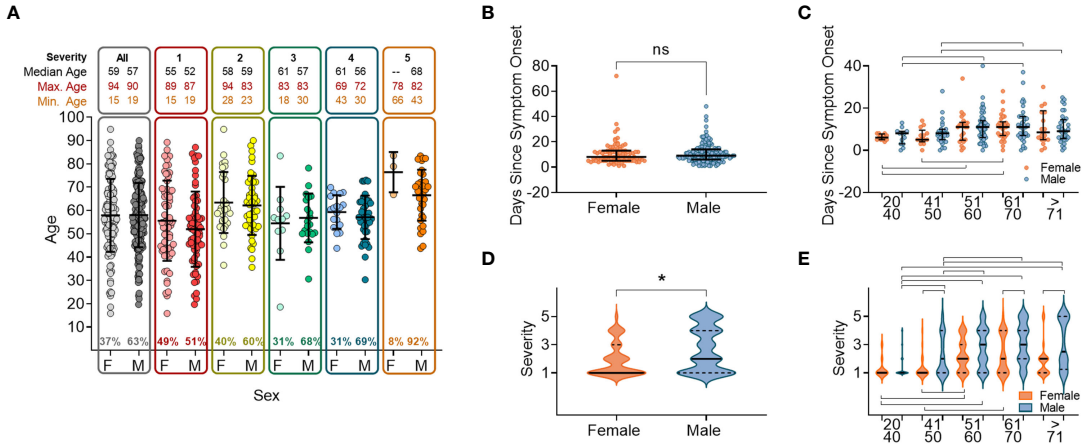


FIGURE 1
Sex and age distribution within groups with relation to days since disease onset and severity. **(A)** Number of individuals, female (F) or male (M), overall and when broken down into disease severity groupings (S1-S5). **(B)** Days since symptom onset split into females (orange) and males (orange) for all individuals. **(C)** Days since symptom onset split into females and males and relative to age groupings. **(D)** Disease severity split into females and males for all individuals. **(E)** Disease severity split into females and males relative to age groupings. In all panels mean values and confidence intervals shown (black lines). Lines above or below the groups indicate significant differences between groups as found by implementing a paired t-test or a non-parametric ANOVA (Kruskal-Wallis test). * indicates statistical significance P < 0.05.

similar profile observed for IgG (Supplementary Figures 3D-F, respectively).

Overall, when comparing antibody responses (DABA, neutralizing, IgG and IgM) at recruitment no differences were found between males and females within age categories but differences were observed between the different age categories. Individuals in age categories 20-40 and >70 had lower antibody titres than those in the intermediate age categories.

## 3.3 Total, neutralizing and class Ab associations

We next analysed the relationship between the antibody classes IgM and IgG against different virus antigens, comparing acute infection with convalescence. During acute infection, IgG responses against Spike protein correlated with IgM antibody levels (P<0.0001), whereas this correlation disappeared during convalescence (Supplementary Figure 4A). This association was not observed when comparing IgG versus IgM responses against S1 or NP antigens during acute infection or convalescence (Supplementary Figures 4B, C, respectively), indicating that antibody class induction is variable across different antigens. Strong correlations were found between Spike-IgM and S1-IgM as well as between Spike-IgG and S1-IgG responses (Supplementary Figures 4D, E) with again no difference between acute infection and convalescence. In contrast, weak correlations were observed when comparing NP with Spike or S1 antibody responses (Supplementary Figures 4F-I).

There were signficant correlations between total anti-RBD binding (DABA) and both IgM and IgG to total spike and S1 (Supplementary Figures 5A-D) during the acute infection phase (<21 days post-symptom onset), which became weaker or not significant during convalescence (>21 days post-symptom onset)

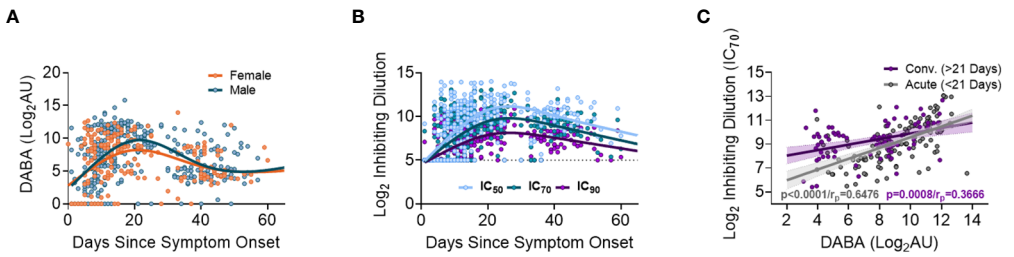


FIGURE 2
Association between anti-RBD as well Ab neutralisation responses with days since disease onset. **(A)** Anti-RBD binding in relation to days since disease onset and split into females (orange) and males (blue). The lines (females orange and males blue) show the spline/LOWESS curves indicating the overtime evolutionary trend of the data. **(B)** Neutralisation antibody responses depict in relation to days since disease onset and curves representing the spline/LOWESS for the $IC_{50}$, $IC_{70}$ and $IC_{90}$ values indicating the overtime evolution trend. **(C)** Association between anti-RBD and neutralisation responses ($IC_{70}$). Spearman correlation test (P<0.0001/$r_p$=0.6476), in acute infection (under 21 days) and (P<0.0001/$r_p$=0.3666) in convalescence (over 21 days).

for IgG, but not IgM. A similar pattern was observed for the correlation between anti-RBD binding and anti-NP binding, indicating that the anti-RBD binding correlated to some extent with the total antibody response, though the magnitude was less for binding to NP (Supplementary Figures 5E, F).

Next, we compared antibody classes IgG and IgM against Spike, NP and S1 to nAb responses ($IC_{70}$) directed against the same antigens. We observed similar profiles during both acute infection and convalescence (Supplementary Figures 5G-L). Collectively, these results suggest that total antibody, as well as class-specific responses (all measured by solid-phase binding ELISA), correlate with nAb activity induced in early infection. The most notable associations between responses were observed when comparing Spike, S1 IgG or IgM levels with nAb responses (Supplementary Figures 5G-J). This would indicate that both IgM and IgG induced during acute infection and convalescence are associated with virus neutralisation with spike, including the RBD domain as the predominant target.

## 3.4 Antibody levels and neutralisation associate with disease severity over time

We next analysed the relationships between anti-RBD and nAb responses ($IC_{70}$) with disease severity (Figure 3). In all severity groups, antibody levels increased over time, but initially relatively lower levels were observed in groups S1 and S5 in week 1, particularly for nAb responses, when compared to intermediate severity groups (Figure 3 and Supplementary Figure 6). By week 3, high levels of anti-RBD and nAbs were measured in all groups, and maintained for the duration of the study period (Figure 3). A similar profile was observed when comparing IgM and IgG responses for Spike, NP and S1 (Supplementary Figure 7). These results indicate that whilst antibody levels rise with time in all severity groups, individuals in the most severe and least severe disease groups developed antibody responses more slowly than those in intermediate groupings.

## 3.5 Differing profiles of antibody responses over time in male and female pariticipants

Sex differences in antibody responses over time were investigated using a mixed effect regression model comparing different antibody measurements. Female participants demonstrated higher initial anti-RBD responses which declined slowly from day 20, whilst male participants had lower early anti-RBD responses that sharply increased up until day 30 before falling to similar levels as females at 50 days post symptom onset (Figure 4A). However, when comparing nAb ($IC_{70}$) responses over the same period (Figure 4B), similar antibody profiles were found for both males and females, suggesting that the higher anti-RBD responses measured by the hybrid DABA observed in males were not associated with higher neutralisation. When comparing IgM and IgG Ab responses against Spike, S1 or NP antigens over the 50 days period following symptom onset, a very similar profile was observed to DABA anti-RBD measurements (Figures 4C-H). However, the most marked differences were observed with IgM between males and females (Figures 4C-E) and especially for the Spike and S1 protein (Figures 4C, D, respectively). These results highlight the differences in antibody response kinetics between male and female participants and in particular in early IgM responses targeted to the dominant antigens for neutralisation.

## 3.6 Upper respiratory tract SARS-CoV-2 viral RNA in relation to demographics, disease severity and Ab responses

We performed SARS-CoV-2 viral transcript measurements on upper respiratory tract samples, taken from 174 participants, at a median of 14 days from date of symptom onset (IQR8-30). There were no differences in viral RNA levels by sex (Figure 5A), nor by age or disease severity (Figures 5B, C, respectively). Viral RNA copy

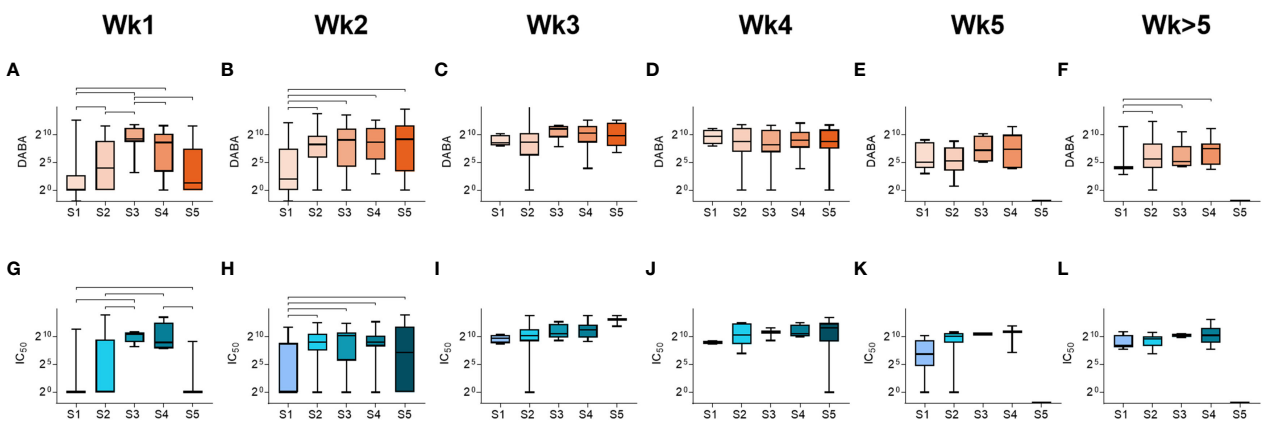


FIGURE 3
Antibody responses by severity groupings and time following disease onset. **(A-F)** Total anti-RBD titres grouped by severity (S1-S5), measured from samples taken at **(A)** week 1, **(B)** week 2, **(C)** week 3, **(D)** week 4, **(E)** week 5 and **(F)** past week 5 post-symptom onset. **(G-L)** Neutralising antibody ($IC_{50}$) titres grouped by severity (S1-S5), measured from samples taken at **(G)** week 1, **(H)** week 2, **(I)** week 3, **(J)** week 4, **(K)** week 5 and **(L)** past week 5 post-symptom onset.Statistically significant differences (non-parametric ANOVA (Kruskal-Wallis test) are indicated by horizontal lines above the groupings.

10.3389/fimmu.2023.1146702

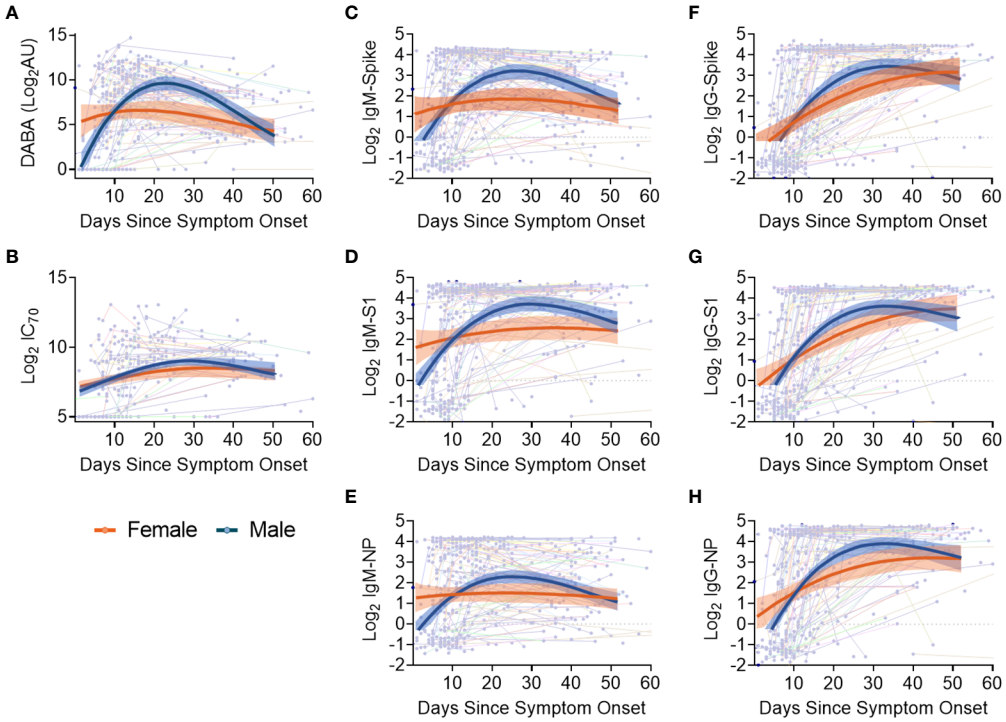


FIGURE 4
Evolution in time of antibody titres following disease onset by sex and subclass. **(A)** Anti-RBD titres. **(B)** nAb ($IC_{70}$) responses. **(C-E)** IgM binding responses against spike **(C)**, S1 **(D)** and NP **(E)**. **(F-H)** IgG binding responses against spike glycoprotein **(F)**, S1 **(G)** and NP **(H)** responses. The thin lines in background indicate individuals with longitudinal samplings with each dot representing a time point collection. For all panels, best-fit curves with 95% confidence intervals are shown for females (orange) and males (blue).

number fell over time from symptom onset (Supplementary Figures 8A, B), but the number of days from symptom onset to when participants first presented at hospital and were sampled at study recruitment did not vary according to age or disease severity (Supplementary Figures 8C, D). We next aimed to identify whether there were associations between viral RNA load and the array of antibody responses previously described. Contemporaneously collected samples showed an inverse correlation between viral RNA measurements and anti-RBD and nAb titres ($IC_{70}$), (Figures 5D, E, respectively). Similar inverse correlations were observed when comparing Spike, NP and S1 antigen directed IgM (Figures 5F-H, respectively) and IgG (Figures 5I-K, respectively). The results indicate that the presence of antibody responses were associated with a reduction in nasal levels of viral RNA, with no difference by sex.

# 4 Discussion

This study of individuals during the early stages of the pandemic (February-May 2020), using several measurements of host responses and viral RNA, has enabled the identification of differences in antibody profiles in an immunologically naïve population. Very early in the SARS-CoV-2 pandemic it was reported that a number of factors such as age, sex, co-morbidities, obesity and ethnicity were associated with the risk of severe disease (2, 5–7). In our cohort, analysis of patient demographics and disease severity showed that males were disproportionately represented in higher severity groups, especially in the age groupings above 50. Further, we showed that 90% of participants who died (severity group 5) were male with a median age of 68, supporting previous reports in which older males were more prone to death (47). Nevertheless, we observed no differences in the mean age between males and females when grouped by disease severity, potentially indicating that age is a stronger determinant of disease severity than sex.

Many other studies have measured antibody responses following acute infection with SARS-CoV-2 (23, 24, 31, 48–50). However, most were either cross-sectional, did not measure such early responses or do not utilise a multitude of comparable antibody assays. Therefore, a strength of this study was the use of an array of assays to measure antibody responses against the two main immunogenic viral proteins S and NP (48). Three different types of binding assays were performed with one quantifying total antibodies against RBD (DABA) and the two other measuring IgM and IgG responses against Spike, S1 and NP. Additionally, a PVP neutralisation assay was also employed to assess the functionality of the antibodies generated. Through comparing these different measurements, we observed an overall robust correlation between binding antibody titres (measured by DABA or ELISA), regardless of IgM or IgG class, to neutralising antibodies which is not affected by age, gender or disease severity. Comparison of total anti-RBD antibodies, as measured by DABA, with IgG and IgM Spike and S1 directed antibodies highlighted a strong correlation between these measurements during the acute

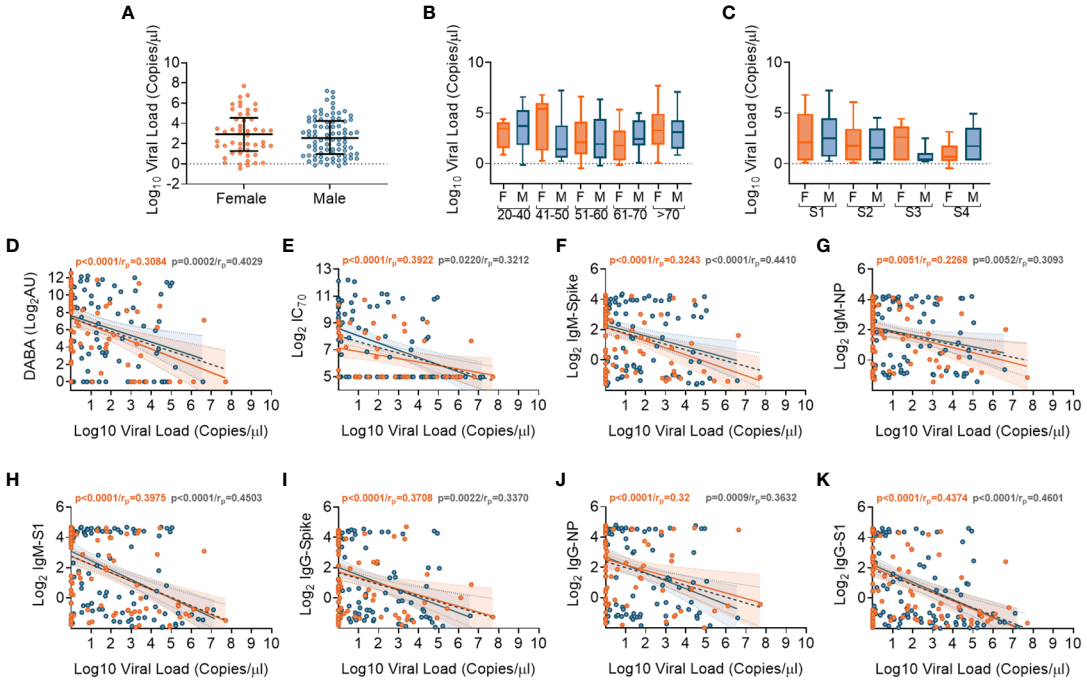


FIGURE 5
Association of SARS-CoV-2 upper respiratory tract viral loads in relation to sex, age and Ab responses at time of sampling. **(A)** Overall viral load measurements in relation to sex. **(B)** Viral loads according to age groupings and between females (orange) and males (blue). **(C)** Viral loads according to disease severity groupings (S1-S4) and between females (orange) and males (blue). **(D)** Associations between viral loads and overall DABA anti-RBD binding responses. **(E)** Associations between viral loads and neutralisation antibody ($IC_{70}$) responses. **(F-H)** Associations between viral loads and IgM antibody binding responses against spike **(F)**, NP **(G)** and S1 **(H)** antigens. **(I-K)** associations between viral loads and IgG antibody binding responses against spike **(I)**, NP **(J)** and S1 **(K)** antigens. **(D-K)** Inverse correlations shown (black dotted line) with males shown in blue and females in orange.

infection phase (Supplementary Figures 5A-D). However, this correlation became significantly weaker when comparing anti-RBD antibodies to spike and S1 directed IgG antibodies during the convalescent phase (Supplementary Figures 5A-D), indicating a strong contribution of IgM to the antibody responses measured by DABA and suggesting a progressive switch to IgG as the predominant class of spike directed antibodies. Similarly, we observed a strong correlation between Spike and S1 directed IgM and IgG antibody responses with nAbs during both acute infection and convalescence, suggesting that both early IgG and IgM posess neutralising activity (Supplementary Figures 5G-J), as has been previously reported (51–53). Together, these results further highlight how this multi-faceted analysis can reveal the evolvoing dynamics serological responses within patients. The associations between different antibody classes and functions observed in this study can be used to provide retrospective insights into humoral immunity in the most vulnerable population during the early stages of the pandemic. Such associations can facilitate further understanding of how inital immune responses can evolve over a pandemic of a novel virus, when population immune responses are not primed by previous exposures or vaccination.

We sought to identify how the timing of antibody responses associates with disease severity. Our data supports previous findings that antibody seroconversion occurs 10-19 days post symptom onset (20–22, 30, 49, 54) and with higher IgM than IgG antibody titres measured during acute infection (Supplementary Figures 4A-C). Despite some differences in the rate of induction of antibody response between males and females (discussed below), we showed that total anti-RBD as well as nAb responses peaked around 3 weeks post-symptom onset for both sexes and across all age groupings. Through comparing antibody titres at hospital presentation in different age groups, we showed that there were higher levels of IgM targeting spike, S1 and NP in indivudals aged between 41-60 than in other age groups (Supplementary Figure 3). Similarly, we also showed that both anti-RBD and nAb responses to all antigens tested were delayed in individuals with lowest disease severity, as previously reported (50, 54, 55) and in those with the highest severity (fatal outcome) (Figures 3, 4 and Supplementary Figure 6, respectively). However, patients in the 51 to 60 age group were recruited up to 4 days later in disease onset than the other groups (Figure 1C), which may account for some of the differences observed. Nevertheless, these data, together with the finding that older males are more prone to severe disease and death, suggests that delayed antibody production is associated with severe disease and death in older patients (>60) but not in younger individuals (<40). A potential explanation for this disparity is that in younger individuals, more robust innate immune responses help to limit virus replication during early infection, reducing the overall viral burden and subsequently delaying the production of Ab responses. Conversely, advanced age is associated with blunted innate immune

responses, which in combination with delayed Ab production likely accounts for the higher risk of severe disease. Indeed, delayed and impaired type 1 IFN responses have been associated with risk of severe COVID-19 (56) and these responses are known to be dysregulated in elderly individuals, contributing to the age related discrepancies in patient outcome (57–59).

When comparing antibody responses between sexes, we observed a more rapid induction of antibody responses in females than was observed in male participants and have associated this with differences in disease severity. Therefore, it is possible that a contributing factor to sex-associated differences in disease severity is the timing of antibody responses, whereby a delay in antibody production may account for increased risk of severe disease outcome. This association between age, sex and disease outcome with antibody kinetics has been previously reported, where females demonstrated more rapid increases in protective IgG responses than males (29) and that in severe cases, females had higher concentrations of virus-specific IgG (28). Here, we identify that the timing of measuring serological responses is important when correlating to disease status and outcome. This should be taken into consideration when comparing results to other studies where levels of IgM have reported contradictory findings between the sexes (60).

Through measuring upper respiratory tract viral RNA transcripts, indicative of localised viral shedding and therefore a surrogate measure for viral load, we observed an inverse correlation between nAb levels which may indicate a critical role of effective serological responses limiting viral replication and leading to clearance of the infection. Nevertheless, our samples were obtained a median of 2 weeks post symptom onset and therefore viral RNA has been predominantly measured during the decline phase of infection (61). Additionally, it is possible that this observation could be a non-causal association with emergence of effective cellular immunity. It should also be noted that viral load in the lower respiratory tract, which may play an important role in defining disease severity, was not measured in this study. Additionally, a formal analysis of the avidity of the anti-RBD serological response following recovery has not been undertaken. Preliminary unpublished data indicate avidity is low after recovery from infection but greatly increased after vaccine administration.

In this study, immunological linkages with disease outcome have been deciphered independently in a naïve host population and with a homogenous viral strain. The analyses of patients early in the pandemic has been vital in enabling description of the associations we have identified. Subsequent multiple exposures to different types of vaccines, natural infections and the emergence of diverse viral variants makes unravelling further host genetic and immune factors associated with disease challenging, meaning that the data presented here are unique, and are unlikely to be obtained as the pandemic evolves.

## Data availability statement

The raw data supporting the conclusions of this article will be made available by the authors, without undue reservation.

## Ethics statement

This analysis included sera from 337 patients admitted to UK hospitals with COVID-19 between February and June 2020 and enrolled in the International Severe Acute Respiratory and emerging Infections Consortium (ISARIC) World Health Organization (WHO) Clinical Characterisation Protocol UK (CCP-UK) study. The patients/participants provided their written informed consent to participate in this study.

## ISARIC4C Investigators

Consortium Lead Investigator: J Kenneth Baillie; Chief Investigator: Malcolm G Semple; Co-Lead Investigator: Peter JM Openshaw; ISARIC Clinical Coordinator: Gail Carson *Co-Investigator*: Beatrice Alex, Petros Andrikopoulos, Benjamin Bach, Wendy S Barclay, Debby Bogaert, Meera Chand, Kanta Chechi, Graham S Cooke, Ana da Silva Filipe, Thushan de Silva, Annemarie B Docherty, Gonçalo dos Santos Correia, Marc-Emmanuel Dumas, Jake Dunning, Tom Fletcher, Christoper A Green, William Greenhalf, Julian L Griffin, Rishi K Gupta, Ewen M Harrison, Julian A Hiscox, Antonia Ying Wai Ho, Peter W Horby, Samreen Ijaz, Saye Khoo, Paul Klenerman, Andrew Law, Matthew R Lewis, Sonia Liggi, Wei Shen Lim, Lynn Maslen, Alexander J Mentzer, Laura Merson, Alison M Meynert, Shona C Moore, Mahdad Noursadeghi, Michael Olanipekun, Anthonia Osagie, Massimo Palmarini, Carlo Palmieri, William A Paxton, Georgios Pollakis, Nicholas Price, Andrew Rambaut, David L Robertson, Clark D Russell, Vanessa Sancho-Shimizu, Caroline J Sands, Janet T Scott, Louise Sigfrid, Tom Solomon, Shiranee Sriskandan, David Stuart, Charlotte Summers, Olivia V Swann, Zoltan Takats, Panteleimon Takis, Richard S Tedder, AA Roger Thompson, Emma C Thomson, Ryan S Thwaites, Lance CW Turtle, Maria Zambon; *Project Manager*: Hayley Hardwick, Chloe Donohue, Fiona Griffiths, Wilna Oosthuyzen; *Project Administrator*: Cara Donegan, Rebecca G. Spencer; *Data Analyst*: Lisa Norman, Riinu Pius, Thomas M Drake, Cameron J Fairfield, Stephen R Knight, Kenneth A Mclean, Derek Murphy, Catherine A Shaw; *Data and Information System Manager*: Jo Dalton, Michelle Girvan, Egle Saviciute, Stephanie Roberts, Janet Harrison, Laura Marsh, Marie Connor, Sophie Halpin, Clare Jackson, Carrol Gamble, Daniel Plotkin, James Lee; *Data Integration and Presentation*: Gary Leeming, Andrew Law, Murray Wham, Sara Clohisey, Ross Hendry, James Scott-Brown; *Material Management*: Victoria Shaw, Sarah E McDonald. *Patient Engagement*: Seán Keating; *Outbreak Laboratory Staff and Volunteers*: Katie A. Ahmed, Jane A Armstrong, Milton Ashworth, Innocent G Asiimwe, Siddharth Bakshi, Samantha L Barlow, Laura Booth, Benjamin Brennan, Katie Bullock, Benjamin WA Catterall, Jordan J Clark, Emily A Clarke, Sarah Cole, Louise Cooper, Helen Cox, Christopher Davis, Oslem Dincarslan, Chris Dunn, Philip Dyer, Angela Elliott, Anthony Evans, Lorna Finch, Lewis WS Fisher, Terry Foster, Isabel Garcia-Dorival, Philip Gunning, Catherine Hartley, Rebecca L Jensen, Christopher B Jones, Trevor R Jones, Shadia Khandaker, Katharine King, Robyn T. Kiy, Chrysa Koukorava, Annette Lake, Suzannah Lant, Diane

Latawiec, Lara Lavelle-Langham, Daniella Lefteri, Lauren Lett, Lucia A Livoti, Maria Mancini, Sarah McDonald, Laurence McEvoy, John McLauchlan, Soeren Metelmann, Nahida S Miah, Joanna Middleton, Joyce Mitchell, Shona C Moore, Ellen G Murphy, Rebekah Penrice-Randal, Jack Pilgrim, Tessa Prince, Will Reynolds, P. Matthew Ridley, Debby Sales, Victoria E Shaw, Rebecca K Shears, Benjamin Small, Krishanthi S Subramaniam, Agnieska Szemiel, Aislynn Taggart, Jolanta Tanianis-Hughes, Jordan Thomas, Erwan Trochu, Libby van Tonder, Eve Wilcock, J. Eunice Zhang, Lisa Flaherty, Nicole Maziere, Emily Cass, Alejandra Doce Carracedo, Nicola Carlucci, Anthony Holmes, Hannah Massey; *Edinburgh Laboratory Staff and Volunteers*: Lee Murphy, Sarah McCafferty, Richard Clark, Angie Fawkes, Kirstie Morrice, Alan Maclean, Nicola Wrobel, Lorna Donnelly, Audrey Coutts, Katarzyna Hafezi, Louise MacGillivray, Tammy Gilchrist; *Local Principal Investigators*: Kayode Adeniji, Daniel Agranoff, Ken Agwuh, Dhiraj Ail, Erin L. Aldera, Ana Alegria, Sam Allen, Brian Angus, Abdul Ashish, Dougal Atkinson, Shahedal Bari, Gavin Barlow, Stella Barnass, Nicholas Barrett, Christopher Bassford, Sneha Basude, David Baxter, Michael Beadsworth, Jolanta Bernatoniene, John Berridge, Colin Berry, Nicola Best, Pieter Bothma, David Chadwick, Robin Brittain-Long, Naomi Bulteel, Tom Burden, Andrew Burtenshaw, Vikki Caruth, David Chadwick, Duncan Chambler, Nigel Chee, Jenny Child, Srikanth Chukkambotla, Tom Clark, Paul Collini, Catherine Cosgrove, Jason Cupitt, Maria-Teresa Cutino-Moguel, Paul Dark, Chris Dawson, Samir Dervisevic, Phil Donnison, Sam Douthwaite, Andrew Drummond, Ingrid DuRand, Ahilanadan Dushianthan, Tristan Dyer, Cariad Evans, Chi Eziefula, Chrisopher Fegan, Adam Finn, Duncan Fullerton, Sanjeev Garg, Sanjeev Garg, Atul Garg, Effrossyni Gkrania-Klotsas, Jo Godden, Arthur Goldsmith, Clive Graham, Elaine Hardy, Stuart Hartshorn, Daniel Harvey, Peter Havalda, Daniel B Hawcutt, Maria Hobrok, Luke Hodgson, Anil Hormis, Michael Jacobs, Susan Jain, Paul Jennings, Agilan Kaliappan, Vidya Kasipandian, Stephen Kegg, Michael Kelsey, Jason Kendall, Caroline Kerrison, Ian Kerslake, Oliver Koch, Gouri Koduri, George Koshy, Shondipon Laha, Steven Laird, Susan Larkin, Tamas Leiner, Patrick Lillie, James Limb, Vanessa Linnett, Jeff Little, Mark Lyttle, Michael MacMahon, Emily MacNaughton, Ravish Mankregod, Huw Masson, Elijah Matovu, Katherine McCullough, Ruth McEwen, Manjula Meda, Gary Mills, Jane Minton, Mariyam Mirfenderesky, Kavya Mohandas, Quen Mok, James Moon, Elinoor Moore, Patrick Morgan, Craig Morris, Katherine Mortimore, Samuel Moses, Mbiye Mpenge, Rohinton Mulla, Michael Murphy, Megan Nagel, Thapas Nagarajan, Mark Nelson, Lillian Norris, Matthew K. O'Shea, Igor Otahal, Marlies Ostermann, Mark Pais, Carlo Palmieri, Selva Panchatsharam, Danai Papakonstantinou, Hassan Paraiso, Brij Patel, Natalie Pattison, Justin Pepperell, Mark Peters, Mandeep Phull, Stefania Pintus, Jagtur Singh Pooni, Tim Planche, Frank Post, David Price, Rachel Prout, Nikolas Rae, Henrik Reschreiter, Tim Reynolds, Neil Richardson, Mark Roberts, Devender Roberts, Alistair Rose, Guy Rousseau, Bobby Ruge, Brendan Ryan, Taranprit Saluja, Matthias L Schmid, Aarti Shah, Prad Shanmuga, Anil Sharma, Anna Shawcross, Jeremy Sizer, Manu Shankar-Hari, Richard Smith, Catherine Snelson, Nick Spittle, Nikki Staines, Tom Stambach, Richard Stewart, Pradeep Subudhi, Tamas Szakmany, Kate Tatham, Jo Thomas, Chris Thompson, Robert Thompson, Ascanio Tridente, Darell Tupper-Carey, Mary Twagira, Nick Vallotton, Rama Vancheeswaran, Lisa Vincent-Smith, Shico Visuvanathan, Alan Vuylsteke, Sam Waddy, Rachel Wake, Andrew Walden, Ingeborg Welters, Tony Whitehouse, Paul Whittaker, Ashley Whittington, Padmasayee Papineni, Meme Wijesinghe, Martin Williams, Lawrence Wilson, Sarah Cole, Stephen Winchester, Martin Wiselka, Adam Wolverson, Daniel G Wootton, Andrew Workman, Bryan Yates, Peter Young.

## Author contributions

EP, JT, KJR, SI, FM, KK, CD, EV, SD, KJ, and NJC performed experiments. EP, JT, KJR, SI, TE, LL, EV, SCM, SD, WP and GP analyzed laboratory and clinical data. NC, JH and PC designed, produced and donated key reagents. LL, CJ, HH, EV, SEM and SCM administered patient specimens and curated clinical data. MS, JB and PO designed and delivered the ISARIC4C consortium project. The study was designed by SI, MM, JB, PO, MS, WP, RT, and GP. The manuscript was written by EP, JT, KJR, SI, TE, LT, AH, MS, WP, RT. and GP. All authors contributed to the article and approved the submitted version.

## Funding

This work is supported by grants from: the National Institute for Health Research (NIHR) [award CO-CIN-01], the Medical Research Council [grant MC_PC_19059, MR/V028979/1 and UKRI CV220-111], the Chief Scientist Office, Scotland, and by the NIHR Health Protection Research Unit (HPRU) in Emerging and Zoonotic Infections at University of Liverpool in partnership with the UK Health Security Agency (UK-HSA), in collaboration with Liverpool School of Tropical Medicine and the University of Oxford [award 200907], NIHR HPRU in Respiratory Infections at Imperial College London with UK-HSA [award 200927], Wellcome Trust and Department for International Development [215091/Z/18/Z], the Bill and Melinda Gates Foundation [OPP1209135], Liverpool Experimental Cancer Medicine Centre (Grant Reference: C18616/A25153), NIHR Biomedical Research Centre at Imperial College London [IS-BRC-1215-20013], EU Platform foR European Preparedness Against (Re-) emerging Epidemics (PREPARE) [FP7 project 602525]. We acknowledge the NIHR Clinical Research Network for providing infrastructure support for this research. This research is part of the Data and Connectivity National Core Study, led by Health Data Research UK in partnership with the Office for National Statistics and funded by UK Research and Innovation (grant ref MC_PC_20029). LT is supported by a Wellcome Trust clinical career development fellowship a [205228/Z/16/Z]. PO is supported by a NIHR Senior Investigator Award [award 201385]. For the purpose of Open Access, the authors have applied a CC-BY public copyright licence to any Author Accepted Manuscript version arising from this submission. The views expressed are those of the authors and not necessarily those of the DHSC, DID, NIHR, MRC, Wellcome Trust or UK-HSA. UKRI support was provided through the following grant: MRC/UKRI grant MC_PC_19078 "nCoV: Serological detection of past SARS-CoV-2 infection by non-

invasive sampling for field epidemiology and quantitative antibody detection".

## Acknowledgments

We thank the study participants and their families for the individual contributions. We also thank all the frontline NHS clinical and research staff as well as volunteer medical students who collected the clinical data in challenging circumstances and aided the collection of the study specimens. We thank Wejdan Albalawi for providing support with virus stock production under pandemic circumstances. This work uses data provided by patients and collected by the NHS as part of their care and support #DataSavesLives.

## Conflict of interest

PO is the Imperial College Lead Investigator of the EMINENT consortium, supported by the Medical Research Council UK MR/R502121/1. This grant supports collaborative testing of compounds developed by GlaxoSmithKline in UK universities. PO is also on advisory boards for Affnivax, Oxford Immunotech, Nestle and Pfizer in relation to immunity to viruses fees paid to Imperial College London. PO is also on an advisory board for Janssen/J&J.

The remaining authors declare that the research was conducted in the absence of any commercial or financial relationships that could be construed as a potential conflict of interest.

## Publisher's note



## Supplementary material

The Supplementary Material for this article can be found online at: https://www.frontiersin.org/articles/10.3389/fimmu.2023.1146702/full#supplementary-material

## References

1. Casanova JL, Su HC, Abel L, Aiuti A, Almuhsen S, Arias AA, et al. A global effort to define the human genetics of protective immunity to SARS-CoV-2 infection. *Cell* (2020) 181:1194–9. doi: 10.1016/J.CELL.2020.05.016

2. Zheng Z, Peng F, Xu B, Zhao J, Liu H, Peng J, et al. Risk factors of critical & mortal COVID-19 cases: A systematic literature review and meta-analysis. *J Infect* (2020) 81: e16–25. doi: 10.1016/J.JINF.2020.04.021

3. Thwaites RS, Uruchurtu ASS, Siggins MK, Liew F, Russell CD, Moore SC, et al. Inflammatory profiles across the spectrum of disease reveal a distinct role for GM-CSF in severe COVID-19. *Sci Immunol* (2021) 6(57):eabg9873. doi: 10.1126/SCIIMMUNOL.ABG9873

4. Kousathanas A, Pairo-Castineira E, Rawlik K, Stuckey A, Odhams CA, Walker S, et al. Whole genome sequencing reveals host factors underlying critical covid-19. *Nature* (2022) 607(7917):97–103. doi: 10.1038/s41586-022-04576-6

5. Deng G, Yin M, Chen X, Zeng F. Clinical determinants for fatality of 44,672 patients with COVID-19. *Crit Care* (2020) 24:1–3. doi: 10.1186/S13054-020-02902-W/FIGURES/1

6. Docherty AB, Harrison EM, Green CA, Hardwick HE, Pius R, Norman L, et al. Features of 20 133 UK patients in hospital with covid-19 using the ISARIC WHO clinical characterisation protocol: prospective observational cohort study. *BMJ* (2020) 369:m1985. doi: 10.1136/BMJ.M1985

7. Williamson EJ, Walker AJ, Bhaskaran K, Bacon S, Bates C, Morton CE, et al. Factors associated with COVID-19-related death using OpenSAFELY. *Nature* (2020) 584:430–6. doi: 10.1038/s41586-020-2521-4

8. Zhang Q, Bastard P, Bolze A, Jouanguy E, Zhang SY, Cobat A, et al. Life-threatening COVID-19: Defective interferons unleash excessive inflammation. *Med* (2020) 1:14–20. doi: 10.1016/J.MEDJ.2020.12.001

9. Norris T, Razieh C, Zaccardi F, Yates T, Islam N, Gillies CL, et al. Impact of cardiometabolic multimorbidity and ethnicity on cardiovascular/renal complications in patients with COVID-19. *Heart* (2022) 108(15):1200–8. doi: 10.1136/HEARTJNL-2021-320047

10. Yates T, Zaccardi F, Islam N, Razieh C, Gillies CL, Lawson CA, et al. Obesity, chronic disease, age, and in-hospital mortality in patients with covid-19: Analysis of ISARIC clinical characterisation protocol UK cohort. *BMC Infect Dis* (2021) 21:1–9. doi: 10.1186/S12879-021-06466-0/FIGURES/3

11. Yates T, Zaccardi F, Islam N, Razieh C, Gillies CL, Lawson CA, et al. Obesity, ethnicity, and risk of critical care, mechanical ventilation, and mortality in patients admitted to hospital with COVID-19: Analysis of the ISARIC CCP-UK cohort. *Obesity* (2021) 29:1223–30. doi: 10.1002/OBY.23178

12. Pairo-Castineira E, Clohisey S, Klaric L, Bretherick AD, Rawlik K, Pasko D, et al. Genetic mechanisms of critical illness in COVID-19. *Nature* (2020) 591:92–8. doi: 10.1038/s41586-020-03065-y

13. The Severe Covid-19 GWAS Group. Genomewide association study of severe covid-19 with respiratory failure. *N Engl J Med* (2020) 383:1522–34. doi: 10.1056/nejmoa2020283

14. David A, Parkinson N, Peacock TP, Pairo-Castineira E, Khanna T, Cobat A, et al. A common TMPRSS2 variant has a protective effect against severe COVID-19. *Curr Res Transl Med* (2022) 70:103333. doi: 10.1016/J.RETRAM.2022.103333

15. Gudbjartsson DF, Norddahl GL, Melsted P, Gunnarsdottir K, Holm H, Eythorsson E, et al. Humoral immune response to SARS-CoV-2 in Iceland. *N Engl J Med* (2020) 383:1724–34. doi: 10.1056/nejmoa2026116

16. Röltgen K, Powell AE, Wirz OF, Stevens BA, Hogan CA, Najeeb J, et al. Defining the features and duration of antibody responses to SARS-CoV-2 infection associated with disease severity and outcome. *Sci Immunol* (2020) 5(54):eabe0240. doi: 10.1126/SCIIMMUNOL.ABE0240

17. Ripperger TJ, Uhrlaub JL, Watanabe M, Wong R, Castaneda Y, Pizzato HA, et al. Orthogonal SARS-CoV-2 serological assays enable surveillance of low-prevalence communities and reveal durable humoral immunity. *Immunity* (2020) 53:925–933.e4. doi: 10.1016/j.immuni.2020.10.004

18. Long Q-X, Tang X-J, Shi Q-L, Li Q, Deng H-J, Yuan J, et al. Clinical and immunological assessment of asymptomatic SARS-CoV-2 infections. *Nat Med* (2020) 26:1200–4. doi: 10.1038/s41591-020-0965-6

19. Siggins MK, Thwaites RS, Openshaw PJM. Durability of immunity to SARS-CoV-2 and other respiratory viruses. *Trends Microbiol* (2021) 29:648–62. doi: 10.1016/j.tim.2021.03.016

20. Isho B, Abe KT, Zuo M, Jamal AJ, Rathod B, Wang JH, et al. Persistence of serum and saliva antibody responses to SARS-CoV-2 spike antigens in COVID-19 patients. *Sci Immunol* (2020) 5(52):eabe5511. doi: 10.1126/SCIIMMUNOL.ABE5511/SUPPL_FILE/ABE5511_TABLE_S4.XLSX

21. Zhao J, Yuan Q, Wang H, Liu W, Liao X, Su Y, et al. Antibody responses to SARS-CoV-2 in patients with novel coronavirus disease 2019. *Clin Infect Dis* (2020) 71:2027–34. doi: 10.1093/cid/ciaa344

22. Long QX, Liu BZ, Deng HJ, Wu GC, Deng K, Chen YK, et al. Antibody responses to SARS-CoV-2 in patients with COVID-19. *Nat Med* (2020) 26:845–8. doi: 10.1038/s41591-020-0897-1

23. Qiu M, Shi Y, Guo Z, Chen Z, He R, Chen R, et al. Antibody responses to individual proteins of SARS coronavirus and their neutralization activities. *Microbes Infect* (2005) 7:882–9. doi: 10.1016/j.micinf.2005.02.006

24. Atyeo C, Fischinger S, Zohar T, Slein MD, Burke J, Loos C, et al. Distinct early serological signatures track with SARS-CoV-2 survival. *Immunity* (2020) 53:524–532.e4. doi: 10.1016/j.immuni.2020.07.020

25. Piccoli L, Park YJ, Tortorici MA, Czudnochowski N, Walls AC, Beltramello M, et al. Mapping neutralizing and immunodominant sites on the SARS-CoV-2 spike receptor-binding domain by structure-guided high-resolution serology. *Cell* (2020) 183:1024–1042.e21. doi: 10.1016/J.CELL.2020.09.037

26. Premkumar L, Segovia-Chumbez B, Jadi R, Martinez DR, Raut R, Markmann AJ, et al. The receptor-binding domain of the viral spike protein is an immunodominant and highly specific target of antibodies in SARS-CoV-2 patients. *Sci Immunol* (2020) 5:8413. doi: 10.1126/SCIIMMUNOL.ABC8413/SUPPL_FILE/ABC8413_TABLES2.XLSX

27. Wajnberg A, Amanat F, Firpo A, Altman DR, Bailey MJ, Mansour M, et al. Robust neutralizing antibodies to SARS-CoV-2 infection persist for months. *Sci (80- )* (2020) 370:1227–30. doi: 10.1126/SCIENCE.ABD7728/SUPPL_FILE/ABD7728_WAJNBERG_SM.PDF

28. Zeng F, Dai C, Cai P, Wang J, Xu L, Li J, et al. A comparison study of SARS-CoV-2 IgG antibody between male and female COVID-19 patients: A possible reason underlying different outcome between sex. *J Med Virol* (2020) 92:2050–4. doi: 10.1002/JMV.25989

29. Huang B, Cai Y, Li N, Li K, Wang Z, Li L, et al. Sex-based clinical and immunological differences in COVID-19. *BMC Infect Dis* (2021) 21:1–10. doi: 10.1186/S12879-021-06313-2/FIGURES/3

30. Orner EP, Rodgers MA, Hock K, Tang MS, Taylor R, Gardiner M, et al. Comparison of SARS-CoV-2 IgM and IgG seroconversion profiles among hospitalized patients in two US cities. *Diagn Microbiol Infect Dis* (2021) 99:115300. doi: 10.1016/J.DIAGMICROBIO.2020.115300

31. Shen L, Wang C, Zhao J, Tang X, Shen Y, Lu M, et al. Delayed specific IgM antibody responses observed among COVID-19 patients with severe progression. *Emerg Microbes Infect* (2020) 9:1096–101. doi: 10.1080/22221751.2020.1766382

32. Collier DA, Ferreira IATM, Kotagiri P, Datir RP, Lim EY, Touizer E, et al. Age-related immune response heterogeneity to SARS-CoV-2 vaccine BNT162b2. *Nature* (2021) 596:417–22. doi: 10.1038/s41586-021-03739-1

33. Müller L, Andrée M, Moskorz W, Drexler I, Walotka L, Grothmann R, et al. Age-dependent immune response to the Biontech/Pfizer BNT162b2 coronavirus disease 2019 vaccination. *Clin Infect Dis* (2021) 73:2065–72. doi: 10.1093/cid/ciab381

34. Wei J, Stoesser N, Matthews PC, Ayoubkhani D, Studley R, Bell I, et al. Antibody responses to SARS-CoV-2 vaccines in 45,965 adults from the general population of the united kingdom. *Nat Microbiol* (2021) 6:1140–9. doi: 10.1038/s41564-021-00947-3

35. Brockman MA, Mwimanzi F, Lapointe HR, Sang Y, Agafitei O, Cheung PK, et al. Reduced magnitude and durability of humoral immune responses to COVID-19 mRNA vaccines among older adults. *J Infect Dis* (2022) 225:1129–40. doi: 10.1093/infdis/jiab592

36. Klein SL, Pekosz A, Park HS, Ursin RL, Shapiro JR, Benner SE, et al. Sex, age, and hospitalization drive antibody responses in a COVID-19 convalescent plasma donor population. *J Clin Invest* (2020) 130:6141–50. doi: 10.1172/JCI142004

37. Shields AM, Faustini SE, Perez-Toledo M, Jossi S, Allen JD, Al-Taei S, et al. Serological responses to SARS-CoV-2 following non-hospitalised infection: clinical and ethnodemographic features associated with the magnitude of the antibody response. *BMJ Open Respir Res* (2021) 8:e000872. doi: 10.1136/BMJRESP-2020-000872

38. Tedder RS, Samuel D, Dicks S, Scott JT, Ijaz S, Smith CC, et al. Detection, characterization, and enrollment of donors of Ebola convalescent plasma in Sierra Leone. *Transfusion* (2018) 58:1289–98. doi: 10.1111/TRF.14580

39. Adaken C, Scott JT, Sharma R, Gopal R, Dicks S, Niazi S, et al. Ebola Virus antibody decay–stimulation in a high proportion of survivors. *Nature* (2021) 590:468–72. doi: 10.1038/s41586-020-03146-y

40. Marshall JC, Murthy S, Diaz J, Adhikari N, Angus DC, Arabi YM, et al. A minimal common outcome measure set for COVID-19 clinical research. *Lancet Infect Dis* (2020) 20:e192–7. doi: 10.1016/S1473-3099(20)30483-7

41. Harris BHL, Zuhair M, Di Giovannantonio M, Rosadas C, Khan M, Short CE, et al. Asymptomatic severe acute respiratory syndrome coronavirus 2 (SARS-CoV-2) infection in a rehabilitation facility: Evolution of the presence of nasopharyngeal SARS-CoV-2 and serological antibody responses. *J Infect Dis* (2021) 223:192–6. doi: 10.1093/INFDIS/JIAA610

42. Rosa A, Pye VE, Graham C, Muir L, Seow J, Ng KW, et al. SARS-CoV-2 can recruit a heme metabolite to evade antibody immunity. *Sci Adv* (2021) 7:17. doi: 10.1126/SCIADV.ABG7607/SUPPL_FILE/SCIADV.ABG7607_SM.PDF

43. Ijaz S, Dicks S, Jegatheesan K, Parker E, Katsanovskaja K, Vink E, et al. Mapping of SARS-CoV-2 IgM and IgG in gingival crevicular fluid: Antibody dynamics and linkage to severity of COVID-19 in hospital inpatients. *J Infect* (2022) 85:152–60. doi: 10.1016/J.JINF.2022.05.033

44. Rosadas C, Khan M, Parker E, Marchesin F, Katsanovskaja K, Sureda-Vives M, et al. Detection and quantification of antibody to SARS CoV 2 receptor binding domain provides enhanced sensitivity, specificity and utility. *J Virol Methods* (2022) 302:114475. doi: 10.1016/J.JVIROMET.2022.114475

45. Carnell G, Grehan K, Ferrara F, Molesti E, Temperton N. An optimized method for the production using PEI, titration and neutralization of SARS-CoV spike luciferase pseudotypes. *Bio-Protocol* (2017) 7(16):e2514. doi: 10.21769/bioprotoc.2514

46. Di Genova C, Sampson A, Scott S, Cantoni D, Mayora-Neto M, Bentley E, et al. Production, titration, neutralisation, storage and lyophilisation of severe acute respiratory syndrome coronavirus 2 (sars-cov-2) lentiviral pseudotypes. *Bio-Protocol* (2021) 11(21):e4236. doi: 10.21769/BioProtoc.4236

47. Huang C, Wang Y, Li X, Ren L, Zhao J, Hu Y, et al. Clinical features of patients infected with 2019 novel coronavirus in wuhan, China. *Lancet* (2020) 395:497–506. doi: 10.1016/S0140-6736(20)30183-5

48. Ni L, Ye F, Cheng ML, Feng Y, Deng YQ, Zhao H, et al. Detection of SARS-CoV-2-Specific humoral and cellular immunity in COVID-19 convalescent individuals. *Immunity* (2020) 52:971–7.e3. doi: 10.1016/j.immuni.2020.04.023

49. Qu J, Wu C, Li X, Zhang G, Jiang Z, Li X, et al. Profile of immunoglobulin G and IgM antibodies against severe acute respiratory syndrome coronavirus 2 (SARS-CoV-2). *Clin Infect Dis* (2020) 71:2255–8. doi: 10.1093/CID/CIAA489

50. Huang AT, Garcia-Carreras B, Hitchings MDT, Yang B, Katzelnick LC, Rattigan SM, et al. A systematic review of antibody mediated immunity to coronaviruses: kinetics, correlates of protection, and association with severity. *Nat Commun* (2020) 11:1–16. doi: 10.1038/s41467-020-18450-4

51. Seow J, Graham C, Merrick B, Acors S, Pickering S, Steel KJA, et al. Longitudinal evaluation and decline of antibody responses in SARS-CoV-2 infection. *Nat Microbiol* (2020) 5:1598. doi: 10.1038/S41564-020-00813-8

52. Dispinseri S, Secchi M, Pirillo MF, Tolazzi M, Borghi M, Brigatti C, et al. Neutralizing antibody responses to SARS-CoV-2 in symptomatic COVID-19 is persistent and critical for survival. *Nat Commun* (2021) 12:1–12. doi: 10.1038/s41467-021-22958-8

53. Lau EHY, Tsang OTY, Hui DSC, Kwan MYW, Chan W, Chiu SS, et al. Neutralizing antibody titres in SARS-CoV-2 infections. *Nat Commun* (2021) 12(1):63. doi: 10.1038/S41467-020-20247-4

54. Wang Y, Zhang L, Sang L, Ye F, Ruan S, Zhong B, et al. Kinetics of viral load and antibody response in relation to COVID-19 severity. *J Clin Invest* (2020) 130:5235–44. doi: 10.1172/JCI138759

55. Rijkers G, Murk J-L, Wintermans B, van Looy B, van den Berge M, Veenemans J, et al. Differences in antibody kinetics and functionality between severe and mild severe acute respiratory syndrome coronavirus 2 infections. *J Infect Dis* (2020) 222:1265–9. doi: 10.1093/infdis/jiaa463

56. Hadjadj J, Yatim N, Barnabei L, Corneau A, Boussier J, Smith N, et al. Impaired type I interferon activity and inflammatory responses in severe COVID-19 patients. *Sci (80- )* (2020) 369:718–24. doi: 10.1126/SCIENCE.ABC6027/SUPPL_FILE/ABC6027-HADJADJ-SM.PDF

57. Acharya D, Liu GQ, Gack MU. Dysregulation of type I interferon responses in COVID-19. *Nat Rev Immunol* (2020) 20:397–8. doi: 10.1038/s41577-020-0346-x

58. Channappanavar R, Perlman S. Age-related susceptibility to coronavirus infections: role of impaired and dysregulated host immunity. *J Clin Invest* (2020) 130:6204–13. doi: 10.1172/JCI144115

59. Beer J, Crotta S, Breithaupt A, Ohnemus A, Becker J, Sachs B, et al. Impaired immune response drives age-dependent severity of COVID-19. *J Exp Med* (2022) 219(12):e20220621. doi: 10.1084/JEM.20220621/213485

60. Chvatal-Medina M, Mendez-Cortina Y, Patiño PJ, Velilla PA, Rugeles MT. Antibody responses in COVID-19: A review. *Front Immunol* (2021) 12:1208. doi: 10.3389/fimmu.2021.633184

61. Cevik M, Tate M, Lloyd O, Maraolo AE, Schafers J, Ho A. SARS-CoV-2, SARS-CoV, and MERS-CoV viral load dynamics, duration of viral shedding, and infectiousness: a systematic review and meta-analysis. *Lancet Microbe* (2021) 2:e13–22. doi: 10.1016/S2666-5247(20)30172-5

frontiers | Frontiers in Immunology

TYPE Original Research
PUBLISHED 19 May 2023
DOI 10.3389/fimmu.2023.1183273



OPEN ACCESS

EDITED BY
Anna Sediva,
University Hospital in Motol, Czechia

REVIEWED BY
Takehito Uruno,
Kyushu University, Japan
Hélène Decaluwe,
University of Montreal, Canada

*CORRESPONDENCE
Cynthia J. Guidos
Cynthia.guidos@sickkids.ca
Evgueni A. Ivakine
zhenya.ivakine@sickkids.ca

†These authors have contributed equally to this work and share senior authorship

RECEIVED 09 March 2023
ACCEPTED 10 May 2023
PUBLISHED 19 May 2023

CITATION
Scott O, Visuvanathan S, Reddy E, Mahamed D, Gu B, Roifman CM, Cohn RD, Guidos CJ and Ivakine EA (2023) The human Stat1 gain-of-function T385M mutation causes expansion of activated T-follicular helper/T-helper 1-like CD4 T cells and sex-biased autoimmunity in specific pathogen-free mice. *Front. Immunol.* 14:1183273. doi: 10.3389/fimmu.2023.1183273



# The human Stat1 gain-of-function T385M mutation causes expansion of activated T-follicular helper/T-helper 1-like CD4 T cells and sex-biased autoimmunity in specific pathogen-free mice

Ori Scott[1,2,3], Shagana Visuvanathan[2], Emily Reddy[4], Deeqa Mahamed[4], Bin Gu[5,6], Chaim M. Roifman[1,7], Ronald D. Cohn[2,3,8†], Cynthia J. Guidos[4,9*†] and Evgueni A. Ivakine[10*†]

[1]Division of Immunology and Allergy, Department of Paediatrics, Hospital for Sick Children and University of Toronto, Toronto, ON, Canada, [2]Program for Genetics & Genome Biology, Hospital for Sick Children Research Institute, Toronto, ON, Canada, [3]Institute of Medical Science, University of Toronto, Toronto, ON, Canada, [4]Program in Developmental and Stem Cell Biology, The Hospital for Sick Children, Toronto, ON, Canada, [5]Department of Obstetrics, Gynecology and Reproductive Biology, Michigan State University, East Lansing, MI, United States, [6]Institute for Quantitative Health Science and Engineering, Michigan State University, East Lansing, MI, United States, [7]The Canadian Centre for Primary Immunodeficiency and The Jeffrey Modell Research Laboratory for the diagnosis of Primary Immunodeficiency, The Hospital for Sick Children, Toronto, ON, Canada, [8]Division of Clinical & Metabolic Genetics, Department of Paediatrics, Hospital for Sick Children and University of Toronto, Toronto, ON, Canada, [9]Department of Immunology, University of Toronto, Toronto, ON, Canada, [10]Department of Physiology, University of Toronto, Toronto, ON, Canada

**Introduction:** Humans with gain-of-function (GOF) mutations in STAT1 (Signal Transducer and Activator of Transcription 1), a potent immune regulator, experience frequent infections. About one-third, especially those with DNA-binding domain (DBD) mutations such as T385M, also develop autoimmunity, sometimes accompanied by increases in T-helper 1 (Th1) and T-follicular helper (Tfh) CD4 effector T cells, resembling those that differentiate following infection-induced STAT1 signaling. However, environmental and molecular mechanisms contributing to autoimmunity in STAT1 GOF patients are not defined.

**Methods:** We generated Stat1T385M/+ mutant mice to model the immune impacts of STAT1 DBD GOF under specific-pathogen free (SPF) conditions.

**Results:** Stat1T385M/+ lymphocytes had more total Stat1 at baseline and also higher amounts of IFNg-induced pStat1. Young mutants exhibited expansion of Tfh-like cells, while older mutants developed autoimmunity accompanied by increased Tfh-like cells, B cell activation and germinal center (GC) formation. Mutant females exhibited these immune changes sooner and more robustly than males, identifying significant sex effects of Stat1T385M-induced immune dysregulation. Single cell RNA-Seq (scRNA-Seq) analysis revealed that Stat1T385M activated transcription of GC-associated programs in both B and T cells. However, it had the strongest

transcriptional impact on T cells, promoting aberrant CD4 T cell activation and imparting both Tfh-like and Th1-like effector programs.

**Discussion:** Collectively, these data demonstrate that in the absence of overt infection, Stat1T385M disrupted naïve CD4 T cell homeostasis and promoted expansion and differentiation of abnormal Tfh/Th1-like helper and GC-like B cells, eventually leading to sex-biased autoimmunity, suggesting a model for STAT1 GOF-induced immune dysregulation and autoimmune sequelae in humans.

KEYWORDS

STAT1, autoimmunity, chronic activation, T helper, immune dysregulation, Specific pathogen free (SPF), mouse model, gain of function (GOF)

# 1 Introduction

Humans with gain-of-function (GOF) mutations in *Signal Transducer and Activator of Transcription (STAT)1* exhibit widespread immune dysregulation. The major function of this STAT family transcription factor is to mediate the biological effects of pro-inflammatory cytokines, such as interferons (IFN), and to a lesser extent interleukin 6 (IL-6), which are produced when certain cells sense microbial products (1, 2). Although transcriptional complexes containing unphosphorylated STAT1 can mediate baseline expression of IFN-stimulated genes (ISG) (3–6), canonical infection-induced STAT1-mediated ISG expression involves a phosphorylation cascade following IFN receptor ligation. Type I IFNα/β cytokines activate Janus kinases (JAK) to phosphorylate STAT1 and STAT2, promoting their dimerization to induce transcription of genes that limit viral replication, enhance CD8 T cell cytotoxic effector function, and induce CD4 T cells to provide B cell help (7). IFNγ (Type II IFN) induces pSTAT1 homodimers to activate macrophage/monocytes and dendritic cell pro-inflammatory functions, enhance antigen presentation and secretion of cytokines that promote differentiation of Th1 cells from naïve CD4 T cells (8). IL6 activates STAT1 and STAT3 to to promote differentiation of naïve CD4 cells into Tfh cells, important mediators of humoral immunity (9). In contrast, IL6 stimulation of activated CD4 cells induces only STAT3, driving differentiation of Th17 cells that orchestrate the immune response to extra-cellular fungi (10, 11). Interestingly, STAT family members often cross-inhibit each other, and the hallmark clinical manifestation of STAT1 GOF is chronic mucocutaneous candidiasis (CMC), resulting from impaired Th17 differentiation due to partial STAT3 loss of function (12). STAT1 GOF patients frequently experience other severe invasive/opportunistic infections, and one third also develop autoimmune disease (13, 14). However, the underlying molecular and cellular mechanisms of autoimmunity in STAT1 GOF patients are unknown.

STAT1 GOF has been linked to dominant mutations in all *STAT1* domains, but most patients have mutations in the coiled-coil domain, essential for protein-protein interactions, or in the DBD, which orchestrates nuclear migration and DNA binding (13, 15, 16). Cells from STAT1 GOF patients typically show elevated pSTAT1 (Tyr701) levels after stimulation with IFNs (15), suggesting that autoimmunity could be linked to IFN hyper-responsiveness. In patients with *STAT1* DBD mutations, the most common of which is T385M (13, 17–19), STAT1 nuclear accumulation can also occur without IFN stimulation, suggesting a constitutive role for unphosphorylated STAT1 in the pathogenesis of these mutations (20). We recently showed that individuals with DBD mutations had a higher prevalence of autoimmunity compared with other STAT1 GOF patients, including endocrinopathies, autoimmune gastrointestinal disease (enteropathy or hepatitis), autoimmune cytopenia's and interstitial lung disease (21). However, these patients also had a high rate of invasive and opportunistic infections that typically preceded autoimmunity. Thus, it is unclear whether abnormal responses to pathogenic microbes promote autoimmunity in STAT1 GOF patients with T385M and other DBD mutations. Many autoimmune disorders are more prevalent in females due to a variety of IFN-dependent and -independent mechanisms (22), so sex may also modulate autoimmunity in STAT1 GOF these patients. However, sex effects on autoimmunity have not been studied in these patients.

In addition to compromising Th17 differentiation, STAT1 GOF may also promote the differentiation of effector CD4 lineages linked to autoimmunity. T cell receptor (TCR) signals plus IFNγ-induced pSTAT1 upregulate Tbet, the regulator of Type I cytotoxic responses (23), driving differentiation of Th1 cells, implicated in inflammatory bowel disease (24) and rheumatoid arthritis (25). Th1 cells are increased in many (26, 27) yet not all (28, 29) STAT1 GOF patients. TCR signals plus IL6-induced pSTAT1 and pSTAT3 regulate early differentiation of Tfh cells, implicated in SLE and

**Abbreviations:** Anti-nuclear autoantibody (ANA), Differentially-expressed genes (DEG), Chronic mucocutaneous candidiasis (CMC), DNA-binding domain (DBD), Gain-of-function (GOF), Germinal center (GC), Inducible co-stimulator (ICOS), Interferon (IFN), Interferon-stimulated genes (ISG), Memory phenotype (MP), Programmed death1 (PD1), Single-cell RNA-sequencing (scRNA-Seq), Systemic lupus erythematosus (SLE), Specific-pathogen free (SPF), Signal transducer and activator of transcription (STAT), T cell receptor (TCR), T-follicular helper (Tfh), T-helper 1 (Th1), Type 1 diabetes (T1D).

Type 1 diabetes (T1D) (30–32). Tfh cell differentiation and function is regulated by inducible T cell co-stimulator (ICOS), programmed death 1 (PD1; *Pdcd1*) and the transcriptional repressor Bcl6 (31). The transcription factors Tcf1 (*Tcf7*) and Lef1 also support Tfh differentiation (33), while restraining expression of co-inhibitory receptors such as *Ctla4* and *Lag3* (30, 33–35). Circulating Tfh-like cells (cTfh) are also increased in some STAT1 GOF patients (27, 28, 36). Foxp3$^{+}$ T-regulatory (Treg) cells are another key subset in autoimmunity (37, 38) that range from low-normal in STAT1 GOF patients (18, 28, 29, 36, 39, 40). Thus, CD4 effector and regulatory subsets are variably affected in STAT1 GOF patients, however it remains unclear if this variability reflects specific STAT1 GOF mutation impacts and/or environmental influences such as infections or immunosuppressive treatments.

Here, we generated a mouse model to identify potential cellular, molecular and environmental mechanisms linked to autoimmunity in STAT1 GOF patients with the DBD T385M mutation. To limit the environmental impact of infection with pathogens, we studied *Stat1*$^{T385M/+}$ mice raised in a specific-pathogen-free (SPF) facility. *Stat1*$^{T385M/+}$ lymphocytes had more total Stat1 at baseline and also higher amounts of IFNγ-induced pStat1. By 15-20 weeks of age, *Stat1*$^{T385M/+}$ mice exhibited excessive splenic GC formation and multiple autoimmune manifestations compared to their co-housed *wild-type* (*WT*) littermates. High parameter immune profiling identified early and sustained expansions of splenic "memory phenotype" (MP) CD4 cells with Tfh-like features, as well as increases in activated B cells. scRNA-Seq analysis suggested that *Stat1*$^{T385M}$ activated transcription of GC-associated programs in both B and T cells, promoted aberrant activation of naïve CD4 cells and induced their differentiation into hybrid Tfh/Th1-like effector cells. Collectively, these data demonstrate that in the absence of overt infection, *Stat1*$^{T385M}$ induced aberrant B cell activation, disrupted CD4 T cell homeostasis and promoted differentiation of abnormal T helper cells, eventually leading to autoimmunity, with both processes occurring sooner and more robustly in females.

# 2 Materials and Methods

Supplementary Tables 1–3 list key reagents and resources used in this study, sequences of the oligonucleotides, primers and repair templates used.

Supplementary Table 2 lists vendors and catalogue numbers for key reagents and antibodies used.

Supplementary Table 3 lists genes included in the BD Rhapsody™ Mouse Immune Response Targeted Panel.

## 2.1 Mouse husbandry

Mice were kept in a specific-pathogen free (SPF) facility (Toronto Centre for Phenogenomics; TCP) on a 12-hour light/dark cycle and provided with food and water ad-libitum. CD1 mice from Charles River (strain code: 022) and C57Bl/6J mice from JAX (strain code 000664) and TCP in-house breeding were used in this study. Mice of both sexes were used; mutants and *WT* littermates of the same sex were co-housed. Mouse procedures were carried out in compliance with the Animal for Research Act of Ontario and Guidelines of the Canadian Council on Animal Care. All procedures were reviewed and approved by the TCP Animal Care Committee, animal use protocol 25-0379H.

## 2.2 Generation of *stat1*$^{t385m/+}$ mice

A single guide RNA (sgRNA; Synthego) was used to target a protospacer adjacent motif within mouse *Stat1* exon 14. A homology-directed repair (HDR) construct (Integrated DNA Technologies) included the human *STAT1* exon 14 with containing the T385M mutation (C>T). The cassette was amplified using 5'-biotinylated primers to generate a repair template. Super-ovulated CD1 females were bred to C57Bl/6J male. Following the two-cell homologous recombination CRISPR approach (41), two-cell embryos collected at 1.5 days post-coitus were microinjected with sgRNA (50ng/μL), Cas9 conjugated with monomeric streptavidin (75ng/μL) and biotinylated repair template (20ng/μL). One day later, embryos were transferred into the oviducts of 0.5-post coitus days pseudo-pregnant CD1 females. Pups were genotyped as described below. After breeding back to C57Bl6/J, verification of congenic status was performed *via* 384-SNP background analysis (Mini Mouse Universal Genotyping Array, Transnetyx). Supplementary Table 1 lists sequences of the oligonucleotides, primers and repair templates used.

## 2.3 Nucleic acid isolation, PCR, Sanger and whole genome sequencing

Genotyping of founder mice, as well as determination of correct splicing, were done *via* a combination of Sanger sequencing, quantitative real-time PCR (qRT-PCR) and whole genome sequencing (WSG). Founder mice underwent genomic DNA isolation followed by PCR amplification and Sanger sequencing. Samples were sequenced on Applied Biosystems SeqStudio Genetic Analyzer (Thermo Fisher). Sequencing files were analyzed using SnapGene version 5.0.8 (Insightful Science; available at snapgene.com). For splicing evaluation, RNA was extracted and reverse-transcribed, followed by qRT-PCR evaluating expression of *Stat1* transcript using QuantStudio Real-Time PCR system (Thermo Fisher). For WGS, DNA samples were extracted as described above and underwent sequencing using the Illumina NovaSeq 6000 system performed by The Centre for Applied Genomics (TCAG) at the Hospital for Sick Children. Analysis was done using Integrative Genomics Viewer (IGV) version 2.9.4 with GRCm38/mm10 as the reference genome. Routine genotyping was done *via* Sanger sequencing as described above.

## 2.4 Immunoblotting for Stat1 and pStat1

Single cell suspensions of splenocytes from 6–12 week-old mice were treated with PBS or murine recombinant IFNγ (100ng/mL) for 30 minutes at 37°CC. To assess Stat1 de-phosphorylation kinetics, splenocytes were IFNγ stimulated for 30 minutes, washed in PBS and transferred to IFNγ-free media. They were then lysed immediately (0 minutes), or cultured for an additional 60 minutes or 120 minutes in IFNγ-free media at 37°C. Cells were lysed in RIPA buffer supplemented with protease and phosphatase inhibitors. Protein lysates (10μg protein/sample) were loaded onto and separated by pre-cast polyacrylamide (4-12% Bis-Tris) gels, and then transferred to a nitrocellulose membrane using iBlot 2 Dry Blotting System (Thermo Fisher). Membranes were blocked for 1 hour at room temperature in Tris-Buffered Saline containing 5% bovine serum albumin prior to incubating overnight with anti-pSTAT1 (pY701) or anti-STAT1 plus anti-β-actin. The following day, membranes were incubated AlexaFluor-647-labelled secondary antibodies. Membranes were imaged using ChemiDoc MP imaging system (Bio-Rad) and analyzed with Image Lab software version 6.0.1 (Bio-Rad). For assessment of pStat1 phosphorylation and de-phosphorylation kinetics, pStat1 normalized to β-actin at the time of IFNγ withdrawal (0 minutes) was designated as the baseline (100%), which was compared to normalized pStat1 levels 60 and 120 minutes after withdrawal of IFNγ. Supplementary Table 2 lists vendors and catalogue numbers for key reagents and antibodies used.

## 2.5 Measurement of serum immunoglobulin isotypes and liver panel

Sera collected from 20 week-old mice were sent to Eve Technologies (Calgary, AB) for immunoglobulin isotyping, using the Custom Mouse Immunoglobulin Isotyping 6-Plex Luminex panel (IgA, IgM, IgG1, IgG2a, IgG2b, IgG3). Liver enzymes and function, including alanine aminotransferase (ALT), aspartate aminotransferase (AST), alkaline phosphatase (ALP) and albumin were assessed in sera from 20 week-old mice by the TCP pathology core.

## 2.6 Histology and ANA detection

Pancreata collected from mice at 15-20 weeks and 49-52 weeks of age were fixed in 10% neutral-buffered formalin, sectioned, stained with hematoxylin and eosin (H&E) using standard techniques. To assess splenic architecture, spleen cryosections from 15–20 week-old mice (6 mice per genotype) were stained with H&E or with a panel consisting of GL7-FITC, CD21-TRITC, Cy5-B220 and DAPI as a nuclear counterstain. Slides were scanned using Olympus VS-120 microscope and images were analyzed using OlyVIA version 2.4 and ImageJ version 2.1.0/1.53c. These procedures were performed by the TCP pathology core. Mouse sera collected at 6-9 weeks and 15-20 weeks were screened at 1/40 for ANA using *via* indirect immunofluorescence on Hep-2 cells, according to the manufacturer's (Bio-Rad) protocol.

## 2.7 Flow and mass cytometric immune profiling

Spleen and mLN were processed into single-cell suspensions. After washing with 1 mL staining media (SM: PBS+ 1% BSA), 1-2x$10^6$ cells/sample were Fc-receptor blocked in SM at RT for 15' prior to staining for mass or flow cytometry. For mass cytometry, cells were then stained with a 50μL cocktail of metal-tagged antibodies (Supplementary Table 2), washed and stained with 1 μM natural abundance Cisplatin as previously described (42). Samples were then barcoded using the Cell-ID 20-Plex PD Barcoding Kit (Fluidigm) following the manufacturer's instructions prior to pooling up to 20 samples/tube and staining of nuclear DNA with $^{191/193}$Iridium. Final washes, addition 4-element EQ normalization beads and Helios acquisition were then performed as previously described (42). Helios software (v7.0.8493) was used to generate and normalize FCS 3.0 datafiles that were uploaded to CytoBank (Beckman Coulter Enterprise version) to perform sample-specific barcode stringency filtering as described (43). Additional gating removed debris, dead cells and doublets, before gating specific populations (Figure S2). For flow cytometry, cells were stained with 50μL of a T cell or B cell antibody cocktail (Supplementary Table 2) in SM (RT, 30'). After 2 PBS washes, T cell panel samples were stained with a fixable viability dye, fixed, permeabilized, and stained with anti-FoxP3 in 50μL (RT, 30'). Cells were washed, resuspended in SM and run on a 5-laser LSRFortessa analyzer running FACS-DIVA v8.0.1 (BD Biosciences). Exported FCS 3.0 files were uploaded to CytoBank, where data were compensated and pre-gated to remove debris, dead cells and doublets, prior to population gating (Figure S3).

## 2.8 Targeted scRNA-Seq analysis of immune gene expression

Single cell mouse splenocyte suspensions from 15 week-old female mice (3 per genotype) were stained with multiplexing antibodies, pooled, and stained with oligonucleotide-barcoded "AbSeq" antibodies. Single cells were paired with barcoded beads in a microwell cartridge using the BD Biosciences Rhapsody Express Single Cell Analysis System and Scanner, which documented retrieval of 36,059 beads with cells (8.3% multiplets). In-well single cell lysis allowed capture of RNA and AbSeq reagents bound to cells by barcoded beads prior to synthesizing cDNA and removing genomic DNA following the manufacturer's instructions. These procedures were performed by SickKids' Center for Advanced Single Cell Analysis (CASCA). Preparation of cDNA and AbSeq libraries followed by paired-end sequencing in an Illumina SP Nova-Seq flow cell (2x100 bp) was carried out by The Center for Genomic Analysis at the SickKids' Research Institute.

After uploading the Fastq sequence files and Fasta mRNA+ AbSeq reference files, the SevenBridges BD Targeted Multiplex Rhapsody Analysis Pipeline (v1.10) was used to filter by read-quality prior to aligning, annotating and combining R1+R2 reads. The pipeline annotated molecules, identified putative cells and originating samples for each molecule, and output files containing expression matrices and sequencing quality metrics, yielding $6.33x10^8$ aligned mRNA reads assigned to 21,583 cells (mean=29,343 RSEC-adjusted molecule counts/cell). The RSEC_MolsperCell.csv file was uploaded to BD's SeqGeq v1.8 where all additional analyses were performed. Briefly, data were normalized (counts/10,000 reads) and cells with low gene expression gated-out (0.4%). Of 397 mouse immune response genes analyzed (Supplementary Table 3), 378 were expressed at ≥100 molecules/cell in ≥ 10 cells.

Sample de-multiplixing was performed using the Lex_BDSMK Plugin (v. 0.6.0) to yield 2,810-3,734 cells/sample. Boolean "Or" gating was then used to combine samples by genotype for gating specific populations based on surface protein expression detected by AbSeq (Figure S4). The Seurat v.4.0.4 plugin was also used to perform unsupervised dimensionality reduction (uniform manifold approximation and projection, UMAP), multimodal (mRNA and AbSeq) clustering and identifying clusters with differentially expressed genes (mRNA) and/or proteins (AbSeq) (44). Differentially-expressed genes (DEG) between samples grouped by genotype for each population were identified using Volcano plots of fold change (FC) difference vs the negative logarithm of false-discovery rate (FDR)-adjusted q-value. The threshold for differential expression was ≥40% FC (corresponding to +/- 0.49 Log2 FC) with FDR-adjusted q-value <0.05.

The MyGeneSet tool from the Immunological Genome Project data-browser (http://rstats.immgen.org/MyGeneSet_New/index.html (45)) was used to visualize how genes over-expressed in mutant CD4 T cells were expressed in reference *WT* CD4 and CD8 T cell subsets from the microarray V1 dataset. Heatmaps were median-normalized by row (gene).

## 2.9 Statistical analysis

Statistical analyses were performed using GraphPad Prism 9 (version 9.3.1). The Shapiro-Wilk method was used to test for normal distribution of data. For normally-distributed data, unpaired two-tailed Student's t-tests with Welch's correction were performed, whereas a Mann-Whitney test was performed for non-normally-distributed data, to evaluate differences between genotypes. Two-way ANOVA was used to identify the main effects of genotype versus sex as well as the interaction between these independent variables on the measured values. *Post-hoc* t-tests were performed *via* a two-stage linear step-up method of Benjamini, Krieger and Yekutieli. A false discovery rate (FDR) adjusted-p value of <0.05 represented discovery. Observed frequencies of serum ANA positivity were compared using Fisher's exact test. Graphical data were represented as means ± standard deviation. Statistical significance was represented as: *p < 0.05, **p < 0.01, ***p < 0.001, ****p < 0.0001.

# 3 Results

## 3.1 *Stat1*$^{T385M/+}$ in mice recapitulates biochemical features of human *STAT1* GOF

We used CRISPR/Cas9 technology to replace the murine *Stat1* exon 14 with the human counterpart, which introduced a C>T substitution to cause the T385M mutation in the *Stat1* DBD (Figure 1A) (13, 17–19). *WT* human and murine exon 14 differ by 11 base-pairs, but encode amino acid sequences which are 100% conserved between species. Exchanging the human for the mouse exon was done so that this model may be used in future studies, to test therapeutic genome-editing strategies specifically targeting the human exon 14. Splenocytes and thymocytes from *Stat1*$^{T385M/+}$ mice showed enhanced induction of pStat1(Y701) in response to acute IFNγ stimulation (Figure 1B). Total Stat1, both at baseline and following stimulation, was also increased as has been observed in STAT1 GOF patients (15, 46) and consistent with the known positive feedback regulation of *STAT1* (6). Importantly, de-phosphorylation in mutants was neither diminished nor delayed (Figure 1C), in agreement with results from STAT1 GOF patient lymphocytes (46). These data demonstrate that, similar to patients with STAT1 GOF, lymphocytes from *Stat1*$^{T385M/+}$ mice exhibited pronounced dysregulation of basal and cytokine-stimulated *Stat1* activation.

## 3.2 Spontaneous GC formation and development of age-dependent autoimmunity in *Stat1*$^{T385M/+}$ mice

Previous mouse models of autoimmunity demonstrated splenic abnormalities including increased spontaneous GC formation (47, 48). Therefore, we evaluated spleen size and histology in roughly equal numbers of male and female mutant mice and their *WT* littermates at different ages. At 6-9 weeks of age, female but not male mutants exhibited significant splenomegaly (Figure S1A). However, by 15-20 weeks of age mutants of both sexes exhibited significant splenomegaly (Figure 2A). To evaluate architecture of B cell follicles and to assess GC formation at this age, we performed immunofluorescence using the B cell marker B220, the mature B cell/follicular dendritic cell marker CD21, and the GC B cell marker GL7. Both male and female mutants showed abnormal splenic architecture with loss of clear follicular borders. Mutant spleens also had increased density (number/mm$^2$) of GL7$^+$ GC, suggesting ongoing GC reactions and B cell activation (Figure 2B). In accordance with this notion, mutants had elevated serum levels of IgM, IgA, and IgG2a, but reduced levels of IgG1 (Figure 2C). These findings, and in particular the changes noted to IgG sub-classes, mirror the reported effect of enhanced IFNγ/Th1 signaling on immunoglobulin isotypes (49). Thus, by ~4 months of age, mutants displayed splenomegaly, increased GC formation and increase serum concentrations of several Ig isotypes, suggesting immune dysregulation.

To evaluate whether *Stat1*$^{T385M/+}$ mice born and raised in a SPF environment developed autoimmune manifestations, we screened sera for the presence of anti-nuclear autoantibodies (ANA) that

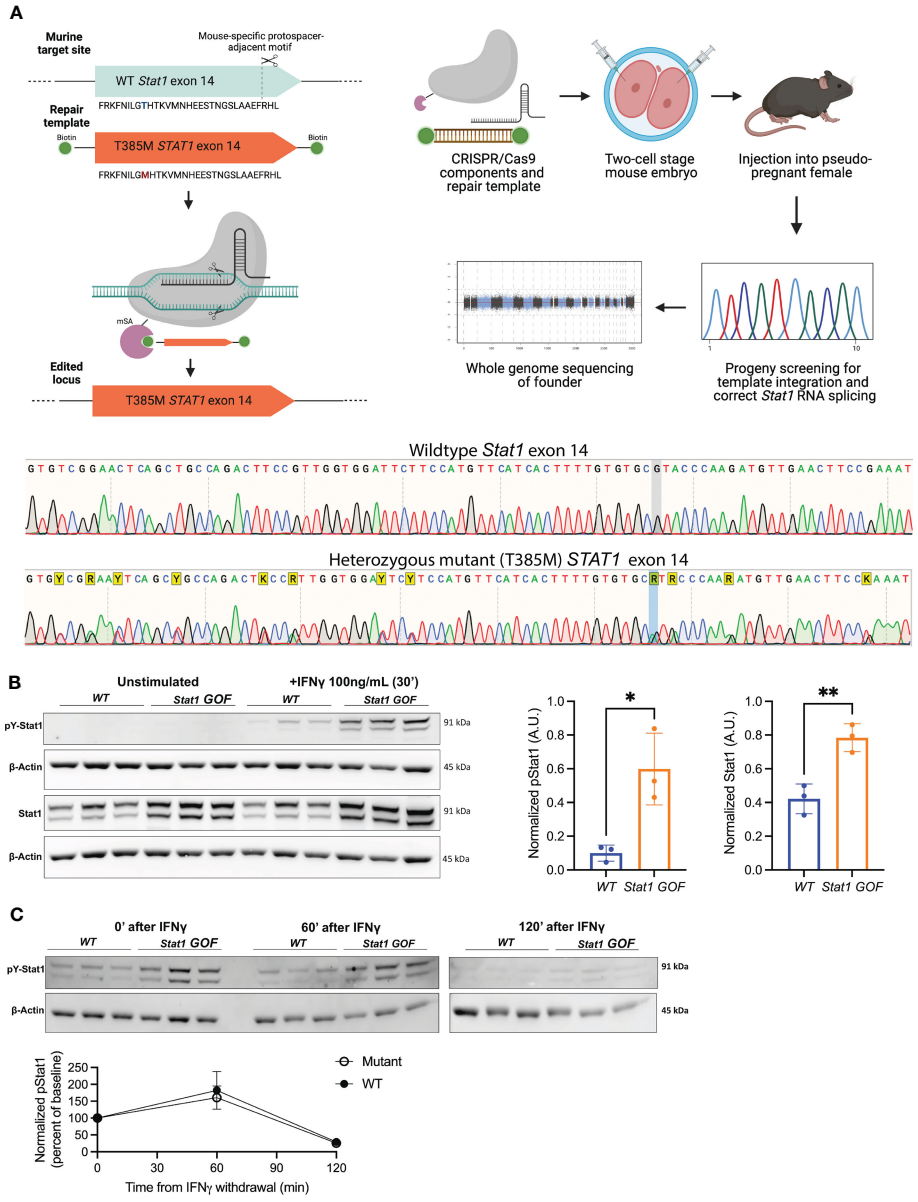


FIGURE 1
*Stat1*$^{T385M/+}$ recapitulates key biochemical hallmarks of human STAT1 gain-of-function (GOF). **(A)** *Top*: Schematic of CRISPR/Cas9 strategy used to replace *WT* murine *Stat1* exon 14 with human exon 14 harboring the T385M point mutation in the DBD. *Bottom:* Sanger sequencing confirmed the *WT* mouse exon 14 with the heterozygous mutant exon 14 in *Stat1*$^{T385M/+}$ mice. Heterozygous changes between mouse and human exon 14 are highlighted in yellow (Y: C/T; A/G; K: G/T). The T385M heterozygous point mutation on the negative strand is highlighted in blue (C>T, resulting in a G>A on the negative strand) **(B)** *Left:* Immunoblotting of splenocytes from 6–12 week-old *WT* and mutant mice (n=3/group) for total Stat1 and pStat1 (Tyr701) at baseline and after *in vitro* stimulation with 100 ng/mL IFNγ for 30 minutes. Stat1 isoforms α (91kDa) and β (84kDa) were detected.Densitometric quantification was performed on total Stat1 from unstimulated cells and on pStat1(Tyr701) from IFNγ-stimulated cells, each normalized to the β-actin loading control. Bar graphs show mean +/- SD. Unpaired 2-tailed student's t-test with Welch's correction: *p<0.05 (pStat1) and **p<0.01 (Stat1). **(C)** *Top:* Immunoblotting of splenocytes from *WT* and mutant mice (n=3/group) for pStat1 (Tyr701) at 0, 60 and 120 minutes following withdrawal of IFNγ stimulation (as above). *Bottom*: densitometry quantification of pStat1 (normalized to β-actin loading control) plotted as percent of starting pStat1 at time 0, immediately after IFNγ withdrawal. Unpaired 2-tailed student's t-test with Welch's correction: p=0.6077 (60 minutes) and p=0.6183 (120 minutes).

bind HEp-2 liver cells, the gold standard method for ANA testing (50). ANA were undetectable in most mice of both genotypes between 6-9 weeks of age (Figure S1B). In contrast, by 15-20 weeks of age significantly more mutants were ANA$^+$ compared with their *WT* littermates (Figure 2D). Importantly, fluorescence intensity of ANA$^+$ sera was higher in mutants (Figure 2D), suggesting higher ANA concentrations.

We used several approaches to assess organ-specific autoimmunity. At 20 weeks of age, sera from *WT* and mutants had similar levels of liver enzymes (ALT, AST, ALP) and albumin, suggesting that mutants did not have autoimmune hepatitis (Figure S1C). In contrast, all mutants at this age displayed leukocytic infiltration in the pancreas manifesting as either peri-insulitis or insulitis of β-cell islets, a typical feature of T1D in mouse models (51),

10.3389/fimmu.2023.1183273

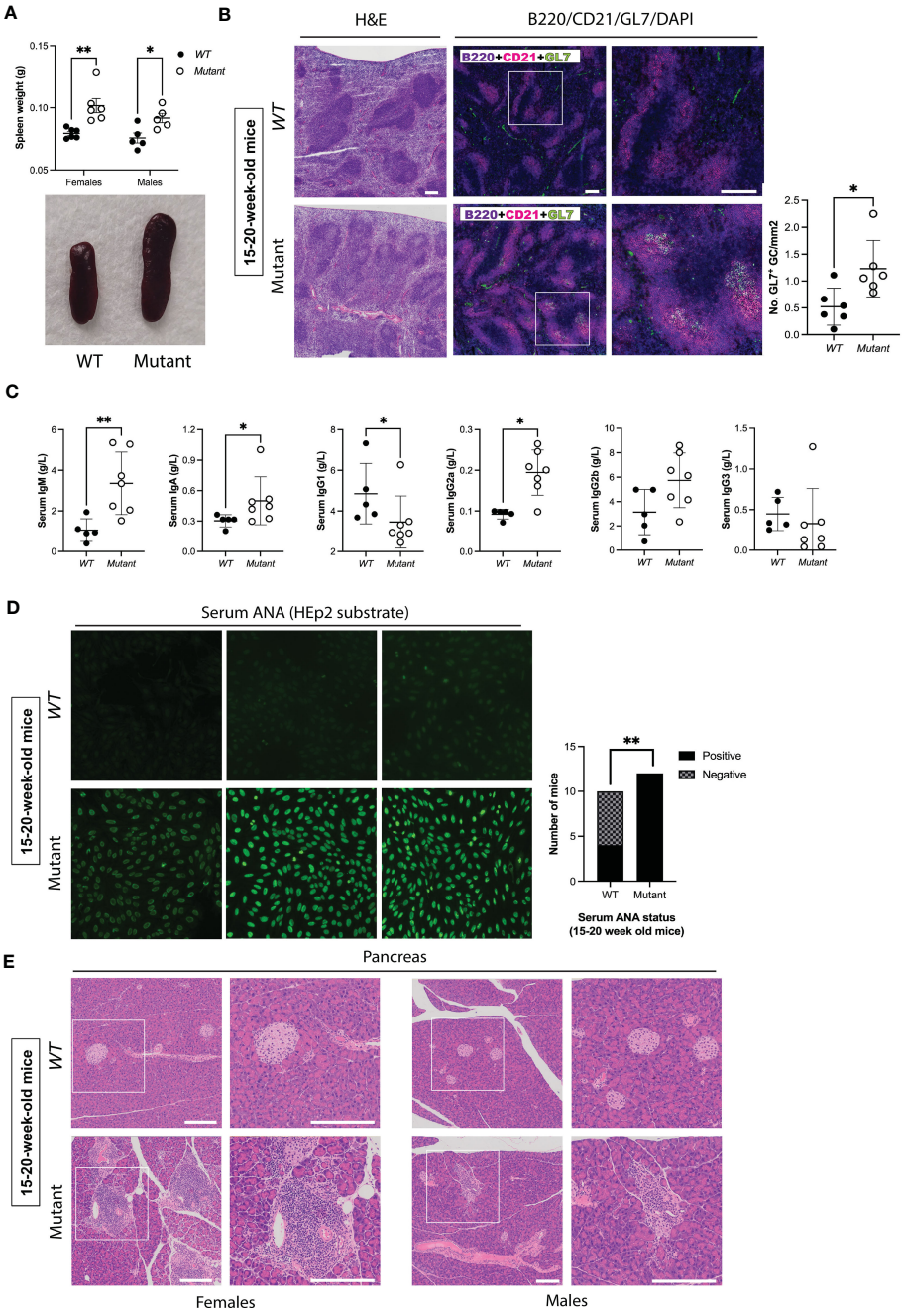


FIGURE 2
*Stat1*$^{T385M/+}$ mice develop spontaneous splenomegaly, increased germinal center formation, abnormal immunoglobulin isotype profiles and autoimmunity between 15-20 weeks of age. **(A)** Dot plots (*left*) show spleen weights in males and females, with means +/- SD indicated. Exemplar pictures are shown on the bottom. Two-way ANOVA FDR-adjusted p-values: **p<0.01 (females) vs *p<0.05 (males). **(B)** *Left*: H&E staining of spleen sections. *Middle:* Immunofluorescence staining of spleen sections with DAPI (blue), B220 (violet), CD21 (magenta) and GL7 (green). Panels on the right show area enlarged view of boxed area shown at lower magnification on the left, scale bar=200µm. *Right*: Quantification of the number of GL7$^{+}$ germinal centers (GC)/mm$^{2}$ per spleen (6 mice per genotype). Mann-Whitney test: *p<0.05. **(C)** Dot plots show serum levels of immunoglobulin isotypes, with means +/- SD indicated. Mann-Whitney p-values: **p<0.01 (IgM), *p<0.05 (IgA, IgG1, IgG2a), p=0.1061 (IgG2b), and p=0.2020 (IgG3). **(D)** Bar graphs (*left*) show the observed number of 20-week-old mice with negative or positive ANA detected by indirect immunofluorescence using HEp-2 cells at a screening dilution of 1:40. Fischer's exact test **p<0.01. Exemplar images shown on the left (40X magnification) demonstrate the spectrum of fluorescence observed for each genotype, and are representative of 12/12 mutants with positive serum ANA, and 6/10 *WT* with no detectable serum ANA at this age. **(E)** Histological assessment of pancreas by hematoxylin and eosin (H&E) staining. *Left:* Exemplar images are representative of 4/4 mutant females and 0/4 *WT* females by 20 weeks of age who developed pancreatic leukocytic infiltration. *Right:* Exemplar images are representative of 3/3 mutant males and 0/4 *WT* males who developed pancreatic leukocytic infiltration by 20 weeks of age. Panels on the right show enlarged views of boxed area shown at lower magnification on the left (scale bar=200µm).

compared with none in *WT* (Figure 2E). Mutant females had higher insulitis grades at 15–20 weeks of age compared with males (Figure 2E), whereas mutant males developed high grade insulitis by 1 year (Figure S1D). Overall, these data demonstrate age-dependent and female-biased excessive spontaneous splenic GC formation and autoimmune manifestations in *Stat1*$^{T385M/+}$ mice raised in SPF conditions.

## 3.3 Expansion of PD1$^+$ "memory phenotype" CD4 T cells precedes development of autoimmunity

To identify immune abnormalities that precede development of frank autoimmunity at 15-20 weeks of age, we used mass cytometry to profile immune cell lineages and activation states in spleen and mesenteric lymph nodes (LN) from a 9-week-old cohort of *Stat1*$^{T385M/+}$and *WT* littermates. *WT* and mutant spleens had similar numbers of B, NK, and most myeloid cell populations, except for a small increase in macrophages in mutants (Figures S2A–D). Although splenic T cell numbers were similar in mutant versus *WT* mice (Figure S2A), the ratios of CD4/CD8 T cell number were significantly higher in mutant females and males (Figure 3A), reflecting significantly more CD44$^+$ CD62L$^-$ CD4 cells in mutants (Figure 3B). These non-naïve "memory phenotype" (MP) cells, also known as "natural memory" T cells, develop in unimmunized mice under SPF conditions in response to low levels of tonic TCR and cytokine signaling (52). Interestingly, more mutant MP CD4 cells expressed PD1, a co-inhibitory receptor that marks the Tfh sub-lineage of CD4 T cells (Figure 3C), and the activation marker CD69 (Figure 3D), suggesting that mutant MP CD4 T cells were more activated. Importantly, numbers of PD1$^+$ CD44$^+$ and CD69$^+$ CD44$^+$ CD4 T cells were significantly increased only in female mutants (Figures 3C, D). Mutants also had more PD1$^+$ MP CD4 T cells in mesenteric LN, but the increase was less pronounced than in spleen (data not shown). In contrast to these significant impacts of *Stat1*$^{T385M}$ on CD4 T cells, PD1 was not elevated in mutant CD8 T cells and they had similar numbers of MP CD8 T cells (defined as CD44$^+$ CD122$^+$) as *WT* (Figure S2E and data not shown). In addition, 2-way ANOVA showed that sex significantly modified the impact of genotype on the abundance of MP CD44$^+$ CD62L$^-$ CD4 cells (interaction P=0.009). These data demonstrate that an early, selective expansion of PD1$^+$ MP CD4 T cells precedes the development of frank autoimmunity in both sexes, but in a more variable and robust fashion in females.

## 3.4 Expansion of ICOS$^+$ Tfh-like cells and activated B cells in 15-week-old mutant mice

Since *Stat1*$^{T385M/+}$ mice exhibited autoimmune manifestations by 15-20 weeks of age, we performed immune profiling on another cohort of *WT* and mutant mice aged to 15 weeks, adding additional markers for Tfh (ICOS) and T regulatory (FoxP3) CD4 cells. The ratio of CD4/CD8 T cell number was again increased, but the number of Foxp3$^+$ CD4 T cells was similar to *WT* (Figures S3A, B), revealing no impact of *Stat1*$^{T385M}$ on abundance of this important immunosuppressive subset. In contrast, mutants had more non-naïve CD62L$^-$ Foxp3$^-$ CD4 T cells (Figure 4A). Within this population, mutants had significantly more CD44$^+$ ICOS$^+$ cells (Figure 4B) and more PD1$^+$ ICOS$^+$ cells (Figure 4B), suggesting expansion of Tfh-like cells. Similar to our findings in 9 week-old mice, T cell differences in 15 week-old mice were generally more significant but also more variable in females (Figures 4A, B). T cell changes in mLN were similar to those identified in spleen, though slightly less robust (Figure S3C).

Tfh cells also promote differentiation and isotype class-switching in GC (31), and our histological analysis revealed increased GC B cells in 15-20 week-old mice (Figure 2B). Therefore, we profiled B cell differentiation states using CD21, IgM, IgD, CD95 and GL7. *WT* and mutant mice had similar numbers of total B cells, as well as classically defined follicular, marginal zone and transitional B cells (Figure S3D). However, mutants had more IgM$^{lo}$ IgD$^{lo}$ class-switched and more activated CD95$^+$ and CD95$^+$ GL7$^+$ GC B cells in the spleen (Figures 4C, D) and mLN (Figure S3E). Mutants also had more splenic CD21$^{lo}$ CD95$^+$ GL7$^-$ B cells (Figure 4E), a phenotype associated with Tbet$^+$ B cells found in certain autoimmune conditions in humans (53). Both CD95$^+$ subsets were greatly enriched among IgM$^{lo}$ IgD$^{lo}$ B cells, suggesting that in mutants, there were more activated B cells engaged in class-switching. Interestingly, in contrast to the T cell data, when the B cell data were dis-aggregated by sex the *Stat1*$^{T385M}$ impacts were only significant in females (Figures 4C–E). However, similar to the T cell data female mutants again showed greater variability than male mutants. Thus at 15 weeks of age, while both sexes exhibited significant expansion of Tfh-like MP CD4 cells, only female *Stat1*$^{T385M/+}$ mice exhibited a significant increase in activated and class-switched B cells.

Collectively, these immune profiling experiments revealed that *Stat1*$^{T385M/+}$ mice raised in SPF conditions exhibit early and prolonged expansion of Tfh-like MP CD4 in both sexes. These effects were more robust on average in females but also more variable and were seen in spleen and mLN. The *Stat1*$^{T385M}$ impacts on B cells were not evident until 15 weeks of age and were restricted to females at this timepoint.

## 3.5 *Stat1*$^{T385M}$ enhances CD4 T cell activation and imparts Tfh-like and Th1-like effector programs

To elucidate the transcriptional impact of *Stat1*$^{T385M}$ in T and B cells, we performed targeted scRNA-seq analysis of splenocytes from 15 week-old *WT* and mutant (n=3/group), quantifying transcripts encoding 397 immune genes as well as surface expression of 10 proteins detected with oligo-nucleotide tagged "AbSeq" antibodies. After de-multiplexing, we gated on CD19$^+$ IgD$^+$ B cells, TCRβ$^+$ CD4$^+$ and TCRβ$^+$ CD4$^-$ T cell subsets (Figure S4A). Importantly, mutants in this small cohort had higher ratios of CD4/CD8 T cells and of CD62L$^-$/CD62L$^+$ cells within the CD4 T cell compartment (Figure S4B), similar to flow cytometric profiling

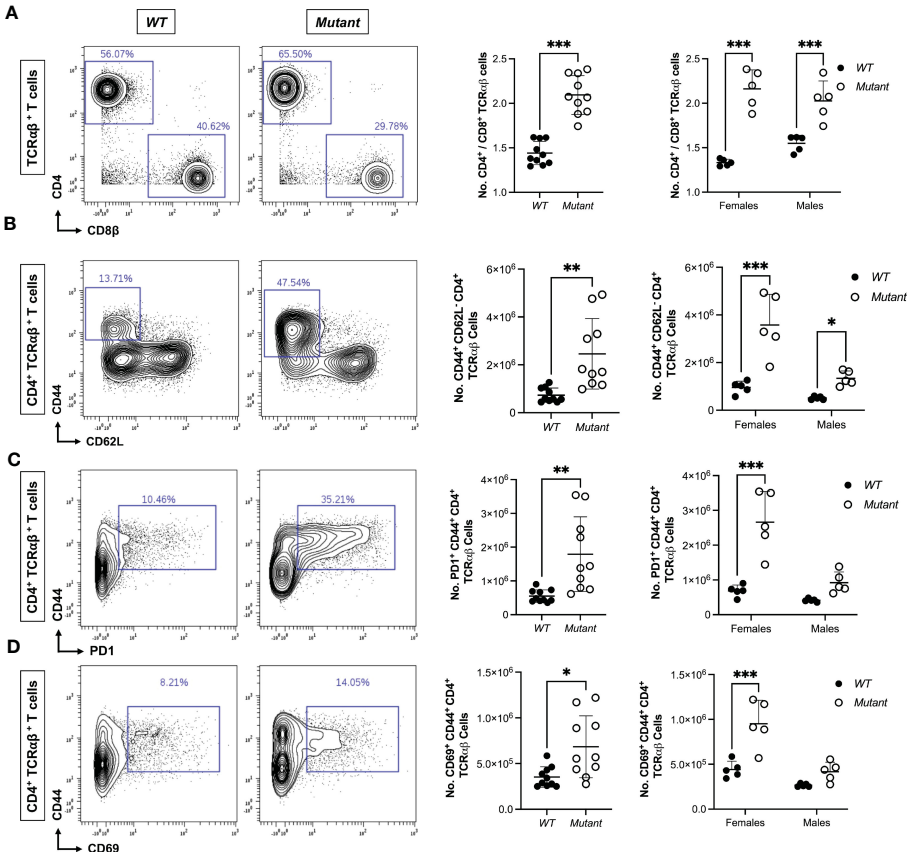


FIGURE 3
Expansion of activated splenic CD4 T cells precedes autoimmunity in *Stat1*$^{T385M/+}$ mice. Mass cytometric immune profiling of splenic T cells in 9 week-old mice. Unpaired Student's t-test with Welch's correction was used for all sex-aggregated genotype comparisons. Two-way ANOVA with *post-hoc* t-test was used for all genotype comparisons dis-aggregated by sex. **(A)** Left: Contour plots show CD4 vs CD8 expression gated on TCRαβ$^+$ splenic T cells from exemplar mice of each strain. Right: summary dot plots show ratio of CD4$^+$/CD8$^+$ T cell numbers in all mice by genotype. Sex-aggregated (***p<0.001) and dis-aggregated [***p<0.001 (mutant vs. *WT* females), ***p<0.001 (mutant vs. *WT* males), interaction *p=0.03] data are shown. **(B)** Left: CD44 vs CD62L expression gated on CD4$^+$ TCRαβ$^+$ splenic T cells from exemplar mice of each strain. Right: summary dot plots show absolute numbers of CD44$^+$ CD62L$^-$ (MP) CD4$^+$ T cells in all mice by genotype. Sex-aggregated (**p<0.01) and dis-aggregated [***p<0.001 (mutant vs. *WT* females), *p<0.05 (mutant vs. *WT* males), interaction **p=0.009] data are shown. **(C)** Left: Contour plots show CD44 vs PD1 expression gated on CD4$^+$ TCRαβ$^+$ splenic T cells from exemplar mice of each strain. Right: summary dot plots show absolute numbers of PD1$^+$ CD44$^+$ CD4$^+$ T cells in all mice by genotype. Sex-aggregated (**p<0.01) and dis-aggregated [***p<0.001 (mutant vs. *WT* females), P=0.11 (mutant vs. *WT* males), interaction **p=0.003] data are shown. **(D)** Left: Contour plots show CD44 vs CD69 expression gated on CD4$^+$ TCRαβ$^+$ splenic T cells from exemplar mice of each strain. Right: summary dot plots show absolute numbers of CD69$^+$ CD44$^+$ CD4$^+$ T cells in all mice by genotype. Sex-aggregated (*p<0.05) and dis-aggregated [***p<0.001 (mutant vs. *WT* females), P=0.07 (mutant vs. *WT* males), interaction *p=0.02] data are shown. For all dot plots, mean +/- SD are presented.

of the larger cohort reported above. We then merged the individual samples from each group to identify genes whose expression differed significantly (≥40% with FDR-adjusted q-value of <0.05) between *WT* vs mutant in each of the 3 subsets. *Stat1* itself was among the top DEG and was over-expressed in all mutant lymphocyte populations (Figure 5A; Figures S4C, D, Tables S1–S3), in keeping with its known capacity to positively regulate its own expression (6). There were more over-expressed than under-expressed genes in mutants relative to *WT*, suggesting that *Stat1*$^{T385M}$ acted primarily as a transcriptional activator in all lineages. Interestingly, *Stat1* was more highly upregulated in mutant T cells relative to mutant B cells. CD4 T cells had ~3-4 times as many DEG as CD8 T cells or B cells and most were over-expressed in mutants (n=33; Figure 5A), suggesting that *Stat1*$^{T385M}$ had the greatest transcriptional impact on CD4 T cells.

Among the genes significantly down-regulated in mutant CD4 T cells were several associated with a naïve quiescent state (54, 55), such as *Sell* (encoding CD62L), *Ccr7, Il6ra, Il7ra*, and *Bach2* (Figure 5B top), suggesting that they were more activated. This group also included *Lef1* and *Tcf7*, which restrain induction of co-inhibitory receptors and promote expression of Tfh genes during anti-virus responses (33–35); *Tcf7* also restrains induction of cytotoxicity genes in CD8 T cells (55). Conversely, mutant CD4 T cells significantly over-expressed several genes encoding immunoregulatory receptors known to be induced during T cell activation (56) (Figure 5C top), including *Tnfrsf4* (encoding Ox40), *Tnfsfr1b* (encoding Tnfr2), *Pdcd1*, *Lag3, Cd200, Tigit, Ctla4* and *Nt5e* (encoding CD73). Mutant CD4 T cells also over-expressed the Tfh-associated genes *Icos, Cxcr5, Il21 and Ikzf2* (31, 57, 58); however, *Bcl6*, the master Tfh regulator (31), was not

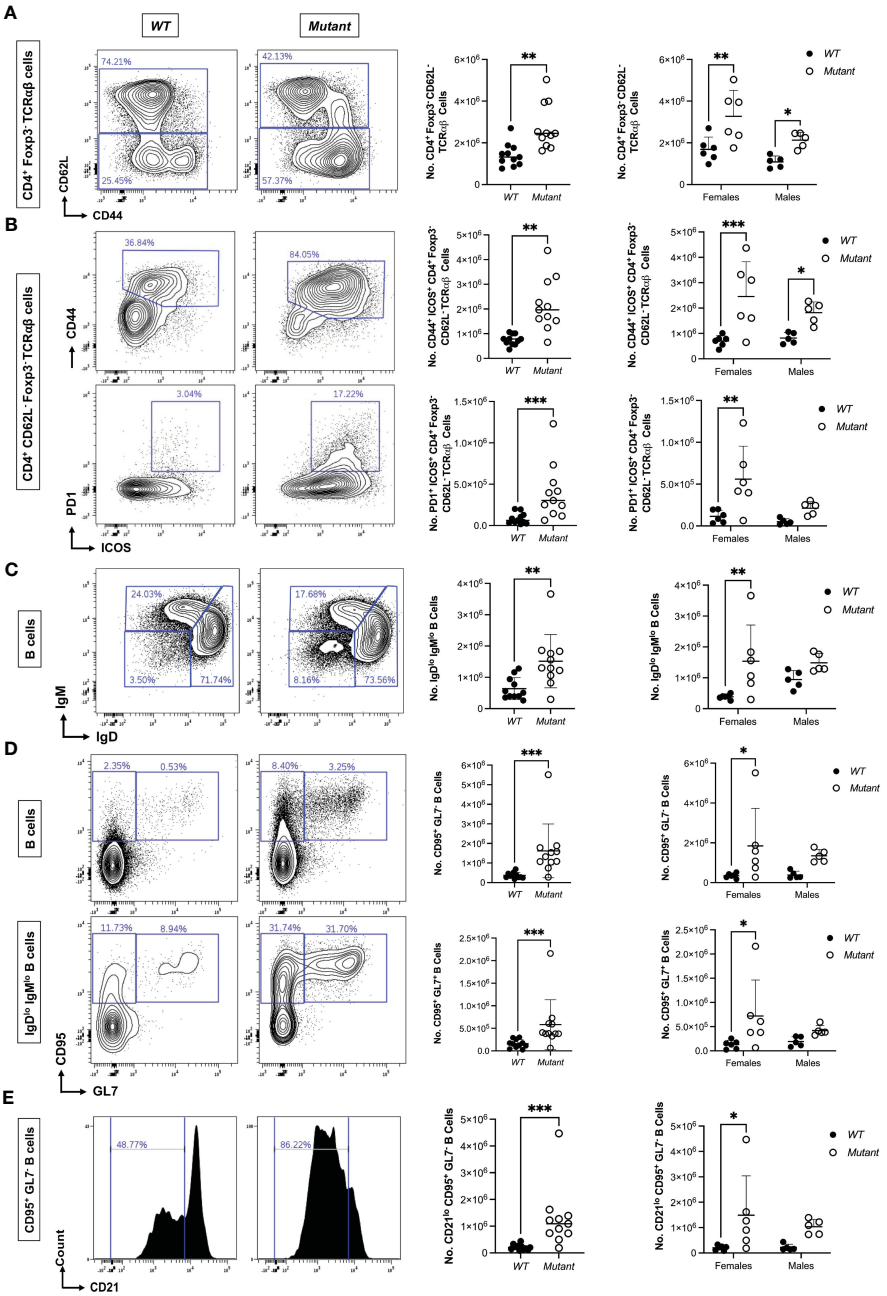


FIGURE 4
Expansion of ICOS$^+$ PD1$^+$ Tfh-like MP CD4 cells and activated B cells in 15 week-old *Stat1*$^{T385M/+}$ mice. Flow cytometric immune profiling of splenic T cells in 15 week-old mice. Unpaired student's t-test with Welch's correction was used for all sex-aggregated genotype comparisons except where Mann-Whitney tests are indicated below. Two-way ANOVA with *post-hoc* t-test was used for all genotype comparisons dis-aggregated by sex. **(A)** *Left:* Exemplar contour plots of CD44 vs CD62L expression gated on CD4$^+$ Foxp3$^-$ TCRαβ$^+$ splenic T cells from each strain. *Right*: Summary dot plots of CD62L$^-$ CD4$^+$ Foxp3$^-$ T cell numbers per spleen by genotype. Sex-aggregated (Mann-Whitney **p<0.01) and dis-aggregated [**p<0.01 (females) vs *p<0.05 (males), interaction p=0.42] data are shown. **(B)** *Top left*: Exemplar contour plots of CD44 vs ICOS expression gated on CD4$^+$ Foxp3$^-$ CD62L$^-$ TCRαβ$^+$ splenic T cells from each strain. *Bottom left:* Exemplar contour plots of PD1 vs ICOS expression gated on CD4$^+$ Foxp3$^-$ CD62L$^-$ TCRαβ$^+$ splenic T cells from each strain. *Top right*: Summary dot plots of numbers of ICOS$^+$ CD44$^+$ CD62L$^-$ CD4 cells per spleen by genotype. Sex-aggregated (**p<0.01) and dis-aggregated [***p<0.001 (females) vs *p<0.05 (males), interaction p=0.27] data are shown. *Bottom right*: Summary dot plots of numbers of ICOS$^+$ PD1$^+$ CD62L$^-$ CD4 cells per spleen by genotype. Sex-aggregated (Mann-Whitey ***p<0.001) and dis-aggregated [**p<0.01 (females) vs p=0.13 (males), interaction p=0.14] data are shown. **(C)** *Left*: Exemplar contour plots of IgM vs IgD gated on CD19$^+$ splenic B cells from each strain. *Right*: Summary dot plots of IgM$^{lo}$ IgD$^{lo}$ B cell numbers per spleen by genotype. Sex-aggregated (**p<0.01) and dis-aggregated [**p<0.01 (females) vs p=0.11 (males), interaction p=0.29] data are shown. **(D)** *Left*: Exemplar contour plots of CD95 vs GL7 expression gated on either total (*top*) or IgM$^{lo}$ IgD$^{lo}$ (*bottom*) splenic B cells. *Right*: Summary dot plots of absolute number of activated CD95$^+$ GL7$^-$ (top) or CD95$^+$ GL7$^+$ (bottom) B cells per spleen. For CD95$^+$ GL7$^-$ B cells, sex-aggregated (Mann-Whitney ***p<0.001) and dis-aggregated [*p<0.05 (females) vs p=0.08 (males), interaction p=0.55] data are shown. For CD95$^+$ GL7$^+$ B cells, sex-aggregated (Mann-Whitney ***p<0.001) and dis-aggregated [*p<0.05 (females) vs p=0.2 (males), interaction p=0.3] data are shown. **(E)** *Left*: Exemplar histogram of CD21 gated on CD95$^+$ GL7$^-$ splenic B cells. *Right*: Summary dot plots of CD21$^{lo}$ CD95$^+$ GL7$^-$ B cell numbers in all mice by genotype. Sex-aggregated (Mann-Whitney ***p<0.001) and dis-aggregated [*p<0.05 (females) vs p=0.07 (males), interaction p=0.52] data are shown. For all dot plots, mean +/- SD are presented.

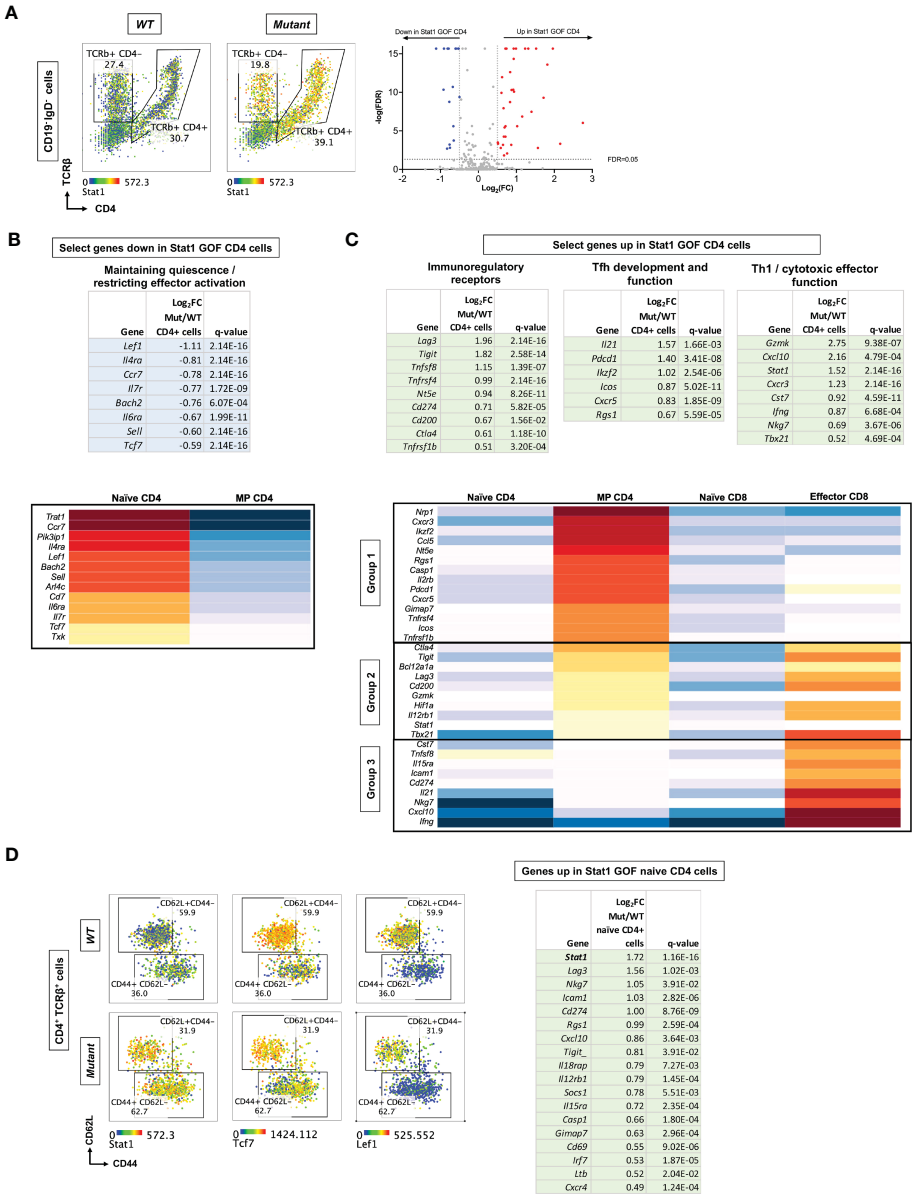


FIGURE 5
scRNA-Seq profiling of immune gene expression in *WT* versus *Stat1*$^{T385M/+}$ spleen cells from 15 week-old mice. **(A)** (*Left*): Dot plots show CD4 and TCRβ expression on CD19$^-$ IgD$^-$ cells, defining CD4 T cells (CD4$^+$ TCRβ$^+$) and CD8 T cells (CD4$^-$ TCRβ$^+$ expressing *Cd8b1*- see Figure S4D). Overlaid heatmap shows *Stat1* expression in CD4 and CD8 T cells. (*Right*): Volcano plots show DEG between mutant and *WT* CD4 T cells, plotted according to Log$_2$fold change [Log$_2$FC (mutant/*WT*)], against the negative logarithmic value of the false discovery rate (-logFDR). Genes up-regulated or down-regulated in mutant are denoted in red and blue, respectively. (B, C) *Top:* Tables show select genes down-regulated **(B)** or up-regulated **(C)** in mutant CD4 T cells by 40% or more. Gene expression tables show Log$_2$FC values and FDR-adjusted q-values <0.05. *Bottom:* Heatmap visualization of genes down-regulated **(B)** or up-regulated **(C)** in mutant CD4 cells in selected splenic T cell reference populations from the Immunological Genome Project (45): naïve CD4 or CD8 cells, MP CD4 cells and effector CD8 cells (isolated 12h following infection with *Listeria*). Upregulated genes were grouped (1–3) according to their pattern of expression in the reference populations. **(D)** *Left:* Dot plots show CD44 vs CD62L expression on CD4$^+$ TCRβ$^+$ cells in mutants and *WT*, distinguishing naïve CD62L$^+$CD44$^-$ from MP CD44$^+$ CD62L$^-$ CD4 cells. Expression levels of genes of interest are overlaid as heatmaps. *Right:* Table shows genes upregulated in mutant naive CD4 T cells by 40% or more. FC values are presented along with FDR-adjusted q-values <0.05.

differentially expressed. Several cytotoxicity/Th1-associated molecules were also overexpressed: *Tbx21* encoding Tbet, *Ifng*, *Cst7*, *Nkg7* and *Gzmk* (Figure 5C top). This signature suggested that *Stat1*$^{T385M}$ may enhance CD4 T cell activation while also imparting both Tfh-like and Th1-like effector programs.

To better understand the unusual differentiation state of CD4 T cells from *Stat1*$^{T385M/+}$ mice, we visualized how the DEG were expressed by reference *WT* CD4 and CD8 T cell populations profiled by the Immunological Genome Project (45). Notably, all genes expressed at lower levels in mutant CD4 cells were more highly expressed by reference naïve compared to reference MP CD4 cells (Figure 5B, bottom). This finding confirms that *Stat1*$^{T385M}$ downregulates genes associated with the naïve state of normal CD4 T cells. We also visualized how genes up-regulated in mutant CD4 T

cells were expressed in reference naïve and MP CD4 subsets. We added a reference effector CD8 subset, since we had observed several cytotoxicity-associated genes among those upregulated by *Stat1*$^{T385M}$. Interestingly, the *Stat1*$^{T385M}$-upregulated genes fell into 3 groups (Figure 5C, bottom). Group 1 genes were most highly expressed by reference MP CD4 cells, and included *Nrp1, Icos, Pdcd1 and Cxcr5*, suggesting that these Tfh-associated genes are also up-regulated as part of the natural CD4 memory program. Group 2 genes were highly expressed by reference MP CD4 and effector CD8 cells, and included *Ctla4, Lag3, Tigit, Stat1, Tbx21* and *Gzmk*. Finally, Group 3 genes were most highly expressed by reference effector CD8 cells, and included *Cst7*, *Nkg7*, *Ifng, Cxcl10, Il21, Il15ra* and *Cd274* (encoding PD-L1). This analysis confirmed that mutant CD4 T cells over-express Tfh-associated and other genes that distinguish *WT* naïve from MP CD4 cells, but they also expressed genes associated with cytotoxic differentiation.

To determine which aspects of the *Stat1*$^{T385M}$-associated gene expression program identified above were already present in the naïve state, we performed DEG analysis comparing WT vs mutant naïve CD62L$^{+}$ CD44$^{-}$ as well as MP CD44$^{+}$ CD62L$^{-}$ CD4 cells (Figure 5D; Tables S4, S5). Interestingly, *Stat1* was the most highly over-expressed gene in mutant naive CD4 T cells, which also over-expressed certain activation (*Lag3, Tigit, Cd69, Icam1*), IFN-regulated (*Cd274, Socs1, Cxcl10*), cytokine receptor (*Il12rb1* and *Il15ra*) and cytotoxicity (*Nkg7*) genes (Figure 5D; Table S2). Indeed, several genes belonging to each of the 3 Groups of up-regulated genes identified in total CD4 cells (Figure 5C) were overexpressed specifically in mutant naive CD4 cells. As expected, many of the up-regulated genes in total mutant CD4 cells were also up-regulated specifically in mutant MP CD4 cells (Table S4). Additionally, mutant MP CD4 cells had decreased expression of *Ccr6* and *Rorc* (encoding RORγt), suggesting that *Stat1*$^{T385M}$ inhibited Stat3 activation and impaired Th17 effector differentiation, as previously observed in STAT1 GOF patients (15). Other lineage-defining transcription factors (*Gata3, Foxp3*) were not differentially expressed between *WT* and mutants.

We also used Seurat to perform unsupervised multimodal (mRNA and AbSeq) dimensionality reduction and clustering to ask whether mutants contained T or B cell subsets with unique immune gene profiles. Among the 14 clusters with >100 cells in merged *WT* or mutant samples, there were two myeloid (macrophages and monocytes), seven B cell and five T cell clusters that were all present in both *WT* and mutant samples (Figures 6A, B and Table S6A). Thus, targeted single cell profiling of immune gene and protein expression by total splenocytes identified multiple clusters of naïve and activated/effector of T and B cells. However, mutant-specific T or B cell clusters were not detected, suggesting that *Stat1*$^{T385M}$ did not promote differentiation of a trancriptionally unique T or B cell effector subset.

All mutant B cell clusters expressed more *Stat1* than their *WT* counterparts (Figure 6C; Table S6C). Five of seven also over-expressed *Tbx21* and/or its target *Cxcr3*; both are known to regulate B cell proliferation and migration to the GC dark zone during malaria infection (59). Indeed, several mutant B cell clusters over-expressed one or more GC-associated genes such as *Fas/CD95* (60), *Irf8* (61) and *Icam1* (62), as well as *Igh* isotypes that result from class-switching. A similar set of GC-associated genes were also up-regulated in our comparison of total mutant versus *WT* B cells (Table S3). GC B cells are highly proliferative, but high levels of cell cycle-associated genes such as *Pclaf, Mki67* and *Pcna*, were restricted to a single small B cell cluster (#14), which was more abundant in mutants (Figure 6C; Table S6B). This unsupervised analysis showed that *Stat1*$^{T385M}$ activated aspects of the GC B cell program, though not *Bcl6*, across multiple B cell subsets.

Among the five T cell clusters, Seurat identified *Sell*$^{+}$ (encoding CD62L) naïve and *Sell*$^{-}$ non-naïve CD4 and CD8 T cell subsets. A comparison of mutant/*WT* CD8 clusters yielded a small number of DEG highly similar to those identified in our analysis of total CD8 T cells, with the addition of *Gzmk* in naïve CD8 cells (Figure S4). The two non-naïve CD4 T cell clusters (6 and 11) expressed high levels of *Il2rb*, *Tbx21, Cxcr3*, together with the Tfh-associated genes *Pdcd1, Icos, Ctal4* and *Tigit*, suggesting a hybrid Tfh/Th1 program (Figure 6C). Mutant clusters 6 and 11 expressed higher levels of these genes and/or proteins together with more *Stat1*, *Gzmk, Cxcl10, Il21, Lag3, Nt5e* and *Tnfrsf4* to name a few (Table S6C). Overall, unsupervised and immunophenotype-guided analysis of single cell immune gene expression identified highly overlapping sets of DEG which collectively suggested that *Stat1*$^{T385M}$ activated transcription of GC-associated programs in both B and T cells. However, *Stat1*$^{T385M}$ had the strongest transcriptional impact on T cells, promoting aberrant activation of naïve CD4 cells and inducing their differentiation into hybrid Tfh/Th1-like effector cells.

# 4 Discussion

We generated and characterized *Stat1*$^{T385M/+}$mice to model the impact of the DBD class of STAT1 GOF mutations on immune homeostasis under SPF conditions in both males and females. Similar to patients with STAT1 GOF (46), *Stat1*$^{T385M/+}$ lymphocytes had more total Stat1 at baseline and also higher amounts of IFNγ-induced pStat1. By 9 weeks of age, *Stat1*$^{T385M/+}$ mice showed expansion of MP CD4 cells expressing Tfh-like markers, in spleen and in gut-draining mLN, with no observed autoimmunity. By 15-20 weeks of age mutants also displayed B cell activation, increased GC formation, abnormal immunoglobulin isotype profiles and development of autoimmunity. Notably, females developed these immune abnormalities sooner and more robustly than males, identifying significant sex effects for this mouse model of STAT1 DBD GOF. Single cell analysis showed that although *Stat1* was significantly up-regulated in both T and B cells from *Stat1*$^{T385M}$ mutants, its most predominant impact was to promote aberrant activation of naïve CD4 cells and induce their differentiation into hybrid Tfh/Th1-like effector cells. Collectively, these data demonstrate that *Stat1*$^{T385M}$ increased basal and cytokine-stimulated Stat1 activation in lymphocytes, disrupting naïve CD4 T cell homeostasis and promoting differentiation of abnormal T helper cells with cytotoxic features (63) as well as GC-like B cells, eventually resulting in autoimmunity in the absence of overt infection. These findings potentially explain how human STAT1 GOF causes immune dysregulation and autoimmunity.

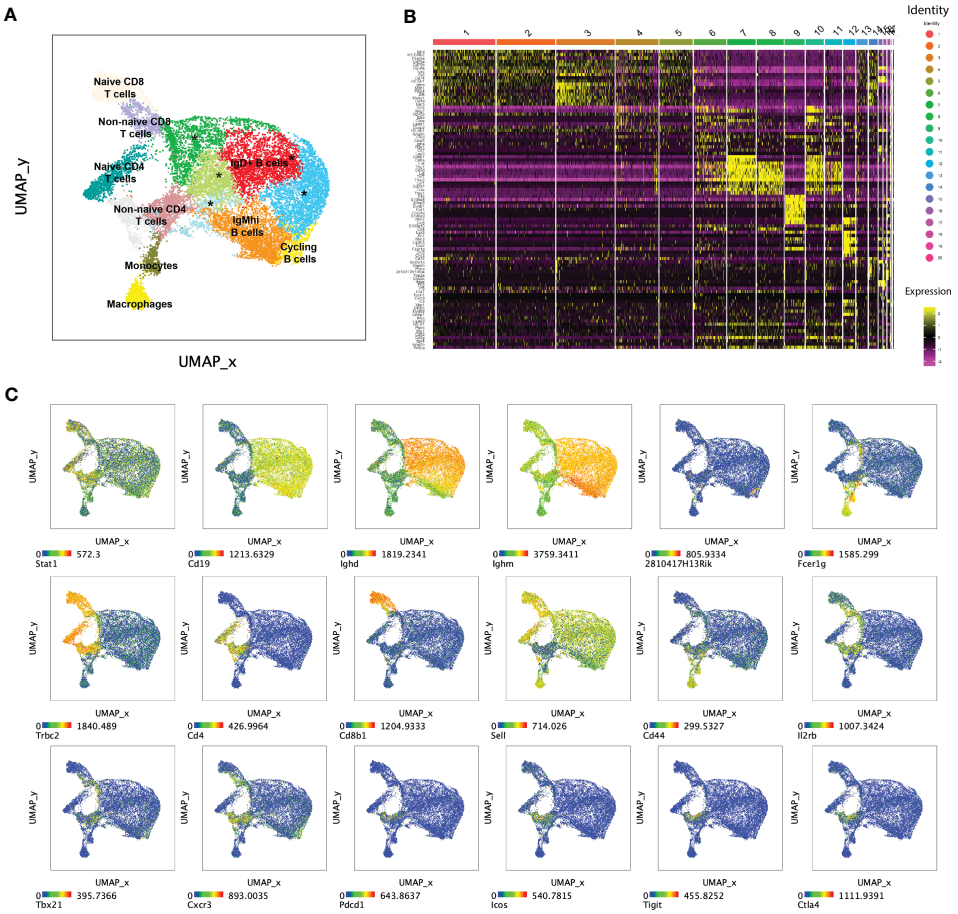


FIGURE 6
Seurat multi-modal clustering of 15 week-old mouse splenocytes. **(A)** Plot shows uniform manifold approximation and projection (UMAP) dimensionality reduction overlayed with Seurat-generated clusters on aggregated WT and mutant cells. Clusters marked with an asterisk (*) represent IgD+ B cells. **(B)** Heatmap shows relative expression of Seurat-defined "marker" genes across 20 Seurat-generated clusters. **(C)** Dot plots show UMAP of aggregated WT and mutant cells colored by expression levels of informative transcripts. Note that 2810417H13Rik encodes Pclaf (PCNA clamp associated factor), a cell cycle regulatory gene.

The biochemical, immunophenotypic and overt autoimmune abnormalities we observed in *Stat1*$^{T385M/+}$ mice differ from previously published studies modeling the immune impacts of STAT1 GOF mutations in the coiled-coil domain. In *Stat1*$^{R274W/+}$ (64) mice, total Stat1 was not increased at baseline, and IFN-induced Stat1 hyper-phosphorylation was noted in T cells; however T cell numbers were normal (64). *Stat1*$^{R274Q/+}$ mice also showed increased IFN-stimulated pStat1 in gut CD4$^{+}$ T-cells (65). However, autoimmunity was not reported in either model, and viral or fungal infection was required to induce overt immunophenotypic or transcriptional changes in both. In contrast, splenocytes from our *Stat1*$^{T385M/+}$ mice had more total Stat1 at baseline and in IFNγ-induced pStat1 but normal Stat1 dephosphorylation kinetics, all in keeping with observations made in patient cells (46). The immunophenotypic and transcriptional profiles of *Stat1*$^{T385M/+}$ mice were also significantly different from *WT* in our SPF colony. These findings suggest that there is differential pathogenicity of STAT1 GOF mutations; the T385M DBD mutation selectively disrupted immune homeostasis and promoted autoimmunity in the absence of deliberate stimulation or infection.

Here we report significant sex effects for both the kinetics and magnitude of immune abnormalities in our *Stat1*$^{T385M/+}$ GOF mouse model. Female mutants developed splenomegaly earlier, and also displayed more robust increases in MP CD4 cells between 9-15 weeks. These cells also expressed significantly higher amounts of PD1 and ICOS, suggesting that MP CD4 cells were more activated than in males. By 15 weeks, activated IgD$^{lo}$ IgM$^{lo}$ GC B cells were significantly elevated only in females. In contrast, studies of humans or other mouse models with STAT1 GOF did not report sex effects on development of immune abnormalities and autoimmunity. Most human autoimmune diseases preferentially affect females due to a combination of factors, including increased expression of X-linked innate and adaptive immune genes, heightened type I IFN secretion mediated by estrogens, and microbiome differences (22, 66). Additionally, *STAT1* contains an estrogen-response element, suggesting an IFN-independent role for estrogens in STAT1 activation (67). However, sex effects identified in mice do not always apply to humans. For instance, while female mice show a higher predisposition than males to developing T1D, whereas

humans of both sexes develop T1D in nearly equal ratios (22). Investigation of the possible sex effect of autoimmunity in human STAT1 DBD GOF is therefore warranted, including assessment of the types of autoimmune manifestation, age of onset and severity.

*Stat1*$^{T385M}$ had the greatest immunophenotypic impact on MP CD4 T cells, which in *WT* mice, differentiate in response to homeostatic TCR signaling and cytokine stimulation. MP CD4 T cells are generated in mice free of all microbes and exogenous food antigens (52), suggesting that they differentiate cell autonomously and/or in response to self-antigens. While we cannot rule out the contribution of commensal microbes to the immune changes observed in our SPF *Stat1*$^{T385M/+}$ mice, these changes were not more prominent in gut-draining mLN, as would be expected if commensal gut microbiota drove CD4 T cell activation. Further studies will be required to determine the role of self- versus foreign-antigens as well TCR and cytokine signaling in driving aberrant MP CD4 T cell differentiation in this mouse model of STAT1 DBD GOF.

*Stat1*$^{T385M}$ had also the greatest transcriptional impact on CD4 T cells, which over-expressed several Tfh-associated genes a well as immunoregulatory receptors associated with Tfh and also with chronic T cell activation and exhaustion. Elevated expression of co-inhibitory activation markers, such as PD-L1 and Fas was previously reported in STAT1 GOF patient CD4 T cells, and was suggested as a mechanism potentially leading to T cell exhaustion over time (39, 68, 69). Although *Stat1*$^{T385M}$ MP CD4 T cells did not over-express *Bcl6*, which encodes the master regulator of Tfh differentiation (70), they over-expressed several other Tfh-associated genes such as *Icos, Pdcd1, Icam1, Ikzf2, Il21*and *Cxcr5*, suggesting that *Bcl6* up-regulation is not required to induce these genes when Stat1 is activated. Similar to early Tfh cells, mutant CD4 T cells also expressed *Il21* but not *Il4*; the latter cytokine is made only by fully differentiated Tfh cells (31). IL21 together with other signals can drive B cell proliferation and differentiation both within and outside of the GC. Therefore, it seems likely that, in addition to a primary impact of *Stat1*$^{T385M}$ on B cells, the expanded Tfh-like cells may also have contributed to the increase in activated B cells and excessive splenic GC formation. Interestingly, T cell-intrinsic overproduction of IFNγ also causes accumulation of Tfh cells, GC B cell activation and SLE (71), phenomena that are likely linked to Stat1 activation. Our scRNA-Seq based immune gene profiling showed that in addition to early Tfh-like features, *Stat1*$^{T385M}$ CD4 T cells also expressed a cytotoxic CD8/Th1-like effector program. Although multiple lines of evidence show that Bcl6 and Tbet cross inhibit each other, infection-induced Tfh cells can transiently express Tbet and Th1 features (70, 72–75). Thus, STAT1 GOF mimics some aspects of infection-induced Tfh differentiation. During acute viral infection, IL6 activates both Stat1 and Stat3, with the latter being required to limit IL2/Stat5-induced Th1 differentiation (9, 76, 77). However, this break on Th1 differentiation may be impaired in *Stat1*$^{T385M}$ CD4 T cells since activated Stat1 inhibits Stat3. Peripheral blood from STAT1 GOF patients shows variable in Th1 cells, circulating Tfh (cTfh) cells as well as cTfh with "Th1-like" features (such as increased Tbet and CXCR3 expression) (26–28, 36, 78). Thus, our *Stat1*$^{T385M/+}$ mouse model recapitulates several features of abnormal CD4 T cell differentiation seen in STAT1 GOF patients, but in the absence of infection.

Interestingly, naïve CD4 T cells highly over-expressed *Stat1* and also displayed some aspects of the *Stat1*$^{T385M}$-driven abnormal program, which became more prominent in MP CD4 T cells. However, these phenotypically naïve cells also exhibited unique transcriptional changes, likely setting the stage for abnormal differentiation. They overexpressed *Il2rb* and *Il15ra*, cytokine receptors that drive differentiation of MP CD4 cells (52). Notably, mutant CD4 T cells expressed significantly lower amounts of *Tcf7* and *Lef1*, transcription factors which restrain expression of the *Ctla4* and *Lag3* co-inhibitory receptors in Tfh cells (35), providing a potential mechanism for over-expression of these genes in mutant CD4 T cells. *Tcf7* and *Lef1* also restrain expression of cytotoxicity genes in naïve CD8 cells (55), so their downregulation, together with Stat1 GOF, could contribute to the up-regulation of a Type I/cytotoxicity program marked by expression of *Tbx21, Gzmk, Nkg7, Cst7*, *Cxcr3* and *Cxcl10. Tcf7* and *Lef1* also critically regulate Tfh differentiation and *Bcl6* induction during infection-induced Tfh differentiation (33, 35), so their *Stat1*$^{T385M}$-induced down-regulation could contribute to the lack of *Bcl6* expression by mutant Tfh-like CD4 cells. *Stat1*$^{T385M}$-induced *Tbx21* could also contribute to the lack of *Bcl6* expression. While the precise molecular mechanisms remain to be elucidated, our findings suggest that *Stat1*$^{T338M}$ alters expression of key transcription factors to aberrantly activate naïve CD4 T and promote their differentiation into hybrid Tfh/Th1-like CD4 cells under homeostatic conditions, ultimately promoting autoimmunity in the absence of infection.

## Data availability statement

The datasets presented in this study can be found in online repositories. The names of the repository/repositories and accession number(s) can be found below: PRJNA949654 (SRA).

## Ethics statement

The animal study was reviewed and approved by The Centre for Phenogemonics Animal Care Committee.

## Author contributions

Study conceptualization by OS, CG, CR, EA, RC. Methodology by OS, SV, BG, CG. Investigation by OS, SV, ER, DM, CG. Data analysis by OS, CG. Visualization by OS, CG. Supervision by RC, CR, CG and EI. Funding acquisition by OS, CR, RC. Writing - original draft by OS. Writing – review and editing by OS, SV, ER, DM, BG, CR, DC, CG, EI. All authors contributed to the article and approved the submitted version.

## Funding

Funding for this work was provided by Rare Disease Models and Mechanisms Network (RDMM) Catalyst Grant (190829-001-002; PIs: CMR and RDC), the Primary Immunodeficiency Treatment Consortium Fellowship Award (PIDTC 12082sc; PI: OS), Canadian Institutes for Health Research Operating Grant 165973 (PI: CJG) and Immunodeficiency Canada Young Investigator Award (PI: OS). Salary support for OS has been provided by the Ontario Ministry of Health Clinician Investigator Program (MOH-CIP), Empowering Next Generation Researchers in perinatal and Child Health (ENRICH), The Hospital for Sick Children Clinician Scientist Training Program (CSTP), and the Canadian Institutes of Health Research (CIHR) Canada Graduate Scholarship Doctoral Award (CGS-D).

## Acknowledgments

Figure 1 was generated using Biorender (app.biorender.com). RNA-Seq was performed at The Centre for Applied Genomics with support from Genome Canada/Ontario Genomics Institute and the Canada Foundation for Innovation (CFI). Flow cytometry, mass cytometry and Rhapsody single cell multi-omics were performed at the SickKids Flow Cytometry Facility and the Centre for Advanced Single Cell Analysis, supported by the SickKids Foundation and a CFI John Evans Fund Leaders grant to CJG.

## Conflict of interest

The authors declare that the research was conducted in the absence of any commercial or financial relationships that could be construed as a potential conflict of interest.

## Publisher's note



## Supplementary material

The Supplementary Material for this article can be found online at: https://www.frontiersin.org/articles/10.3389/fimmu.2023.1183273/full#supplementary-material

SUPPLEMENTARY FIGURE 1
Autoimmune manifestations in Stat1T385M/+ mice from 6 weeks to 1 year of age. (A) Dot plots show spleen weights in 9-week-old males and females, with means +/- SD indicated. Two-way ANOVA: FDR-adjusted p-values: *p<0.05 (females) vs p=0.42 (males). (B) Bar graphs show the observed frequency of serum positivity for anti-nuclear antibodies (ANA) as detected in 6-9-week-old mice via indirect immunofluorescence using HEp-2 substrate, at a screening dilution of 1:40. Fischer's exact test **p>0.999. (C) Dot plots show serum values of liver parameters including alanine amino transferase (ALT), aspartate aminotransferase (AST), alkaline phosphatase (ALP) and albumin in 20 week-old mutants and *WT* littermates, with means +/- SD indicated. Mann-Whitney test: p=0.5224 (ALT), p=0.6482 (AST), p=0.6601 (ALP) and p=0.8911 (albumin). (D) Histological assessment of pancreas from 1-year-old males by H&E staining. Data shown are representative of 3/3 mutants and 0/3 *WT* mice who developed pancreatic insulitis. Panels on the right show area-enlarged view of boxed area shown at lower magnification on the left, scale bar= 200μm.

SUPPLEMENTARY FIGURE 2
Mass cytometric immune profiling of splenocytes in 9 week-old mice. (A) *Left:* Exemplar contour plots show CD3 vs CD19 expression gated on live single splenic cells from each strain. Two-way ANOVA with post-hoc t-test was used for all genotype comparisons dis-aggregated by sex. *Right:* summary dot plots show absolute numbers of B, T, and non-T, non-B cells by sex and genotype. B cells: p=0.06 (females) vs p=0.34 (males). T cells: p=0.72 (females) vs p=0.72 (males). Non-T, non-B cells: p=0.56 (females) vs p=0.41 (males). (B) *Left:* Exemplar contour plots show CD122 vs NK1.1 expression gated on non-T non-B cells from each strain. *Right:* summary dot plots show absolute numbers of NK cells by sex and genotype: p=0.79 (females) vs p=0.79 (males). (C) *Left:* Exemplar contour plots show Sirpα vs Ly6G expression gated on non-T/B/NK cells from each strain. *Right:* summary dot plots show absolute numbers of granulocytes by sex and genotype: p=0.53 (females) vs p=0.11 (males). (D) *Left:* Exemplar contour plots show SiglecF vs CD64 expression gated on Sirpα$^+$ Ly6G- non-dendritic cells from each strain. *Right:* summary dot plots show absolute numbers of SiglecF-CD64+ macrophages by sex and genotype: *p<0.05 (females) vs *p>0.05 (males). (E) *Left:* Exemplar contour plots show CD44 vs CD122 expression gated on CD8$^+$ TCRαβ$^+$ cells from each strain. *Right:* summary dot plots show absolute numbers of MP CD44$^+$ CD122$^+$ CD8 T cells by sex and genotype: p>0.99 (females) vs p=0.85 (males). For all dot plots, mean +/- SD are presented.

SUPPLEMENTARY FIGURE 3
Flow cytometric immune profiling of splenocytes and mLN in 15 week-old mice. Two-way ANOVA with post-hoc t-test was used for all genotype comparisons dis-aggregated by sex. (A) *Left:* Exemplar contour plots show CD4 vs CD8a expression gated on live single splenic CD3$^+$ TCRβ$^+$ cells from each strain. *Right:* summary dot plots show ratios of CD4/CD8 cells by sex and genotype. *p=0.01 (females) vs *p=0.01 (males). (B) *Left:* Exemplar contour plots show CD25 vs Foxp3 expression gated on CD4$^+$ TCRβ$^+$ T cells from each strain. *Right:* summary dot plots show absolute numbers of Foxp3$^+$ T regulatory cells (Treg) cells by sex and genotype: p=0.53 (females) vs p=0.53 (males). (C) Summary dot plots show absolute numbers of CD62L-Foxp3$^-$ CD4 T cells, and ICOS$^+$ CD44$^+$ CD62L$^-$ CD4 T cells, from mLN by sex and genotype. Non-naïve CD4 cells: p=0.11 (females) vs p=0.14 (males). ICOS$^+$ MP CD4 cells: **p=0.005 (females) vs *p=0.04 (males). (D) *Left:* Summary dot plots show absolute numbers of splenic CD19$^+$ B220$^+$ B cells by sex and genotype: p=0.15 (females) vs p=0.67 (males). *Middle:* Exemplar contour plots show CD21 vs CD24 expression gated on B cells from each strain. *Right:* summary dot plots show absolute numbers of follicular (CD21$^{med}$ CD24$^{lo}$), T1 (CD24$^{hi}$ CD21$^{lo}$) and T2 plus marginal zone (CD21$^{hi}$ CD24$^{hi}$) B cells by sex and genotype. Follicular B cells: p=0.09 (females) vs p=0.4 (males). T1 B cells: p=0.41 (females) vs p=0.94 (males). T2$^+$marginal zone B cells: p=0.56 (females) vs p=0.79 (males). (E) Summary dot plots show absolute numbers of class-switched (IgM$^{lo}$ IgD$^{lo}$) B cells, activated pre-germinal center (GC; CD95$^+$ GL7$^-$) and GC (CD95$^+$ GL7$^+$) B cells, from mesenteric LN by sex and genotype. IgM$^{lo}$ IgD$^{lo}$ B cells: **p=0.002 (females) vs p=0.02 (males). CD95$^+$ GL7$^-$ B cells: **p=0.003 (females) vs p=0.15 (males). CD95$^+$ GL7$^+$ B cells: **p=0.001 (females) vs p=0.1 (males). For all dot plots, mean +/- SD are presented.

SUPPLEMENTARY FIGURE 4
ScRNA-seq analysis of 15 week-old mouse splenocytes. (A) Pre-gating strategy for each subset is shown on aggregated *WT* cells. *Left:* Dot plots show CD19 vs IgD protein expression showing gates for B cells (CD19$^+$IgD$^+$) vs. non-B cells (CD19$^-$IgD$^-$). Overlayed heatmap display *Ighm* expression which guided gating. *Middle:* CD4 vs TCRβ protein expression gated on CD19$^-$IgD$^-$ non-B cells with overlayed heatmaps showing Trac expression

which guided gating decisions for CD4 cells (TCRβ$^+$ CD4$^+$) and CD8 (TCRβ$^+$ CD4$^-$) cells. *Right:* CD44 vs CD62L protein expression gated on CD4$^+$ TCRβ$^+$ T cells. Gates used for CD62L$^+$CD44$^-$ (naïve) and CD44$^+$ CD62L$^-$ MP CD4 cells are shown with overlayed heatmap of *Sell* encoding CD62L. (B) *Left:* summary dot plots show ratios of CD4/CD8 cells by genotype. Unpaired Student's t-test with Welch's correction p=0.16. *Right:* summary dot plots show ratios of CD62L$^+$CD44$^-$ / CD44$^+$ CD62L$^-$ CD4 cells by genotype, unpaired Student's t-test with Welch's correction **p<0.01. For all dot plots, mean +/- SD are presented. (C) *Left:* IgD vs CD44 protein expression on B cells from each strain, overlayed with heatmap of *Stat1*. *Middle:* Volcano plots show DEG between mutant and *WT* B cells, plotted according to $Log_2$ fold change [$Log_2$FC (mutant/*WT*)], against the negative logarithmic value of the false discovery rate [-log(FDR)]. Genes up- and down-regulated in mutant are denoted in red and blue, respectively. *Right:* Tables show genes up- or down regulated in mutant B cells by 40% or more. $Log_2$FC values are presented along with FDR-adjusted q-values <0.05. (D) *Left:* dot plots show CD4 vs TCRβ protein expression gated on CD19$^-$IgD$^-$ non-B cells for aggregated samples from each strain, with overlayed heatmaps showing *Cd8b1* expression. *Middle:* Volcano plots show DEG between mutant and *WT* CD8 T cells, plotted according to Log2FC (mutant/*WT*)] against -log(FDR). Genes up- and down-regulated in mutant are denoted in red and blue, respectively. *Right:* Tables show genes up- or down regulated in mutant CD8 T cells by 40% or more. $Log_2$FC values are presented along with FDR-adjusted q-values <0.05.

# References

1. Stark GR, Darnell JE. The JAK-STAT pathway at twenty. *Immunity* (2012) 36 (4):503–14. doi: 10.1016/j.immuni.2012.03.013

2. Hirahara K, Onodera A, Villarino AV, Bonelli M, Sciumè G, Laurence A, et al. Asymmetric action of STAT transcription factors drives transcriptional outputs and cytokine specificity. *Immunity* (2015) 42(5):877–89. doi: 10.1016/j.immuni.2015.04.014

3. Chatterjee-Kishore M, Wright KL, Ting JP, Stark GR. How Stat1 mediates constitutive gene expression: a complex of unphosphorylated Stat1 and IRF1 supports transcription of the LMP2 gene. *EMBO J* (2000) 19(15):4111–22. doi: 10.1093/emboj/19.15.4111

4. Cheon H, Stark GR. Unphosphorylated STAT1 prolongs the expression of interferon-induced immune regulatory genes. *Proc Natl Acad Sci U S A* (2009) 106 (23):9373–8. doi: 10.1073/pnas.0903487106

5. Majoros A, Platanitis E, Szappanos D, Cheon H, Vogl C, Shukla P, et al. Response to interferons and antibacterial innate immunity in the absence of tyrosine-phosphorylated STAT1. *EMBO Rep* (2016) 17(3):367–82. doi: 10.15252/embr.201540726

6. Michalska A, Blaszczyk K, Wesoly J, Bluyssen HAR. A positive feedback amplifier circuit that regulates interferon (IFN)-stimulated gene expression and controls type I and type II IFN responses. *Front Immunol* (2018) 9:1135. doi: 10.3389/fimmu.2018.01135

7. Wang BX, Fish EN. Global virus outbreaks: interferons as 1st responders. *Semin Immunol* (2019) 43:101300. doi: 10.1016/j.smim.2019.101300

8. Burke JD, Young HA. IFN-γ: a cytokine at the right time, is in the right place. *Semin Immunol* (2019) 43:101280. doi: 10.1016/j.smim.2019.05.002

9. Choi YS, Eto D, Yang JA, Lao C, Crotty S. Cutting edge: STAT1 is required for IL-6–mediated Bcl6 induction for early follicular helper cell differentiation. *J Immunol* (2013) 190(7):3049–53. doi: 10.4049/jimmunol.1203032

10. Stepkowski SM, Chen W, Ross JA, Nagy ZS, Kirken RA. STAT3: an important regulator of multiple cytokine functions. *Transplantation* (2008) 85(10):1372–7. doi: 10.1097/TP.0b013e3181739d25

11. Teague TK, Schaefer BC, Hildeman D, Bender J, Mitchell T, Kappler JW, et al. Activation-induced inhibition of interleukin 6–mediated T cell survival and signal transducer and activator of transcription 1 signaling. *J Exp Med* (2000) 191(6):915–26. doi: 10.1084/jem.191.6.915

12. Zheng J, van de Veerdonk FL, Crossland KL, Smeekens SP, Chan CM, Al Shehri T, et al. Gain-of-function STAT1 mutations impair STAT3 activity in patients with chronic mucocutaneous candidiasis (CMC). *Eur J Immunol* (2015) 45(10):2834–46. doi: 10.1002/eji.201445344

13. Toubiana J, Okada S, Hiller J, Oleastro M, Lagos Gomez M, Aldave Becerra JC, et al. Heterozygous STAT1 gain-of-function mutations underlie an unexpectedly broad clinical phenotype. *Blood* (2016) 127(25):3154–64. doi: 10.1182/blood-2015-11-679902

14. Depner M, Fuchs S, Raabe J, Frede N, Glocker C, Doffinger R, et al. The extended clinical phenotype of 26 patients with chronic mucocutaneous candidiasis due to gain-of-Function mutations in STAT1. *J Clin Immunol* (2016) 36(1):73–84. doi: 10.1007/s10875-015-0214-9

15. Liu L, Okada S, Kong XF, Kreins AY, Cypowyj S, Abhyankar A, et al. Gain-of-function human STAT1 mutations impair IL-17 immunity and underlie chronic mucocutaneous candidiasis. *J Exp Med* (2011) 208(8):1635–48. doi: 10.1084/jem.20110958

16. van de Veerdonk FL, Plantinga TS, Hoischen A, Smeekens SP, Joosten LAB, Gilissen C, et al. *STAT1* mutations in autosomal dominant chronic mucocutaneous candidiasis. *N Engl J Med* (2011) 365(1):54–61. doi: 10.1056/NEJMoa1100102

17. Sampaio EP, Hsu AP, Pechacek J, Bax HI, Dias DL, Paulson ML, et al. Signal transducer and activator of transcription 1 (STAT1) gain-of-function mutations and disseminated coccidioidomycosis and histoplasmosis. *J Allergy Clin Immunol* (2013) 131(6):1624-1634.e17. doi: 10.1016/j.jaci.2013.01.052

18. Uzel G, Sampaio EP, Lawrence MG, Hsu AP, Hackett M, Dorsey MJ, et al. Dominant gain-of-function STAT1 mutations in FOXP3 wild-type immune dysregulation–polyendocrinopathy–enteropathy–X-linked–like syndrome. *J Allergy Clin Immunol* (2013) 131(6):1611–23. doi: 10.1016/j.jaci.2012.11.054

19. Verbsky JW, Chatila TA. Immune dysregulation, polyendocrinopathy, enteropathy, X-linked (IPEX) and IPEX-related disorders: an evolving web of heritable autoimmune diseases. *Curr Opin Pediatr* (2013) 25(6):708–14. doi: 10.1097/MOP.0000000000000029

20. Scott O, Lindsay K, Erwood S, Mollica A, Roifman CM, Cohn RD, et al. STAT1 gain-of-function heterozygous cell models reveal diverse interferon-signature gene transcriptional responses. *NPJ Genom Med* (2021) 6(1):34. doi: 10.1038/s41525-021-00196-7

21. Scott O, Dadi H, Vong L, Pasternak Y, Garkaby J, Willett Pachul J, et al. DNA-Binding domain mutations confer severe outcome at an early age among STAT1 gain-of-function patients. *Pediatr Allergy Immunol* (2022) 33(1):e13694. doi: 10.1111/pai.13694

22. Rubtsova K, Marrack P, Rubtsov AV. Sexual dimorphism in autoimmunity. *J Clin Invest* (2015) 125(6):2187–93. doi: 10.1172/JCI78082

23. Lazarevic V, Glimcher LH, Lord GM. T-Bet: a bridge between innate and adaptive immunity. *Nat Rev Immunol* (2013) 13(11):777–89. doi: 10.1038/nri3536

24. Imam T, Park S, Kaplan MH, Olson MR. Effector T helper cell subsets in inflammatory bowel diseases. *Front Immunol* (2018) 9. doi: 10.3389/fimmu.2018.01212

25. Skapenko A, Leipe J, Lipsky PE, Schulze-Koops H. The role of the T cell in autoimmune inflammation. *Arthr Res Ther* (2005) 7(2):S4. doi: 10.1186/ar1703

26. Baris S, Alroqi F, Kiykim A, Karakoc-Aydiner E, Ogulur I, Ozen A, et al. Severe early-onset combined immunodeficiency due to heterozygous gain-of-Function mutations in STAT1. *J Clin Immunol* (2016) 36(7):641–8. doi: 10.1007/s10875-016-0312-3

27. Weinacht KG, Charbonnier LM, Alroqi F, Plant A, Qiao Q, Wu H, et al. Ruxolitinib reverses dysregulated T helper cell responses and controls autoimmunity caused by a novel signal transducer and activator of transcription 1 (STAT1) gain-of-function mutation. *J Allergy Clin Immunol* (2017) 139(5):1629–40. doi: 10.1016/j.jaci.2016.11.022

28. Chen X, Xu Q, Li X, Wang L, Yang L, Chen Z, et al. Molecular and phenotypic characterization of nine patients with STAT1 GOF mutations in China. *J Clin Immunol* (2020) 40(1):82–95. doi: 10.1007/s10875-019-00688-3

29. Bloomfield M, Kanderová V, Paračková Z, Vrabcová P, Svatoň M, Froňková E, et al. Utility of ruxolitinib in a child with chronic mucocutaneous candidiasis caused by a novel STAT1 gain-of-Function mutation. *J Clin Immunol* (2018) 38(5):589–601. doi: 10.1007/s10875-018-0519-6

30. Qin L, Waseem TC, Sahoo A, Bieerkehazhi S, Zhou H, Galkina EV, et al. Insights into the molecular mechanisms of T follicular helper-mediated immunity and pathology. *Front Immunol* (2018) 9:1884. doi: 10.3389/fimmu.2018.01884

31. Crotty S. T Follicular helper cell biology: a decade of discovery and diseases. *Immunity* (2019) 50(5):1132–48. doi: 10.1016/j.immuni.2019.04.011

32. Gensous N, Charrier M, Duluc D, Contin-Bordes C, Truchetet ME, Lazaro E, et al. T Follicular helper cells in autoimmune disorders. *Front Immunol* (2018) 9:1637. doi: 10.3389/fimmu.2018.01637

33. Wu T, Shin HM, Moseman EA, Ji Y, Huang B, Harly C, et al. TCF1 is required for the T follicular helper cell response to viral infection. *Cell Rep* (2015) 12(12):2099–110. doi: 10.1016/j.celrep.2015.08.049

34. Li F, Zhao X, Zhang Y, Shao P, Ma X, Paradee WJ, et al. TFH cells depend on Tcf1-intrinsic HDAC activity to suppress CTLA4 and guard b-cell help function. *Proc Nat Acad Sci* (2021) 118(2):e2014562118. doi: 10.1073/pnas.2014562118

35. Choi YS, Gullicksrud JA, Xing S, Zeng Z, Shan Q, Li F, et al. LEF-1 and TCF-1 orchestrate TFH differentiation by regulating differentiation circuits upstream of the transcriptional repressor Bcl6. *Nat Immunol* (2015) 16(9):980–90. doi: 10.1038/ni.3226

36. Breuer O, Daum H, Cohen-Cymberknoh M, Unger S, Shoseyov D, Stepensky P, et al. Autosomal dominant gain of function STAT1 mutation and severe bronchiectasis. *Respir Med* (2017) 126:39–45. doi: 10.1016/j.rmed.2017.03.018

37. Cepika AM, Sato Y, Liu JMH, Uyeda MJ, Bacchetta R, Roncarolo MG. Tregopathies: monogenic diseases resulting in regulatory T-cell deficiency. *J Allergy Clin Immunol* (2018) 142(6):1679–95. doi: 10.1016/j.jaci.2018.10.026

38. Shevyrev D, Tereshchenko V. Treg heterogeneity, function, and homeostasis. *Front Immunol* (2020) 10. doi: 10.3389/fimmu.2019.03100

39. Sharfe N, Nahum A, Newell A, Dadi H, Ngan B, Pereira SL, et al. Fatal combined immunodeficiency associated with heterozygous mutation in STAT1. *J Allergy Clin Immunol* (2014) 133(3):807–17. doi: 10.1016/j.jaci.2013.09.032

40. Tanimura M, Dohi K, Hirayama M, Sato Y, Sugiura E, Nakajima H, et al. Recurrent inflammatory aortic aneurysms in chronic mucocutaneous candidiasis with a gain-of-function STAT1 mutation. *Int J Cardiol* (2015) 196:88–90. doi: 10.1016/j.ijcard.2015.05.183

41. Gu B, Posfai E, Rossant J. Efficient generation of targeted large insertions by microinjection into two-cell-stage mouse embryos. *Nat Biotechnol* (2018) 36(7):632–7. doi: 10.1038/nbt.4166

42. Fortin J, Chiang MF, Meydan C, Foox J, Ramachandran P, Leca J, et al. Distinct and opposite effects of leukemogenic idh and Tet2 mutations in hematopoietic stem and progenitor cells. *Proc Natl Acad Sci U S A* (2023) 120(4):e2208176120. doi: 10.1073/pnas.2208176120

43. Fread KI, Strickland WD, Nolan GP, Zunder ER. AN UPDATED DEBARCODING TOOL FOR MASS CYTOMETRY WITH CELL TYPE-SPECIFIC AND CELL SAMPLE-SPECIFIC STRINGENCY ADJUSTMENT. *Pac Symp Biocomput* (2017) 22:588–98. doi: 10.1142/9789813207813_0054

44. Hao Y, Hao S, Andersen-Nissen E, Mauck WM, Zheng S, Butler A, et al. Integrated analysis of multimodal single-cell data. *Cell* (2021) 184(13):3573-3587.e29. doi: 10.1016/j.cell.2021.04.048

45. Heng TSP, Painter MW, Elpek K, Lukacs-Kornek V, Mauermann N, Turley SJ, et al. The immunological genome project: networks of gene expression in immune cells. *Nat Immunol* (2008) 9(10):1091–4. doi: 10.1038/ni1008-1091

46. Zimmerman O, Olbrich P, Freeman AF, Rosen LB, Uzel G, Zerbe CS, et al. STAT1 gain-of-Function mutations cause high total STAT1 levels with normal dephosphorylation. *Front Immunol* (2019) 10:1433. doi: 10.3389/fimmu.2019.01433

47. Vinuesa CG, Cook MC, Angelucci C, Athanasopoulos V, Rui L, Hill KM, et al. A RING-type ubiquitin ligase family member required to repress follicular helper T cells and autoimmunity. *Nature* (2005) 435(7041):452–8. doi: 10.1038/nature03555

48. Yang BH, Wang K, Wan S, Liang Y, Yuan X, Dong Y, et al. TCF1 and LEF1 control treg competitive survival and tfr development to prevent autoimmune diseases. *Cell Rep* (2019) 27(12):3629–45. doi: 10.1016/j.celrep.2019.05.061

49. Snapper CM, Peschel C, Paul WE. IFN-gamma stimulates IgG2a secretion by murine b cells stimulated with bacterial lipopolysaccharide. *J Immunol* (1988) 140 (7):2121–7. doi: 10.4049/jimmunol.140.7.2121

50. Meroni PL, Schur PH. ANA screening: an old test with new recommendations. *Ann Rheum Dis* (2010) 69(8):1420–2. doi: 10.1136/ard.2009.127100

51. Markle JGM, Mortin-Toth S, Wong ASL, Geng L, Hayday A, Danska JS. γδT cells are essential effectors of type 1 diabetes in the NOD mouse model. *J Immunol* (2013) 190(11):5392–401. doi: 10.4049/jimmunol.1203502

52. Kawabe T, Yi J, Sprent J. Homeostasis of naive and memory T lymphocytes. *Cold Spring Harb Perspect Biol* (2021) 13(9):a037879. doi: 10.1101/cshperspect.a037879

53. Keller B, Strohmeier V, Harder I, Unger S, Payne KJ, Andrieux G, et al. The expansion of human T-bethighCD21low b cells is T cell dependent. *Sci Immunol* (2021) 6(64):eabh0891. doi: 10.1126/sciimmunol.abh0891

54. Cano-Gamez E, Soskic B, Roumeliotis TI, So E, Smyth DJ, Baldrighi M, et al. Single-cell transcriptomics identifies an effectorness gradient shaping the response of CD4 + T cells to cytokines. *Nat Commun* (2020) 11(1):1801. doi: 10.1038/s41467-020-15543-y

55. Danilo M, Chennupati V, Silva JG, Siegert S, Held W. Suppression of Tcf1 by inflammatory cytokines facilitates effector CD8 T cell differentiation. *Cell Rep* (2018) 22 (8):2107–17. doi: 10.1016/j.celrep.2018.01.072

56. Chen L, Flies DB. Molecular mechanisms of T cell co-stimulation and co-inhibition. *Nat Rev Immunol* (2013) 13(4):227–42. doi: 10.1038/nri3405

57. Serre K, Bénézech C, Desanti G, Bobat S, Toellner KM, Bird R, et al. Helios Is associated with CD4 T cells differentiating to T helper 2 and follicular helper T cells *In vivo* independently of Foxp3 expression. *PloS One* (2011) 6(6):e20731. doi: 10.1371/journal.pone.0020731

58. Hale JS, Youngblood B, Latner DR, Mohammed AUR, Ye L, Akondy RS, et al. Distinct memory CD4+ T cells with commitment to T follicular helper- and T helper 1-cell lineages are generated after acute viral infection. *Immunity* (2013) 38(4):805–17. doi: 10.1016/j.immuni.2013.02.020

59. Ly A, Liao Y, Pietrzak H, Ioannidis LJ, Sidwell T, Gloury R, et al. Transcription factor T-bet in b cells modulates germinal center polarization and antibody affinity maturation in response to malaria. *Cell Rep* (2019) 29(8):2257–2269.e6. doi: 10.1016/j.celrep.2019.10.087

60. Hao Z, Duncan GS, Seagal J, Su YW, Hong C, Haight J, et al. Fas receptor expression in germinal-center b cells is essential for T and b lymphocyte homeostasis. *Immunity* (2008) 29(4):615–27. doi: 10.1016/j.immuni.2008.07.016

61. Wang H, Jain S, Li P, Lin JX, Oh J, Qi C, et al. Transcription factors IRF8 and PU.1 are required for follicular b cell development and BCL6-driven germinal center responses. *Proc Natl Acad Sci USA* (2019) 116(19):9511–20. doi: 10.1073/pnas.1901258116

62. Zaretsky I, Atrakchi O, Mazor RD, Stoler-Barak L, Biram A, Feigelson SW, et al. ICAMs support b cell interactions with T follicular helper cells and promote clonal selection. *J Exp Med* (2017) 214(11):3435–48. doi: 10.1084/jem.20171129

63. Cenerenti M, Saillard M, Romero P, Jandus C. The era of cytotoxic CD4 T cells. *Front Immunol* (2022) 13. doi: 10.3389/fimmu.2022.867189

64. Qian W, Miner CA, Ingle H, Platt DJ, Baldridge MT, Miner JJ. A human STAT1 gain-of-Function mutation impairs CD8 $^{+}$ T cell responses against gammaherpesvirus 68. *J Virol* (2019) 93(19):e00307–19. doi: 10.1128/JVI.00307-19

65. Tamaura M, Satoh-Takayama N, Tsumura M, Sasaki T, Goda S, Kageyama T, et al. Human gain-of-function STAT1 mutation disturbs IL-17 immunity in mice. *Int Immunol* (2020) 32(4):259–72. doi: 10.1093/intimm/dxz079

66. Laffont S, Guéry JC. Deconstructing the sex bias in allergy and autoimmunity: from sex hormones and beyond. *Adv Immunol* (2019) 142:35–64. doi: 10.1016/bs.ai.2019.04.001

67. Young NA, Valiente GR, Hampton JM, Wu LC, Burd CJ, Willis WL, et al. Estrogen-regulated STAT1 activation promotes TLR8 expression to facilitate signaling *via* microRNA-21 in systemic lupus erythematosus. *Clin Immunol* (2017) 176:12–22. doi: 10.1016/j.clim.2016.12.005

68. Romberg N, Morbach H, Lawrence MG, Kim S, Kang I, Holland SM, et al. Gain-of-function STAT1 mutations are associated with PD-L1 overexpression and a defect in b-cell survival. *J Allergy Clin Immunol* (2013) 131(6):1691–3. doi: 10.1016/j.jaci.2013.01.004

69. Zhang Y, Ma CA, Lawrence MG, Break TJ, O'Connell MP, Lyons JJ, et al. PD-L1 up-regulation restrains Th17 cell differentiation in STAT3 loss- and STAT1 gain-of-function patients. *J Exp Med* (2017) 214(9):2523–33. doi: 10.1084/jem.20161427

70. Choi J, Crotty S. Bcl6-mediated transcriptional regulation of follicular helper T cells (TFH). *Trends Immunol* (2021) 42(4):336–49. doi: 10.1016/j.it.2021.02.002

71. Lee SK, Silva DG, Martin JL, Pratama A, Hu X, Chang PP, et al. Interferon-γ excess leads to pathogenic accumulation of follicular helper T cells and germinal centers. *Immunity* (2012) 37(5):880–92. doi: 10.1016/j.immuni.2012.10.010

72. Nakayamada S, Kanno Y, Takahashi H, Jankovic D, Lu KT, Johnson TA, et al. Early Th1 cell differentiation is marked by a tfh cell-like transition. *Immunity* (2011) 35 (6):919–31. doi: 10.1016/j.immuni.2011.11.012

73. Oestreich KJ, Mohn SE, Weinmann AS. Molecular mechanisms that control the expression and activity of bcl-6 in TH1 cells to regulate flexibility with a TFH-like gene profile. *Nat Immunol* (2012) 13(4):405–11. doi: 10.1038/ni.2242

74. Weinstein JS, Laidlaw BJ, Lu Y, Wang JK, Schulz VP, Li N, et al. STAT4 and T-bet control follicular helper T cell development in viral infections. *J Exp Med* (2018) 215 (1):337–55. doi: 10.1084/jem.20170457

75. Fang D, Cui K, Mao K, Hu G, Li R, Zheng M, et al. Transient T-bet expression functionally specifies a distinct T follicular helper subset. *J Exp Med* (2018) 215 (11):2705–14. doi: 10.1084/jem.20180927

76. Papillion A, Powell MD, Chisolm DA, Bachus H, Fuller MJ, Weinmann AS, et al. Inhibition of IL-2 responsiveness by IL-6 is required for the generation of GC-TFH cells. *Sci Immunol* (2019) 4(39):eaaw7636. doi: 10.1126/sciimmunol.aaw7636

77. Osum KC, Jenkins MK. Toward a general model of CD4+ T cell subset specification and memory cell formation. *Immunity* (2023) 56(3):475–84. doi: 10.1016/j.immuni.2023.02.010

78. Ma CS, Wong N, Rao G, Avery DT, Torpy J, Hambridge T, et al. Monogenic mutations differentially affect the quantity and quality of T follicular helper cells in patients with human primary immunodeficiencies. *J Allergy Clin Immunol* (2015) 136 (4):993–1006.e1. doi: 10.1016/j.jaci.2015.05.036

frontiers | Frontiers in Immunology

TYPE Original Research
PUBLISHED 25 May 2023
DOI 10.3389/fimmu.2023.1133358



OPEN ACCESS

EDITED BY
Urszula Krzych,
Walter Reed Army Institute of Research, United States

REVIEWED BY
Paulina Niedźwiedzka-Rystwej, University of Szczecin, Poland
Bartłomiej Grygorcewicz, Pomeranian Medical University, Poland

*CORRESPONDENCE
Magdalena Podlacha
magdalena.podlacha@ug.edu.pl

RECEIVED 03 January 2023
ACCEPTED 16 May 2023
PUBLISHED 25 May 2023

CITATION
Grabowski Ł, Pierzynowska K, Kosznik-Kwaśnicka K, Stasiłojć M, Jerzemowska G, Węgrzyn A, Węgrzyn G and Podlacha M (2023) Sex-dependent differences in behavioral and immunological responses to antibiotic and bacteriophage administration in mice. *Front. Immunol.* 14:1133358. doi: 10.3389/fimmu.2023.1133358



# Sex-dependent differences in behavioral and immunological responses to antibiotic and bacteriophage administration in mice

Łukasz Grabowski[1], Karolina Pierzynowska[2], Katarzyna Kosznik-Kwaśnicka[1,3], Małgorzata Stasiłojć[2,4], Grażyna Jerzemowska[5], Alicja Węgrzyn[6], Grzegorz Węgrzyn[2] and Magdalena Podlacha[2]*

[1]Laboratory of Bacteriophage Therapy, Institute of Biochemistry and Biophysics, Polish Academy of Sciences, Gdansk, Poland, [2]Department of Molecular Biology, Faculty of Biology, University of Gdansk, Gdansk, Poland, [3]Department of Medical Microbiology, Faculty of Medicine, Medical University of Gdansk, Gdansk, Poland, [4]Department of Cell Biology and Immunology, Intercollegiate Faculty of Biotechnology of University of Gdansk and Medical University of Gdansk, Gdansk, Poland, [5]Department of Animal and Human Physiology, Faculty of Biology, University of Gdansk, Gdansk, Poland, [6]Phage Therapy Center, University Center of Applied and Interdisciplinary Research, Gdansk, Poland

**Introduction:** The problem of antibiotic resistance is a global one, involving many industries and entailing huge financial outlays. Therefore, the search for alternative methods to combat drug-resistant bacteria has a priority status. Great potential is seen in bacteriophages which have the natural ability to kill bacterial cells. Bacteriophages also have several advantages over antibiotics. Firstly, they are considered ecologically safe (harmless to humans, plants and animals). Secondly, bacteriophages preparations are readily producible and easy to apply. However, before bacteriophages can be authorized for medical and veterinary use, they must be accurately characterized *in vitro* and *in vivo* to determinate safety.

**Methods:** Therefore, the aim of this study was to verify for the first time the behavioral and immunological responses of both male and female mice (C57BL/6J) to bacteriophage cocktail, composed of two bacteriophages, and to two commonly used antibiotics, enrofloxacin and tetracycline. Animal behavior, the percentage of lymphocyte populations and subpopulations, cytokine concentrations, blood hematological parameters, gastrointestinal microbiome analysis and the size of internal organs, were evaluated.

**Results:** Unexpectedly, we observed a sex-dependent, negative effect of antibiotic therapy, which not only involved the functioning of the immune system, but could also significantly impaired the activity of the central nervous system, as manifested by disruption of the behavioral pattern, especially exacerbated in females. In contrast to antibiotics, complex behavioral and immunological analyses confirmed the lack of adverse effects during the bacteriophage cocktail administration.

**Discussion:** The mechanism of the differences between males and females in appearance of adverse effects, related to the behavioral and immune functions, in the response to antibiotic treatment remains to be elucidated. One might imagine that differences in hormones and/or different permeability of the blood-brain barrier can be important factors, however, extensive studies are required to find the real reason(s).

KEYWORDS

**antibiotics, bacteriophage, males and females, behavior, immune system, mice**

# 1 Introduction

While the threat of antibiotic resistance is increasing, the interest in the use of bacteriophages to treat bacterial infections, known as bacteriophage therapy, has rapidly grown, especially in the context of veterinary (1), poultry industry (1) and public health (2). There are 2.8 million infections with antibiotic-resistant bacteria in the United States each year, with a minimum of 35.000 cases resulting in death (3). It is projected that by 2050, the annual number of deaths worldwide caused by this type of infection will be at ten million people (4). It is worth nothing that at the root of the antibiotic crisis, it is not only their use in medicine, but also in the treatment of livestock. Indeed, about two-thirds of the tonnage of global antibiotic use are commonly employed to combat bacterial infections in food-animal production (5). *Salmonella enterica* is one of the most common pathogens causing gastrointestinal diseases in the European Union. In United States, based on data obtained from the Center for Disease Control and Prevention, it is estimated that this bacterium causes about 1.2 million cases of food product contamination, which translates into 23.000 hospitalizations and 450 deaths each year (3). Although the level of antibiotic resistance of different *Salmonella* serovars varies from country to country (6), the problem is global and requires the implementation of alternative methods to control the infection (7).

Bacteriophage therapy uses the natural ability of bacteriophages to kill bacterial cells. Bacteriophages have also several advantages over antibiotics, as they are considered ecologically safe (harmless to humans, plants and animals), and bacteriophage preparations are readily producible and easy to apply. The concentration of an antibiotic introduced into the human organism decreases with time (due to natural drug clearance from the body), whereas bacteriophages continue to multiply, decreasing as soon as sensitive bacterial cells are eliminated (8). However, before bacteriophages can be authorized for medical and veterinary use, they must be accurately characterized *in vitro* and then *in vivo* to determinate their safety. Despite bacteriophages being specific to their bacterial hosts, there are a growing number of reports about interactions of bacteriophages with eukaryotic cells. These impacts can, to varying degrees, involve not only tissues or organs, but even entire systems, including the immune system or central nervous system, as reviewed recently (9). While there are reports on the characterization and safety of bacteriophages tested *in vitro*, animal studies are still in the minority, and systematic comparison of effects of administration of bacteriophages and antibiotics *in vivo* is, to our knowledge, absent in the literature, especially regarding functions of the brain and the immune system.

Therefore, the aim of this study was to verify the behavioral and immunological responses to a bacteriophage cocktail, composed of two bacteriophages, and to two commonly used antibiotics, enrofloxacin and tetracycline, in female and male C57BL/67 mice. Animal behavior, the percentage of lymphocyte populations and subpopulations, cytokine concentrations, blood hematological parameters, gastrointestinal microbiome analysis and the size of internal organs, were evaluated.

# 2 Materials and methods

## 2.1 Animals

The experiments were conducted with male (n=24) and female (n=24) C57BL/6J mice. At the start of the experiment, all animals were 6 months old. The experiments were performed with animals of both sexes, to assess any differences in responses to administration of different types of bacteriophages and antibiotics (Figure 1).

The mice were housed in a ventilated animal room (15 air changes per hour) in a laboratory setting. Stable conditions were maintained: artificial lighting (12 hours light/12 hours dark), ambient temperature (22 ± 2°C), humidity (50 ± 5%) with access to food and tap water *ad libitum*. Mice were maintained in approved laboratory cages 15 cm high and at least 400 $cm^2$ in size. To ensure the most optimal enrichment of the environment, suitable attractants and accessories for rodents were used.

The animal house in which the mice were placed meets the requirements of the Law on the Protection of Animals Used for Scientific or Educational Purposes, dated on January 15, 2015 (Journal of Laws dated on February 26, 2015), as well as the recommendations of the European Commission on the welfare of

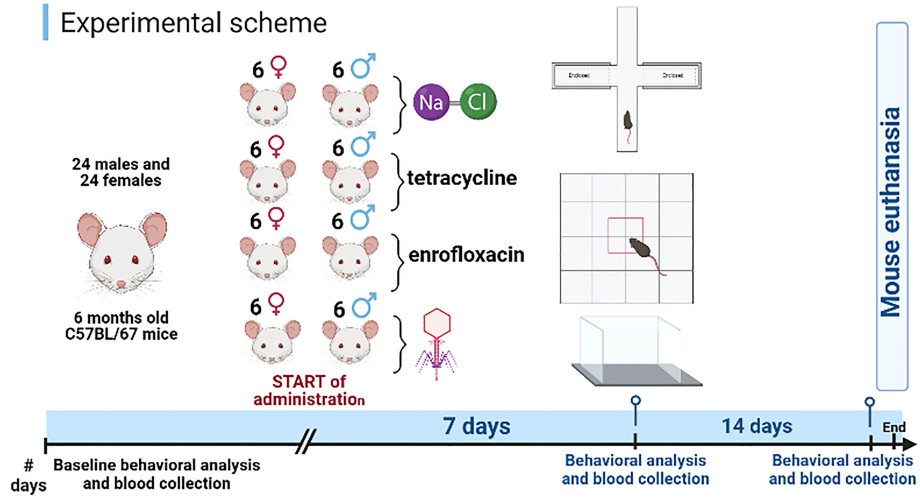


FIGURE 1
Schematic diagram of the experiment. Created using BioRender software.

animals used in scientific experiments. All experiments were approved by the Local Ethics Committee for Experimental Animals in Bydgoszcz (permission number 02/2022, dated on January 19, 2022).

## 2.2 Preparation and purification of high-titer bacteriophage lysates

Due to huge diversity of bacteriophages, we aimed to study bacteriophages representing various types of viruses, which differ in head morphology and genome size. Therefore, the following bacteriophages isolated from the environment, were employed: vB_ Sen-TO17 and vB_SenM-2. Bacteriophage vB_ Sen-TO17 is a caudate bacteriophage with a virion composed of head and tail (head diameter: 48 x 46 nm, tail length: 121 nm), bearing dsDNA as a genetic material (genome size is 41,658 bp), and infecting *Salmonella enterica* strains (10, 11). vB_SenM-2 is a *S.enterica* – specific, caudate bacteriophage (head diameter: 84 x 79 nm, tail length: 111 nm) with a dsDNA genome (the genome size is 158,986 bp) (10, 12).

The bacteriophages included in the bacteriophage cocktail were prepared according to the protocol described previously (13). Briefly, all bacteriophages were propagated in susceptible bacterial strains to obtain high titer. To avoid contamination with bacteria-derived products, including lipopolysaccharide (LPS) which reveals toxic features to eukaryotic cells, bacteriophages were concentrated with polyethylene glycol (PEG8000) (BioShop, Burlington, Ontario, Canada) and purified by ultracentrifugation at 95,000 × *g* for 2.5 hours, at 4°C (Avanti JXN-26, rotor JLA-8000, Beckman Coulter, Indianapolis, USA) in a CsCl density gradient (14). Purified bacteriophages were tested for a lack of toxic contaminants using Purified Thermo Scientific™ Pierce ™ LAL Chromogenic Endotoxin Quantitation Kit (catalog number: 12117850; Thermo Fisher Scientific Inc., Paisley, UK). To remove residual CsCl, 1 ml of bacteriophages were dialyzed against 300 ml of 3M NaCl, using a dialysis membrane (ZelluTrans, MWCO: 12.000-14.000, serial number: E674.1; Roth, Germany) for 7 days at 4°C. The NaCl was replaced every 12 hours (15).

The bacteriophages were characterized in terms of survival under various physicochemical conditions (stability in pH range between 1.8 and 12; stability in ethanol, chloroform, DMSO and acetone; stability in temperature range between -80°C and 95°C), and their effectiveness in combating various *Salmonella enterica* serovars *in vitro* was verified (10, 16).

## 2.3 Experimental groups

Experiments were conducted with eight groups for male and female mice, (i) control (receiving saline (0.9% NaCl), 0.1 ml), (ii) tetracycline, (iii) enrofloxacin, and (iv) bacteriophage cocktail. Each group consisted of six mice. The cocktail was administered at $10^9$ PFU/ml (0.1 ml), whereas enrofloxacin (Scanflox, Scanvet, Warsaw, Poland) at 5 mg/kg body weight and tetracycline (catalog number: 200-481-9; Merck, Darmstadt, Germany) at 20 mg/kg body weight, orally every day by using an oro-gastric probe, for fourteen days.

## 2.4 Locomotor activity in actometers

The locomotor activity of animals was measured using actometers (Opto Varimex Minor, Columbus, USA). The actometer consists of four plexiglass walls measuring 43 x 43 x 20 cm. At the moment of movement, a photocell is used to record each interruption of the infrared beam, which is then counted by a digital counter. The movements analyzed in this test are divided into horizontal (movements in the horizontal plane), vertical (movements in the vertical plane), and ambulatory (such as during body cleaning). The animals' locomotor activity was recorded for 10 minutes three times, before the start of administration, after one week, and after fourteen days of

administration of bacteriophage cocktail, antibiotic or saline. Measurements were taken at a fixed time, between 4 p.m. and 6 p.m., according to the method described previously (17).

## 2.5 Analysis of anxiety behavior in the open field test

The open field test allows for the assessment of the severity of the level of fear towards the stress factor of the open space, and also determines locomotor activity and the degree of exploration in a new hostile environment. Rodents are inherently prone to darkened, enclosed spaces, fear of open spaces and heights, so the test was conducted in a 100 x 100 x 60 cm box (usually made of white – colored boards), additionally exposed to a light source which intensifies the sense of fear. The floor of the box was divided into equal parts, among which central and peripheral squares were distinguished. Mice were placed in the test, always in the same position (e.g. with their head to one of the corners). The experiments were carried out at a fixed time, between 2 and 3 p.m. The locomotor activity of the exploring animal was measured by the number of squares crossed. The level of stress was determined by the number of all entries to the central squares and the time spent in the central part of the test. A bright, open space is a strong stressor for mice, so crossing the central fields of the box and staying there longer was considered as a sign of the animal's courage (rodents with higher sensitivity to stress generally stay in the peripheral fields of the test). All categories of animal behavior were recorded using a camera and the Ethovision XT 10 software (Noldus, Wagenigen, the Nederlands) for 10 minutes, three times: before the start of administration, after one week and after fourteen days of administration of bacteriophage cocktail, antibiotic or saline.

## 2.6 Analysis of anxiety behavior and memory processes in the elevated plus-maze test

Similar to the above-described open field test, the elevated plus-maze test allows assessment of the anxiety response, based on the natural tendency of rodents to actively explore new environment, which is limited by the aversive properties of the elevated plus open part of the test. This test can also be used to record memory processes under anxiety conditions by recording the transfer latency from the open to the closed arm. In addition, the implementation of a re-test (repeat measurement) procedure, allows the evaluation of memory processes. The apparatus used to carry out the test, consisted of a cross-shaped (plus) platform raised about 50 cm above the ground. Two of the platform's arms were shielded by walls, while two remained open. The dimensions of the arms were 5 x 10 cm, respectively. During the test, the procedure was carried out three times for each group. During the intervals, the apparatus was washed with 70% ethanol after each trial and allowed to dry for five minutes so that the smell of other animals would not affect the experiment. The first trial was considered as a baseline measurement, allowing to exclude the individuals whose results deviate from the average value for the group. In further stages of the experiment, the baseline measurement was also considered as a reference point. The second trial was performed after seven days of the administration onset, while the third trial was carried out after fourteen days of the treatment with the bacteriophage cocktail, antibiotics or saline. All trials were recorded using an analog camera and EthoVision XT 10 software (Noldus, Wageningen, the Netherlands). Reactions considered were: time spent in the open/closed arms; number of entries into the open/closed arms; as well as exploration and immobilization.

## 2.7 Blood collection

Blood was collected from mice at three time points: under baseline conditions (before the start of administration, but also before behavioral testing – baseline measurement) and after seven and then fourteen days from orally administration onset of the bacteriophage cocktail, antibiotics or saline. This procedure was performed under short-term ketamine (87.5 mg/kg body weight) and xylasine (12.5 mg/kg body weight) anesthesia from the *venous plexus* inside the orbit behind the eyeball. Blood was collected in a volume representing 6% of the animal's body weight into EDTA-containing tubes using capillaries 2 cm in length, approximately 1 mm in diameter with the interiors coated with the same anticoagulant. Each blood sample collected was immediately divided according to the course of further determination: 700 µl of whole blood was used to obtain the results of flow cytometry and hematological parameters, while the remaining blood was centrifuged (10 minutes, 2000 × *g*, 4°C) to obtain plasma, which was subjected to deep freezing (-80°C) until further analysis.

## 2.8 Analysis of selected blood hematological parameters

The hematological analysis of previously collected whole blood (200 µl) was performed in a Horiba ABX Micros ES 60 automatic analyzer (Horiba Medical, Japan). Following parameters were monitored: number of leukocytes, lymphocytes, monocytes and granulocytes, as well as the red blood cell system indexes: erythrocyte count, hemoglobin (HGB) level, hematocrit (HCT) level, mean red cell volume (MCV), mean corpuscular hemoglobin (MCH), mean corpuscular hemoglobin concentration (MCHC), and platelet (PLT) number.

## 2.9 Determination of the percentage of lymphocyte population and subpopulations of T helper (Th, TCD4+) and T cytotoxic (Tc, TCD8+) in peripheral blood by flow cytometry

Cytometric analysis of the lymphocyte population was performed after centrifugation of blood in a Ficoll gradient (1,113 × *g*, 30 minutes,

4°C) and uropollin according to the procedure described previously (18). Peripheral blood mononuclear cells (PBMCs, mainly lymphocytes and monocytes), isolated by this method, were suspended at a final concentration of $10^7$ cells/ml. For cytometric verifications, 25 µl of prepared PBMC cell suspension and 25 µl of antibodies selected from two kits, AntiMouse CD3-FITC/CD45RA-PC7/CD161a-APC or CD3-FITC/CD4-PC7/CD8-APC (Beckman Coulter, California, USA), were employed. The samples were incubated for 20 minutes in the dark at room temperature. After incubation, 700 µl of buffered saline (PBS) and 25 µl of fixative solution (Fixative Solution IOTest O3, Beckman Coulter, California, USA) were added. The percentage of lymphocyte population and subpopulations was determined by flow cytometry using the FACSVerese cytometer (Becton Dickson) and BD FACSuite software version 1.0.5. The separation into subpopulations was based on the surface expression of CD4 (helper T cells, Th, TCD4+) or CD8 (cytotoxic T cells, Tc, TCD8+). The total number of lymphocytes and their subpopulations was calculated based on the total number of leukocytes and the percentage of T, TCD4+ and TCD8+ lymphocytes.

## 2.10 Determination of pro-inflammatory (IL-6, TNF-α) and anti-inflammatory (IL-10) cytokine concentrations in blood plasma

Plasma IL-6, TNF-α and IL-10 concentrations were determined by enzyme–linked immunoassay (ELISA) using a commercially available kit (My BioSource Inc., San Diego, USA) according to the manufacturer's instructions and using a Multiskan Fc microplate reader (Thermo Fisher Scientific, Massachusetts, USA), coupled with Skanlt 6.1.1 RE software, which analyzes spectrophotometric color intensity, plots a standard curve based on the standards used, and reads the concentration values of the particular cytokines in the plasma samples tested. The results obtained are presented in pg/ml.

## 2.11 Mice weighing procedure

Mice were weighed three times: at the beginning of the experiment (before blood collection and behavioral tests performed under baseline conditions), then after seven and fourteen days after bacteriophage cocktail, antibiotic or saline administration onset, depending on the experimental group. After removal from the home cage, the animal was placed in a plastic container, 15 cm in diameter and 18 cm high, which was then placed on the scale (Soehlnc Professional, Nassau, Germany). The total duration of the activity did not exceed 30 seconds.

## 2.12 Mice euthanasia

Mice were given a lethal intraperitoneal dose of pentobarbital anesthesia at 120 mg/kg body weight, and internal organs were harvested. To minimize the animal's discomfort during the procedure, immediately before the injection, the mouse was additionally anesthetized with isoflurane inhalation anesthesia (2.5%, flow rate 0.5 l/minute).

## 2.13 Weighing internal organs

Briefly, all organs: thymus, spleen, brain, kidney, heart, liver, intestines and stomach subjected to the weighing procedure were taken entirely from each animal. They were then purified (removal of residual fat) by washing in buffered saline solution (PBS). The intestines were cut off immediately after the stomach, at the level of the *pylorus*, and were taken as far as the *rectum*. Intestines before weighing were cleaned off any remaining digestive contents.

## 2.14 Preparation of homogenates

All organs were sliced with a sterile scalpel into smaller pieces, the size of which dependent on the tissue type. In the case of the brain and kidney, their fragments were 50 mg, the heart and spleen 5 mg, and the liver 100 mg. In order to remove any external contamination (blood, vessels, fat), the organs were rinsed three times in 1 ml PBS. Homogenization was performed using a Bullet Blender Tissue Homogenizer (Next Advance, NY, USA), according to protocols, dedicated to the specific tissue type. The appropriate type of grinding beads was added to the microcentrifuge tubes. In the case of brain and liver, glass beads (0.5 mm, product number GB05) were used. For the homogenization of the heart, stainless steel beads (1.6 mm, product number SSB16) were used. The zirconium oxide beads (0.5 mm, product number ZROB05) were used to homogenize the kidney and spleen. The weight of the beads used had to be equal to the weight of the homogenized organ. The next step was to add two volumes of homogenization buffer (T-PER Tissue Protein Extraction Reagent, Thermo Scientific, product number 78510, Massachusetts, USA), containing protease inhibitors (Thermo Scientific, product number A32955, Massachusetts, USA) for every 100 mg of organ. The organ prepared in this way was centrifuged for 5 minutes at maximum speed (level 12; 10,000 RPM), then the supernatant was collected and frozen until further analysis.

## 2.15 Isolation of total DNA

Homogenates from brains, hearts, livers, spleens and kidneys were used to isolate total DNA. RNase (final concentration 5 µg/µl; EURx, Poland) was added to 300 µl of the lysate and incubated at 37°C for 30 minutes. Next, thermal inactivation of RNase was performed for 10 minutes at 65°C. To samples obtained in this way, 400 µl of Tissue Cell Lysis Solution (Lucigen, USA) and 5 µl of Proteinase K (concentration 25 mg/ml; EURx, Poland) were added, and then incubated for 30 minutes at 65°C. Samples were cooled in ice for 5 minutes, then 300 µl MPC Protein Precipitation Reagent (Lucigen, USA) was added and centrifuged (8,000 x *g*, 10 minutes,

4°C). Five hundred µl of isopropanol (POCH, Poland) were added to the supernatant and incubated at -20°C for 24 hours. Then, the samples were centrifuged (9,600 x *g*, 20 minutes, 4°C), the supernatant was removed, and 700 µl of 70% ethanol (POCH, Poland) were added to the resulting colorless pellet. The samples were centrifuged (9,600 x *g*, 40 minutes, 4°C), the supernatant was removed, and 500 µl of 70% ethanol were added to the white pellet. The supernatant was removed, and the pellet was dried for 20 minutes under vacuum at 30°C. The pellet was suspended in 30 µl of nuclease free water (Roth, Germany) and incubated for 15 minutes at 37°C to dissolve. The obtained samples were stored at -20°C.

## 2.16 Primer design

Specific primers were designed by Primer-BLAST software, with parameters set to exclude *Mus musculus* (taxid: 10090), Caudoviricetes (taxid: 2731619), and Viral (taxid: 10239) sequences. Forward (5'AGCGTTAGTTCTGTCCACCC3') and reverse (5'CGCTGGCACTAATTTCGGTG3') primers of the length of 20 nucleotides are complementary to positions flanking the 37654-38634 nucleotides region of the *Salmonella* bacteriophage vB_Sen-TO17 genome, which encodes hypothetical tail and neck proteins. As for *Salmonella* bacteriophage vB_SenM-2, primers (Forward primer: 5'GCGCGACTTGTAAGATGCTG3', Reverse primer: 5'CCAATCAAGGGGCTTCTCGT3') were designed to target the nucleotide span 157621-157987 within the genome, encoding a hypothetical neck protein.

## 2.17 Bacteriophage DNA identification using PCR

The PCR reaction was performed for the identification of bacteriophage DNA. The reaction was performed using Color Taq PCR Master Mix (EURx, Poland), specific primers (listed in Section 2.15, Genomed, Poland), nuclease free water (Roth, Germany) and the matrix (isolated according to the section 2.14.). The reaction was conducted with the following parameters: denaturation – 15 seconds, 94°C; annealing – 15 seconds, 55°C; extension – 60 seconds, 72°C; number of cycles: 30.

## 2.18 Electrophoresis and gel visualization

The obtained PCR reaction products were visualized in a 1.5% agarose gel (agarose solution in Tris-Octane-EDTA buffer (Bioshop, Canada) supplemented with SimplySafe™ (EURx, Poland) solution according to the manufacturer's instructions). Electrophoresis was conducted for 30 minutes at 100 V. The gels were then visualized using a gel documentation system (FastGene FAS-DIGI PRO, Nippon Genetics Europe, Germany). Parameters of the images taken: aperture 9 AV, exposure 1/50 TV, ISO 1600.

## 2.19 Determination of bacteriophage numbers in mouse organs

Ten µl of the lysate of the appropriate organ was diluted in 90 µl of 0.89% NaCl. Serial dilutions (1:9 v/v each) were then prepared in 0.89% NaCl. Then, 100 µl of each dilution were added to 200 µl of the overnight culture of *Salmonella* Typhimurium in LB medium and incubated for 10 min, to adsorb bacteriophages at the bacterial surface. Then, 4 ml of the Taq medium (0.7% bacteriological agar (BTL, Poland) in LB medium (Bioshop, Canada) was added and poured into Petri dishes with LB-agar medium (1% Agar-Agar (BTL, Poland) in LB medium). The plates were incubated at 37°C for 24 hours. The bacteriophage titer was then counted on the basis of number of plaques appearing on plates. The bacteriophage titer was then counted according to the formula: $PFU/g = A \times \frac{1000}{V} \times 10^n$, where: A - plaque number in a particular plate, V - volume of bacteriophage stock, $10^n$ - bacteriophage dilution factor.

## 2.20 Microbiome analysis

Bacterial genomic DNA extracted from the gastrointestinal tract was purified according to the method described previously (12), using a commercially available reagent kit (Invitrogen, Carlsbad, CA, USA). The obtained DNA samples were sent (Genomed S.A., Warsaw, Poland) for 16S rRNA gene PCR amplification, library preparation, illumina MiSeq sequencing, and bioinformatics taxonomy analysis. The Shannon diversity index, taking into account the OTU (the abundance of each operational taxonomic unit) value, was calculated using the PAST software version 4.09. The Shapiro-Wilk test was used to determine the normality of the diversity index data, and a comparison of the variability of the bacterial families in the experimental groups and the control group was carried out using the paired samples T-test. The final step was to perform a frequency analysis and the chi square test to determine the relative contribution of the particular bacterial families in the microbiome of each experimental group. All the aforementioned comparisons were performed using IBM SPSS 21.0 software (SPSS Inc., Amonk, USA).

## 2.21 Statistical analysis

The results are presented as mean ± standard deviation (SD). For statistical analyses of the results, SPSS 21.0 (SPSS Inc., Amonk, USA) software was used. The normality of the distribution of variables was checked with the Kolmogorov-Smirnov test, and the homogeneity of the variances with the Levene test. When the outcome of the Kolmogorov-Smirnov test indicated that the data were not distributed normally, we used non-parametric Kruskal-Wallis and Dunn tests for further analysis. For other parameters, two-way ANOVA and Tukey's *post hoc* tests were performed. The *p* value lower than 0.05 was considered statistically significant.

# 3 Results

## 3.1 Antibiotic therapy induces hyperactivity in the actometers which is more pronounced in females

To test effects of administrations of the bacteriophage cocktail and antibiotics on functions of the central nervous system (memory and learning processes, anxiety reactions, locomotor activity), behavioral assays were performed. Number of horizontal, vertical and ambulatory movements were determined at various times during the treatment (Figure 2). Unexpectedly, we found that antibiotic therapy led to severe behavioral disturbances, already after seven days of the administration, which were manifested by hyperactivity, expressed by an increased number of the three types of movement. The observed deviation from the natural behavioral pattern persisted throughout the whole antibiotic treatment period (fourteen days). Interestingly, this feature was significantly more severe in females than in males. Such a disturbed behavioral phenotype may be an indication of a seriously impaired central nervous system function, following the use of antibiotics, particularly the enrofloxacin. In contrast, both males and females

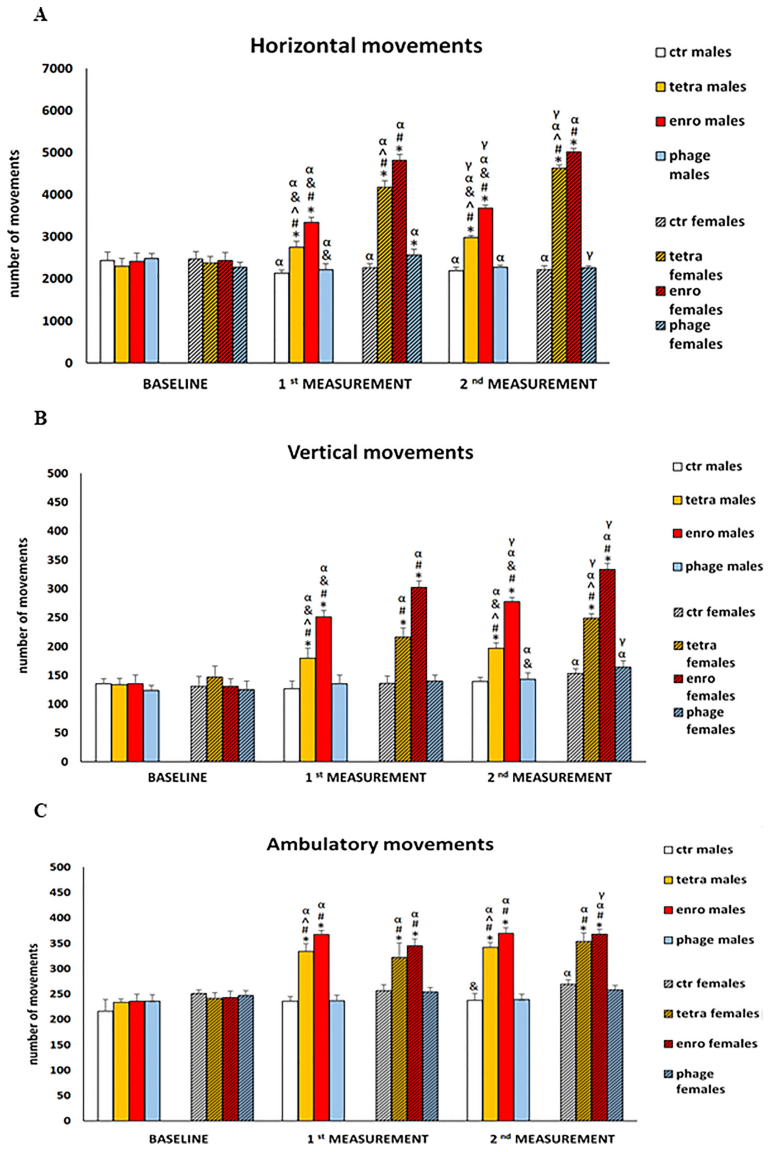


FIGURE 2
Changes in the number of three types of movements performed in 10 minutes in actometers: **(A)** horizontal, **(B)** vertical and **(C)** ambulatory in male and female mice receiving saline, antibiotics or bacteriophage cocktail. Results are presented as mean values ± SD. Statistical analyses were performed by ANOVA and *post-hoc* Tukey test for horizontal and vertical movements and by Kruskal-Wallis test and *post-hoc* Dunn test for ambulatory movements. The significance of differences between controls and particular treated groups are marked by: asterisks (*) vs. saline control males or saline control females group; (#) vs. bacteriophage males or bacteriophage females group; (^) vs. enrofloxacin males or enrofloxacin females group; (δ) vs. females; (α) vs. baseline value; (γ) vs. 7 days.

receiving the bacteriophage cocktail did not differ in their locomotor behavior from animals in the control groups throughout the supplementation period.

## 3.2 Antibiotics generate anxiety behaviors that are more severe in females

The results of anxiety behavior in the open field test are shown in Figure 3, and in Supplementary Figures S1, S2. Another indication of antibiotic-mediated central nervous system dysfunction was an increase in the anxiety behavior. The central squares, which are open spaces that are further illuminated by bright light, are a factor for rodents to induce severe stress and anxiety. Animals that, despite the aversive nature of this test zone, stay in it for a longer period of time are characterized by lower levels of anxiety. High level of stress was mainly manifested by shorter duration of stay, fewer entrances, and shorter distance travelled in the central (inner) quadrants by mice. In addition, the administration of antibiotics, especially enrofloxacin, caused hyperactivity similar to that observed in actometers. All of these disturbances were evident after only seven days of administration and, noteworthy, they were particularly severe in females. In contrast, the behavior of both males and females receiving the

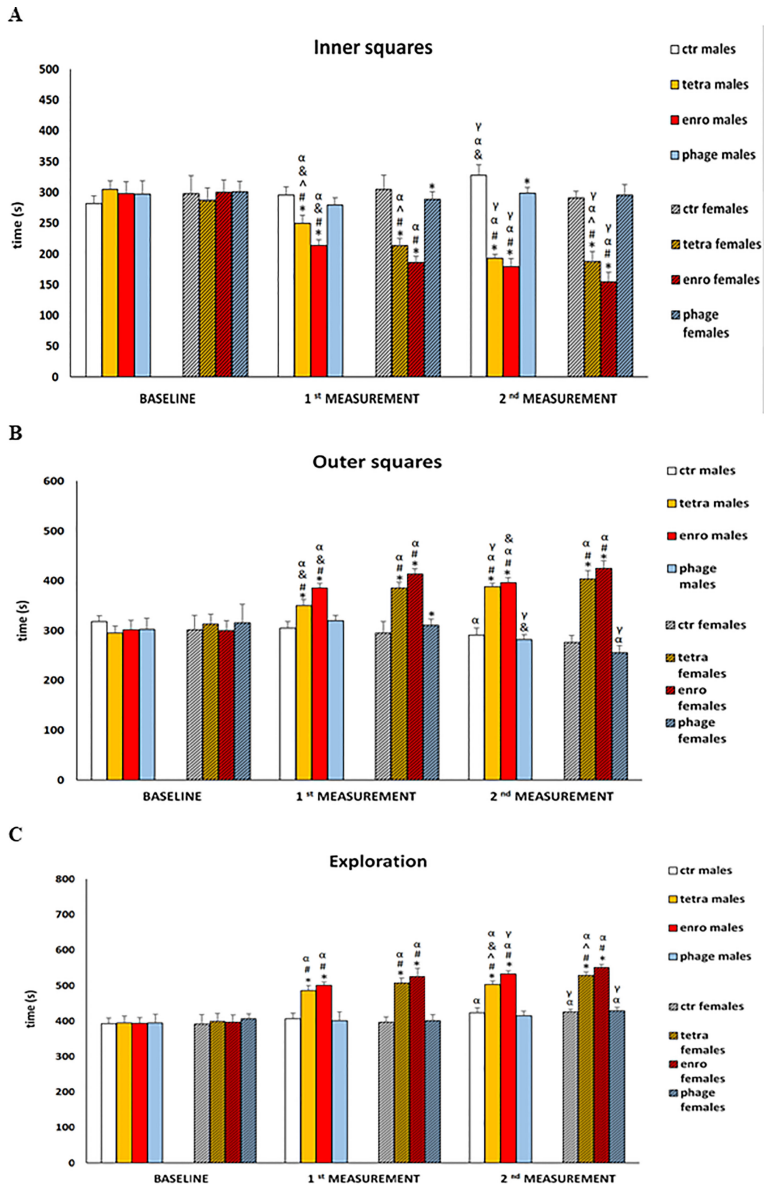


FIGURE 3
Changes in the anxiety behavior in the open field test (10-minute recording): **(A)** time spent in the inner squares, **(B)** time spent in the outer squares, **(C)** exploration in male and female mice receiving saline, antibiotics or bacteriophage cocktail. Results are presented as mean values ± SD. Statistical analyses were performed by ANOVA and *post-hoc* Tukey test. The significance of differences between controls and particular treated groups are observed and marked by: asterisks (*) vs. saline control males or saline control females group; (#) vs. bacteriophage males or bacteriophage females group; (^) vs. enrofloxacin males or enrofloxacin females group; (&) vs. females; (α) vs. baseline value; (γ) vs. 1st measurement value.

bacteriophage cocktail did not differ from that of the control groups and did not show symptoms of increased anxiety.

## 3.3 Short-term memory impairment following antibiotics administration

The results of assessment of the anxiety level and memory processes in the elevated plus-maze test (EPM) are presented in Figure 4 and Supplementary Figure S3. Analysis of the rate of movement of mice from the open, aversive arm to the closed (safe) arm makes it possible to study the course of working (short-term) memory, which is disrupted not only in the course of neurodegenerative diseases, but also under the influence of strong stimuli, such as stress/anxiety. A more complex behavioral analysis, including not only anxiety levels but also memory processes, carried out in the EPM test, confirmed previous observations of nervous system dysfunction after antibiotic therapy. Statistical analysis after

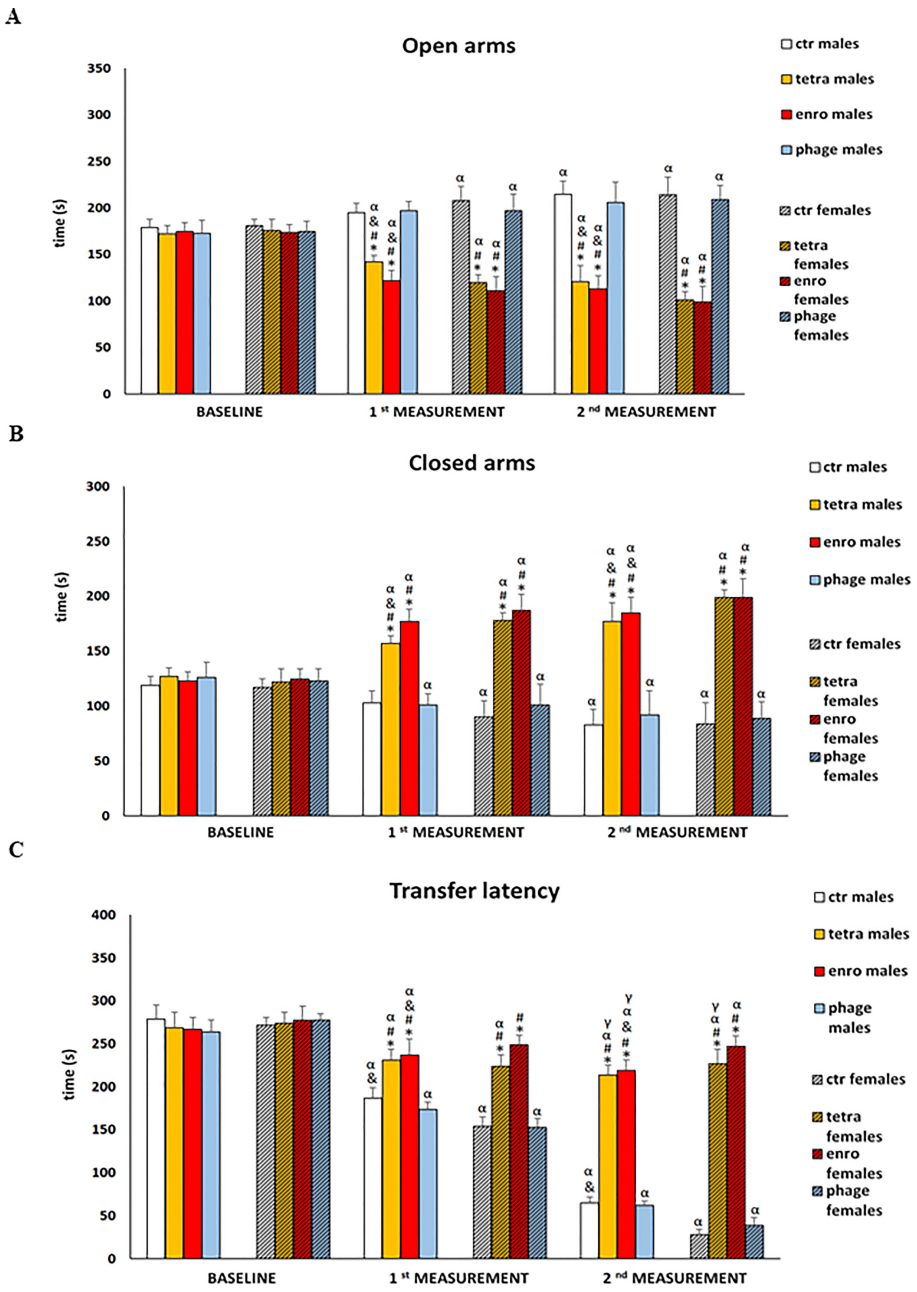


FIGURE 4
Changes in the anxiety behavior and memory processes in the elevated plus-maze test (5 minutes): **(A)** time spent in the open arms, **(B)** time spent in the closed arms, **(C)** transfer latency in male and female mice receiving saline, antibiotics or bacteriophage cocktail. Results are presented as mean values ± SD. Statistical analyses were performed by Kruskal-Wallis test and *post-hoc* Dunn test. The significance of differences between controls and particular treated groups are observed and marked by: asterisks (*) vs. saline control males or saline control females group; (#) vs. bacteriophage males or bacteriophage females group; (&) vs. females; (α) vs. baseline value; (γ) vs. 1st measurement value.

just seven days of the administration onset showed significantly reduced number of entries and shorter time spent in the open arms of the maze by mice. Furthermore, both antibiotics (though especially enrofloxacin) interfered with appropriate learning and memory processes, expressed by a prolongation of the transfer latency from the aversive (open) to the closed (safe) arms. In addition, non-natural locomotor activity was noted. All these abnormalities persisted throughout the supplementation period and were significantly more severe in females. For the group receiving the bacteriophage cocktail, both male and female mice did not differ from the control animals in the analyzed parameters.

## 3.4 Antibiotic therapy results in leukocytosis which is more severe in males

The absolute numbers and relative numbers of leukocytes, lymphocytes, monocytes, as well as red blood cell parameters, measured in all tested groups, are shown in Supplementary Table S1 and in the Supplementary Table S2. The absolute number of leukocytes (especially lymphocytes, but also granulocytes and monocytes) was elevated after tetracycline and enrofloxacin supplementation. Elevated lymphocyte levels indicate chronic or severe bacterial/viral infections, the development of inflammation, dehydration or neurological injury. In turn, increased granulocyte production occurs during inflammation. Elevated monocytes often appear after past infections, at a time when there is an intense renewal of leukocytes after infection. In contrast to behavioral studies, the negative effects of the antibiotic therapy on hematological parameters were more severe in males than in females. When the bacteriophage cocktail was used, the values observed did not differ significantly from those noted in the control groups. The same conclusion applied to the relative values. As for erythrocyte indices, the statistically significant reduction was noted in both females and males after administration of both antibiotics. Such results may indicate the initial phase of anaemia, but also bone marrow failure.

## 3.5 Decrease in the percentage of T lymphocytes and their key subpopulations (Tc, TCD8+ and Th, TCD4+) after antibiotic therapy

The results of cytometric analyses are presented in Figure 5. Interestingly, these analyses showed a statistically significant reduction in the percentage of T lymphocytes, as well as key cytotoxic and T helper subpopulations, in antibiotic-treated animals. This adverse effect of the antibiotic therapy (which was more severe after enrofloxacin administration) was seen at comparable levels in animals of both sexes. An insufficient proportion of T cytotoxic lymphocytes may hinder the elimination of cells infected by viruses or other intracellular parasites. In turn, a deficiency of T helper lymphocytes may reduce the release of cytokines, which are important mediators of differentiation and antibody release by B lymphocytes. We noted the opposite effect after administration of bacteriophages, namely, such a treatment did not affect the percentage of key immune cells in mice.

## 3.6 Antibiotic therapy results in cytokine imbalance which is more severe in females

The results of measurements of pro-inflammatory (IL-6, TNF-α) and anti-inflammatory (IL-10) cytokine concentrations in plasma are presented in Figure 6. Statistical analysis showed a significant cytokine imbalance induced by the administration of both antibiotics. As with most other parameters, this negative effect was especially pronounced during enrofloxacin supplementation, and showed a greater severity in females. The changes consisted of not only a decrease in the concentration of both pro-inflammatory cytokines (TNF-α and IL-6), but also IL-10. One should note that TNF-α and IL-6 are particularly important for the regulation of memory processes, and IL-10 exerts an anti-inflammatory effect. In contrast, the use of bacteriophages did not induce any changes in levels of investigated cytokines.

## 3.7 Weight loss following the antibiotics administration

The average weight of the mice at the start of the experiments was 29 ± 2 g and 25 ± 2 g for males and females, respectively. After fourteen days of saline or bacteriophage cocktail supplementation, there was an increase in the weight of mice by an average of 2 g, while the antibiotic treatment groups showed a statistically significant decrease in weight by an average of 2 (tetracycline) or 4 (enrofloxacin) g.

## 3.8 Antibiotic therapy leads to a reduction in organ weights which is more severe in females

The results of the weight of particular internal organs after fourteen days of antibiotic or bacteriophage administration are presented in the Supplementary Figure S4. Statistically significant reduction in weight was seen in the spleen, thymus, kidneys, intestines and stomach. In all of these organs, the reduction of weight was evident after the antibiotic therapy, particularly when the administration of enrofloxacin was performed, and there was more pronounced in females. Interestingly, the opposite situation was found for the heart and liver, as after the antibiotic therapy, there was an increase in heart and liver weight in females and in mice of both sexes treated with enrofloxacin. Only for the brain, it was no difference in the organ weight between groups and sexes. In the groups receiving the bacteriophage cocktail, the organs' weights did not differ from those in the control groups.

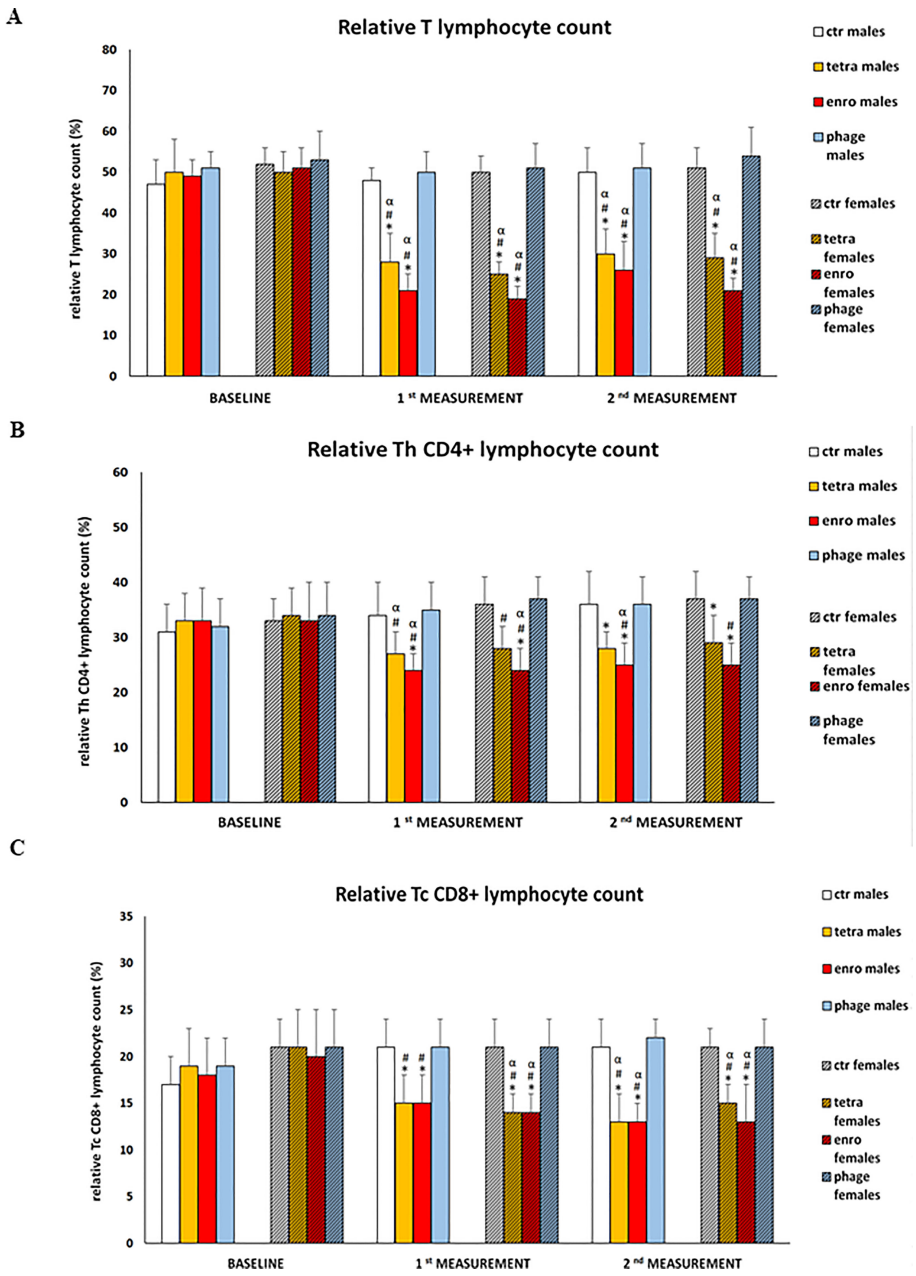


FIGURE 5
Changes in relative T lymphocyte **(A)**, relative Th TCD4+ **(B)** and relative Tc TCD8+ **(C)** counts in the blood of male and female mice receiving saline, antibiotics or bacteriophage cocktail. Results are presented as mean values ± SD. Statistical analyses were performed by ANOVA and *post-hoc* Tukey test. The significance of differences between controls and particular treated groups are observed and marked by: asterisks (*) vs. saline control males or saline control females group; (#) vs. bacteriophage males or bacteriophage females group; (&) vs. females; (α) vs. baseline value.

## 3.9 Confirmation of the presence of bacteriophages in the examined organs

Identification of bacteriophages in organs of mice treated with the bacteriophage cocktail was performed by PCR. The organs were homogenized, and then total DNA was isolated.

Specific products of 988 bp (bacteriophage vB_SenM-2) and 736 bp (bacteriophage vB_Sen-TO17) were confirmed in the brains of female mice, however, no specific product was obtained for bacteriophage vB_SenM-2 in the brains of male mice (Figure 7). Moreover, products specific for both bacteriophages were obtained in spleens, livers and kidneys of males and females. However, products specific for bacteriophages vB_SenM-2 and vB_Sen-TO17 were observed in male hearts, while they were not detected in hearts of female mice (Supplementary Figure S5).

The number of bacteriophages in the liver, spleen, kidney, heart and brain was also determined by the titration method. The presence of bacteriophage vB_Sen-TO17 in the liver, spleen, kidney, heart and

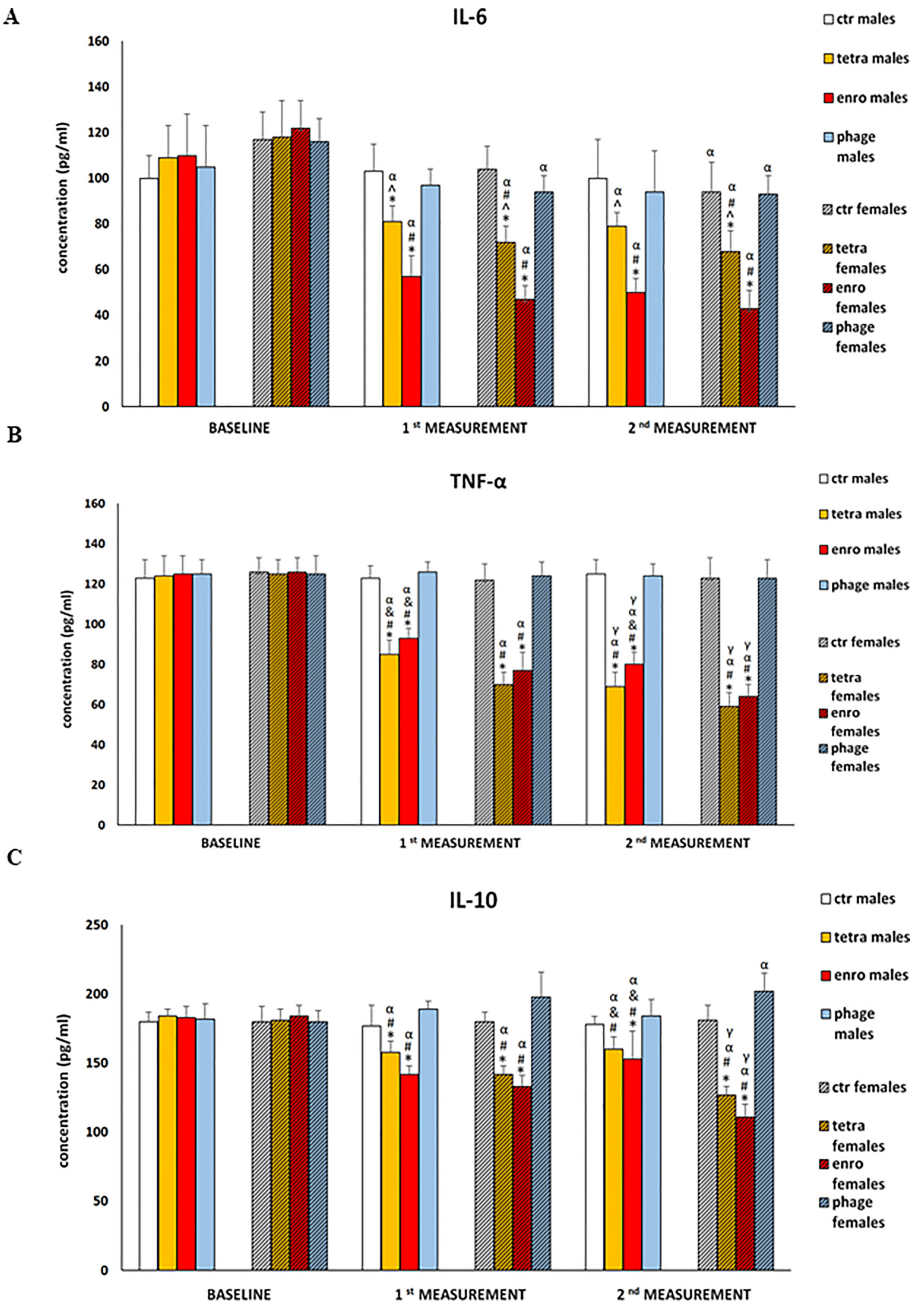


FIGURE 6
Changes in the cytokine concentrations: Il-6 **(A)**, TNF-α **(B)**, and IL-10 **(C)** in the blood plasma of male and female mice receiving saline, antibiotics or bacteriophage cocktail. Results are presented as mean values ± SD. Statistical analyses were performed by ANOVA and *post-hoc* Tukey test. The significance of differences between controls and particular treated groups are observed and marked by: asterisks (*) vs. saline control males or saline control females group; (#) vs. bacteriophage males or bacteriophage females group; (ϑ) vs. females; (α) vs. baseline value; (γ) vs. 1st measurement value.

brain of females and males was found. Interestingly, the bacteriophage vB_SenM-2 was present in the livers, spleens, kidneys and hearts of males. The titer of bacteriophage vB_SenM-2 was 5 times lower than that of bacteriophage vB_Sen-TO17 in the livers of females and 2.5 times lower in the livers of males. In the kidneys and spleens, the titer of bacteriophage vB_Sen-TO17 was 10 times higher than that of bacteriophage vB_SenM-2 in females and males. In addition, the presence of bacteriophages vB_Sen-TO17 and vB_SenM-2 in the brains of females was noted. However, bacteriophage vB_SenM-2 was not detected in the brains of males.

## 3.10 Microbiome changes following bacteriophage and antibiotic administration

As indicated in Figure 8 and Supplementary Figure S6, the most significant changes in the microbiome were observed after fourteen days of the antibiotic or bacteriophage supplementation, respectively. Interestingly, after treatment with enrofloxacin, *Muribaculaceae* predominated in males. In contrast, in bacteriophage-treated females, this bacterial family dominated

10.3389/fimmu.2023.1133358

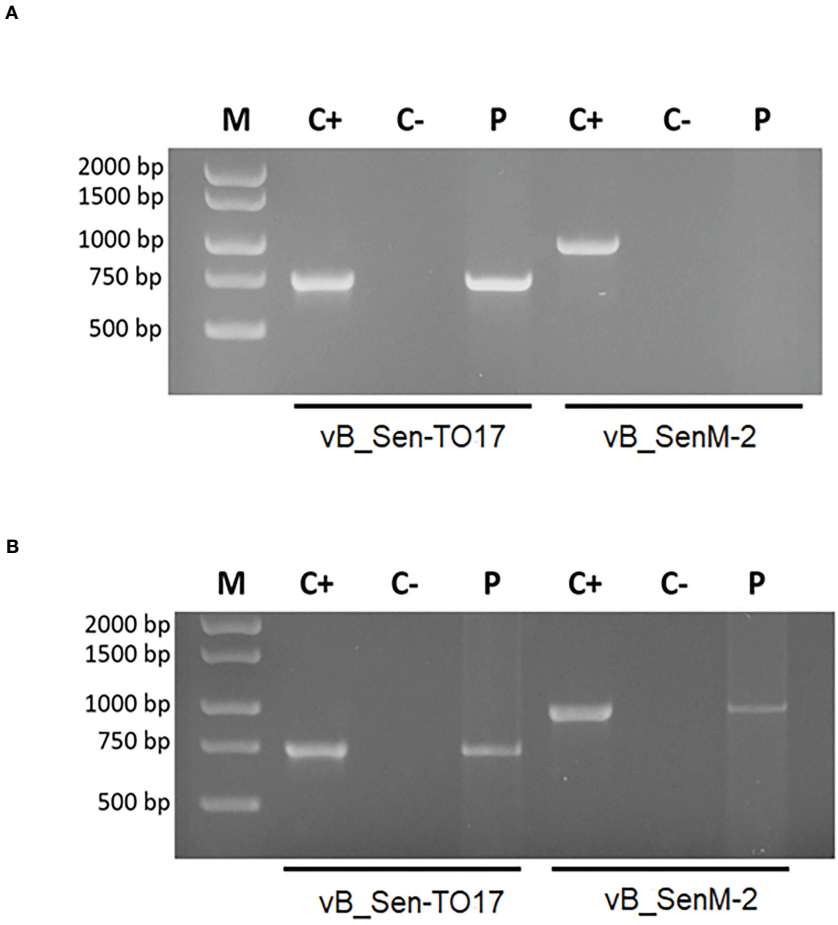


FIGURE 7
Identification of bacteriophages in brains of male **(A)** and female **(B)** mice treated with the bacteriophage cocktail. Specific products of 988 bp (bacteriophage vB_SenM-2) and 736 bp (bacteriophage vB_Sen-TO17) were analyzed by the PCR method. The matrix in the positive control was DNA isolated from purified bacteriophage lysate (PFU/ml=$10^9$). For the negative control, water was added instead of matrix.

after only seven days of supplementation. In turn, enrofloxacin-treated females had a microbiome dominated by bacteria from the *Lactobacilaceae* family. Similar distribution of bacteria was observed in mice of both sexes from the control groups and those receiving bacteriophage cocktail.

## 4 Discussion

In the present study, we compared effects of administration of antibiotics (enrofloxacin and tetracycline) and bacteriophage therapy in a mouse model. We demonstrated, for the first time, a sex-dependent negative effect of antibiotic therapy, which not only involved the functioning of the immune system, but also significantly impaired the activity of the central nervous system, as manifested by a disruption of the behavioral pattern, particularly exacerbated in females. On the other hand, the complex behavioral and immunological analyses confirmed the lack of adverse effects after the bacteriophage cocktail administration.

The issue concerning the differences in the presence of bacteriophages in the various organs in males and females undoubtedly requires further research. Nevertheless, it can be speculated that, as with the bioavailability of nanomedicines, the differences between the sexes are on the cellular and molecular levels. Physiological differences between the sexes are also not limited to body fat and water content, plasma volume or the amount of blood reaching particular organs. For example, it has been confirmed that there are differences between men and women in the expression of thousands of genes that determine the functions of the liver, adipose tissue or skeletal muscle. In turn, the kidneys showed the presence of transporters which expression levels differ between males and females. Transcriptomic analysis of human kidneys confirmed the presence of twenty-one genes with male dominance and two transporter genes with female dominance. Further differentiating factors which role should not be overlooked are sex hormones (19). Moreover, analyses carried out on the heart showed that the profiles of functionally relevant proteins and their isoforms differed in animals of both sexes. These differences, included more than twenty-two proteins and increased significantly with the age of the mice (20). Male-specific expression of Y-linked genes was observed not only in mouse heart, but also in the human myocardium (e.g. Ddx3y, Eif2s3y and Jarid1d). Higher expression levels of X-linked genes were detected in female mice for Xist, Timp1, Car5b, XIST, EIF2S3X and GPM6B.

10.3389/fimmu.2023.1133358

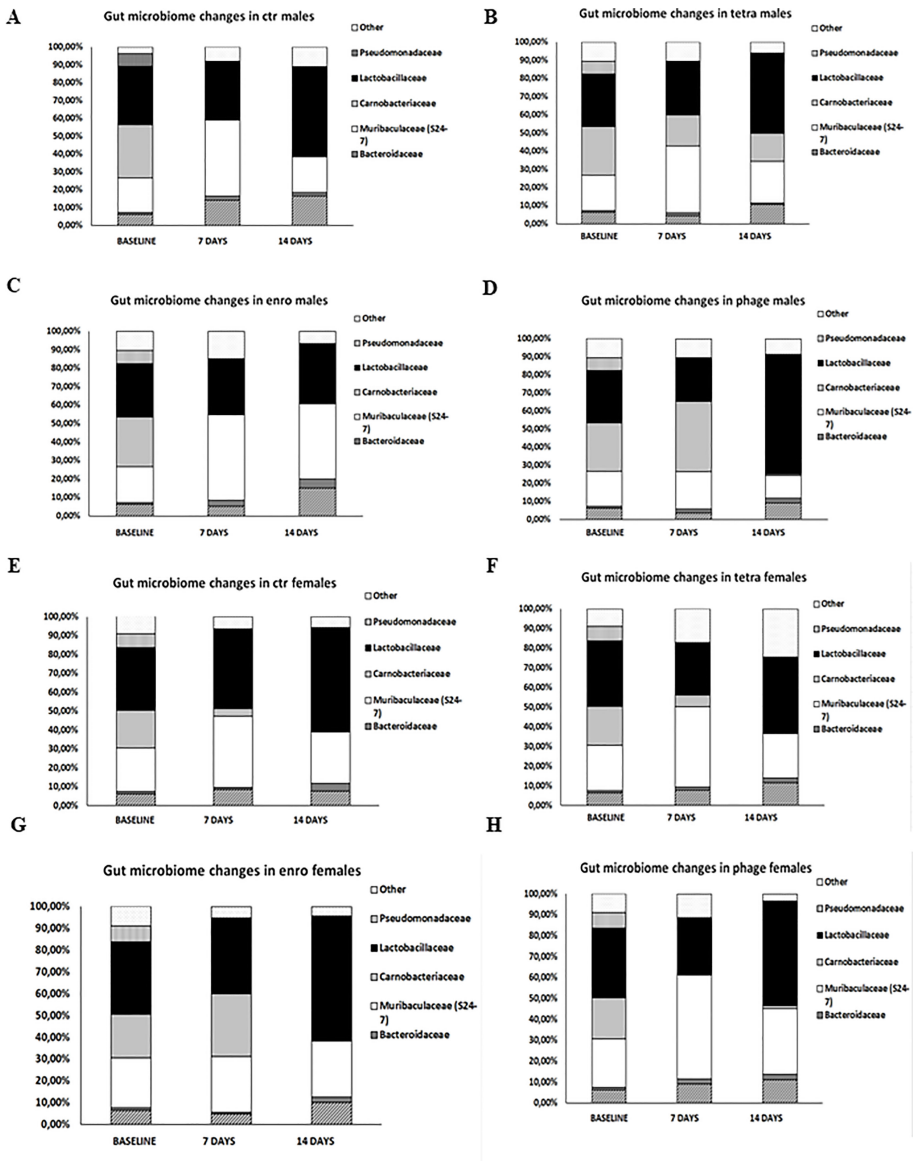


FIGURE 8
Differences in mice intestinal microbiome in particular groups: **(A)** males saline control group; **(B)** males tetracycline group; **(C)** males enrofloxacin group; **(D)** males bacteriophage group; **(E)** females saline control group; **(F)** females tetracycline group; **(G)** females enrofloxacin group; **(H)** females bacteriophage group.

In addition, genes on autosomal chromosomes encoding cytochromes of the monoxygenase family (e.g. Cyp2b10), carbonic anhydrases (e.g. Car2 and Car3) and natriuretic peptides (e.g. Nppb) were identified with sex- and/or age-specific expression levels (21). Furthermore, only female mice showed differences in the expression of important genes, including those regulating DNA metabolism, which showed a strong dependence on tissue/organ type following exposure to low doses of radiation (22). What is more, previous studies have shown that DNA isolates obtained from different types of organs from female mice confirmed significant differences in the level of damage as a result to exposure to organic wood preserving waste extracts. Adduct profiles were tissue-specific and displayed a multitude of non-polar DNA (23). Interestingly, the response to viral infection is strongly dependent on hormonal regulation and differs between males and females. Experiments with non-gonadectomized rats have shown that infection with Seoul virus results in the elevated levels of viral RNA, which was detected in males, but not in females. In contrast, removal of the gonads in males resulted in comparable levels of viral RNA to that observed in intact females. The opposite effect was noticed in females, in which the levels were significantly higher. Induction of pattern recognition receptors (PRRs, TLR7 and Rig-1), expression of antiviral genes (Myd88, Visa, Jun, IRF7, IFNβ, Ifnar1, Jak2, Stat3 and Mx2), and production of Mx protein were elevated in the lungs of intact females compared with intact males. Hormone cycle activity appears to have a significant impact primarily on the induction of PRRs than downstream IFNβ or Mx2 expression (24). However, the mechanism underlying the

differences in bacteriophage location in particular organs in animals of both sexes requires additional investigation. Although sex-dependent, central nervous system-related differences in response of animals to treatment with antibiotics were not – to our knowledge - described previously, indications of changed behaviors after antibiotic therapy were reported recently. Namely, it was showed that administration of clindamycin and/or amoxicillin caused severe behavioral disturbances (25). First of all, a deterioration of cognitive processes in the novel object recognition test and an increase in the percentage of depressive behavior episodes were noted in the tail suspension test. In contrast to our study, those experiments were conducted only with females. It was proposed that an indirect cause of the observed behavioral disturbances was a dysbiosis of the gut microbiome induced by antibiotics (11). One should note that such adverse effects may increase the risk of neurodegenerative diseases in the long term (26). Similar conclusions were included in the report describing investigations of the effects of antibiotic therapy on anxiety behavior in mice (27). Although the authors of that report also did not take into account differences between animals of both sexes, they observed that streptomycin treatment significantly increased anxiety in mice in the light-dark box test and in the elevated plus-maze test. Again, they also suggested a dysbiosis of the gut microbiome as a potential cause of the observed disturbances (27). The long-term effects of the low-dose penicillin intake by pregnant mice on these animals and their offspring shortly after the birth were also studied (28). Gut microbiome, blood-brain barrier permeability, central (brain) cytokine expression and behavior were analyzed to demonstrate that the use of antibiotics at an early stage of development can have negative and long-term side effects (28). Among other changes, a disruption of cytokine expression in the frontal cortex, which directly translated into behavioral disturbances (manifested by increased aggression, anxiety, and decreased social interaction), was evident. The behavioral pattern of the antibiotic-treated animals resembled autism spectrum disorders in children (28). Therefore, one might speculate that the lack of an adequate diversity of beneficial bacteria forming a part of the gut microbiome increases the permeability of the blood-brain barrier, thus negatively affecting the microglia immune response, myelination, the neurochemical structure of the brain or the activity of the hypothalamic-pituitary-adrenal stress axis (28).

In the case of our study, the most pronounced change in the microbiome was the increase in the percentage of bacteria from the still poorly understood *Muribaculaceae* family, both in males after enrofloxacin treatment and in females receiving the bacteriophage cocktail. Previous studies have shown that the *Muribaculaceae* family is associated with the formation of the inner mucus layer in the colon and the proper functioning of the intestinal barrier, and its abundance was strongly correlated with the level of propionate, a kind of short-chain fatty acid negatively correlating with the colorectal cancer in mice (29). In addition, these bacteria are important in adaptation to hypoxia-induced stress and in response to the inflammatory process (30). Although we did not analyze the central immune response, the cytokine imbalance we demonstrated in the plasma in mice after the antibiotic therapy might be an indirect indicator of the negative effects of the tested antibiotics on neuroimmune parameters. We demonstrated that as short as two-week treatment with antibiotic may result in a severely disturbed behavioral pattern. Therefore, it is tempting to speculate that repeated or prolonged administration of antibiotics or their use early in life might have negative consequences in the form of metabolic disorders, allergies or neurodegenerative diseases.

Obviously, there are limitations of our studies. The foremost one is that the central immune response and histological changes in the brain were not analyzed, and the persistence and severity of the observed abnormalities were not verified. Only in the case of the female heart both methods used did not give a conclusive result. As the plaque counting method allows the detection of viable bacteriophages and the results indicated a low number of them in the heart of females, the PCR performed from the deep-frozen material proved to be an insensitive method with too many limitations in this experimental scheme. The detection limit of PCR method is usually in the range of $10^3$- $10^5$ PFU/ml. Furthermore, for the procedure we carried out, no additional steps were used to increase the sensitivity, such as magnetic capture hybridization, which could have contributed to discrepant results with the titration method. Nevertheless, the presented results are important indications of the risks that the antibiotic use may entail. In addition, to our knowledge, this is the first demonstration that the gender factor can be included in such a complex analysis as an important determinant, conditioning the course of the immune and behavioral response to the administered compounds. The mechanism of the differences between males and females in appearance of adverse effects, related to the behavioral and immune functions, in the response to antibiotic treatment remains to be elucidated. One might imagine that differences in hormones and/or different permeability of the blood-brain barrier can be important factors, however, extensive studies are required to find the real reason(s). Nevertheless, it is also important to note that this study confirmed the general safety of the use of bacteriophages *in vivo* which is a promising sing in the light of potential approval of bacteriophage therapy as a therapeutic procedure that might be used in clinical practice and in veterinary use.

## Data availability statement

The datasets presented in this study can be found in online repositories. The names of the repository/repositories and accession number(s) can be found below: NCBI database, BioProject ID PRJNA967510.

## Ethics statement

The animal study was reviewed and approved by the Local Ethics Committee for Experimental Animals in Bydgoszcz (permission number 02/2022, dated on January 19, 2022).

## Author contributions

ŁG prepared the bacteriophage cocktail, participated in behavioral tests and sections of mice, prepared blood for future experiments, performed the analysis of levels of cytokines in mice blood plasma, performed the analysis of levels of blood morphological parameters, analyzed the percentage of lymphocytes in peripheral blood, performed the PCR reactions, statistical analysis, co-drafted the manuscript, and prepared the visualization of the results. GW participated in sections of mice and participated in analyses of results and co-drafted the manuscript. AW participated in sections of mice, participated in the analysis of levels of cytokines, analyzed data, and co-drafted the manuscript. KP participated in behavioral tests, analyzed data and co-drafted the manuscript. KK-K and MS participated in preparing the material for the microbiome analysis. MG participated in designing the primers. GJ participated in behavioral tests. MP presented the concept of the study, planned and coordinate experiments, participated and coordinated the sections of mice, participated in the behavioral analysis and analysis of levels of cytokines in mice blood plasma, participated in the analysis of levels of blood morphological parameters and participated in the analysis of the percentage of lymphocytes in peripheral blood, and co-drafted the manuscript. All authors contributed to the article and approved the submitted version.

## Funding

This work was supported by the National Science Centre (Poland) within project grant no. 2021/05/X/NZ4/00221.

## Conflict of interest

The authors declare that the research was conducted in the absence of any commercial or financial relationships that could be construed as a potential conflict of interest.

## Publisher's note



## Supplementary material

The Supplementary Material for this article can be found online at: https://www.frontiersin.org/articles/10.3389/fimmu.2023.1133358/full#supplementary-material

SUPPLEMENTARY FIGURE 1
Changes in the anxiety behavior in the open field test (10 minutes): **(A)** frequency of entries to the inner squares; **(B)** frequency of entries to the outer squares; **(C)** immobility in male and female mice receiving saline, antibiotics or bacteriophage cocktail. Results are presented as mean values ± SD. Statistical analyses were performed by ANOVA and *post-hoc* Tukey test. The significance of differences between controls and particular treated groups are observed and marked by: asterisks (*) vs. saline control males or saline control females group; (#) vs. bacteriophage males or bacteriophage females group; (^) vs. enrofloxacin males or enrofloxacin females group; (&) vs. females; (α) vs. baseline value; (γ) vs. 1$^{st}$ measurement value.

SUPPLEMENTARY FIGURE 2
Changes in the anxiety behavior in the open field test (10 minutes): **(A)** distance in the inner squares; **(B)** distance in the outer squares in male and female mice receiving saline, antibiotics or bacteriophage cocktail. Results are presented as mean values ± SD. Statistical analyses were performed by ANOVA and *post-hoc* Tukey test. The significance of differences between controls and particular treated groups are observed and marked by: asterisks (*) vs. saline control males or saline control females group; (#) vs. bacteriophage males or bacteriophage females group; (^) vs. enrofloxacin males or enrofloxacin females group; (&) vs. females; (α) vs. baseline value.

SUPPLEMENTARY FIGURE 3
Changes in the anxiety behavior and memory processes in the elevated plus-maze test (5 minutes): **(A)** number of entries to open arms, **(B)** number of entries to closed arms, **(C)** exploration in male and female mice receiving saline, antibiotics or bacteriophage cocktail. Results are presented as mean values ± SD. Statistical analyses were performed by ANOVA and *post-hoc* Tukey test for number of entries to open arms and exploration and by Kruskal-Wallis test and *post-hoc* Dunn test for number of entries to closed arms. The significance of differences between controls and particular treated groups are observed and marked by: asterisks (*) vs. saline control males or saline control females group; (#) vs. bacteriophage males or bacteriophage females group; (&) vs. females; (α) vs. baseline value; (γ) vs. 1$^{st}$ measurement value.

SUPPLEMENTARY FIGURE 4
Changes in the weights of particular internal organs: **(A)** brain, **(B)** spleen, **(C)** thymus, **(D)** heart, **(E)** liver, **(F)** kidneys, **(G)** intestines and **(H)** stomach, after fourteen days of antibiotic or bacteriophage administration in male and female mice. Results are presented as mean values ± SD. Statistical analyses were performed by ANOVA and *post-hoc* Tukey test. The significance of differences between controls and particular treated groups are observed and marked by: asterisks (*) vs. saline control males or saline control females group; (#) vs. bacteriophage males or bacteriophage females group; (&) vs. females.

SUPPLEMENTARY FIGURE 5
Identification of bacteriophages in particular organs: **(A)** livers of male, **(B)** livers of female, **(C)** kidneys of male, **(D)** kidneys of female, **(E)** spleens of male, **(F)** spleens of female, **(G)** hearts of male, **(H)** hearts of female mice treated with the bacteriophage cocktail. Specific products of 988 bp (bacteriophage vB_SenM-2) and 736 bp (bacteriophage vB_Sen-TO17) were analyzed by the PCR method.

SUPPLEMENTARY FIGURE 6
The Shannon diversity index, taking into account the OTU (the abundance of each operational taxonomic unit) value.

SUPPLEMENTARY TABLE 1
Changes in the absolute ($10^3$/μl) counts of leukocytes, lymphocytes, monocytes and granulocytes and relative (%) values of lymphocytes, monocytes and granulocytes in blood of male and female mice receiving saline, antibiotics or bacteriophage cocktail. Results are presented as mean values ± SD. Statistical analyses were performed by Kruskal-Wallis test and *post-hoc* Dunn test. The significance of differences between controls and particular treated groups are observed and marked by: asterisks (*) vs. saline control males or saline control females group; (#) vs. bacteriophage males or bacteriophage females group; (&) vs. females; (α) vs. baseline value.

SUPPLEMENTARY TABLE 2
Changes in the erythrocyte number ($10^6$/$mm^3$), hemoglobin (g/dL) and hematocrit (%) level as well as erythrocyte indicators: MCV (Mean Corpuscular Volume, fL), MCH (Mean Corpuscular Hemoglobin, pg), MCHC (Mean Corpuscular Hemoglobin Concentration, g/L) and platelet number ($10^3$/$mm^3$) in blood of male and female mice receiving saline, antibiotics or bacteriophage cocktail. Results are presented as mean values ± SD. Statistical analyses were performed by Kruskal-Wallis test and *post-hoc* Dunn test. The significance of differences between controls and particular treated groups are observed and marked by: asterisks (*) vs. saline control males or saline control females group; (#) vs. bacteriophage males or bacteriophage females group; (&) vs. females; (α) vs. baseline value.

# References


1. Loponte R, Pagnini U, Iovane G, Pisanelli G. Bacteriophage therapy in veterinary medicine. *Antibiotics* (2021) 10(4):421. doi: 10.3390/antibiotics10040421

2. Brix A, Cafora M, Aureli M, Pistocchi A. Animal models to translate bacteriophage therapy to human medicine. *Int J Mol Sci* (2020) 21(10):3715. doi: 10.3390/ijms21103715

3. CDC. *Antibiotic resistance threats in the united states, 2019* (2019). Atlanta, GA: U.S. Department of Health and Human Services, CDC (Accessed 04.02.2023).

4. Murray CJ, Ikuta KS, Sharara F, Swetschinski L, Robles Aguilar G, Gray A, et al. Global burden of bacterial antimicrobial resistance in 2019: a systematic analysis. *Lancet* (2022) 399:629–55. doi: 10.1016/S0140-6736(21)02724-0

5. Patel SJ, Wellington M, Shah RM, Ferreira MJ. Antibiotic stewardship in food-producing animals: challenges, progress, and opportunities. *Clin Ther* (2020) 42:1649–58. doi: 10.1016/j.clinthera.2020.07.004

6. Yang X, Huang J, Wu Q, Zhang J, Yang S, Wang J, et al. Occurrence, serovars and antibiotic resistance of salmonella spp. in retail ready-to-eat food products in some Chinese provinces. *LWT* (2022) 154:112699. doi: 10.1016/j.lwt.2021.112699

7. Nadi ZR, Salehi TZ, Tamai IA, Foroushani AR, Sillanpaa M, Dallal MMS. Evaluation of antibiotic resistance and prevalence of common *Salmonella enterica* serovars isolated from foodborne outbreaks. *Microchem J* (2020) 155:104660. doi: 10.1016/j.microc.2020.104660

8. Kortright KE, Chan BK, Koff JL, Turner PE. Bacteriophage therapy: a renewed approach to combat antibiotic-resistant bacteria. *Cell Host Microbe* (2019) 25:219–32. doi: 10.1016/j.chom.2019.01.014

9. Podlacha M, Grabowski Ł., Kosznik-Kawśnicka K, Zdrojewska K, Stasiłojć M, Węgrzyn G, et al. Interactions of bacteriophages with animal and human organisms–safety issues in the light of bacteriophage therapy. *Int J Mol Sci* (2021) 22(16):8937. doi: 10.3390/ijms22168937

10. Kosznik-Kwaśnicka K, Stasiłojć M, Grabowski Ł., Zdrojewska K, Węgrzyn G, Węgrzyn A. Efficacy and safety of bacteriophage therapy against *Salmonella enterica* serovars typhimurium and enteritidis estimated by using a battery of *in vitro* tests and the *Galleria mellonella* animal model. *Microbiol Res* (2022) 261:127052. doi: 10.1016/j.micres.2022.127052

11. Kosznik-Kwaśnicka K, Ciemińska K, Grabski M, Grabowski Ł., Górniak M, Jurczak-Kurek A, et al. Characteristics of a series of three bacteriophages infecting *Salmonella enterica* strains. int. *J Mol Sci* (2020) 21:1–26. doi: 10.3390/ijms21228821

12. Jurczak-Kurek A, Gasior T, Nejman-Faleńczyk B, Bloch S, Dydecka A, Topka G, et al. Biodiversity of bacteriophages: morphological and biological properties of a large group of bacteriophages isolated from urban sewage. *Sci Rep* (2016) 6:1–17. doi: 10.1038/srep34338

13. Kosznik-Kwaśnicka K, Podlacha M, Grabowski Ł., Stasiłojć M, Nowak-Zaleska A, Ciemińska K, et al. Biological aspects of bacteriophage therapy versus antibiotics against *Salmonella enterica* serovar typhimurium infection of chickens. *Front Cell Infect Microbiol* (2022) 12:941867. doi: 10.3389/fcimb.2022.941867

14. Green MR, Sambrook J, Sambrook J. *Molecular cloning: a laboratory manual. 4th ed*. Cold Spring Harbor, N.Y: Cold Spring Harbor Laboratory Press (2012).

15. Hurwitz BL, Deng L, Poulos BT, Sullivan MB. Evaluation of methods to concentrate and purify ocean virus communities through comparative, replicated metagenomics. *Environ Microbiol* (2012) 15:1428–40. doi: 10.1111/j.1462-2920.2012.02836.x

16. Kosznik-Kwaśnicka K, Grabowski Ł., Grabski M, Kaszubski M, Górniak M, Jurczak-Kurek A, et al. Bacteriophages vb_Sen-TO17 and vb_Sen-e22, newly isolated viruses from chicken feces, specific for several *Salmonella enterica* strains. *Int J Mol Sci* (2020) 21:1–21. doi: 10.3390/ijms21228821

17. Podlacha M, Pierzynowska K, Gaffke L, Jerzemowska G, Piotrowska E, Węgrzyn G. Behavioral- and blood-based biomarkers for huntington's disease: studies on the R6/1 mouse model with prospects for early diagnosis and monitoring of the disease. *Brain Behav Immun - Heal* (2022) 23:100482. doi: 10.1016/j.bbih.2022.100482

18. Listowska M, Glac W, Grembecka B, Grzybowska M, Wrona D. Changes in blood CD4+T and CD8+T lymphocytes in stressed rats pretreated chronically with desipramine are more pronounced after chronic open field stress challenge. *J Neuroimmunol* (2015) 282:54–62. doi: 10.1016/j.jneuroim.2015.02.015

19. Madla CM, Gavins FK, Merchant HA, Orlu M, Murdan S, Basit AW. Let's talk about sex: differences in drug therapy in males and females. *Adv Drug Deliv Rev* (2021) 175:113804. doi: 10.1016/j.addr.2021.05.014

20. Dela Justina V, Miguez JS, Priviero F, Sullivan JC, Giachini FR, Webb RC. Sex differences in molecular mechanisms of cardiovascular aging. *Front Aging* (2021) 2:725884. doi: 10.3389/fragi.2021.725884

21. Isensee J, Witt H, Pregla R, Hetzer R, Regitz-Zagrosek V, Ruiz Noppinger P. Sexually dimorphic gene expression in the heart of mice and men. *J @ Mol Med* (2008) 86:61–74. doi: 10.1007/s00109-007-0240-z

22. Lee WJ, Majumder ZR, Jeoung DI, Lee HJ, Kim SH, Bae S, et al. Organ-specific gene expressions in C57BL/6 mice after exposure to low-dose radiation. *Radiat Res* (2006) 165(5):562–9. doi: 10.1667/RR3549.1

23. Randerath E, Zhou GD, Donnelly KC, Safe SH, Randerath K. DNA Damage induced in mouse tissues by organic wood preserving waste extracts as assayed by 32P-postlabeling. *Arch Toxicol* (1996) 70:683–95. doi: 10.1007/s002040050329

24. Hannah MF, Bajic VB, Klein SL. Sex differences in the recognition of and innate antiviral responses to Seoul virus in Norway rats. *Brain Behav Immun* (2008) 22 (4):503–16. doi: 10.1016/j.bbi.2007.10.005

25. Kwon HJ, Mohammed AE, Eltom KH, Albrahim JS, Alburae NA. Evaluation of antibiotic-induced behavioral changes in mice. *Physiol Behav* (2020) 223:113015. doi: 10.1016/j.physbeh.2020.113015

26. Roy Sarkar S, Banerjee S. Gut microbiota in neurodegenerative disorders. *J Neuroimmunol* (2019) 328:98–104. doi: 10.1016/j.jneuroim.2019.01.004

27. Park K, Park S, Nagappan A, Ray N, Kim J, Yoon S, et al. Probiotic *Escherichia coli* ameliorates antibiotic-associated anxiety responses in mice. *Nutrients* (2021) 13:1–10. doi: 10.3390/nu13030811

28. Leclercq S, Mian FM, Stanisz AM, Bindels LB, Cambier E, Ben-Amram H, et al. Low-dose penicillin in early life induces long-term changes in murine gut microbiota, brain cytokines and behavior. *Nat Commun* (2017) 8(1):15062. doi: 10.1038/ncomms15062

29. Zhang Z, Cao H, Song N, Zhang L, Cao Y, Tai J. Long-term hexavalent chromium exposure facilitates colorectal cancer in mice associated with changes in gut microbiota composition. *Food Chem Toxicol* (2020) 138:111237. doi: 10.1016/j.fct.2020.111237

30. Zhang Y, Luo H, Niu Y, Yang X, Li Z, Wang K, et al. Chronic intermittent hypoxia induces gut microbial dysbiosis and infers metabolic dysfunction in mice. *Sleep Med* (2022) 91:84–92. doi: 10.1016/j.sleep.2022.02.003

# Frontiers in Immunology

**Explores novel approaches and diagnoses to treat immune disorders.**

The official journal of the International Union of Immunological Societies (IUIS) and the most cited in its field, leading the way for research across basic, translational and clinical immunology.

## Discover the latest Research Topics

See more →


**Frontiers**

Avenue du Tribunal-Fédéral 34
1005 Lausanne, Switzerland
frontiersin.org

**Contact us**

+41 (0)21 510 17 00
frontiersin.org/about/contact